

THE EFFECTS OF SPATIO-TEMPORAL VARIATION IN ESTUARINE CONTAMINATION

Thesis submitted in accordance with the requirements of the University of Stirling for
the degree of Doctor of Philosophy by Christopher Richard Sneddon

January 2017

Abstract

With the coastal environment likely to be affected by climate change induced modifications to storminess (both frequency and intensity), sea level rise and increased precipitation in the near future, changes in sediment dynamics in terms of erosion, accretion and movement is expected. Given the important role coastal sediments play as sinks for environmental contaminants, understanding the fate and behaviour of these sediments is crucial in determining any potential impacts on humans and wildlife. This project investigates long-term trends in sediment movement in the Ribble estuary and how disturbance events might affect these trends.

The rate of erosion of sediment within the coastal environment is a concern as the diverse array of sediment deposits in the coastal margins are vital habitat for a range of wildlife. They also act as a substantial sink of radioactive contaminants from current and past discharge practices. Remobilisation and any consequent changes in bioavailability of these contaminants is of potential concern and a key reason for this research. There is an emerging view that the reworking of sediment bound contaminants either already is or will soon become the dominant factor in the extent of inter-annual variation in estuarine contamination.

Within the Ribble estuary NW, England, the physical, spatial and temporal characteristics of the exchange of contaminated sediment between different sediment deposits was investigated at the micro and macro scale. Monthly observations of changes in the sediment physical properties and contaminant concentration were conducted. These observations determined that contaminants remained strongly associated with fine grained sediments, though this association varied temporally and spatially and could become decoupled in response to a substantial siltation event.

Analysis of historic data for the Ribble estuary revealed that the nature of the relationship the radiogenic contaminants ^{137}Cs and ^{241}Am had with the fine-grained sediments differed between the contaminants over time. For example, the activity concentration of ^{137}Cs in the fine-grained sediments was found to decline between 1995 and 2014 and has been put down to radioactive decay and reduced inputs of ^{137}Cs into the estuary from the Irish Sea. In contrast, ^{241}Am activity concentrations did not show a statistically significant decline over the same time period. This was interpreted as being a function of the longer half-life of ^{241}Am , its ingrowth from ^{241}Pu and a reduced rate of re-dissolution.

A time series statistical analysis was used to determine if storminess and high riverine discharge events could explain variation in sediment properties. The analysis showed that riverine discharge was the dominant factor. Storminess was still a statistically significant driver of change in sediments but was less so in comparison to riverine discharge. These results confirm that discrete high impact disturbance events are substantial factors in the reworking of estuarine sediments.

A three-dimensional spatial analysis of the sediment movements within the Ribble estuary was conducted from 1999 – 2015 through a novel LiDAR geostatistical methodology, with the purpose of determining the nature of sediment movements within the Ribble estuary. The Ribble was confirmed to be a very dynamic estuary and exhibited substantial morphological change that was interpreted as large-scale sediment remobilisations. The geostatistical analysis of the Ribble Interestingly showed that the estuary fluctuated between erosion and accretion. The saltmarshes were observed within the 16-year study period to be more significant than the mudflats in terms of sediment erosion and accretion which is of interest given that saltmarshes are concentrated in radiogenic contaminants.

Natural disturbance events are very difficult to study given the uncertainty of when they may occur, the resources and time needed to sample before and after the event. In contrast planned anthropogenic disturbance can be easier to study and can still allow conclusions to be drawn on the impacts of largescale disturbance events. To this end, the disturbance effects of a managed realignment scheme were investigated specifically the modification of saltmarsh creek hydrodynamics. The managed realignment scheme was implemented in 2009 at the Hesketh Outmarsh in the Ribble estuary. Over the following years, the scheme has been shown to promote localised erosion within the larger creeks inside the breached area. A novel geostatistical methodology was used to estimate the quantity of radiogenic contaminants (^{137}Cs and ^{241}Am) remobilised from the breached area. This research estimates that, from a baseline in 2007, some 52 GBq of ^{137}Cs and 20.9 GBq of ^{241}Am were remobilised – up to 2015.

The Ribble Estuary is dynamic at the micro and macro scale and under current circumstance the contaminant enriched saltmarshes are functioning as a diffuse source of radiogenic contaminants to the wider estuary and potentially beyond. Sediment remobilisations are believed to be responsible for significant variation in contaminant sediment matrix relationships. Where climate change will see an increase in disturbance events there will also be an enhanced rate of contaminant redistribution.

Acknowledgements

Without the continued support of my principal supervisor Professor David Copplestone the completion of this project would not have been possible, time and again he has gone the extra mile regardless of the challenges thrown up over the past four years. Professor David Copplestone and my co supervisor Professor Andrew Tyler have both given me numerous opportunities which have allowed me to work my way towards this point, for this hand up I'm eternally grateful. My co-supervisor Dr Peter Hunter is the quintessence of a solid work ethic and has been an example of excellence for me to strive towards. I would also like to thank my Industrial supervisor Dr Nick Smith whose passion for geology is both inspiring and intriguing.

I would like to thank my family for their support over the years, without my Mum, Gran Papa and Davie I would not have been able to get to this point and devote such a large amount of time to my studies. My Mum and Gran were there through every disaster, setback and problem I encountered and with their support I was able to overcome all.

My brother Ross and cousin Tam have my thanks for agreeing to spend their free time with me at distant parts of the country and in interesting conditions. They have also helped me design and build innovative lab equipment on more times than I can remember over the past few years.

I would like to acknowledge the good humour and assistance of Stuart Bradley over the past four years. Working with Stuart was always a good time.

I would like to extend my thanks to the technical staff at the biological and environmental science department for their assistance over the years; especially Ronnie Balfour, Scott Jackson, James Weir, Ian Washbourne, Lorna English and John MacArthur

My fellow PhD cohort have my thanks for their assistance and stimulating debate; Amani Becker, Adam Varley, Junyao Sun, Diana McLaren and Kat Raines.

The undergraduate and postgraduate students that spent week-long periods in the field with me working sun up to sun down deserve special recognition. Thank you Marius Stokke Sønneland and Alan Steen together we collected some great data.

Table of Contents

| | |
|---|-----------|
| Abstract | i |
| Acknowledgments | ii |
| Table of contents | iv |
| Table of figures | ix |
| Table of tables | xvi |
| | |
| 1. Introduction | 1 |
| 1.1. The ARCoES Project | 3 |
| 1.2. Climate change implications for sediment remobilisation | 3 |
| 1.3. Environmental contaminants | 4 |
| 1.4. Thesis rationale and Aims | 6 |
| 1.5. Summary | 9 |
| | |
| 2. Literature review of estuarine sediment movement and associated radioactive contaminants | 10 |
| 2.1. Sediment | 12 |
| 2.1.1. Sediment types | 12 |
| 2.1.2. Managed realignment | 15 |
| 2.1.3. Sediment movement within the Ribble estuary | 16 |
| 2.2. Radioactive contaminants within the estuarine and marine environment | 17 |
| 2.2.1. Historic and current discharges of radioactive contaminants | 17 |
| 2.2.2. Properties of contaminant sink radionuclides ^{137}Cs , ^{241}Am and $^{239+240}\text{Pu}$ / ^{241}Pu | 18 |
| 2.2.3. Sediment-bound contaminants | 21 |
| 2.3. The role of climate change in contaminant remobilisation | 22 |
| 2.4. Conclusion | 24 |

| | | |
|-----------|---|-----------|
| 3. | Spatio-temporal characteristics of radioactive contaminants in the Ribble estuary | 25 |
| 3.1. | Aims | 28 |
| 3.2. | Methods | 28 |
| 3.2.1. | Site selection | 28 |
| 3.2.2. | Field work | 29 |
| 3.2.3. | Sediment preparation | 31 |
| 3.2.4. | Sediment properties | 31 |
| 3.2.5. | Contaminants | 32 |
| 3.2.6. | Dosimetry | 34 |
| 3.2.7. | DGPS | 35 |
| 3.2.8. | Statistical analysis | 35 |
| 3.3. | Results | 38 |
| 3.3.1. | Temporal and spatial variability | 38 |
| 3.3.2. | Contaminant sediment relationships | 47 |
| 3.3.3. | Temporal variability in radioactive contaminant sediment relationships | 58 |
| 3.3.4. | 20-year trend in radioactive contaminant sediment relationship | 61 |
| 3.4. | Discussion | 65 |
| 3.4.1. | Sediment spatio-temporal variability | 65 |
| 3.4.2. | Contaminant spatio-temporal variability | 66 |
| 3.4.3. | Long term trend 1995 - 2014 | 68 |
| 3.5. | Conclusions | 69 |
| 4. | The impact of disturbance events on estuarine sediment properties over a two-year period | 71 |
| 4.1. | Aims | 73 |
| 4.2. | Data sets | 73 |
| 4.2.1. | Ribble estuary sediment properties | 74 |
| 4.2.2. | Significant wave height as a proxy for storminess | 76 |

| | |
|---|-----------|
| 4.2.3. Ribble riverine discharge | 76 |
| 4.3. Methods | 77 |
| 4.3.1. Granger causality test as it relates to the data sets | 77 |
| 4.3.2. Preparation of data subsets for analysis | 77 |
| 4.3.3. Granger causality analysis within R | 80 |
| 4.4. Results | 82 |
| 4.4.1. Storminess proxy | 83 |
| 4.4.2. The Ribble riverine discharge | 87 |
| 4.4.3. Reciprocal causation: Storminess proxy and Ribble riverine discharge | 88 |
| 4.5. Discussion | 89 |
| 4.5.1. Storminess proxy | 89 |
| 4.5.2. Ribble riverine discharge | 91 |
| 4.5.3. Storminess proxy and riverine discharge | 92 |
| 4.6. Conclusion | 92 |
| | |
| 5. The spatial-temporal characteristics of long term Ribble estuary sediment movements | 94 |
| 5.1. Aims | 97 |
| 5.2. Data sets | 97 |
| 5.2.1. LiDAR overview | 97 |
| 5.2.2. Available LiDAR data | 98 |
| 5.2.3. Study sites | 99 |
| 5.3. Methods | 101 |
| 5.3.1. Raster processing framework | 101 |
| 5.3.2. Raster of difference – Limit of detection | 104 |
| 5.3.3. Cluster analysis | 106 |
| 5.3.4. Volume determination | 108 |
| 5.4. Results | 109 |

| | | |
|--------|--|-----|
| 5.4.1. | 1999 – 2009 full estuary coverage | 109 |
| 5.4.2. | 1999 – 2015 mid estuary coverage | 113 |
| 5.4.3. | Localised site 1 – Sandbanks | 127 |
| 5.4.4. | Localised site 2 – Mudflats | 129 |
| 5.4.5. | Localised site 3 – Hesketh Outmarsh | 132 |
| 5.5. | Discussion | 148 |
| 5.5.1. | 1999 – 2009 full estuary coverage | 148 |
| 5.5.2. | 1999 – 2015 mid estuary coverage | 149 |
| 5.5.3. | Localised site 1 – Sandbanks | 151 |
| 5.5.4. | Localised site 2 – Mudflats | 152 |
| 5.5.5. | Localised site 3 – Hesketh Outmarsh | 152 |
| 5.6. | Conclusions | 154 |
| 6. | Sediment-bound radioactive contaminant remobilisation in response to an anthropogenic disturbance event | 155 |
| 6.1. | Aims | 157 |
| 6.2. | Methods | 158 |
| 6.2.1. | Field work at Hesketh Outmarsh | 160 |
| 6.2.2. | Sediment processing | 161 |
| 6.2.3. | DGPS data processing | 161 |
| 6.2.4. | Dosimetry | 162 |
| 6.2.5. | MoGSS | 162 |
| 6.2.6. | Radiogenic contaminant horizontal spatial analysis | 162 |
| 6.2.7. | Radiogenic contaminant vertical spatial analysis | 167 |
| 6.2.8. | Inferred sediment movement | 167 |
| 6.2.9. | Radiogenic contaminant remobilisation | 167 |
| 6.3. | Results | 169 |
| 6.3.1. | Horizontal spatial properties of radiogenic contaminants | 169 |

| | |
|--|-----|
| 6.3.2. Radiogenic contaminant vertical profiles | 177 |
| 6.3.3. Mass balance of contaminants | 180 |
| 6.4. Discussion | 181 |
| 6.4.1. Saltmarsh radiogenic contamination | 181 |
| 6.4.2. Remobilised radiogenic contamination | 184 |
| 6.5. Conclusion | 186 |
| | |
| 7. Conclusions | 188 |
| 7.1. Research questions | 189 |
| 7.1.1. Radiogenic contaminants and the sediment matrix | 189 |
| 7.1.2. Mechanisms of disturbance and the sediment matrix | 192 |
| 7.1.3. Ribble estuary sediment movement | 193 |
| 7.1.4. Hesketh Outmarsh managed realignment scheme | 196 |
| 7.1.5. Saltmarshes as sources of contaminants | 197 |
| 7.2. Implications for contaminant movement | 199 |
| 7.3. Future work | 200 |
| 7.3.1. Daily sediment morphological change and sediment movement | 200 |
| 7.3.2. Radiogenic contaminant remobilisation method application to other estuaries | 201 |
| 7.3.3. Revisiting storminess granger causality at a higher temporal resolution | 202 |
| 7.3.4. Modelling saltmarsh diffuse radiogenic contaminant releases | 203 |
| 7.4. Summary | 203 |
| | |
| Appendix 1 | 206 |
| Appendix 2 | 276 |
| Appendix 3 | 279 |
| | |
| References | 288 |

List of Figures

- Figure 1.1** Composite satellite image of the Ribble estuary, Northwest England. Map produced in Google Earth pro using composite Landsat data across 2017. 6
- Figure 2.2** Map of the Ribble estuary with digitised overlays highlighting the three main sediment deposit types; Sandbanks, Mudflats and Saltmarsh. 13
- Figure 3.1** The top map shows the area of mudflat in front of the Lytham St Anne's lifeboat jetty with transects marked in red. Transects are numbered 1-3. The bottom map shows the location of these mudflats within the Ribble estuary, highlighted by a red polygon. 29
- Figure 3.2** March 2014 log vs log plots (ln) showing the natural log transformed data and fitted linear model. Data were regressed with ^{137}Cs Bq kg⁻¹ as the response variable and percentage clay, silt, sand and organic matter acting as predictor variables. 49
- Figure 3.3** March 2014 log vs log plots (ln) showing the natural log transformed data and fitted linear model. Data were regressed with ^{241}Am Bq kg⁻¹ as the response variable and percentage clay, silt, sand and organic matter acting as predictor variables. 50
- Figure 3.4** May 2014 log vs log plots (ln) showing the natural log transformed data and fitted linear model. Data were regressed with ^{137}Cs Bq kg⁻¹ as the response variable and percentage clay, silt, sand and organic matter acting as predictor variables. 51
- Figure 3.5** May 2014 log vs log plots (ln) showing the natural log transformed data and fitted linear model. Data were regressed with ^{241}Am Bq kg⁻¹ as the response variable and percentage clay, silt, sand and organic matter acting as predictor variables. 52
- Figure 3.6** September 2014 log vs log plots (ln) showing the natural log transformed data and fitted linear model. Data were regressed with ^{137}Cs Bq kg⁻¹ as the response variable and percentage clay, silt, sand and organic matter acting as predictor variables. 54

| | | |
|--------------------|--|----|
| Figure 3.7 | September 2014 log vs log plots (ln) showing the natural log transformed data and fitted linear model. Data were regressed with ^{241}Am Bq kg ⁻¹ as the response variable and percentage clay, silt, sand and organic matter acting as predictor variables. | 55 |
| Figure 3.8 | December 2014 log vs log plots (ln) showing the natural log transformed data and fitted linear model. Data were regressed with ^{137}Cs Bq kg ⁻¹ as the response variable and percentage clay, silt, sand and organic matter acting as predictor variables. | 56 |
| Figure 3.9 | December 2014 log vs log plots (ln) showing the natural log transformed data and fitted linear model. Data were regressed with ^{241}Am Bq kg ⁻¹ as the response variable and percentage clay, silt, sand and organic matter acting as predictor variables. | 57 |
| Figure 3.10 | Monthly models for 2014 plotted on a log vs log plots (ln). Data were modelled with ^{137}Cs Bq kg ⁻¹ as the response variable and percentage clay, silt, sand and organic matter acting as predictor variables. | 58 |
| Figure 3.11 | Monthly models for 2014 plotted on a log vs log plots (ln). Data were modelled with ^{241}Am Bq kg ⁻¹ as the response variable and percentage clay, silt, sand and organic matter acting as predictor variables. | 59 |
| Figure 3.12 | Annual models plotted on a log vs log plots (ln). Data were modelled with ^{137}Cs Bq kg ⁻¹ as the response variable and percentage Clay acting as the predictor variable. | 63 |
| Figure 3.13 | Annual models plotted on a log vs log plots (ln). Data were modelled with ^{241}Am Bq kg ⁻¹ as the response variable and percentage Clay acting as the predictor variable. | 64 |
| Figure 4.1 | Map of the Ribble estuary with the four sampling locations denoted by a red circle. | 75 |
| Figure 4.2 | Wave direction rose, the bars show the direction that the waves are traveling towards. The concentric rings denote what percentage of the waves the bars represent. The colours on the bars denote the proportion of the waves that have the stated wave height. | 79 |

- Figure 4.3** Example of a wave height (Hs) time series that has had seasonal and first differencing applied to the data a) raw Hs time series, b) seasonal differencing has been applied to these data, c) first differencing has been applied to the time series found in b. 81
- Figure 5.1** Map outlining the different types of sediment deposits of the Ribble estuary. A blue line has been drawn around the outer estuary sandbanks, a red line has been drawn around the mudflats and purple lines have been drawn around the north shore and south shore saltmarshes. 95
- Figure 5.2** The Ribble estuary is shown with two boxes denoting the areas that the localised focus sites are based. The sandbanks studied are located at the Lytham beach site in the outer estuary, with the mudflats and saltmarshes being studied at the Hesketh Outmarsh site in the mid estuary. 100
- Figure 5.3** This schematic flow diagram showing the data processing stages to convert raw ASCII data to a form useful in the current study. 102
- Figure 5.4** The Ribble estuary is shown with a classified intertidal zone, green = saltmarshes, grey = mudflats and blue is water that is below low tide. These classifications were derived from averaged tide data from 2015. These data are used to assign habitat type to the LiDAR data. 104
- Figure 5.5** This schematic flow diagram shows the stages incorporated into the clustering analysis which used the ArcGIS suite to conduct processing. 107
- Figure 5.6** Map of change in volume (m³) of sediment from 1999 – 2009 for the Ribble estuary, each pixel has an area of 4 m². 110
- Figure 5.7** Frontal saltmarsh erosion resulting in a retreat of the saltmarsh extent for an area of the Hesketh Outmarsh saltmarshes (OSGB; 340000,426000). 114
- Figure 5.8** Map of change in volume (m³) of sediment from 1999 – 2007 for the mid Ribble estuary, each pixel has an area of 4 m². 115

- Figure 5.9** Map of change in volume (m^3) of sediment from 2007 – 2009 for the mid Ribble estuary, each pixel has an area of 0.0625 m^2 . 116
- Figure 5.10** Map of change in volume (m^3) of sediment from 2009 – 2010 for the mid Ribble estuary, each pixel has an area of 0.0625 m^2 . 117
- Figure 5.11** Map of change in volume (m^3) of sediment from 2010 – 2011 for the mid Ribble estuary, each pixel has an area of 0.0625 m^2 . 118
- Figure 5.12** Map of change in volume (m^3) of sediment from 2011 – 2014 for the mid Ribble estuary, each pixel has an area of 0.25 m^2 . 119
- Figure 5.13** Map of change in volume (m^3) of sediment from 2014 – 2015 for the mid Ribble estuary, each pixel has an area of 0.25 m^2 . 120
- Figure 5.14** A fixed extent comparison for the periods 2007 – 2009 and 2009 – 2010. The scale used for the colour ramp is the same for both data sets and only significant change is displayed through the application of a limit of detection. The areas shown represent saltmarsh creeks and surface marsh ponds. 123
- Figure 5.15** An example of a marsh pond on the Ribble saltmarshes. Marsh ponds are bare patches of sediment that retain water after the ebb tide. (Photo taken of the New marsh site in 2015). 124
- Figure 5.16** Photograph of a creek that was undercutting the sides of the saltmarsh on either side at the Hesketh Outmarsh site (Photo taken of the New marsh site in 2015). 125
- Figure 5.17** The mid estuary sediment significant change data is shown as the average volume of change per 1 m^2 area. Faded blue and orange boxes are used to represent the time period from which each data set is derived. The Green (saltmarsh) and Grey (mudflat) bars are placed at the end of the time period as the volume of change is relative to the start and end of the time period. 126
- Figure 5.18** Map of change in volume (m^3) of sediment from 2013 – 2014 for the outer Ribble estuary sandbanks, each pixel has an area of 4 m^2 . These data have had a limit of detection applied to them so that only significant movement is shown. 127

| | | |
|--------------------|--|-----|
| Figure 5.19 | Map of change in volume (m ³) of sediment from 1999 to 2007 for the mid Ribble estuary, each pixel has an area of 4 m ² . These data have had a limit of detection applied to them so that only significant movement is shown. | 130 |
| Figure 5.20 | Map of change in volume (m ³) of sediment from 2007 to 2009 for the mid Ribble estuary, each pixel has an area of 0.0625 m ² . These data have had a limit of detection applied to them so that only significant movement is shown. | 131 |
| Figure 5.21 | Overview of the mid estuary localised site Hesketh Outmarsh. The site is split into an area of mature saltmarsh designated Old marsh and an area of emergent saltmarsh designated New marsh. | 132 |
| Figure 5.22 | Map of significant change in sediment volume from 2007 to 2009 for the Hesketh Outmarsh managed realignment site. | 134 |
| Figure 5.23 | Map of significant change in sediment volume from 2009 to 2010 for the Hesketh Outmarsh managed realignment site. | 135 |
| Figure 5.24 | Map of significant change in sediment volume from 2010 to 2011 for the Hesketh Outmarsh managed realignment site. | 136 |
| Figure 5.25 | Map of significant change in sediment volume from 2011 to 2014 for the Hesketh Outmarsh managed realignment site. | 137 |
| Figure 5.26 | Map of significant change in sediment volume from 2014 to 2015 for the Hesketh Outmarsh managed realignment site. | 138 |
| Figure 5.27 | Map of significant change in sediment volume from 1999 to 2007 for the Hesketh Outmarsh old marsh site. | 140 |
| Figure 5.28 | Map of significant change in sediment volume from 2007 to 2009 for the Hesketh Outmarsh old marsh site. | 141 |
| Figure 5.29 | Map of significant change in sediment volume from 2009 to 2010 for the Hesketh Outmarsh old marsh site. | 142 |
| Figure 5.30 | Map of significant change in sediment volume from 2010 to 2011 for the Hesketh Outmarsh old marsh site. | 143 |

| | | |
|--------------------|---|-----|
| Figure 5.31 | Map of significant change in sediment volume from 2011 to 2014 for the Hesketh Outmarsh old marsh site. | 144 |
| Figure 5.32 | Map of significant change in sediment volume from 2014 to 2015 for the Hesketh Outmarsh old marsh site. | 145 |
| Figure 6.1 | This aerial photograph was collected by the Environment Agency Geomatics group in 2007 prior to the realignment scheme. The Hesketh study area is denoted by a red polygon within which there are two sub categories Old marsh (green polygon / points) and New marsh (Blue polygon / points). | 158 |
| Figure 6.2 | Example photograph of undercutting action that is typical of saltmarsh lateral erosion from the Hesketh saltmarshes (Photo taken of the Old marsh site in 2015). | 159 |
| Figure 6.3 | Total counts for the ^{137}Cs window from the MoGSS dataset are plotted against the ^{137}Cs Bq kg ⁻¹ of the sediment scrapes from the new marsh. A regression model which used the log transformed MoGSS data was fitted to the data with 95% confidence intervals. | 165 |
| Figure 6.4 | Comparison of estimated activity for ^{137}Cs in the new marsh (x axis) and measured activity (y axis) a linear model is fitted to these data to show the general trend in comparison to the 1:1 prediction line. | 166 |
| Figure 6.5 | The left image shows the MoGSS derived map of surface activity and the map on the right shows the sediment scrape derived map of surface activity for ^{137}Cs at the new marsh site. | 170 |
| Figure 6.6 | The left image shows the MoGSS derived map of surface activity and the map on the right shows the sediment scrape derived map of surface activity for ^{241}Am at the new marsh site. | 171 |
| Figure 6.7 | Plot of the new marsh MoGSS ^{137}Cs activity concentration data against the ^{137}Cs predicted by the spatial statistics model fitted to the sediment scrape data. The colour ramp from red to blue indicates the number of points at that location. | 172 |

- Figure 6.8** The left image shows the MoGSS derived map of surface activity and the map on the right shows the sediment scrape derived map of surface activity for ^{137}Cs at the old marsh site. 174
- Figure 6.9** The left image shows the MoGSS derived map of surface activity and the map on the right shows the sediment scrape derived map of surface activity ^{241}Am at the old marsh site. 175
- Figure 6.10** Activity concentration depth profiles for ^{137}Cs Bq kg⁻¹ for four cores collected from the new marsh site. 177
- Figure 6.11** Activity concentration depth profiles for ^{241}Am Bq kg⁻¹ for four cores collected from the new marsh site. 177
- Figure 6.12** Activity concentration depth profiles for ^{137}Cs Bq kg⁻¹ for two cores collected from the old marsh site. 178
- Figure 6.13** Activity concentration depth profiles for ^{241}Am Bq kg⁻¹ for two cores collected from the old marsh site. 178
- Figure 6.14** Photograph of the large main creek which ran adjacent to the old marsh site. This creek expanded in size as a result of the managed realignment, the rough areas seen in the creek are sections of marsh that have been undercut (Photo taken of the Old marsh site in 2015). 183

List of Tables

| | | |
|-------------------|---|----|
| Table 3.1 | % clay content summary statistics for each of the four monthly sampling campaigns. MAD = median absolute deviation, n = 36. | 38 |
| Table 3.2 | % silt content summary statistics for each of the four monthly sampling campaigns. MAD = median absolute deviation, n = 36. | 39 |
| Table 3.3 | % sand content summary statistics for each of the four monthly sampling campaigns. MAD = median absolute deviation, n = 36. | 40 |
| Table 3.4 | % organic matter content summary statistics for each of the four monthly sampling campaigns. MAD = median absolute deviation, n = 36. | 41 |
| Table 3.5 | % carbonates content summary statistics for each of the four monthly sampling campaigns. MAD = median absolute deviation, n = 36. | 41 |
| Table 3.6 | pH summary statistics for each of the four monthly sampling campaigns. MAD = median absolute deviation, n = 36. | 42 |
| Table 3.7 | ¹³⁷ Cs summary statistics for each of the four monthly sampling campaigns. MAD = median absolute deviation, n = 36. | 43 |
| Table 3.8 | ²⁴¹ Am summary statistics for each of the four monthly sampling campaigns. MAD = median absolute deviation, n = 36. | 44 |
| Table 3.9 | As summary statistics for each of the four monthly sampling campaigns. MAD = median absolute deviation, n = 36. | 45 |
| Table 3.10 | Fe summary statistics for each of the four monthly sampling campaigns. MAD = median absolute deviation, n = 36. | 45 |
| Table 3.11 | Sr summary statistics for each of the four monthly sampling campaigns. MAD = median absolute deviation, n = 36. | 46 |
| Table 3.12 | Air kerma summary statistics for each of the four monthly sampling campaigns. MAD = median absolute deviation, n = 19. | 47 |
| Table 3.13 | Coefficients of determination (R^2) for each monthly regression model for ¹³⁷ Cs. | 60 |

| | | |
|-------------------|---|----|
| Table 3.14 | Coefficients of determination (R^2) for each monthly regression model for ^{241}Am . | 60 |
| Table 3.15 | Regression model parameters for % clay / ^{137}Cs for 1995, 1997, 2002, 2003 and 2014. % clay / ^{241}Am was only applied to 1995, 1997 and 2014. | 65 |
| Table 4.1 | Upper estuary Granger causality matrix. For each transect the matrix reports whether the sediment variable was as a pass (green) or fail (grey). A pass denotes that the trend in the storminess proxy data was found in the corresponding sediment property data at p-value = < 0.05. | 83 |
| Table 4.2 | Lower estuary Granger causality matrix. For each transect the matrix reports whether the sediment variable was as a pass (green) or fail (grey). A pass denotes that the trend in the storminess proxy data was found in the corresponding sediment property data at p-value = < 0.05. | 84 |
| Table 4.3 | Upper estuary Granger causality matrix. For each transect the matrix reports whether the sediment variable was as a pass (green) or fail (grey). A pass denotes that the trend in the storminess proxy data was found in the corresponding sediment property data at p-value = < 0.05. This matrix has M = mean storminess and S = sum of storminess. | 85 |
| Table 4.4 | Lower estuary Granger causality matrix. For each transect the matrix reports whether the sediment variable was as a pass (green) or fail (grey). A pass denotes that the trend in the storminess proxy data was found in the corresponding sediment property data at p-value = < 0.05. This matrix has M = mean storminess and S = sum of storminess. | 86 |
| Table 4.5 | Upper estuary Granger causality matrix. For each transect the matrix reports whether the sediment variable was as a pass (green) or fail (grey). A pass denotes that the trend in the riverine discharge data was found in the corresponding sediment property data at p-value = < 0.05. | 87 |

| | | |
|------------------|---|-----|
| Table 4.6 | Lower estuary Granger causality matrix. For each transect the matrix reports whether the sediment variable was as a pass (green) or fail (grey). A pass denotes that the trend in the riverine discharge data was found in the corresponding sediment property data at p-value = < 0.05. | 88 |
| Table 5.1 | The LiDAR data sets used in this chapter are listed here with their accompanying spatial resolution and RMSE. A description of the extent of the spatial coverage is also provided. | 99 |
| Table 5.2 | Summary statistics for the movement of sediment in the Ribble estuary between 1999 and 2009. | 111 |
| Table 5.3 | Ribble mid estuary summary statistics for 1999 – 2015 for the significant change data using the limit of detection method. Total change was derived from the sum of all pixels. Survey area was the geometry of the survey area and was calculated independently of the volume determination. | 121 |
| Table 5.4 | Ribble mid estuary summary statistics for 1999 – 2015. These are total values and use no limit of detection. Total change is equal to the sum of all pixels. Survey area is the geometry of the survey area and is calculated independently of the volume determination. | 122 |
| Table 5.5 | Lytham beach site summary statistics for four data sets ranging from 1999 – 2014. Total change was equal to the sum of all pixels. Survey area was the geometry of the survey area and was calculated independently of the volume determination. | 128 |
| Table 5.6 | Hesketh Outmarsh new marsh site summary statistics for the volume of change (m ³) in sediment. | 139 |
| Table 5.7 | Hesketh Outmarsh old marsh site summary statistics for the volume of change (m ³) in sediment. | 146 |
| Table 6.1 | Summary of the four regression models produced to estimate ¹³⁷ Cs and ²⁴¹ Am concentration from MoGSS data at the two marsh sites. | 163 |

| | | |
|------------------|--|-----|
| Table 6.2 | Summary statistics for the new marsh site for ^{137}Cs (Bq Kg^{-1}) and ^{241}Am (Bq Kg^{-1}), prefix SM = MoGSS data, prefix SC = sediment scrape. MAD = median absolute deviation. | 173 |
| Table 6.3 | Summary statistics for the old marsh site for ^{137}Cs (Bq Kg^{-1}) and ^{241}Am (Bq Kg^{-1}), prefix SM = MoGSS data, prefix SC = sediment scrape. MAD = median absolute deviation. | 176 |
| Table 6.4 | Sediment budget data for the Hesketh Outmarsh site from 2007 to 2015. | 180 |
| Table 6.5 | Calculated volumes of remobilised contaminants for the Hesketh Outmarsh site from 2007 to 2015. | 181 |

[This page is intentionally left blank]

1. Introduction

Estuaries are a complex exchange environment where the marine and terrestrial environment interface to form a distinct system of sediment deposits with a range of biological and physical properties (Jickells and Rae, 1997). The unique physical properties of these sediments create a unique habitat that is of great importance to a range of biota such as resident and migratory bird species (Still et al., 2014). The historic, economic and social value of estuaries to humanity has often resulted in conflicts of use, traditionally with the importance of natural habitat provision being a secondary concern. The recognition of the socioeconomic value that ecosystem services from these habitats can provide however has resulted in changing attitudes in how estuaries should be managed (Boerema and Meire, 2017).

Anthropogenic modifications to estuaries occur at many spatial scales the most evident example is the physical modification of the estuaries morphology through heavy engineering works. Channel straightening through the emplacement of training walls and repeated dredging substantially increases river discharge velocities. The emplacement of sea walls for the purpose of historic land reclamations affect estuaries by reducing the extent of the intertidal zone. Such modifications greatly affect the estuary hydrodynamics, which in turn modifies how sediments are transported within the estuary and the spatial pattern of sediment deposits, at a longer time scale this will impact how the estuaries morphology will evolve (e.g. Azevedo et al., 2010; Browne, 2017; Wolanski et al., 2001).

As a sediment deposition environment an exchange of marine and terrestrial sediments occurs to form the estuarine sediment deposits such as the mudflats and saltmarshes (Pye and Blott, 2014). This estuarine sediment is the result of extensive mixing via sediment resuspension and transport with these sediments being deposited according to the particle size of the sediment and the energy of the flood and ebb flows (e.g. Azhikodan and Yokoyama, 2015). The water current velocities of the flood and ebb flows of the tides, the shape of the tidal frame as well as the disruptive effect of the tidal bore combine to dictate how sediments are remobilised at a daily rate (Choi and Kim, 2016; Gleizon et al., 2003; Pieterse et al., 2017; Stark et al., 2017). These factors can be generalised as the hydrodynamics of the system which in its simplest definition is how a fluid body such as the tidal water will interact with the estuarine sediment deposits (Merriam-Webster, 2017). The hydrodynamics will have feed back to the estuary surface morphology and influence over time where different sediment deposits

are formed e.g. sandbanks, mudflats saltmarshes (Choi and Kim, 2016; Luo et al., 2013).

Therefore, changes in the amount of hydrodynamic energy in the system effects the estuary, resulting in a modified sediment spatial distribution. Whether modifications to the hydrodynamics are through natural or anthropogenic circumstances the result will likely be the same, which is changes to how sediments are remobilised within the estuary. Furthermore, there are new potential stressors, such as the long-term effects of climate change that are predicted to see rates of sea level rise and storminess increase in coming years (Barker, 2007). Given the important role coastal sediments play as sinks for environmental contaminants, understanding the fate and behaviour of these sediments is crucial in determining any potential impacts on humans and wildlife.

Estuarine and marine sediments can act as sinks for contaminants, with industrial discharges of metals and radiogenic contaminants being concentrated within clay and silt deposits within estuaries as well as within the marine environment (Brown, 1997; Brown et al., 1999; Clifton et al., 1999; Mackenzie and Scott, 1993; Rainey et al., 1999). Saltmarshes in particular by virtue of their formation processes act as a stratified environmental store of radiogenic contaminants such as ^{241}Am and ^{137}Cs (Assinder et al., 1997; Brown et al., 1999). It is the sediment stores of contaminants that create interest in better understanding the nature of sediment morphological change and sediment movement. Changing concentrations of radiogenic contaminants will affect radiological risk for human and non-human biota which is in part a function of the activity concentration of radioactive contaminants (Hunt, 1997; Rahman et al., 2013). Anthropogenic modifications and climate change have the potential to alter the amount of energy within the estuary and its hydrodynamics which in turn will impact how sediments are remobilised and cycled within and out with the estuary (e.g. Brown et al., 2016; Azevedo et al., 2010; Browne, 2017; Wolanski et al., 2001). The question that is of interest is what do these sediment movements mean in terms of radiogenic contaminant remobilisation and what is the radiological significance of these remobilisations?

1.1. The ARCoES Project

The research described here is linked to the Engineering and Physical Sciences Research Council (EPSRC) funded Adaptation and Resilience of Coastal Energy Supply (ARCoES) project (<https://www.liverpool.ac.uk/geography-and-planning/research/adaptation-and-resilience-of-coastal-energy-supply/>), which aims to identify the challenges facing the future security of the UK nuclear energy sector and coastal energy supply as a result of changing patterns of temperature and rainfall, sea-level rise and storms. In particular, it aims to determine threats posed to future energy generation and the distribution network, as well as the surrounding coastline and coastal waters, by flooding, erosion, changing patterns of sedimentation, water temperature and the distribution of flora and fauna in the coastal zone. This is being achieved through modelling of coastal processes (e.g. coastal hydrodynamics) to predict likely changes to estuaries, beaches, dunes and cliffs in terms of future flooding, erosion, sedimentation, water quality and habitats. There is a focus on the North West of England as a test case and this is one of the reasons why the work conducted here was focused on the Ribble estuary and its sediment.

1.2. Climate change implications for sediment remobilisation

At present there is a consensus found within the literature that the North Atlantic region surrounding the British Isles and parts of western Europe will experience an increase in storm frequency and intensity in coming years (Möller et al., 2016). Such findings are partially based on studies of the North Atlantic Oscillation (NAO), which is an index of the local climate that has been linked to storminess (Bader et al., 2011; Bengtsson et al., 2006; Greeves et al., 2007; Keim et al., 2004) and in some cases variation in erosion and accretion rates (Esteves et al., 2011).

Put simply sea level rise and storminess are the two mechanisms through which climate change is likely to impact the estuarine environment. Sea level rise, which is more widely studied, will impact erosion and accretion, tidal surge frequency and intensity and shore line retreat (Allen and Pye, 1992). Individual extreme storm events are known to cause significant estuary wide changes to sediment deposits, though their significance relative to the long term narrative of estuarine sediment movement remains uncertain (Blott et al., 2006).

Classic beach theory tells us that an intertidal profile will flatten in response to increased storminess and otherwise steepen during low energy seasons, though engineered defences can prevent an overall expansion of the intertidal profile resulting

in saltmarsh edge erosion (e.g. Allen and Pye, 1992). This idealised transfer of material in response to storminess may be complicated by sea level rise as an enhanced tidal frame or storm surge will see hydrodynamic energy increased, which may result in increased sediment being ejected from the estuary during the ebb tide (van der Wal et al., 2002).

The way in which an estuarine environment will respond to climate change enhanced sea level rise and storminess is determined by a range of factors such as; local wind climate, local sediment transport, sediment supply, estuary morphology and extent of anthropogenic modification (Brown et al., 2016; Adams et al., 2011; Esteves et al., 2011; Luo et al., 2015). Storminess has been linked to erosion in the short to medium term at a number of sites (Adams et al., 2011; Esteves et al., 2011; Gutiérrez et al., 2016). At a longer time scale storminess has been linked to increases in the rate of saltmarsh critical sea level rise rate, in effect given an adequate supply of fine grained material, saltmarshes in some cases may be able to keep pace with sea level rise (Schuerch et al., 2013). However, potential modifications to wave climate; wave height (H_0), wave period (T) and wave direction (Θ_0) will result in significant modification to sediment supply via longshore sediment transport and sediment erosion rates via cross-shore sediment transport (Sierra and Casas-Prat, 2014).

Understanding how storminess will impact estuaries is an active area of research and there is great uncertainty in generalising the effects of sporadic high impact disturbance events. Despite the uncertainty of where this sediment will be (re)mobilised to, it is commonly agreed that in the short (years) to medium term (decades) storminess will result in an enhanced rate of sediment remobilisation.

1.3. Environmental contaminants

The changes in estuarine sediment deposit spatial distribution is of great importance to a multitude of research strands, such as the study of how coastal processes evolve. However, within this project, it is the fate of historic stores of anthropogenic contaminants within the marine environment that is of primary interest. The predicted increase in sediment disturbance and remobilisation means that historically deposited contaminants will also be remobilised and moved within and out with the estuary (Aldridge et al., 2003; Gleizon and McDonald, 2010; Hunt et al., 2013; Marsden et al., 2006). This raises questions about what the environmental and health risks might be of these remobilisations and that of a general trend of enhanced remobilisation (Rahman et al., 2013).

The time integrated discharges of contaminants that are present within sediment deposits such as the clay and silt dominated saltmarshes represent substantial coastal contaminant sinks (Gleizon and McDonald, 2010; Rainey, 1999; Wakefield, 2005). These contaminant sinks are often referred to as being part of the environmental store of radioactivity and are thought to be stored within sediments.(Rahman et al., 2013). It is possible to subdivide the sediment deposits of the estuary based on the sediment properties and contaminant concentration. We would expect sandbanks, mudflats and saltmarshes to have distinct sediment properties and contaminant concentrations as a result of sediment particle size (MacKenzie et al., 1999; Rainey et al., 1999). These contaminant sinks also have varying residency periods governed by the frequency of disturbance, this can range from days (low lying mudflats), months (high tidal frame mudflats) and years (saltmarshes) (van der Wal et al., 2002).

Coastal contaminant sinks are known to be acting as sources to other near shore environments within the Irish sea (Hunt et al., 2013). At the saltmarsh scale, remobilisation within the estuary and saltmarsh itself is also known to be occurring (Lindahl et al., 2011; Morris et al., 2000; Oh et al., 2009). With authorised discharges from nuclear facilities being much reduced compared to historic levels, remobilisation of radioactive contaminants from coastal contaminant sinks will, and in some cases already has, emerged as the dominant source of radionuclides to the environment (Aldridge et al., 2003; Goshawk et al., 2003; Hunt et al., 2013; Leonard et al., 1999; Lindahl et al., 2011; Mackenzie and Scott, 1993).

Given that the nature of estuarine remobilisation is principally a morphological process, which is likely to be highly spatially variable then an integrated spatial solution is required to determine the extent of remobilisation of contaminated sediments. Combining this with an evaluation of the risks from the contaminants will allow the long-term consequences of large scale sediment remobilisation to be determined.

1.4. Thesis rationale and Aims

Understanding how the environmental store of radioactivity will be impacted by the effects of climate change is a substantial challenge, in part due to the complexity of the environmental store of radioactivity. This complexity is emphasised by the range of constituents, such as the wide range of radiogenic contaminants that compose this store. These radionuclides will not react uniformly to remobilisation from disturbance due to radionuclide specific chemical properties (Mackenzie and Scott, 1993; McDonald et al., 2001). Studying the environmental store of radioactivity is a trade-off between scale and depth of study. The particle reactive radionuclides ^{241}Am and ^{137}Cs are studied in this work, which explores their remobilisation and concentrations within the sediments of an estuary on the North-west coast of England.



Figure 1.1 Composite satellite image of the Ribble estuary, Northwest England. Map produced in Google Earth pro using composite Landsat data across 2017.

At the Ribble estuary (figure 1.1) this work explores sediment remobilisation and associated contaminant redistribution in a focused way that should allow the findings to be relevant not just to the wider Irish Sea but estuaries in general.

The Ribble estuary was selected because it is an expansive, highly modified, high energy system (van der Wal et al., 2002). Through studying the Ribble, an insight into changes at the extremes of estuary scale, geomorphological diversity and extent of anthropogenic modification will be gained. The Ribble estuary has also been surveyed

a number of times since 1995 by the University of Stirling. Remote sensing techniques were developed here to estimate mudflat (Rainey et al., 2003) and suspended sediment bound (Atkin, 2000) contaminant inventory for 1995 (Rainey, 1999) and 2003 (Wakefield, 2005). The Ribble estuary is included in the Radioactivity in Food and the Environment (RIFE) (Cefas, 2005) and the Environment Agency's UK Mapping program. This also means that there is an extensive volume of historic data for the Ribble available through open data commitments, published reports and the literature. Therefore, a multidecadal analysis of radiogenic contaminant interaction with the sediment matrix is possible at this site.

There are five main questions that this research will answer that are important to understand the past, present and likely future nature of sediment bound radiogenic contaminant redistribution. These questions are the focus of my four research data chapters.

- Are the relationships between estuarine radiogenic contaminants and the sediment matrix temporally and spatially stable in the short to medium term?
- Are mechanisms of disturbance significantly correlated with changes in the sediment matrix and radiogenic contaminant concentration?
- What is the nature of sediment movement within the Ribble Estuary?
- How do saltmarshes respond to the emplacement of a managed realignment scheme within their locality?
- How much contamination is remobilised from saltmarshes in response to an analogue for disturbance?

The relationships between the radiogenic contaminant and the sediment matrix was studied extensively in the 1990s (MacKenzie et al., 1999; Rainey, 1999; Rainey et al., 1999) and most recently in the early 2000s (Atkin, 2000; Wakefield, 2005; Wakefield et al., 2011). Particle reactive radionuclides bind to sediments and predominantly remain there with only a small fraction being vulnerable to redissolution, though this fraction is often resorbed by sediment within the water column (McDonald et al., 2001). The work of Wakefield (2005) on radiogenic contaminant association with fine sediment fractions at the Ribble however challenged this view, showing that such relationships could be temporally variable and even unstable in certain circumstances. It is unknown if this variability is a function of disturbance or a result of Irish sea sediments with time moving away from historically high sediment radiogenic contaminant activity concentrations. I investigate the physical, spatial and temporal properties of the

sediment matrix, to resolve the current status of the estuarine radiogenic contaminant interaction with the sediment.

A changing climate is expected to increase the amount of disturbance sediment bound contaminants are exposed to through an increase in storminess (Brown et al., 2016; Luo et al., 2015), this will likely accelerate the rate at which sediment bound contaminants are remobilised (Hunt et al., 2013). This is an important mechanism of my research which forms part of the wider rationale for pursuing this work as well as interproject links with the ARCoES project. Addressing the question of what is the significance of single high impact disturbance events or the long-term pattern of disturbance is therefore key. To do this, a time series analysis was conducted using modelled storminess data and repeated measurements of sediment property data.

The Ribble estuary is a deposition environment and is reported within the literature to be accreting sediments (van der Wal et al., 2002). However, estuaries are exchange environments and it is possible that although the long-term trend is that of accretion there may be variability over shorter time scales with differing patterns of accretion and erosion. The macrotidal status, funnel shape and linear channel of the Ribble estuary result in a pronounced tidal pumping cycle that results in substantial transfers of sediments within and out with the estuary on the ebb and flood tide (Wakefield et al., 2011). These sediment movements will translate to sediment bound contaminant movement, therefore to better understand the spatio-temporal properties of radiogenic contaminants a deeper understanding is required of sediment movements within the Ribble estuary. Using a novel geostatistical analysis of LiDAR data, a hind cast from 1999 – 2015 was used to answer the question, what is the nature of sediment morphological change and movement within the Ribble estuary?

The Hesketh Outmarsh managed realignment scheme represents a substantial anthropogenic modification to the saltmarshes and their adjoining creeks as a single major disturbance event. The realignment expanded the tidal frame into the new marsh site, this resulted in increased water velocities within the main saltmarsh creeks during the ebb tide, this is a modification to the site hydrodynamics and is a longer-term effect of this singular disturbance event (Stark et al., 2017). Both the initial disturbance and the modification to the hydrodynamics are viewed as an analogue for disturbance, specifically a high impact event that could be caused by storminess and which will be more common under current climate change expectations (Mölter et al., 2016). This analogue for a disturbance event is used to determine how much sediment and radiogenic contamination is remobilised from the Hesketh Outmarsh saltmarshes as a

result of a singular disturbance event. In effect, this represents a hind cast of radiogenic contaminant remobilisation in response to a single disturbance event.

1.5. Summary

Given the established view that climate change will enhance the frequency of high impact disturbance events, this work agrees that the rate at which sediment deposits are remobilised within and out with estuarine and marine environments will be accelerated. Therefore, using historic data, a hind-cast of past sediment morphological change and inferred sediment movement from 1999- 2015 is conducted. This hind-cast uses fine resolution spatial data and accounts for lateral and vertical changes within the estuary sediment system.

The questions this research will answer are stated here, the accompanying chapter in brackets denotes where this research is contained;

- Are the relationships between estuarine radiogenic contaminants and the sediment matrix temporally and spatially stable in the short to medium term? (Chapter 3)
- Are mechanisms of disturbance significantly correlated with changes in the sediment matrix and radiogenic contaminant concentration? (Chapter 4)
- What is the nature of sediment movement within the Ribble Estuary? (Chapter 5)
- How do saltmarshes respond to the emplacement of a managed realignment scheme within their locality? (Chapter 5)
- How much contamination is remobilised from saltmarshes in response to an analogue for disturbance? (Chapter 6)

2. Literature review of estuarine sediment movement and associated radioactive contaminants

BNFL Sellafield (NW, England), which incorporates the legacy sites of Windscale and Calder Hall, began making authorised radioactive discharges to the marine and terrestrial environments in the 1950s, with authorised discharges peaking around 1975 for most nuclides (e.g. ^{137}Cs and ^{241}Am) (Cefas, 2005). In addition, there have been past accidental releases such as those resulting from the 1957 Windscale pile fire. Those radionuclides discharged to the marine environment, can travel with ocean currents in the dissolved phase or attached to suspended matter, they may either fall out of the water column or travel as part of the Irish Sea's sediment transport systems (Gleizon and McDonald, 2010). Radionuclides that enter the sediment transport system can be deposited within marine sediment beds or transported to coastal contaminant sinks such as saltmarshes (Hunt et al., 2013; Lansard et al., 2005; Leonard et al., 1999).

Despite being a relatively scarce habitat in the UK (~450km² around the UK coastline), saltmarshes are of global importance as a coastal contaminant sink of heavy metals (Ridgway, 2001) and radionuclides (e.g. Horrill 1983). This scarce habitat is also vital for supporting an important assemblage of biota, which makes saltmarshes nationally and internationally important for conservation (Habitats Directive 92/43/ EEC).

UK saltmarsh extent is estimated to be declining by around 2.2% per year (Beaumont et al., 2014) due to a combination of factors including; sea-level rise, regional postglacial rebound, modifications to sediment supply, emplacement of engineered sea wall defences and high impact storm events (e.g. Allen & Pye 1992). The loss of mature saltmarsh to erosion will result in the remobilisation and resuspension of sediment bound radiogenic contaminants (Rahman et al., 2013b), which up until that point had been stored and buried at depth within the saltmarsh sediment matrix (Brown et al., 1999).

Contaminants such as ^{137}Cs , ^{241}Am and $^{239+240}\text{Pu}$ are typically bound to the clay fraction of the saltmarsh (Oh *et al.*, 2009). The vertical distribution of these sediment bound contaminants within the marsh is described as the activity depth profile, which typically takes the form of a gaussian distribution, with the contaminant concentration exhibiting a rise, peak and decline (Brown et al., 1999). The peak is the depth at which contaminant concentration is highest and is referred to as the subsurface maxima and it is the remobilisation of this part of the saltmarsh that would represent the highest

radiological risk (Marsden et al., 2006; Rahman et al., 2013b). This activity depth profile can deviate from the above definition and this is often the result of disturbance during marsh formation or post deposition remobilisation either within the saltmarsh or out with the saltmarsh (Harvey *et al.*, 2007). The remobilisation of off-shore marine sediment bound radionuclides and estuarine sediment bound radionuclides within the Irish Sea by physical and biogeochemical processes (Leonard *et al.*, 1999; McDonald *et al.*, 2001; Oh *et al.*, 2009) can result in a more complex vertical and horizontal distribution of radionuclides within estuaries and specifically saltmarshes (Morris *et al.*, 2000; Finegan *et al.*, 2009).

At the landscape scale, coastal contaminant sinks found in estuaries near the Sellafield complex are currently acting as sources to other nearshore environments within the Irish sea (Hunt *et al.*, 2013). At the saltmarsh scale, remobilisation within the estuary and saltmarsh itself is occurring (e.g. Morris *et al.*, 2000; Oh *et al.*, 2009; Lindahl *et al.*, 2011). With authorised discharges from nuclear facilities being much reduced compared to historic levels, remobilisation of contaminants from coastal sinks will, and in some cases already has, emerged as the dominant source of radionuclides to the environment (Mackenzie & Scott 1993; Leonard *et al.*, 1999; Aldridge *et al.*, 2003; Goshawk *et al.*, 2003; Lindahl *et al.*, 2011; Hunt *et al.*, 2013).

The OSPAR Convention (1998) advocates that radionuclide discharges to the North East Atlantic Ocean should "...maintain background levels..." or "...be close to zero..." for naturally occurring radionuclides and those released via anthropogenic activities respectively. While these requirements are for current discharges, the role of coastal contaminant sinks in inter-annual variability of estuarine contaminant concentration will be of increasing interest and importance as routine discharges decline further.

The implications for humans of future remobilisation of saltmarsh sediment and its associated store of environmental contaminants within these exchange environments is dependent on the extent of sediment reworking under natural and anthropogenic induced disturbance (Rahman et al., 2013b). At present, there is a paucity of literature investigating the same issue for non-human biota, which given the global significance of the biologically diverse communities that depend on saltmarshes (Still et al., 2014), does give cause for a need for further information.

The Ribble Estuary

The Ribble estuary is situated 70km south of the Sellafield complex and contains a discharge point for the nuclear licensed site at Springfields, the estuary has long

served as a store for radioactive contaminants (Assinder et al., 1997). Furthermore, the area of the Ribble catchment results in terrestrial inputs of heavy metals from a range of historic mining sites and agricultural practices (Ridgway, 2001). Hydrological processes have also resulted in nuclear weapons testing derived contaminants from upland environments being transported to river systems and then estuaries such as the Ribble estuary (Tyler and Heal, 2000).

The Ribble estuary is highly relevant to the current issues facing coastal contaminant sinks, it is a highly modified estuary that is being allowed to return to a natural state in line with the current policy of adaption to coastal change (DEFRA, 2012). The Ribble's main channel has been allowed to re-establish itself within its delta by the decision to abandon maintenance of the Victorian training walls which have maintained the straightened river channel for the past 150 years. The former sea defences have been breached as part of managed realignment scheme, to promote new saltmarsh formation (discussed further in chapters 5 and 6). These changes have in effect resulted in disturbance to the estuaries hydrodynamics by modifying the morphology of the tidal frame. The result is that sediment distribution within the estuary is altered so that previously stable areas are now acting as sources of sediment to the wider estuary. These events provide the opportunity to use anthropogenic disturbance within the Ribble as an analogue for disturbance mechanisms that may be associated with climate change induced modifications to the coastal system such as altered patterns of storminess and sea level rise.

2.1. Sediment

The remobilisation of marine and estuarine sediments as well as the nature of spatio-temporal variation of these sediment deposits has substantial implications for radiogenic contaminant remobilisation. The nature of sediment types, their definitions and the issues affecting sediment remobilisations, both internationally and at the Ribble estuary level are discussed here.

2.1.1. Sediment types

Estuaries are exchange environments where the terrestrial and marine environment interface resulting in substantial mixing and deposition. In these environments catchment-derived, marine-derived sediments and estuarine sediments are mixed and either deposited within the estuary or transported out with to the Irish Sea through sediment transfer mechanisms. The morphology of estuaries is characterised by deposition features (e.g. sandbanks, mudflats and saltmarshes), with their formation

being determined by the sediment grain size and the available at the time of formation. Sediment grain size is a vital measurement when it comes to defining how sediments behave and is defined throughout this thesis in accordance with ISO 14688 -1:2002 (2013); clay < 2 µm, silt 2 µm – 63 µm, sand 63 µm – 2000 µm. In this thesis (and particularly in chapter 3) sand is referred to as sand or fine sand. Fine sand is a fraction which has a particle size range of 63 µm – 200 µm.

The marine environment is the primary source of the Ribble estuary sediments, with landward migration of marine sediments and partial littoral migration of reworked estuarine sediments south of the estuary being the main sediment sources for the Ribble estuary (Holden et al., 2011). Sources of marine sediments occur across the bottom of the Irish Sea and consist of a mix of sands (> 63 µm) (Wright et al., 1971) and muds (< 2 µm) deposits that are derived originally from glacial processes (van der Wal et al., 2002). These sediments are transported to the estuarine environment where they undergo size specific sorting based on their respective grain sizes and the energy available to transport those sediments, the result is the formation of deposition features such as sandbanks, mudflats and saltmarshes.



Figure 2.1 Map of the Ribble estuary with digitised overlays highlighting the three main sediment deposit types; Sandbanks, Mudflats and Saltmarsh.

The funnel shaped Ribble estuary exhibits clear longitudinal stratification of the three main sediment deposit types as demonstrated by figure 2.1, this stratification occurs along the length of the Ribble main channel as well as with the elevation within the tidal frame. At the mouth of the Ribble estuary there are expansive sets of sand banks which exhibit dynamic sand wave features (Rainford, 1997) that have the visual appearance of ripples in the surface. It has been suggested that these sand deposits are under a constant state of reworking towards the estuary channel and substantial sediment movements occur here (van der Wal et al., 2002). These sand dominated sediment deposits are therefore subject to substantial spatio-temporal variability, however this variability likely translates to a marginal radiological impact (Rainey et al., 1999).

The mudflats and saltmarshes are the two sediment deposit types that are radiologically significant due to their sediment bound radiogenic contaminants (Clifton et al., 1999). In the Ribble mudflats are found in the high tidal frame above the main channel where energy conditions are lower, and are distributed from the mouth of the estuary near Lytham up to Preston docks, they are the dominant surface type in the mid estuary (figure 2.1). Mudflats are formed by the process of flocculation which is where marine and catchment derived mineral material such as clays and organic matter in various stages of decomposition join to form a cohesive sediment (Manning et al., 2011). Mudflats are dynamic in that the process of flocculation is a mix of aggregation of flocs, which causes accretion and the breakup of flocs which causes erosion. The clay and organic fractions of the sediment during erosion are released back into the estuaries water column, this process is called remobilisation and represents the physical transport of sediments (Lee et al., 2011). Once these remobilised clays are returned to the water column they are available to the flocculation process again and can become incorporated back in the sediment deposit in a cyclic process mediated by any disturbance that might have occurred within the estuary.

The Ribble estuary has a large collection of fringing saltmarshes, these are an evolution of mudflats in that this sediment deposition feature begins as a mudflat. Through physical sedimentation of an area high in the tidal frame, a mudflat with a higher elevation is formed that is above water for a sufficient length of time to promote cyanobacterial and microphytobenthos growth (Coles, 1979). Cyanobacteria are photosynthetic bacteria found in sediments that are exposed for prolonged periods of time during low tide (Friend et al., 2003). Microphytobenthos are algae that reside in the sediments and are responsible for the formation of biofilms, an important source of

organic matter for the sediment matrix (Santos et al., 1997). Cyanobacterial, as well as microphytobenthos, growth stabilises the mudflats and helps them resist erosion by increasing the cohesion of the sediment through the production of extracellular polymeric substances (Friend et al., 2003). The net effect is a positive feedback whereby physical sedimentation allows biological factors such as vegetation growth to promote increased sediment accumulation that in turn raises the height of the mudflat eventually forming a saltmarsh (Allen and Pye, 1992).

The saltmarshes are halophytic and generally have a poor diversity of vegetation, the vegetation will exhibit zonation from the front to the back of the marsh caused by differences in frequency and intensity of inundation and salinity. These different zones also, in effect, reflect slight differences in the elevation gradient (Adam, 1993; Doody, 2008). Within the marsh there are branching networks of tidal creeks that drain the marsh during the ebb tide and flood it during the flood tide. The saltmarsh creeks are in fact regarded as being part of the mudflat and emphasise the extent to which the mudflats and saltmarshes are interconnected. The saltmarsh and the fronting mudflats interact through hydrodynamics, when one of these sediment deposits is substantially modified by a disturbance event (e.g. storminess) sediment transfers will occur by erosion and deposition forces, as the hydrodynamics force a correction in the sediment deposits morphology (Pethick, 1992).

2.1.2. Managed realignment

The extent of saltmarsh within the UK is currently in decline, with erosion of mature saltmarsh outpacing the creation of new saltmarsh (e.g. Beaumont et al., 2014). Coastal squeeze the process in which saltmarshes are prevented from retreating inland by sea wall defences and human development, is considered as a present and future contributing factor to the problem of declining saltmarsh extent (Masselink and Russell, 2013; Symonds, 2006). The increasing eutrophication in the estuaries globally is also considered a likely factor as it is leading to a population boom in the ragworm, *Nereis Diversicolor*, which is causing increased rates of bioturbation and herbivory of the saltmarsh vegetation roots. This enhanced rate of herbivory and bioturbation can cause vegetation diebacks which in turn destabilise the saltmarsh sediments thus making them vulnerable to erosion (Wolters et al., 2005a). The consequence of such vegetation loss will be the removal of the dampening effect of vegetation on the flood and ebb flows which will in turn increase water flow velocities and may cause enhanced saltmarsh erosion (Stark et al., 2017).

This erosion and loss of saltmarsh must be overcome to prevent a decline in overall saltmarsh area and associated habitat for wild birds and other wildlife (Speakman et al., 2013). The Hesketh Outmarsh site at the Ribble estuary is an example of a managed realignment scheme, which has reconnected a 1980's land reclamation site to the Ribble estuary (Tovey et al., 2009). Such schemes aim to create new saltmarsh often by the removal of old sea walls and the reconnection of previously reclaimed saltmarshes to the estuary (Wolters et al., 2005b). While managed realignment addresses the issue of coastal squeeze there is some debate of the effectiveness of these schemes given the potential impact of the ragworm *Nereis Diversicolor* (Wolters et al., 2005a).

Managed realignment schemes have been shown to trigger changes in sediment transport with localised erosion and accretion occurring at a non-spatially uniform pattern within the managed realignment, likely due to modifications to the site's hydrodynamics (Symonds, 2006). Disturbance and the physical modification to saltmarsh morphology has been shown to promote erosion (Browne, 2017; Pieterse et al., 2017), though the full effects of managed realignment remain unknown. These localised erosion/accretion events and the overall loss of saltmarsh sediments are however radiologically important due to saltmarshes being a concentrated coastal contaminant sink.

2.1.3. Sediment movement within the Ribble estuary

The Ribble estuary is believed to be accreting overall, with long term sediment budgets showing a positive trend of accretion up until 1999 (van der Wal et al., 2002) since 1999 there has been no further sediment budgets. Through a series of multispectral remote sensing images processed to show suspended sediment concentration, the Ribble estuary was shown to exhibit a pump and flush mechanism of sediment transport (Wakefield, 2005). This mechanism in effect means that, partly due to the linear morphology of the Ribble estuary, sediments are redistributed to the water column by disturbance of the flood tide and then pumped to the upper estuary (e.g. Choi and Kim, 2016). On the ebb tide there is a partial back wash, though it is the effects of high river discharge and possibly storminess that cause a flushing of sediments to the estuary mouth, which are then pumped back into the estuary on the next flood tide (Wakefield et al., 2011).

2.2. Radioactive contaminants within the estuarine and marine environment

The radionuclides ^{137}Cs and ^{241}Am were the focus of this work as they provided contrasting information due to their differing behaviour in the marine and estuarine environments as they have different levels of conservativeness in the water column and are known to be readily detectable. These properties mean that they act as good geochemical tracers in Irish Sea sediments and allow inferences of sediment movements to be formed based on the concentration and ratios of these radiogenic contaminants within the sediment matrix.

2.2.1. Historic and current discharges of radioactive contaminants

Westinghouse Springfields Fuel Limited located on the northern bank of the Ribble estuary is responsible for the manufacture of uranium fuel for the UK civil nuclear programme. The Springfields site makes authorised discharges of radionuclides from the uranium decay series directly to the Ribble estuary, these do not include ^{137}Cs and ^{241}Am . Therefore, the ^{137}Cs and ^{241}Am found within the Ribble estuary is derived from atmospheric deposition, Ribble river catchment concentration and Irish Sea sources, with the latter being by the far the largest source.

Sellafield Limited manages and operates the Sellafield nuclear fuel reprocessing complex on the North West English coast. The Sellafield site is complex and undertakes nuclear decommissioning, nuclear fuel reprocessing and waste management and storage activities. Sellafield is considered to be the primary source of ^{137}Cs and ^{241}Am , along with a number of other radionuclides, to the Irish Sea and its surrounding estuaries (Gleizon and McDonald, 2010; Vintró et al., 2000). The site historically had an emphasis on nuclear weapons development and to a lesser extent domestic nuclear power research and later production. Consequentially Sellafield, as the UK's pre-eminent nuclear material research, production and reprocessing facility, is the main source of radioactive discharges to the Irish Sea.

The 1957 Windscale accident was the most severe Sellafield non-authorised discharge according to the international atomic energy agency's (IAEA) international nuclear and radiological event scale (INES), which ranked the accident as INES 5. This accident resulted in radioactive deposition equivalent to around 1/30th of that deposited by the Chernobyl accident, with deposition occurring predominantly in the North West of England (Bonnett and Cambray, 1991). Authorised marine discharges via the Sellafield pipeline over the past 60 years however represent the more substantial impact Sellafield has had on the environment and understanding any risks to humans and

wildlife from these historic discharges is needed (Hunt et al., 2013; Rahman et al., 2013).

The Sellafield authorised discharges to the Irish Sea are bulk diluted and discharged over 2.5km off shore. Discharged radionuclides travel with coastal and shallow shelf sea currents as a dissolved phase or they attach to suspended matter where by they either fall out of the water column or travel as part of the Irish Sea's sediment transport systems. With Sellafield discharges currently in decline in comparison to the 1970's, future variability in environmental radioactivity levels may be dominated more so by remobilisation of the radionuclides currently stored within the environment (Hunt et al., 2013).

2.2.2. Properties of contaminant sink radionuclides ^{137}Cs , ^{241}Am and $^{239+240}\text{Pu}$ / ^{241}Pu

An overview of how ^{137}Cs and ^{241}Am have been observed behaving within the marine and estuarine environment is provided, this overview also includes $^{239+240}\text{Pu}$ / ^{241}Pu . Plutonium was included as current activity concentrations of ^{241}Am are significantly affected today by ingrowth – the decay of a parent radionuclide and production of a daughter radionuclide – from ^{241}Pu . Therefore, the plutoniums are covered as they represent a source of ^{241}Am to the marine and estuarine environment.

Plutonium

Located in the north eastern Irish Sea the Sellafield mud patch is the primary environmental store of plutonium radionuclides and via remobilisation contributes to rising concentrations of plutonium around the Irish Sea (e.g. Kershaw *et al.* 1999a) as well as the North Sea and Arctic Sea (Kershaw *et al.*, 1999b). Mud patch plutonium has been shown to have a relatively low re-dissolution rate (<1%) which can be enhanced via disturbance; with the disturbance believed to be a combination of bioturbation and tidal/storm events (Leonard *et al.*, 1999; McDonald *et al.*, 2001).

Aldridge *et al.* (2003) successfully (validated via hind casting) investigated $^{239+240}\text{Pu}$ remobilisation via a modelling approach that attempts to account for the physical, chemical and biological mechanisms of remobilisation. $^{239+240}\text{Pu}$ is remobilised from the eastern Irish Sea mud patches via pore water exchange and tide and storm activity. It is then transported as a dissolved phase as part of the Irish Sea ocean currents whilst being scavenged from the water column by fine grained sediments and suspended material. The importance of these sediment transport processes is such that

$^{239}\text{Pu}/^{240}\text{Pu}$ remobilisation can to a great extent be accounted for by sediment transport modelling (Gleizon and McDonald, 2010).

$^{239+240}\text{Pu}$ sediment concentrations have been declining by an order of magnitude less than the rate of decline seen in Sellafield discharges; the implication being that the remobilisation of the environmental store of $^{239+240}\text{Pu}$ is responsible for this trend (Hunt *et al.*, 2013). Concentrations of $^{239+240}\text{Pu}$ at sites further away from the immediate Sellafield vicinity have in some cases not experienced a significant decline or have increased. Consequently, the study by Hunt *et al.* (2013), which used a 50-year time series, supports the assertions in the literature that Sellafield derived radionuclides are being remobilised and this is a significant process in the inter-annual variation of anthropogenic radionuclide spatial distribution (Mackenzie & Scott 1993; Leonard *et al.*, 1999; Aldridge *et al.*, 2003; Goshawk *et al.*, 2003; Lindahl *et al.*, 2011).

Americium

By 2009 630 TBq of ^{241}Am had been produced within the environment through the process of radioactive ingrowth compared to 510 TBq that has been discharged by Sellafield since 1963 (Hunt *et al.*, 2013). Ingrowth adds 8 TBq y^{-1} to the environmental store of ^{241}Am compared to direct discharges of 0.04 TBq y^{-1} (Hunt *et al.*, 2013). Effectively ^{241}Am concentration within the environment is now more affected by the decay production from ^{241}Pu than by to authorised discharges.

^{241}Am has very similar environmental behaviour to plutonium, with it being highly particle reactive and binding to the organic and carbonate fractions of the sediment (Desideri *et al.*, 2001). Consequently the mud patches store large quantities of ^{241}Am as a time integrated source (Finegan *et al.*, 2009). ^{241}Am is slightly less soluble than plutonium but shares a vulnerability to enhanced remobilisation via a combination of bioturbation and tidal/storm events (Leonard *et al.*, 1999; McDonald *et al.*, 2001). The remobilisation of ^{241}Am from the mud patch is believed to occur as part of a wider sediment transport system within the Irish Sea (Aston and Stanners, 1982), with sediment transport being more important for ^{241}Am remobilisation than other particle reactive radionuclides such as $^{239+240}\text{Pu}$ (Marsden *et al.*, 2006) due to ^{241}Am having a lower distribution coefficient.

Agreement is found in the literature that ^{241}Am is being remobilised from the environmental stores and this remobilisation is a significant cause of inter-annual variation in ^{241}Am concentrations (Mackenzie & Scott, 1993; Gleizon & McDonald, 2010; Kershaw *et al.*, 1999a). ^{241}Am exhibits the same process of remobilisation as

seen in $^{239+240}\text{Pu}$, which is characterised by declines in the immediate vicinity of Sellafield and a spreading of activity away from Sellafield (Hunt *et al.*, 2013).

Caesium

Irish sea radioceasium discharges peaked in 1977 and had levelled off by 1985, as ^{137}Cs has a half-life of 30.17 years it would be reasonable to expect present (2017) concentrations in the environment to have declined substantially. The low rate of decline and lack of a decline in some cases was, like ^{241}Am , interpreted as evidence that a source of ^{137}Cs other than discharges was in operation. The Sellafield mud patch is believed to be this source, as it is for ^{241}Am and plutonium (e.g. Hunt *et al.*, 2013). ^{137}Cs is a conservative radionuclide and as such most of the discharges were within the dissolved phase, which facilitated transport of a significant amount to the Northern Atlantic and Arctic waters (Kershaw *et al.*, 1999). Large amounts of ^{137}Cs are located within the Sellafield mud patch though this has been declining via a combination of re-dissolution and sediment transport (Hunt *et al.*, 2013).

^{137}Cs enters deposition sites such as estuaries as a mixed time integrated source transported by adhesion to clays and silts (e.g. Brown *et al.*, 1999). Deposition within estuaries is dependent on site micro-topography (Bradley and Clapham, 1998) and the clay/silt bound caesium is then re-distributed frequently within this system (Assinder *et al.*, 1997). Once deposited within temporally stable sediment deposits such as saltmarshes the ^{137}Cs is usually fixed, though the most labile elements have been found to show a degree of mobility (Morris *et al.*, 2000).

It is likely that the ^{137}Cs signal found within Irish Sea sediment will homogenise over time as the significance of mud patch remobilisation which is dominant at present declines in its importance and factors such as half-life decay and re-dissolution become more significant (Hunt *et al.*, 2013; Mackenzie & Scott, 1993; Vives I Batlle *et al.*, 2008). At present remobilisation is causing a degree of scatter in ^{137}Cs concentrations at sites further away from Sellafield, this has been shown to be affected by Irish Sea sediment transport systems as ^{137}Cs bound to finer grained fraction of the sediment is less likely to be transported out of the eastern Irish sea (MacKenzie *et al.*, 1999)

Coastal contaminant sinks

Coastal contaminant sinks are known to be acting as sources to other near shore environments within the Irish sea (Hunt et al., 2013). At the saltmarsh scale, remobilisation within the estuary and saltmarsh itself is also known to be occurring (Lindahl et al., 2011; Morris et al., 2000; Oh et al., 2009). With authorised discharges from nuclear facilities being much reduced compared to historic levels, remobilisation of radioactive contaminants from coastal contaminant sinks will, and in some cases already has, emerged as the dominant source of radionuclides to the environment (Aldridge et al., 2003; Goshawk et al., 2003; Hunt et al., 2013; Leonard et al., 1999; Lindahl et al., 2011; A. B. Mackenzie and Scott, 1993).

The predicted increase in sediment disturbance and remobilisation means that historically deposited contaminants will also be remobilised and moved within and out with the estuary (Aldridge et al., 2003; Gleizon and McDonald, 2010; Hunt et al., 2013; Marsden et al., 2006). The time integrated discharges of radiogenic contaminants that are present within sediment deposits such as the clay and silt dominated saltmarshes represent substantial coastal contaminant sinks (Gleizon and McDonald, 2010; Rainey, 1999; Wakefield, 2005).

2.2.3. Sediment-bound contaminants

The distribution of radioactivity within the intertidal environment is closely correlated with the distribution of fine sediments due to radionuclide sorption to the surface of clay particles (Clifton et al., 1999; MacKenzie et al., 1999). Therefore, sediment deposition environments will also be sites of radionuclide accumulation; this is best emphasised with saltmarshes, which act as a temporal record of estuarine contaminant levels (Morris et al., 2000). ^{137}Cs and ^{241}Am differ in their chemical conservativeness and as such sediment bound ^{137}Cs is more vulnerable to redissolution as it is more likely to be in disequilibrium with the ^{137}Cs concentration within the overlying water this is less the case for ^{241}Am (MacKenzie et al., 1999; McDonald et al., 2001).

At the Ribble estuary the association of ^{137}Cs and ^{241}Am with the clays and silts of the sediment matrix was investigated by Rainey (1999) and later Wakefield (2005). They established significant correlations between the percentage of clays and silts and the concentrations of ^{137}Cs and ^{241}Am . These correlations were strong enough to allow a proxy relationship to be derived that allowed prediction of ^{137}Cs and ^{241}Am as a function of the percentage clay. These proxy relationships were applied to multispectral data collected by airborne remote sensing for the extent of the mudflats of the Ribble

estuary and resulted in the mapping of surface contaminant distribution within the Ribble estuary.

Given the strong association of contaminants with fine grained sediment within the estuary and as part of the wider Irish Sea sediment transport system, the question to be answered is will remobilisation of sediments result in the remobilisation of contaminants? There is some evidence to suggest that sediment remobilisation from storms and other physical processes may be responsible for the remobilisation of contaminants (e.g. Morelli and Gasparon, 2015). Should estuarine stores of contaminants be remobilised then it may be the case that the tidal processes that govern sediment reworking will see remobilised sediment concentrations sufficiently diluted (Periáñez, 2005).

Saltmarshes represent the most concentrated coastal contaminant sink with historic discharges of contaminants stored as vertical stratified deposits (Fox et al., 1999). The implications of saltmarsh erosion and the redistribution of the sediment-bound contaminants is of great interest, particularly if this redistribution is likely to be a pulse or diffuse source (Allen and Pye, 1992). There is currently a paucity of literature exploring such scenarios. One of the few examples of research on these issues is the work of Rahman et al (2013) who determined that that such remobilisations could result in a three - to four - fold increase in best estimate doses for saltmarsh users. How sediment bound contaminants will be affected by changes in the estuarine environment is particularly relevant given the potential impacts of climate change in the coastal environment.

2.3. The role of climate change in contaminant remobilisation

The fine grained estuarine sediment deposits are in effect coastal contaminant sinks, therefore modifications to the coastal system that promote enhanced sediment remobilisation will result in accelerated contaminant remobilisation. At present there is a consensus found within the literature that the North Atlantic region surrounding the British Isles and parts of western Europe will experience an increase in storm frequency and intensity in coming years (Mölter et al., 2016). Such findings are partially based on studies of the North Atlantic Oscillation (NAO), which is an index of the local climate that has been linked to storminess (Bader et al., 2011; Bengtsson et al., 2006; Greeves et al., 2007; Keim et al., 2004) and in some cases variation in erosion and accretion rates (Esteves et al., 2011).

Sea level rise, which is more widely studied, will impact sediment erosion and accretion, tidal surge frequency and intensity and shore line retreat (Allen and Pye, 1992). Sea-level rise will result in the landward migration of the estuarine environment, the change in coastal policy towards managed realignment is indicative of the acceptance of this reality as it is a climate change adaptation strategy (Robins et al., 2016). It is hoped that managed realignment will allow the estuarine environment to migrate inland, though should this not be the case then the sediment would be remobilised to the marine environment.

Sea level rise and storminess are the two mechanisms through which climate change is likely to impact the estuarine environments sediment deposits. Individual extreme storm events are known to cause significant estuary wide changes to sediment deposits, though their significance relative to the long term narrative of estuarine sediment movement remains uncertain (Blott et al., 2006). Classic beach theory tells us that an intertidal profile will flatten in response to increased storminess and otherwise steepen during low energy seasons, though engineered defences can prevent an overall expansion of the intertidal profile resulting in saltmarsh edge erosion (e.g. Allen and Pye, 1992). This idealised transfer of material in response to storminess may be complicated by sea level rise as an enhanced tidal frame or storm surge will see hydrodynamic energy increased, which may result in increased sediment being ejected from the estuary during the ebb tide (van der Wal et al., 2002; Wakefield, 2005).

The way in which an estuarine environment will respond to climate change enhanced sea level rise and storminess is determined by a range of factors such as; local wind climate, local sediment transport, sediment supply, estuary morphology and extent of anthropogenic modification (Brown et al., 2016; Adams et al., 2011; Esteves et al., 2011; Luo et al., 2015). Storminess has been linked to erosion in the short to medium term at a number of sites (Adams et al., 2011; Esteves et al., 2011; Gutiérrez et al., 2016). At a longer time scale storminess has been linked to increases in the rate of saltmarsh critical sea level rise rate, in effect given an adequate supply of fine grained material, saltmarshes in some cases may be able to keep pace with sea level rise (Schuerch et al., 2013). However, potential modifications to wave climate; wave height (H_0), wave period (T) and wave direction (Θ_0) will result in significant modification to sediment supply via longshore sediment transport and sediment erosion rates via cross-shore sediment transport (Sierra and Casas-Prat, 2014).

Understanding the effects of climate change for sediment transport, estuary evolution and specifically the remobilisation of contaminated sediments is an active area of

research. The best knowledge view derived from the above, is that climate change will result in conditions that are known to promote sediment erosion such as modifications to the estuaries hydrodynamics (Azevedo et al., 2010; Choi and Kim, 2016; Gleizon et al., 2003; Luo et al., 2015; Stark et al., 2017). Therefore, it is reasonable to state that climate change will likely result in an enhanced rate of sediment remobilisation from estuarine sediment deposits.

2.4. Conclusion

Contaminants have long been known to be preferentially bound to sediments within coastal margins and thus the potential for contaminant redistribution has always existed. The anticipated changes in climate have however given a new emphasis to understanding how such contaminants will be remobilised in response to disturbance. The lack of understanding of exactly how the anticipated changes to the coastal system will affect coastal contaminant sinks is a concern that needs to be resolved. Through studying how coastal contaminant sinks behave temporally and spatially under current circumstance and how they respond to disturbance perhaps insight into how they may react to the potential challenges of climate change may be gained.

3. Spatio-temporal characteristics of radioactive contaminants in the Ribble estuary

The Ribble estuary contains deposition features notably mudflats, saltmarshes and sandbanks created by the inputs of Irish Sea derived marine sediments and North West England derived riverine sediments (van der Wal et al., 2002). The presence of these sand banks, mudflats and saltmarshes, is evidence that supports the view that the estuary is a sink for marine sediments and the predominant balance of sediment transfers is towards accretion within the estuary (Luo et al., 2013). The bulk of Ribble estuarine contamination originates from the Irish Sea (e.g. Brown, 1997), particle reactive contaminants will either enter the estuary bound to fine grained sediments or those that are unbound will bind to fine grained sediments or the organic fraction of the sediment matrix within the estuary (Brown et al., 1999). Estuaries in general and specifically the Ribble estuary are viewed as a sink for marine contamination with contaminants being concentrated within the mudflats and saltmarshes (Assinder et al., 1997; Rainey et al., 1999).

It is important for us to understand estuarine contamination as estuaries are an exchange environment between the terrestrial and marine environments. How marine derived contaminants affect humans, wildlife and the functioning of that ecosystem is of great importance (Bolívar et al., 2002; Villa et al., 2009). For example, the spatial distribution and concentration of contaminants will determine the dose of radiation that organisms receive from radionuclides, therefore understanding the characteristics of contaminants allows us to understand their effects (Hunt, 1997; Stark et al., 2017).

Understanding how contaminants are incorporated into the estuary, specifically the estuaries saltmarshes and mudflats, will deepen our understanding of likely contaminant behaviour. Such knowledge will allow a better understanding of how contaminants may react to changes in the estuary, for example a shift in sediment transport dynamics will likely modify the spatial distribution of sediment bound contaminants (Schoellhamer et al., 2007; Chen et al., 2017). The ability to observe trends in these movements requires an understanding of the natural variability in the system that the contaminants are part of (Gosnell et al., 2016) and therefore monitoring is required to characterise the estuaries contaminant characteristics which is explored in this chapter.

Known contaminant relationships with different fractions of the sediment matrix such as clay, silt, sand and organic matter, mean that changes within these sediment fractions

can be reliably inferred as changes in the concentration of contaminants within the sediment matrix (Atkin, 2000; Ben-Dor et al., 2002; Deronde et al., 2008, 2006; Rainey, 1999; Wakefield, 2005; Wal and Herman, 2006). It is widely reported that contaminants such as ^{241}Am and ^{137}Cs will bind to the clay, silt and organic fractions of the sediment matrix, with varying degrees of ease e.g. ^{241}Am binds more readily to organic matter than ^{137}Cs (Clifton et al., 1999; MacKenzie et al., 1999; McDonald et al., 2001). These relationships when quantified as a ratio provide a measure of the amount of contamination associated with a specific sediment fraction. Where change within this sediment fraction is measured, then these ratios through inference allow estimates of the associated change in contamination concentration. Analysing variability in this ratio accounts for variability in the sediment matrix composition in contrast to bulk sediment contaminant concentrations, which are influenced by variation in the sediment matrix composition.

Changes in the ratio of contamination to a fraction of the sediment matrix can be the result of changes in the concentration of the contaminant or changes in the overall sediment matrix composition. The concentration of contaminants can vary due to the increase of available contaminants to be fixed to this part of the sediment matrix or chemical remobilisation of contaminants from that sediment matrix. Such a change that is contaminant driven would be characterised by a change in contaminant concentration without a corresponding change in the sediment matrix.

Alternatively, such changes in the ratio can be driven by a more complex process of sediment remobilisation in which sediment erosion and/or accretion can result in changes to the sediment matrix composition. This process can be described as the mixing of sediments with differing contaminant concentrations resulting in a new sediment matrix with altered contaminant concentrations. This type of scenario was recently observed at the near shore sediments of Fukushima, Japan where vertical mixing has resulted in reduced ^{137}Cs concentrations (Otosaka, 2017). In this case the ratio change would be characterised by a change in the sediment matrix as well a corresponding change in the contaminant concentration.

By observing variability in such sediment-contaminant relationships, it is possible to differentiate between monthly variability in contamination as a result of sediment reworking and real increases and decreases in estuarine contamination and this will be shown in the following chapter.

Contaminant-sediment relationships are generally thought to be temporally stable and this has been the case for when contamination levels were significantly higher than at present (2017) (Rainey, 1999). However, as the UK has undergone continuous improvement in environmental legislation, contamination levels are falling (Leonard et al., 2017). In particular, radioactive contaminant discharge levels are now significantly lower than historic releases e.g. Sellafield ^{137}Cs discharge 1980 = 5000 TBq | 2015 = 3.1 TBq. Consequently the remobilisation of marine sediment deposits enriched by historic discharges (the environmental store) is now a significant cause of inter annual variability in contamination levels around the Irish Sea (Hunt et al., 2013).

As environmental contamination levels move away from their historically high levels the nature of these contaminant sediment matrix relationships may change. This is evidenced by the work of Wakefield (2005) through repeated observations of the clay/ ^{137}Cs relationship at the Ribble estuary. Wakefield (2005) identified that the ratios could be significantly affected and in some cases decoupled through disturbance mechanisms such as high levels of precipitation and/or high riverine discharge. It was believed that resuspension of ^{137}Cs followed by sediment erosion may have resulted in significant changes to these ratios that would in effect challenge the assertion that ^{137}Cs is significantly correlated with fine sediments (Wakefield, 2005). There is a lack of further work following up on the implications of lower estuarine contamination levels on the strength of such contaminant sediment matrix ratios.

Long term radioactive decay and sediment reworking with less contaminated sediments from the marine environment and catchments can lead to a long-term trend of declining radiogenic contaminant concentration (Gleizon and McDonald, 2010). As estuarine contamination, has already moved away from the historically high levels of past years, the uncertainty of the nature of contaminant sediment matrix relationships is a significant issue. Such relationships are vital for informing estuary wide analysis of contaminant redistribution and understanding the likely implications of such remobilisations.

The presence of contaminant relationships with the sediment matrix are important when linking estuarine and coastal morphological change to contaminant remobilisation. Without understanding these fundamental relationships, it is not possible to infer contaminant remobilisation from sediment movement. Developing an understanding of how contaminants interact with the estuaries sediment matrix has implications for upscaling to coastal sediment transport models and predictions of climate change impacts.

3.1. Aims

This chapter aims to characterise the spatial and temporal characteristics of radioactive contaminants within the different fractions of the sediment matrix. The following questions will be examined:

- Is there a significant relationship between contaminants and particle size distribution?
- Is there a significant relationship between contaminants and percentage organic matter?
- Is the contaminant sediment property ratios temporally stable? and at what scales do these ratios exist at?

3.2. Methods

3.2.1. Site selection

Within the Ribble estuary an area of mudflat located around the Lytham St Anne's lifeboat jetty (Figure 3.1) was selected for this work due to the presence of a diverse range of sediment types across an elevation range from 0 – 3m. The area had sediment deposits that transitioned from fine grained deep mud deposits towards coarse silty sand deposits. This sediment diversity at this location reflects those found across the whole estuary and this means that the results from the field site can be applied to the entire estuary.

The elevation range present means that there will be sediment deposits that vary in the frequency in which they are subjected to disturbance, as sediments higher in the tidal frame are disturbed less frequently due to a lack of energy (Jickells and Rae, 1997). Therefore, transects were set out across the gradient of elevation within the tidal frame, with the purpose to target this survey across sediments that have varying rates of disturbance. This ensures that this work incorporates sample sites with a range of diversity in sediment composition and disturbance frequency, which is important to ensure my findings are applicable more widely to the estuary.

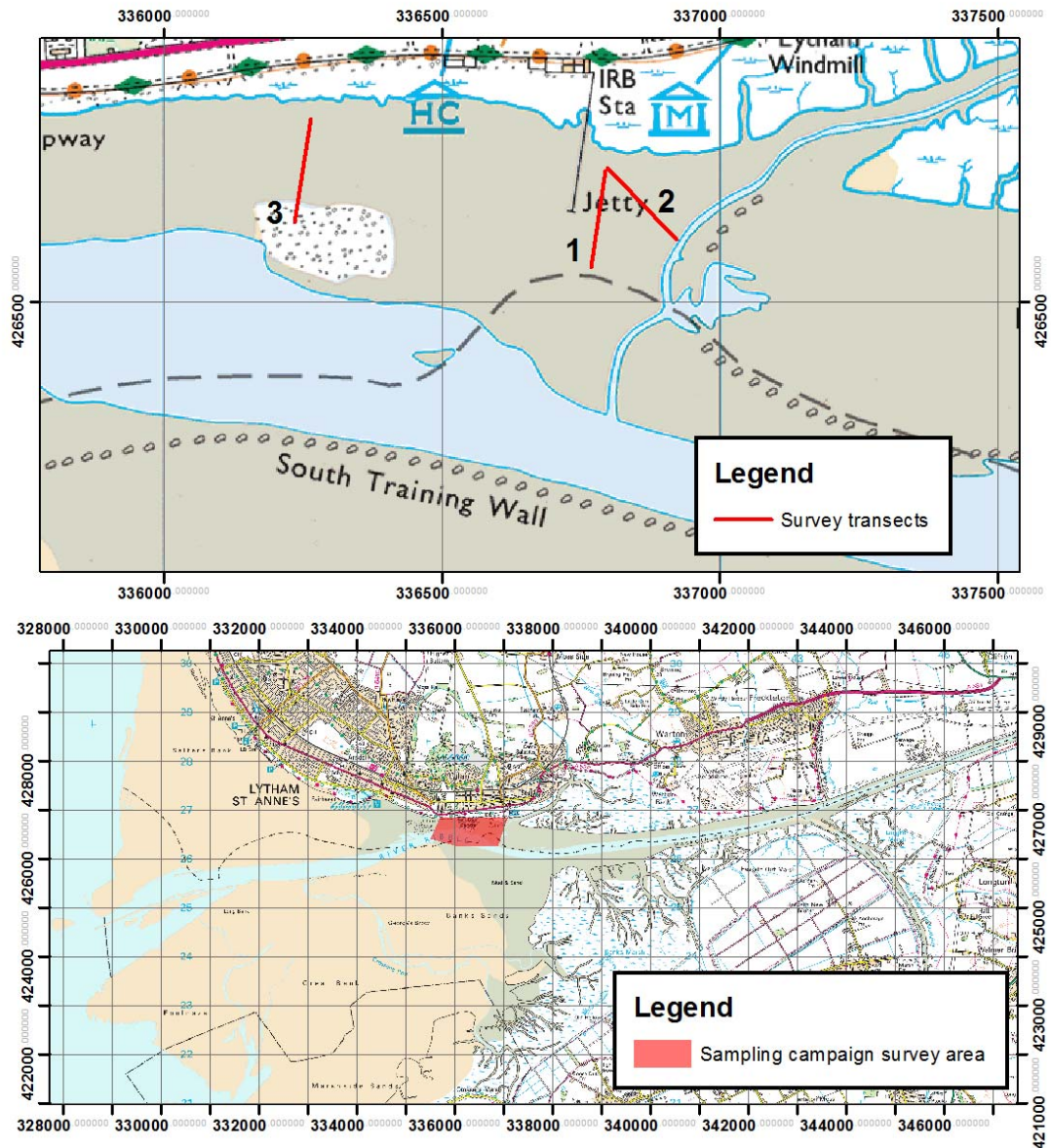


Figure 3.1 The top map shows the area of mudflat in front of the Lytham St Anne's lifeboat jetty with transects marked in red. Transects are numbered 1-3. The bottom map shows the location of these mudflats within the Ribble estuary, highlighted by a red polygon.

3.2.2. Field work

Three transects were set out across the mudflats as shown in Figure 3.1. The transects were laid out using a tape measure beginning at the edge of the Lytham St Anne's saltmarsh and terminating at the water's edge of the Ribble's main channel at low tide. Every 15m a coloured flag and bamboo cane were inserted into the sediment, to mark the samples location. The setting out of transects was to ensure evenly spaced

sampling along an environmental gradient, this targeted approach was to ensure diversity in the sediment types.

Located to the East of the Lytham St Anne's lifeboat jetty transect 1 consisted of 12 sample points and was oriented from North to South beginning at the saltmarsh edge and terminating at the Ribble's main channel. There was a band of relatively deep, fine grained sediments that ran through the middle of this transect; for this reason, transect 2 was orientated to cut diagonally across this band to increase sampling of these sediments. Transect 2, which consisted of 13 points, began 5m east of the top of transect 1 at the saltmarsh edge and ran south east towards a small tributary of the Ribble's main channel, terminating at a steep (60°) decline.

Transect 3 consisting of 11 points was located over 500m west of the Lytham St Anne's lifeboat jetty and was orientated North - South beginning at the saltmarsh edge and terminating at the Ribble's main channel. Where the transect terminated there was a large mussel bed and these sediments were the coarsest observed across all three transects.

At each flag a 1m² quadrat was used to define the sampling area. The quadrat was placed so that when facing the Ribble's main channel (South) and sighting along the row of flags the sample point's flag was always in the northwest corner of the quadrat. Within each 1m² area a sediment scrape was collected by running a trowel over the surface of the sediment (collecting the upper 5mm of sediment) and placing the material collected into a pre-labelled plastic bag. Coordinates of each sample point were surveyed using a Leica 1200 differential global positioning system (DGPS), a one hour preliminary site calibration was used to ensure high spatial accuracies when post processing the data.

At each sample site the amount of ionising radiation was measured using a Thermo-scientific Radeye® and MC71 probe air kerma unit at a standard height of 1m. The air kerma unit was pre-calibrated using an IAEA traceable sealed ¹³⁷Cs source following a method designed to be compliant with the University of Stirling's Environmental Radioactivity Laboratory's (ERL) United Kingdom Accreditation Service (UKAS) accredited quality control system.

The sample points located on these three transects were sampled in March 2014, May 2014, September 2014 and December 2014. At each repeat visit observations about noticeable physical changes at the site were recorded. Care was taken to ensure that

field workers operated outside the collection points' quadrats to minimise disturbance during sampling.

3.2.3. Sediment preparation

The plastic bag containing the sediment sample from the field work was emptied into a 2000µm calibrated test sieve and the sample was sieved in accordance with a United States Environmental Protection Agency (US EPA) methodology (EPA, 2001). Across the four sampling campaigns there was a negligible amount of material above 2000µm, often blades of grass, pieces of plastic or some crushed mussel shells. The sieved sediment was placed in a large tin foil tray and homogenised further by gloved hands and chemically inert plastic paddles.

3.2.4. Sediment properties

After sieving and homogenising each individual sediment sample, subsamples for the following analytical methods were collected as, while wet, the sediment fractions will separate under gravity with time.

pH

The sediment pH was measured using a standard 1:1 ratio method, where by 20g of sediment was mixed with 20ml of distilled water and agitated by hand for a minute and allowed to settle for 15 minutes. A combi pH meter, calibrated with pH buffers 4 and 7, was placed in the soil/water solution and the meter and beaker agitated gently to promote movement around the probe, when a stable reading was displayed it was recorded.

Particle size distribution

Particle size distribution was determined using a Beckman Coulter Counter LS 230, which is a laser diffraction system that produces an estimate of particle size based on Mie theory (Wriedt, 2012). The system records the intensity and angle of light scattered by the sample when a laser is fired at it, through modelling how light would reflect from a homogenous sphere (Mie theory), the system can estimate the size of the particles the laser is being fired at.

15g of sediment, 30ml of distilled water and 2ml of sodium hexametaphosphate solution was added to a 60ml polypropylene bottle. This bottle was placed on a mechanical agitator for 30 minutes to ensure the sediment was disaggregated. The

bottle was then placed on a magnetic stirring plate and 2ml of sample was extracted by pipette and added to the sample loader on the Beckman Coulter Counter LS 230.

To improve the accuracy of the Mie theory based approach to estimating particle size distribution, an optical module was parametrised using the refractive indexes of the major mineral constituents that composed the Ribble estuary sediment. Five repeat measurements were made to ensure that the estimation was reliable and sizing was reported as percentage of sediment that is less than ($\%<$) 2, 63, 212, 630 and 2000 μm .

Organic matter and carbonates

The sequential loss on ignition (LOI) method was used, this method allows the assessment of the percentage organic matter and carbonates within the sample by a controlled ignition of the sample in a furnace. A full method review was conducted by Wang et al., (2011); they produced ideal temperature profiles for various sediment types that would allow successful sequential loss on ignition. I selected their temperature profile for estuarine sediment for my sequential loss on ignition, which consisted of 475°C for 15 hours for organic matter determination followed by 800°C for 12 hours for carbonate determination.

20g of sediment was placed within a dry pre-weighed crucible then placed in a furnace set to 105°C for 24 hours, the sample was removed and weighed, the percentage decrease in weight of the sample is the percentage moisture. The sample was then placed in the furnace set to 475°C for 15 hours, the sample was removed and weighed, the percentage decrease in weight is the percentage organic matter. The sample was returned to the furnace at 800°C for 12 hours, the final percentage decrease in weight is the percentage carbonates of the sediment.

3.2.5. Contaminants

After the sieved homogenised sediment within the tin tray was subsampled for the analyses in section 3.2.4, the tray was weighed and placed in an oven set to 105°C for 24 hours. The tray was weighed after 24 hours and the percentage decrease in weight was the percentage moisture content of the sample. The dried sample was disaggregated using mortar and pestle then homogenised, the sample was placed as a cone then quartered and quartered again and folded over on itself (Schumacher, 1990).

Metals

Metal concentrations within the sediment were determined using Inductively Coupled Plasma-Optical Emission Spectrometry (ICP-OES). The ICP-OES uses plasma to excite the elements within a sample to trigger the emission of electromagnetic radiation. The position on the electromagnetic spectrum and intensity of this emission allows the calculation of the identity of the element and its concentration. The system was pre-calibrated using TraceCERT® certified reference materials for the following elements; Al, Ba, Be, Cd, Co, Cr, Cu, Fe, Ga, K, Mg, Mn, Ni, Pb, Rb, Sr, V, Zn, As, Hg and Sn.

A subsample of the homogenised sediment was placed in a mortar and pestle and ground to a fine powder then placed in a new pre-marked sample bag. 0.25g (+/- 0.005g) of this sediment was placed into a Polytetrafluoroethylene tube and 2ml of concentrated nitric acid was added to each tube and the actual weight used recorded. The tubes were carefully sealed and placed inside a MARS 5 microwave digestion system and a pre-programmed sediment digestion programme was run. Following cooling the tubes were rinsed using 100ml of deionised water into a funnel lined with a filter paper (Whatman grade no 2) over a 100ml volumetric flask. Additional deionised water was added to each volumetric flask to make up the solution to 2% nitric acid.

Quality control samples were analysed with each sample batch. These included two blanks to check for residual contamination in the Polytetrafluoroethylene tubes and 0.25g (+/-0.005g) of a NIST-SRM certified sandy clay soil (CRM049-50G). All digested samples were agitated and 15ml of sample was decanted into a 15ml centrifuge tube and placed on an automated sampler connected to the ICP-OES. The data were then processed using calibration curves derived from standards which were run for each sample batch through the ICP-MS to convert the emissivity data to parts per billion.

Gamma spectrometry

The remaining homogenised sediment was placed inside a large mechanical grinding dish and placed inside the mechanical grinder which was then run for 3 minutes. The sample was checked to ensure it had been ground thoroughly to a fine texture, if not it was reground for an additional 3 minutes. The ground sediment was placed on a clean steel tray and homogenised by mixing with chemically inert plastic paddles with the sample being quartered and quartered again and folded over on itself.

The ground sediment was added to a pre-weighed plastic container of known geometry; the sample was added incrementally then tapped to ensure a consistent settling of the ground sediment. Once the container was filled it was levelled off with a knife and any sediment around the threads was brushed off. A lid was placed on the container, which then had molten wax placed around the seal to ensure it was air tight. The sealed containers were left for 2 weeks to allow the natural decay chain to reach equilibrium within the sealed container.

The sealed containers were transferred to the University of Stirling's Environmental Radioactivity Laboratory (ERL) for quantification of the full range of gamma emitting radionuclides by gamma ray spectrometry (Knoll, 2010). The ERL is operated in accordance with a UKAS accredited ISO/IEC 17025:2015 management system. A suite of ORTEC® GMX N Type 35% pure High Purity Germanium (HPGe) detectors, which are routinely calibrated with National Physical Laboratory (NPL) certified standards used for gamma ray spectrometry.

Each sealed container was placed on top of the HPGe detector, which is surrounded by a lead lined structure to minimise background interference. The detector measures the number of gamma ray emissions from radioactive decay of the radionuclides present within the sample. The proprietary ORTEC software Gammavision was used to analyse the sample; the software uses radionuclide libraries, geometry calibrations, energy calibrations and efficiency calibrations to calculate the amount present for a number of gamma emitting radionuclides with energies ranging from 20 to 2000 keV. This study has focused on two of the radionuclides – ^{137}Cs and ^{241}Am . The results for each sample were decay corrected to the date the sample was collected and reported as activity for each nuclide in Bq kg^{-1} .

3.2.6. Dosimetry

The dosimetry results collected in the field from a height of 1m over a 600 second duration were entered into an ERL prepared template that calculates the absorbed dose rate in air for each location in $\mu\text{Gy hr}^{-1}$. The air kerma equipment was calibrated by Cavendish Nuclear Ltd in accordance with their UKAS accredited methods. Shortly before field visits a ^{137}Cs check source was used to check that the air kerma equipment was functioning correctly.

3.2.7. DGPS

The DGPS data were extracted to propriety Leica software (Leica Geooffice) for post processing with Ordnance Survey (OS) base station data. Four base stations from the OS-Net were selected, these were Giggleswick, Blackpool, Manchester and Daresbury, these were the closet to the Lytham field site. The DGPS data were shifted towards a reference point that was averaged from the four base stations and processed, allowing a ± 1.5 -3cm accuracy to be achieved. These data are exported as x, y, z coordinates on the British National Grid coordinate system.

3.2.8. Statistical analysis

Data exploration

The investigation of the radiometric and metals data in combination with the discussion in section 2.2 highlighted a number of contaminants that would be ideally suited for the analysis here. ^{137}Cs is conservative in nature as it does not readily bind to particulates such as sediments with a half-life of 30.17 years' contrasts ^{241}Am which does readily bind to sediments and has a half-life of 432.2 years. These radionuclides lend themselves to rapid in situ characterisation and are excellent proxies of other sediment bound contaminants, therefore where chosen for focused analysis.

A BGS report (Ridgway, 2001) which investigated the distinctions between natural and anthropogenic sources of metals within the Ribble estuary and catchment determined that the Ribble was polluted with Mg, Ca, Fe, V, Cr, AS, Rb and Sr. Contaminants that represented groups of metals were selected for this study, these included a naturally occurring metal (Fe), anthropogenic metal (Sr) and metalloid (As).

Summary statistics were calculated using the describe by function of the psych package (Revelle, 2016) within the R programming environment. The reported data describe the central tendency (mean and median), dispersion (min, max and range), variance (standard deviation and median absolute deviation) and shape of the distribution (skew and kurtosis). These statistical outputs were calculated for each of the sample parameters: ^{137}Cs , ^{241}Am , As, Fe, Sr, % clay, %silt, %sand, %OM, %Carbonates and pH in each month (March, May, September and December. The summary statistics were also calculated for all points along each transect for each month.

A correlation matrix was produced using the `cor()` function in R, this produces a matrix of calculated Pearson correlation coefficients ranging from -1 to +1. The closer to the value of 1 (negative or positive) denotes the strength of the correlation with ± 1 being perfect correlation the sign (\pm) tells you whether it is a positive or negative correlation. This is a measure of linear dependence between x and y and is useful for quantifying which variables may be correlated. The `plot()` function was also used to produce a large graph matrix such as that shown in Appendix 1.1, which is a visual representation of the correlation matrix. This was used as a tool to aid the selection of metals to be profiled as representing the general trend in metal concentration.

Fe was correlated at > 80% with As, Cd, Co, Cr, K, Mg, Mn, Ni, P, V and Zn was selected to represent naturally abundant metals. As was correlated with Al, Cd, Co, Cr, Fe, K, Mg, Ni, P and V at > 80% and represents a metalloid. Sr was correlated with As, Cr and V and represents a metal that is likely to be present at anthropogenically enhanced levels. These three metals through cross correlation allow the results of the metals analysis to be presented in a concise fashion.

Temporal and spatial variability

Analysis of variance was used to determine if there was significant difference between subsets of the variables using the grouping variables month and transect number. The month grouping aggregated the three transect data from each of the four months March, May, September and December. The transect grouping compared individual transects (e.g. 1, 2 and 3) against each other for each month. These two grouping arrangements allowed the spatial variation across the Lytham sediments and temporal variation in the Lytham sediments to be assessed for statistically significant change.

The ANOVA requires the assumption of normality in the data distribution, however there is evidence to suggest that ANOVA will outperform the nonparametric alternative Kruskal Wallis H test even in cases where this assumption is not correct (e.g. McDonald et al., 2014). Post hoc tests to further interpret the results in the case of the Kruskal Wallis H test can result in error propagation through the manual adjustment of p - values (Zar, 2010). Therefore, data transformation has been applied to achieve a normal distribution, however where the deviation from normality was not substantial an ANOVA was used.

The `aov()` function was used to conduct the ANOVA in R with the results of the model being stored as a model object which in turn had a Tukey-Kramer test conducted on it

using the TukeyHSD() function. This test allowed the differences at the group level to be examined.

Contaminant sediment relationships

The radioactive contaminants ^{137}Cs and ^{241}Am were found to have variability that was similar to the variability in the sediment matrix specifically the particle size distribution and there were substantial concentrations present. The metals contaminants however were present in negligible quantities and did not exhibit significant change similar to that seen with the radioactive contaminants. For these reasons this work focused on the radioactive contaminants ^{137}Cs and ^{241}Am and used these contaminants to narrate the nature of statistically significant variability in the contaminant sediment relationships within the Ribble.

^{137}Cs and ^{241}Am relationships with the sediment properties are explored to quantify the nature of the detected correlation from section 3.3.1. Regression analysis was conducted for both contaminants against the sediment properties % clay, % silt, % sand and % organic matter. All data was transformed by natural logarithm and mallows statistics and residual diagnostics plots were used as part of model simplification. Linear regression models that used log transformed data were produced that predicted contaminant concentration from the sediment property data. Regression models were produced for the individual transect and for each of the four months.

Annual regression models were fitted to the full data set and compared to historic data sets from the work of Rainey (1999) from 1995 and 1997 and Wakefield (2005) from 2002 and 2003. These regression models were statically compared by a dummy variable regression, which used a numeric stand in for the categorical variable in this case the year the data was collected (Rogerson, 2008). The data for 1995, 1997, 2002, 2003 and 2014 were compared and grouped based on statistical difference.

3.3. Results

The results are presented here firstly as a descriptive interpretation of the sediment properties (clay, silt, sand, organic matter, pH), the contaminants (^{137}Cs , ^{241}Am , Fe, Sr and As) and measured dose. The results are interpreted in terms of temporal change across the year 2014 and spatial change between the different transects.

This analysis then goes on to explore key relationships between the sediment properties and the contaminants ^{137}Cs and ^{241}Am across different spatial and temporal scales. These relationships are then contrasted with historic data to evaluate how contaminants sediment relationships have changed over the past 20 years.

3.3.1. Temporal and spatial variability

Summary statistics and ANOVA analysis with post hoc tests were used to determine how the sediment matrix and contamination concentration of that matrix varied temporally. The full model outputs are in Appendix 1 as a list of R console print formatted outputs for each ANOVA analysis, F statistics are referenced within the following text when referring to the significance of any change.

Sediment properties (% clay, %silt, %sand, %OM, %Carbonates, pH)

Table 3.1 % clay content summary statistics for each of the four monthly sampling campaigns. MAD = median absolute deviation, n = 36.

| Month | Mean % | SD % | Median % | MAD % | Min % | Max % | Skew | Kurtosis |
|-------|--------|------|----------|-------|-------|-------|------|----------|
| Mar | 3.60 | 2.32 | 2.90 | 1.77 | 0.87 | 8.81 | 0.97 | -0.30 |
| May | 4.98 | 2.46 | 4.78 | 2.23 | 1.22 | 10.30 | 0.44 | -0.70 |
| Sep | 7.86 | 2.05 | 7.76 | 2.19 | 4.73 | 14.00 | 0.70 | 0.26 |
| Dec | 6.28 | 2.16 | 6.13 | 2.17 | 2.85 | 12.20 | 0.70 | 0.06 |

The site accumulated fine grained clays throughout the year until September, then those fine-grained clays were eroded away as the winter begins as shown in Table 3.1. The percentage of clay within the sediment was significantly higher for September in

comparison to March and May ($F(3,140) = 23.52, p < 0.001$). The post September decline was also significant ($F(3,140) = 23.52, p < 0.05$), furthermore the percentage clay for December was not significantly higher than May. The data were positively skewed towards low clay values (Table 3.1) however the range was consistent across all four months, which means that in September the whole site saw a uniform increase in percentage clay. The September to December decline was also uniform in that the range remained the same but a 2% decrease in the minimum was observed.

In March there was spatial variation at the site with transect 2 covering sediments that were significantly higher in clay content and transect 3 covering sediments that had the least amount of clay ($F(2,33) = 5.504, p < 0.01$). By May this significant spatial variation had disappeared apart from at transect 3 which still had significantly less clay, though the alpha level of this difference was <0.05 as opposed to <0.01 in March. For September and December there was no significant spatial variation detected in these data.

The site saw a positive trend of 87% increase in the amount of fine grained silts at the site, with this accumulation occurring exclusively between May and September from 20.4% to 37.5% silt. Changes in silt content between September and December were not significantly different, similarly for March and May. However, May and September do differ significantly ($F(3,140) = 21.5, p < 0$), therefore between May and September the amount of silt at the site increased and it has remained so until the end of the survey campaign.

Table 3.2 % silt content summary statistics for each of the four monthly sampling campaigns. MAD = median absolute deviation, $n = 36$.

| Month | Mean % | SD % | Median % | MAD % | Min % | Max % | Skew | Kurtosis |
|-------|--------|-------|----------|-------|-------|-------|-------|----------|
| Mar | 17.62 | 10.76 | 16.91 | 9.83 | 2.59 | 41.68 | 0.73 | -0.31 |
| May | 20.46 | 16.15 | 17.58 | 13.90 | 2.60 | 76.54 | 1.42 | 2.22 |
| Sep | 37.53 | 12.36 | 37.74 | 16.69 | 15.95 | 60.80 | -0.09 | -1.27 |
| Dec | 36.36 | 14.04 | 36.58 | 16.43 | 12.95 | 61.25 | 0.17 | -1.21 |

Table 3.3 % sand content summary statistics for each of the four monthly sampling campaigns. MAD = median absolute deviation, n = 36.

| Month | Mean % | SD % | Median % | MAD % | Min % | Max % | Skew | Kurtosis |
|--------------|-------------------|-----------------|---------------------|------------------|------------------|------------------|-------------|-----------------|
| Mar | 67.55 | 10.18 | 69.76 | 10.24 | 41.67 | 82.80 | -0.58 | -0.41 |
| May | 66.67 | 14.16 | 70.35 | 8.97 | 12.70 | 83.10 | -1.86 | 4.04 |
| Sep | 51.19 | 13.36 | 48.65 | 15.79 | 24.70 | 75.50 | 0.25 | -1.13 |
| Dec | 53.09 | 15.11 | 51.75 | 20.09 | 26.00 | 81.20 | -0.03 | -1.12 |

The month of May stands out with a large positive skew and a high maximum value relative to the mean (Table 3.2), this suggests there was a small number of samples that had a large amount of silt present. Spatially, in March the site had significant difference between transect 2 which had a high accumulation of silts and transect 3 which had a low accumulation of silts ($F(2,33) = 6.189, p < 0.001$). From May to December there was no significant difference between transects.

There was a negative trend present in the fine sand data with a 20% decline over the 1-year survey period, this decline occurred between May and September. September and December were not significantly different, and March and May were not significantly different. However, May and September did differ significantly ($F(3,140) = 15.28, p < 0$), therefore between May and September the amount of fine sand at the site decreased from a median of 70% to around 50%.

There was no significant spatial variation between transects therefore the summary data in Table 3.3 are a good approximation of the Lytham sites trend in sand. The month of March stands out as having a distribution that was partially skewed by sites with low sand content. The patterns of changing percentage sand reported here share a number of trends with percentage silt and clay, the nature of how these trends fit together is discussed in section 3.4.1.

Table 3.4 % organic matter content summary statistics for each of the four monthly sampling campaigns. MAD = median absolute deviation, n = 36.

| Month | Mean % | SD % | Median % | MAD % | Min % | Max % | Skew | Kurtosis |
|-------|--------|------|----------|-------|-------|-------|------|----------|
| Mar | 0.76 | 0.46 | 0.68 | 0.44 | 0.22 | 1.73 | 0.73 | -0.67 |
| May | 2.05 | 1.49 | 1.86 | 0.92 | 0.70 | 8.78 | 2.74 | 9.24 |
| Sep | 4.20 | 1.75 | 3.67 | 1.64 | 1.95 | 7.91 | 0.70 | -0.83 |
| Dec | 2.84 | 1.43 | 2.37 | 1.12 | 1.21 | 6.16 | 0.79 | -0.80 |

The amount of organic matter within the sediment increased across the year, peaking in September but declined in December. The percentage organic matter was variable between the months with all months being significantly different apart from December and May ($F(3, 140) = 39.58$ $p < 0$). The range for the data was also highly variable with the greatest difference observed in March which resulted in the data being highly skewed by a few samples with large (e.g. 8%) amounts of organic matter (Table 3.4).

Spatial variation was not significant though; generally speaking transect 2 had more organic matter (4.8%) followed by transect 1 (3.7%) then transect 3 (3.1%). In March and December, the ANOVA results suggested that transect 3 had significantly less organic matter than transects 2 and 1.

Table 3.5 % carbonates content summary statistics for each of the four monthly sampling campaigns. MAD = median absolute deviation, n = 36.

| Month | Mean % | SD % | Median % | MAD % | Min % | Max % | Skew | Kurtosis |
|-------|--------|------|----------|-------|-------|-------|-------|----------|
| Mar | 2.16 | 0.37 | 2.12 | 0.44 | 1.49 | 2.86 | 0.06 | -1.00 |
| May | 3.85 | 0.66 | 3.83 | 0.83 | 2.70 | 5.16 | 0.01 | -1.12 |
| Sep | 3.64 | 0.77 | 3.51 | 0.62 | 2.53 | 5.58 | 0.85 | -0.05 |
| Dec | 4.11 | 0.41 | 4.16 | 0.39 | 3.19 | 4.93 | -0.33 | -0.38 |

Table 3.6 pH summary statistics for each of the four monthly sampling campaigns.
MAD = median absolute deviation, n = 36.

| Month | Mean | SD | Median | MAD | Min | Max | Skew | Kurtosis |
|--------------|-------------|-----------|---------------|------------|------------|------------|-------------|-----------------|
| Mar | 8.28 | 0.42 | 8.29 | 0.21 | 7.12 | 9.50 | 0.36 | 1.96 |
| May | 8.17 | 0.23 | 8.20 | 0.30 | 7.60 | 8.50 | -0.53 | -0.65 |
| Sep | 7.70 | 0.13 | 7.70 | 0.15 | 7.44 | 7.98 | 0.06 | -0.80 |
| Dec | 7.86 | 0.13 | 7.88 | 0.12 | 7.47 | 8.19 | -0.11 | 1.48 |

During the survey period the percentage carbonates increased from March to May, then remained consistent across the spring and summer before increasing again in the winter (December). The differences in means shown in Table 3.5 were not significant for May and September. Spatially the data were subject to a great deal of intersessional variation with the percentage carbonates being different across the sites and there being no particular trend in the data.

The pH of the sediment declined through March and May and then began to increase again in September and December. The decline seen in March to May was not significant, though the decline from May to September was significant ($F(3,140) = 39.36$ $p < 0$). There was a great deal of variation in the distribution of the data between months (Table 3.6), with March having two to four times the range of the other months.

At the site the spatial variability of these data can be defined as the following, transect 3 was the most acidic at 7.86 in March and 8.13 in May ($F(2,33) = 14.76$ $p < 0$) and transect 2 8.02 in May was the second most acidic with this being significant in May and December.

Contaminants (¹³⁷Cs, ²⁴¹Am, As, Fe, Sr)

Table 3.7 ¹³⁷Cs summary statistics for each of the four monthly sampling campaigns. MAD = median absolute deviation, n = 36.

| Month | Mean Bq kg ⁻¹ | SD Bq kg ⁻¹ | Median Bq kg ⁻¹ | MAD Bq kg ⁻¹ | Min Bq kg ⁻¹ | Max Bq kg ⁻¹ | Skew | Kurtosis |
|-------|-----------------------------|---------------------------|-------------------------------|----------------------------|----------------------------|----------------------------|------|----------|
| Mar | 42.64 | 31.46 | 32.05 | 20.98 | 9.80 | 110.00 | 1.01 | -0.40 |
| May | 38.22 | 31.20 | 30.75 | 19.90 | 0.15 | 168.44 | 2.17 | 6.12 |
| Sep | 67.09 | 53.35 | 56.83 | 34.28 | 2.63 | 311.11 | 2.71 | 9.60 |
| Dec | 54.82 | 30.18 | 48.12 | 29.67 | 20.53 | 139.91 | 1.13 | 0.81 |

The ¹³⁷Cs concentration of the sediment increased across the year peaking in September but declined between September and December. The activity concentration of ¹³⁷Cs was significantly higher in September than March and May (F (3,140) = 4.247, p < 0.01) however the decline from September to December seen in Table 3.7 was not statistically significant. All months had a positive skew, which means that for all months there were a number of samples that had high ¹³⁷Cs activity concentrations. The range in these data increased across the year with a large increase between May and September followed by an equally large decrease between September and December.

In March there was spatial variation at the site with transect 2 covering sediments that were significantly higher in ¹³⁷Cs activity concentration and transect 3 covering sediments that had the smallest concentration of ¹³⁷Cs (F (2,33) = 6.031, p < 0.01). By May this significant spatial variation had disappeared apart from at transect 2 which still had significantly less ¹³⁷Cs, though the alpha level of this difference was <0.05 opposed to <0.01 in March. For September and December there was no significant spatial variation detected in these data.

The ²⁴¹Am activity concentration of the sediment increases across the year peaking in September and goes into decline between September and December. The activity concentration of ²⁴¹Am was significantly higher in September than March and May (F (3,140) = 6.577, p < 0.01) however the decline seen in Table 3.8 between September and December was not significant. All months had a positive skew, which means that

for all months there were a number of samples that had high ^{241}Am concentrations. The range of these data increased across the year with a large increase between May and September which is followed by an equally large decrease between September and December.

Table 3.8 ^{241}Am summary statistics for each of the four monthly sampling campaigns. MAD = median absolute deviation, n = 36.

| Month | Mean Bq kg ⁻¹ | SD Bq kg ⁻¹ | Median Bq kg ⁻¹ | MAD Bq kg ⁻¹ | Min Bq kg ⁻¹ | Max Bq kg ⁻¹ | Skew | Kurtosis |
|-------|-----------------------------|---------------------------|-------------------------------|----------------------------|----------------------------|----------------------------|------|----------|
| Mar | 39.33 | 27.17 | 31.65 | 15.86 | 10.60 | 108.00 | 1.07 | -0.11 |
| May | 34.34 | 24.93 | 30.66 | 19.23 | 0.00 | 132.12 | 1.72 | 4.36 |
| Sep | 63.07 | 40.59 | 53.53 | 29.70 | 0.00 | 221.45 | 1.69 | 4.15 |
| Dec | 48.90 | 22.20 | 45.61 | 23.89 | 20.42 | 113.08 | 0.94 | 0.47 |

In March there was spatial variation at the site with transect 2 covering sediments that were significantly higher in ^{241}Am activity concentration and transect 3 covering sediments that had the smallest activity concentration of ^{241}Am ($F(2,33) = 7.097$, $p < 0.01$). By May this significant spatial variation had disappeared apart from at transect 2 which still had significantly less ^{241}Am , though the alpha level of this difference was <0.05 opposed to <0.01 in March. For September and December there was no significant spatial variation detected in these data. It should be noted that the temporal and spatial variation seen in ^{241}Am was identical to that of ^{137}Cs .

The As concentration did not exhibit a particular trend; it fluctuated sometimes increasing and sometimes decreasing with month, though between May and September there was a large increase in As concentration relative to the other months. Statistically the increase in As concentration from May to September was the only significant change ($F(3,140) = 11.8$, $p < 0.01$) as the declines seen for March and December were not significant. The range between months was consistent and the months have similar minimum and maximum values, though March stands out as having a large positive skew which is the result of its elevated maximum value. Understanding the site's spatial trends was limited because the As concentration was so low for transect 3 in March and December.

Table 3.9 As summary statistics for each of the four monthly sampling campaigns.

MAD = median absolute deviation, n = 36.

| Month | Mean ppb | SD ppb | Median ppb | MAD ppb | Min ppb | Max ppb | Skew | Kurtosis |
|-------|-------------|-----------|---------------|------------|------------|------------|------|----------|
| Mar | 5.09 | 1.31 | 4.91 | 1.00 | 3.24 | 8.80 | 0.91 | 0.29 |
| May | 4.39 | 1.22 | 4.17 | 0.43 | 3.32 | 10.59 | 3.71 | 15.67 |
| Sep | 6.27 | 1.48 | 6.12 | 1.60 | 3.87 | 9.42 | 0.31 | -1.02 |
| Dec | 5.89 | 1.77 | 5.38 | 1.90 | 3.47 | 9.85 | 0.70 | -0.51 |

Table 3.10 Fe summary statistics for each of the four monthly sampling campaigns.

MAD = median absolute deviation, n = 36.

| Month | Mean ppb | SD ppb | Median ppb | MAD ppb | Min ppb | Max ppb | Skew | Kurtosis |
|-------|-------------|-----------|---------------|------------|------------|------------|------|----------|
| Mar | 5455 | 2471 | 5143 | 2138 | 1858 | 10554 | 0.60 | -0.52 |
| May | 6692 | 2477 | 6422 | 1607 | 4088 | 17622 | 2.47 | 8.11 |
| Sep | 8698 | 2822 | 8056 | 2832 | 3996 | 13436 | 0.21 | -1.24 |
| Dec | 7968 | 2766 | 7317 | 2546 | 4455 | 14790 | 0.69 | -0.61 |

The Fe concentration of the sediment increased throughout the year peaking in September and then experienced a decrease between September and December. The Fe concentration of the sediment was significantly higher for September in comparison to March and May ($F(3,140) = 10.57, p < 0.001$). The post September decline was not significant in this case though the mean and median shown in Table 3.10 did show a decrease. Therefore, the Fe concentration can be said to have increased between May and September and the concentrations remained at the elevated levels for the remainder of the survey period. Spatial variability in the Fe concentration was confined to March where transect 2 was significantly higher and transect 3 was significantly lower, there were no other spatial trends for Fe during the survey period.

Table 3.11 Sr summary statistics for each of the four monthly sampling campaigns.

MAD = median absolute deviation, n = 36.

| Month | Mean ppb | SD ppb | Median ppb | MAD ppb | Min ppb | Max ppb | Skew | Kurtosis |
|--------------|---------------------|-------------------|-----------------------|--------------------|--------------------|--------------------|-------------|-----------------|
| Mar | 93.86 | 18.90 | 95.53 | 17.52 | 53.62 | 125.33 | -0.17 | -0.71 |
| May | 79.73 | 17.16 | 79.79 | 20.10 | 50.94 | 125.20 | 0.32 | -0.49 |
| Sep | 109.84 | 23.10 | 109.39 | 22.34 | 60.36 | 154.67 | -0.03 | -0.79 |
| Dec | 99.41 | 18.98 | 97.43 | 26.01 | 73.52 | 138.16 | 0.35 | -1.15 |

The shape of the data distribution as indicated by the skew factor and Kurtosis factor indicated that for March there were a few samples that had relatively high concentrations of Fe.

The Sr concentration within the sediment was variable between months, with the concentration increasing and decreasing between each month. The concentration significantly decreased from March to May and then significantly increased from May to September ($F(3,140) = 14.67, p < 0$). From September to December there was a slight decrease but this was within the expected variability given the stated standard deviation of these data and was not significant. The data distribution did not appear to be substantially impacted by the few samples with high Sr concentration and the range observed was consistent across all months, though in September it was elevated. There were few spatial trends found in the data other than transect 3 being significantly lower in Sr concentration in December.

Air kerma

The air kerma data varied across the sampling period however this variation was within what would be expected by the standard deviation (Table 3.12). There was no significant difference between the data sets for the monthly groupings, therefore the air kerma data does not vary temporally for these data. Transect 3 was significantly higher in air kerma measurements than transects 1 and 2 for March, September and December ($F(3,72) = 1.182, p < 0.01$).

Table 3.12 Air kerma summary statistics for each of the four monthly sampling campaigns. MAD = median absolute deviation, n = 19.

| Month | Mean μGy h⁻¹ | SD μGy h⁻¹ | Median μGy h⁻¹ | MAD μGy h⁻¹ | Min μGy h⁻¹ | Max μGy h⁻¹ | Skew | Kurtosis |
|--------------|------------------------------------|----------------------------------|--------------------------------------|-----------------------------------|-----------------------------------|-----------------------------------|-------------|-----------------|
| Mar | 0.05 | 0.01 | 0.05 | 0.01 | 0.04 | 0.06 | -0.01 | 0.12 |
| May | 0.05 | 0.01 | 0.05 | 0.01 | 0.02 | 0.06 | -1.12 | 0.35 |
| Sep | 0.05 | 0.01 | 0.05 | 0 | 0.04 | 0.06 | 0.27 | -0.63 |
| Dec | 0.05 | 0.01 | 0.05 | 0.01 | 0.04 | 0.06 | 0.11 | -1.47 |

3.3.2. Contaminant sediment relationships

The analysis of the variables in 3.3.1 revealed that there were some common trends throughout the data sets, particularly between the particle size distribution and the contaminants ¹³⁷Cs and ²⁴¹Am. The theory that sediment movement accounts for the monthly variation in these contaminants is discussed in section 3.4.1, here this theory is tested by exploring the spatial and temporal variability in this relationship.

The monthly trends for ¹³⁷Cs and ²⁴¹Am association with clay, silt, sand and organic matter are presented here for March, May, September and December. The analysis used the coefficient of determination (R^2) as a measure of the strength of the contaminant sediment relationship. Summary statistics are reported in section 3.3.1 for reference. A total of 136 regression analyses were conducted, these data are given in appendix 1. The results were interpreted at the monthly level, though reference is made to transect variability, for the purpose of being concise these transect data are not presented here and are only discussed when relevant.

March 2014

The regression analysis conducted for the March 2014 data is presented in Figures 3.2 and 3.3, the plots show the regression model with the data plotted around it to give an idea of the goodness of fit of the regression models. Based on the scatter of the data in the plots silt appeared to be the best predictor of both ¹³⁷Cs and ²⁴¹Am concentration. This was supported by the data with the silt regressions returning a coefficient of determination of $R^2 = 89\%$ ($p < 0.01$) for both relationships. Clay also performed well as

a predictor of contamination levels with 74% of the variability in the contamination data explained by clay. The observed relationship between clays and silts and the contaminants ^{137}Cs and ^{241}Am is that as the amount of fine sediment increase so does the quantity of contaminants.

Sand acted as a negative predictor variable were by as the percentage of sand increased the concentration of contamination decreased. Transect 3 had significantly less contamination however did not have significantly more fine sands, the site did have significantly less clay and silt ($F(2,33) = 5.504, p < 0.01$). Therefore, it is reasonable to suggest that fine sand was not an appropriate predictor as it is a case of correlation not equalling causation. The presence of sand means the area will have a coarse particle size distribution, and consequently, less clay and silt, which were positively correlated with ^{137}Cs and ^{241}Am .

The relationship between organic matter and ^{137}Cs and ^{241}Am exhibited a lot of scatter as shown in Figures 3.2 and 3.3, the coefficients of determination were 68% for ^{137}Cs and 72% for ^{241}Am . The data, however were, subject to high spatial variation with the transect 1 and 3 regressions failing to explain a sufficient amount of variance (>70%). This contrasted with transect 2 which explained some 93% and 95% of the variance in ^{137}Cs and ^{241}Am data respectively.

For March 2014 the data showed that silt and clay performed as strong predictors of ^{137}Cs and ^{241}Am concentration within the sediment. Organic matter and sand underperformed as predictors for the reasons discussed in section 3.4.).

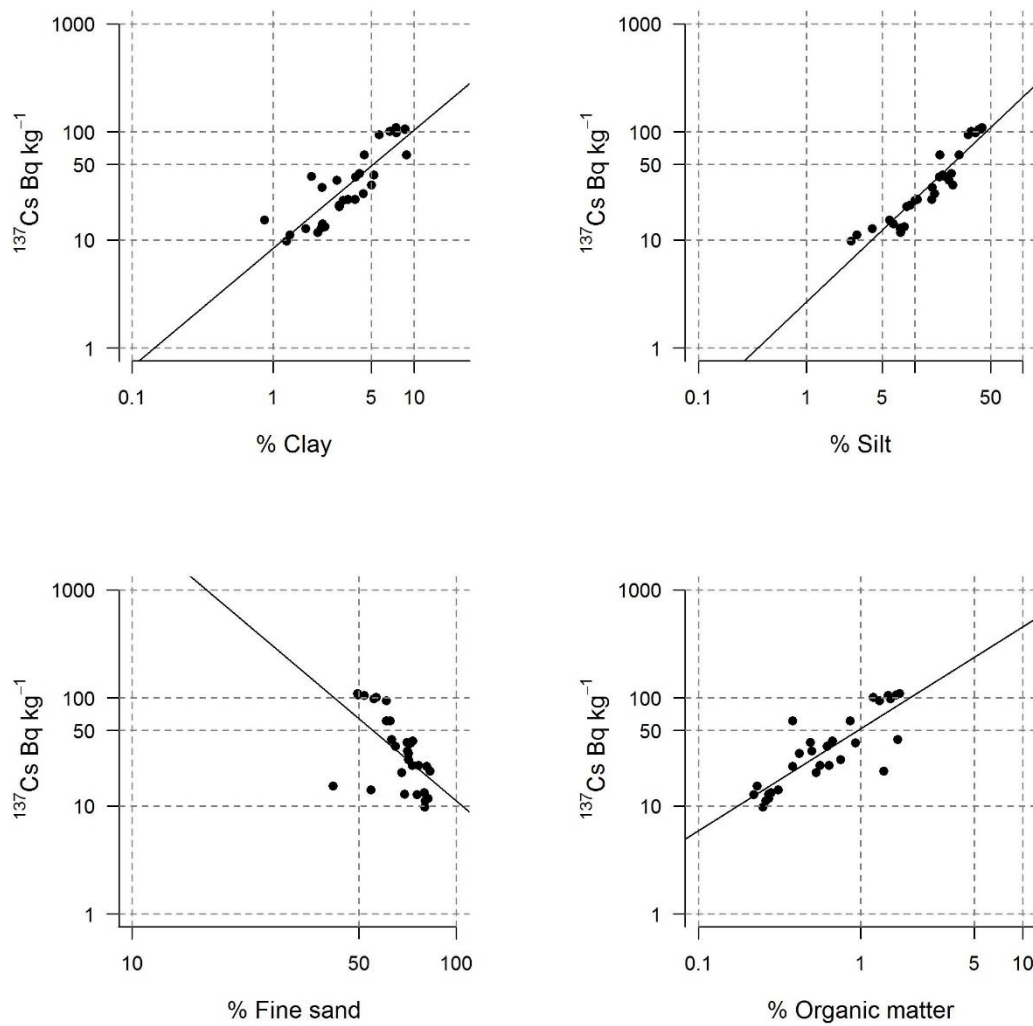


Figure 3.2 March 2014 log vs log plots (ln) showing the natural log transformed data and fitted linear model. Data were regressed with $^{137}\text{Cs Bq kg}^{-1}$ as the response variable and percentage clay, silt, sand and organic matter acting as predictor variables.

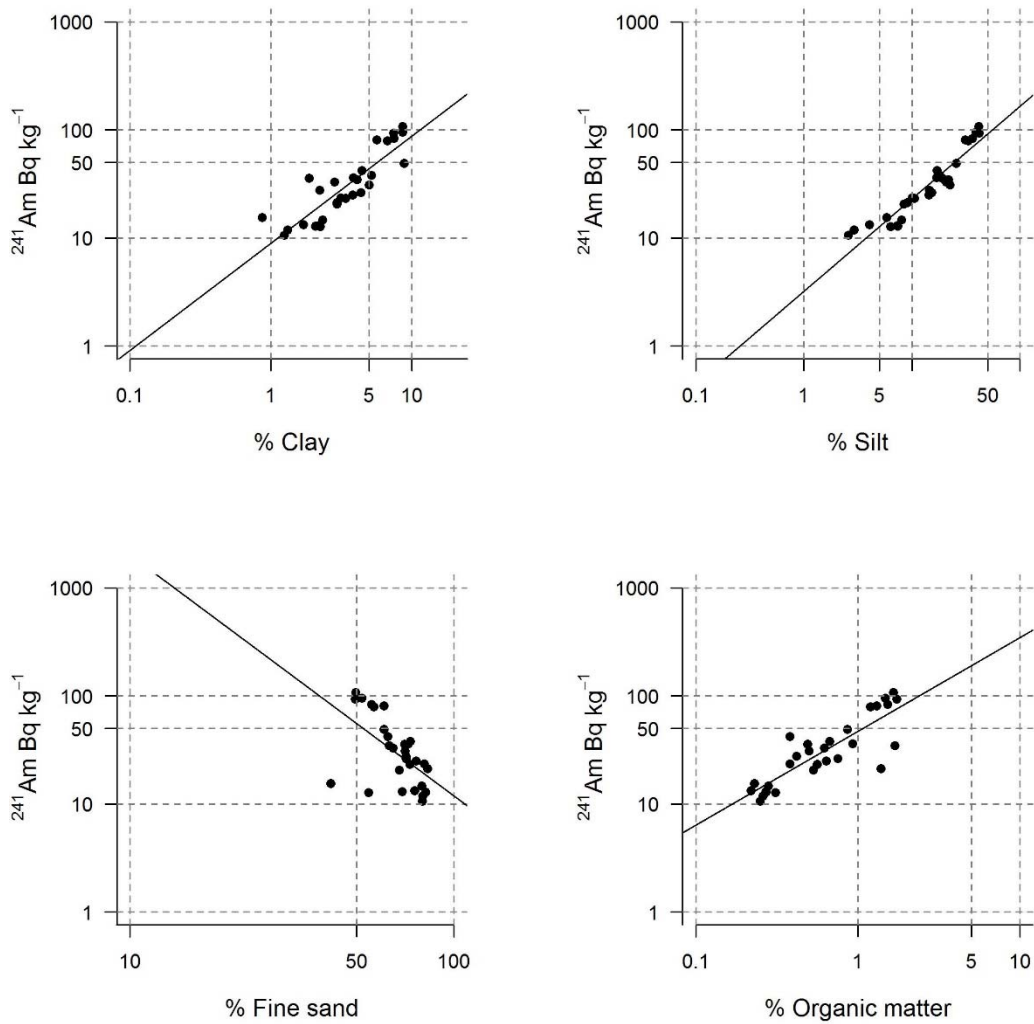


Figure 3.3 March 2014 log vs log plots (ln) showing the natural log transformed data and fitted linear model. Data were regressed with $^{241}\text{Am Bq kg}^{-1}$ as the response variable and percentage clay, silt, sand and organic matter acting as predictor variables.

May 2014

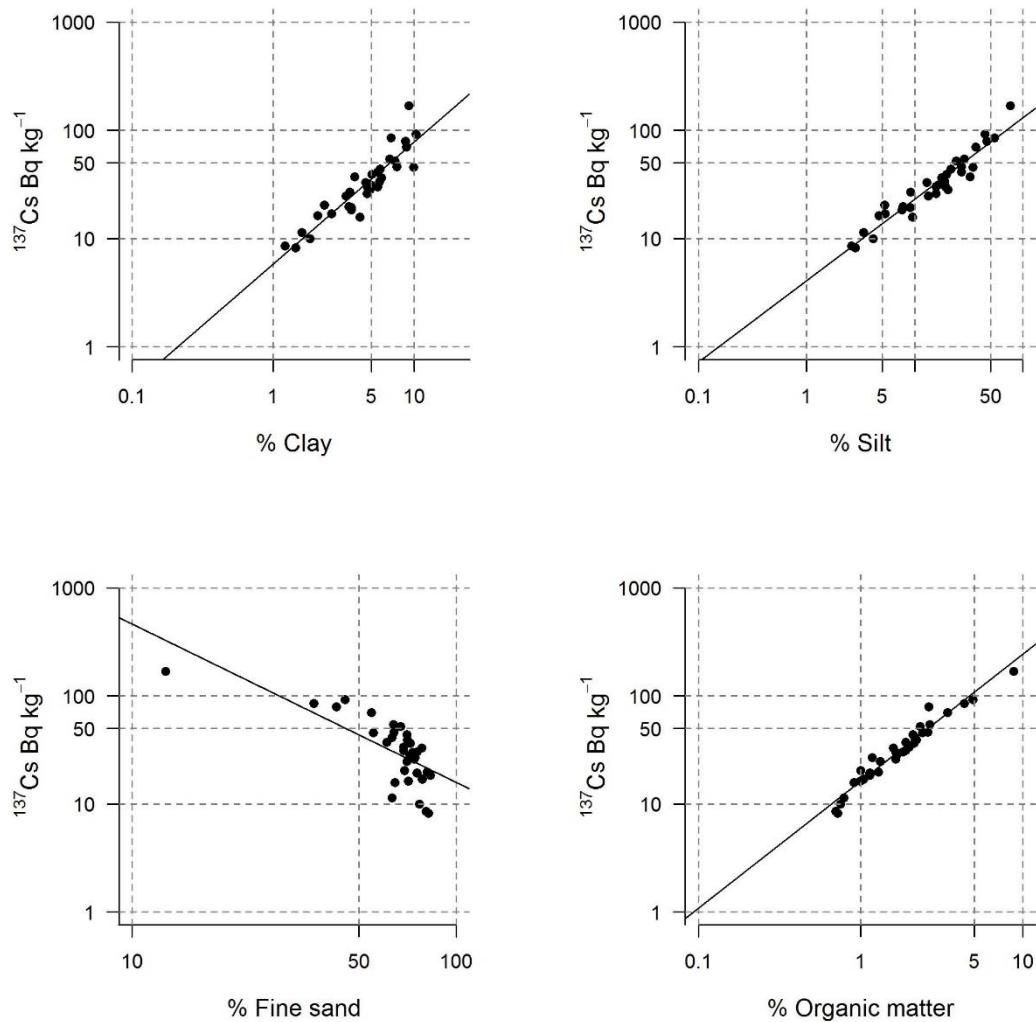


Figure 3.4 May 2014 log vs log plots (ln) showing the natural log transformed data and fitted linear model. Data were regressed with $^{137}\text{Cs Bq kg}^{-1}$ as the response variable and percentage clay, silt, sand and organic matter acting as predictor variables.

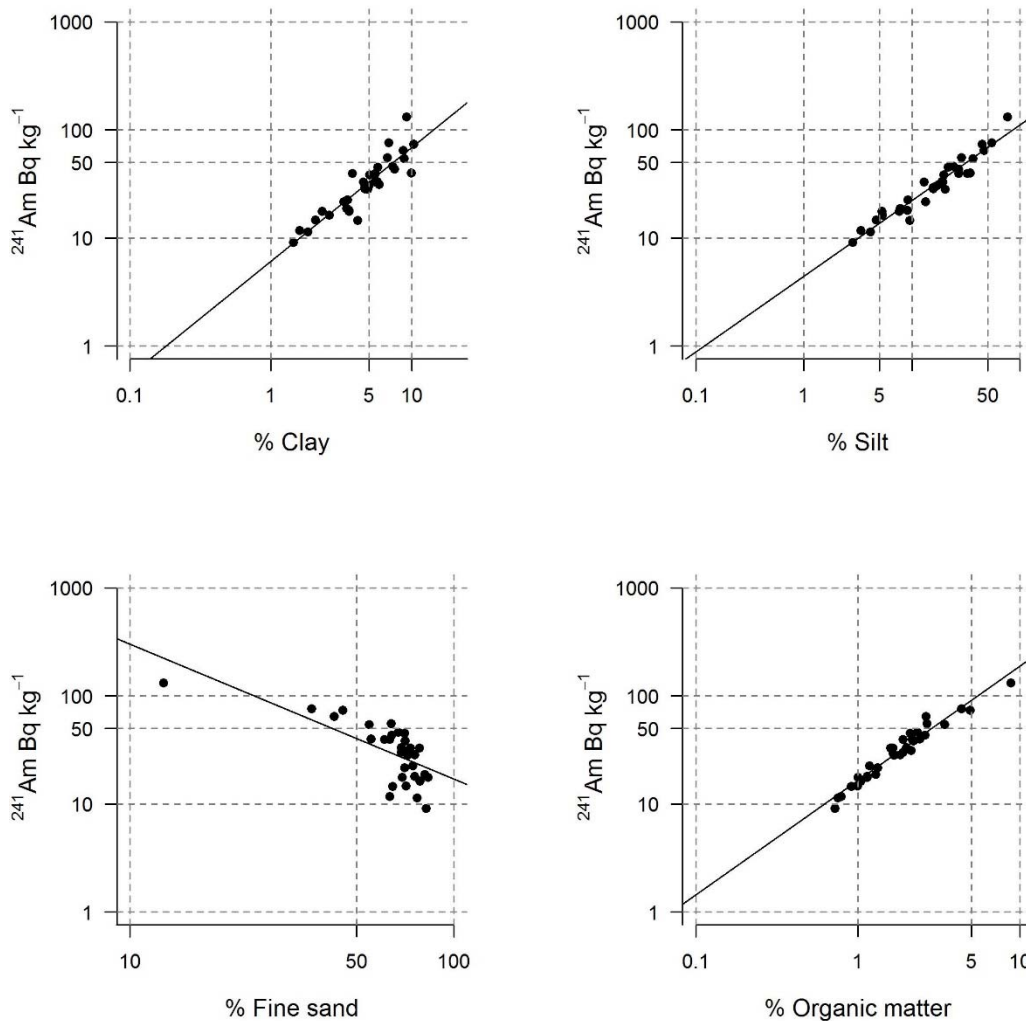


Figure 3.5 May 2014 log vs log plots (ln) showing the natural log transformed data and fitted linear model. Data were regressed with ^{241}Am Bq kg $^{-1}$ as the response variable and percentage clay, silt, sand and organic matter acting as predictor variables.

The data for May had noticeably less scatter around the fitted linear regression models for clay, silt and organic matter against ^{137}Cs and ^{241}Am (Figures 3.4 and 3.5). Organic matter and silt were the best predictors of ^{137}Cs and ^{241}Am concentration within May with coefficients of determination ranging between 91% and 95%. This increase in the predictive power of organic matter for May was in contrast to March where there was significant variation between the transects that hindered successful regression. In May there was no significant variation between transects percentage organic matter (section 3.3.1). The lack of significant variation between transects resulted in the average monthly regression model fitting the data with minimum deviance.

The relationship between clay and the contaminants was stronger in May with more of the variation in ^{137}Cs ($R^2 = 80\%$) and ^{241}Am ($R^2 = 83\%$) data explained by variation in percentage clay content than in March. However, there was greater inter-transect variability that was not accounted for by a significant change in the amount of clay present in each transect. It is true that transect level regression models were more vulnerable to the effects of outliers due to having fewer data points, therefore the residuals of individual points have more power. These differences highlight that a general model that includes spatial variability such as the monthly models can approximate the relationship between contaminants and the sediment matrix.

The sand regression models performed at ^{137}Cs $R^2 = 47\%$ and ^{241}Am $R^2 = 50\%$ which means that variation in sand explained more variability in the contaminants than was the case for March's sand regression models. The lack of predictive power was not surprising given the same pattern of wide scatter shown in Figures 3.4 and 3.5 however clay, silt and organic matter performed as strong predictors of ^{137}Cs and ^{241}Am for May 2014.

September 2014

The September data exhibited more scatter than was seen in March and May for clay, silt and organic matter, though there was less scatter for sand (Figures 3.6 and 3.7). The scatter around the fitted regression models was more severe in the ^{137}Cs plots (Figure 3.6) than the ^{241}Am plots (Figure 3.7). The regressions of organic matter produced the best predictive models for September with the following coefficients of ^{137}Cs $R^2 = 64\%$ and ^{241}Am $R^2 = 81\%$. The principal difference between the regression models in September was between the contaminants and not the predictor variables. Regressions of clay, silt, sand and organic matter against ^{241}Am produced coefficients of determination between 75% and 82% in contrast ^{137}Cs coefficients ranged from 47% to 66%.

One of the key findings of section 3.3.1 was the significant increase in fine sediments at the Lytham site between May and September, the significance is discussed in section 3.4.1. The transect level regression did reveal spatial variability that was evident with good fitting ($R^2 > 77\%$) regression models for transects 1 and 2 but no significant fits being obtained from transect 3. Between May to September transect 3 went from having the least amount of silt to having the most, which may explain the difficulty in modelling contaminants at this site from the particle size distribution (discussed further in section 3.4.2).

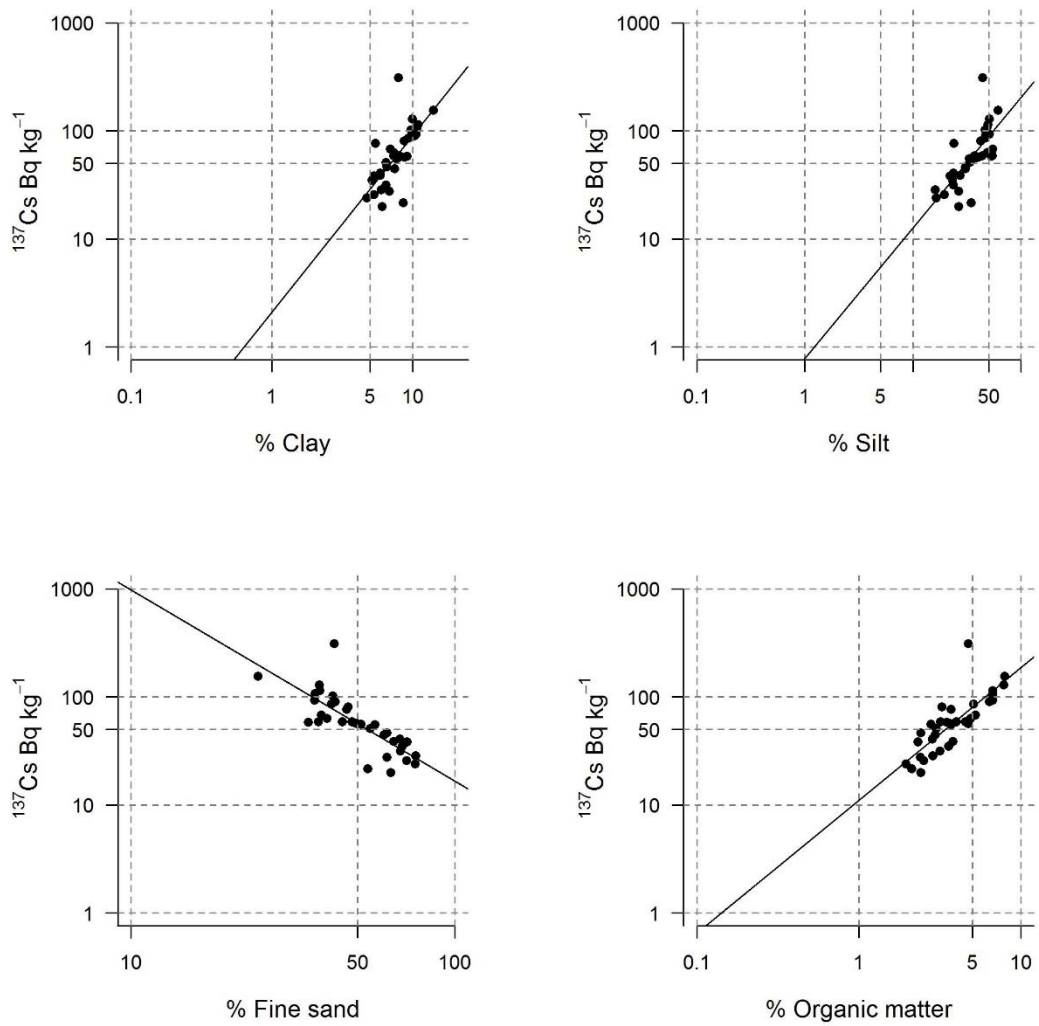


Figure 3.6 September 2014 log vs log plots (ln) showing the natural log transformed data and fitted linear model. Data were regressed with $^{137}\text{Cs Bq kg}^{-1}$ as the response variable and percentage clay, silt, sand and organic matter acting as predictor variables.

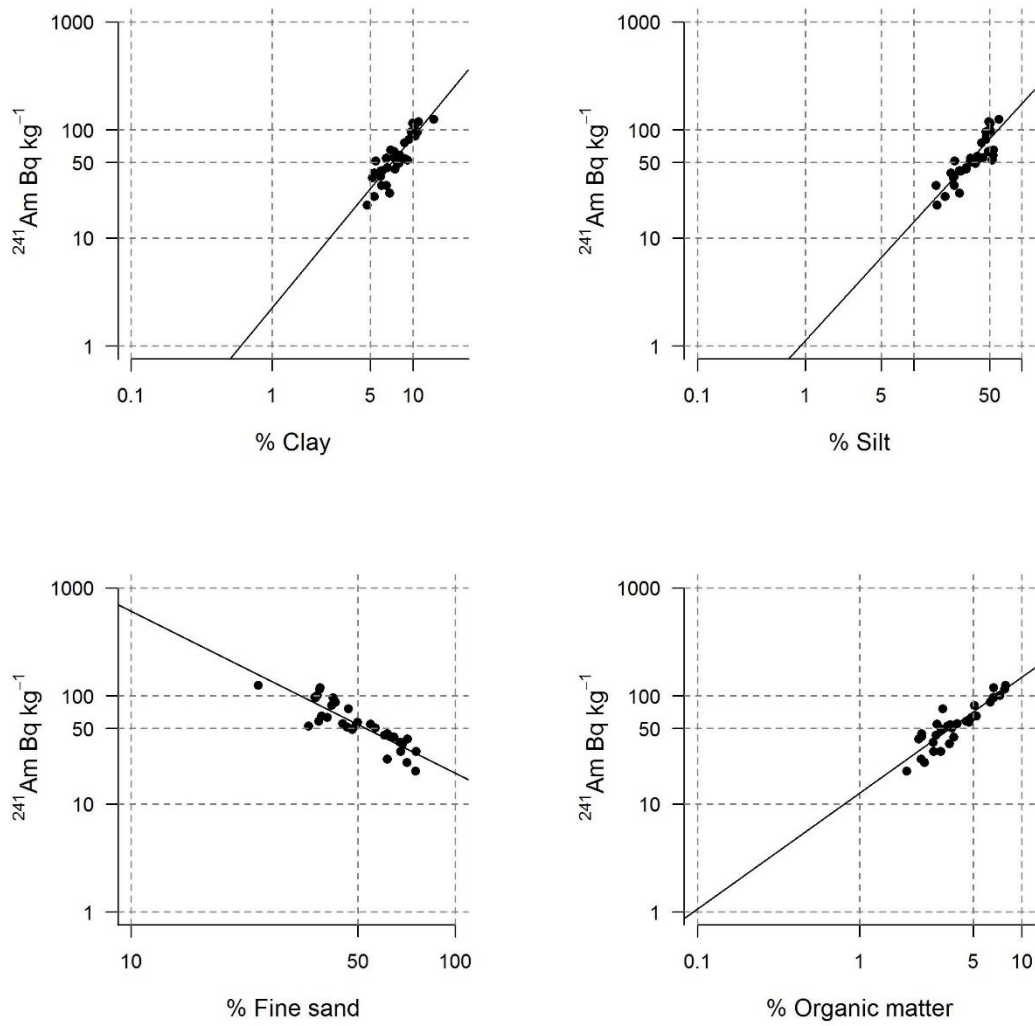


Figure 3.7 September 2014 log vs log plots (ln) showing the natural log transformed data and fitted linear model. Data were regressed with $^{241}\text{Am Bq kg}^{-1}$ as the response variable and percentage clay, silt, sand and organic matter acting as predictor variables.

December 2014

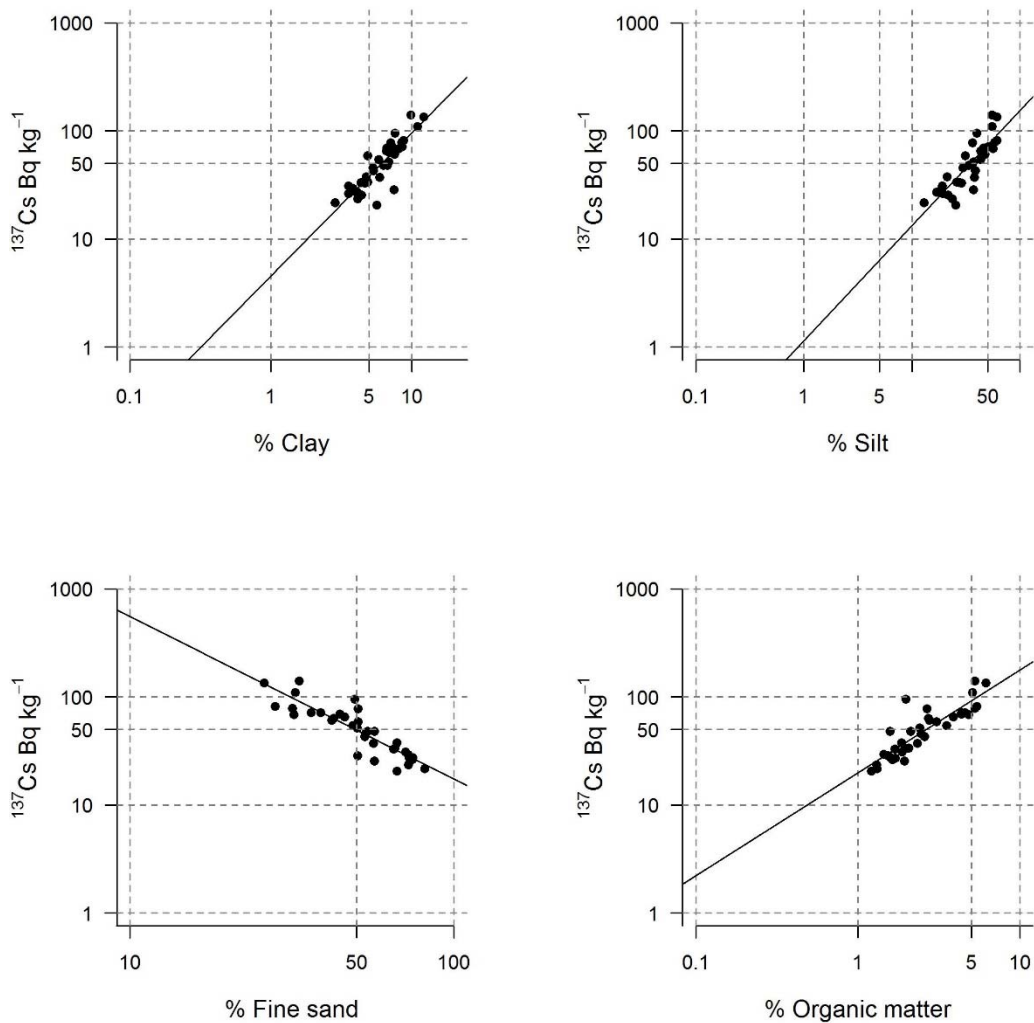


Figure 3.8 December 2014 log vs log plots (ln) showing the natural log transformed data and fitted linear model. Data were regressed with $^{137}\text{Cs Bq kg}^{-1}$ as the response variable and percentage clay, silt, sand and organic matter acting as predictor variables.

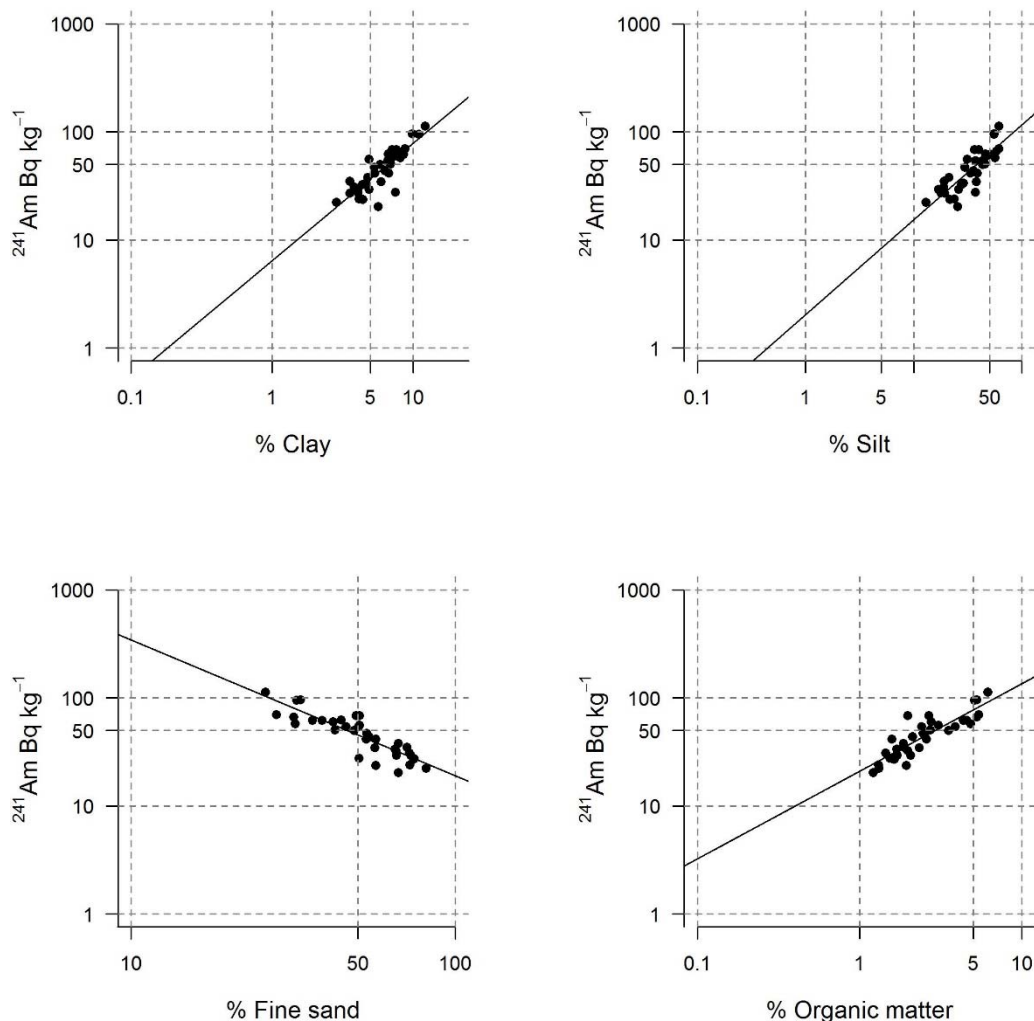


Figure 3.9 December 2014 log vs log plots (ln) showing the natural log transformed data and fitted linear model. Data were regressed with ^{241}Am Bq kg^{-1} as the response variable and percentage clay, silt, sand and organic matter acting as predictor variables.

Data for December showed more scatter in ^{241}Am particularly for the organic matter plot. In contrast, the ^{137}Cs data showed less scatter than was seen in September (Figures 3.8 and 3.9). The sediment property contaminant relationships at transect 3 that were absent in September returned in December, however the regression models have unacceptable coefficients of determination that range from $R^2 = 45\%$ to $R^2 = 55\%$. Though the site wide average regression models returned coefficients of determination for ^{137}Cs between 73% and 78% and for ^{241}Am between 70% and 77%. Therefore, the sediment property regression models account for a similar amount of variance in ^{241}Am in December as they did in September and there was a marked improvement for ^{137}Cs .

3.3.3. Temporal variability in radioactive contaminant sediment relationships

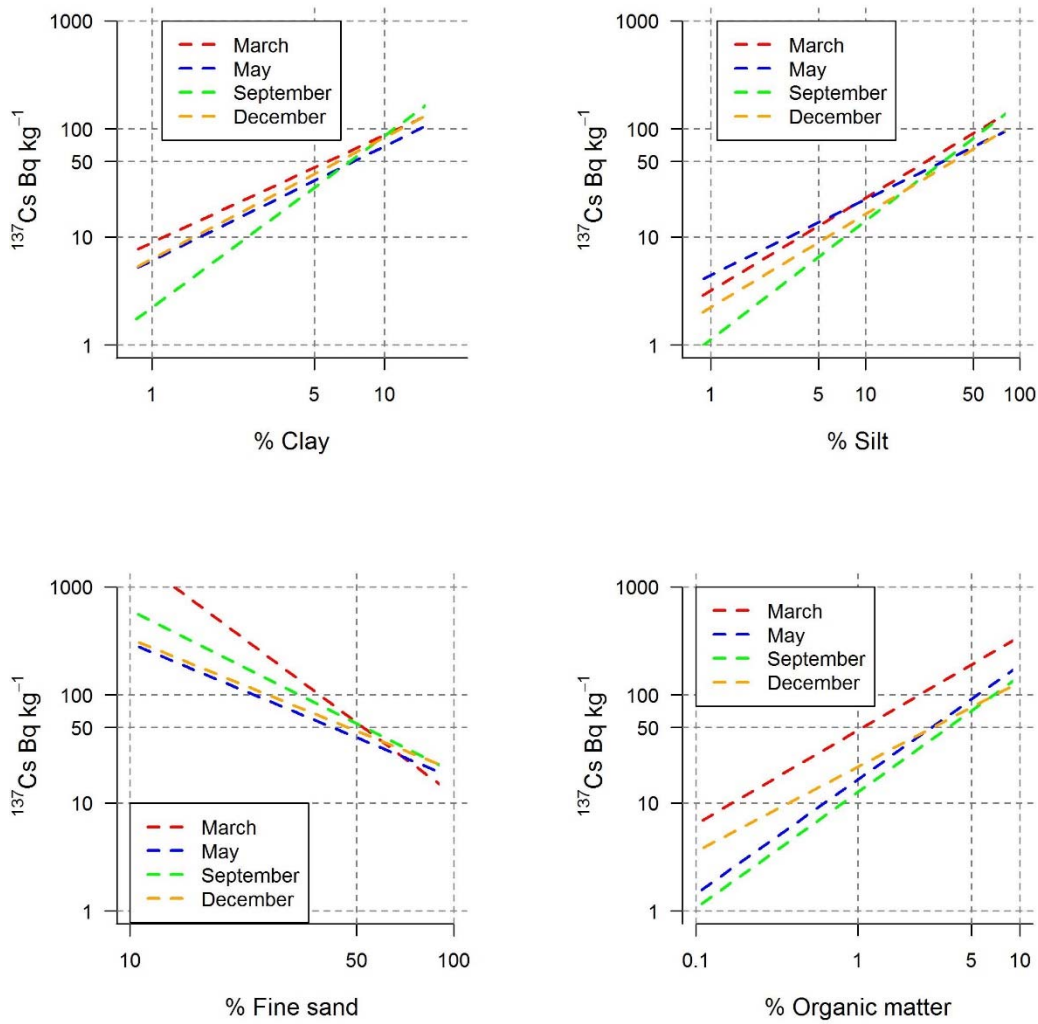


Figure 3.10 Monthly models for 2014 plotted on a log vs log plots (ln). Data were modelled with $^{137}\text{Cs Bq kg}^{-1}$ as the response variable and percentage clay, silt, sand and organic matter acting as predictor variables.

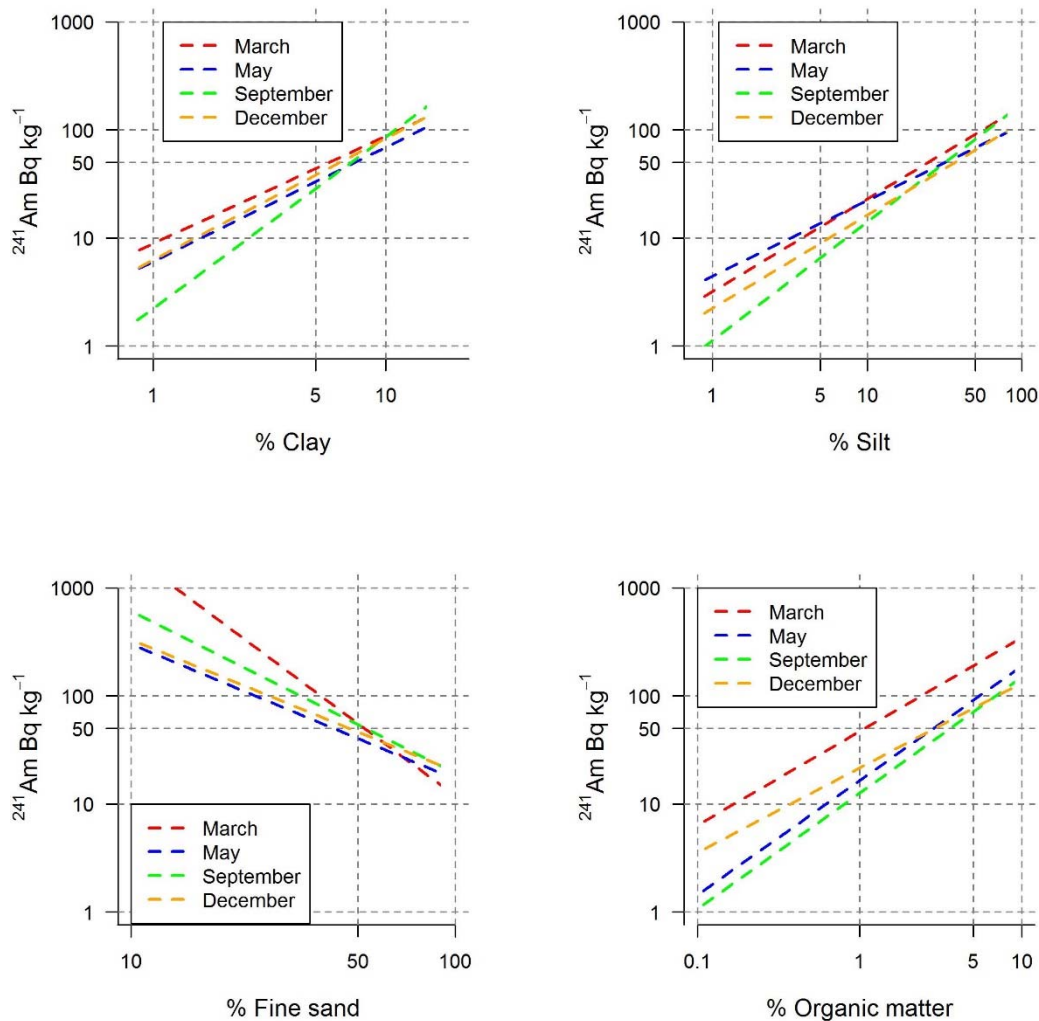


Figure 3.11 Monthly models for 2014 plotted on a log vs log plots (ln). Data were modelled with ^{241}Am Bq kg $^{-1}$ as the response variable and percentage clay, silt, sand and organic matter acting as predictor variables.

The temporal trend between the four months is explored here, to provide a narrative of how the monthly models compared to each other. The sediment property relationships were defined by a regression model that predicted ^{137}Cs and ^{241}Am activity concentrations in Bq kg $^{-1}$ from measurements of the sediment particle size distribution or organic matter content were calculated for four months of the year 2014. These monthly models are plotted in Figures 3.10 and 3.11. The regression models are linear models plotted in a log-log format and like above the coefficient of determination is used to describe how well the regression models accounts for variation in the contaminant data.

Table 3.13 Coefficients of determination (R^2) for each monthly regression model for ^{137}Cs .

| ^{137}Cs | Clay | Silt | Fine sand | Organic matter |
|-------------------|------|------|-----------|----------------|
| Mar | 75 | 89 | 33 | 70 |
| May | 84 | 92 | 52 | 95 |
| Sep | 47 | 54 | 62 | 65 |
| Dec | 75 | 73 | 78 | 77 |

Table 3.14 Coefficients of determination (R^2) for each monthly regression model for ^{241}Am .

| ^{241}Am | Clay | Silt | Fine sand | Organic matter |
|-------------------|------|------|-----------|----------------|
| Mar | 76 | 89 | 31 | 72 |
| May | 81 | 93 | 50 | 95 |
| Sep | 78 | 76 | 76 | 82 |
| Dec | 70 | 70 | 75 | 77 |

The clay regression models showed that March and May had similar slopes though March had a higher intercept, December had the same intercept as May but its slope was slightly larger (Figures 3.10 and 3.11). However, September was substantially different with a much lower intercept and a far steeper slope. This was tested statistically using a dummy variable regression which confirmed that the September ^{137}Cs and ^{241}Am regression models were distinct ($p < 0.05$). This variability resulted in a noted decline in the coefficient of determination for the ^{137}Cs model in September as shown in Table 3.13.

The March and December silt regression models had similar slopes though December had a lower intercept, May had the highest intercept but had a shallower slope than March and December. September was again substantially different to the other models

with a much lower intercept and larger slope. The dummy variable regression confirmed that the September silt regression models for ^{137}Cs and ^{241}Am were distinct ($p < 0.05$). The variation in the coefficients of determination (Tables 3.13 and 3.14) showed that the ^{137}Cs model was most affected by the increase in silts that occurred in September.

The fitted regression models presented in Figures 3.10 and 3.11 showed that December and May were visually similar in terms of slope and intercept with September and March being distinct. Due to the wide variability in these data and poor fit of the fitted models, it is not appropriate to conduct a dummy variable regression. As previously stated, the sand regression models are not likely to be robust predictors, their coefficients were shown to range from $R^2 = 31\%$ to $R^2 = 78\%$. Their coefficients were highest in September and December and lowest in March and May contrasting with the results for clay and silt (Table 3.13 and 3.14)

The organic matter regression models were all distinct according to the dummy variable regression analysis, though visually May and September had similar intercepts and slopes, while March and December had higher intercepts and slightly shallower slopes. The organic matter regression models had similar or identical coefficients of determination across all months apart from September when the ^{137}Cs model produced low coefficients of determination.

3.3.4. 20-year trend in radioactive contaminant sediment relationship

The percentage clay sediment property relationship was explored using data from 1995 – 2014 for both ^{137}Cs and ^{241}Am . The data were decay corrected to the 2014 data set before regression analysis was conducted to ensure the effect of radioactive decay was accounted for. Decay correcting allowed the 2014 data to be compared to the historic data sets as it removes reductions in ^{137}Cs which would occur from radioactive decay, therefore changes in activity levels will be the result of accumulation or remobilisation.

A visual inspection of the ^{137}Cs regression models given in Figure 3.12 showed that the earlier models 1995 and 1997 appear to be very similar to the 2003 model although this had a slightly higher intercept. The 2002 and 2014 models have the same intercept (Table 3.15) though 2002 had a steeper slope, these models appeared to be similar despite the 12-year time difference between when these data were collected. 2003 had the highest intercept though the low slope distinguished it from the 1995 and 1997 models. A dummy variable regression analysis confirmed this visual split in the model

groupings determining that 1995 and 1997 were not dissimilar from each other. The 2002, 2003 and 2014 models were not statistically different ($p < 0.05$) but were distinct from the 1995 and 1997 models. Therefore, the nature of the percentage clay / ^{137}Cs relationship within these data changed temporally between the early 1990s but not significantly between 2003 and 2014.

The ^{241}Am regression models given in Figure 3.13 showed a great deal of overlap, model 2014 and 1995 were more similar in terms of their slopes than 1997 is to 1995. This was contrary to observations of the ^{137}Cs models whereby the models from the 1990s were distinct from those models in the 2000s and 2014. There was also a large amount of variability in the model intercepts as seen in Table 3.15 and the coefficient of determination of the more recent 2014 regression model was similar to that of the 1995 regression model (77% compared to 82%). The models were not statistically distinct however the 2014 data that were used to build the regression model were lower though not significantly so. Therefore, in contrast to the percentage clay / ^{137}Cs relationship the percentage clay/ ^{241}Am relationship has remained temporally stable from 1995 to 2014.

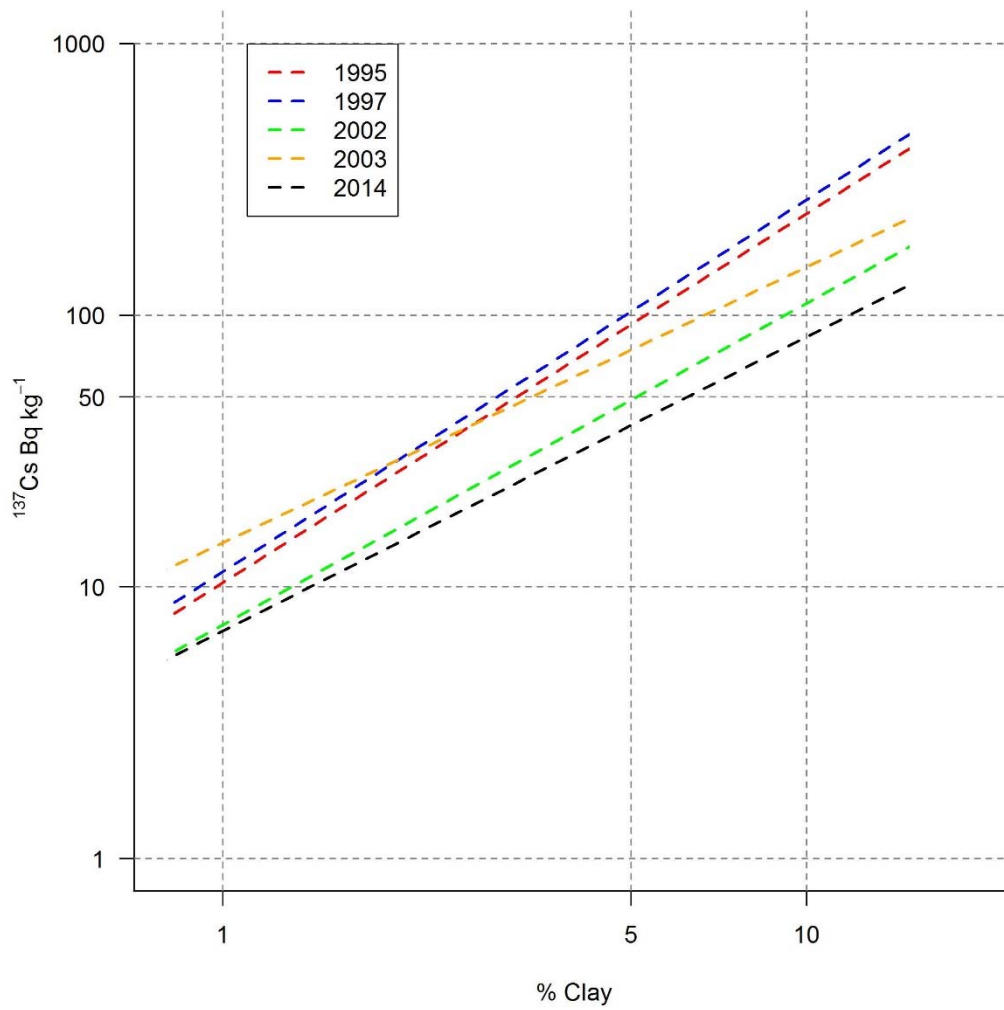


Figure 3.12 Annual models plotted on a log vs log plots (ln). Data were modelled with ^{137}Cs Bq kg⁻¹ as the response variable and percentage Clay acting as the predictor variable.

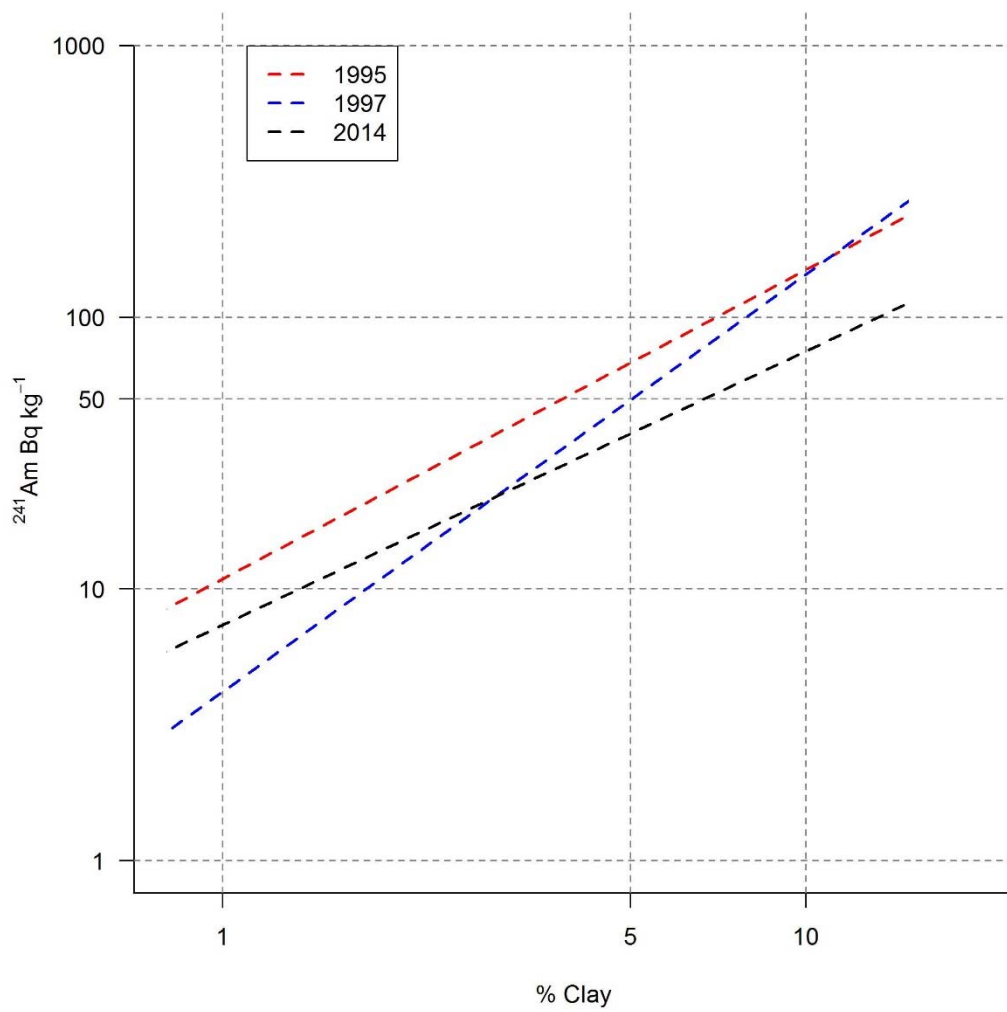


Figure 3.13 Annual models plotted on a log vs log plots (ln). Data were modelled with ^{241}Am Bq kg⁻¹ as the response variable and percentage Clay acting as the predictor variable.

Table 3.15 Regression model parameters for % clay / ^{137}Cs for 1995, 1997, 2002, 2003 and 2014. % clay / ^{241}Am was only applied to 1995, 1997 and 2014.

| Nuclide | Parameter | 1995 | 1997 | 2002 | 2003 | 2014 |
|-------------------|----------------|------|------|------|------|------|
| ^{137}Cs | R ² | 93 | 93 | 88 | 92 | 71 |
| | Slope | 1.36 | 1.37 | 1.18 | 1.01 | 1.08 |
| | Intercept | 2.34 | 2.43 | 1.98 | 2.68 | 1.93 |
| ^{241}Am | R ² | 82 | 91 | NA | NA | 77 |
| | Slope | 1.14 | 1.54 | NA | NA | 1.01 |
| | Intercept | 2.39 | 1.43 | NA | NA | 2.00 |

3.4. Discussion

The temporal and spatial characteristics of a range of sediment properties were analysed from March 2014 to December 2014. The analysis focused on the association of contaminants, principally ^{137}Cs and ^{241}Am , with the sediment matrix. These analyses attempted to establish if it is correct to treat sediment movement as contaminant movement.

3.4.1. Sediment spatio temporal variability

The particle size distribution of the Lytham site over time has shifted towards finer sediments with increases in the amount of silt and clay and decreases in the amount of sands. This change occurred between May and September, suggesting that fine grained sediments were being preferentially deposited at the site. After September, there was a decline in the amount of fine grained sediments present though this decline was only significant for clay.

During March and May fine sediments such as clay accumulated within the mudflats located higher in the tidal frame, In September and December these fine sediments were remobilised. A model for sediment deposition within the Ribble estuary advanced by Wakefield (2005) suggests sediments are deposited during low energy conditions and then remobilised to the outer estuary to then be deposited again when energy

conditions permit. The data collected here may support this trend in the fine-grained sediments as they were deposited until September and then experienced a decline as the winter season began, which is characterised by enhanced disturbance (Esteves et al., 2011).

That the reduction in clay fraction was significant, unlike the reduction in silt, is due to the clays being finer and more vulnerable to remobilisation. The silts and sands do undergo change though with lower statistical significance, this is likely due the energy changes within the estuary not being high enough. This energy required to remobilise clays can be provided by heavy precipitation events during low tide that will disproportionately washout the finer and lighter clays opposed to the heavier silts.

There was a substantial siltation event at transect three in the September data. The increase in the percentage of the sediment that was silts can only be explained by the addition of sediments representing the silt fraction or the remobilisation of the coarse sand sediments which were then lost from the area. The remobilisation of sands is not likely as the sand fraction, being larger, simply requires more energy to remobilise and the energy that would remobilise sands would also have remobilised the silt and clay fractions which we know increased in quantity. Therefore, the silt and clay fractions must have been deposited at a higher rate relative to the sand fraction in the months between May and September. This deposition will likely be a result of continued accretion of fine sediments at the site from the Irish sea or from other parts of the estuary.

3.4.2. Contaminant spatio-temporal variability

The metals Fe and Sr and metalloid As were found at concentrations far below the National Oceanic and Atmospheric Administration (NOAA) screening quick reference table (SQiRTs) values (Warren et al., 2012); they also exhibited a great deal of temporal variability. It is therefore reasonable to say that the observed Fe, Sr and As concentrations within the site are not likely to pose a threat to human health at current concentrations and the site would not be considered contaminated.

Spatially these metals were found at higher concentrations at transects 2 and lowest concentrations at transect 3, this is in agreement with the general spatial distribution of ^{137}Cs and ^{241}Am . Weak ($R^2 = 40\% - 55\%$) linear relationships exist between these three metals and ^{137}Cs and ^{241}Am and the clay and silt fractions. As the contaminant concentrations were so low, this causes uncertainty in the temporal and spatial data, which was responsible for the high amount of scatter that was encountered when trying

to conduct a regression analysis. The lower contaminant concentrations are thought to mean that a less contaminated sediment has been added to the site and that this has occurred at different levels across the tidal frame, resulting in a spatially uneven dilution.

The radionuclides ^{137}Cs and ^{241}Am were found to have identical spatial and temporal variation in the sediment concentration of these contaminants. The contaminants had a strong correlation with each other with a ^{137}Cs to ^{241}Am ratio of 5:4 being present across the full sampling period. Their temporal variation mimicked that of the clays and silts, which was to be expected as these contaminants are known to bind to clays and silts (MacKenzie et al., 1999). Consequently, as the quantity of fine sediments increase, so should the activity concentration of ^{137}Cs and ^{241}Am (Rainey et al., 1999). This association with the fine fraction of the sediments was tested by a large number of regression analyses, that aimed to determine if these associations were spatially and temporally stable, they were found to be stable temporally and spatially though with the following caveats.

There was some spatial variation observed between transects that was not found in the monthly comparisons that were used to assess temporal variation. Part of this will be due to the reduction in the number of samples (following removal of outliers) included in the modelling for transects. However, there was one incident in September that significantly affected the performance of the monthly models, this was the September siltation event. The substantial accumulation of silts at the site decoupled the contaminant fine sediment relationship for sites located lower down in the tidal frame.

From May to September transect 3 transitioned from having the coarsest sediment and lowest ^{137}Cs and ^{241}Am activity concentrations of the three transects to having the highest clay and silt percentages and ^{137}Cs and ^{241}Am activity concentrations. The significant increase in clays and silts for September is believed to have been caused by deposition as opposed to sand erosion for the reasons given earlier. This has resulted in a new sediment mix with different activity concentrations of ^{137}Cs and ^{241}Am being added to the site. This caused scatter in the regression model as the two types of sediment would be expected to take some time to mix thoroughly (Brown et al., 2015). This time to mix may also explain the high amount of variability in this month's regression models.

There are two possible explanations for the September siltation events' effects on the contaminant sediment property relationships. 1) That the continued gradual accretion

of sediments from the Irish Sea at the site over summer caused an enrichment of fine sediments that had higher contaminant concentrations than those sediments found in March and May. However, this does seem unlikely as the Irish Sea sediment is being deposited year-round and its contaminant concentration is similar to those sediments that are already present. 2) such a significant change in the sediment mix, is caused by a sediment with significantly higher contaminant concentration being deposited at this site. The effects of such a deposition would be that the sediment contaminant relationship would exhibit greater scatter whilst seeing bulk contaminant concentrations increase, which they did for this site.

The likely source of fine-grained sediments which have a higher concentration of radioactive contaminants such as ^{137}Cs and ^{241}Am is the Ribble estuary saltmarshes (Assinder et al., 1997; Clifton et al., 1999; Mudge et al., 1997). A probable explanation is that sediments from these saltmarshes may have been redistributed to the mudflats which owing to their significantly higher concentration of contaminants resulted in the decoupling of the contaminant relationship during the siltation event. This further highlights the need to better understand the nature of inter estuary transfers of sediment, perhaps through the use of better remote sensing techniques and sediment transport modelling.

In 2014 the estuarine sediments activity concentration of ^{137}Cs and ^{241}Am was significantly related to how much clay and silt was present at the site. Fine grained sediments can therefore be said to act as a proxy for these contaminants. The results demonstrated that the contaminant proxy relationships were subject to temporal and spatial variation. The data showed that variation occurred between different transects with those such as transect 3 which were lower down in the tidal frame having more scatter in the data. The data also showed that the proxy relationships were not temporally stable with the coefficients of determination varying temporally for some transects. However, in only one incidence (September's siltation event) did this variability disprove the statement that ^{137}Cs and ^{241}Am activity concentration was determined by the percentage of fine sediments present.

3.4.3. Long term trend 1995 - 2014

The analysis of annual data sets spanning a 20-year period aimed to investigate the long-term trend of estuarine contamination. The prior assumption of this work was that radioactive contaminant concentration was dependent upon three variables; radioactive decay, remobilisation from the site and accumulation at the site.

Remobilisation could result in the relocation of contaminants to other parts of the estuary or out with the estuary to the Irish Sea sediment transport system, though it could also be the bulk dilution of contaminants with uncontaminated sediments. Accumulation would be the increase in contaminant concentration within a particular fraction of the sediment matrix (e.g. % clay), the source of this increase in contamination could be sediments with a higher contaminant concentration such as the Ribble saltmarshes (Assinder et al., 1997; Clifton et al., 1999; Mudge et al., 1997) or contaminant concentrated marine sediment deposits such as the Sellafield mud patch located in the eastern Irish Sea (Kershaw et al., 1999; Lindahl et al., 2011; Marsden et al., 2006).

As radioactive discharges are much reduced to the environment, (Coughlan et al., 2015) the effect of these physical mixing processes should be a downward trend in estuarine contamination. However, the data showed that this downward trend occurred until 2002 but that from 2002 – 2014 these data are not statistically distinct after the effect of radioactive decay is accounted for.

Possible explanations for this could be that diffuse sources of contaminants from the Irish Sea or other parts of the estuary are 'topping up' the contaminant concentration at the rate it is being diluted (e.g. Hunt et al., 2013). Estuary wide sediment budgets are required to better understand why the long-term data do not show a gradual downward trend in contamination by identifying additional sources of contaminated sediment present in the estuary. Sediment transport modelling for the Ribble estuary would reveal how sediments are redistributed within the estuary and may shed light on likely sources or at the minimum the nature of sediment transfers within the estuary. At the coastal scale sediment transport modelling for the North West of England would shed light on the nature of the reworking of sediments from higher concentration deposits near Sellafield to less concentrated areas such as the Ribble (Gleizon and McDonald, 2010; Periañez, 2005, 2003).

3.5. Conclusions

The activity concentration of the contaminants ^{137}Cs and ^{241}Am was found to be determined by the variation of fine sediments in the mudflats. Organic matter was also a good predictor though it had more inter-transect variability, which made building a general model for the estuary more difficult. The findings are consistent with the view found in the literature that contaminants in general are associated with fine sediments (MacKenzie et al., 1999; Rainey et al., 1999). Furthermore, they agree with Wakefield's

(2005) data which show that disturbance can cause a decoupling in these relationships, which in this case was most likely through physical remobilisation of the sediments from the saltmarshes to the mudflats.

Estuarine contamination levels were shown to have declined significantly from 1995 to 2014 though from 2003 to 2014 there was not a significant decline. This lack of a significant decline was interpreted as the estuaries contaminant levels being topped up at the same rate of dilution, though ultimately such sources would have to be identified to confirm this. These sources are likely to be the estuarine saltmarshes and Irish sea deposits which are believed to be undergoing reworking and hence releasing sediments, which is then traveling towards estuaries along the Irish Sea coast (Hunt et al., 2013). The nature of estuarine contamination was clearly linked to changes in sediment particle size distribution. Therefore, it would be reasonable to suggest that the physical drivers of sediment remobilisation are also influential in monthly and annual variation in sediment contaminant concentration.

4. The impact of disturbance events on estuarine sediment properties over a two-year period

Within the context of this work disturbance events are considered to be discrete incidents that cause a change to the sediment matrix or some of its properties over a short time frame. These events can include, though are not limited to, storminess, high riverine discharge and high precipitation. Typically, such an event will modify the energy dynamics of the estuary or a part of the estuary, which in turn can affect the estuaries sediment transport system (Masselink and Russell, 2013). The underlying theory being that had the disturbance event not occurred the properties of the sediment matrix would be as it was before disturbance.

Storm events have been observed to cause sediment remobilisation from the mudflats to the saltmarsh surface, where such sudden changes in elevation of the saltmarshes relative to the mudflats can trigger erosion processes due to modified local hydrodynamic processes (e.g. Pethick, 1992). In this example, the immediate bulk remobilisation of sediment from the mudflat to the saltmarsh is evident in the short term but over a longer time scale a secondary effect is also present. This secondary effect is a change in the local energy regime that results in local sediment transport being changed such that saltmarsh edge erosion can be promoted resulting in a transfer of sediment to the mudflats over a longer period.

Disturbance events are described here as discrete events that cause an accelerated modification to the sediment properties away from what would be seen as part of daily variability. The daily and seasonal variability of the sediment is governed by the long-term Irish Sea coastal sediment transport to the Ribble estuary and the estuary wide sediment transport system that dictates how terrestrial, estuarine and marine sediments are distributed within the Ribble estuary (Luo et al., 2015). The ebb and flow of the tide will see sediments sorted through out the tidal frame according to the mass, cohesiveness of the sediments and the available energy of the tides (Choi and Kim, 2016; Pamba et al., 2016). Disturbance events are a deviation from these daily processes as they represent an injection of excess energy to the hydrodynamics of the area and can modify coastal morphology and the sediment transport system by increasing sediment supply (Brooks et al., 2017; Pye and Blott, 2008; Sierra and Casas-Prat, 2014).

It is important to understand the significance of these events in the seasonal and annual variability of the estuary's sediments so as to deepen our understanding of how

such estuarine stores of sediment may behave in the future (Dissanayake et al., 2015; Pye and Blott, 2016). As discussed in section 3.4, the association of radioactive contaminants namely ^{137}Cs and ^{241}Am with clays and silts, means that the seasonal and annual variability of some contaminants is to a great extent governed by the processes that rework sediments (Hunt et al., 2013; Leonard et al., 1999; McDonald et al., 2001). A deeper understanding of the role of these infrequent high energy events occupy will have implications for those interested in the reworking of sediment bound contaminants.

Increased moisture in the atmosphere due to rising temperatures, will likely see an increase in the frequency and intensity of storm events globally and this is predicted to be the case for the Irish Sea as well (Möller et al., 2016). Consequently, the frequency and intensity of high impact disturbance events that can see an injection of energy to the regional (Irish Sea) and local (Ribble estuary) sediment transport systems will likely also increase (Blott et al., 2006; Esteves et al., 2011). High riverine discharge events represent a disturbance event that can promote the remobilisation of sediments to the mouth of the Ribble estuary, and where several of these events occur within a short period, it is believed that they will promote the remobilisation of sediments to the Irish Sea, to be redistributed by the Irish sea sediment transport system (Wakefield, 2005). Wave climate has been highlighted as an understudied aspect of climate change induced changes to storminess that may lead to significant changes to the coastal system (Sierra and Casas-Prat, 2014; Stive et al., 2002). Though there is uncertainty, it is generally agreed that the frequency of these high impact disturbance events will increase (Robins et al., 2016).

The implication of sediment remobilisation is that those sediments may be transported to new areas within or outwith the Ribble estuary. This is of concern as the relocation of sediments will mean that any associated contaminants will also be relocated given the relationships between contaminants (^{137}Cs and ^{241}Am) and sediment fractions that were shown in chapter 3, these associations are also widely reported within the literature (Inoue et al., 2017; Lansard et al., 2005).

The spatio-temporal stability of the contaminant sediment proxy relationships established in chapter 3 was reported as being influenced by the September siltation event. The causes of this variability in the sediments is explained in chapter 3 as being a combination of daily and seasonal processes that dictate long term trend along with short high impact disturbance events. These events cause substantial initial change that can be followed up by a longer-term modification to how sediment is transported

within the local area (Adams et al., 2011; Blott et al., 2006; Gutiérrez et al., 2016; Robins et al., 2016). The assumption that disturbance events e.g. storminess and high riverine discharge are significant out with the natural seasonal variability, as discussed above, are explored in this chapter to determine the significance of discrete disturbance events on sediment remobilisation and consequently contaminant remobilisation.

4.1. Aims

This chapter then aims to determine if measurements of climate driven disturbance events such as storminess and high riverine discharge can be used to explain part of the variability in measurements of sediment properties. The following research questions will be investigated:

- Does storminess cause variation in the sediment particle size distribution?
- Does storminess cause variation in the sediment contaminant levels?
- Does storminess cause variation in the sediment elevation?
- Does high riverine discharge cause variation in the sediment particle size distribution?
- Does high riverine discharge cause variation in the sediment contaminant levels?
- Does high riverine discharge cause variation in the sediment elevation?

4.2. Data sets

The questions being investigated here are not necessarily that storminess and high riverine discharge cause variation in the sediment of the estuary as, from the literature discussed in chapter 2.3, it is reasonable to assume this to be the case (Adams et al., 2011; Blott et al., 2006; Gutiérrez et al., 2016; Robins et al., 2016). It is the context of detecting a statistically significant effect of these disturbance variables on the properties of the sediment that is of interest. Consequently, the analysis here focuses on those discrete high impact disturbance events and ignores the cumulative effects from processes that occur daily. The presence of a significant effect when ignoring the ebb and flow tides and variation in tidal height indicates that high impact events such as storminess, can cause a significant effect that it is detectable through the masking of seasonal and daily reworking of the sediments.

A statistical analysis of sediment property time series is the only viable method that can reasonably answer these questions, though this does introduce issues of time series

duration, temporal resolution and the variables that should be measured. It is important that the duration of the study is long enough to include multiple seasons so that any trend is truly detected and not just down to seasonal fluctuations, therefore at least two years of data are required. Understanding temporal resolution is more complicated though as sampling constraints are a significant factor; for example, an ideal time series would have daily measurements as the shorter the duration between points the smaller the assumption about how that system changed between being monitored. However, this is simply not practicable in most studies given available resources. A compromise in sampling frequency was, therefore, used in this analysis. The factors to be used in this analysis are significant wave height as a proxy for storminess (Brooks et al., 2016; Rangel-Buitrago et al., 2016), riverine discharge and variation in the Ribble estuary's sediment properties.

4.2.1. Ribble estuary sediment properties

The sediment properties data were provided by Dr Richard Wakefield from a larger data set collected during his PhD studies into temporal trends in estuary sedimentation within the Ribble between 2002 and 2004. This large data set consisted of 74 individual time series at a 4 week frequency for a two year duration, with these data coming from upper and lower estuary sites. Included variables were particle size distribution, ^{137}Cs concentration, and bed elevation changes. The decision to use these data was formed by two factors, the practical limitations of duplicating such an extensive data set and the availability of coincident wave height data.

When planning, this work, I was faced with the option of using the pre-existing sediment property data provided by Dr Richard Wakefield, or expanding the sampling campaign from chapter 3 to include a longer duration and finer temporal resolution. To expand the chapter 3 sampling campaign would have allowed a finer temporal resolution and eliminated the coarseness in Dr Wakefield's data set introduced by aggregating sampling measurements. However, fine scale monthly changes in sediment properties have already been studied by past workers (Atkin, 2000; Rainey, 1999; Wakefield, 2005) and there would be marginal benefits in producing a monthly time series for the Ribble. Therefore, the collection of such a data set would have come at the cost of chapters 5 and 6 and would have greatly limited my ability to study large scale sediment movement and consider its implications.

Modelled wave property data from the National Oceanographic Centre (NOC), as discussed below in section 4.2.2, covered the time frame from 1996 - 2007, which was

coincident with the sediment property data and were extracted for a fixed point at the mouth of the Ribble estuary (Brown et al., 2010). An alternative to this modelled data would have been to get these data from a series of wave buoys in the Irish Sea, though during the course of this project there was technical issues with these wave buoys that created data gaps. Therefore, the availability of wave height data was a strong part of the decision to use the Wakefield 2002-2004 data set.

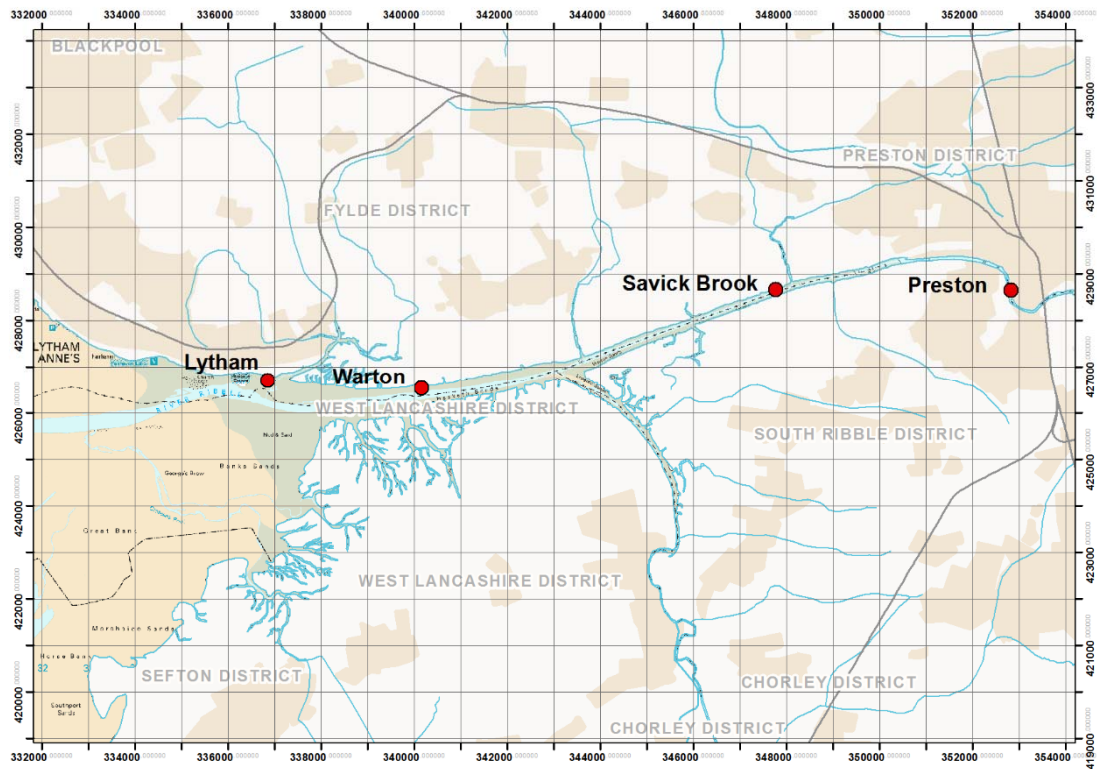


Figure 4.1 Map of the Ribble estuary with the four sampling locations denoted by a red circle.

The field properties data were collected by Wakefield (2005) from four locations within the Ribble estuary; Preston, Savick Brook, Warton bank and Lytham (figure 4.1) during 2002 - 2004. At each location, Wakefield laid out a number of transects dependant on the size of the site Preston (2), Savick Brook (3), Warton (5) and Lytham (3). Transects were deployed across the mudflat horizontally to the Ribble main channel and numbered with transect 1 being farthest from the main channel and transect 2 being second farthest. Along each transect poles were inserted to denote sampling stations, it is from these sampling stations that sediment scrapes and observations of elevation change relevant to the top of the pole were made. These measurements were repeated every month beginning in March 2002 and ending in February 2004.

The sediment scrapes were processed in the same fashion to section 3.2.3 to determine particle size distribution (% clay, % silt, %sand) and ^{137}Cs (Bq kg^{-1}) concentration, with the difference in height measurements indicating the magnitude of erosion or accretion.

4.2.2. Significant wave height as a proxy for storminess

Through the ARCoES project, the National Oceanography Centres (NOC) Proudman Oceanographic Laboratory provided an extract from an 11-year wave simulation of the Irish Sea (Brown et al., 2010). The model was a 1.85km nested 3rd generation spectral wave model (WAM) coupled with the Proudman Oceanographic Laboratory Coastal Ocean Modelling System (POLCOMS). At the mouth of the Ribble estuary hourly estimates of significant wave height (H_s), second moment period (TM_02), peak wave period (TP) and mean wave direction (Θ_m) were made from 1996 - 2007.

From the wave property data, the significant wave height (H_s) was targeted for use as an indicator of storminess within the Irish Sea. Where a pattern of waves observed for a period of time would form a positively skewed Gaussian or Rayleigh distribution, the H_s is defined as the mean of the highest one third of this distribution. This gives a good approximation of the average height of the highest waves for the given time interval, however it is still likely that waves in excess of twice the reported H_s will occur (National Oceanic and Atmospheric Administration, 2017). I use H_s as a proxy for storminess in this work due to it being a measurement of the extreme wave climate that would be present during a storm event (e.g. Valchev et al., 2012). In effect this analysis assumes that wave height will be elevated during storms (Rangel-Buitrago et al., 2016).

4.2.3. Ribble riverine discharge

The riverine discharge is defined in this work as the total volume (m^3) of water that passed an Environment Agency (EA) gauging station at Preston in any given 24-hour period. The station used is located above the tidal reach of the Ribble. The data were formatted with a total river discharge value for each calendar day from 2002 - 2005.

4.3. Methods

This section describes a time series statistical analysis with the Granger causality test chosen as the statistical test of choice. This test and the data preparation and processing steps are discussed in detail below. As all this analysis was conducted within the R programming environment it is important to note that a time series is a vector of data points that are indexed at different times.

4.3.1. Granger causality test as it relates to the data sets

Simply put the Granger casualty test is a hypothesis test of whether values of time series x can be used to predict values of time series y . The test evaluates if the structure of time series storminess is significantly present in the structure of time series % clay after a period of temporal lag. It is important to note that this test does not determine causality despite the name or statistically determine that storminess causes variation in % clay. This method compares the underlying trend in time series storminess and compares it to the underlying trend in time series % clay and determines if the structure of time series storminess is present in time series % clay. Should it be the case that this structure is present, then reasonable interpretation must be used to determine what is likely the cause for this positive result.

The Granger causality test is a bivariate hypothesis test used to assess temporal ordering in two data sets. The Granger causality test and variations of it (Attanasio and Triacca, 2011; Toda and Yamamoto, 1995) have been used extensively for investigating presumed bivariate hypotheses e.g. the causal relationship between global greenhouse gas emissions and global temperatures (Attanasio et al., 2013).

4.3.2. Preparation of data subsets for analysis

The three time series data sets were not of the same temporal resolution; the wave height data were given in one hour increments, the riverine discharge data were in 24 hour increments and the sediment property data were in monthly increments. This is an issue as, in order to conduct the time series analysis, the two data sets that are being tested against each other must be equidistant. The options to rectify this problem are to interpolate the data sets so that they are equidistant or to degrade one of the data sets to achieve equidistance. I chose to create four data subsets that would undergo granger causality testing to better understand the effects of coarseness in temporal resolution.

The four subsets are listed here with a subset ID which is used throughout to avoid confusion as all these data subsets are derived from the three source data sets described in section 4.2. The method used to create each subset follows this list.

- 1) Sub^{IntSP} = the interpolated sediment property data set, the original significant wave height data and original riverine discharge data.
- 2) Sub^{MeanHs} = the Mean of the Significant wave height data for a four-week period, the original sediment property data and the original riverine discharge data.
- 3) Sub^{SumHs} = the Sum of the Significant wave height data for a four-week period, the original sediment property data and the original riverine discharge data.
- 4) Sub^{ScenHs} = the high significant wave height scenario data set, the original sediment property data and the riverine discharge data.

Sub^{IntSP} was created by applying an exact linear interpolation to the sediment property data using the wave height data as a reference, the method was similar to the simple linear interpolation conducted by Kang and Larsson (2014) to correct non equidistant data. This exact interpolator uses a straight line between sampled points to estimate values for time points that were not sampled. This ensured that for every point of the wave height data, a new point for the sediment property data was generated using an exact linear interpolation algorithm meaning both data sets were then equidistant in their observations. These transformations were conducted using the zoo time series package (Zeileis et al., 2016) within the R environment, with the zoo function `na.approx()` being modified to conduct the linear interpolation.

The Subsets Sub^{MeanHs} and Sub^{SumHs} are data sets which have degraded the significant wave height data to the same temporal resolution as the sediment property data. Each data point in the sediment property data represents a site visit on which samples of sediment were collected from locations within the Ribble estuary. The degradation applied aggregates the significant wave height data for the time period between site visits. Two methods of aggregation are used which results in two subsets. Sub^{MeanHs} takes the Mean of all waves in the four-week period before each site visit and Sub^{SumHs} totals the wave heights of all waves in the four-week period before each site visit.

As the significant wave height data is being used as a proxy for storminess this aggregation can be problematic in that storminess is defined here as a disturbance event that is short in duration and infrequent in occurrence. Therefore, by degrading the significant wave height data the signature of these short-term events may be removed. This potentially circumvents the purpose of this chapter, however these

analyses where conducted as it checks for rigour in the methods and ensures a robust analysis by not relying on one method of data analysis. These pair of degraded data subsets also offer a counter to the potential issue of the interpolated subset dataset (Sub^{IntSP}) which whilst preserving the signature of the storminess proxy may be over analysing the sediment property dataset.

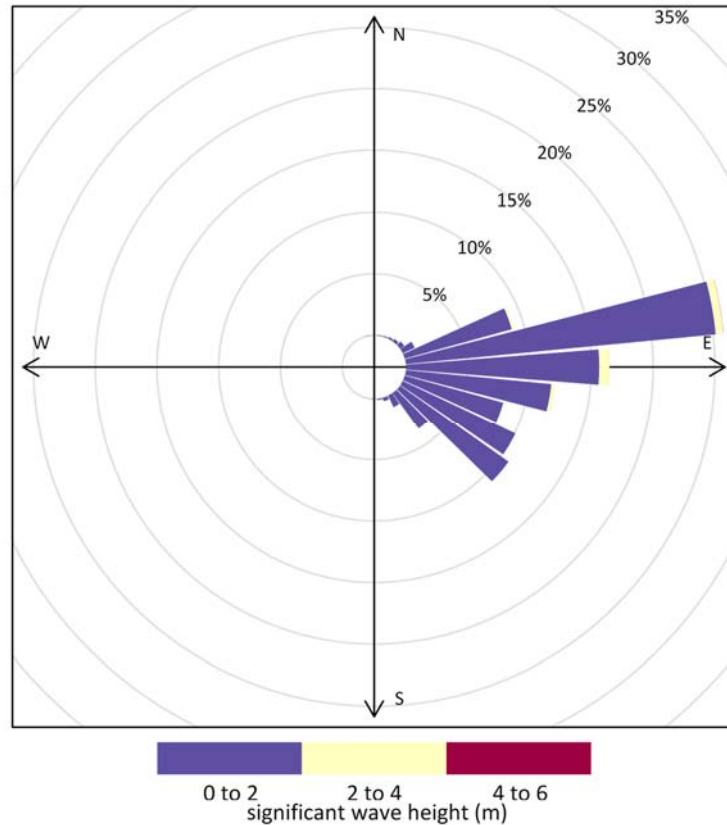


Figure 4.2 Wave direction rose, the bars show the direction that the waves are traveling towards. The concentric rings denote what percentage of the waves the bars represent. The colours on the bars denote the proportion of the waves that have the stated wave height.

The fourth data subset created (Sub^{ScenHs}) was an attempt to isolate the underlying nature of storminess by specifically targeting a subset of the significant wave height dataset which is used as a proxy for storminess here. Figure 4.2 represents the distribution of wave directions and magnitude of waves for the point at the estuary mouth where the wave climate was modelled. From this diagram, it is clear that an arc of 45° and 135° included the waves with the highest wave heights and it also

represented the waves that are angled towards the mouth of the Ribble estuary and are therefore likely to impact it.

Sub^{ScenHs} is a subset of those wave heights that had a direction between 45° and 135° and a size greater than 1m which is the equivalent of the mean of all wave height data plus one standard deviation. This subset was also aggregated to produce a mean of these specifically selected waves for the four-week period before each field visit. This aggregated subset does degrade the data, but by using a scenario which accounts for wave direction and size it is more likely this subset will maintain the underlying trend in storminess. Therefore, this scenario of direction and wave height is believed to isolate elements of the significant wave height data that are most likely to be a good proxy for storminess. This is supported by the work of Luo et al., (2015) whom suggested that for the Ribble Estuary storm waves directed towards the estuary may cause enhanced disturbance by eroding the inner estuary and therefore the direction of waves is an important factor.

4.3.3. Granger causality analysis within R

For each of the four data subsets their three constituent time series datasets were loaded into the R programming environment and all-time series were converted to POSIXt objects using as.POSIX function, which is required to read these data for the analysis. Dates were converted to represent the number of seconds since a fixed epoch; in this case, it was the number of seconds since 00:00am January 1st 1974, which is a default time point used by many applications. The Zoo time series package and lmtest statistical analysis package were loaded and the Granger causality analysis was conducted (Zeileis and Hothorn, 2002).

The time series data were tested for stationarity, which is when the properties of a time series do not depend on the time at which the series was observed. Stationarity can be achieved through the process of differencing, this involves calculating the difference between consecutive observations and conducting the analysis on this new differenced data set. Unit root tests revealed that seasonal and then first differencing was required to achieve stationarity, this was conducted using the lmtest differencing function. An example of a differenced time series is presented in figure 4.3, the storminess time series in this example had the seasonal trend removed by seasonal differencing. However, it was not stationary so had first differencing applied and was tested with unit roots test, the result was a time series that can be said to be stationary.

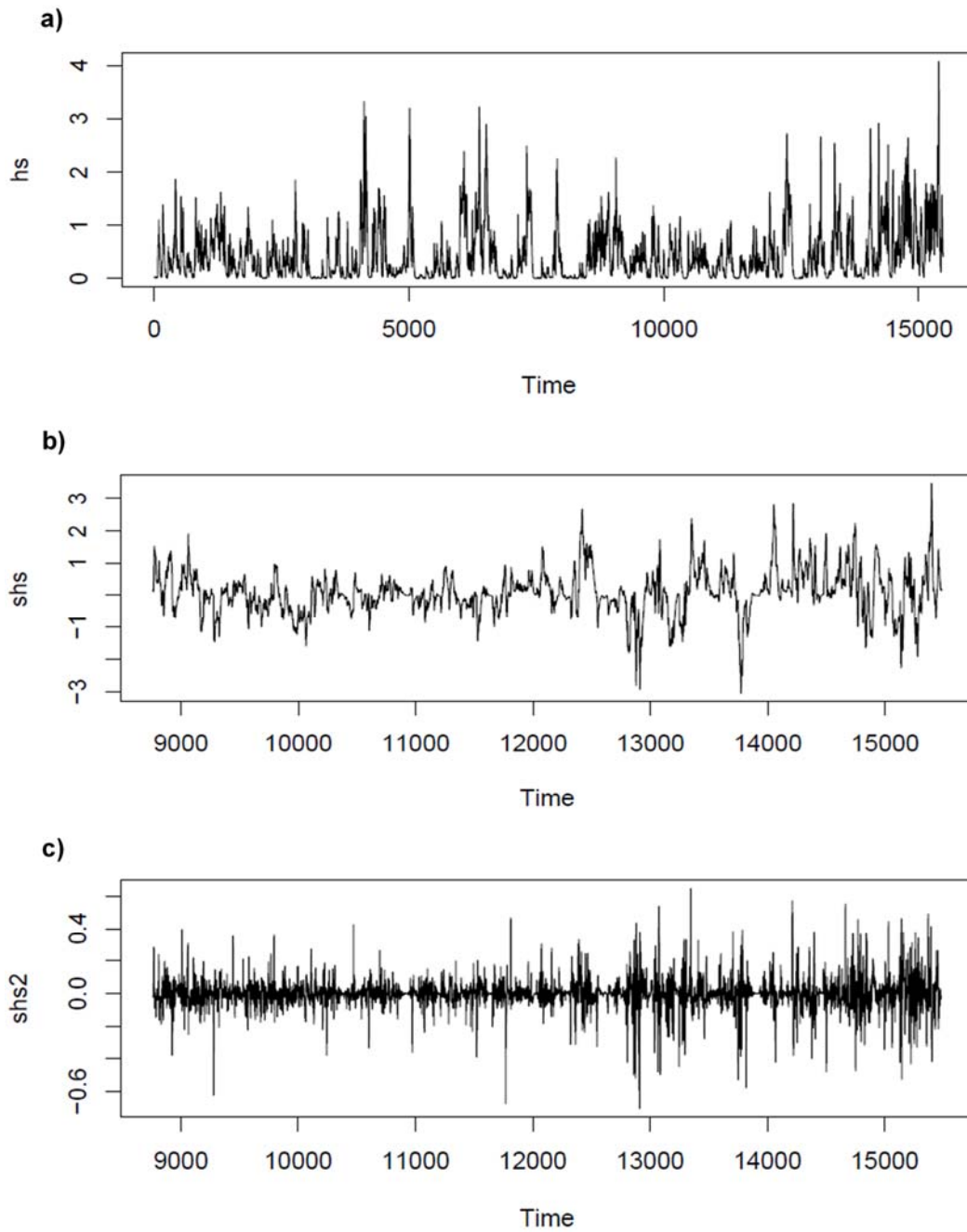


Figure 4.3 Example of a wave height (Hs) time series that has had seasonal and first differencing applied to the data a) raw Hs time series, b) seasonal differencing has been applied to these data, c) first differencing has been applied to the time series found in b.

The differenced data sets were then used for a Granger causality test which tested the hypothesis that x causes y and the reverse that y causes x . These results were then interpreted as passes or fails.

4.4. Results

Each iteration of the Granger causality test evaluated the following null and alternate hypotheses at a significance level of p-value = < 0.05 to determine a pass or fail.

Causation is referred to as “Granger cause” below to emphasise that it is causation within the confines of this particular statistical test and not true causation.

- H_0 Disturbance mechanism does not Granger cause variation in sediment properties
- H_1 Disturbance mechanism does Granger cause variation in sediment properties

I tested two disturbance mechanisms here; a time series of riverine discharge and a time series of significant wave height which is used as a proxy for storminess. The storminess proxy consisted of four data subsets; Sub^{IntSP} , Sub^{MeanHs} , Sub^{SumHs} and Sub^{ScenHs} . Each subset interpolated, aggregated or specifically subset the three source time series to produce four subsets that would allow this analysis to test for a temporal trend in the storminess proxy and sediment properties data sets.

The sediment properties data consists of the particle size distribution, the ^{137}Cs activity concentration and the change in sediment bed elevation. The hypotheses were tested for each sediment property against each disturbance mechanism for each transect. This allows the effects of these disturbance mechanism to be assessed at a spatial scale that ranges from the mouth of the estuary to the extent of the Ribble’s tidal reach. These results are presented as tables below and discussed in section 4.5.

4.4.1. Storminess proxy

Sub^{IntSP}: Interpolated sediment properties

Through the granger causality analysis, the underlying temporal trend within the significant wave height data was compared to the underlying trend within an interpolated time series of the sediment properties data. The results of this analysis are displayed in tables 4.1 and 4.2 as a pass or fail at a significance level of p-value = < 0.05. These data showed that none of the sediment property variables from the five transects located in the upper estuary had any similarity in temporal trend with the significant wave height data. In the lower estuary three of the eight transects; Lytham 1, Lytham 2 and Warton 3 showed positive results indicating that the trend in the significant wave height data sets was partially replicated in the trend of the sediment properties data at these sites. A test for reciprocal causation found that the Lytham 1 sand data exhibited reverse causation across the significant wave height data and the sediment property data.

Table 4.1 Upper estuary Granger causality matrix. For each transect the matrix reports whether the sediment variable was as a pass (green) or fail (grey). A pass denotes that the trend in the storminess proxy data was found in the corresponding sediment property data at p-value = < 0.05.

| Transect | % Clay | % Silt | % Sand | PSD | ¹³⁷ Cs | Elevation change |
|-----------|--------|--------|--------|-----|-------------------|------------------|
| Preston 1 | | | | | | |
| Preston 2 | | | | | | |
| Savick 1 | | | | | | |
| Savick 2 | | | | | | |
| Savick 3 | | | | | | |

Table 4.2 Lower estuary Granger causality matrix. For each transect the matrix reports whether the sediment variable was as a pass (green) or fail (grey). A pass denotes that the trend in the storminess proxy data was found in the corresponding sediment property data at p-value = < 0.05.

| Transect | % Clay | % Silt | % Sand | PSD | ¹³⁷ Cs | Elevation change |
|----------|--------|--------|--------|------|-------------------|------------------|
| Warton 1 | Fail | Fail | Fail | Fail | Fail | Fail |
| Warton 2 | Fail | Fail | Fail | Fail | Fail | Fail |
| Warton 3 | Pass | Pass | Pass | Pass | Fail | Fail |
| Warton 4 | Fail | Fail | Fail | Fail | Fail | Fail |
| Warton 5 | Fail | Fail | Fail | Fail | Fail | Fail |
| Lytham 1 | Pass | Fail | Pass | Fail | Fail | Fail |
| Lytham 2 | Fail | Fail | Fail | Fail | Fail | Pass |
| Lytham 3 | Fail | Fail | Fail | Fail | Fail | Fail |

Sub^{MeanHs} and Sub^{SumHs}: Degraded storminess proxy

Through the granger causality analysis, the underlying temporal trend within the sediment properties data was compared to two subsets of the significant wave height data. The results of this analysis are displayed in tables 4.3 and 4.4 as a pass or fail at a significance level of p-value = < 0.05.

Sub^{MeanHs} demonstrated that for the upper estuary at transect Preston 2 there was a significant temporal trend found in both the significant wave height data and particle size distribution. In the lower estuary, the full particle size distribution and ¹³⁷Cs data at transect Warton 2 showed there was significant similarity between the temporal trend in the Sediment property data and significant wave height data. Within these data reciprocal causation was not found though reverse causation was present.

The Sub^{SumHs} data set showed that transect Preston 1's elevation change data had significant temporal trend along with the particle size distribution data and elevation change data from transects Warton 2 and Warton 5. Like Sub^{MeanHs} reciprocal

causation was absent but reverse causation was present. These subsets which degraded the significant wave height data through aggregation appeared to offer no real advantage over the interpolated data set.

Table 4.3 Upper estuary Granger causality matrix. For each transect the matrix reports whether the sediment variable was as a pass (green) or fail (grey). A pass denotes that the trend in the storminess proxy data was found in the corresponding sediment property data at p-value = < 0.05. This matrix has M = mean storminess and S = sum of storminess.

| Transect | % Clay | % Silt | % Sand | PSD | ¹³⁷ Cs | Elevation change |
|-----------|--------|--------|--------|-----|-------------------|------------------|
| Preston 1 | | | | | | S |
| Preston 2 | | | M | M | | |
| Savick 1 | | | | | | |
| Savick 2 | | | | | | |
| Savick 3 | | | | | | |

Table 4. 4 Lower estuary Granger causality matrix. For each transect the matrix reports whether the sediment variable was as a pass (green) or fail (grey). A pass denotes that the trend in the storminess proxy data was found in the corresponding sediment property data at p-value = < 0.05. This matrix has M = mean storminess and S = sum of storminess.

| Transect | % Clay | % Silt | % Sand | PSD | ¹³⁷ Cs | Elevation change |
|----------|--------|--------|--------|-----|-------------------|------------------|
| Warton 1 | | | | | | |
| Warton 2 | M | M | M | S | M +S | |
| Warton 3 | | | | | | |
| Warton 4 | | | | | | |
| Warton 5 | | | | | | S |
| Lytham 1 | | | | | | |
| Lytham 2 | | | | | | |
| Lytham 3 | | | | | | |

Sub^{ScenHs}: High wave height scenario data set

The Sub^{ScenHs} data set failed to identify the presence of significant temporal trend between the significant wave height data and the sediment property data. This was primarily due to differencing reducing the length of some of the time series and thus making them unsuitable for this analysis. The distribution of storminess was primarily located in the second half of the data October 2002 – February 2004, this meant that differencing which causes a reduction in the length of the data also reduced the length of the temporal trend which the method tried to isolate. As under 50% of the data could not be included as the modified data sets failed unit root test it was impossible to achieve stationarity and thus this analysis failed.

4.4.2. The Ribble riverine discharge

Through the granger causality analysis, the underlying temporal trend within the riverine discharge data was compared to the underlying trend within the sediment properties data. The results of this analysis are displayed in tables 4.5 and 4.6 as a pass or fail at a significance level of p-value = < 0.05. There was a strong spatial component with the riverine discharge data's temporal trend being found within the sediment properties of transects in the lower estuary more so than the upper estuary. In the upper estuary transect Preston 1 showed significant trend for the silt and ¹³⁷Cs data. In the lower estuary, all transects but Warton 2 showed some extent of significant presence of temporal trend. The absence of reciprocal causation and reverse causation within these data sets means that I can accept the alternate hypothesis for these data. I can also state that the underlying temporal trend in the River Ribble's discharge volume was significantly present within the properties of the sediments in the lower estuary.

Table 4.5 Upper estuary Granger causality matrix. For each transect the matrix reports whether the sediment variable was as a pass (green) or fail (grey). A pass denotes that the trend in the riverine discharge data was found in the corresponding sediment property data at p-value = < 0.05.

| Transect | % Clay | % Silt | % Sand | PSD | ¹³⁷ Cs | Elevation change |
|-----------|--------|--------|--------|------|-------------------|------------------|
| Preston 1 | Grey | Green | Grey | Grey | Green | Grey |
| Preston 2 | Grey | Grey | Grey | Grey | Grey | Grey |
| Savick 1 | Grey | Grey | Grey | Grey | Grey | Grey |
| Savick 2 | Grey | Grey | Grey | Grey | Grey | Grey |
| Savick 3 | Grey | Grey | Grey | Grey | Grey | Grey |

Table 4.6 Lower estuary Granger causality matrix. For each transect the matrix reports whether the sediment variable was as a pass (green) or fail (grey). A pass denotes that the trend in the riverine discharge data was found in the corresponding sediment property data at p-value = < 0.05.

| Transect | % Clay | % Silt | % Sand | PSD | ¹³⁷ Cs | Elevation change |
|----------|--------|--------|--------|-------|-------------------|------------------|
| Warton 1 | Grey | Green | Green | Grey | Grey | Grey |
| Warton 2 | Grey | Grey | Grey | Grey | Grey | Grey |
| Warton 3 | Green | Green | Green | Green | Grey | Grey |
| Warton 4 | Green | Green | Green | Green | Grey | Green |
| Warton 5 | Green | Green | Green | Green | Green | Grey |
| Lytham 1 | Green | Grey | Grey | Green | Grey | Green |
| Lytham 2 | Grey | Grey | Grey | Grey | Grey | Green |
| Lytham 3 | Green | Grey | Green | Grey | Green | Grey |

4.4.3. Reciprocal causation: Storminess proxy and Ribble riverine discharge

Through the granger causality analysis, the underlying temporal trend within the riverine discharge data was compared to the underlying trend within the significant wave height data. This test aims to determine if there is significant temporal trend reproduced in both data sets, the presence of such trend in the case of these data would suggest they are influenced by similar factors. It is believed that the regional climate will determine the amount of precipitation and hence the amount of riverine discharge. It is also believed the regional climate will influence the extent of storminess and hence the wave climate at the mouth of the Ribble estuary. Therefore, here I test the hypotheses that the regional climate influences disturbance. The results of this analysis were that a highly significant reciprocal causation was present at lag = -1. The significant wave height and riverine discharge time series both have the same underlying temporal trend present.

4.5. Discussion

4.5.1. Storminess proxy

The underlying temporal trend of the significant wave height data was detected in the particle size distribution of two transects at the mouth of the estuary. This can be interpreted as the sediments at these transects have their particle size distribution modified in response to the size of the waves at the mouth of the Ribble estuary on a monthly timescale. The data suggest that storminess does cause variation in the particle size distribution of the sediment, which is in line with what would be expected from the literature (Brooks et al., 2017; Pye and Blott, 2008; Sierra and Casas-Prat, 2014). However, the role of significant wave height as a proxy for the magnitude of storminess is more complex.

The absence of significant detection in the upper estuary and the few transects that passed the statistical test in the lower estuary would lead to the conclusion that, whilst significant wave height is a key influencing factor, it is not a substantial reason for why sediment properties change within the Ribble estuary. There are however other factors that the data revealed which complicate the simplistic interpretation that storminess, through its' proxy, is a significant disturbance mechanism. These other factors identified from the analysis are reciprocal causation, reverse causation and data temporal resolution.

Reciprocal causation was present for sand at transect Lytham 1 though reverse causation was a more substantial issue and its dominance offers clues to what is likely to be occurring within these data. Reciprocal causation is defined by the Granger causality framework as the storminess proxy causes the variation in sediment properties and the properties of the sediment cause the variation in the storminess proxy, both these statements are true in reciprocal causation. Generally, when reciprocal causation is present it means that there is a third unknown variable that is governing the temporal trend in both data sets. Reverse causation however is when the Granger hypothesis 'the properties of the sediment cause the variation in the storminess proxy' is found to be true alone. Clearly, where this is present it is counter intuitive and therefore suggests that there may be an interpolation error that is distorting the data. This error is the interpolation applied to the grain size data to force it to a finer temporal resolution through an exact linear interpolator.

The main effect of interpolation is that an assumption is made about the rate of change at which a property transitions from one measured point to another measured point i.e.

it is assumed to be steady and is represented by a straight line between two points. For example, should 100% of the change in a measured value occur one day before the point was measured again, then an exact linear interpolator is forecasting that change back in time because it assumes that change occurred at a consistent rate. As the Granger causality test attempts to detect a duplication of a trend in one-time series at a temporal lag in the other, the above interpolation error will cause failure and in some cases reverse causation.

Alternatively, the data can be degraded so that interpolation is not required however doing so did not appear to offer any particular advantage over the interpolation method in this particular case. The analytical results (tables 4.3 and 4.4) showed that there was completely different output to the interpolation methods results (tables 4.1 and 4.2), even though transects identified as significant were the same transects identified by the interpolation methods reverse causation.

On the basis of the results obtained from all four storminess proxy subsets it is likely that there was a temporal trend being replicated in the sediment property data sets in the transects located at the mouth of the estuary. However, the analysis does not support this assertion strongly, merely indicates that there may be some trend that would be worthy of further investigation. The difference in temporal resolutions of the data sets is the cause of this problem when trying to compare the long-term trend of sediment property variation to short infrequent storm events through a proxy.

This analysis is pushing the limit of what can be achieved with physical sampling. Furthermore, the issues discussed above are primarily a result of the coarseness of the temporal resolution of the field data. A monthly sampling campaign is likely to be the limit for the frequency of field visits to the same point given the resource implications. Therefore, to take this work forward along with the underlying idea of observing the temporal trend of storminess being reproduced in the sediments of an estuary a truly non-invasive/intensive technique is required.

In theory non-invasive/intensive techniques that allow the collection of fine temporal resolution data of the estuaries sediments exist in the form of hyperspectral remote sensing, which can quantifiably measure the properties of sediments (e.g. Rainey et al., 2003). However, despite there being many techniques (Ben-Dor et al., 2002; Deronde et al., 2006; Rainey, 1999; Wal and Herman, 2006) that allow the measurement of particle size distribution, organic matter and surface contaminant concentration available since the mid 1990's these methods have rarely been applied

outside a method development paper. With the advent of the availability of relatively inexpensive air borne drones and development of lightweight spectral sensors and advanced automated image processing algorithms perhaps the ability to collect fine temporal resolution data of the sediment properties may be on the horizon.

4.5.2. Ribble riverine discharge

The temporal trend seen in the riverine discharge data was significant in the particle size distribution of transects Warton 1, 3, 4, 5 and Lytham 1 and 3, this suggests that the riverine discharge is a significant factor in the remobilisation and deposition of sediments. The results for the upper transects (table 4.5) show that the riverine discharge played less of a role here than in the lower estuary (table 4.6). The alternate hypotheses that riverine discharge caused significant variation in the sediment properties of the estuarine sediment can be accepted. It is clear that the riverine discharge mainly affects the lower estuary with only one of the five upper estuary transects reporting a significant effect.

This spatial split in transect response to riverine discharge does seem counter intuitive at first glance, though it may be a result of the lower estuaries wider width meaning that those sites are only affected by large riverine discharge events in comparison to the upper estuary which is affected by all discharge events. The daily riverine discharges may be hiding longer term monthly effects on the sediment matrix in the upper estuary by disturbing the sediment at a higher frequency. Where the lower estuary daily riverine discharges that are unremarkable in magnitude do not have the opportunity, due to a wider channel, to hide the longer-term trend in the sediment matrix.

The presence of the Douglas tributary, which is located downstream of the upper estuary transects but upstream of the lower estuary transects, may also play a role here. This additional source of discharge may compensate for the widening of the channel at the lower estuary, which would be expected to reduce the energy of the river water as it is spread over a greater area (e.g. Gleizon et al., 2003; Luo et al., 2015; van der Wal et al., 2002).

The temporal characteristics of these discharge events are controlled by the extent of urbanisation and modification to the River Ribble, as these factors control the rate at which water enters the River Ribble. The effect of these factors is that the temporal profile of the discharge events is substantially different to the storminess proxy temporal profiles. Where a storm occurs and high waves are generated, once the storm fades the waves will dissipate (Brooks et al., 2017), though due to the holding capacity

of the catchment the effects of high rainfall that causes these high riverine discharge events can be stretched out (Stapleton et al., 2008). The difference in temporal characteristics of these two disturbance mechanisms is likely why the riverine discharge data did not experience reciprocal causation or reverse causation. In this case, the findings strongly indicate that the riverine discharge is a highly significant disturbance mechanism which is responsible for remobilisation of sediments.

4.5.3. Storminess proxy and riverine discharge

The significant wave height and riverine discharge data had the same temporal trend present in both data sets at a highly significant level with minimal temporal lag (lag = -1), meaning the data's underlying trend was significantly similar. It is not surprising that when the meteorological conditions exist that promote stormy waves, these conditions also cause high precipitation; therefore, it would be expected that both these mechanisms would have a similar trend. The exact interpretation of the Granger causality hypothesis tests is that when reciprocal causation is present a third unknown variable is responsible for this temporal trend in both of the disturbance mechanism data sets. This third unknown variable would be the regional climate which dictates local weather patterns. Therefore, climate is likely to be a significant mechanism governing disturbance in riverine discharge as well as a possible mechanism of disturbance in stormy wave climate.

4.6. Conclusion

This chapter has investigated whether temporal trends in the two-time series of the disturbance mechanisms significant wave height as a proxy for storminess and riverine discharge could be detected in the behaviour of sediment properties at a number of different locations within the Ribble estuary. What was important about this analysis was that it ignored the long-term mechanisms of daily reworking by ebb and flow tides etc. and focused solely on the short-term high impact disturbance events. The implication being that if significant trend was found whilst ignoring the other complex factors that operate within the estuary, it gives an idea of the importance of these short-term factors on the temporal fluctuations of the tested sediment properties.

The riverine discharge was clearly found to be a significant factor in modifying sediment properties over the two-year time period that data were analysed for in the lower estuary. Storminess, through its proxy was not found to be a substantial factor though it is likely that it is influencing some of the transects at the lower estuary. However, this was not to a degree sufficient to see its temporal trend repeated in the

overall temporal trend of the sediment properties at many sites throughout the estuary. The storminess proxy whilst not being a substantial disturbance mechanism, a weak statistically significant trend was detected. It is possible that the storminess data may require a finer resolution sediment property data set to fully explain what is happening within the estuarine sediments. The role of storminess may not have been resolved fully in this chapter however the results have illustrated a case for further work preferably using a higher resolution data set collected through a non-invasive/intensive method.

These results have demonstrated that individual high impact disturbance mechanisms can be significant in determining how the estuarine sediments are reworked. If climate is accepted as the third variable responsible for the presence of reciprocal causation between the discharge and storminess proxy data, then we are investigating not only the impact of stormy waves and high riverine discharge on sediment properties but also the effect of climate as a disturbance mechanism for sediment remobilisation.

5. The spatio-temporal characteristics of long term Ribble estuary sediment movements

The importance of variation in sediment particle size distribution and the remobilisation of sediments in determining the concentration of estuarine contaminants such as ^{137}Cs and ^{241}Am was discussed in chapter 3. The effects of a substantial siltation event in September 2014 resulted in a degradation in the proxy relationship between $^{137}\text{Cs}/^{241}\text{Am}$ and % clay and this was believed to be the result of silts with a distinctly different contaminant concentration being deposited at the site. Chapter 4 has highlighted that the effects of disturbance mechanisms have a strong spatial component. Together these points highlight the need to develop an understanding of sediment movement within the Ribble estuary especially the spatial and temporal characteristics of sediment movement.

Sediment movement within the Ribble estuary is not a closed system as it is an extension of the Irish Sea sediment transport system (van der Wal et al., 2002). Marine sediments from the Irish Sea, particularly from the Liverpool bay area, are known to be deposited within the Ribble estuary (Luo et al., 2015). Likewise, it is known that Ribble estuarine sediments are remobilised to the Irish sea (Atkin, 2000; Wakefield, 2005). However, the general prevailing trend in most estuaries is deposition, as evidenced by the presence of the extensive sandbanks, mudflats and saltmarsh, which are all sediment deposition features (Jickells and Rae, 1997). Although post deposition remobilisation will see these sediments subject again to the prevailing sediment transport system as governed by the local energy, river discharges and hydrodynamic processes (Azevedo et al., 2010; Falconer and Lin, 1997; Wolanski et al., 2001). The sediment bound contaminants that are remobilised and redistributed within the estuary or perhaps out with the estuary as part of these sediment movements is the reason why sediment movement is of interest. The temporal and spatial variability of sediment bound contaminants can be understood by exploring the nature of sediment movements (Atkin, 2000; Rainey et al., 1999; Wakefield et al., 2011). This has implications in turn for those interested in investigating potential health impacts from these contaminants on humans and wildlife (e.g. Hunt, 1997).

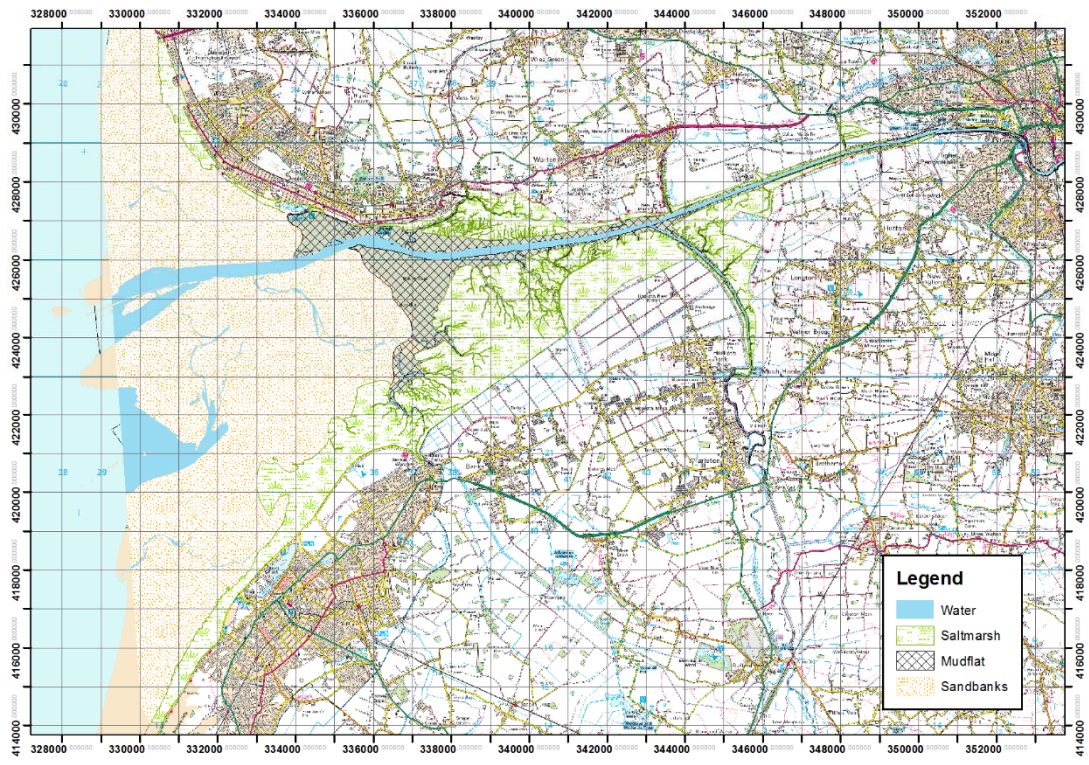


Figure 5.1 Map outlining the different types of sediment deposits of the Ribble estuary. A blue line has been drawn around the outer estuary sandbanks, a red line has been drawn around the mudflats and purple lines have been drawn around the north shore and south shore saltmarshes.

Though estuaries can be viewed as one large deposition feature, within them, there is stratification particularly by particle size (e.g. van der Wal et al., 2002). For example, in the Ribble estuary sand banks dominate at the outer estuary transitioning to mudflats from the mouth of the estuary up till Preston and finally to areas of saltmarsh in the upper tidal frame (Figure 5.1). This stratification is the result of how the following interact; the mass of the sediment, the available tidal energy and the estuaries morphology. These processes can be generalised as the estuary hydrodynamics, which is how the tide flood and ebb cycle along with its suspended sediments interacts with the estuary surface. These three sediment deposit categories allow the sediments of the Ribble estuary to be categorised by their sediment grain size as well as their likely contaminant concentration. For example, the sandbanks at the outer estuary are composed of coarse sandy sediments, which the analysis from chapter three illustrated would have low contaminant concentrations.

The mudflats contain a mixture of clays, silts and sands, with the mixture being controlled by elevation with those mudflats higher in elevation containing a larger

percentage of clays and silts (Rainey et al., 2003). These sediment deposits are disturbed daily with the ebb and flow of the tidal cycle, though the extent of disturbance will be lower in the upper tidal frame (higher elevations) where the mudflats begin to transition into the saltmarshes and deposition via tidal pumping is dominant (Gleizon et al., 2003; Lyons, 1997). The mudflats have been shown in chapter 3 to exhibit substantial variability in contaminant values, ranging from 3 Bq kg⁻¹ to 311 Bq kg⁻¹ for ¹³⁷Cs (table 3.7). The mudflats represent an exchange environment where catchment, Irish Sea and estuarine sediments and their associated contaminants are mixed, therefore mudflats serve as a good indicator of the current levels of contamination.

The Ribble saltmarshes are located on the north bank (Warton marshes) and south bank (Longton and Hesketh marshes) of the main channel. Saltmarshes are considered to be relatively stable and representative of contaminant levels in the past especially deeper down in the sediment vertical profile and consequently these often have higher levels of contamination reflecting past discharge practices (Brown et al., 1999; Lindahl et al., 2011; Rahman et al., 2013). The long-term behaviour of the saltmarshes is important for those interested in understanding the possible radiological implications of increased sediment remobilisation as saltmarshes can be substantial stores of contaminants (Hunt et al., 2013; Rahman et al., 2013).

One feature within the Ribble which will be used to explore the long-term changes in sediments in saltmarshes is the presence of a managed realignment scheme. The scheme was implemented in 2009 at Hesketh Outmarsh to expand the area of saltmarsh habitat for wading birds. Sediments have been eroded and accumulated within the managed realignment area since the initial breach in 2009, these movements may reveal information about how saltmarsh sites may react to disturbance. As it is not possible to study the consequences of a natural disturbance event owing to complexity of the logistics, this chapter aims to use this anthropogenic disturbance event as an analogue for general disturbance and specifically sediment remobilisation. This chapter focuses on the consequence for sediment movement, while chapter 6 explicitly deals with contaminant remobilisation at the Hesketh Outmarsh.

5.1. Aims

Morphological change and inferred movement of sediment within the intertidal area is explored here from 1999 – 2015. The analysis focuses on the specific sediment categories; the sandbanks, mudflats and saltmarshes. The nature of this section is exploratory and therefore attempts to answer the following questions to deepen the understanding of sediment transport in the Ribble estuary.

- Is the long-term trend in estuary sedimentation positive (accretion dominant) or negative (erosion dominant)?
- What are the morphological characteristics of sediment movement for the sandbanks, mudflats and saltmarshes?
- How has the Hesketh Outmarsh managed realignment scheme affected the estuary's sediment deposits and transport of sediments?

5.2. Data sets

The analysis used to answer this chapter's questions about the Ribble estuary's long-term sediment movement, relied on the use of remotely sensed topographic survey data. These data allow large spatial areas of the estuary to be reliably surveyed, with multiple data sets from measurements made in different years it was possible to interpret long term trends in estuary sediment movements. A brief overview of the principles of remotely sensed topographic data, the data sets that were collected and the locations which were surveyed is given below.

5.2.1. LiDAR overview

Light Detection and Ranging (LiDAR) is a widely used remote sensing topographic survey technology and LiDAR data sets form the basis for this Chapter. A comprehensive explanation of LiDAR technology is found in Bossler et al. (2010).

A short explanation of LiDAR is that the technology maps the surface topography by firing a laser along a sweeping arc from, in this case, the underside of an aircraft which flies over the intended survey area. These pulses of laser light are reflected back to the LiDAR system by the land surface, the return time is recorded and given the known speed of light a linear distance can be calculated by the system. Aircraft aeronautics provide information about the aircraft position, pitch and roll, which allow the LiDAR system to determine the 3D coordinates at which the laser beam was emitted. With a known start position of the beam of light as well as the beams arc and length it is

possible to construct and solve a geometry equation to determine the coordinates of the surface from which the beam was reflected.

The LiDAR data are then represented as a list of coordinates (x, y and z) for each point that returned a signal. This format is called a point cloud and it is from these data that a useful digital terrain model (DTM) or digital surface model (DSM) can be derived.

These data will often have geostatistical models (an interpolation method) fitted, the nature of the model used will determine whether it is a DSM or DTM that is produced.

DSM's fit a geostatistical model that passes through all the points in the point cloud.

Where vegetation is known to be present, as in the case of the saltmarshes, within the Ribble estuary it is best to use a DTM, which fits a 'bare earth surface' model that ignores the data determined to be vegetation returns.

Equation 5.1
$$RMSE = \sqrt{\frac{1}{n} \sum_{i=1}^n (y_i - \hat{y}_i)^2}$$

The processed models are then geo-corrected with data provided by a ground based survey team that has collected highly accurate positional data for a number of points within the estuary. The Root Mean Square Error (RMSE) is then calculated (Eq. 5.1) as a measure of the accuracy of the data product. The size of the RMSE is proportional to the quality of the validation survey and consequently the smaller this value is the more confidence there is in the DSM or DTM.

5.2.2. Available LiDAR data

The environmental regulator for England and Wales, the Environment Agency (EA), through its Geomatics Group has been collecting topographic survey data of the coastal areas and river systems in England and Wales since 1998. The Geomatics Group flies two aircraft outfitted with LiDAR systems to collect these data and it processes these data as DSMs and DTMs. In response to the high impact storms seen in 2014, the EA has made these data open access as of August 2015, with the aim of improving flood modelling in England and Wales.

Multi-year DTM data from the EAs data archives were extracted for this project, the exact data sets are listed in table 5.1. There were differences in the observed RMSE and spatial resolution levels over the past 18 years. These differences are associated with improvements in survey technology and LiDAR instrumentation over this time.

Table 5.1 The LiDAR data sets used in this chapter are listed here with their accompanying spatial resolution and RMSE. A description of the extent of the spatial coverage is also provided.

| Year | RMSE (m) | Resolution (m) | Description |
|-------------|-----------------|-----------------------|------------------------------|
| 1999 | 0.15 | 2 | Full estuary coverage |
| 2005 | 0.15 | 1 | Partial outer estuary |
| 2006 | 0.15 | 1 | Partial outer estuary |
| 2007 | 0.05 | 0.25 | Mid estuary coverage |
| 2009 | 0.05 | 0.25 | Full estuary coverage |
| 2010 | 0.05 | 0.25 | Mid estuary coverage |
| 2011 | 0.05 | 0.25 | Mid estuary coverage |
| 2014 | 0.05 | 0.5 | Mid estuary coverage |
| 2015 | 0.05 | 0.5 | Partial mid estuary coverage |

In addition to these data, the ARCoES project commissioned NERC's Airborne Research and Survey Facility (ARSF) to collect LiDAR data covering the full extent of the estuary. The flight survey was conducted in October 2015. However, the data processing steps required meant that the data were not released until the end of October 2016 by which point it was too late to include in this chapter. These data will be used during the preparation of this work for publication.

5.2.3. Study sites

With the available data sets (table 5.1), it was determined that two approaches would be taken to interpreting sediment changes; 1) is an evaluation of the full estuary coverage from 1999-2009 and 2) a similar evaluation of the changes observed mid estuary from 1999-2015. The full estuary data set covered all areas of saltmarsh, mudflats and most of the sandbanks but there are only two full LiDAR data sets available (in 1999 and 2009). The mid-estuary covered an area that spans from Longton marshes to Banks marshes on the south of the estuary and included the

mudflats located north and south of the main river channel and the surrounding saltmarshes. There were available data sets for 1999, 2005, 2006, 2007, 2009, 2010, 2011, 2014 and 2015. In addition, three localised areas that represented specifically the three sediment deposit categories (sand banks, mudflats and saltmarshes) were investigated.

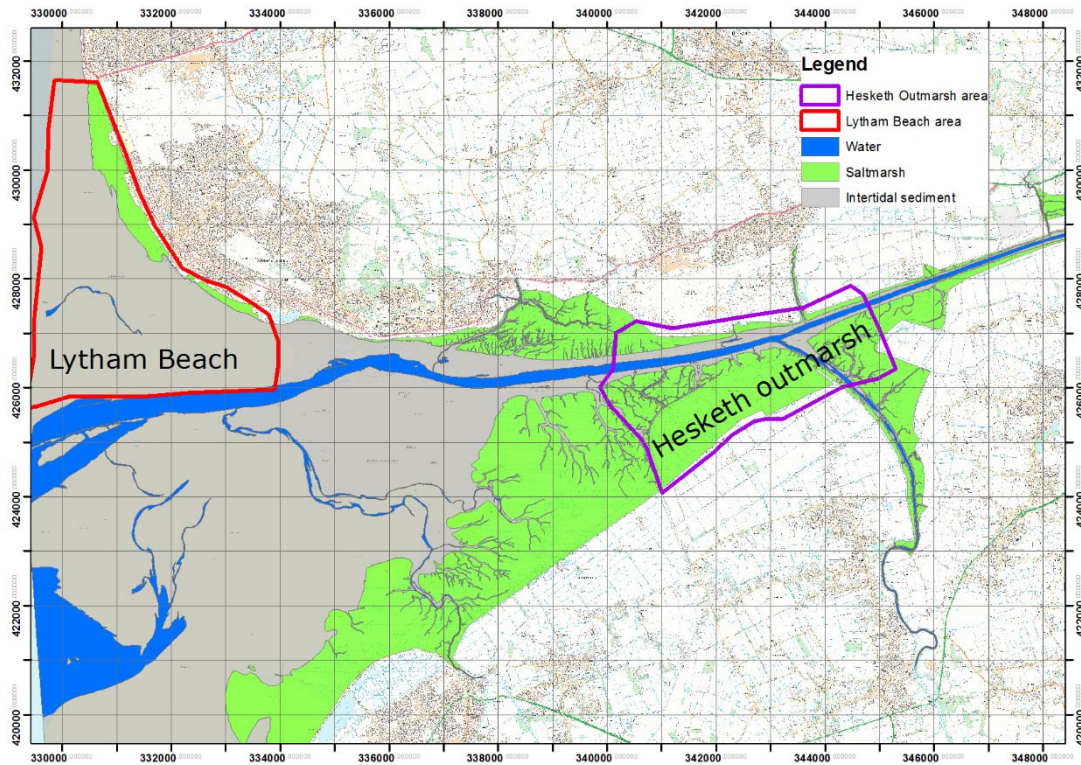


Figure 5.2 The Ribble estuary is shown with two boxes denoting the areas that the localised focus sites are based. The sandbanks studied are located at the Lytham beach site in the outer estuary, with the mudflats and saltmarshes being studied at the Hesketh Outmarsh site in the mid estuary.

The Lytham beach site, which acted as a localised focus site for the sandbanks, was a constrained sand dominated part of the outer estuary with large concrete seawall defences which considerably restricts the ability of the tidal frame to adapt to change. The Hesketh Outmarsh site covers saltmarshes and mudflats located in the mid estuary, it is these sediments that are enriched in contaminants and of most interest to this work. This is also the location of the managed realignment site, which this work treats as analogue for a disturbance event.

5.3. Methods

The DTM data sets were processed here to determine the change in sediment volume between different years. Cluster analysis of the data was conducted for each time period to allow the physical properties of morphological change to be measured. The five sets of data that were analysed are listed below.

- 1999 – 2009 full estuary coverage
- 1999 – 2015 mid estuary coverage
- Localised site 1 – sand banks
- Localised site 2 - mudflats
- Localised site 3 – Hesketh Outmarsh

5.3.1. Raster processing framework

The EA DTM products were delivered as 1km ASCII Grid tiles with varying resolutions. Whilst it is possible to apply a spatial analysis to raster products split across multiple tiles, few open source tools support this and doing so unnecessarily complicates the processing chain. Therefore, the decision was made to develop a raster processing framework that would convert these raw data to a stage that analysis could be conducted. The following software and applications were used in this analysis; ESRI ArcGIS, QGIS and the R statistical programming language with the packages SDMTTools and Maptools. Figure 5.3 presents the data processing steps that were performed.

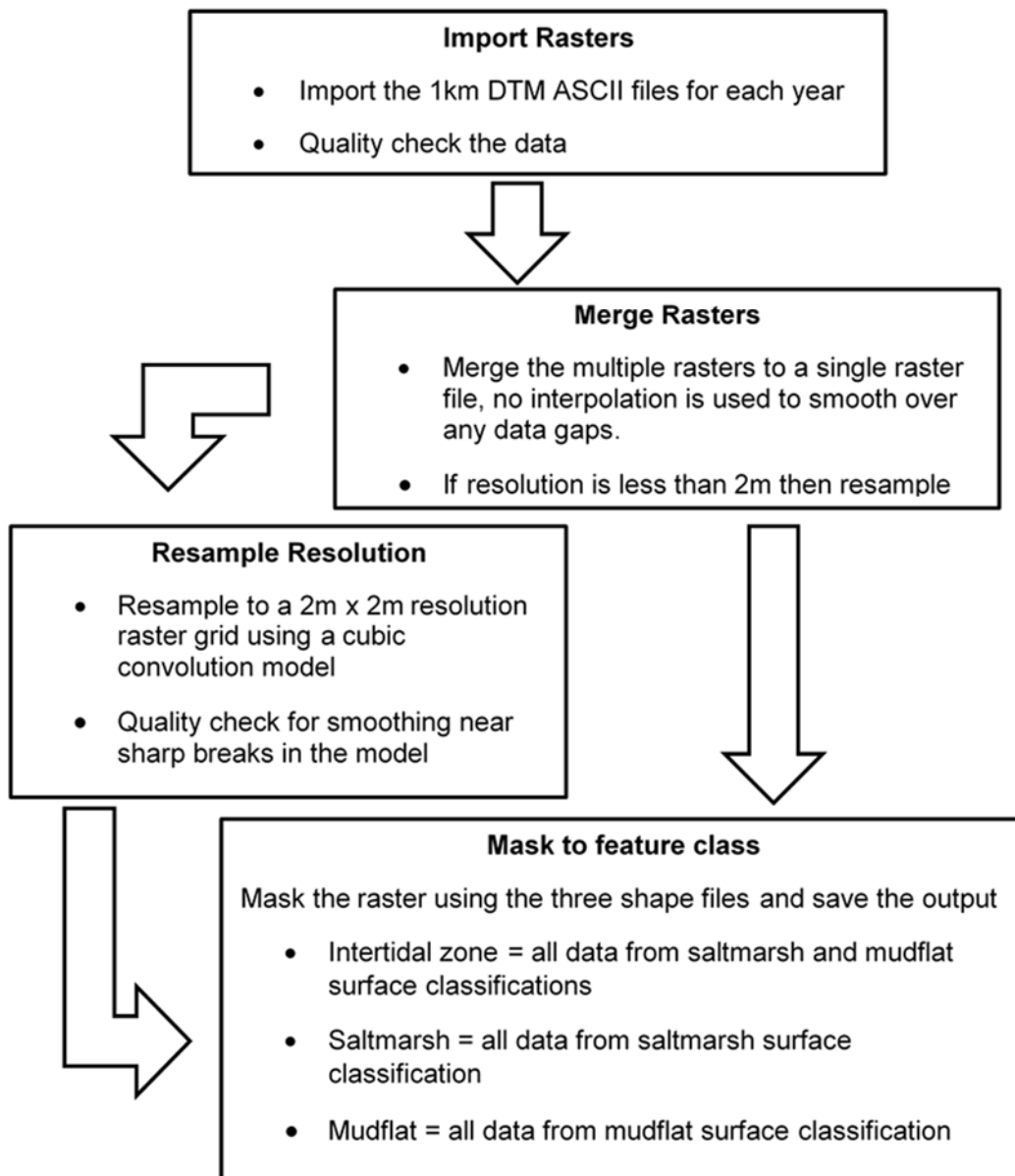


Figure 5.3 This schematic flow diagram showing the data processing stages to convert raw ASCII data to a form useful in the current study.

The raster processing framework devised (figure 5.3) consisted of four stages in data processing.

1. The first stage involved loading each year's data and manually inspecting the data for possible errors such as large areas of missing data or discontinuity between the individual 1km tiles. There were no issues with the initial data quality checks and all available data sets were deemed suitable.
2. The next step involved merging all the 1km individual raster tiles to a single data set using an automated ArcGIS model which was constructed to carry out

this task. This was conducted for each year where there were data available. A number of the tiles had data gaps between tiles where there were lines of pixels with no data, it was decided not to interpolate across these areas as this analysis did not require a continuous topography to function.

3. The 1999 data set was the most spatially comprehensive and was selected as the template to assess all other data against however, this is a 2m x 2m grid resolution whereas the other data sets are available at much higher resolution (table 5.1). The data for years other than 1999 were therefore resampled to a 2 x 2m grid to ensure consistent comparison of the data between years clearly the newer data sets with a finer spatial resolution lost data as a part of this degradation. Where the 1999 data set was not required however, the data sets were resampled so that all data had a finer 25cm raster grid resolution instead.
4. The spatial extent of the data sets often included areas that were of no interest for this analysis and therefore these were masked. This was achieved by creating three feature class files; intertidal zone, saltmarsh and mudflat. These files were created from a surface classification of the estuary which used the Mean High Water (MHW) and Mean Low Water (MLW) lines calculated for 2015 in the Ordnance survey master map product (figure 5.4).

The master map MHW and MLW polylines were produced using ARCGIS editor tools and the QGIS polygoniser tool to manually create masks that encompassed saltmarsh surface type, mudflat surface type and a file that represented the whole intertidal zone (figure 5.4). The main channel was also digitised and used to remove areas that are regarded as always being under water as the LiDAR derived topography is inaccurate in these areas.

The result of this processing chain was that for each year where data were available, an intertidal zone, mudflat and saltmarsh raster file was created containing elevation data relative to the ordnance survey datum.

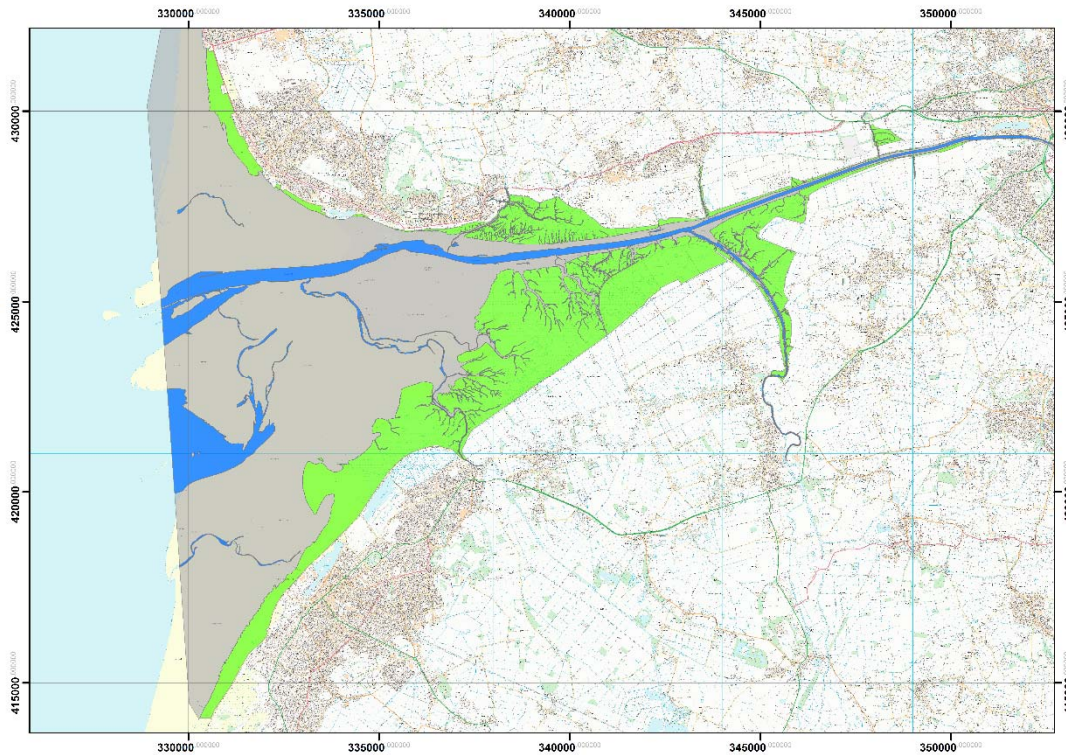


Figure 5.4 The Ribble estuary is shown with a classified intertidal zone, green = saltmarshes, grey = mudflats and blue is water that is below low tide. These classifications were derived from averaged tide data from 2015. These data are used to assign habitat type to the LiDAR data.

5.3.2. Raster of difference – Limit of detection

For each time period (e.g. 1999 and 2009) that a volume of change was required, the pair of rasters produced using the approach outlined above were processed to calculate a new raster called the raster of difference (ROD). Within the ROD raster, each pixel contained a value for the change in height (in mm) between the dates of the two input rasters. Given that the data sets are using the same raster grid it is possible to use raster math functions to produce the ROD using the following equation (Eq. 5.2) applied to each pixel in the target rasters.

Equation 5.2
$$ROD = New\ Raster - Old\ Raster.$$

This subtracts the pixel value in the older of the two datasets from its corresponding pixel value in the newer of the two data sets. Where there is discontinuity in spatial extent between the source data sets, the ROD pixel value was filled with a NA value, therefore the ROD only contains differenced values.

The newly produced ROD contains change in elevation data for each 2m x 2m pixel, as mm above or below the ordnance survey datum. The following equation (Eq. 5.3) was then used to convert the change in height (mm) to a change in volume (m³).

$$\text{Equation 5.3} \quad \text{Volume of change (m}^3\text{)} = (\text{ROD} \div 1000) \times \text{pixel area (m}^2\text{)}$$

This equation will calculate the volume of material that was eroded or deposited for each pixel area, in the case of a 2 x 2 m source data product this volume applies to a 4m² area.

The root mean square error (RMSE) measures the difference between ground survey data and the airborne survey data, it is a standard method of reporting the accuracy of a spatial data set and the equation is given in Eq. 5.4. The source DTM's have differing RMSE, which is associated with improvements in survey technology used to collect and process the data, therefore the RMSE was lower with newer data sets. A common approach to managing uncertainties in the DTMs is to apply a minimum level of detection threshold to the raster of difference, to distinguish between significant elevation change and noise introduced by error in the source DTMs.

$$\text{Equation 5.4} \quad \text{RMSE} = \sqrt{\frac{1}{n} \sum_{i=1}^n (y_i - \hat{y}_i)^2}$$

$$\text{Equation 5.5} \quad \delta u_{\text{ROD}} = \sqrt{(\delta z_{\text{new}})^2 + (\delta u_{\text{old}})^2}$$

The initial error from the source DTMs may be propagated in the raster of difference, therefore the above equation (Eq. 5.5) is given as a method for calculating this error propagation (Montreuil et al., 2014). δu_{ROD} is the propagated error in the raster of difference and $\delta z_{\text{new}}/\delta u_{\text{old}}$ is the error in the source new and old DTMs, old being the chronologically first data set. Therefore δu_{ROD} acts as a modified version of the RMSE that accounts for error propagation and was set as the limit of detection (Eq 5.6).

$$\text{Equation 5.6} \quad \text{ROD}_{\text{LOD}} = (\text{ROD}_{\text{pixels}} \leq -\delta u_{\text{ROD}}) + (\text{ROD}_{\text{pixels}} \geq \delta u_{\text{ROD}})$$

Equation 5.6 was implemented in ArcGIS using the attributes tool to determine the ROD values. The calculation excluded any value that were deemed to be below confidence level which was determined for each case as it is dependent upon the RMSE of the source data. These RMSEs are lower with newer data sets as survey technology has improved substantially from 1999 (first data set) to present (2016), resulting in less error in ground truthing the data. The result was a limit of detection that was applied to each ROD. The resulting raster of difference limit of detection

(RODLOD) may be overly conservative, however it ensures that any conclusions drawn from further analysis provide confidence that the data are representative of sediment volume change in the estuary.

5.3.3. Cluster analysis

The RODLODs represent the volume of sediment that has either eroded or accreted within each pixel between the two dates when the LiDAR data were collected. These data can also be used to visually identify morphological changes within the estuary that have distinguishing physical attributes. To quantify these physical attributes without relying too heavily on user interpretation, which can be subjective, a statistical method was developed to identify and quantify such events. The clustering algorithm was applied to each RODLOD and the results of this clustering were exported as a feature class that contained polygons which denoted the shape of each significant changed morphological feature. The steps in the clustering analysis are given in figure 5.5 and were:

1. The first step in this process was to generate a feature point for the centre of every pixel, this feature point stored the pixel value within the features attribute table. This processing was conducted using the ArcGIS raster to feature tool.
2. Clustering was then performed using the ArcGIS hot spot analysis tool, which is an implementation of the Getis-Ord local statistic (Ord and Getis, 2010). For every feature point, a z and p value is calculated. These data were used to determine feature points that were clustered within the global dataset by comparing a local sum of z-scores with a global sum of z-scores. Z-scores above 1.96 or below -1.96 which also have a p-value of < 0.05 represent statistically significant features at 95% confidence that exhibit clustering. These are either positive (> 1.96 and are accumulating sediment) or negative (< -1.96 and are losing sediment). The magnitude of the z-score was proportional to the strength of the localised clustering relative to the global data.
3. A zone of indifference was used to conceptualise the spatial relationship for these data. This conceptualisation is similar to that of spatial autocorrelation in that, as distance between features increases, their relationship declines. However, this model incorporated a fixed distance band of 6m (equal to 2.5 pixels) to form a search area for calculating the local z scores, this will ensure the scores are not skewed by data that is located at distance.

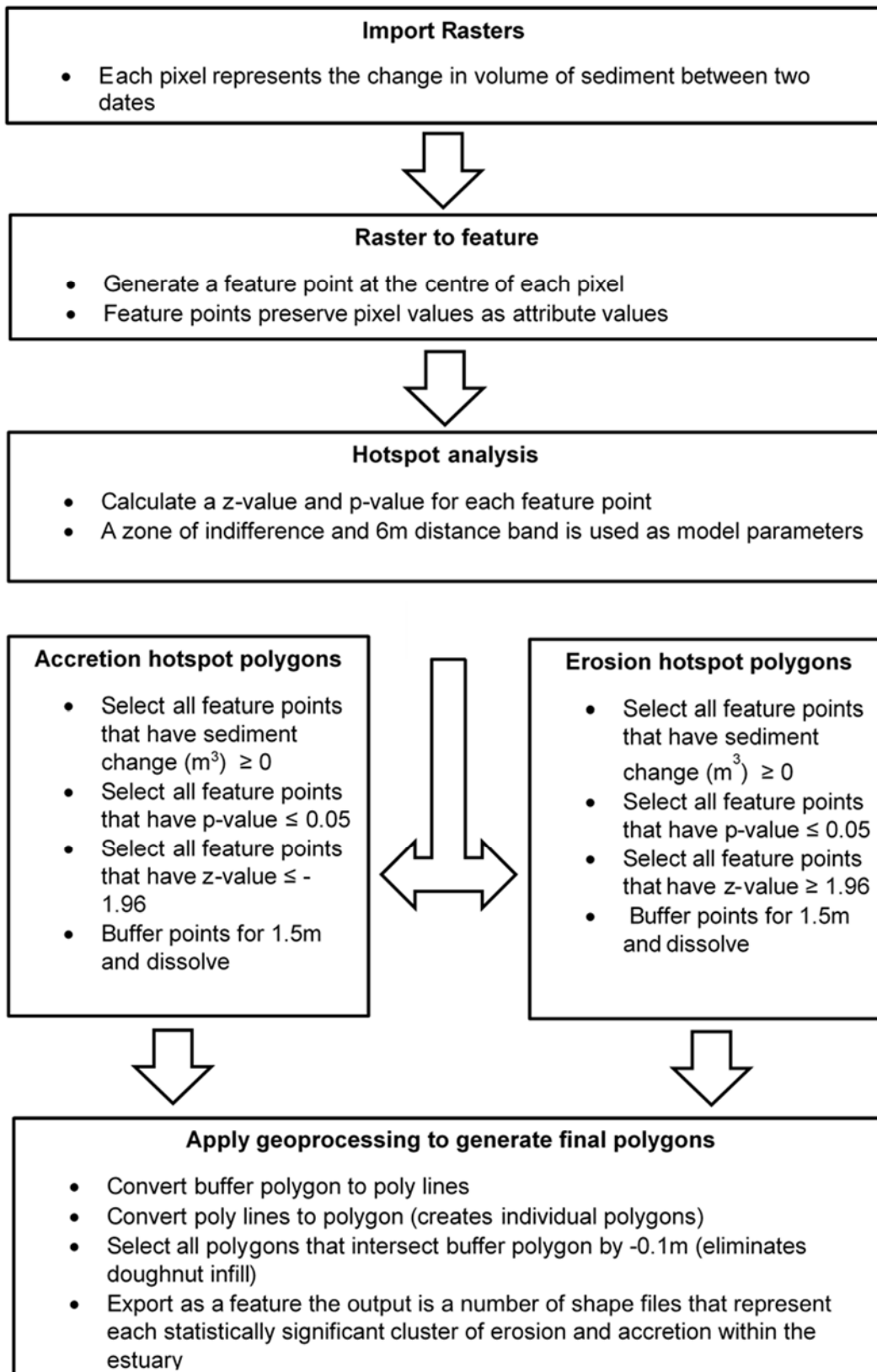


Figure 5.5 This schematic flow diagram shows the stages incorporated into the clustering analysis which used the ArcGIS suite to conduct processing.

Two ArcGIS process models were constructed using the model builder tool to subdivide the processing chain (figure 5.5). This was a precaution as the data processing took several weeks of computing time and consequently the risk of the computers crashing mid process was high. The first model imported the RODLOD, converted it to a feature class file and began the clustering analysis via the Getis-Ord local statistic hotspot analysis. The results of the analysis were added to the feature class attribute table.

The second model used the calculated z-values and p-values to cluster the data through a combination of attribute and spatial selection criteria. Geoprocessing techniques were then applied to the clustered feature points to generate a bounding polygon and this polygon was converted to a number of spatially distinct features with geometric properties added to their respective attribute tables.

The clustering methodology provided a robust spatial statistics approach to interpreting change within the estuary that overcame potential subjectivity associated with user interpretation of the rasters of difference. The polygons generated can be used in conjunction with the source raster and zonal statistic functions to determine the magnitude of erosion and accretion events.

5.3.4. Volume determination

The rasters of difference produced by sections 5.3.2 and the sediment morphological feature bounding geometries produced by the cluster analysis in section 5.3.4 provided appropriate tools to calculate the change in volume of sediment between years. These tools also allowed the physical features of the sediment movements to be calculated as follows.

Using the zonal statistics tool in ArcGIS and the intertidal sediment mask and saltmarsh mask as a defined search area, zonal statistics were calculated, this represented the sum, mean and number of pixels present within the defined search area. This was also applied using the clustering analysis bounding geometries, all results were exported to Microsoft® Excel files, and an R script was written to aggregate all data together as tables.

A limitation of this analytical approach was the spatial discontinuity of the data, which had implications for the sum of change measurements and resulted in some uncertainty in assertions of temporal trend, as it was not appropriate to compare volumes of change. To reduce this introduced error all measurements are reported

with regard to the surveyed area and the figures produced highlight localised change so that the interpretation was not overreaching. This emphasis was also placed on averaged per pixel values, which are not subject to this discontinuity issue as they are an average and can thus be compared to other time points.

5.4. Results

The nature of sediment change within the Ribble estuary is described with reference to the five datasets outlined at the start of section 5.3. Only figures that are relevant to the narrative are included in this section, those that are not given here are presented in Appendix 2. The full print out of the zonal statistics can also be found in Appendix 2 with relevant excerpts summarised in this section.

5.4.1. 1999 – 2009 full estuary coverage

The 1999 and 2009 LiDAR data represent almost full estuary coverage, absent only for some areas of the Ribble sand banks in the outer estuary. The sand banks represent stores of coarse grained sediment that as previously established (chapter 3.3.2) have a negative correlation with estuarine radiogenic contamination. Therefore, for the purposes of conducting a sediment budget for the Ribble estuary, which will ultimately be used to look at contaminant movement (chapter 6), the available data were regarded as sufficient.

Between 1999 and 2009 the data analysed show that generally erosion is dominant between these two survey dates. Figure 5.6 shows the full map of sediment movements, the outer sandbanks were dominated by trends of substantial sediment movement, it is here that many of the large sediment volume changes were detected as these large sand banks migrated across the estuary. The mudflats were a patch work of erosion and accretion with the Lytham mudflats showing a general trend of accretion. The saltmarshes showed a mix of accretion and erosion in the main creeks with erosion being a dominant factor in the smaller branches of creeks.

The Ribble saltmarshes showed erosion overall (-0.3 m^3), this means that from 1999 - 2009 the volume of saltmarsh declined on average by $0.3 \text{ m}^3/\text{m}^2$ (table 5.2). The saltmarsh erosion is shown in figure 5.6 and characterised by front of marsh erosion; this is where the front of the saltmarsh is eroded resulting in the retreat of the saltmarsh by a few meters. There was also wide spread creek based erosion, which takes the form of lateral erosion where creeks widen their channel causing bank collapse by

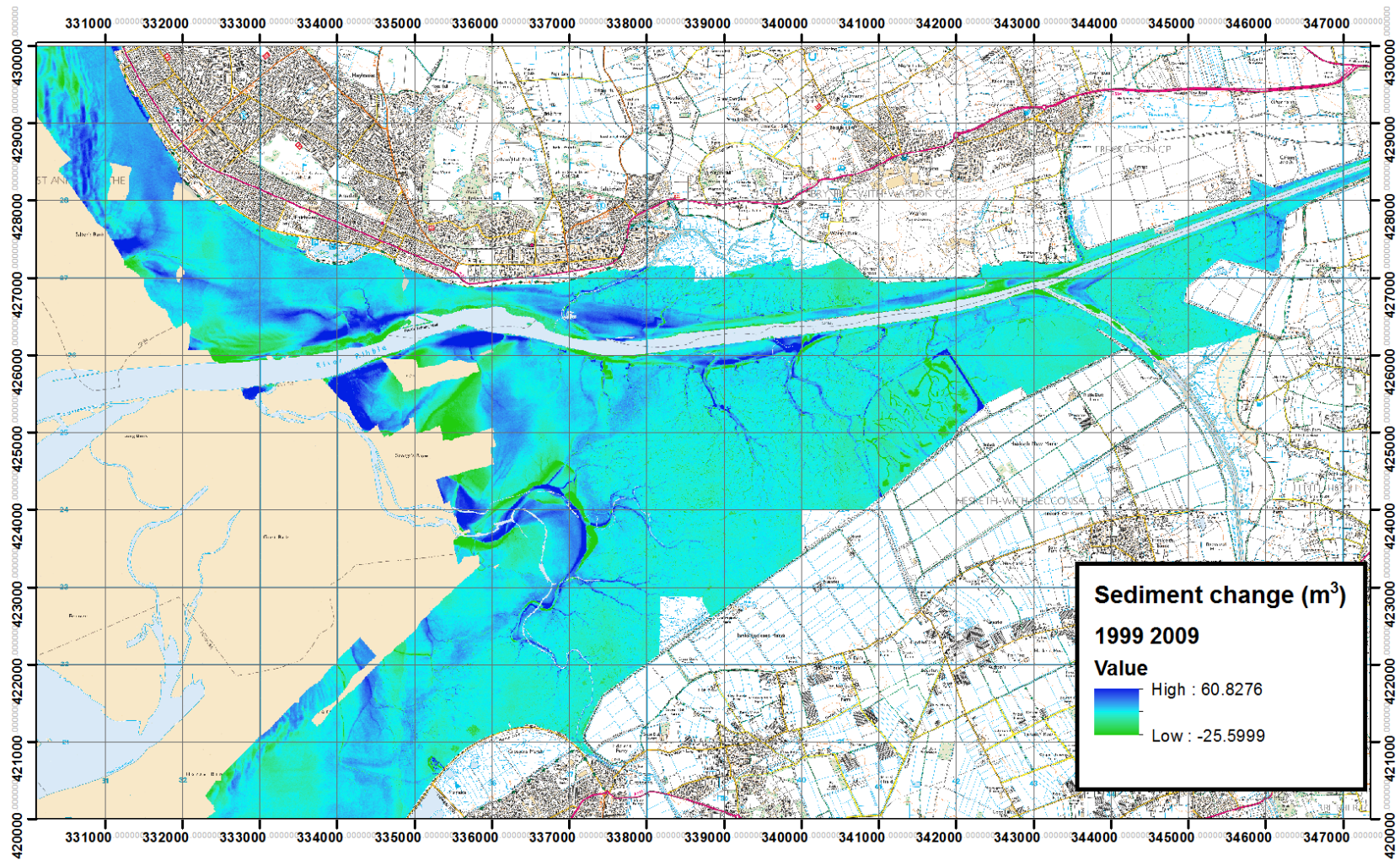


Figure 5.6 Map of change in volume (m^3) of sediment from 1999 – 2009 for the Ribble estuary, each pixel has an area of 4 m^2 .

Table 5.2 Summary statistics for the movement of sediment in the Ribble estuary between 1999 and 2009.

| Description | Total change (m ³) | Survey area (m ²) | Average change (m ³ /m ²) |
|---|--------------------------------|-------------------------------|--|
| Significant change in Saltmarshes | -5.6E+06 | 1.9E+07 | -0.30 |
| Significant change in Mudflats | -2.5E+06 | 1.5E+07 | -0.17 |
| Total change in Saltmarshes | -5.9E+06 | 2.4E+07 | -0.24 |
| Total change in Mudflats | -2.7E+06 | 2.3E+07 | -0.11 |
| Significant change in realignment site | -6.3E+05 | 1.5E+06 | -0.42 |
| Total change in realignment site | -6.4E+05 | 1.7E+06 | -0.38 |
| Significant change in Saltmarshes minus realignment | -4.9E+06 | 1.7E+07 | -0.29 |
| Total change in Saltmarshes minus realignment | -5.3E+06 | 2.2E+07 | -0.23 |

undercutting (Figure 5.6). The creeks also showed a pattern of increasing their length by eroding deeper in to the interior of the saltmarsh.

The impact of the Hesketh Outmarsh realignment scheme is considered in table 5.2 to determine if this scheme was skewing the saltmarsh erosion figures. The data showed that the Hesketh site accounted for 11.3% of the saltmarsh erosion during the 10-year period. Excluding the realignment scheme contribution, resulted in the long-term trend in saltmarsh erosion changing only marginally – a reduction to 0.29 m³/m².

The Ribble mudflats showed an average trend of erosion (-0.17 m³/m²), though erosion here was nearly half that of the average saltmarsh erosion. Mudflat erosion is characterised by reworking of large sediment features such as sand bars and mudflat features found near saltmarsh creeks. Furthermore, a section of the Ribble training wall appears to have collapsed in the mid-section of the Ribble resulting in the erosion of a large section of mudflat. There is also considerable variability at the Ribble confluence with its tributary the Douglas. The Douglas has seen large movements of mudflat features over the ten-year period probably caused by fluctuations in the flow of the two rivers. These changes can be seen in the LiDAR data. It is worth also noting that the Lytham mudflats, which were surveyed in chapter 3, showed a trend of sediment accumulation.

Table 5.2 presents the significant change values and the total values for the different sites and sediment types in the Ribble estuary. The total values presented are the sum of pixel values without using the limit of detection method. The significant change values do use the limit of detection method, which can be seen to skew the data towards higher values as it filtered out values of slight change which fell within the associated error of the LiDAR product. This translated to 23.2% of the saltmarsh data being filtered out reducing the volume of sediment being eroded by 5.5%. The change in mudflats was more subtle, with 37% of the data being filtered out, reducing the volume estimate by 6.5%.

The Ribble estuary had a general trend of sediment erosion from the saltmarshes which are not accounted for by subsequent accumulation within the mudflats suggesting that there is a trend of sediment transfer out from the estuary during 1999 to 2009.

5.4.2. 1999 – 2015 mid estuary coverage

The mid estuary area had repeat coverage of LiDAR data for the years 1999, 2007, 2009, 2010, 2011, 2014 and 2015, this provided additional time points between 1999 – 2015. Therefore, it was possible to construct six pairs of data that chronicled sediment movement within this area to see whether there was a general trend of erosion at all time points as indicated by the 1999 to 2009 data. The mid estuary contained most (> 70%) of the sediments that were expected to be enriched in contaminants based on the findings of chapter 3.3.2, therefore this subsection allows the study of the movement of the Ribble's most contaminated sediment. These data are presented below as full page images of the calculated raster of differences, which show where sediment was lost or accumulated between the date ranges.

For the period 1999 to 2007, as shown in figure 5.8 and reported in table 5.3, the average trend was of significant erosion at the rate of $-0.3 \text{ m}^3/\text{m}^2$ for the saltmarshes and $-0.32 \text{ m}^3/\text{m}^2$ for the mudflats over the 8-year time period. Mudflat erosion occurred predominantly along the north bank of the main channel near the Warton aerodrome as well as those mudflats near the confluence point of the Ribble and Douglas. In contrast to the patterns of erosion at the north bank, the south bank mudflats accumulated substantial amounts of sediments and the mudflats on the south of the river that are located closer to the mouth of the estuary experienced less erosion than those further upstream.

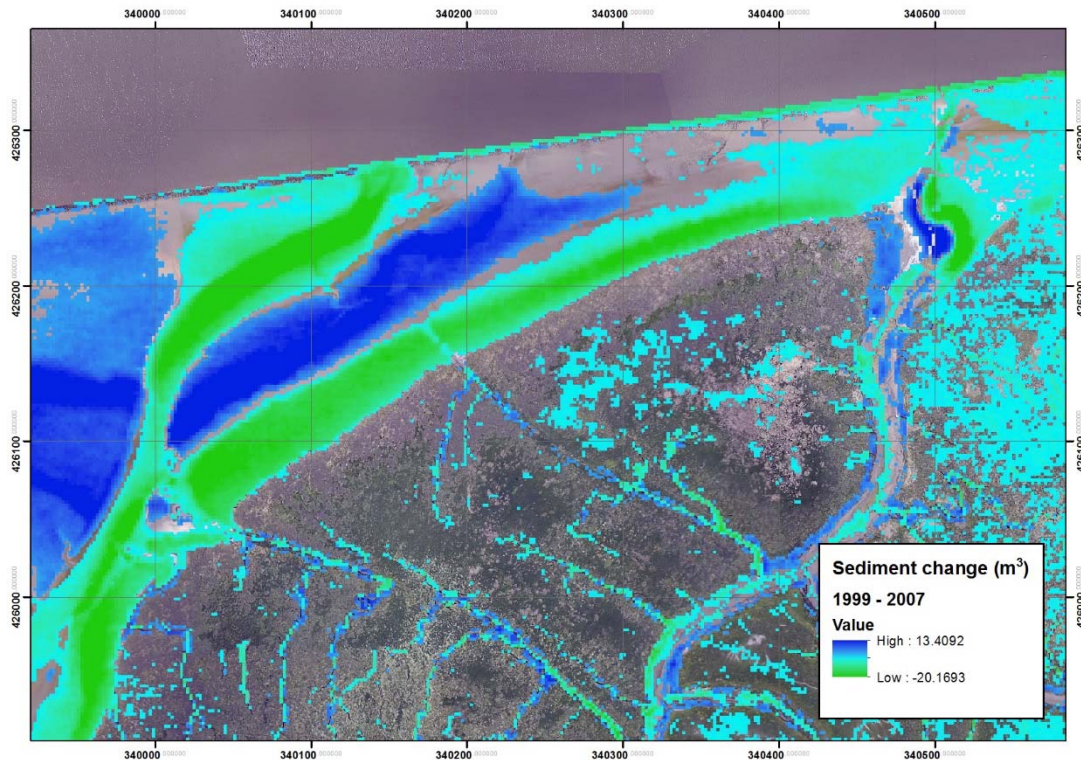


Figure 5.7 Frontal saltmarsh erosion resulting in a retreat of the saltmarsh extent for an area of the Hesketh Outmarsh saltmarshes (OSGB; 340000,426000).

Saltmarsh erosion was characterised by the retreat of the marsh face due to erosion, a good example of this is seen in figure 5.7. As a result of extensive erosion likely through undercutting, the front of the saltmarsh marsh has receded by up to 20m in this particular case, this type of erosion was observed at multiple sites within these data. The surface of the marsh accumulated sediments predominantly near the creek systems, this has the appearance of a darkened blue halo around the creeks. The creeks were diverse in terms of their erosion with accretion being seen generally but with some creeks clearly eroding deeper into the saltmarsh while others showed signs of infilling.

The trend of erosion was still present in the 2007 – 2009 data set although the rates declined slightly in the saltmarshes ($-0.27 \text{ m}^3/\text{m}^2$) and substantially for the mudflats ($-0.13 \text{ m}^3/\text{m}^2$) (table 5.3). The mudflats again showed intense erosion at the confluence of the Douglas and Ribble, and at the Warton marshes. It is suspected that the Warton marshes mudflat erosion (based on its location (figure 5.6 339000, 426000) and the geometry of the event) were a partial collapse of the Ribble training wall. The middle mudflats near the Warton Aerodrome showed a general trend of accretion throughout this period.

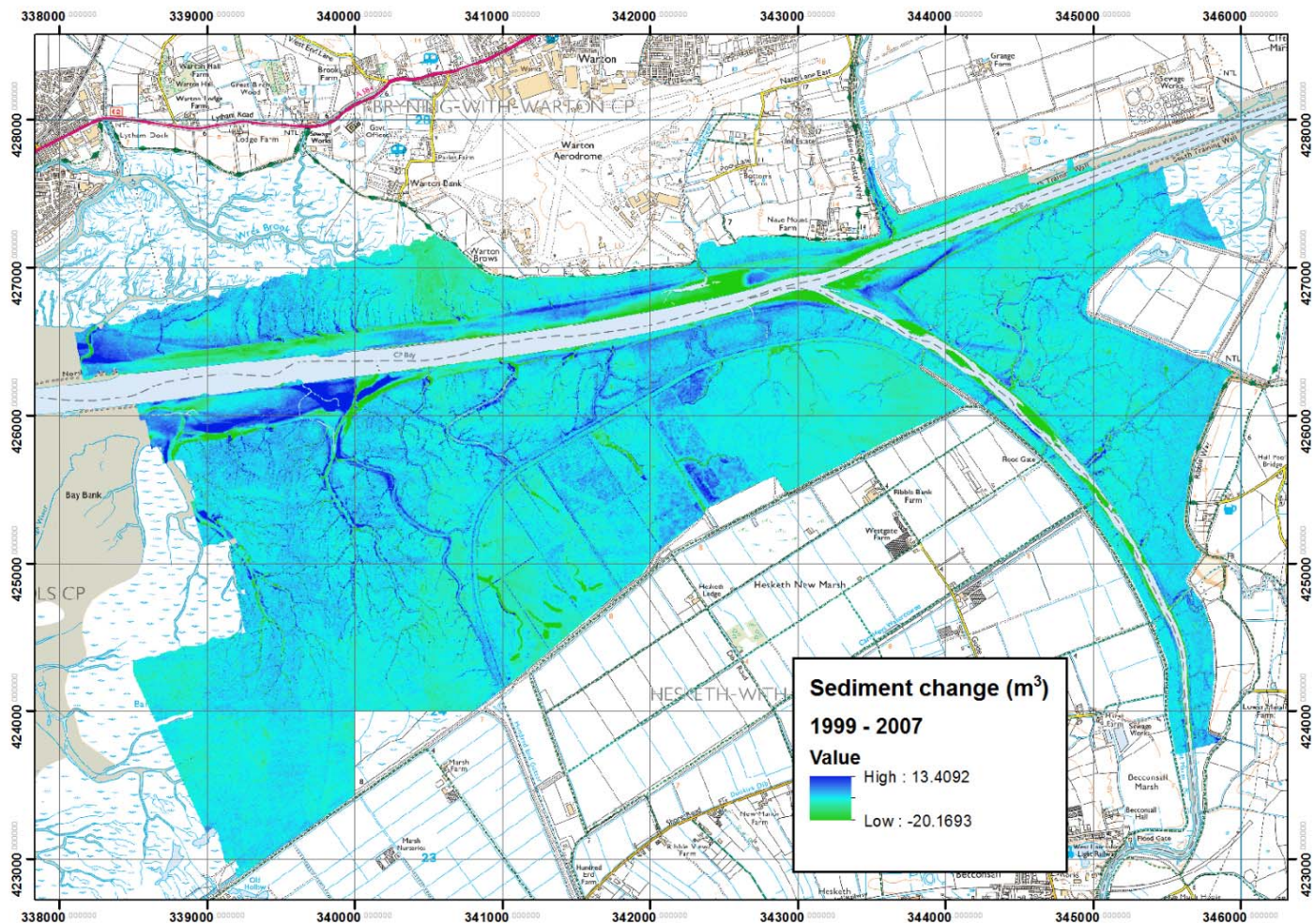


Figure 5.8 Map of change in volume (m³) of sediment from 1999 – 2007 for the mid Ribble estuary, each pixel has an area of 4 m².

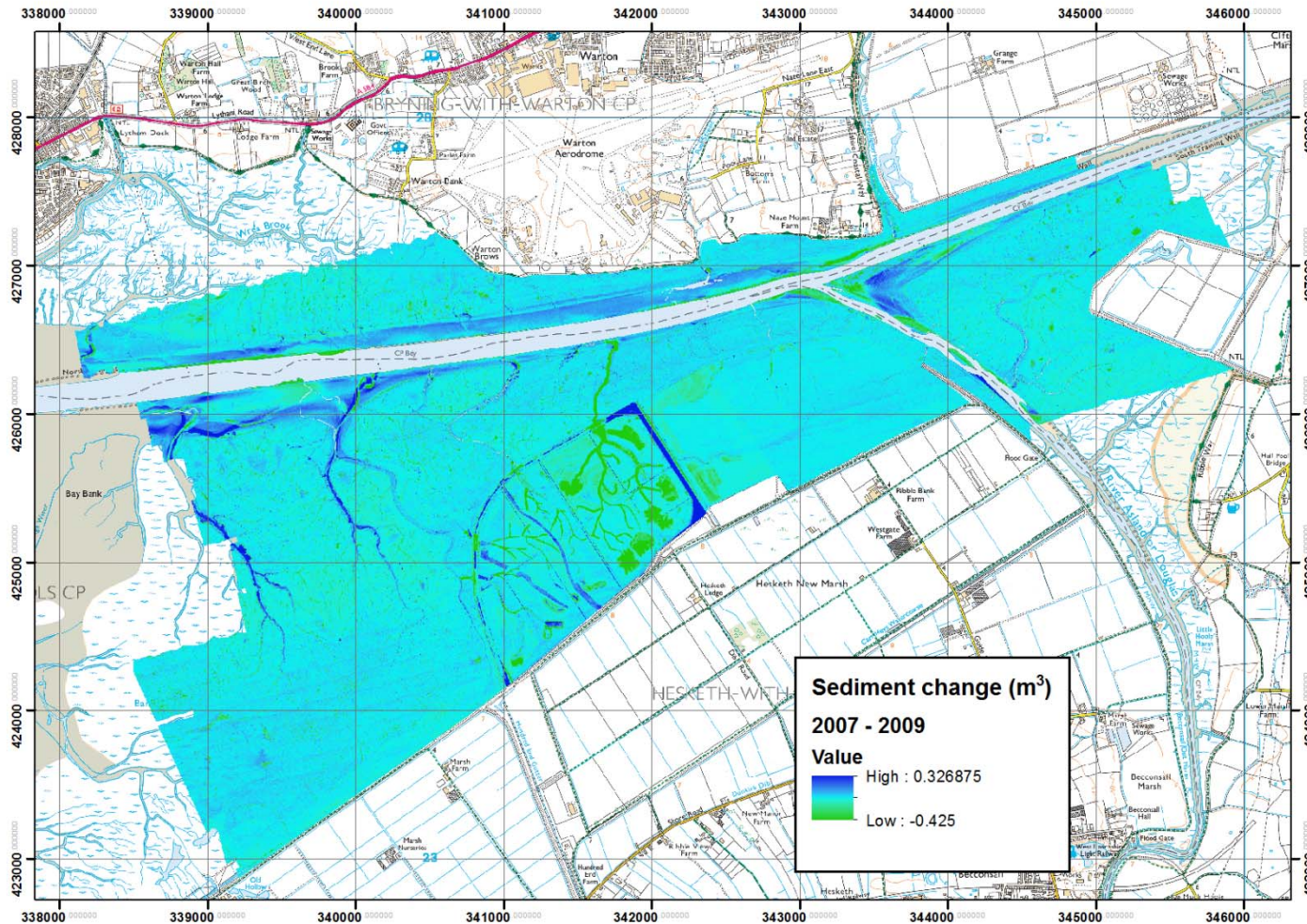


Figure 5.9 Map of change in volume (m^3) of sediment from 2007 – 2009 for the mid Ribble estuary, each pixel has an area of $0.0625 m^2$.

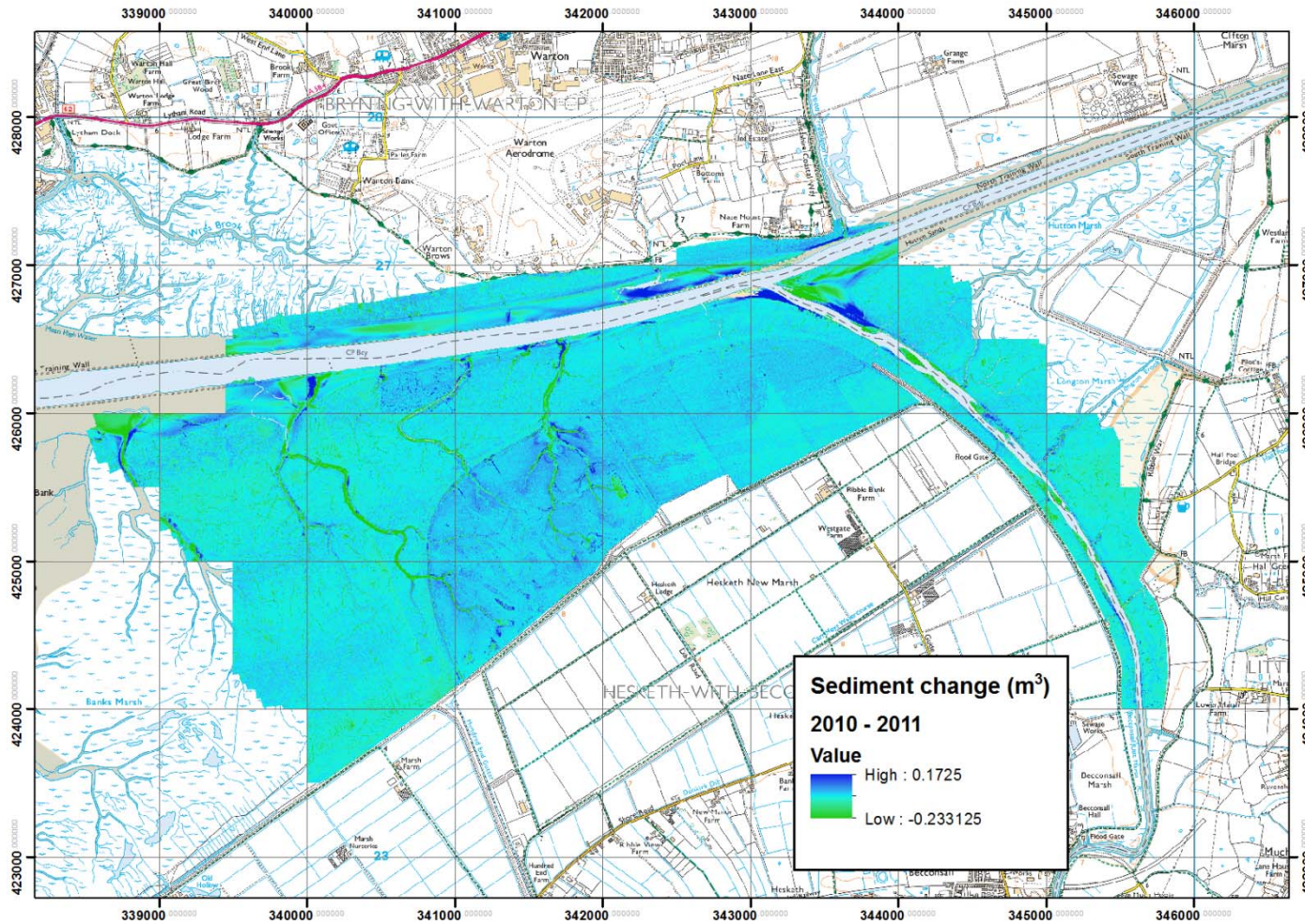


Figure 5.11 Map of change in volume (m³) of sediment from 2010 – 2011 for the mid Ribble estuary, each pixel has an area of 0.0625 m².

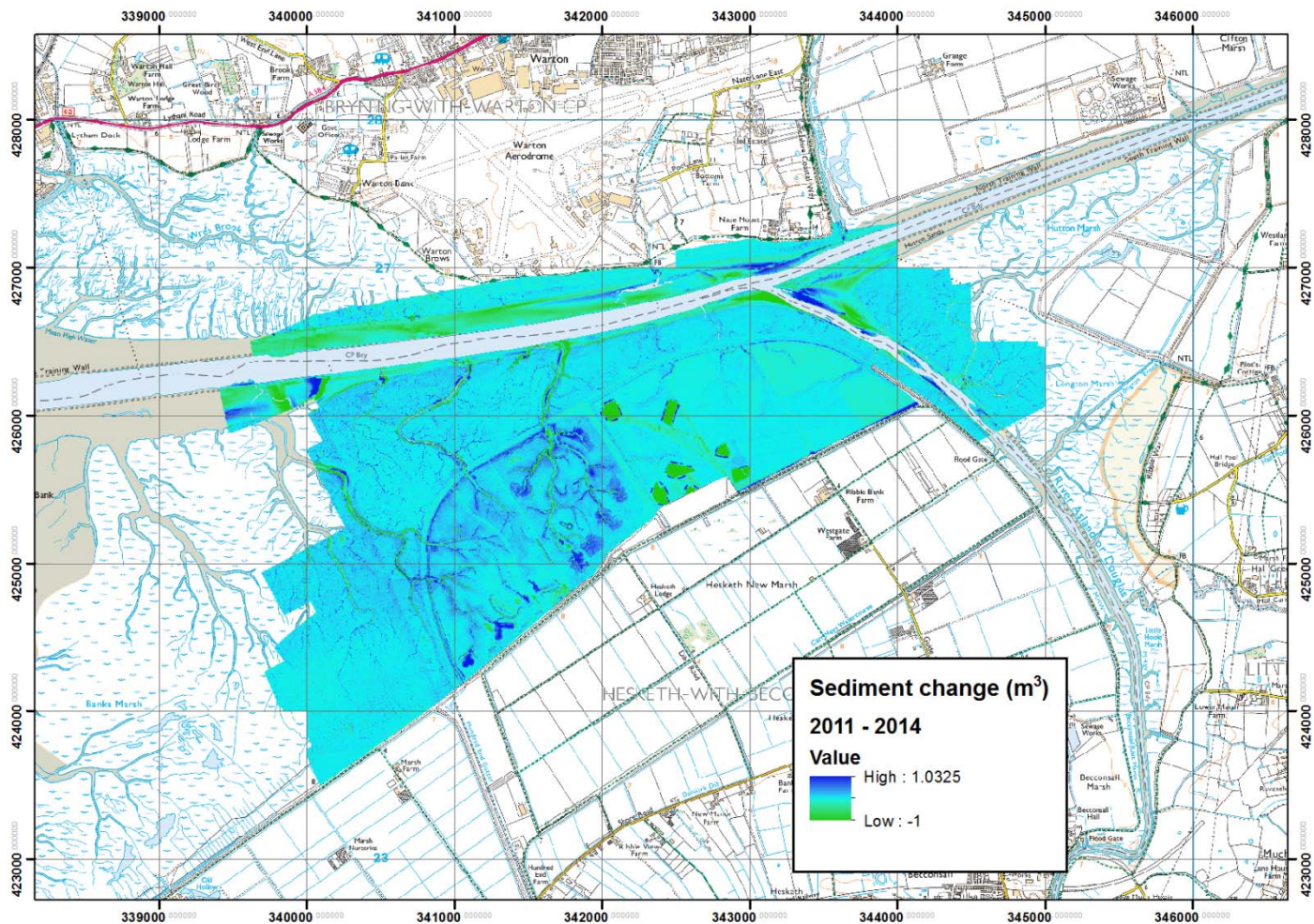


Figure 5.12 Map of change in volume (m³) of sediment from 2011 – 2014 for the mid Ribble estuary, each pixel has an area of 0.25 m².

Table 5.3 Ribble mid estuary summary statistics for 1999 – 2015 for the significant change data using the limit of detection method. Total change was derived from the sum of all pixels. Survey area was the geometry of the survey area and was calculated independently of the volume determination.

| Year range | Habitat | Total change (m³) | Survey area (m²) | Average change (m³/m²) |
|--------------------|----------------|-------------------------------------|------------------------------------|---|
| 1999 - 2007 | Saltmarsh | -1.4E+06 | 4.7E+06 | -0.30 |
| 1999 - 2007 | Mudflat | -5.3E+05 | 1.7E+06 | -0.32 |
| 2007 - 2009 | Saltmarsh | -7.1E+05 | 2.6E+06 | -0.27 |
| 2007 - 2009 | Mudflat | -1.2E+05 | 9.1E+05 | -0.13 |
| 2009 - 2010 | Saltmarsh | 4.3E+05 | 1.7E+06 | 0.25 |
| 2009 - 2010 | Mudflat | 1.6E+05 | 8.4E+05 | 0.19 |
| 2010 - 2011 | Saltmarsh | -4.5E+04 | 5.5E+05 | -0.08 |
| 2010 - 2011 | Mudflat | -7.6E+04 | 6.6E+05 | -0.11 |
| 2011 - 2014 | Saltmarsh | 1.5E+05 | 1.2E+06 | 0.12 |
| 2011 - 2014 | Mudflat | -1.2E+05 | 9.3E+05 | -0.12 |
| 2014 - 2015 | Saltmarsh | 5.5E+04 | 3.9E+05 | 0.17 |
| 2014 - 2015 | Mudflat | 2.4E+04 | 3.4E+05 | 0.07 |

Table 5.4 Ribble mid estuary summary statistics for 1999 – 2015. These are total values and use no limit of detection. Total change is equal to the sum of all pixels. Survey area is the geometry of the survey area and is calculated independently of the volume determination.

| Year range | Habitat | Total change (m³) | Survey area (m²) | Average change (m³/m²) |
|--------------------|----------------|-------------------------------------|------------------------------------|---|
| 1999 - 2007 | Saltmarsh | -2.3E+06 | 1.3E+07 | -0.18 |
| 1999 - 2007 | Mudflat | -5.6E+05 | 3.0E+06 | -0.18 |
| 2007 - 2009 | Saltmarsh | -1.4E+06 | 1.2E+07 | -0.12 |
| 2007 - 2009 | Mudflat | -1.4E+05 | 2.9E+06 | -0.05 |
| 2009 - 2010 | Saltmarsh | 9.7E+05 | 9.0E+06 | 0.11 |
| 2009 - 2010 | Mudflat | 2.4E+05 | 2.2E+06 | 0.11 |
| 2010 - 2011 | Saltmarsh | 2.2E+05 | 9.0E+06 | 0.02 |
| 2010 - 2011 | Mudflat | -2.7E+04 | 2.3E+06 | -0.01 |
| 2011 - 2014 | Saltmarsh | 4.3E+05 | 7.0E+06 | 0.06 |
| 2011 - 2014 | Mudflat | -1.1E+05 | 1.8E+06 | -0.06 |
| 2014 - 2015 | Saltmarsh | 8.9E+04 | 4.7E+06 | 0.02 |
| 2014 - 2015 | Mudflat | 8.3E+03 | 1.3E+06 | 0.01 |

Between 2007 -2009 the saltmarshes showed a uniform trend across all areas at the mid estuary with erosion in the small creeks and accumulation in the larger creeks. The most striking change shown in figure 5.9 was the excavations at the Hesketh Outmarsh management realignment site. As discussed in section 5.4.1, these excavations accounted for 11.3% of sediment movements in the saltmarshes during this time period. The Hesketh managed realignment scheme will be the focus of section 5.4.5 where these fine scale changes will be considered further.

The changes between 2009 and 2010 were dominated by substantial accretion in both sediment categories, the mudflats showed accretion at the rate of $0.19 \text{ m}^3/\text{m}^2$ while the saltmarsh saw an average accretion of $0.25 \text{ m}^3/\text{m}^2$ (table 5.3). The mudflats also saw large scale accretion at the confluence of the Douglas and Ribble though throughout the rest of the mid estuary the mudflats were a mosaic patchwork of zones of accretion and erosion.

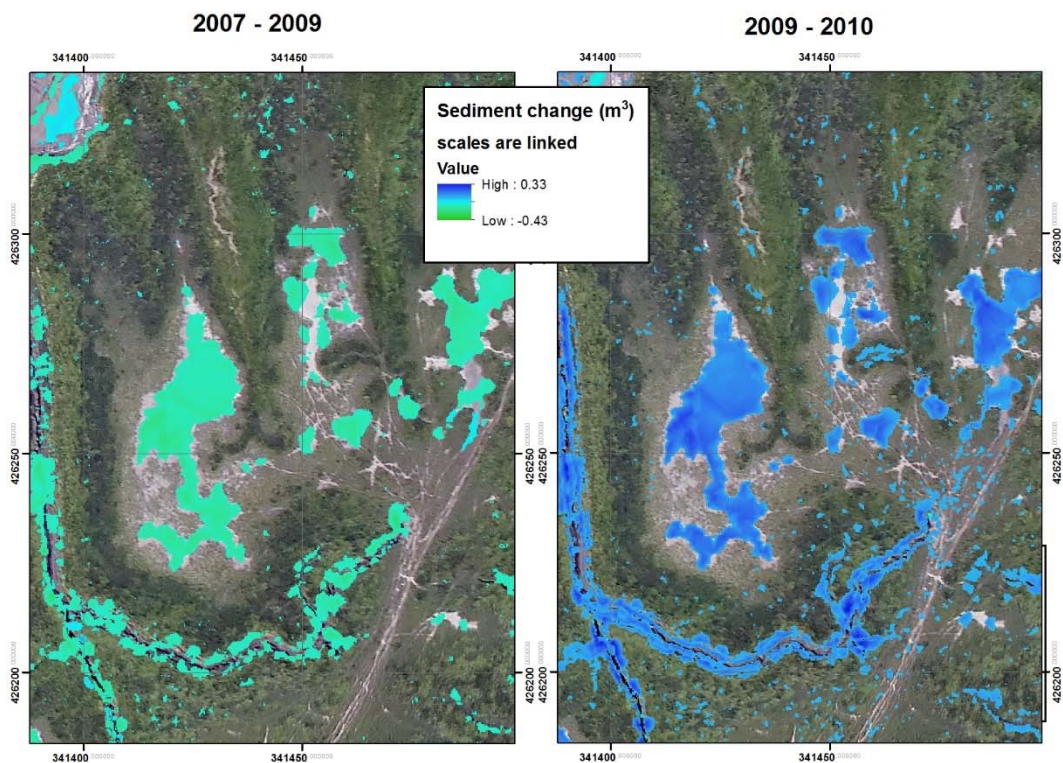


Figure 5.14 A fixed extent comparison for the periods 2007 – 2009 and 2009 – 2010. The scale used for the colour ramp is the same for both data sets and only significant change is displayed through the application of a limit of detection. The areas shown represent saltmarsh creeks and surface marsh ponds.

The saltmarshes showed a distinct accretion trend across all of the mid estuary between 2009 and 2010. The accretion occurred in the small creeks (figure 5.10, where the smaller creeks are shown as a blue lines). The three main creeks that are connected to the Hesketh site were dominated by erosion from the sides and bottoms of these creeks. On the marsh surface, there were signs of vertical accretion. There was for example, a distinctive infilling of marsh ponds (figure 5.15) compared with figure 5.10 which showed the presence of the marsh ponds at grid reference 340500,426700. Figure 5.14 highlights this contrast with a side by side comparison for

different time periods, the figure demonstrates that the mid Ribble estuary has shifted from a general trend of erosion to a general trend of accretion.

Erosion returned to the mid estuary during 2010 and 2011 with $-0.8 \text{ m}^3/\text{m}^2$ for the saltmarshes and $-0.11 \text{ m}^3/\text{m}^2$ for the mudflats (table 5.3). However, the total values (table 5.4) indicated that the average change per m^2 (i.e. without the limit of detection consideration), for saltmarsh was just $0.02 \text{ m}^3/\text{m}^2$ and mudflat value of $-0.01 \text{ m}^3/\text{m}^2$. This suggests that between 2010 and 2011 there was no real significant change. Figure 5.11 shows this visually. The mudflats showed a mix of accretion and erosion events spread across the mudflats at this site. Within the saltmarshes for 2010-2011 the creeks changed from accreting as seen in 2009 – 2010 to eroding, with most of this occurring in the three main creeks attached to the managed realignment site.



Figure 5.15 An example of a marsh pond on the Ribble saltmarshes. Marsh ponds are bare patches of sediment that retain water after the ebb tide. (Photo taken of the New marsh site in 2015)

2011 – 2014 was the only time period in which the saltmarshes and mudflats differed in terms of accreting or eroding regimes, with the mudflats eroding by $-0.12 \text{ m}^3/\text{m}^2$ and the saltmarshes accreting by $0.12 \text{ m}^3/\text{m}^2$ (table 5.3). The majority of the mudflat erosion occurred from the north bank of the mid estuary. For example, figure 5.12 shows a long band of mudflat that has eroded between the 2011 and 2014. Along the south bank mudflats there was also a general trend of erosion, though there are intermittent patches of accretion near the mouths of the three large creeks.



Figure 5.16 Photograph of a creek that was undercutting the sides of the saltmarsh on either side at the Hesketh Outmarsh site (Photo taken of the New marsh site in 2015).

The saltmarshes between 2011 and 2014 accumulated large amounts of sediment within ($0.12 \text{ m}^3/\text{m}^2$) the managed realignment site. The sediment was deposited on the marsh surface in the immediate vicinity of the major creeks in this area. The three main creeks that connect the Hesketh Outmarsh site to the wider estuary showed erosion was dominant at the sides of the creeks, which were cutting into the marsh sides with the middle of these creeks accumulating sediment. Figure 5.16 shows an example of a creek at the Hesketh saltmarshes that is in the process of undercutting the sides of the saltmarsh on either side, this is the type of process occurring at these creeks.

2014 -2015 was marked by a return to accretion with $0.17 \text{ m}^3/\text{m}^2$ seen in the saltmarshes and $0.07 \text{ m}^3/\text{m}^2$ for the mudflats (table 5.3), these values were heavily influenced by extreme events as the table 5.4 values showed much reduced values of

0.02 m³/m² for the saltmarshes and 0.01 m³/m² for the mudflats. There was a large amount of accretion seen near the main channel, and some large accretion events were observed at the confluence of the Ribble and Douglas (figure 5.13). Within the saltmarshes at this time a complex mix of accretion and erosion events are occurring.

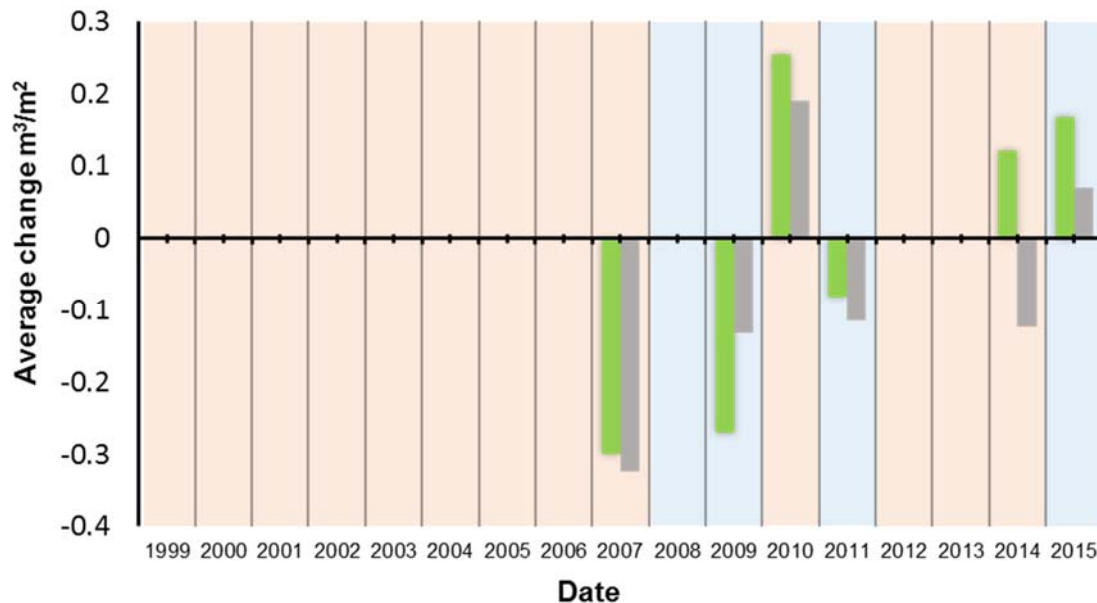


Figure 5.17 The mid estuary sediment significant change data is shown as the average volume of change per 1 m² area. Faded blue and orange boxes are used to represent the time period from which each data set is derived. The Green (saltmarsh) and Grey (mudflat) bars are placed at the end of the time period as the volume of change is relative to the start and end of the time period.

Between 1999 and 2014 the mid estuary of the Ribble experienced a great deal of variability in the sediment deposits of the estuary (Figure 5.17). The mudflats experienced substantial changes in this time period with the mudflat surface often being a patch work of accretion and erosion events. These events were characterised as elongated shapes that often ran parallel to the main channel. Saltmarsh erosion was dominated by erosion and accretion in the creeks that flipped between eroding and accreting between different time periods although the main creeks did show some consistency in that they were predominantly being eroded.

The Lytham beach site is a sand dominated environment. Four time points beginning in 1999 and ending in 2014 were constructed from the available LiDAR data for this area. Figure 5.18 is an enhanced image of the 2013 to 2014 data and showed a typical example of the type of sediment movement observed at the Lytham beach site. This site can be characterised as having large sand bars that run parallel to the immediate coast. The dominant mechanism of change appears to be sandbar migration towards the mouth of the estuary and the nearshore. The sandbars appeared to diminish in size as distance from the near shore reduced. The pattern of layered erosion and accretion shown in figure 5.18 does suggest that the sediment in this area may be moving towards the coast.

Table 5.5 Lytham beach site summary statistics for four data sets ranging from 1999 – 2014. Total change was equal to the sum of all pixels. Survey area was the geometry of the survey area and was calculated independently of the volume determination.

| Year range | Total change (m³) | Survey area (m²) | Average change (m³/m²) |
|--------------------|-------------------------------------|------------------------------------|---|
| 1999 - 2005 | 2.3E+06 | 1.4E+06 | 1.56 |
| 2005 - 2009 | -9.6E+05 | 8.7E+05 | -1.11 |
| 2009 - 2013 | 9.5E+04 | 5.5E+05 | 0.17 |
| 2013 - 2014 | 4.1E+04 | 5.2E+05 | 0.08 |

The data contained in Table 5.5 are a summation of the individual zonal statistics data calculated for each raster. They show a varied picture of sediment movement between 1999 and 2014. The first time point 1999 – 2005 showed an average increase of 1.56 m³/m² of sediment over the 6-year time period assuming an even rate of accumulation this equates to 0.26 m³/m² of deposition per year. In contrast the second time point had a negative average change value suggesting that for these data erosion was dominant. The average change between 2005 and 2009 was -1.11 m³/m² which, assuming an even rate of erosion, equated to a very similar -0.28 m³/m² of erosion each year. The rate of sediment movement was much reduced for the time period 2009 -2013 with average deposition being 0.17 m³/m² which gave an annual rate of deposition of 0.04

m^3/m^2 . From 2013 – 2014 the annual deposition was $0.08 \text{ m}^3/\text{m}^2$ almost double the presumed annual rate from the preceding data set.

5.4.4. Localised site 2 – Mudflats

This section focused on a subset of the mid estuary mudflat area to explore the nature of morphological change in the mudflat sediments. The data shown give significant movement (m^3) values, which are data that has exceeded the limit of detection. The focus is on the Warton mudflats that are located on the north bank of the Ribble's main channel and the Hesketh mudflats located on the south bank of the Ribble main channel.

1999 – 2007 represents a long-term trend in sediment movement with 8 years between the data sets. Figure 5.18 shows that the north bank mudflats have eroded over this time period; this has occurred across all of the mudflats in the eastern extent of the study site, though in the west the change was not significant. There were areas of accretion in the north bank mudflats located at the mouths of a number of creeks. The south bank accreted substantial amounts of sediment around the mouth of a large creek. The large areas of erosion at the south bank site were in fact saltmarsh erosion, with the marsh retreating by up to 20 meters at this site. The north and south bank can be said to be substantially different in terms of their sediment movement between 1999 and 2007.

2007 -2009 highlights the spatial variability in sediment movement, figure 5.20 shows on the north banks areas of erosion siting side by side with areas of accretion. The mudflats for this time period were composed of a complex patchwork of accretion and erosion events. The impact of the saltmarsh creeks on the mudflats is seen in this dataset although in this case it was erosion associated with the saltmarsh creek mouths opposed to the previous accretion seen between 1999 and 2007.

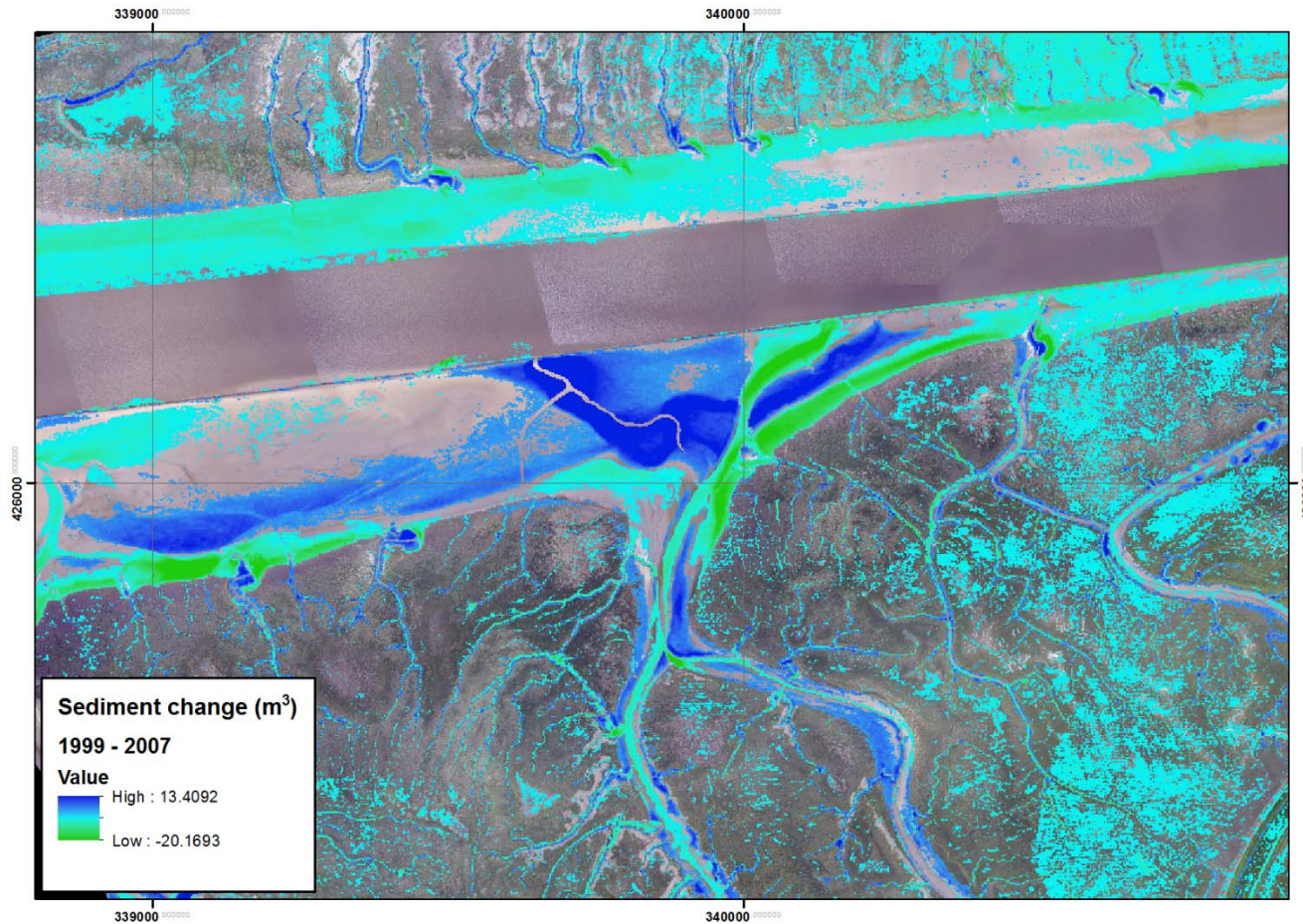


Figure 5.19 Map of change in volume (m^3) of sediment from 1999 to 2007 for the mid Ribble estuary, each pixel has an area of 4 m^2 . These data have had a limit of detection applied to them so that only significant movement is shown.

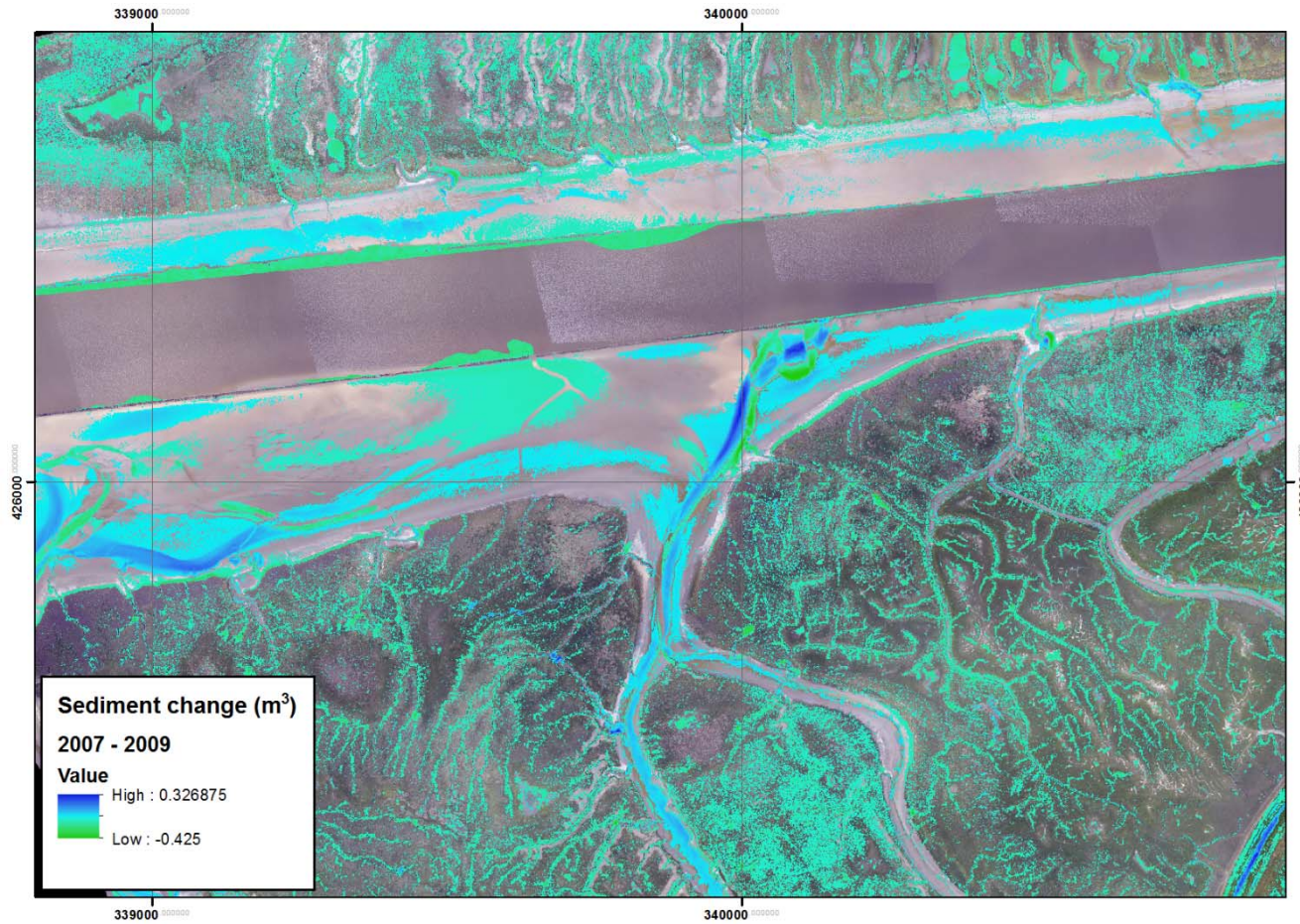


Figure 5.20 Map of change in volume (m³) of sediment from 2007 to 2009 for the mid Ribble estuary, each pixel has an area of 0.0625 m². These data have had a limit of detection applied to them so that only significant movement is shown.

5.4.5. Localised site 3 – Hesketh Outmarsh

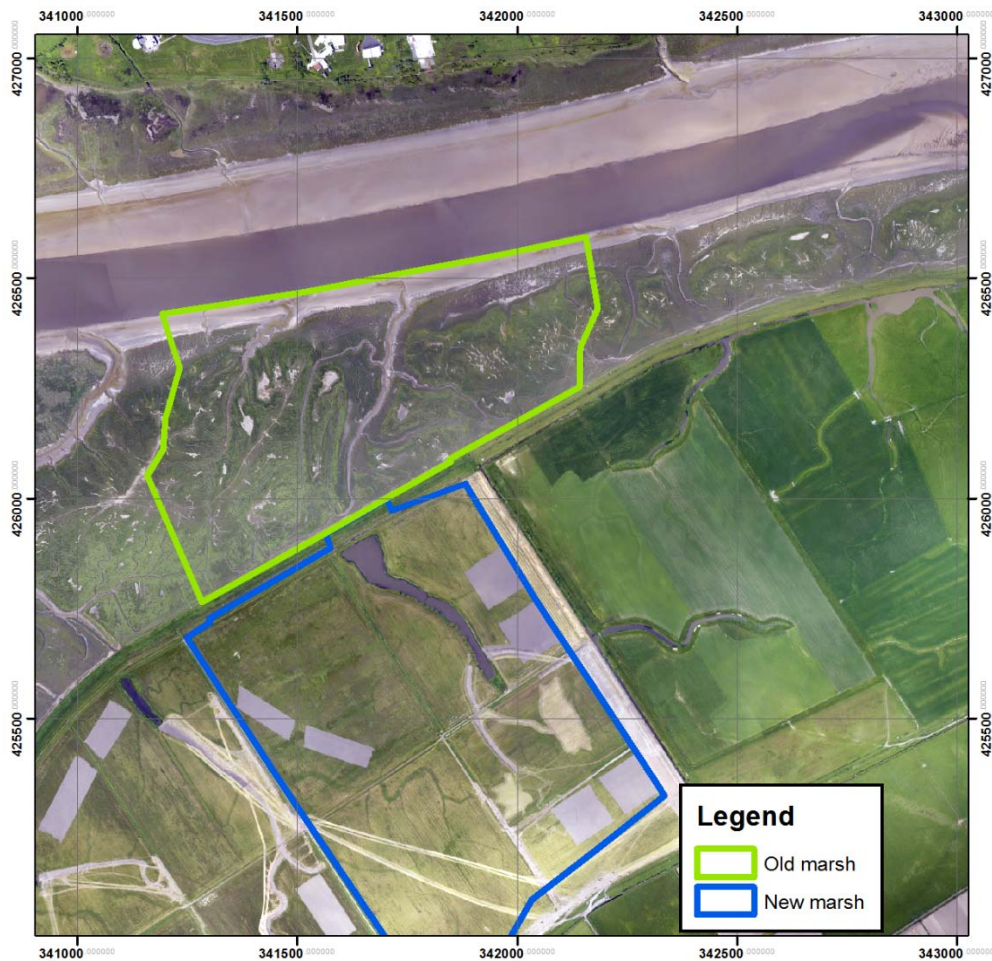


Figure 5.21 Overview of the mid estuary localised site Hesketh Outmarsh. The site is split into an area of mature saltmarsh designated Old marsh and an area of emergent saltmarsh designated New marsh.

Results are presented here for an analysis of the long-term trends seen in the Hesketh Outmarsh managed realignment site, data were available for the years 1999, 2007, 2009, 2010, 2011, 2014 and 2015. The inner site is referred to as the new marsh as it represents new saltmarsh formation and the outer site beyond the sea wall is referred to as the old marsh as it consists of older mature saltmarsh (figure 5.21). Two sets of data are presented to detail the sediment changes that have occurred in response to this anthropogenic disturbance event. Volume of change values cited here were calculated for this local site alone i.e. only data within the localised site respectively (new marsh and old marsh) are used. These data are used in the contaminant analysis in chapter 6.

Figure 5.22 shows the Hesketh Outmarsh new marsh site post realignment, the strong green outline of the trenches that have been excavated to re-establish the connection of the saltmarsh to the estuary are distinct. These excavations are characterised by a branching network of creeks that were excavated and a deepening of the central creek that runs through the old saltmarsh site near the Ribble main channel. Unsurprisingly the data showed an average change value (table 5.6) of $-0.56 \text{ m}^3/\text{m}^2$ due to the excavation of the saltmarsh main creeks and breaching of the sea walls during this time period.

2009 - 2010 (figure 5.23) is the first-time step since initial realignment. This returned an average change value of $0.21 \text{ m}^3/\text{m}^2$. This accretion was seen occurring as widespread deposition of sediment across the new marsh site. Erosion at the site was confined to the main channels and not the sub channels, suggesting that the main channels were eroding at a faster rate than the smaller sub channels. In fact, there was some infilling of the smaller channels, possibly due to their elevation resulting in them acting as sediment traps.

The data between 2010 and 2011 (Figure 5.24) showed a much-reduced deposition value of $0.02 \text{ m}^3/\text{m}^2$ for this time period. Accretion took the form of deposition concentrated around the main creeks, with deposition reducing as distance from the saltmarsh creeks increased. Within the saltmarsh creeks, particularly the main channels, the sedimentation pattern evolved to be more complex, exhibiting both erosion and accretion side by side. The creeks show a braided pattern of erosion which was interrupted by the deposition of a sediment bar (Fig 5.24 341680, 425700).

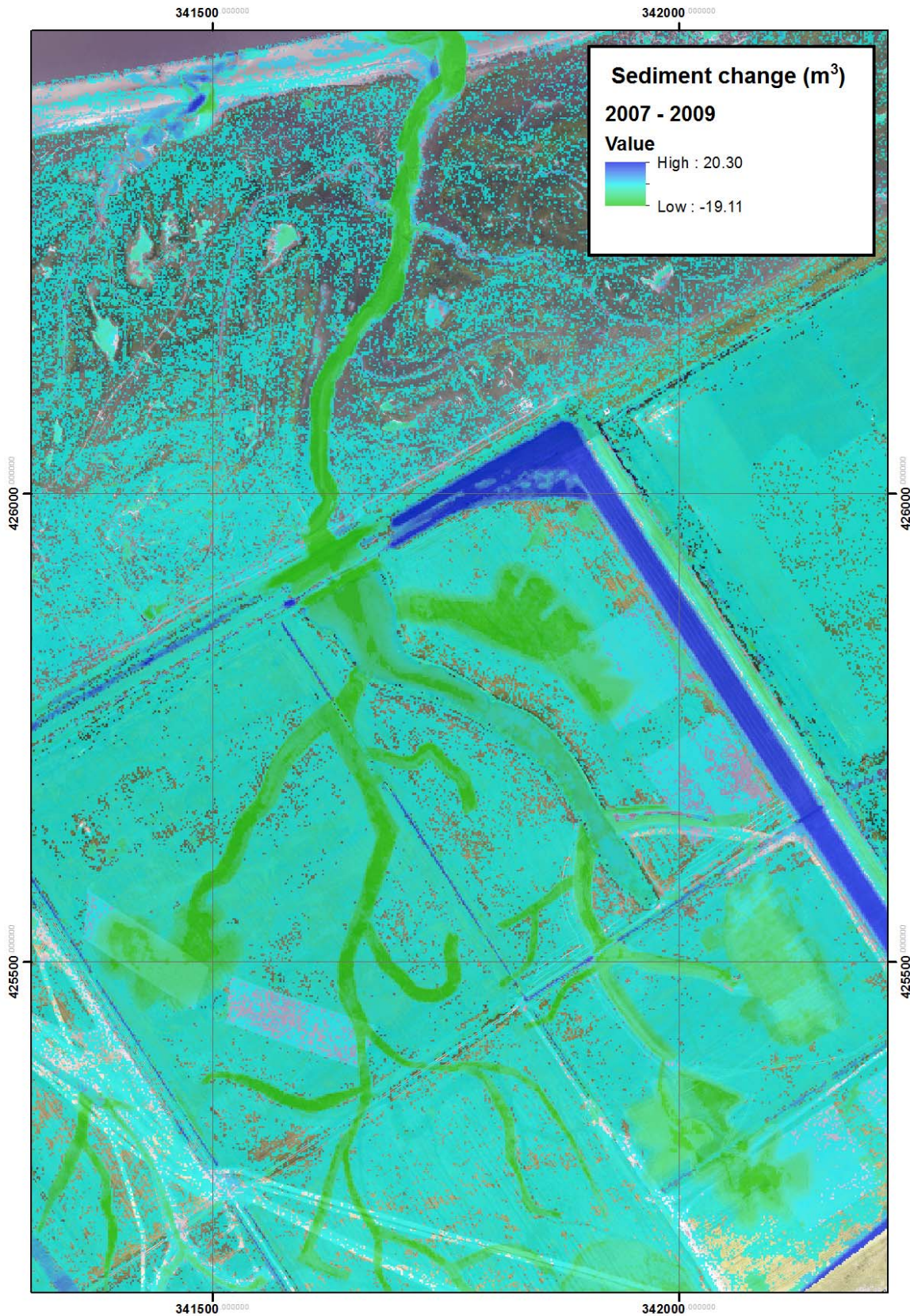


Figure 5.22 Map of significant change in sediment volume from 2007 to 2009 for the Hesketh Outmarsh managed realignment site.

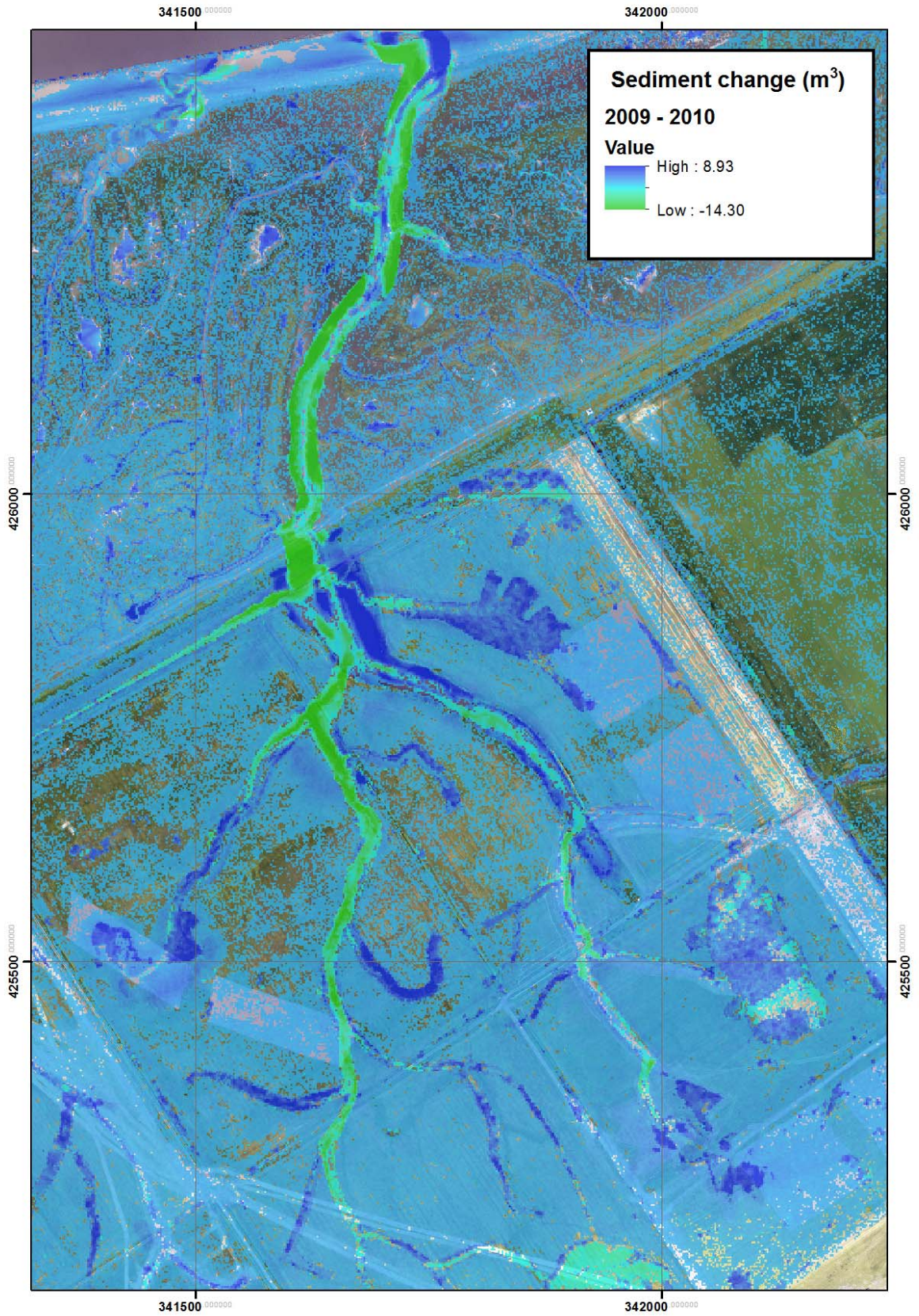


Figure 5.23 Map of significant change in sediment volume from 2009 to 2010 for the Hesketh Outmarsh managed realignment site.

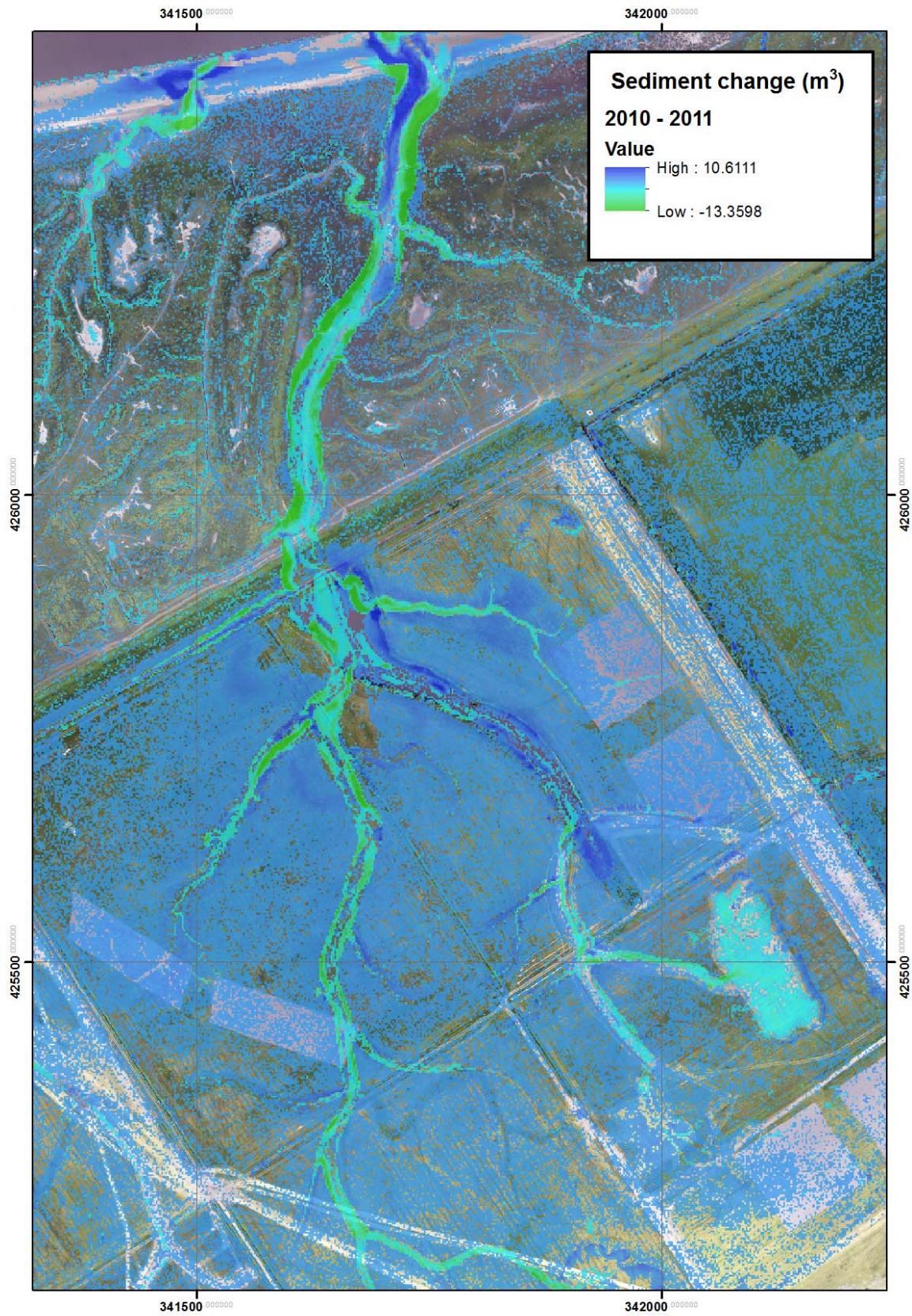


Figure 5.24 Map of significant change in sediment volume from 2010 to 2011 for the Hesketh Outmarsh managed realignment site.

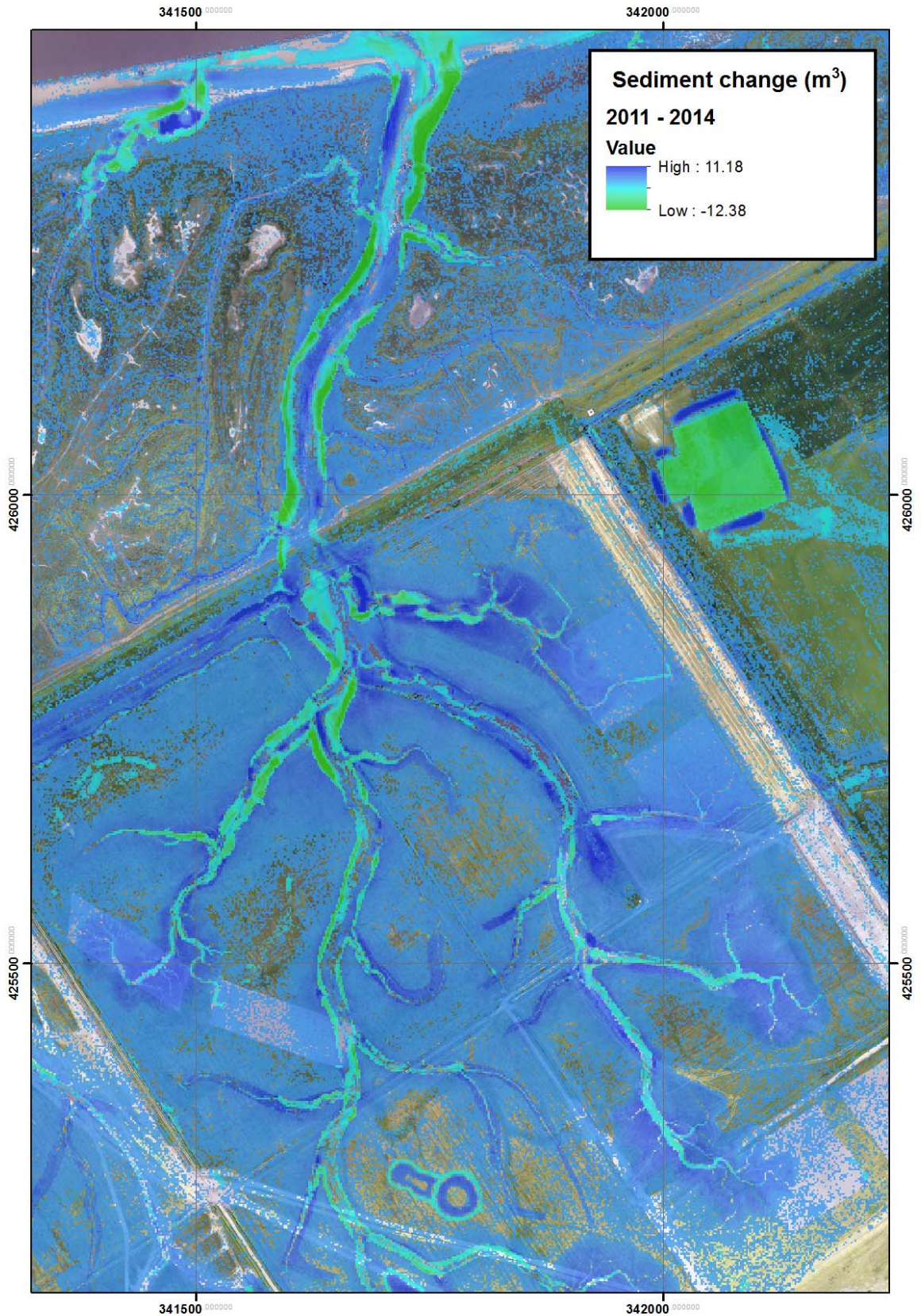


Figure 5.25 Map of significant change in sediment volume from 2011 to 2014 for the Hesketh Outmarsh managed realignment site.

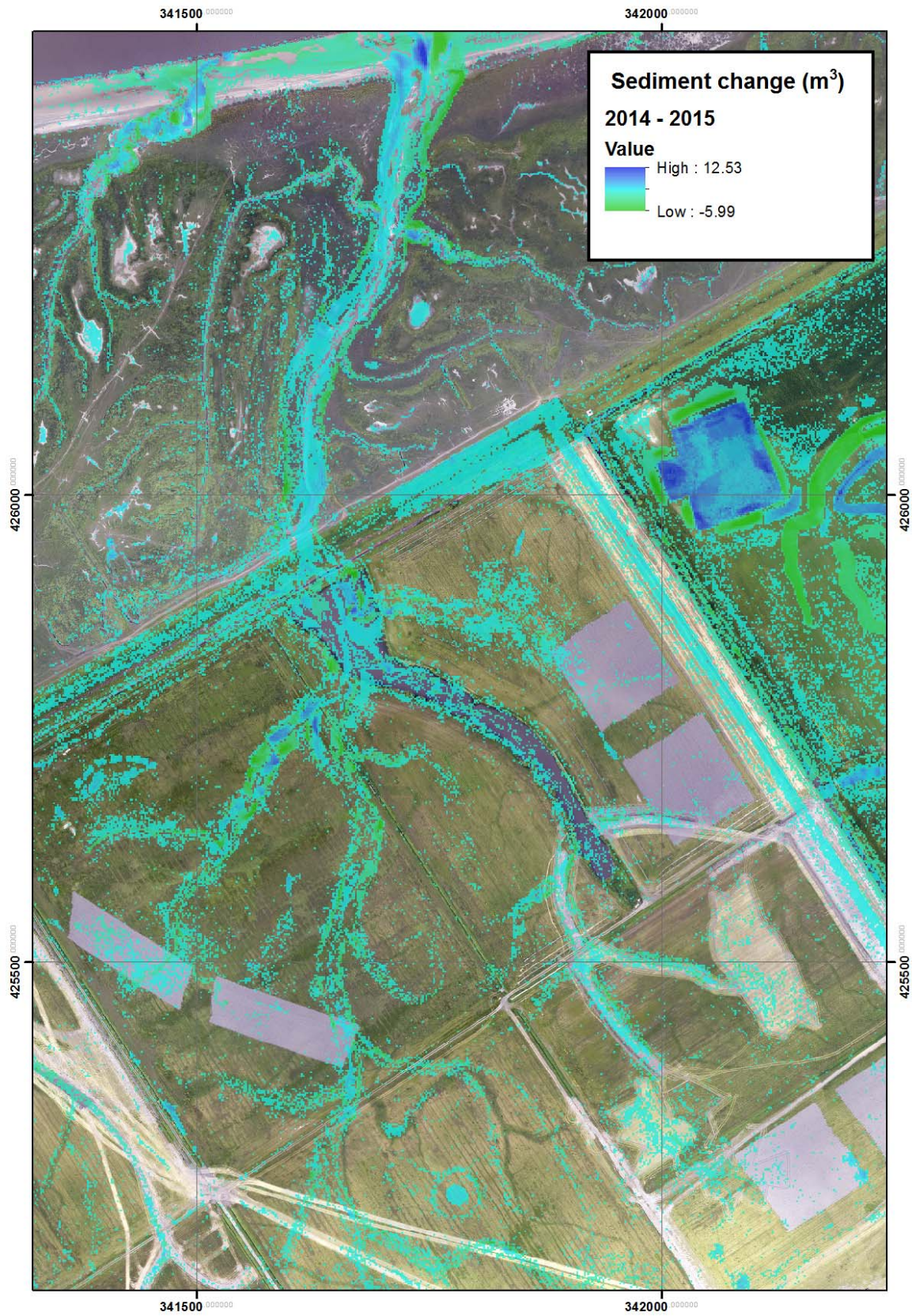


Figure 5.26 Map of significant change in sediment volume from 2014 to 2015 for the Hesketh Outmarsh managed realignment site.

Table 5.6 Hesketh Outmarsh new marsh site summary statistics for the volume of change (m³) in sediment.

| Year range | Volume of change (m³) | Average change (m³/m²) |
|--------------------|---|---|
| 2007 – 2009 | -2.2E+05 | -0.56 |
| 2009 – 2010 | 5.3E+04 | 0.21 |
| 2010 – 2011 | 1.9E+03 | 0.02 |
| 2011 – 2014 | 6.9E+04 | 0.21 |
| 2014 – 2015 | -5.3E+02 | -0.01 |

During the 2011 to 2014 period (Figure 5.25), expansion of creek erosion occurred, with erosion branching into the smaller creeks. This expansion led to the formation of numerous small sub creeks that are typically seen in a natural saltmarsh. Deposition covered a wider area of the marsh but was still concentrated around the creek network. Erosion concentrated along the edges of the marshes for this time period and appeared to be eroding laterally as opposed to vertically.

2014 – 2015 (Figure 5.26) contrasts with the previous data sets due to the relatively small average change value of -0.01 m³/m² meaning that deposition had been substantially reduced. There was very little deposition out with the creeks, in fact most deposition was occurring solely within the creeks at this point in time.

1999 – 2007: (figure 5.27) shows the sedimentation patterns at the old marsh site before the realignment scheme at Hesketh was implemented. There was accumulation along the saltmarsh creeks with the greatest accumulation being at the saltmarsh edge. There was a lesser amount of accumulation in the creek/channel middle. This accumulation was causing saltmarsh creeks to be infilled with sediment. There was also accumulation at the front of the saltmarsh suggesting that the marsh was expanding. On the surface of the saltmarshes there was general accumulation from gradual build-up of sediment. The mudflats showed a mix of erosion and accumulation

of sediment as a combination of long ellipsoid features which ran parallel to the main channel.

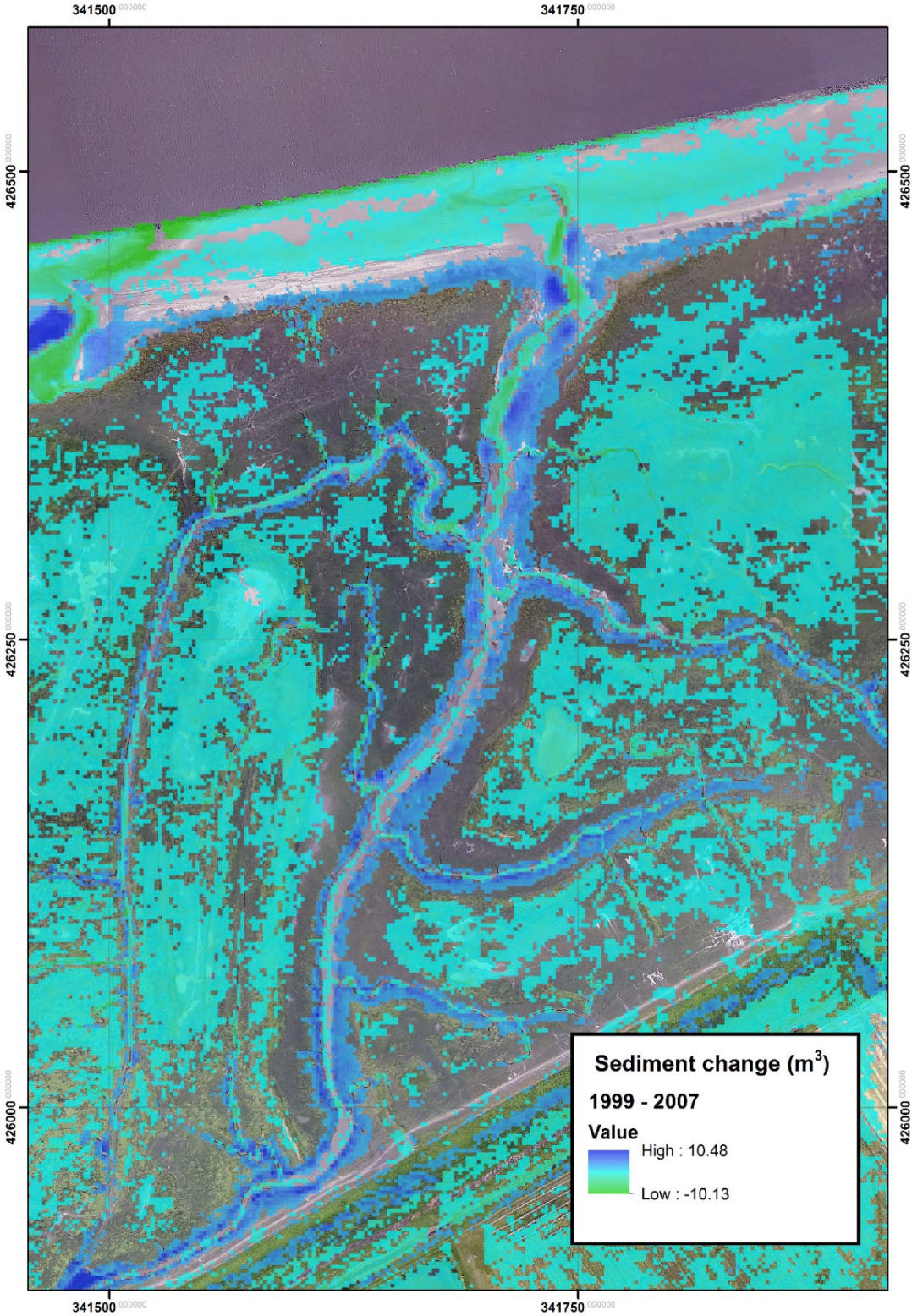


Figure 5.27 Map of significant change in sediment volume from 1999 to 2007 for the Hesketh Outmarsh old marsh site.

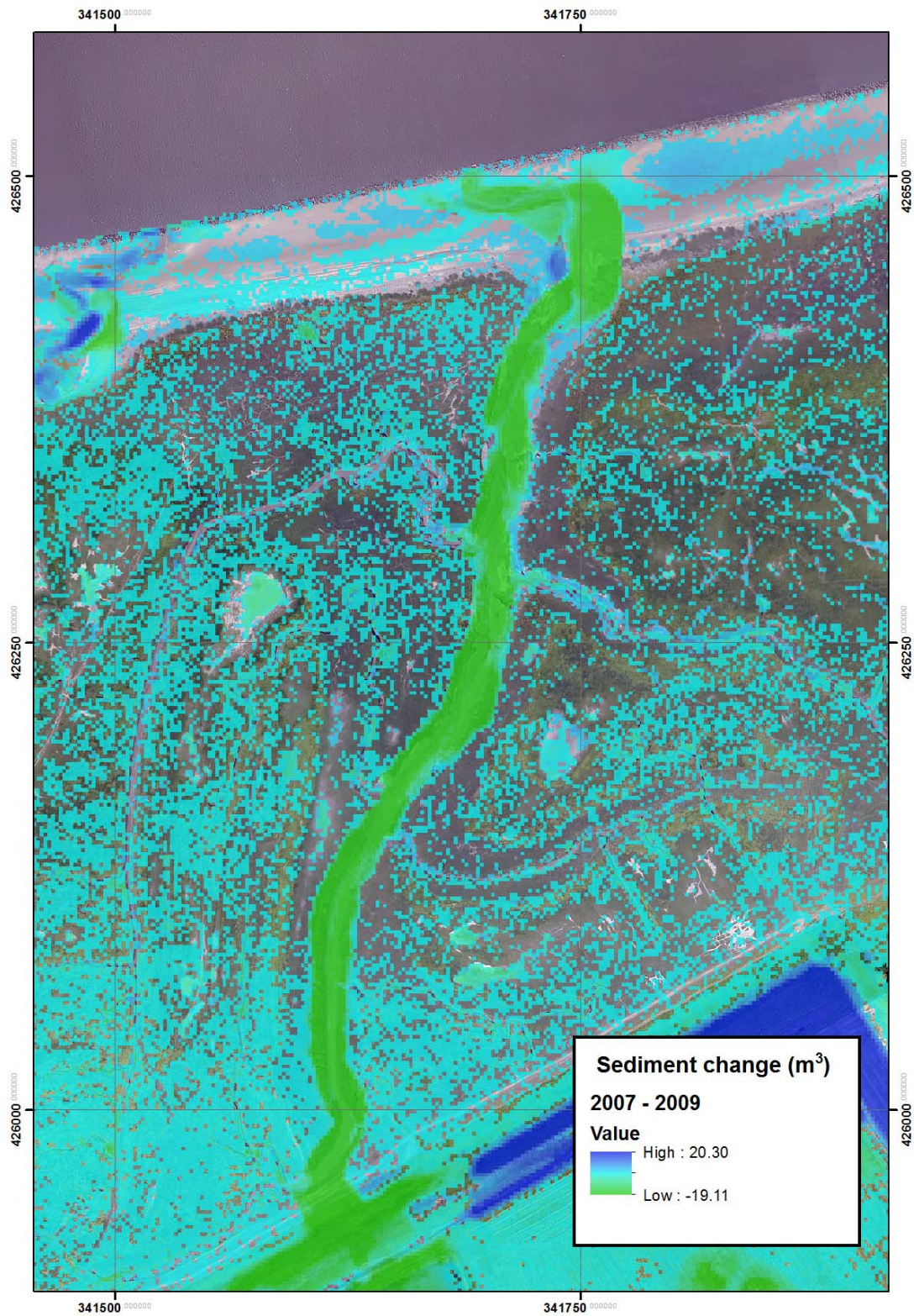


Figure 5.28 Map of significant change in sediment volume from 2007 to 2009 for the Hesketh Outmarsh old marsh site.

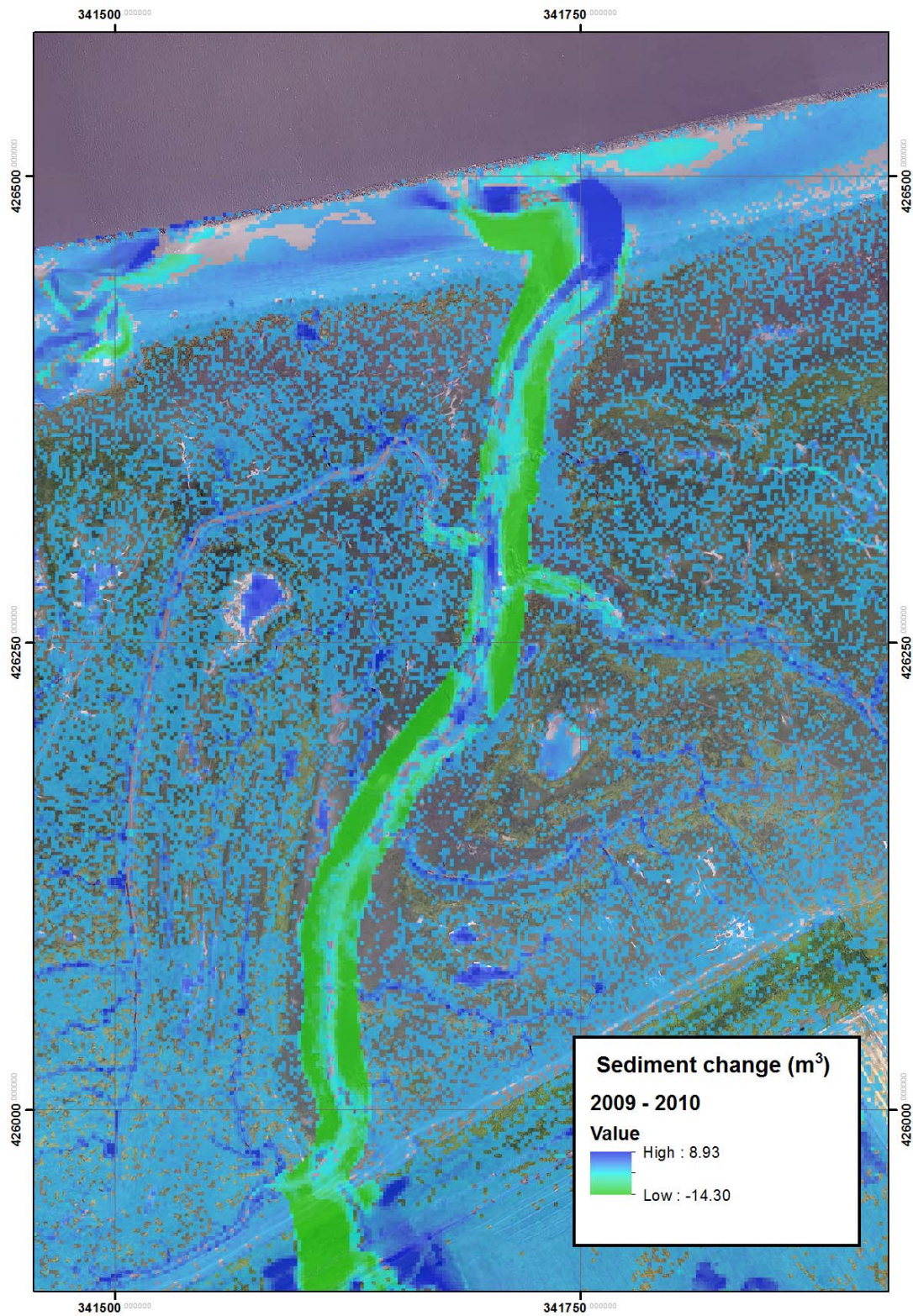


Figure 5.29 Map of significant change in sediment volume from 2009 to 2010 for the Hesketh Outmarsh old marsh site.

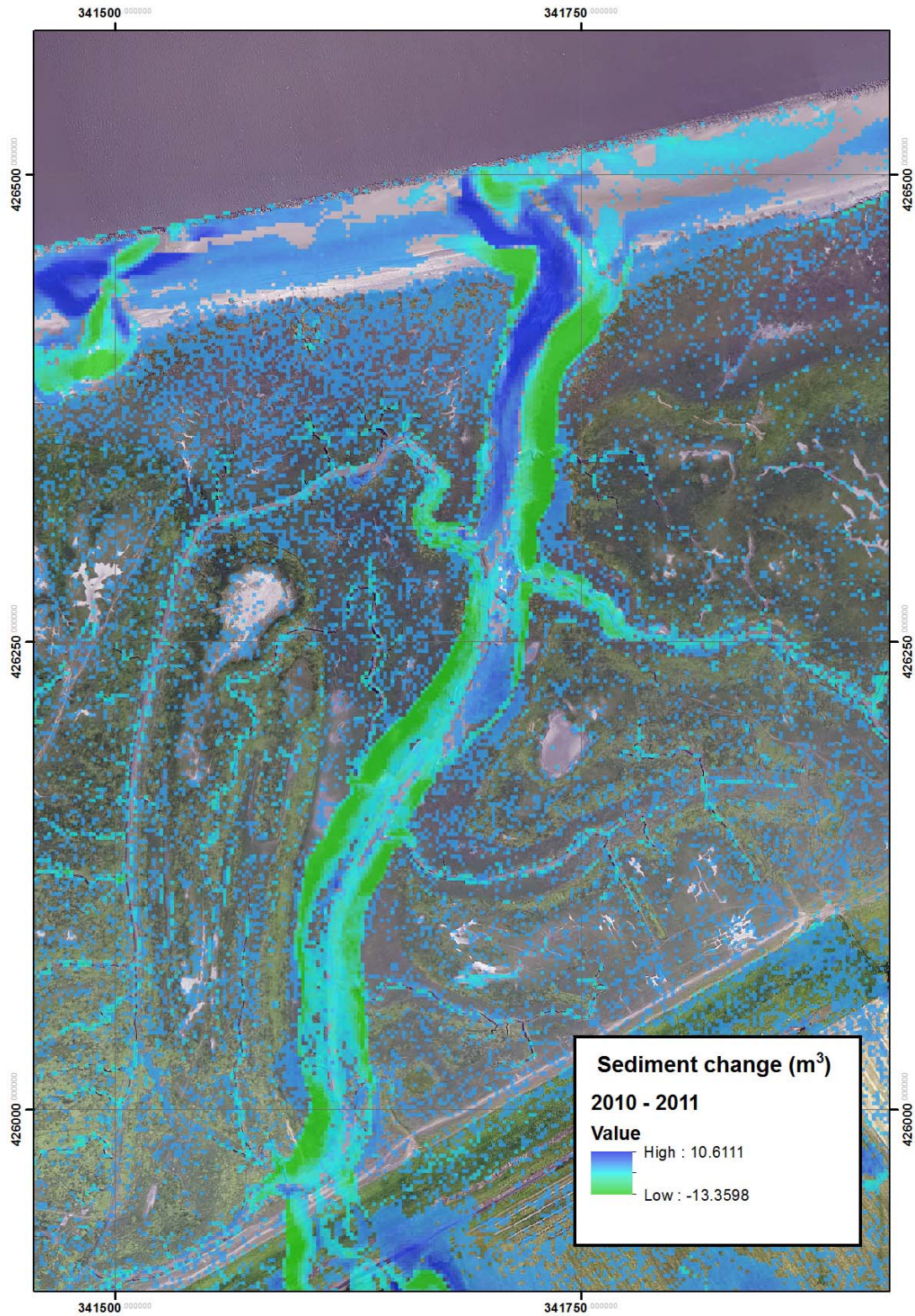


Figure 5.30 Map of significant change in sediment volume from 2010 to 2011 for the Hesketh Outmarsh old marsh site.

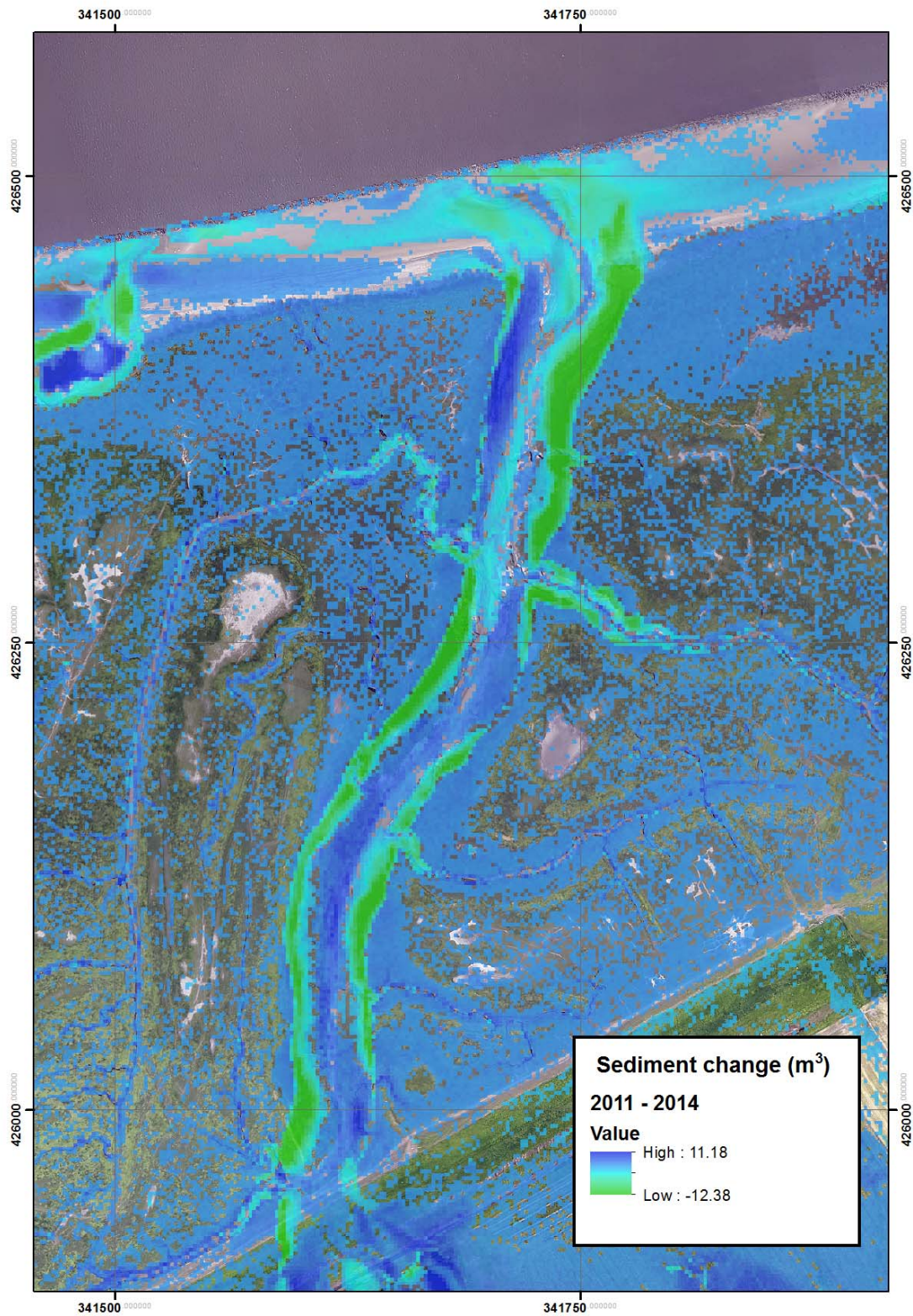


Figure 5.31 Map of significant change in sediment volume from 2011 to 2014 for the Hesketh Outmarsh old marsh site.

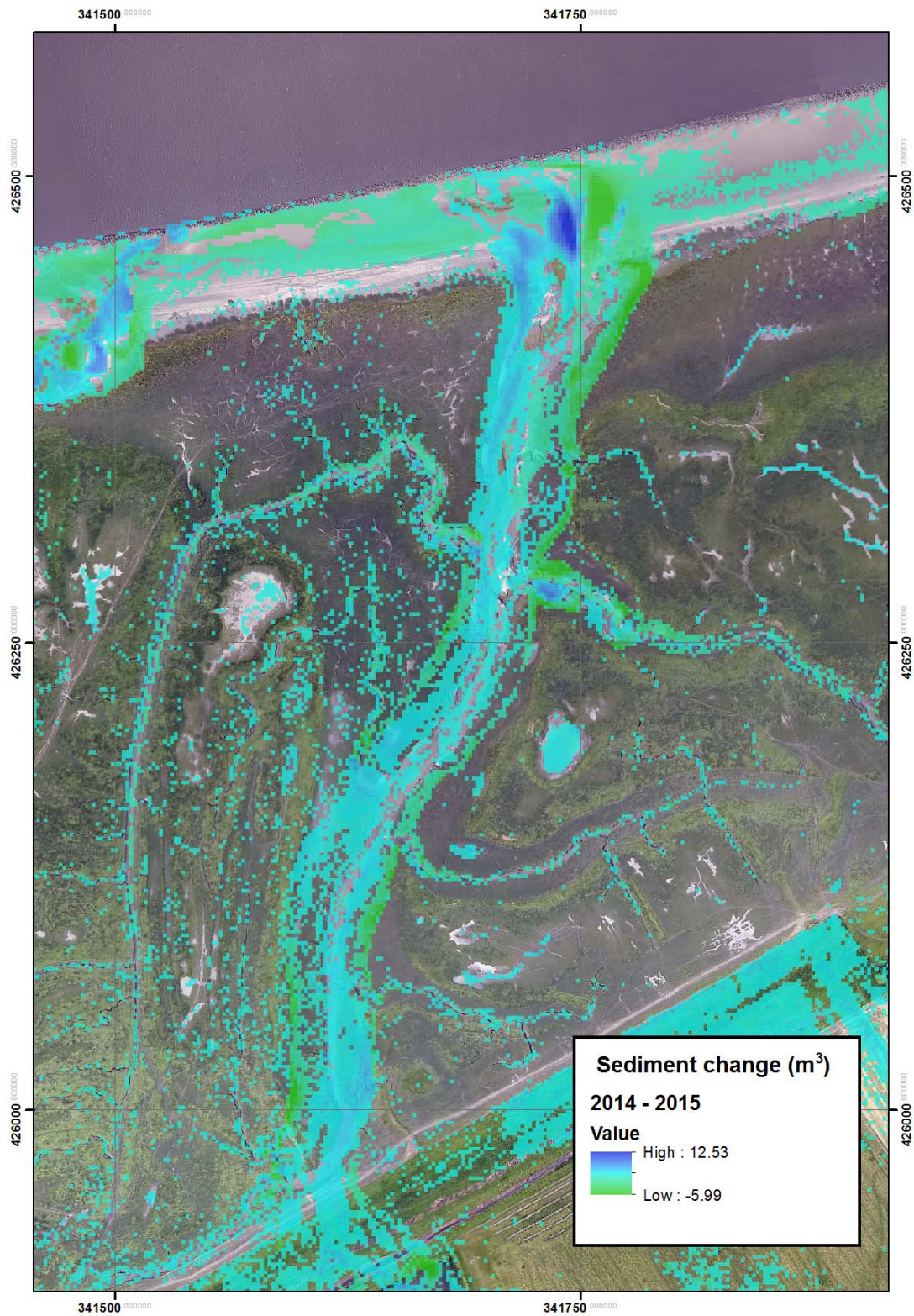


Figure 5.32 Map of significant change in sediment volume from 2014 to 2015 for the Hesketh Outmarsh old marsh site.

Table 5.7 Hesketh Outmarsh old marsh site summary statistics for the volume of change (m³) in sediment.

| Year range | Volume of change (m³) | Average change (m³/m²) |
|--------------------|---|---|
| 1999 - 2007 | 2.6E+03 | 0.20 |
| 2007 – 2009 | -4.1E+04 | -0.61 |
| 2009 – 2010 | 6.1E+03 | 0.06 |
| 2010 – 2011 | -1.5E+04 | -0.31 |
| 2011 – 2014 | -1.1E+04 | -0.12 |
| 2014 – 2015 | -2.7E+03 | -0.07 |

2007 to 2009 (figure 5.28) shows the site after the realignment; the main creek that runs through the mature saltmarsh of the old marsh site was deepened substantially and this carried on to the mudflat where it joined the main river channel. There appeared to be erosion between these time points along the sides of the main saltmarsh channel, likely due to it widening in response to the changes in hydrodynamics. The accretion previously seen at the front of the marsh and within its creek network has stopped at this time.

2009 -2010 (figure 5.29) shows the site after initial disturbance. The main saltmarsh channel has started to accrete. Erosion in the main channel was occurring still at the sides of the main channel and was likely to be from the channel widening as it adapted to the new hydrodynamics of the area. The mudflats at the front of the marsh were predominantly accreting during this time period although as previously seen, there were a number of erosion areas also present. The smaller creeks in the marsh were generally accreting, which was a trend shared by the marsh surface. A number of depressions (marsh ponds) in the marsh surface were observed to be accreting at a greater rate than the surrounding marsh surface as they were likely to be acting as sinks for sediment.

For 2010 to 2011 (figure 5.30) the erosion in the main channel was still going on although now it was primarily confined to the edges of the marsh near the front and back. There was also some minor erosion occurring in the minor creeks across the marsh area and surface accretion was much reduced apart from at the front of the saltmarsh. Across the mudflat accretion was occurring though the extent of accretion is highly variable, mudflat erosion at this point was confined to the areas in front of the mouths of large saltmarsh creeks.

2011 - 2014 (figure 5.31) showed the same trends as those seen between 2010 and 2011 with erosion mainly occurring along the sides of the main creek channels and in the same locations. However, surface deposition was much increased though it was greatest at the front of the marsh it also occurred near the back for areas close to large creeks. There was more erosion of the sub creeks in this time period particularly along their sides, which suggests that these creeks were widening. The mudflats remained much the same as 2010 - 2011 with a general trend of accretion.

2014 – 2015 (figure 5.32) is the most complex data with the main channel showing a braided pattern of erosion and accretion spots. The main channel creek was still undergoing lateral erosion along the sides especially at the front of the marsh but it was not as extensive as in previous years. The mudflats were exhibiting more erosion at this point with the mudflats being composed of compartments of erosion and accretion that were spatially complex. For this time point there was comparably less sediment movement.

5.5. Discussion

Section 5.4 described a detailed investigation into the three main sediment categories - sandbanks, mudflats and saltmarshes - within the Ribble estuary. The investigation inferred the movements of sediment over different time periods where LiDAR data were available. Where possible, the change in sediment volumes were quantified and average values calculated that represented the state of sediment flux for the given time period and given location within the estuary.

5.5.1. 1999 – 2009 full estuary coverage

The large-scale analysis conducted using data from 1999 to 2009 demonstrated that there was a net sediment loss of $8.1 \text{ E}+6 \text{ m}^3$. This means that the volume of sediment within the survey area in 2009 was less than that in the survey area from 1999. As the survey area fully covered the mudflats and saltmarshes, it is known that this is not a case of sediment simply being transferred to another part of the estuary. This suggests that the missing sediment may have been remobilised to the Irish Sea through the interconnected sediment transfer systems that are responsible for sediment redistribution around the Irish Sea (Luo et al., 2015; van der Wal et al., 2002; Wakefield et al., 2011).

As the outer estuary beyond the sand banks was not included within this analysis as it was out with the available data, it is possible that this may be where the lost sediment has been transferred to, though this is just speculation. Determining where these sediments and their sediment bound contaminants have gone would require development of more advanced sediment transport models to improve past estimates of sediment movements in this part of the Irish Sea (Gleizon et al., 2003; Gleizon and McDonald, 2010; Luo et al., 2015; Lyons, 1997; van der Wal et al., 2002). This would be an interesting area for future work and allow the fate of remobilised sediment to be examined and theorised.

Given that this analysis was based on the measurement of two data sets, it is possible that on the two LiDAR survey days the estuary was substantially different by chance as a result of events that had occurred in the immediate period before the LiDAR measurements were made. Furthermore, it is well known that within the Ribble estuary sediment moves in and out from the offshore areas beyond the mouth of the estuary (Atkin, 2000; Wakefield, 2005). This is therefore an important point to consider as it is a limitation of this analysis.

In the Ribble estuary the ebb and flow of the tide creates a tidal bore which will cause turbulent conditions that promote sediment remobilisation, such remobilisation will be more pronounced on the mudflats (Atkin, 2000; Wakefield, 2005). Therefore the mudflats are expected to be more dynamic in their morphological change as they are exposed to more disturbance. As 65% of the reported lost sediment came from saltmarshes which are believed to be comparatively more stable, it seems plausible that the observed trend of erosion was dominant during this 10-year time period.

There were also a number of discreet, large sediment movement events that may have contributed to this trend of erosion. These include:

- The retreat of a section of mature marsh front 5.4.1.
- The collapse of a section of the Ribble training wall which allowed more movement of sediment on the north bank mid estuary mudflats.
- The fact that the Hesketh site accounted for 11% of all erosion during this time period and that this estimate did not include the effects of modified hydrodynamics causing erosion in mature saltmarshes and mudflats.

Despite year on year fluctuations and likely transfers of sediment between the surveyed estuary and the outer estuary and Irish Sea itself, a general trend of erosion over the 10 years from 1999 -2009 is supported by the observed sediment movements from the mudflats and saltmarshes. Therefore, it is likely that sediment bound contaminants (mainly from the saltmarshes) have been relocated during this time-period. In effect the saltmarshes would have been acting as a source of time-integrated, sediment-bound contaminants to the estuary and the Irish Seas sediment transfer system (Brown, 1997; Hunt et al., 2013; Mudge et al., 1997). This will be discussed further in chapter 6.

5.5.2. 1999 – 2015 mid estuary coverage

The mid estuary analysis considered an area of extensive mudflats and saltmarshes, therefore, the sediment movements here in these clay and silt rich deposits will have implications for sediment associated contaminant transfers (Assinder et al., 1997; Rainey et al., 2003; Wakefield, 2005). This section aimed to explore the trend in sediment movement as it was an area that covered around 35% of the estuary yet 65% of the mudflats and saltmarshes are found here. Sediment movements were shown to be variable between the different time periods, exhibiting inter-annual variability (figure 5.17).

The early data sets for 1999 to 2007 and 2007 to 2009 showed erosion to be the dominant form of sediment movement, this corroborated the findings of the long-term sediment budget in section 5.5.1. However, by the 2009 to 2010 time period, the mid Ribble area had shifted to a pattern of accumulating sediments. Given this accumulation occurred over a 1-year period, this was the most substantial sedimentation event seen within the period of study. After this substantial accretion event the pattern of erosion and accretion took on a great deal of variability within the study area, shifting from erosion to accretion for each of the following data sets.

What was of interest was that the saltmarshes tended to be the largest contributors to either the erosion or accretion, with the saltmarshes losing or gaining more sediment than the mudflats in most cases. This is significant for this work as previously mentioned, because saltmarshes store relatively high concentrations of historic radiogenic contaminants, for example, nuclear sector discharged ^{137}Cs and ^{241}Am (e.g. Brown et al., 1999).

Sediment movement in the saltmarshes tended to show erosion in the small creek networks while accretion occurred in the large creeks as well as the mudflats near large creeks (e.g. figure 5.9). This is interpreted as the eroded sediment from the saltmarsh small creeks accumulating in the large creeks and then being remobilised to the mudflats. This process was observed in reverse whereby when erosion was dominant in the large creeks and the mudflats near these creeks, accretion was occurring in the saltmarsh small creeks (e.g. figure 5.10). The data appear to show a long-term back and forth mechanism of sediment being cycled between the saltmarshes and the mudflats.

This cycling process is caused by saltmarsh creek bank migration. Bank migration within the small creek networks involves undercutting up to the point the creek bank collapses, thus creating a temporal profile which appears to show erosion happening suddenly as a single event. When such erosion from undercutting occurs, the excess of sediment within the creeks will be carried towards the mudflats by the daily ebb flows over a period of time (Hu et al., 2017; Pieterse et al., 2017). Therefore, as the eroded sediment from the small creeks converges at the large creeks, accretion will be observed in these large creeks and the nearby mudflats. This accounts for the transfer of sediment from the small creeks to the large creeks as well as the nearby mudflats.

These systems are complex in terms of their spatio-temporal properties and a second process that is the opposite of the bank migration driven process was observed to be in operation at these saltmarshes. Erosion of the sediment in the fronting mudflats as well as the large creeks and accretion in the small creek network was observed in the data. The bank migration process discussed above was driven by an excess supply of sediment in the small creeks and the ebb tide, this second process is believed to be driven by an excess of sediment in the large creeks and nearby mudflats and the flood tide. Where the flood tides have been reported as being the dominant energy mechanism the overall trend in sediment transfer within saltmarsh will be towards the small creeks (e.g. Pieterse et al., 2017). Therefore, from the data it appears that a cyclic sediment transfer process is in operation which exhibits inter annual variability.

5.5.3. Localised site 1 – Sandbanks

The first localised site investigated was the sandbanks located near Lytham St Anne's. As previously mentioned, and based on the findings of chapter 3.3.2, these sand deposits are not expected to be significant in terms of contaminant remobilisation as they are inversely correlated with estuarine radiogenic contaminants such as ^{137}Cs and ^{241}Am . However, they form one of the three main sediment deposit categories of the estuary and it was important to study all aspects of the estuary, to ensure a complete accounting of the estuaries sediment volumes. As these sites were found to have substantial morphological change and inferred sediment movement, it was also important to quantify these so that they did not skew observations of any mudflat sediment volume change.

The sandbank sediment remobilisation took the form of clearly distinct sandbank migration with deposits of sand having a morphology of classic sandbanks that appeared to be migrating towards the estuary mouths (Figure 5.18; 330500, 429500). The distinct morphology of these feature leads me to believe that the pattern of layered erosion and accretion features towards the near shore and mouth of the Ribble estuary may in fact be evidence of the sandbanks direction of travel. This chapters observations of these sandbank features confirm the postulated theory of channel ward migration (Rainford, 1997), which suggests these sands are migrating to the main channel and infilling it (van der Wal et al., 2002). The sandbanks whilst probably not significant to contaminant remobilisation had a relatively simple pattern of spatial variation, with a clearly defined structure to sediment movement.

5.5.4. Localised site 2 – Mudflats

Chapter 3 explored the temporal and spatial variability of the Ribble mudflats and showed that the mudflats preferentially store contaminants due to a positive correlation with percentage clay. However, contaminant values ranged from 2.6 Bq kg⁻¹ to 311 Bq kg⁻¹ for ¹³⁷Cs and 2 Bq kg⁻¹ to 171 Bq kg⁻¹ for ²⁴¹Am across the study sites and across the length of the study period. The conclusion being that variation in sediment particle size distribution was responsible for this variability and that sediment movements were a significant factor in determining contaminant concentration.

The mudflats were shown to exhibit a high degree of spatial variability and there was little to no long-term trend in these sediments, with erosion and accretion being highly spatially variable. This is likely due to the drivers of sediment movement within the mudflats operating at a fine temporal scale with the daily ebb/flow of the tides and the tidal bore being responsible for a large extent of mixing in the mudflats (Azhikodan and Yokoyama, 2015). The data did show that accretion of the mudflats, particularly those in front of the saltmarsh, tended to coincide with erosion of the saltmarsh creek system. These coincident morphological changes represent a transfer of sediment from the saltmarshes to the mudflats. This can be further supported by the presence of a delta fan shape at the mouth of the saltmarsh creeks – a common feature of sediments being laid down by hydrological processes as they are washed out of a creek or channel. Moreover, these areas were spatially distinct from the typical parallel ellipsoid that was observed dominating mudflat sediment movements.

The sediment in the saltmarsh creeks typically had contaminant values of 159 Bq kg⁻¹ to 576 Bq kg⁻¹ for ¹³⁷Cs and 122 Bq kg⁻¹ to 188 Bq kg⁻¹ for ²⁴¹Am (see chapter 6.3 for further details). Therefore, these transfers of sediment from saltmarshes to mudflats constitute a source of radiogenic contaminants to the mudflats. The identification of this sediment source and its average levels of contamination is important for this work's aims of evaluating the significance of sediment bound contaminant remobilisation.

5.5.5. Localised site 3 – Hesketh Outmarsh

It is difficult to observe how an estuary will respond to a natural disturbance event such as a high impact storm or prolonged sea level rise without information prior to and after the event. Difficulties such as the unpredictability of such storms, the logistical difficulties involved in mobilising a response prior to and after such an event, and the uncertainty in knowing which events will have a suitably large impact that could be detected and therefore should be studied. Consequently, this study has taken

advantage of the Hesketh Outmarsh managed realignment scheme as an example of a significant anthropogenic disturbance event that modified the local hydrodynamics and triggered sediment erosion and deposition mechanisms in the local vicinity.

The initial excavation works saw the historic creeks that were infilled during the 1980s land reclamation re-established. This was done to reconnect the site to the estuary to accelerate marsh formation and encourage sediment accretion across the marsh surface. The site underwent a period of creek formation which saw lateral and vertical erosion across the site as a dense network of saltmarsh creeks were formed. These erosion events persisted for the first three years after the breaching of the sea walls and have led to sediment bound contaminants in these eroded sediments being remobilised and redistributed by the estuary wide sediment transfer system.

The trend of sediment accumulation seen from 2009 onwards will likely mean that those time integrated stores of contaminants have been deposited on the marsh surface near the creeks. This will be considered further in chapter 6 where sediment cores taken at different locations in the estuary are used to estimate the historic levels of contaminants. These transfers of sediments and by consequence sediment bound contaminants were in response to the physical disturbance of the excavations.

The mature marsh located north of the breached sea wall did not have the physical disturbance of excavations applied to it, instead the creation of a new saltmarsh resulted in what was a previously a dead-end creek becoming a main creek connecting the new saltmarsh to the estuary (figure 5.22). These modifications to the saltmarsh creeks altered the hydrodynamics of the area, resulting in increased water velocities and drainage times that caused creek erosion (Browne, 2017; Pieterse et al., 2017). This erosion continued for some time after the disturbance event. The erosion caused the main creek to widen substantially (over 10 times wider in 2015 than 2007) and deepen to a depth of 7m. This erosion has also led to bank collapse along the creek with large sections of marsh being undercut, these sediments were then removed by the ebb tide and represent a time integrated source of sediment bound contaminants that will have been remobilised and redistributed within the estuary.

In the most recent data set available (for 2014 – 2015), the rates of erosion were much reduced and accretion has occurred in the new marsh site, though erosion was still clearly present in the old marsh site. This is significant as the mature saltmarshes present at the old marsh site are expected to be the most concentrated store of contaminants in the estuary (see chapter 6). Follow up topographic surveys are

recommended to monitor if these marshes have entered a stage of recovery from disturbance or if the reduced rates of erosion are just a lull in a larger temporal trend.

5.6. Conclusions

The long-term trends in sedimentation patterns within the Ribble estuary from 1999 - 2015 show complex patterns of erosion and accretion which varied over the different time periods for which LiDAR data were available. For example, erosion was clearly dominant from 1999 – 2009, though from 2009 – 2015 the pattern of sedimentation was very variable. The implications are that there was a great deal of movement in the sediment types, with the saltmarsh sediments being subject to more movement than was originally thought.

Looking at the differences in sediment movement over shorter timescales, highlighted the fact that sediments were being eroded from the small creek networks possibly due to bank migration as part of saltmarsh evolution. With the sediment being temporarily remobilised to the larger creeks as well as the nearby mudflats. The mudflat sediments were then subject to great spatial and temporal variability and likely to mix the mature saltmarsh sediments with new sources from the river, marine and the existing sediment stocks within the estuary. Consequently, this is likely to dilute any historic contaminant levels originating in the saltmarsh sediments (e.g. Rahman et al., 2013). In some cases, these mixed sediments were observed to be deposited back in the saltmarsh creeks or on the marsh surface surrounding this network of creeks.

The managed realignment site has prompted the erosion of mature saltmarsh by causing the lateral and vertical expansion of three large creeks that are connected to the new marsh site. This is believed to be caused by a modification to the local hydrodynamic conditions, similar to the processes reported by Browne (2017) that were responsible for long term erosion of Long Island, USA saltmarshes. The consequence is that the time integrated store of contaminants stored in these marshes has seen its rate of transfer to the mudflats accelerated. This in turn has seen an acceleration in the rate at which sediment bound contaminants have been remobilised to the estuary and in turn the Ribble and Irish Sea's sediment transfer systems.

6. Sediment-bound radioactive contaminant remobilisation in response to an anthropogenic disturbance event

The Ribble estuary experiences a great deal of morphological variability, which translates to a large amount of sediment movement. The estuary is known to receive constant inputs of Irish Sea marine sediment, transported primarily from the Liverpool bay area (Luo et al., 2015; van der Wal et al., 2002). It has also been shown that the estuary transfers sediments back to the Irish sea sediment transfer system, with the full estuary sediment budget from chapter five highlighting that a substantial volume of estuarine sediment was likely transferred to the marine environment. Therefore, the Ribble estuary is clearly an open system and given the large-scale transfers of marine and estuarine sediments can be viewed as an exchange environment of sediment bound radiogenic contaminants.

The principal mechanisms of sediment transfer within the estuary are believed to be the estuary hydrodynamics and discrete high impact disturbance events (Azevedo et al., 2010; Azhikodan and Yokoyama, 2015). The estuaries hydrodynamics and river discharges are responsible for daily remobilisation of sediments within the estuary and the sorting of sediments within the Ribble by particle size and the energy available to move those particles (Azevedo et al., 2010; Pamba et al., 2016). On a longer time scale, discrete high impact disturbance events such as storms and high riverine discharge as a result of heavy precipitation within the river catchment represent an injection of excess energy that can cause large scale sediment remobilisations (e.g. Allen and Duffy, 1998; Chen et al., 2017). These mechanisms underpin the idea that the sediments within the estuary, specifically the mudflat sediments and the newly deposited saltmarsh sediments are a product of sediment mixing (Azhikodan and Yokoyama, 2015).

With substantially reduced liquid discharges from Sellafield and sediment mixing with fresh uncontaminated material that is known to occur during sediment transport, it would be reasonable to expect estuarine contaminant levels to be declining (Gleizon and McDonald, 2010; Marsden et al., 2006). In the case of the Ribble estuary where the primary source of radiogenic contamination is from the Irish sea sediment transfer system, mixing of sediments should dilute concentrations of radiogenic contaminants (Hunt et al., 2013; Rainey et al., 1999; Wakefield, 2005). Where concentrations of these radiogenic contaminants are not reducing and radionuclide ingrowth can not explain the lack of a reduction then a possible explanation is that a concentrated

source of sediment bound contaminants may be toping up these sediments contamination levels (Hunt et al., 2013; Marsden et al., 2006). Such an example of a lack of decline was reported in chapter 3 for ^{241}Am which may have been due to a combination of the top up of ^{241}Am from in growth from ^{241}Pu and from sediment remobilisation from more concentrated sources such as the Ribble saltmarshes and Irish sea sediments.

In chapter 5 a series of saltmarsh and mudflat morphological changes was interpreted as sediment moving back and forth between the saltmarsh creeks to the mudflats as a result of creek bank collapse. The implication of these observations is that there is back and forth movement of sediment from the saltmarshes to the mudflats and the wider Ribble estuary sediment transport system. This redistribution of sediments and their associated sediment bound contaminants represents a source of diffuse radiogenic contaminants to the estuary and by extension the Irish Sea sediment transfer system.

The Ribble saltmarsh sediments are known to contain contaminant concentrations that can be up to 179% higher than the highest concentration mudflat sediments (section 3.3.1). Therefore, transfer of fine grained sediments, which are known to act as vehicles for contaminant transport, will also lead to contaminant movement from the saltmarshes to the mudflats (Brown, 1997; Hunt et al., 2013; Wakefield et al., 2011). That the saltmarshes have been acting as a source of contaminants to the estuarine environment is supported by the following three findings of this work so far: 1) the lack of a significant decline in ^{241}Am and ^{137}Cs in mudflat sediments (3.3.4); 2) the detection of a mechanism of sediment transfer between the mudflats and the saltmarshes (5.5.2); and, 3) the quantification of substantial saltmarsh erosion (Table 5.2).

The identification and quantification of these diffuse sources of contaminants to the estuarine environment is important given the context of current historically low point source contaminant discharges, as seen in the significant reduction in Sellafield discharges of the radionuclides ^{137}Cs and ^{241}Am (Ray, 2013). This means that inter-annual variation in contaminant concentration within the estuarine environment will be partially influenced by the rate of diffuse releases of contaminants from concentrated sediment deposits within the estuary and around the Irish Sea (Hunt et al., 2013). These diffuse environmental sources are more complicated to quantify than point source discharges and therefore mechanisms of sediment remobilisation are important for understanding the nature of contaminant remobilisation.

The anticipated implications of climate change highlights the need to better understand the significance of the transfer of radiogenic contaminant concentrated sediments from saltmarshes to the estuary and beyond. It is believed that the effects of climate change particularly for the North Atlantic area will be an increase in the amount of energy within the climate system and an accelerated rate of sea level rise (Mölter et al., 2016). These factors have the potential to modify the estuary hydrodynamics and increase the frequency of high impact disturbance events (Azevedo et al., 2010; Gleizon et al., 2003; Luo et al., 2015). The result would be a modification to the temporal and spatial patterns of sediment redistribution at sites such as the Ribble estuary (Dissanayake et al., 2015; Esteves et al., 2011).

The Hesketh Outmarsh managed realignment site was investigated in chapter 5 as an example of a known disturbance event whose impacts can be measured. In chapter 5 it's the morphological change which occurred at the site which was analysed to infer sediment movements, prior knowledge of the particle size of these sediments was then used to estimate radiogenic contaminant remobilisation. The disturbance caused by the realignment is believed to have modified the local hydrodynamics and it is the effects of those modified hydrodynamics that are of particular interest to this work. Comparing the old and new marsh sites, offered the most information about the consequences of modifying local hydrodynamics particularly of the saltmarsh creeks. The findings of the study reported here in chapter 6 consider the wider implications of managed realignment as well as the implications of increasing disturbance for sediment bound radiogenic contaminants.

6.1. Aims

The spatial dynamics of saltmarsh contamination are explored here for the purpose of determining a robust method for estimating contaminant remobilisation from the site. The method is developed to estimate likely contaminant remobilisation in response to the disturbance event triggered by the implementation of the managed realignment scheme. Using a focused sediment budget, sediment movement is converted to an estimation of sediment bound contaminant movement.

- Is there significant spatial variation in saltmarsh contaminant concentration?
- How much historic contamination has been remobilised as part of sediment movements at the Hesketh out marsh site?
- How has the temporal trend in contaminant remobilisation changed since disturbance?

6.2. Methods

Site selection

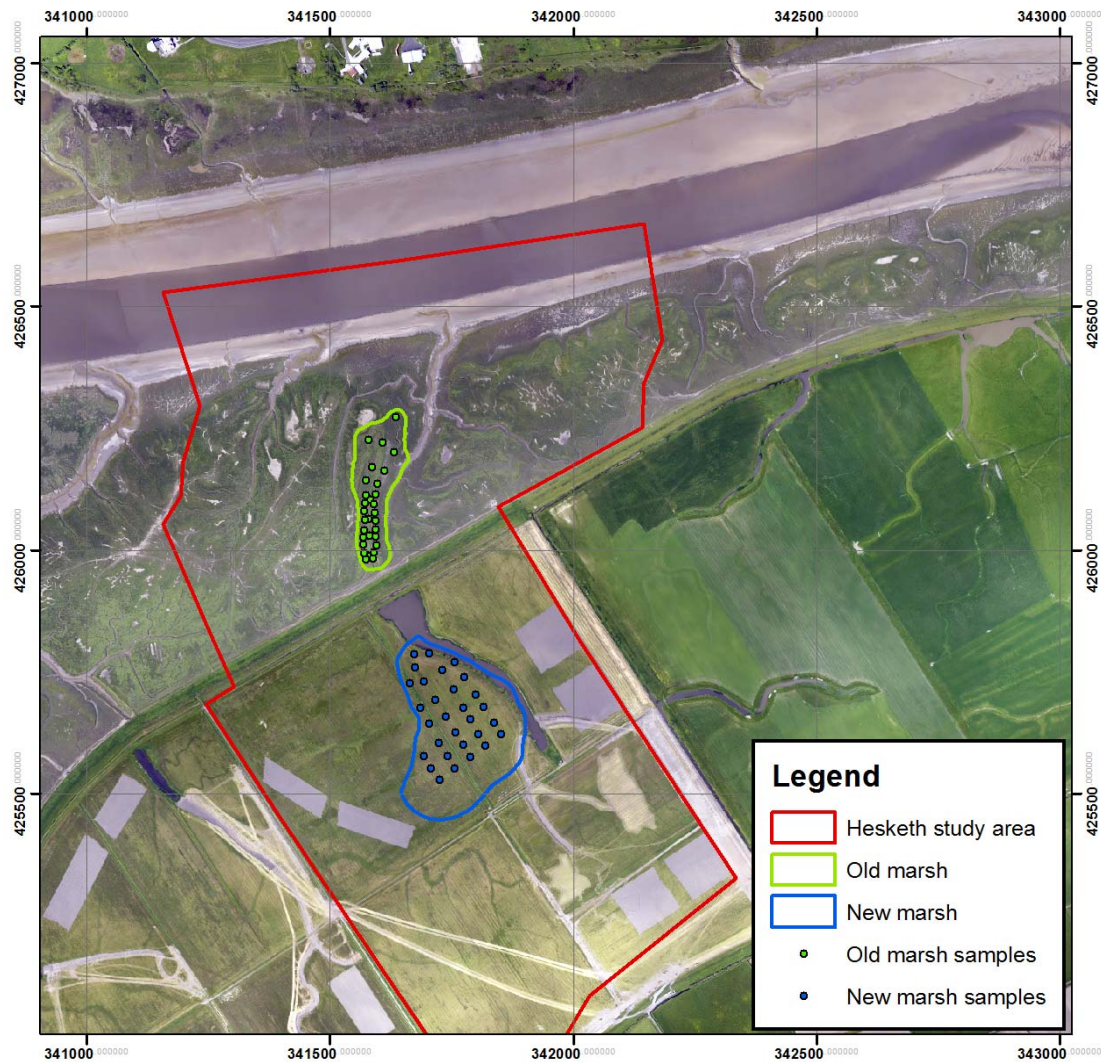


Figure 6.1 This aerial photograph was collected by the Environment Agency Geomatics group in 2007 prior to the realignment scheme. The Hesketh study area is denoted by a red polygon within which there are two sub categories Old marsh (green polygon / points) and New marsh (Blue polygon / points).

The Hesketh Outmarsh, as discussed in section 6.1, was the ideal site for a case study of sediment bound contaminant remobilisation. The new marsh site is located to the south of the breached sea wall and the old marsh site is to north (figure 6.1). Targeted areas were selected within each of the new and old marsh sites to give two focused areas to conduct this research (figure 6.1). The reasoning for this was that for the

remobilised sediment data to be converted to an estimate of contaminant remobilisation it was vital that the marsh that is being eroded be thoroughly characterised.



Figure 6.2 Example photograph of undercutting action that is typical of saltmarsh lateral erosion from the Hesketh saltmarshes (Photo taken of the Old marsh site in 2015).

The selected areas within the Hesketh Outmarsh are highlighted in figure 6.1, they are discrete compartments of their respective saltmarshes with creeks on all sides. This was a desirable feature as this study was conducted post the 2009 breach and so no data were available from before the sea defences were breached. Given the stated aims of this chapter, it was important to investigate an area of saltmarsh that was known to have experienced net erosion. The nature of the erosion at these sites was creek based undercutting of the sides (figure 6.2), which in turn resulted in a contraction of the marsh surface area. Therefore, the two field sites selected for investigation provide a compartment of saltmarsh which is known to be undergoing erosion but is not excessive in size so that it can be fully characterised in terms of its contaminant properties.

The new marsh site was reclaimed from the estuary in the 1980's, which is contemporary with the peak discharges of Sellafield (e.g. Vintró et al., 2000), it was therefore reasonable to assume lower sediment concentrations of ^{137}Cs and ^{241}Am should be expected than in the mature saltmarsh found in the Ribble estuary. The agricultural practices associated with wheat production, which was carried out at this

site, involved routine ploughing and infrequent deep ploughing. This means that the contaminants activity depth profile at the new marsh site can be expected to deviate from the classic saltmarsh activity depth profile (e.g. Brown et al., 1999) that would be expected to be found at the old marsh.

6.2.1. Field work at Hesketh Outmarsh

At each of the field sites, thirty sampling points were distributed across the marsh surface in a 35 m grid. Thirty sample points per field area was decided to offer the best trade-off in terms of sampling density and sample processing times. At each sampling point a survey flag was inserted to mark the location and a sediment scrape of the upper 10 mm of sediment was collected with a trowel and placed in a new pre-labelled plastic bag. Coordinates of each sample point were recorded using a Leica 1200 differential global positioning system (DGPS), a one-hour duration was used for raw data logging at the base station.

At each sample site the amount of ionising radiation was measured using a Thermo-scientific Radeye© air kerma unit at a standard height of 1m. The air kerma unit was pre-calibrated using an IAEA traceable sealed ^{137}Cs source following the method compliant with the University of Stirling's Environmental Radioactivity Laboratory's (ERL) United Kingdom Accreditation Service (UKAS) accredited quality control system.

A Mobile Gamma Spectrometry System (MoGSS) was then used to survey the marsh surface. MoGSS is a rapid mobile in situ gamma spectrometry system that logs gamma ray counts and geographic coordinates every one second. The user simply walks the site area of interest whilst holding the Na-I (TI) about 20 cm from the ground surface. Preliminary data from this system were used to identify high and low areas of radioactive contamination. This information was then used to identify sites for coring, so that both high contaminant sites and low contaminant sites would be sampled.

Two sediment cores of a length of 1 m and diameter of 0.10 m were collected from each site to give a total of four cores. These cores were extracted by hammering a section of drain pipe into the marsh surface with a sledgehammer. The core and tube were then extracted using a hydraulic jack and ball clamp. These deep cores were then given sample numbers and sealed with durable sticky tape.

6.2.2. Sediment processing

The deep cores were stored in the University of Stirling's -40 °C freezers from the end of the field campaign until sediment processing could be began. The cores were placed in a custom built cryogenic chamber, which flash froze the cores to -80 °C, this was required to ensure the cores remain in one piece during sediment extraction from the casings. The core casings were cut along their length using a circular saw with a depth of cut slightly less than the casing thickness to prevent smearing occurring.

Once the intact sediment cores were removed from their casings the cores were sectioned using a knife in increments measured from the top of the core. Cores were sectioned at 5cm increments, though one core from each site was sectioned at 1cm increments to observe finer scale change. Care was taken to ensure no cross-contamination occurred by cleaning equipment between sections. The extracted sections were then subsampled by pressing a circular aluminium cookie cutter device into the sediment to extract a disc of known volume, this also removed the outer layer of sediment which may have been smeared during the process of driving the corer tube into the marsh. The core sample was then placed in a pre-weighed aluminium tray and placed in an oven for 24 hours at 105°C and then weighed once dry, these measurements allowed the % moisture and bulk density of the sediment to be calculated.

The sediment scrapes were removed from the departmental cold store room where they had been stored since the completion of the field campaign. These samples were placed in a pre-weighed aluminium tray and placed in an oven for 24 hours at 105°C and then weighed once dry. The dried core sediment and the dried scrape sediment were then ground, containerised and counted for gamma emitting radionuclides using the same methodologies described in section 3.2.3 and 3.2.5.

6.2.3. DGPS data processing

The DGPS data were extracted to propriety Leica software Leica Geoffice for post processing with Ordnance Survey (OS) base station data. Four base stations from the OS-Net were selected, these are Giggleswick, Blackpool, Manchester and Daresbury. The DGPS data were shifted towards a reference point that was formed from an average of the four base stations and processed, due to the 1 - hour duration of raw data collection $\pm 1.5 - 3$ cm accuracy is achieved. These data were presented as x, y and z coordinates on the British National Grid coordinate system.

6.2.4. Dosimetry

The dosimetry results collected in the field from a height of 1m over a 600 second duration were entered into standard spreadsheet that calculated the absorbed dose rate in air for each site as $\mu\text{Gy hr}^{-1}$. The air kerma equipment was calibrated by Cavendish Nuclear Ltd in accordance with their UKAS accredited methods. Shortly before field visits the calibration of the air kerma equipment was checked using a ^{137}Cs source to ensure the equipment was functioning correctly.

6.2.5. MoGSS

Mobile Gamma Spectrometry System (MoGSS) is a rapid mobile in situ gamma spectrometry system that logs gamma ray counts and geographic coordinates every one second. With the aid of pre-programmed stripping algorithms total counts for user defined target windows can be measured that minimise the effect of high energy nuclides contributing to lower energy nuclide counts. User defined windows for ^{137}Cs and ^{241}Am were used to extract the data from the surveys. As counts are proportional to the amount of gamma emitting radionuclides within the vicinity of the Na-I (TI) detector this system allows the relative mapping of gamma emitting radionuclides.

The data were processed using the R statistical analysis environment, where a script was written to aggregate all the thousands of spectral data points for each field site (new marsh/old marsh). These data were checked for quality, the main issue found with these data was that at the time of sampling this was an experimental system, which would infrequently result in the DGPS receiver failing to record coordinate data. This error could be easily identified by plotting the data within a geographical information system and following the data's time stamps, data which did not follow the known site survey walk pattern were identified as errors and removed.

6.2.6. Radiogenic contaminant horizontal spatial analysis

The spatial distribution of the surface contaminant concentrations for both saltmarsh areas were calculated using data from the MoGSS in situ Na-I (TI) logging system. This required the development of regression models that could convert the raw MoGSS data to an estimation of ^{137}Cs and ^{241}Am activity concentrations (Bq kg^{-1}). As this MoGSS method is novel, widely accepted spatial statistics approaches were also used to convert the sediment scrape data to an interpolated surface, for the purpose of validation and comparison of spatial trends (Bossler et al., 2010; Ouyang et al., 2003).

Sediment scrape

The sediment scrape data were loaded into ArcGIS with accompanying coordinate data provided by the DGPS, these data were projected to a feature class file before being analysed. The ArcGIS implementation of Empirical Bayesian Kriging (EBK) was used to fit a geostatistical model to these data. The EBK method was selected as it allowed an automatic generation of a semivariogram through a process of subsetting and simulations (Esri, 2012). This simulated semivariogram can be modified by the user in a defined number of simulations so that the, spatial conceptualisation of the underlying geostatistical model is refined through processing. This method is more suitable for smaller data sets, with the primary limitation being its long processing times. The output of these data was four rasters depicting contaminant concentration (Bq kg^{-1}) for ^{137}Cs and ^{241}Am for the new marsh and old marsh site.

In situ Gamma spectrometry data

Using the sediment scrape data and the pre-processed MoGSS data four predictive models were constructed using regression analysis and spatial statistics. The method presented here uses the new marsh ^{137}Cs data set as an example, the analytical steps were conducted for each of the four data sets and the associated figures for the other three data sets can be found in appendix 3.

Table 6.1 Summary of the four regression models produced to estimate ^{137}Cs and ^{241}Am concentration from MoGSS data at the two marsh sites.

| Data set | Regression equation | R ² | P-Value |
|-----------------------------|--------------------------------|----------------|---------|
| ^{137}Cs New Marsh | $y = -496 + \log(188.57x)$ | 80% | <0.001 |
| ^{241}Am New Marsh | $y = -870 + \log(203.9x)$ | 79% | <0.001 |
| ^{137}Cs Old Marsh | $y = -331.96 + \log(130.79x)$ | 74% | <0.001 |
| ^{241}Am Old Marsh | $y = -1141.58 + \log(244.82x)$ | 60% | <0.001 |

The data analysis was conducted within the R statistical analysis environment. Using the dplyr package random sampling algorithm (sample n) the data set was split into two parts; a modelling data set and a validation dataset. Each of the two parts had MoGSS data for ^{137}Cs and the sediment scrape ^{137}Cs activity concentration (Bq kg^{-1}) data. The

modelling dataset was subjected to a regression analysis; a simple log transformation of the predictor variable was seen to produce the simplest regression model that explained the most variance in y with x. This regression model was fitted to the data in figure 6.3 and a summary of the regression equation and parameters is given in table 6.1.

Using the ^{137}Cs counts from the validation data set estimates of ^{137}Cs Bq Kg^{-1} were calculated using the regression equation. These estimated concentrations were plotted against the observed sediment concentrations in figure 6.4, a linear model was fitted to the data for the purpose of visualising the general trend in comparison to a 1:1 prediction line. The general trend in this case was seen to be slightly overestimating at high values and underestimating at low values, this was primarily caused by two points which deviated from the mean. I chose not to remove points that could be considered outliers from visual diagnostic analysis as the NaI (TI) system is known to produce a degree of scatter, therefore my model should try to fit for that scatter. With this scatter the regression model fitted to the data returned $R^2 = 82\%$ p-value <0.001 , therefore the regression model estimates surface activity to within an acceptable margin of error.

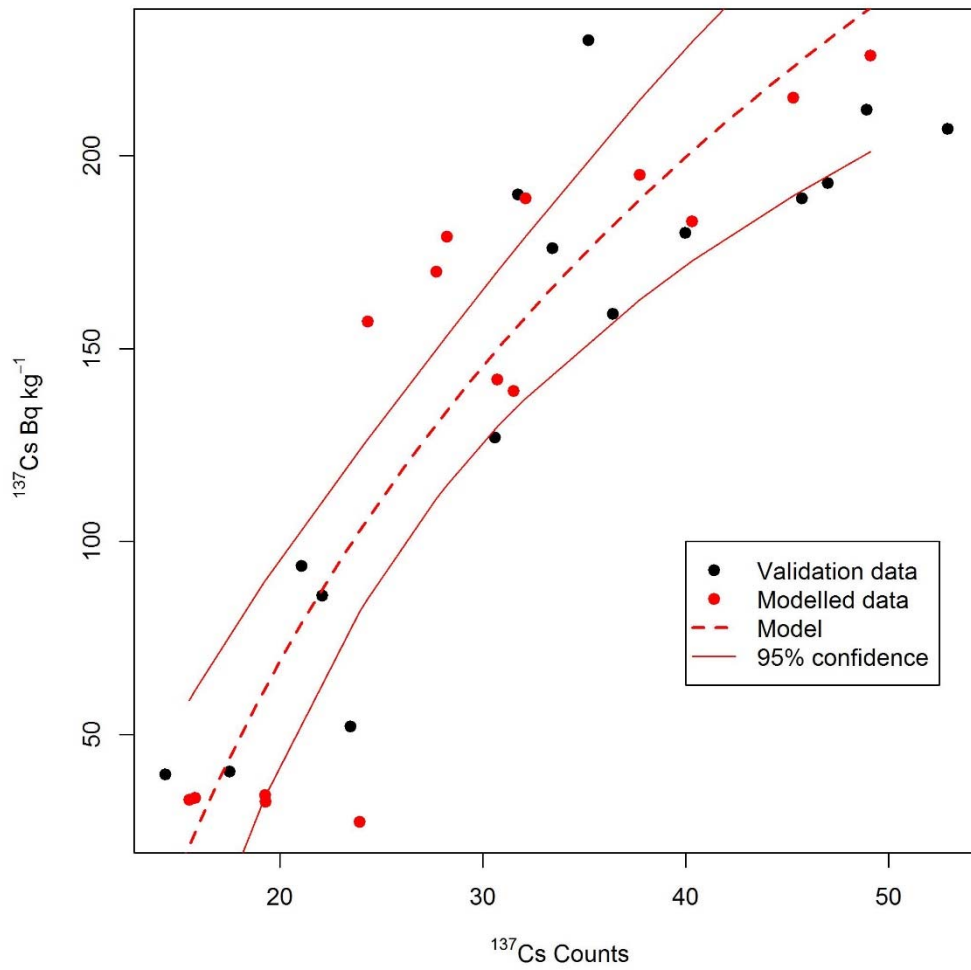


Figure 6.3 Total counts for the ^{137}Cs window from the MoGSS dataset are plotted against the ^{137}Cs Bq kg $^{-1}$ of the sediment scrapes from the new marsh. A regression model which used the log transformed MoGSS data was fitted to the data with 95% confidence intervals.

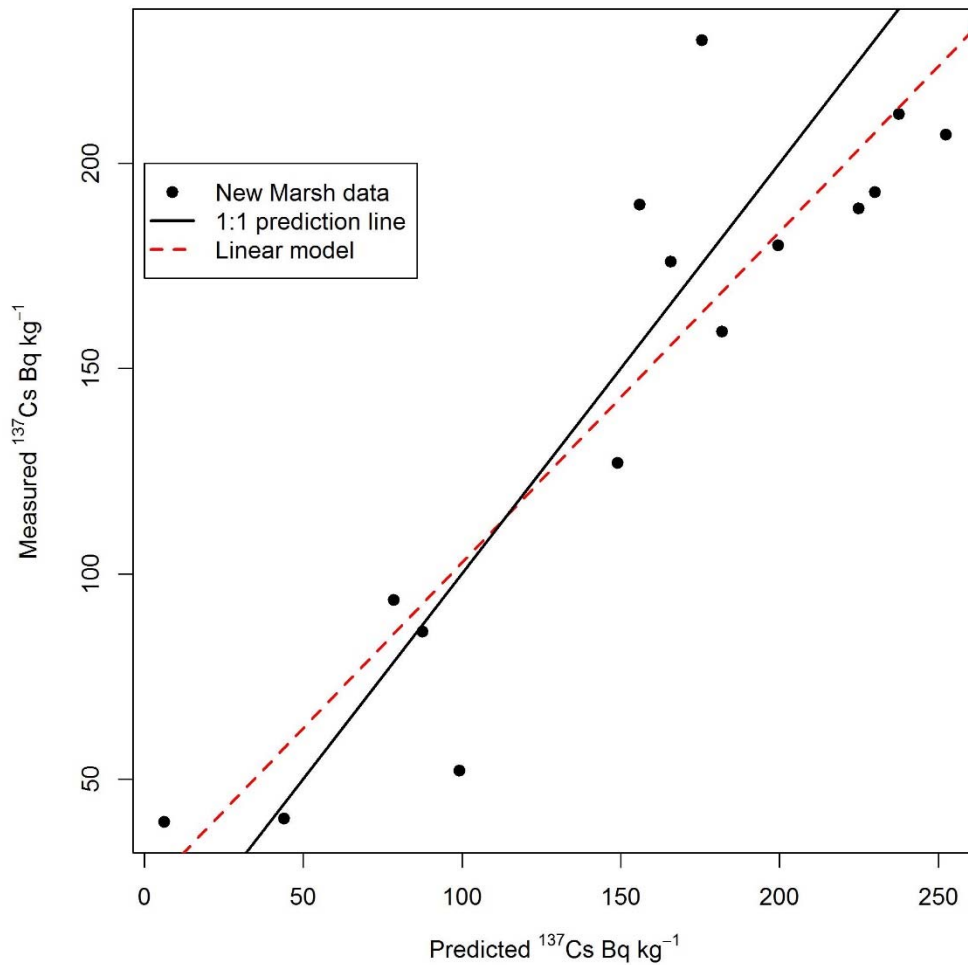


Figure 6.4 Comparison of estimated activity for ^{137}Cs in the new marsh (x axis) and measured activity (y axis) a linear model is fitted to these data to show the general trend in comparison to the 1:1 prediction line.

Having validated these regression models, they were used to make estimations of ^{137}Cs and ^{241}Am activity concentrations for both the new marsh and old marsh sites. These data were then imported in to ArcGIS and had a geostatistical model fitted to them using the Empirical Bayesian Kriging function. A resolution of 0.5 m was set so that the data would be aggregated for most points to smooth out spikes in the data. As the fitted model takes on a nonlinear shape at values of less than 10 counts the model adopts a curve that estimates negative values at less than 10 counts. The adopted solution was to treat negative values as zero contamination and to average them out by using a slightly coarse interpolation of 0.5 m.

6.2.7. Radiogenic contaminant vertical spatial analysis

The four cores collected in this work plus two cores collected from an earlier visit to this site in late 2013 as part of a pilot study were combined and analysed in the R statistical environment. Descriptive statistics were calculated and activity depth profiles were plotted, the interpretation of these data is found below in section 6.3.2. From these data, average contaminant reference values were derived using the mean of the core depth integrated mean. These average contaminant reference values were used in conjunction with the surface activity data to derive reference values for section 6.2.9.

6.2.8. Inferred sediment movement

Morphological change was analysed and inferences of sediment movement were produced from 2007 to 2015 (chapter 5), the estimation of the volumes of sediment that were remobilised within this time period were derived from a subset of the data presented in section 5.4.5. The evaluation here only considered locations in the estuary which were eroding (e.g. where negative values were available in chapter 5 as positive values represent deposition of material) as the focus of this section is on the remobilisation of stored contaminants to the estuarine environment. These sediment movements were fed into section 6.2.9 and used to calculate the volumes of contaminated sediment that had been remobilised.

6.2.9. Radiogenic contaminant remobilisation

The estimation of the quantity of contaminants that were remobilised from the new marsh and old marsh sites required three pieces of information; the volume of sediment that was remobilised, the density of the sediment and an estimate of how much contamination was present in the remobilised sediment. With these three pieces of information, it is possible to estimate the quantity of saltmarsh stratified contaminants that have been remobilised.

The volume of sediment remobilised was determined on a 0.5 x 0.5m basis for the Hesketh Outmarsh site using the raster of difference products with the limit of detection applied (from chapter 5). For every 0.25m² area of the study site a volume of change m³ was provided for this analysis.

The bulk density value of 1230 kg m⁻³ with a standard deviation of 264 kg m⁻³ was determined to be suitable for a reference value of the bulk density of the saltmarsh

sediment. This was based on the descriptive statistics of all the cores collected from the site with this value being agreed as a representative value.

Contaminant reference values were taken from the average of the five cores taken within the marshes and the average surface activity concentrations of the two saltmarshes. Core 17 was not used due to its activity depth profile being representative of a disturbed site, this is explained further in the discussion. The cores that were taken from areas of the marsh that were not disturbed were again favoured as examples of an activity depth profile before disturbance. Contaminant reference values of 233 Bq kg⁻¹ for ¹³⁷Cs and 141 Bq kg⁻¹ for ²⁴¹Am were selected. These values were lower than the undisturbed core sites and higher than the old marsh sites. The ²⁴¹Am value was in line with current surface activities though the ¹³⁷Cs value was higher than current surface activities.

A method that used the ArcGIS raster calculator was developed to determine the amount of contamination remobilised based on bulk density (BD) and contaminant reference values (CRV). The equation below (Eq. 6.1) was typed into the raster calculator and run for every pixel of the volume of change rasters of difference. The raster calculator extracted the pixel value and inserted it as the volume of change (VOC) in the below equation and produced a new raster with each cell containing the amount of contamination that was calculated to have been remobilised. Zonal statistics were used to quantify the total amount of contaminants that has been remobilised since the 2007 disturbance event for the new marsh and old marsh site.

Equation 6.1:

$$\text{Remobilised contamination Bq kg}^{-1} = (\text{VOC } m^3 \times \text{BD kg}/m^3) \times \text{CRV Bq kg}^{-1}$$

6.3. Results

The analysis conducted in this chapter produced an estimation of contaminant remobilisation using Eq. 6.1. To make this estimation the saltmarsh vertical and horizontal variation in contaminant concentration was characterised. The results of these characterisations are presented first then the estimation which uses the characterisation data is presented.

6.3.1. Horizontal spatial properties of radiogenic contaminants

Subsets of the descriptive statistics and model output are presented where necessary, the full printout can be obtained for each model and data set within Appendix 3.

The rasters produced from the geostatistical analysis for both the MoGSS data and the sediment scrape data are displayed as maps in figures 6.5 and 6.6. These maps show that the MoGSS geostatistical models showed a great deal of site variation in comparison to the sediment scrape geostatistical models. The sediment scrape data characterised the sites' surface contamination as a trend of high values in the south and east of the site and low values in the north and west of the site. In comparison the two map products characterised the same spatial trend but the difference is of resolution, with the MoGSS geostatistical model providing a greatly enhanced view of sites' contaminant distribution. A per pixel comparison between these maps is shown in figure 6.7, this figure shows a great deal of variation though the general trend is reproduced here in both data sets ($R^2 = 46\%$ p-value < 0.001).

It should be noted that ^{137}Cs and ^{241}Am share a statistically significant correlation with a regression analysis determining that ^{137}Cs and ^{241}Am activity concentrations had a strong linear relationship ($R^2 = 98\%$, p-value < 0.001), the result is that the spatial trends for figures 6.5 and 6.6 are almost identical.

The descriptive statistics for MoGSS and sediment scrape data show that both methods returned similar means and medians for the concentration of the ^{137}Cs and ^{241}Am (table 6.2). The MoGSS data were less influenced by extremes and had a more normal distribution than the sediment scrape data. From these results the surface sediments of the new marsh site are represented by concentration values of 136 Bq kg^{-1} for ^{137}Cs and 125 Bq kg^{-1} for ^{241}Am .

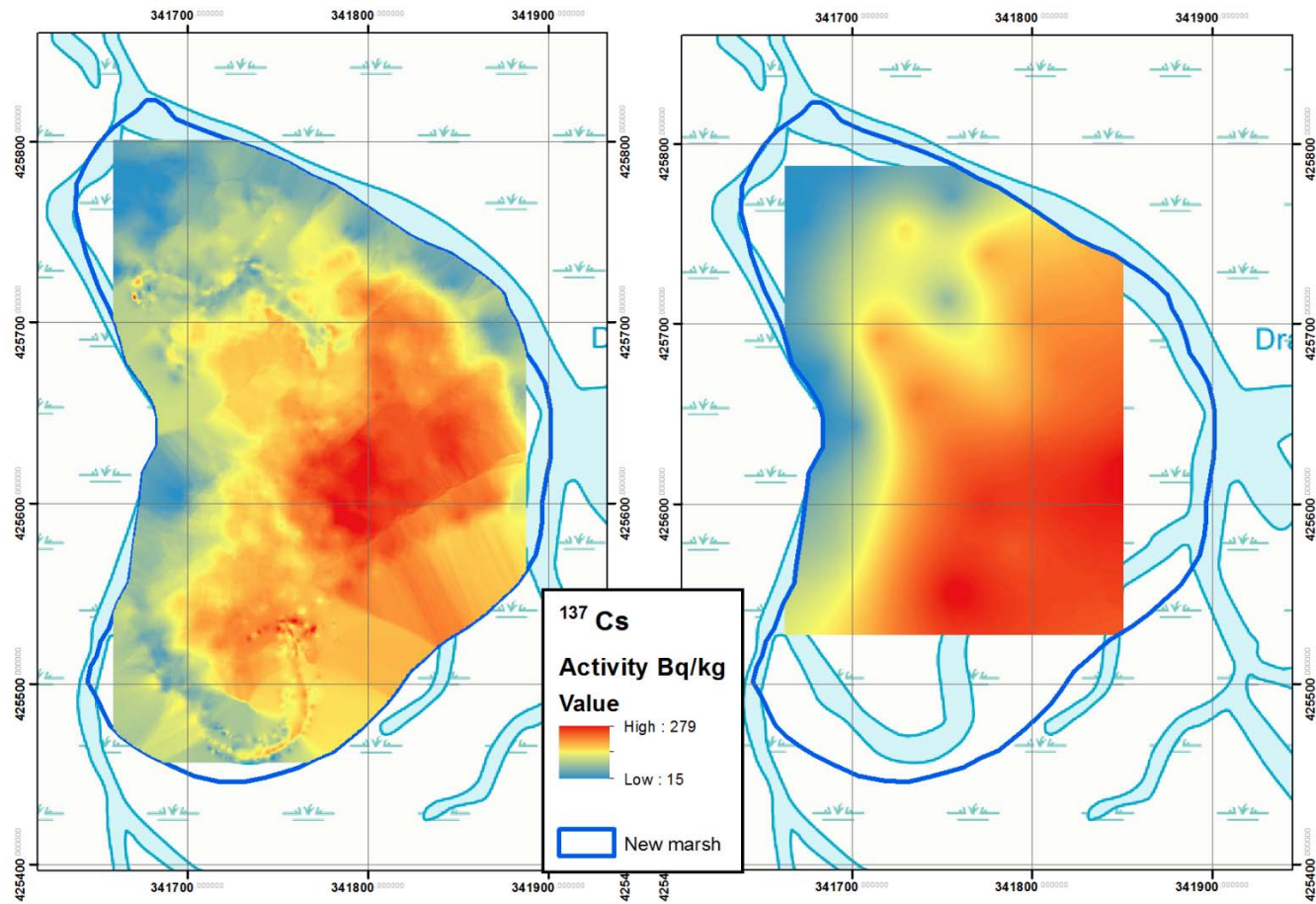


Figure 6.5 The left image shows the MoGSS derived map of surface activity and the map on the right shows the sediment scrape derived map of surface activity for ^{137}Cs at the new marsh site.

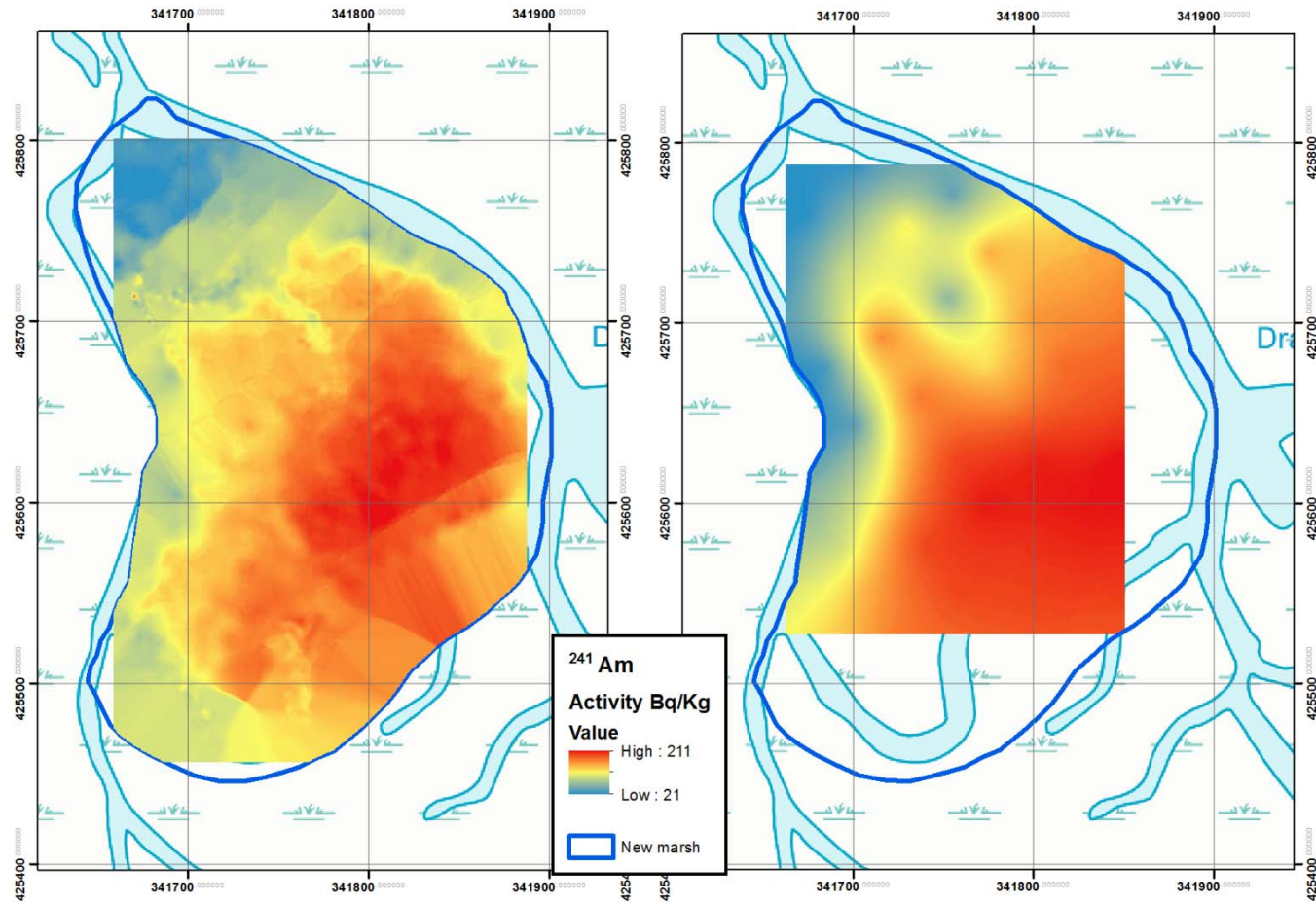


Figure 6.6 The left image shows the MoGSS derived map of surface activity and the map on the right shows the sediment scrape derived map of surface activity for ^{241}Am at the new marsh site.

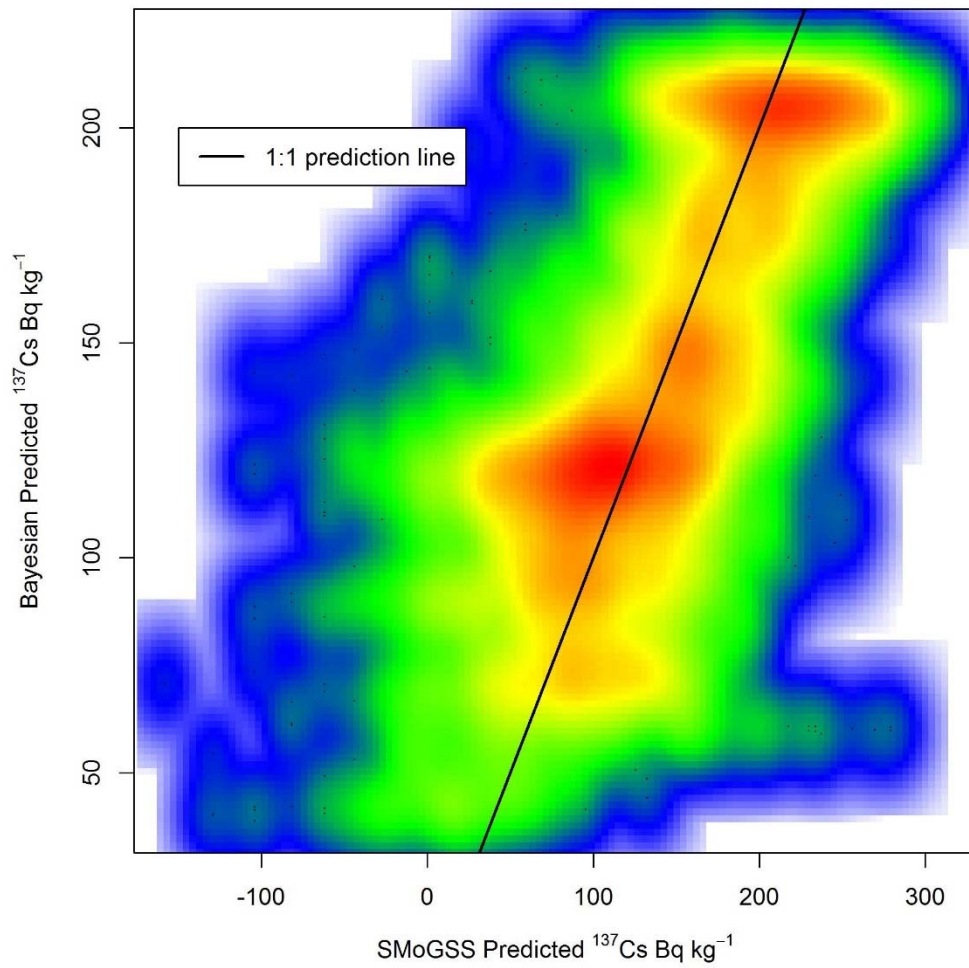


Figure 6.7 Plot of the new marsh MoGSS ^{137}Cs activity concentration data against the ^{137}Cs predicted by the spatial statistics model fitted to the sediment scrape data. The colour ramp from red to blue indicates the number of points at that location.

Table 6.2 Summary statistics for the new marsh site for ^{137}Cs (Bq Kg^{-1}) and ^{241}Am (Bq Kg^{-1}), prefix SM = MoGSS data, prefix SC = sediment scrape. MAD = median absolute deviation.

| Data type | Mean | SD | Median | MAD | Min | Max | Skew | Kurtosis |
|-------------------------------|-------------|-----------|---------------|------------|------------|------------|-------------|-----------------|
| $^{137}\text{Cs}_{\text{SM}}$ | 136 | 62 | 139 | 68 | 1.7 | 313 | -0.07 | -0.57 |
| $^{241}\text{Am}_{\text{SM}}$ | 125 | 42 | 125 | 44 | 1.9 | 235 | -0.17 | -0.37 |
| $^{137}\text{Cs}_{\text{SC}}$ | 138 | 70 | 165 | 59 | 27 | 230 | -0.46 | -1.42 |
| $^{241}\text{Am}_{\text{SC}}$ | 119 | 56 | 144 | 44 | 31 | 183 | -0.54 | -1.43 |

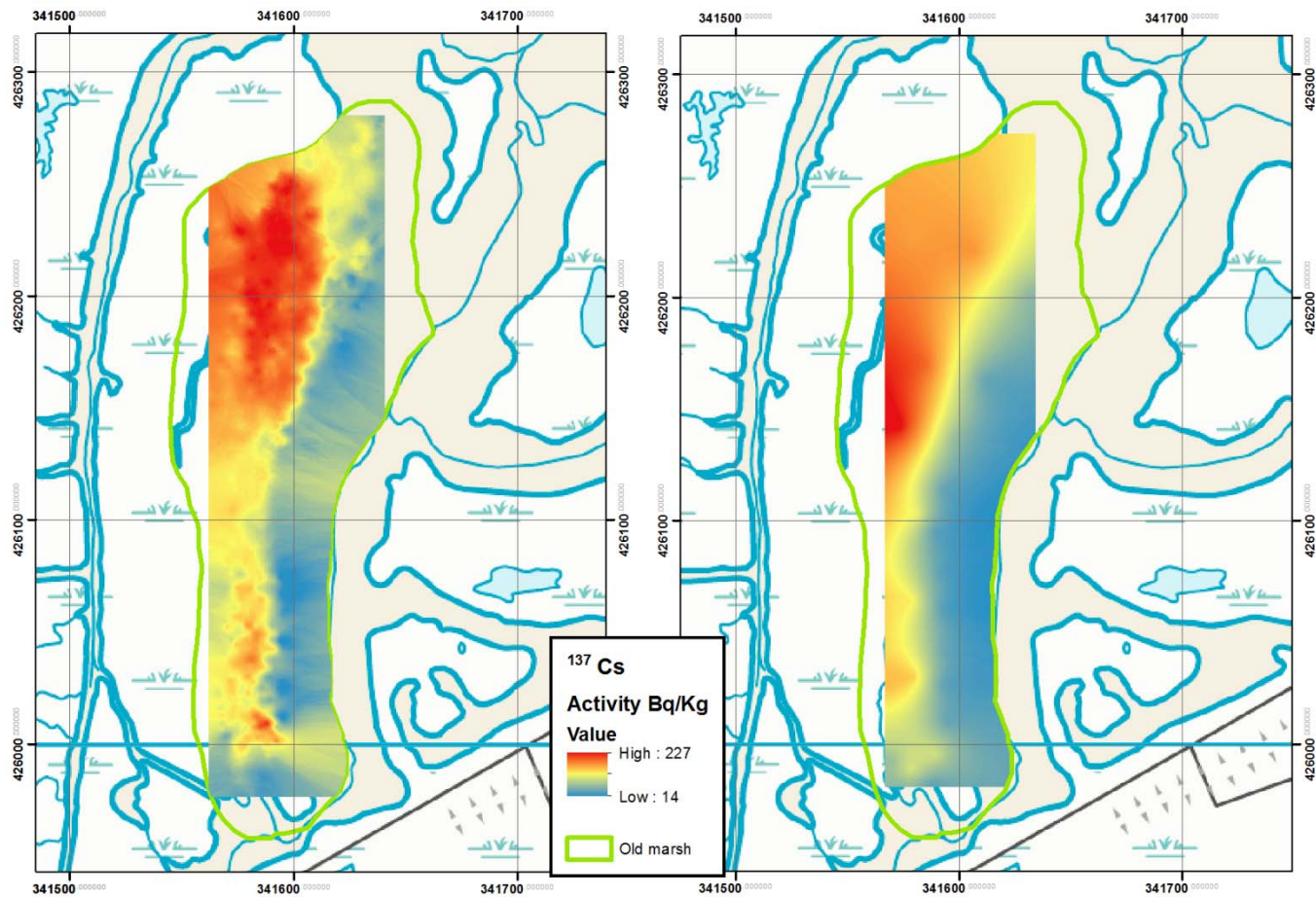


Figure 6.8 The left image shows the MoGSS derived map of surface activity and the map on the right shows the sediment scrape derived map of surface activity for ¹³⁷Cs at the old marsh site.

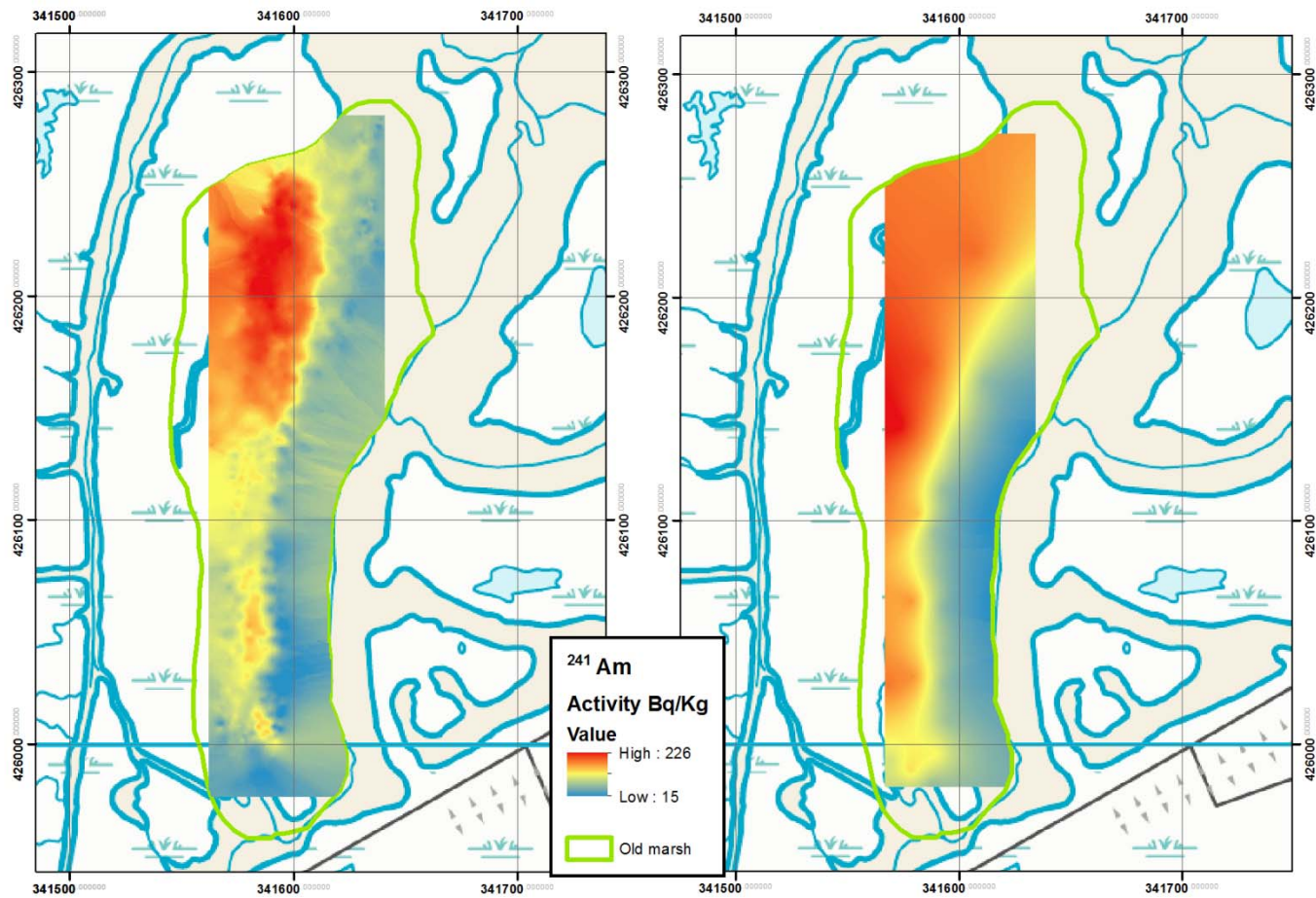


Figure 6.9 The left image shows the MoGSS derived map of surface activity and the map on the right shows the sediment scrape derived map of surface activity ^{241}Am at the old marsh site.

The geostatistical models fitted to the data sets for the old marsh site have good agreement on what the spatial distribution of ^{137}Cs and ^{241}Am is within the old marsh site (figures 6.8 and 6.9). Within the site there was a difference in activity levels with a west east divide clearly present, the western side of the marsh had higher activities. This area with higher activities had a slightly higher elevation and it had a key feature which was a large patch of exposed sediment that drained from north to south across this area.

Table 6.3 Summary statistics for the old marsh site for ^{137}Cs (Bq Kg^{-1}) and ^{241}Am (Bq Kg^{-1}), prefix SM = MoGSS data, prefix SC = sediment scrape. MAD = median absolute deviation.

| Data type | Mean | SD | Median | MAD | Min | Max | Skew | Kurtosis |
|-------------------------------|------|----|--------|-----|-----|-----|-------|----------|
| $^{137}\text{Cs}_{\text{SM}}$ | 114 | 50 | 113 | 52 | 3.5 | 234 | -0.04 | -0.64 |
| $^{241}\text{Am}_{\text{SM}}$ | 107 | 54 | 101 | 57 | 0.1 | 259 | 0.25 | -0.7 |
| $^{137}\text{Cs}_{\text{SC}}$ | 96 | 58 | 108 | 76 | 26 | 235 | 0.36 | -0.86 |
| $^{241}\text{Am}_{\text{SC}}$ | 87 | 44 | 99 | 57 | 28 | 172 | 0.03 | -1.46 |

The MoGSS and sediment scrape data's descriptive statistics show that both methods returned similar means and medians (table 6.3). There was less variability in the old marsh sediment scrape data compared to the new marsh site. From these results the surface sediments of the old marsh site are represented by concentration values of 114 Bq kg^{-1} for ^{137}Cs and 125 Bq kg^{-1} for ^{241}Am .

6.3.2. Radiogenic contaminant vertical profiles

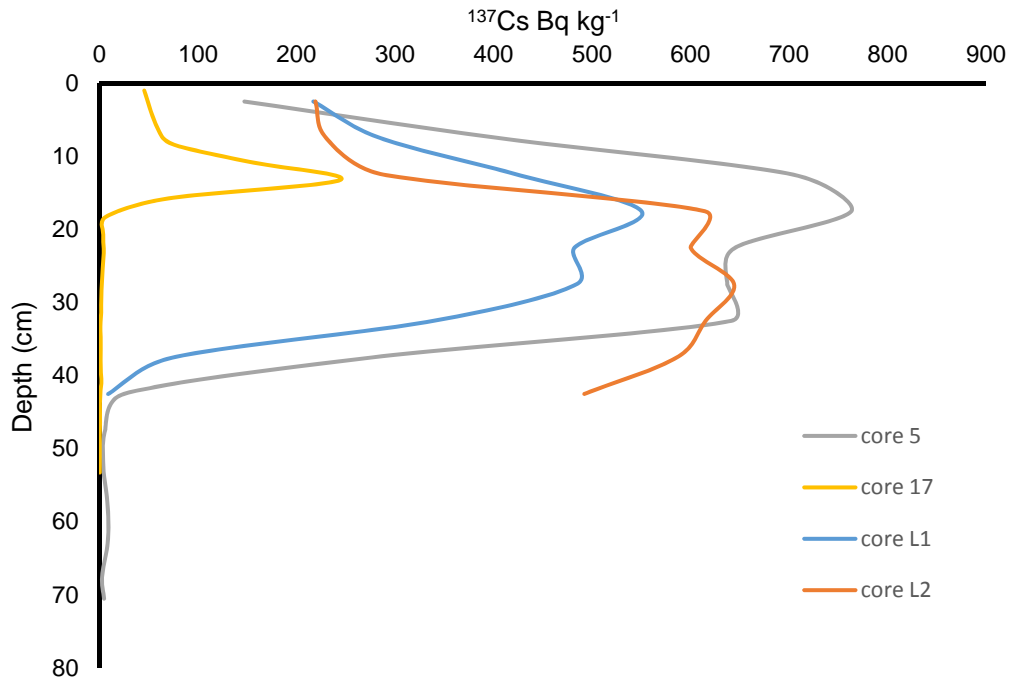


Figure 6.10 Activity concentration depth profiles for ^{137}Cs Bq kg^{-1} for four cores collected from the new marsh site.

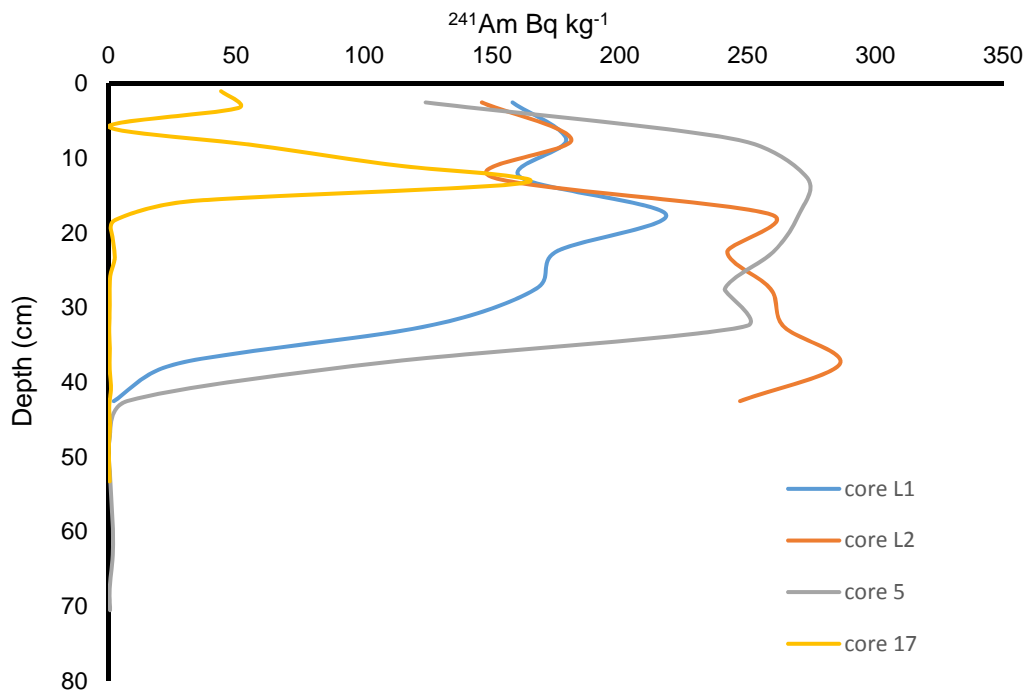


Figure 6.11 Activity concentration depth profiles for ^{241}Am Bq kg^{-1} for four cores collected from the new marsh site.

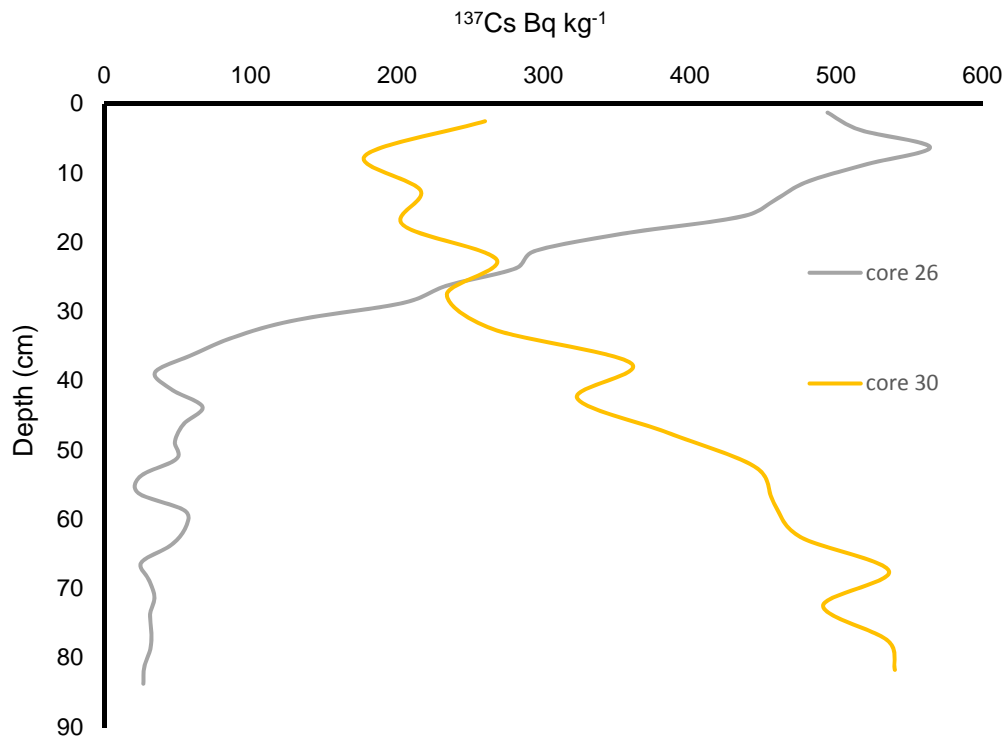


Figure 6.12 Activity concentration depth profiles for ^{137}Cs Bq kg^{-1} for two cores collected from the old marsh site.

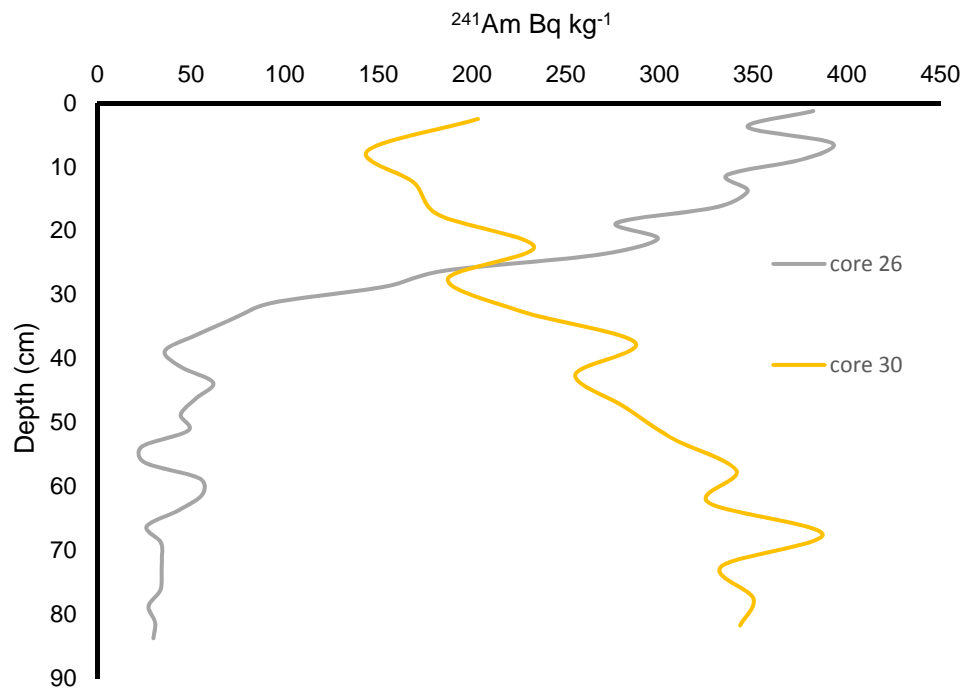


Figure 6.13 Activity concentration depth profiles for ^{241}Am Bq kg^{-1} for two cores collected from the old marsh site.

Figures 6.10 to 6.13 all present core activity concentration depth profiles for ^{137}Cs or ^{241}Am . The figures are a graphical representation of the vertical distribution of the contamination. The saltmarsh surface is represented by a depth 0 cm, contaminant concentration is reported down to 1 m for the long cores and 0.5 m for the shallow cores, in this study two shallow cores (L1 and L2) and four long cores (5, 17, 26 and 30) were collected and analysed. This graphical representation of core contaminant data is standard in the environmental radioactivity literature (e.g. Brown et al., 1999; Mackenzie and Scott, 1993). The cores were compared using their respective elevations to attempt to produce a narrative that incorporated sedimentation rates, however more cores would have been needed for this narrative and thus it was not used. Descriptive statistics for each core were calculated and the relevant statistics for each core are stated in this section where appropriate.

The new marsh site had four cores available. Cores L1 and L2 were collected around 20 m south of the new marsh focus area (figure 6.1). These cores were categorized as undisturbed marsh and were taken as an example of the marshes activity depth profile before disturbance. Core 5 represents a semi disturbed marsh example and core 17 represents a fully disturbed core example. These categorisations of these cores are relevant for deriving the contaminant reference values, the justification and reasoning for the categorisation of these cores is explained fully in the discussion section (6.5.2).

At the new marsh site there was a clear distinction between the activity depth profiles of the sediments, where cores 5, L1 and L2 were similar but core 17 distinctly different. Core 17 was taken from an area of marsh that has seen in excess of 0.5m of erosion as a creek was formed and consequently represents a partial activity depth profile. Cores 5, L1 and L2 have mean activities ranging from 285 Bq kg⁻¹ to 476 Bq kg⁻¹ for ^{137}Cs and 118 Bq kg⁻¹ to 226 Bq kg⁻¹ for ^{241}Am .

The old marsh cores are more complex and on initial inspection core 30 appears suspect, with the likely physical factors that may have accounted for core 30's unique profile described in the discussion section. These cores provide mean activities ranging from 172 Bq kg⁻¹ to 363 Bq kg⁻¹ for ^{137}Cs and 137 Bq kg⁻¹ to 267 Bq kg⁻¹ for ^{241}Am .

These data show that the sediments of the new marsh in terms of the radioactive contaminants had a lower range than the old marsh but the peaks of the activity depth profiles were broader and thus the sediments were more homogeneous in comparison to the old marsh sediments.

6.3.3. Mass balance of contaminants

The volume of change data used to drive the estimation of contaminant remobilisation was processed as a sediment budget for the site. These data are reported in table 6.4. The new marsh site experienced most of its erosion from 2007 to 2009, this was driven by the large scale earth works as part of the realignment scheme. From 2009 to 2014 the site was in a state of accretion with smaller amounts of erosion occurring between 2014 and 2015. The old marsh site experienced less loss of sediment however it remained in a state of erosion for a longer period from 2010 to 2015.

The new marsh and old marsh calculated quantities of ^{137}Cs and ^{241}Am that have been remobilised from the site are presented in table 6.5. These data show 67.3 GBq of ^{137}Cs and 40.9 GBq of ^{241}Am was remobilised in the initial period from the new marsh. 12.5 GBq of ^{137}Cs and 7.6 GBq of ^{241}Am was remobilised in the initial period from the old marsh. In the following years since the managed realignment scheme was implemented a downward trend in the quantity of contamination remobilised for each following year is present.

Table 6.4 Sediment budget data for the Hesketh Outmarsh site from 2007 to 2015.

| Year range | Volume of change (m ³) | | Average (m ³ /m ²) | |
|-------------|------------------------------------|------------------|---|------------------|
| | <i>New marsh</i> | <i>Old marsh</i> | <i>New marsh</i> | <i>Old marsh</i> |
| 2007 – 2009 | -2.2E+05 | -4.1E+04 | -0.56 | -0.61 |
| 2009 – 2010 | 5.3E+04 | 6.1E+03 | 0.21 | 0.06 |
| 2010 – 2011 | 1.9E+03 | -1.5E+04 | 0.02 | -0.31 |
| 2011 – 2014 | 6.8E+04 | -1.1E+04 | 0.21 | -0.12 |
| 2014 – 2015 | -5.3E+02 | -2.7E+03 | -0.01 | -0.07 |

Table 6.5 Calculated volumes of remobilised contaminants for the Hesketh Outmarsh site from 2007 to 2015.

| Year range | Remobilised ¹³⁷ Cs (GBq) | | Remobilised ²⁴¹ Am (GBq) | |
|-------------|-------------------------------------|------------------|-------------------------------------|------------------|
| | <i>New marsh</i> | <i>Old marsh</i> | <i>New marsh</i> | <i>Old marsh</i> |
| 2007 – 2009 | 67.3 | 12.5 | 40.9 | 7.6 |
| 2009 – 2010 | 5.6 | 6.1 | 3.4 | 3.7 |
| 2010 – 2011 | 4.8 | 5.8 | 2.9 | 3.5 |
| 2011 – 2014 | 6.1 | 7.8 | 3.7 | 4.7 |
| 2014 – 2015 | 1.8 | 2.4 | 1.1 | 1.4 |

6.4. Discussion

The saltmarshes were characterised using a novel in-situ technique and these characterisations were used to produce saltmarsh contaminant reference values. These values in conjunction with a multiyear LiDAR derived sediment budget were used to calculate the volume of contaminants that were remobilised in response to the Hesketh Outmarsh managed realignment scheme.

6.4.1. Saltmarsh radiogenic contamination

The developed MoGSS method was validated by using a subset of the data. The results of this validation showed favourable results and proved its predictive ability. As an additional step the data were compared to a geostatistical model; in effect comparing predictions from a Bayesian kriging function to predictions from the MoGSS method. Such kriging functions are used as standard practice (Bossler et al., 2010; Smith et al., 2008) therefore comparing this method to what is in effect a widely accepted practice (e.g. Oh et al., 2009) was seen as a second way of assessing the quality of the method. The results produced the same underlying trend though the MoGSS method allowed finer detail to be mapped, which resulted in a better characterisation of the site.

The new marsh site was in effect an island attached to the rest of the marsh by a narrow isthmus, with large creeks on all sides and two smaller creeks penetrating in to the marsh. The smaller creeks had lower levels of contamination this is likely due to them being some 0.5 m below the marsh surface therefore the subsurface maxima of contamination, which was around 0.1 – 0.2 m in depth, would have been almost entirely remobilised from these locations. The activity depth profile of core 17, which was taken from a creek site supports this as the activity depth profile of the core is much reduced in ^{137}Cs Bq kg⁻¹ activity concentration for the whole core compared to cores such as core 5 which are known to have not experienced erosion.

Core 17 also exhibited an interesting feature in that ^{241}Am had two peaks one at depth with ^{137}Cs and a second located at the marsh surface. This second ^{241}Am peak is the result of deposition of sediments that have enriched ^{241}Am values and not ingrowth as ingrowth would have affected the activity depth profile at all depths where ^{241}Pu and ^{241}Am are found. As the second ^{241}Am peak is in the upper 5cm of sediment it is likely that this second peak was formed by sediment deposition. Such sediments could have come from saltmarshes that have been eroded, which is the case for this site. These enriched sediments could have also come from the estuary or the Irish sea, as ^{241}Am in particular is affected by remobilisations from the environmental store of radioactivity and ingrowth from ^{241}Pu decay (Aston and Stanners, 1982; Hunt et al., 2013; Leonard et al., 1999; Lindahl et al., 2011). This cores activity depth profile proves that the subsurface maxima of historic contamination has been remobilised through erosion and that post deposition remobilisation of radiogenic contaminants is occurring.



Figure 6.14 Photograph of the large main creek which ran adjacent to the old marsh site. This creek expanded in size as a result of the managed realignment, the rough areas seen in the creek are sections of marsh that have been undercut (Photo taken of the Old marsh site in 2015).

The old marsh was an island of saltmarsh surrounded on all sides by creeks. Just under half of its perimeter was adjacent to the main creek, which caused substantial erosion at this site (figure 6.14). The site surface appeared to be composed of two saltmarshes of different age, they are identifiable from aerial photographs by a distinct colour change and in the field, this is identifiable by a step down in elevation. The data showed the site contaminant activity concentration was highest in the westward area which had a higher elevation reflecting the older, more established nature of the saltmarsh.

It is likely that the 1980's land reclamation is responsible for these two different aged marshes at the old marsh site. When the main creek was converted to a dead end by the placement of sea walls it will have begun a process of sediment accretion that was observed to be in operation from 1999 - 2007 prior to the breach (chapter 5.4.5). This accretion would have seen the marshes expand on either side of the main creek, exactly as they were seen to be doing in figure 5.24.

Cores 26 and 30 offer more evidence in support of this theory that the old marsh is in fact two marshes of a different age. Both cores had unusual activity depth profiles that deviated from what would be expected to be found for a mature saltmarsh that had

been accreting sediment and sediment bound contaminants from the beginning of the nuclear age to present day. They also had a high content of sand present which again is unusual, as clays and silts should be dominant. These unusual activity depth profiles are not likely to be caused by smearing as the outer edge of the core slices was removed to avoid smearing during the coring process. This suggests that the old marsh sites contaminant distribution is spatially complex.

The surface of the new marsh showed a great deal of relative variability in contamination with ranges of 311 Bq kg⁻¹ for ¹³⁷Cs and 233 Bq kg⁻¹ for ²⁴¹Am. This variation was true for the old marsh site as well which exhibited similar ranges for both ¹³⁷Cs and ²⁴¹Am. Therefore, there is substantial variability in contaminant concentration across the saltmarsh surfaces. This variability highlights the need to characterise the saltmarshes for this work before determining a reasonable contaminant reference value for the marsh surfaces. As this reference value should incorporate the spatial dynamics of the radiogenic contaminants found at the saltmarshes.

6.4.2. Remobilised radiogenic contamination

The method developed for assessing the quantity of contaminants that were remobilised was a simple linear equation that used saltmarsh contaminant reference values, saltmarsh bulk density values and sediment change values. As this equation was implemented as a per pixel iteration across the study site, there was a great deal of flexibility in which data sets could be used to drive this equation, as the quality of the input data dictated the scope and complexity of the output. Where high frequency data were available for all three parameters then it was possible to produce a high-resolution simulation.

The contaminant reference values were set by conducting an in-depth characterisation of the saltmarshes and generating average values, which were weighted towards the subsurface sediment bound contaminants. They were weighted in that there were three subsurface values for every one surface value and it was the average of these that formed the contaminant reference value. The reasoning behind this was that the current surface spatial distribution of contaminants may be indicative of past spatial distributions of contaminants that were present during marsh formation. This characterisation was conducted to incorporate the spatial trend of contaminant distribution into the contaminant reference values for the site.

The sediment change values were derived from an eight-year sediment budget conducted for the Hesketh Outmarsh site at five time steps, this was part of the Ribble

sediment analysis conducted in chapter 5. These data allowed the assessment of contaminant remobilisation at the relatively fine resolution of 0.5 m. The analysis used an intense characterisation exercise and applied conservative limits of detection that accounted for error propagation in the source data sets to produce a robust method of contaminant estimation.

The new marsh site, as discussed in chapter five, was characterised by high erosion values from 2007 - 2009, these data were skewed by the earth works and landscaping conducted as part of the managed realignment. In this initial period some 67 GBq of ^{137}Cs and 41 GBq of ^{241}Am was lost from the site due to the reestablishment of the main creeks. 2009 - 2010 represents the first year of erosion induced sediment remobilisation that was not caused by the excavation works, though the site was accreting from this point onwards. For this year the quantity of remobilised contaminants was much reduced from the previous time step at 5.6 GBq of ^{137}Cs and 3.4 GBq of ^{241}Am . The rate of contaminant remobilisation continued to decline until 2014 - 2015 with a yearly value of 1.8 GBq of ^{137}Cs and 1.1 GBq of ^{241}Am that was remobilised. These remobilisations were dominated by creek induced erosion of the sides of the marshes by undercutting the saltmarsh creek banks. At present based on the downward trend in erosion it appears that the marsh site has reached some form of equilibrium and is no longer subject to substantial sediment change in the form of major accretion or erosion events.

The old marsh site, which was not subject to the substantial excavation works seen at the new marsh site, was primarily affected by erosion by the widening of the newly reconnected main creek. The initial 2007 – 2009 period reported remobilisation values of 12.5 GBq of ^{137}Cs and 7.6 GBq of ^{241}Am and like the new marsh these values have continued to decline probably as result of the main creek reaching an equilibrium point in terms of its width.

These observations of the quantity of contaminants that have been remobilised and the rates at which they have been remobilised are exactly as they are described, they are remobilised contaminants and not contaminant budgets. The method expressly ignores accretion and focuses on erosion for a number of reasons, erosion is the remobilisation of a volume of the marsh to the intertidal environment. As it is possible to quantify this volume and the likely contaminant concentration of the marsh, then a reasonable estimate of the quantity of contaminants is possible.

Accretion however is more complex the remobilisation mechanism (chapter 5.5) of sediment transfers from the saltmarshes to the mudflats and back to the saltmarsh again involves a mixing and dilution process in the mudflats. Chapter 3 revealed that the concentration of contaminants within the mudflats was highly variable temporally and spatially, in contrast to the vertically stratified saltmarshes. Therefore, producing a reasonable contaminant reference value for these accretions would be fraught with uncertainty. For these reasons this work focused on identifying how much contaminants were being remobilised from the saltmarshes to the Ribble estuary sediment transport system, in effect quantifying these sources of contaminants.

6.5. Conclusion

This work has shown that there was significant spatial variation in how the contaminants were stored within the saltmarshes both in terms of surface spatial variability and the vertical distribution of the contaminants at depth. This spatial variability was measured and incorporated into a contaminant reference value which was used to estimate the quantity of contaminants that have been remobilised from the Hesketh Outmarsh to the Ribble estuary.

From 2007 to 2015 85.6 GBq of ^{137}Cs and 34.6 GBq of ^{241}Am were estimated to have been remobilised at the new marsh site and 52 GBq of ^{137}Cs and 20.9 GBq of ^{241}Am were estimated to have been remobilised at the old marsh site. The rates of remobilisation have reduced substantially over the years, which is believed to be due to the sites reaching equilibrium with the new energy regime caused by the managed realignment scheme.

Based on the data presented, the remobilised sediment and its associated radiogenic contaminants would have been remobilised first to the wider estuary, where it would have mixed with sediment from other sources resulting in a change to the contaminant concentration ratio of this sediment. The 'new' sediment could then have been moved out of the estuary or deposited in other parts of the estuary. A sediment transport model of the Ribble estuary would be required to determine which of these two processes is most likely to have happened. Based on the evidence presented here though, remobilisation of the sediment and its' associated radiogenic contaminants are most likely to enter the Ribble's sediment transfer system and then the Irish sea sediment transfer system. By entering these systems, they are likely deposited according to the hydrodynamics during the time of remobilisation, supporting the idea

of producing a sediment transport model as a potentially useful tool for further work at this site.

Remobilisation of the environmental store of radioactivity from radiogenic contaminant enriched sediments such as saltmarshes has been demonstrated to occur at an accelerated rate for a site that has undergone anthropogenic disturbance (managed realignment). The old marsh site acted as an analogue for understanding the impacts of changing hydrodynamics as a result of a disturbance event. The disturbance and saltmarsh response were somewhat similar to the findings of Browne (2017) whom investigated the post disturbance erosion of saltmarshes. There is however a lack of work looking at these types of disturbance events at a landscape scale with novel results therefore being presented here. The findings at the old marsh site provide evidence that increasing disturbance to the coastal margins, either through an increase in storminess or sea level rise, will likely accelerate the rate of radiogenic contaminant remobilisation to the marine environment.

7. Conclusions

Estuarine and marine sediments can act as sinks for contaminants, with industrial discharges of radiogenic contaminants being concentrated within clay and silt deposits within estuaries as well as within the marine environment (Brown, 1997; Brown et al., 1999; Clifton et al., 1999; Mackenzie and Scott, 1993; Rainey et al., 1999).

Saltmarshes by virtue of their formation processes act as a stratified environmental store of radiogenic contaminants such as ^{241}Am and ^{137}Cs (Assinder et al., 1997; Brown et al., 1999). The time integrated discharges of contaminants that are present within saltmarshes represent substantial coastal contaminant sinks (Gleizon and McDonald, 2010; Rainey, 1999; Wakefield, 2005). These contaminant sinks are often referred to as being part of the environmental store of radioactivity and have previously been thought to be locked within sediments (Rahman et al., 2013b).

Coastal contaminant sinks are now accepted to be acting as sources to other near shore environments within the Irish sea (Hunt et al., 2013). At the saltmarsh scale, remobilisation within the estuary and saltmarsh itself is also known to be occurring (Lindahl et al., 2011; Morris et al., 2000; Oh et al., 2009). With authorised discharges from nuclear facilities being much reduced compared to historic levels, remobilisation of radioactive contaminants from coastal contaminant sinks will, and in some cases already has, emerged as the dominant source of radionuclides to the environment (Aldridge et al., 2003; Goshawk et al., 2003; Hunt et al., 2013; Leonard et al., 1999; Lindahl et al., 2011; Mackenzie and Scott, 1993).

It is the store of contaminants in the sediments that creates interest in better understanding the nature of sediment morphological change and sediment movement. Anthropogenic modifications and climate change have the potential to alter the amount of energy within the estuary and its hydrodynamics, which in turn will impact how sediments are remobilised and cycled within and out with the estuary (e.g. Brown et al., 2016; Azevedo et al., 2010; Browne, 2017; Wolanski et al., 2001). The current expectation that climate change will result in an increasing frequency of storminess is linked to sediment remobilisation (e.g. Mølter et al., 2016). The significance of sediment movements for radionuclide remobilisation was explored throughout his work.

The problem of climate change induced acceleration to the rate of sediment bound radiogenic contaminant remobilisation was considered and the following five research questions have been addressed.

- Are the relationships between estuarine radiogenic contaminants and the sediment matrix temporally and spatially stable in the short to medium term? (Chapter 3)
- Are mechanisms of disturbance significantly correlated with changes in the sediment matrix and radiogenic contaminant concentration? (Chapter 4)
- What is the nature of sediment movement within the Ribble Estuary? (Chapter 5)
- How do saltmarshes respond to the emplacement of a managed realignment scheme within their locality? (Chapter 5)
- How much contamination is remobilised from saltmarshes in response to an analogue for disturbance? (Chapter 6)

7.1. Research questions

7.1.1. Radiogenic contaminants and the sediment matrix

Chapter 3's findings confirmed the established contaminant sediment relationships (MacKenzie et al., 1999; Rainey, 1999) that show ^{137}Cs and ^{241}Am are particle reactive. These findings are important because the expected increase in sediment remobilisation rates under climate change scenarios will have implications for contaminant transport. These particle reactive relationships also underpin the quantification of saltmarsh radionuclide remobilisations conducted within chapter 6 and therefore it was important to establish that these relationships are present at the Ribble estuary. The following questions were asked in chapter 3:

- Are the relationships between estuarine radiogenic contaminants and the sediment matrix temporally and spatially stable in the short to medium term?
- Is there a significant relationship between contaminants and particle size distribution?
- Is there a significant relationship between contaminants and percentage organic matter?
- Is the contaminant sediment property ratios temporally stable? and at what scales do these ratios exist at?

The radionuclides ^{137}Cs and ^{241}Am were found to exhibit strong statistical associations with the particle size distribution, in that as the clay and silt content of the sediment matrix increased so did the concentration of these contaminants. The findings confirm those in the literature that contaminants in general are associated with fine sediments (MacKenzie et al., 1999; Rainey et al., 1999). They also agree with Wakefield (2005) in that disturbance can cause a decoupling in these relationships which I believe in the case of my data was through physical remobilisations of the sediments between deposits (September siltation event).

Organic matter was also a good predictor though it had more inter-transect variability, which made building a general model for the estuary more difficult. ^{241}Am is known to be preferentially bound to organic matter which is why the relationship with organic matter was explored. Percentage of organic matter in the sediment can change seasonally with the influx of detritus from leaf fall in the autumn as well as microphytobenthos production (de Jonge et al., 2012; van der Wal et al., 2008). Therefore, this parameter was assessed over the year to investigate whether these seasonal changes might affect radionuclide concentrations.

The ^{137}Cs and ^{241}Am contaminant sediment property ratios were found to be spatially and temporal variable between transects. The data showed that variation occurred between different transects with transect 3, which was lower down in the tidal frame, having less clay and silt. The data also showed that the contaminant ratios were not temporally stable with the coefficients of determination varying temporally for all transects. However, the data from transect 3 during the September siltation event was the only incidence of variability in the sediment particle size distribution and contaminant concentration rendering the contaminant ratio not statistically significant.

The substantial accumulation of silts during the event described as the September siltation event, decoupled the contaminant fine sediment relationship for sites located lower down in the tidal frame. From May to September transect 3 transitioned from having the coarsest sediment and lowest ^{137}Cs and ^{241}Am activity concentrations of the three transects to having the highest clay and silt percentages and ^{137}Cs and ^{241}Am activity concentrations. The event clearly had higher deposition of fine sediment in comparison with coarse sediment at this site. These finer sediments had higher activity concentrations of ^{137}Cs and ^{241}Am and there had been insufficient time for the two types of sediment to mix thoroughly (Brown et al., 2015). The consequence was that there was too much scatter in the surveyed data for the relationship between radiogenic contaminants and clay/silt to be statistically significant.

There are two possible explanations for the effects of this siltation event on the contaminant sediment property relationships:

1. That the continued gradual accretion of sediments from the Irish Sea at the site over summer caused an enrichment of fine sediments that had higher contaminant concentrations than those sediments found in March and May. However, this does seem unlikely as the Irish Sea sediment is being deposited year-round and its contaminant concentration is similar to those sediments that are already present.
2. A sediment with significantly higher contaminant concentration has been deposited here. The effects of such a deposition would be that the sediment contaminant relationship would exhibit greater scatter whilst seeing bulk contaminant concentrations increase, which they did for this site.

The second explanation is more plausible given the weight of the evidence of the observed changes during the seasonal sampling campaign.

The long-term trend in ^{137}Cs and ^{241}Am contamination at the Ribble estuary is a downward trend in contamination levels until 2002 but from 2002 to 2014 there has not been a significant change in the levels of sediment contamination. This is likely to be the result of diffuse sources of contaminants from the Irish Sea or other parts of the estuary 'topping up' the contaminant concentration at the same rate it is being diluted by sediment mixing (e.g. Hunt et al., 2013). The September siltation event is an example of such an introduction of sediment with a higher contaminant concentration from an area such as the Ribble saltmarshes. It should be noted that these types of remobilisations of saltmarsh sediment to the mudflats were described in chapter 5 in the form of bank migration promoting saltmarsh erosion towards the mudflats.

The research described in chapter 3 confirmed that the relationship between the estuarine radiogenic contaminants and the sediment matrix are temporally and spatially stable with a few notable caveats. For, example the first caveat is that there is variability both spatially and temporally, but this variability does not fundamentally challenge the established wisdom that, as clay and silt increase within the sediment matrix, so does the activity concentration of ^{137}Cs and ^{241}Am . The September siltation event is evidence of sediment bound contaminant transfer from a concentrated sediment deposit (saltmarsh) to a less concentrated sediment deposit (mudflat). The lack of a significant decline in ^{137}Cs and ^{241}Am concentration post 2002 is also evidence

that these activity concentration levels are being inflated by remobilisations from more concentrated deposits within the estuary and from the Irish Sea (e.g. Hunt et al., 2013).

7.1.2. Mechanisms of disturbance and the sediment matrix

The significance of discreet high impact disturbance events that contribute to the short-term modification of the sediment matrix properties as well as the cumulative effect on longer term trends is my second key underpinning mechanism. Storminess is widely regarded as a factor that will become more significant as the frequency of high impact storms increases in future years (Mölter et al., 2016), however its effects are yet to be fully understood (Adams et al., 2011; Esteves et al., 2011; Gutiérrez et al., 2016; Schuerch et al., 2013; Sierra and Casas-Prat, 2014). There is a view that whilst it is not a significant driver at present it may become so in the near future especially for estuaries such as the Ribble that may or may not be at a state of dynamic equilibrium (Pye and Blott, 2014; van der Wal et al., 2002). The following question was asked in chapter 4:

- Are mechanisms of disturbance significantly correlated with changes in the sediment matrix and radiogenic contaminant concentration?

Storminess was found to cause variation in the particle size distribution, sediment elevation and contaminant concentration of the sediment, which is in line with what would be expected from the literature (Brooks et al., 2017; Pye and Blott, 2008; Sierra and Casas-Prat, 2014). The data showed statistically significant causation though this was not repeated at many sites within the Ribble estuary, therefore storminess is considered a minor factor and reciprocal causation in the data was an issue. An interpolation artefact is the likely cause of the presence of the reciprocal causation in these data. The main effect of the interpolation is that an assumption is made about the rate of change at which a property transitions from one measured point to another measured point i.e. it is assumed to be steady and is represented by a straight line between two points. Therefore, I think that the results are valid and that what has been analysed is the long-term trend of how the estuarine sediment matrix responds to successive disturbance from storm events. The cumulative effect of storm events at Southport near the mouth of the Ribble Estuary has been shown to be a significant factor in beach morphological evolution (e.g. Pye and Blott, 2016).

There is a clear causal linkage between storminess / riverine discharge data and the sediment bed elevation change as well as sediment matrix properties such as particle size and contaminant concentration. The Ribble riverine discharges were revealed to be a substantial driver of change within the Ribble estuarine sediments. These

discharges will influence the estuary hydrodynamics and promote seaward erosion during peak river discharges. The riverine discharge will also impact the sediment matrix properties by preventing accretion in the upper estuary as increased river flow will impact sediment deposition from the incoming flood tide (Azevedo et al., 2010; Gleizon et al., 2003). The fact that this disturbance mechanism was predominantly correlated with lower estuary transects, suggests that riverine discharge impacts these sites by eroding sediments from the upper estuary to those lower estuary sites during heavy river discharge periods.

The analysis of reciprocal causation showed that the storminess data, and riverine discharge data was affected by regional climate which influences the precipitation patterns as well as the extent of storminess for the Irish Sea and specifically the Ribble estuary. However, the linkages between the multiple drivers of sediment disturbance and remobilisation should be further explored to yield a fuller understanding of how sediments and the sediment bound contaminants will behave in the coming years. The impact of storminess on the properties of the sediment matrix should also be revisited using higher temporal resolution data sets, specifically to quantify the measurable impact of storminess (Brooks et al., 2017; Esteves et al., 2011; Robins et al., 2016).

7.1.3. Ribble estuary sediment movement

Within estuaries sediments from the marine, estuarine and terrestrial environment are mixed and deposited within mudflats, saltmarshes and sandbanks or transported out with the estuary (Wakefield et al., 2011). This known variability in the sediment deposits, means that environmental stores of radioactivity will at some time scale be vulnerable to remobilisation (e.g. Rahman et al., 2013). The loss of large sections of saltmarsh at Arnside, North West England due to shifting river channels caused by high riverine discharge during the 2013 winter storms, is an example of these stores of radioactivity being remobilised to the Irish Sea. The uneven distribution of radiogenic contaminants within estuarine sediment deposits such as mudflats (Gleizon et al., 2003; Lyons, 1997; Rainey et al., 2003) and saltmarshes (Brown et al., 1999; Lindahl et al., 2011) means that the impact of exposure to radiological contaminants can be variable and dependent upon which sediments are remobilised. To understand the nature of sediment bound contaminant remobilisation the morphological change and sediment movement of the Ribble estuary was explored in chapter 5.

- What is the nature of sediment movement within the Ribble Estuary?
- Is the long-term trend in estuary sedimentation positive (accretion dominant) or negative (erosion dominant)?

- What are the morphological characteristics of sediment movement for the sandbanks, mudflats and saltmarshes?

Characterisation of the Ribble Estuary's sediment spatio-temporal properties was conducted over 16 years from 1999 – 2015, making this estuary one of the best characterised in the world. The analysis focused on sediment morphological change which can be used to infer sediment movement. Where a negative (erosion) or positive (positive) change in sediment morphology was detected the sediment can be said to have moved. This distinction is important as true movement would require repeated daily LiDAR surveys and the incorporation of hyperspectral data (Deronde et al., 2008, 2006).

The geospatial analysis used geo-statistics and clustering algorithms to allow computational delineation of sediment morphological features. This was key to defining the morphological characteristics of the Ribble estuaries sediment movements objectively, as it removed user bias in determining what features were of note. Similar approaches should be applied to future data sets as a means of quantifying morphological change within a complex sediment system.

The analysis of the Ribble Estuary sandbanks in the context of radiogenic contaminant remobilisation is of little interest due to contaminants not binding to coarse grained sediments such as sand. However, the morphological characterisation of these features is perhaps an interesting finding of this research. These features confirm the postulated theory of channel ward migration (Rainford, 1997), which suggests these sands are migrating to the main channel and infilling it (van der Wal et al., 2002). The detected pattern of layered erosion and accretion features shown in figure 5.18 is a clear example of sand migration towards the nearshore and Ribble channel.

The Ribble mudflats and saltmarshes were found to be interconnected, I identified features that suggest a back and forth transfer of sediment between the mudflats and the saltmarshes. Within the mudflats a highly variable pattern of sediment morphological change was interspersed with occasional ellipsoids running parallel to the main channel and delta fans originating from a saltmarsh creek.

The ellipsoids were interpreted as evidence of the ebb tide deposition of sediment as they are formed along the same direction as the receding Ribble ebb tide. The ellipsoids are significant as they highlight how the September siltation event from chapter 3 could have occurred. Transect 3 which ran from saltmarsh edge towards the Ribble main channel is interpreted as having sampled across such an ellipsoid.

Therefore transect 3 sampled two distinct types of sediment with contrasting contaminant activity concentrations resulting in excess scatter in the data. This occurs because the two types of sediment have not had sufficient time to mix from time of deposition to time of sampling.

The delta fans at the mouths of saltmarsh creeks are a deposition feature formed by sediment that has been washed out of the saltmarsh creeks by the ebb tide. The saltmarsh sediments undergo erosion via bank migration and marsh retreat, which causes sediment to be deposited within the large creeks and mudflats in front of the saltmarsh. Bank migration is the process in which undercutting of the saltmarsh that runs parallel to the creeks results in collapse of the saltmarsh bank. This collapse represented the deposition of saltmarsh sediment into the creeks which is then eroded via flood and ebb tides. The presence of extensive erosion within the large network of saltmarsh creeks and the formation of a delta fan at the mouth of the saltmarsh creek, provides evidence of the transfer of saltmarsh sediments to the mudflats.

Some of these remobilised sediments are redeposited within the creeks and on the saltmarsh surface due to the flood and ebb tides of the Ribble estuary. The great spatial and temporal variability of the mudflats will likely mix the mature saltmarsh sediments with new sources from the river, marine and the existing sediment stocks within the estuary. Consequently, this is likely to dilute any historic contaminant levels originating in the saltmarsh sediments, such that the sediment redeposited within the saltmarshes creeks and surface will be distinct from that which was remobilised (e.g. Rahman et al., 2013).

My findings support the views of Rahman et al., (2013) and Hunt et al., (2013) that the environmental store of radioactivity should not be considered 'safely stored' and the implications of remobilisation should be further investigated. Over a ten-year period from 1999 – 2009 the estuary was observed to have undergone a net trend of erosion with some $8.1 \text{ E}+6 \text{ m}^3$ of sediment being un accounted for. Interestingly the effects of marsh retreat and bank migration caused by the evolution of the saltmarsh creek systems resulted in saltmarshes accounting for some 65% of the erosion measured. This is significant as radiogenic contaminants are concentrated in the saltmarshes and such remobilisations confirm the saltmarshes as a source of such contaminants to the estuarine environment.

The dominance of accretion and erosion was found to be temporally variable and that the estuary could switch between either for different years. This is likely evidence of a larger Irish Sea sediment transfer system mechanism and should be investigated in

further research. This is why sediment remobilisation, through the detection of deposition features that reveal a cycling of sediment between the saltmarshes and mudflats are emphasized over sediment budgets, which are fraught with the risk of over interpretation.

7.1.4. Hesketh Outmarsh managed realignment scheme

The Hesketh Outmarsh case study provides the opportunity to study the impacts of a managed realignment scheme on the nearby saltmarshes and sediment deposition in the locality. This is important as such schemes will become more common internationally as governments seek to preserve coastal habitat in response to sea level rise. This scheme represents an anthropogenic modification to the local hydrodynamics of the mid estuary and therefore provided the opportunity to study what may be considered an analogue for disturbance. The Hesketh Outmarsh was explored as a case study of a managed realignment scheme and as an analogue for disturbance, by monitoring the changing morphology of the realignment site and nearby sediment deposits. Using a hindcast the following research question was answered;

- How do saltmarshes respond to the emplacement of a managed realignment scheme within their locality?

Using multiple LiDAR data sets from 1999 – 2015 the sites morphological change and sediment movement were analysed from the initial breach in 2007 to 2015. The analysis focussed on two sites; the first was the area of new saltmarsh created by the scheme (new marsh site) and the second was an area of mature saltmarsh just outside the scheme (old marsh site).

The new marsh site was reconnected to the Ribble estuary via series of landscaping projects that included the excavation of the main historic saltmarsh creeks and the breaching of the sea wall defences. The site underwent extensive erosion for the initial three years after the breach, which was characterised by the formation of a dense network of creeks. The sites creeks widened and deepened through bank migration which resulted in undercutting of the marsh along the creek networks and the subsequent remobilisation of the saltmarsh sediments. At the same time, there was substantial deposition of sediment on the marsh surface from 2009 onwards. The dramatic reduction in sediment movement by 2014 and 2015 suggests that the effects of the initial disturbance of realignment have diminished such that the site is now nearing equilibrium with the estuary.

The old marsh site was most interesting to this work as it represented a response to modified hydrodynamics, which means those findings are generalised easier than the new marsh site which experienced excavations. The old marsh site responded to the main creek that ran through the site transforming from a dead end to being connected to a newly forming saltmarsh. These modifications to the saltmarsh creeks create altered hydrodynamics, that result in increased water velocities and drainage times that will cause creek erosion that can continue for some time after the point of disturbance (Browne, 2017; Pieterse et al., 2017). The old marsh site had previously been accreting within the creeks, specially at the ends of the creeks which were infilling suggesting that this was a long-term trend in response to the initial construction of the sea walls that made these creeks a dead end in the 1980s.

It has been suggested in the literature that modifications to the hydrodynamics of an estuary can result in changes to sediment deposition and rates of erosion (Azevedo et al., 2010; Gleizon et al., 2003; Stark et al., 2017). At the old marsh site, such erosion and deposition of sediment was quantified in response to a change in hydrodynamics, and it can be concluded that the site underwent extensive erosion in response to the managed realignment scheme. As climate change is anticipated to modify estuary hydrodynamics (e.g. Blott et al., 2006) then these findings support the assertion that climate change may result in enhanced saltmarsh erosion.

7.1.5. Saltmarshes as sources of contaminants

The detected remobilisation of sediments from the Ribble saltmarshes will result in the transfer of sediment bound radiogenic contaminants to the mudflats where they are mixed and redistributed either within the estuary or out with the estuary. Saltmarshes therefore act as a diffuse source of radionuclides to the wider estuary. Understanding the nature of these remobilisations first requires an understanding of the spatial distribution of radionuclides within the saltmarsh, as the spatial distribution can be complex (Oh et al., 2009). The following research questions were addressed:

- How much contamination is remobilised from saltmarshes in response to an analogue for disturbance?
- Is there significant spatial variation in saltmarsh contaminant concentration?
- How much historic contamination has been remobilised as part of sediment movements at the Hesketh out marsh site?
- How has the temporal trend in contaminant remobilisation changed since disturbance?

The old marsh site appeared to be composed of two saltmarshes of different ages, identifiable from aerial photographs and as a change in elevation. The data showed the site contaminant activity concentration was highest in the westward area which had a higher elevation and was probably the older saltmarsh. This would also be consistent with being formed during the initial land reclamation in the 1980s, with the eastern part of the marsh accreting substantially due to the construction of the sea walls.

The new marsh site surface activities of ^{241}Am and ^{137}Cs support the assumption that remobilised contaminants are mixed and diluted before being deposited on the marsh surface. This was evident in the lower surface activities found in areas off the new marsh site that are known to have undergone erosion and then deposition. The increased activities of ^{241}Am within some surface sediments however do suggest that a source of ^{241}Am , likely the sub surface maxima of eroded saltmarsh sediments elsewhere in the estuary is being deposited on the marsh surface with marginal mixing. This conflicting evidence suggests that the deposition of remobilised sediments and the associated radionuclides is variable and likely subject to the prevailing hydrodynamics and energy within the system at the time of erosion.

The complex spatial variability of contaminant distribution within the saltmarshes supports the decision to develop a novel measurement driven geostatistical approach to quantify the spatial properties of the saltmarsh contaminants. The approach taken allowed contaminant remobilisation to be estimated from high resolution radionuclide characterisation and sediment movement data products. Remobilisation in this context is important as it referred to the movement of contaminants from a vertically stratified source as it is within the saltmarshes, to the creeks and mudflats where it may be mixed and deposited on the marsh surface. This is important as without a daily time series it is not possible to quantify contaminant movements post remobilisation, even if those movements were to be transfers back to the saltmarsh. Therefore, this method quantified the amount of ^{137}Cs and ^{241}Am that was removed from the saltmarshes as stratified deposits.

Radionuclide transfers to the estuary from 2007 – 2015 were estimated as 86 and 52 GBq of ^{137}Cs and 35 and 21 GBq of ^{241}Am , from the new and old marsh sites respectively. These remobilisations were substantially reduced in later years with most movement occurring in the initial years after the realignment (e.g. 2007 – 2009). This quantification of remobilised ^{137}Cs and ^{241}Am is the first time such a remobilisation has been physically measured opposed to past modelling/inference approaches and is a

valuable contribution towards efforts to improve our understanding of the environmental store of radioactivity (Gleizon and McDonald, 2010; Hunt et al., 2013).

The peak Sellafield discharges during the 1980's were approximately 5000 TBq for ^{137}Cs and 140 TBq for ^{241}Am , the particle reactive discharges are now incorporated within sediment deposits around the Irish sea such as saltmarshes. Now with current discharges being 3.1 TBq of ^{137}Cs and 30 GBq of ^{241}Am (Cefas, 2015), diffuse remobilisations of environmental radioactivity from sediment deposits are likely to be the main source of radionuclides to the environment.

7.2. Implications for contaminant movement

In this work, it has been shown that radionuclides are being remobilised into the environment as a result of reworking of sediments in mudflats and saltmarshes. This is occurring at a range of spatial and temporal scales. The reworking mechanisms are likely to be exacerbated by the impacts of climate change which will increase disturbance through an increasing frequency of high impact storms. Using a managed realignment scheme as an example of disturbance to an area of saltmarsh, strong evidence has been gained for what the impacts of such a disturbance would be specially the implications of altered hydrodynamics.

The managed realignment scheme at the Hesketh Outmarsh resulted in substantial erosion from 2007 -2009 at both the new marsh site and the old marsh site. At the old marsh site this erosion occurred due to an increase in the water velocities and drainage times of the main creeks caused by the expansion of the tidal frame into the new marsh site. These increased water velocities result in modified hydrodynamics at the old marsh site, such that there is more energy in the system which promotes bank migration as the main creeks widen and deepen resulting in saltmarsh sediment that borders these creeks being eroded.

There is enhanced erosion within the main creeks, but the modifications to the hydrodynamics have caused the branching network of smaller creeks to accelerate their development and expand having previously been in a state of infilling (pre-2007). Saltmarsh erosion at this site is a function of undercutting within the creeks, which leads to sections of marsh collapsing into the creek. This bank migration is very similar to how a river meanders across its flood plain. The marsh sediment that is eroded represents a vertical cross section of the saltmarsh and therefore encapsulates a full depth profile of radionuclides contained and laid down within the saltmarsh over the past 60 years that Sellafield has been operating. These sediments and their associated radionuclides are eroded by the flood and ebb tides with material moving between the

main creeks and nearby mudflats. At the old marsh site, it is estimated that some 52 GBq of ^{137}Cs and 21 GBq of ^{241}Am has been remobilised in this fashion between 2007 and 2015.

The eroded sediment accumulates within the main creeks and the nearby mudflats where it forms delta fans at the mouths of the main creeks. These eroded sediments can be remobilised from the creeks to the marsh surface; where this occurs shortly after erosion, it results in increased activities of ^{241}Am at deposition sites on the marsh surface. The eroded sediment is however eventually washed out by the ebb tides to the mudflats where a combination of flood/ebb tides, tidal bores and riverine discharge promote the redistribution of these sediments within the wider estuary. These factors will also promote the mixing of the saltmarsh sediments with mudflat sediments and the eventual dilution of the sediment bound radiogenic contaminants.

The transfer of these saltmarsh sediments to the mudflat will result in an initial period where the newly arrived sediment is significantly different in particle size distribution and contaminant concentration to the sediments already at the site. The deposition of such sediments as bulk deposits has been identified as 'mud drapes' in the literature (Choi and Kim, 2016; Wakefield, 2005) and was also seen in the September siltation event described in chapter 3. Such transfers of concentrated sediment bound contaminants to the mudflats represents the remobilisation of the environmental store of radioactivity.

These remobilisations can have significant effects on the inter annual variation in radioactivity levels of the receiving site. At the Lytham mudflats, the lack of a significant decline in ^{241}Am and ^{137}Cs concentrations from 2002 to 2014 despite 12 years of mixing and dilution is believed to be in part caused by the addition of contaminants from the environmental stores of radioactivity in the estuary, such as the saltmarshes and from the Irish sea mud patch.

7.3. Future work

A number of research activities should be considered in the future:

7.3.1. Daily sediment morphological change and sediment movement

LiDAR measurements of the Ribble estuary at frequent time intervals would allow a more detailed study of sediment morphological change to be undertaken. In the current work, the shortest time period between observations was one year and in some cases, there were gaps of several years between measurements. It is desirable to observe sediment morphological change and movement in direct response to mechanisms of

disturbance so ideally on short time scales for example pre and post major storm disturbance events. The daily flood and ebb tidal cycle operates at the finest temporal resolution of these mechanisms of disturbance. Therefore, future work should aim to explore sediment morphological change and sediment movement at a daily time scale for the purpose of evaluating the 3D effects of the flood ebb tidal cycle. This would contribute to a refinement of the knowledge of the extent of daily sediment remobilisations as present estimations rely on inferences from modelled hydrodynamics and 2D quantifications (Wakefield et al., 2011).

Recognising however the logistical difficulties associated with this recommendation, it is further recommended that advanced airborne LiDAR systems be developed to survey the Ribble estuary in its entirety using drones for example to reduce the logistical difficulties associated with aircraft based LiDAR. At present LiDAR data is economically expensive to acquire for large areas such as estuaries and therefore a cheaper alternative could use recent advances in photogrammetry (Brunier et al., 2016; Jaud et al., 2016).

Such work would however reveal the extent of morphological change and sediment movement and would produce a high-resolution sediment budget for a single flood ebb tidal cycle. This would have the added advantage of allowing the quantification of daily radiogenic contaminant remobilisations using the methods described in chapter 6. Understanding the effects of the daily flood and ebb tidal cycle on the remobilisation of sediments and sediment bound contaminants should be an area for further study in the coming years.

7.3.2. Radiogenic contaminant remobilisation method application to other estuaries

The method developed to estimate the quantity of radiogenic contaminants remobilised from the Hesketh Outmarsh saltmarshes in chapter 6 should be applied to a more radioactively contaminated saltmarsh site such as those found in the Ravenglass estuary. As the UK's most radioactively contaminated estuary, remobilisation of Ravenglass sediments could be used as a worst-case scenario, in determining whether there is a significant risk to humans or the environment from the relocation of the radionuclides within the estuary. If the risk is low here, then there should be little concern from radioactive contaminants in other estuaries. The findings of Rahman et al., (2013) showed that remobilisations of contaminants could approach safety thresholds in a dosimetry based risk assessment at saltmarshes that were more concentrated in contaminants. So such an evaluation using the tools developed here would be beneficial. In recent years there is evidence to suggest that Ravenglass is

acting as a sink for remobilised Sellafield mud patch radiogenic contaminants and also as a diffuse source to the wider Irish Sea (Aston and Stanners, 1982; Goshawk et al., 2003; Hunt et al., 2013; Lindahl et al., 2011; Oh et al., 2009).

7.3.3. Revisiting storminess granger causality at a higher temporal resolution

Chapter 4 explored the nature of disturbance mechanisms on the sediment matrix of the Ribble estuary mudflats. The analysis did show that increased storminess was significant however this was not a substantial factor in explaining the variation in the sediment matrix. Past modelling and field investigations have both concluded that storminess, specifically in the form of high amplitude waves, is expected to be a significant factor in sediment remobilisation in the Ribble estuary (Luo et al., 2015; Rainford, 1997; Robins et al., 2016; van der Wal et al., 2002). However, the temporal resolution of my sediment property data in this project was too coarse and therefore only the underlying trend in the storminess data was only partially detected.

Sediment property data collected at a higher temporal resolution should be collected to enable a proper time series analysis to determine if storminess specifically the associated high amplitude waves are responsible for detectable modifications to the sediment matrix. The best approach would be to place sensors along a section of saltmarsh to measure changes in it and the fronting mudflat. Topographic data and optical reflectance spectra data would allow both the quantification of the sediment particle size distribution as well as quantification of sediment movement (Montreuil et al., 2014; Rainey et al., 2003; Wal and Herman, 2006). The work of Deronde et al. (2006; 2008) highlights how such data can be used to explore sediment movement along a section of sand dominated coast and these same methods would be applicable to a mudflat.

The recent advances in automatic image stack adjustment based photogrammetry would allow a relatively low-cost alternative to the above proposed work (Brunier et al., 2016; Jaud et al., 2016). The emplacement of high resolution cameras at multiple points could yield daily estimates of mudflat morphological change. This approach would allow a time series analysis to be conducted as was done in chapter 4 but with a much higher spatial and temporal resolution data. The downside to this approach is that it would be computationally intense however with advances in processing algorithms the associated time of this type of processing has been reduced. Daily time series analysis might result in a different outcome from that of chapter 4 but either way the effect of storminess on the mudflat sediment matrix would be better quantified.

7.3.4. Modelling saltmarsh diffuse radiogenic contaminant releases

Repeated measurements of the sediment matrix and estuary morphology were used to infer temporal change in the Ribble's sediment deposits from a 1 m² quadrat scale up to landscape scale. This approach produced three datasets: 1) a 19-year hindcast of mudflat ²⁴¹Am and ¹³⁷Cs relationships with sediment particle size; 2) a 16-year hindcast of estuary morphological change; and 3) a 10-year estimation of the Ribble's sediment budget. By observing changes in the past, it is possible to predict what changes might occur in the future.

Work conducted using similar geospatial modelling approaches to those used here would provide an excellent training data set for advanced modelling. A sediment transport model that can resolve the nature of diffuse radiogenic contaminant remobilisation from environmental stores of radioactivity would be a useful tool, with applications for a wider range of estuarine contaminants. Production of such a tool may be possible in the near future given recent advances in coastal modelling (e.g. van Maanen et al., 2016) resulting in a new ability to quantify the sediments of the intertidal environment at a high spatial resolution and to observe fine scale changes at a high temporal resolution.

Such an advanced model would take the form of a machine learning framework similar to a neural network, which would use continued observations of how the estuarine and marine sediments are changing to improve its predictive power (Buyukyildiz and Kumcu, 2017; Lagos-Avid and Bonilla, 2017; van Maanen et al., 2010). A limiting factor on the implementation of such a model though is the lack of high spatial and temporal resolution data. With increasing availability of high-resolution topographic data sets and the availability of new airborne sensing platforms such as UAV LiDAR and photogrammetry, this may no longer be the case.

The creation of a routine survey programme at the Ribble saltmarshes that used UAV derived topographic surveys or sensors in situ to observe daily changes in the saltmarsh is desirable. An ideal field site for this would be the eastern Hesketh Outmarsh, which is undergoing managed realignment in 2017. The coupling of high spatial and temporal resolution topographic data with advanced machine learning may reveal new insights into saltmarsh sediment transfers in response to disturbance.

7.4. Summary

In summary, a multidisciplinary approach was used to analyse the spatio-temporal characteristics of Ribble estuary sediment and its associated sediment bound radiogenic contaminants. The morphological changes within the saltmarshes and

mudflats were identified and showed saltmarsh sediment erosion with subsequent transfer of this eroded sediment to the mudflats. The sediment matrix and associated contaminants were temporally variable and sensitive to disturbance mechanism such as high riverine discharge and storminess. The evidence collected shows that there are spatial and temporal trends which indicate post deposition remobilisation of radiogenic contaminants is occurring.

The environmental store of radioactivity is functioning as a diffuse source of radionuclides to the Ribble estuary and by extension to the Irish Sea. This is likely to be accelerated by disturbance which is anticipated to increase as a consequence of climate change. While the full implications of disturbance are not yet understood, it is known that events which modify local hydrodynamics can in turn lead to changes in sediment transport and erosion rates. Therefore, increasing the frequency of high impact storm events associated with climate change will most likely result in an accelerated rate of radionuclide remobilisation from the environmental store of radioactivity.

There should be further work investigating the radiological significance of these remobilisations for human and non-human biota that utilise estuaries and other coastal environments. This should be investigated further at sites with more concentrated radiogenic contaminant sinks than those of the Ribble estuary such as the saltmarshes found in the Ravenglass estuary.

[This page is intentionally left blank]

Appendix 1

Appendix T1.1 Correlation matrix for a range of sediment metal concentrations

| | Al | As | Ba | Cd | Co | Cr | Cu | Fe | Hg | K | Mg | Mn | Ni | P | Pb | Sr | V | Zn | Ca | Mo |
|----|-------|-------|-------|-------|-------|-------|-------|-------|-------|-------|-------|-------|-------|-------|-------|-------|-------|-------|-------|-------|
| Al | 1.00 | 0.88 | 0.85 | 0.65 | 0.78 | 0.96 | 0.37 | 0.80 | -0.12 | 0.91 | 0.76 | 0.69 | 0.80 | 0.69 | -0.19 | 0.80 | 1.00 | 0.55 | 0.42 | 0.46 |
| As | 0.88 | 1.00 | 0.71 | 0.82 | 0.90 | 0.94 | 0.63 | 0.89 | -0.01 | 0.90 | 0.87 | 0.77 | 0.92 | 0.80 | 0.13 | 0.79 | 0.90 | 0.78 | 0.52 | 0.48 |
| Ba | 0.85 | 0.71 | 1.00 | 0.52 | 0.62 | 0.80 | 0.19 | 0.67 | -0.11 | 0.73 | 0.68 | 0.61 | 0.56 | 0.59 | -0.28 | 0.77 | 0.85 | 0.40 | 0.52 | 0.40 |
| Cd | 0.65 | 0.82 | 0.52 | 1.00 | 0.96 | 0.78 | 0.73 | 0.95 | -0.11 | 0.75 | 0.93 | 0.85 | 0.89 | 0.88 | 0.49 | 0.70 | 0.66 | 0.92 | 0.60 | 0.31 |
| Co | 0.78 | 0.90 | 0.62 | 0.96 | 1.00 | 0.89 | 0.73 | 0.98 | -0.13 | 0.85 | 0.97 | 0.88 | 0.95 | 0.90 | 0.37 | 0.76 | 0.79 | 0.91 | 0.60 | 0.35 |
| Cr | 0.96 | 0.94 | 0.80 | 0.78 | 0.89 | 1.00 | 0.55 | 0.89 | -0.13 | 0.94 | 0.88 | 0.77 | 0.90 | 0.83 | 0.04 | 0.84 | 0.96 | 0.74 | 0.57 | 0.44 |
| Cu | 0.37 | 0.63 | 0.19 | 0.73 | 0.73 | 0.55 | 1.00 | 0.67 | -0.09 | 0.51 | 0.69 | 0.60 | 0.74 | 0.67 | 0.55 | 0.51 | 0.38 | 0.85 | 0.54 | 0.23 |
| Fe | 0.80 | 0.89 | 0.67 | 0.95 | 0.98 | 0.89 | 0.67 | 1.00 | -0.14 | 0.82 | 0.95 | 0.88 | 0.90 | 0.86 | 0.26 | 0.76 | 0.80 | 0.85 | 0.57 | 0.33 |
| Hg | -0.12 | -0.01 | -0.11 | -0.11 | -0.13 | -0.13 | -0.09 | -0.14 | 1.00 | -0.11 | -0.14 | -0.13 | -0.11 | -0.11 | -0.04 | -0.14 | -0.12 | -0.12 | -0.12 | 0.21 |
| K | 0.91 | 0.90 | 0.73 | 0.75 | 0.85 | 0.94 | 0.51 | 0.82 | -0.11 | 1.00 | 0.82 | 0.67 | 0.88 | 0.80 | 0.11 | 0.77 | 0.92 | 0.71 | 0.50 | 0.54 |
| Mg | 0.76 | 0.87 | 0.68 | 0.93 | 0.97 | 0.88 | 0.69 | 0.95 | -0.14 | 0.82 | 1.00 | 0.89 | 0.90 | 0.94 | 0.37 | 0.80 | 0.77 | 0.89 | 0.74 | 0.31 |
| Mn | 0.69 | 0.77 | 0.61 | 0.85 | 0.88 | 0.77 | 0.60 | 0.88 | -0.13 | 0.67 | 0.89 | 1.00 | 0.78 | 0.85 | 0.26 | 0.72 | 0.68 | 0.77 | 0.59 | 0.12 |
| Ni | 0.80 | 0.92 | 0.56 | 0.89 | 0.95 | 0.90 | 0.74 | 0.90 | -0.11 | 0.88 | 0.90 | 0.78 | 1.00 | 0.85 | 0.36 | 0.75 | 0.81 | 0.88 | 0.54 | 0.40 |
| P | 0.69 | 0.80 | 0.59 | 0.88 | 0.90 | 0.83 | 0.67 | 0.86 | -0.11 | 0.80 | 0.94 | 0.85 | 0.85 | 1.00 | 0.42 | 0.77 | 0.70 | 0.86 | 0.75 | 0.24 |
| Pb | -0.19 | 0.13 | -0.28 | 0.49 | 0.37 | 0.04 | 0.55 | 0.26 | -0.04 | 0.11 | 0.37 | 0.26 | 0.36 | 0.42 | 1.00 | 0.04 | -0.17 | 0.59 | 0.36 | -0.01 |
| Sr | 0.80 | 0.79 | 0.77 | 0.70 | 0.76 | 0.84 | 0.51 | 0.76 | -0.14 | 0.77 | 0.80 | 0.72 | 0.75 | 0.77 | 0.04 | 1.00 | 0.81 | 0.64 | 0.80 | 0.30 |
| V | 1.00 | 0.90 | 0.85 | 0.66 | 0.79 | 0.96 | 0.38 | 0.80 | -0.12 | 0.92 | 0.77 | 0.68 | 0.81 | 0.70 | -0.17 | 0.81 | 1.00 | 0.56 | 0.45 | 0.47 |
| Zn | 0.55 | 0.78 | 0.40 | 0.92 | 0.91 | 0.74 | 0.85 | 0.85 | -0.12 | 0.71 | 0.89 | 0.77 | 0.88 | 0.86 | 0.59 | 0.64 | 0.56 | 1.00 | 0.65 | 0.30 |
| Ca | 0.42 | 0.52 | 0.52 | 0.60 | 0.60 | 0.57 | 0.54 | 0.57 | -0.12 | 0.50 | 0.74 | 0.59 | 0.54 | 0.75 | 0.36 | 0.80 | 0.45 | 0.65 | 1.00 | 0.12 |
| Mo | 0.46 | 0.48 | 0.40 | 0.31 | 0.35 | 0.44 | 0.23 | 0.33 | 0.21 | 0.54 | 0.31 | 0.12 | 0.40 | 0.24 | -0.01 | 0.30 | 0.47 | 0.30 | 0.12 | 1.00 |

Appendix T1.2 Model output for March seasonal differences

```
[1] "clay"
      Df Sum Sq Mean Sq F value Pr(>F)
y      2  47.19  23.597   5.504 0.00866 **
Residuals 33 141.49  4.287
---
Signif. codes:  0 '***' 0.001 '**' 0.01 '*' 0.05 '.' 0.1 ' ' 1
Tukey multiple comparisons of means
 95% family-wise confidence level

Fit: aov(formula = x ~ y, data = test)

$y
      diff      lwr      upr      p adj
2-1  2.387371795  0.3533863  4.4213573 0.0185147
3-1  0.007651515 -2.1132334  2.1285364 0.9999568
3-2 -2.379720280 -4.4612267 -0.2982139 0.0221869

[1] "silt"
      Df Sum Sq Mean Sq F value Pr(>F)
y      2  1105  552.4  6.189 0.00522 **
Residuals 33  2945  89.3
---
Signif. codes:  0 '***' 0.001 '**' 0.01 '*' 0.05 '.' 0.1 ' ' 1
Tukey multiple comparisons of means
 95% family-wise confidence level

Fit: aov(formula = x ~ y, data = test)

$y
      diff      lwr      upr      p adj
2-1 11.7161538  2.435849 20.996459 0.0107760
3-1  0.3927273 -9.284067 10.069521 0.9945482
3-2 -11.3234266 -20.820551 -1.826302 0.0165616

[1] "fine_sand"
      Df Sum Sq Mean Sq F value Pr(>F)
y      2  678.5  339.2  3.792 0.0329 *
Residuals 33 2951.9  89.5
---
Signif. codes:  0 '***' 0.001 '**' 0.01 '*' 0.05 '.' 0.1 ' ' 1
Tukey multiple comparisons of means
 95% family-wise confidence level

Fit: aov(formula = x ~ y, data = test)

$y
      diff      lwr      upr      p adj
2-1 -10.214423 -19.504873 -0.9239734 0.0286424
3-1  -7.205682 -16.893054  2.4816903 0.1771452
3-2  3.008741  -6.498765 12.5162478 0.7198483

[1] "organic_matter"
      Df Sum Sq Mean Sq F value Pr(>F)
y      2  2.026  1.0128  6.27 0.00492 **
Residuals 33  5.330  0.1615
---
Signif. codes:  0 '***' 0.001 '**' 0.01 '*' 0.05 '.' 0.1 ' ' 1
Tukey multiple comparisons of means
 95% family-wise confidence level

Fit: aov(formula = x ~ y, data = test)

$y
      diff      lwr      upr      p adj
2-1  0.3849359 -0.009857969  0.7797298 0.0572036
3-1 -0.1794697 -0.591130620  0.2321912 0.5391830
3-2 -0.5644056 -0.968423203 -0.1603880 0.0045765

[1] "carbonates"
      Df Sum Sq Mean Sq F value Pr(>F)
```

```
y      2  1.769  0.8845  9.742 0.000473 ***
Residuals 33  2.996  0.0908
---
Signif. codes:  0 '***' 0.001 '**' 0.01 '*' 0.05 '.' 0.1 ' ' 1
Tukey multiple comparisons of means
 95% family-wise confidence level

Fit: aov(formula = x ~ y, data = test)

$y
      diff      lwr      upr      p adj
2-1  0.5083974  0.21241187  0.8043830 0.0005220
3-1  0.4073485  0.09871732  0.7159796 0.0075150
3-2 -0.1010490 -0.40394976  0.2018519 0.6943051

[1] "airkerma"
      Df Sum Sq Mean Sq F value Pr(>F)
y      2  29418  14709  8.76 0.00269 **
Residuals 16 26866  1679
---
Signif. codes:  0 '***' 0.001 '**' 0.01 '*' 0.05 '.' 0.1 ' ' 1
17 observations deleted due to missingness
Tukey multiple comparisons of means
 95% family-wise confidence level

Fit: aov(formula = x ~ y, data = test)

$y
      diff      lwr      upr      p adj
2-1 51.35714 -7.467972 110.1823 0.0923827
3-1 99.00000 37.954293 160.0457 0.0019129
3-2 47.64286 -11.182258 106.4680 0.1235721

[1] "ph"
      Df Sum Sq Mean Sq F value Pr(>F)
y      2  2.790  1.3950 13.47 5.27e-05 ***
Residuals 33  3.416  0.1035
---
Signif. codes:  0 '***' 0.001 '**' 0.01 '*' 0.05 '.' 0.1 ' ' 1
Tukey multiple comparisons of means
 95% family-wise confidence level

Fit: aov(formula = x ~ y, data = test)

$y
      diff      lwr      upr      p adj
2-1 0.0624359 -0.2536245  0.3784963 0.8789997
3-1 -0.5692424 -0.8988061 -0.2396787 0.0004880
3-2 -0.6316783 -0.9551230 -0.3082337 0.0000987

[1] "CS137"
      Df Sum Sq Mean Sq F value Pr(>F)
y      2  9273  4637  6.031 0.00586 **
Residuals 33 25370  769
---
Signif. codes:  0 '***' 0.001 '**' 0.01 '*' 0.05 '.' 0.1 ' ' 1
Tukey multiple comparisons of means
 95% family-wise confidence level

Fit: aov(formula = x ~ y, data = test)

$y
      diff      lwr      upr      p adj
2-1 30.649359  3.41298 57.885738 0.0246525
3-1 -5.194697 -33.59471 23.205321 0.8952594
3-2 -35.844056 -63.71677 -7.971342 0.0093050

[1] "Al"
      Df Sum Sq Mean Sq F value Pr(>F)
y      2  319.2  159.58  9.957 0.000413 ***
Residuals 33  528.9  16.03
---
Signif. codes:  0 '***' 0.001 '**' 0.01 '*' 0.05 '.' 0.1 ' ' 1
Tukey multiple comparisons of means
```

95% family-wise confidence level

Fit: aov(formula = x ~ y, data = test)

```
$y
      diff      lwr      upr    p adj
2-1 5.7992351 1.866758 9.731712 0.0027437
3-1 -0.7671987 -4.867686 3.333288 0.8907017
3-2 -6.5664338 -10.590787 -2.542081 0.0009474
```

[1] "As"

| | Df | Sum Sq | Mean Sq | F value | Pr(>F) |
|-----------|----|-----------|-----------|---------|------------|
| y | 2 | 2.031e-05 | 1.015e-05 | 8.494 | 0.00106 ** |
| Residuals | 33 | 3.945e-05 | 1.195e-06 | | |

Signif. codes: 0 '***' 0.001 '**' 0.01 '*' 0.05 '.' 0.1 ' ' 1
Tukey multiple comparisons of means
95% family-wise confidence level

Fit: aov(formula = x ~ y, data = test)

```
$y
      diff      lwr      upr    p adj
2-1 0.001161217 8.722391e-05 0.0022352092
0.0318003
3-1 -0.000643887 -1.763765e-03 0.0004759906
0.3470606
3-2 -0.001805104 -2.904188e-03 -0.0007060187
0.0008801
```

[1] "Ba"

| | Df | Sum Sq | Mean Sq | F value | Pr(>F) |
|-----------|----|---------|----------|---------|-------------|
| y | 2 | 0.03878 | 0.019391 | 10.65 | 0.00027 *** |
| Residuals | 33 | 0.06009 | 0.001821 | | |

Signif. codes: 0 '***' 0.001 '**' 0.01 '*' 0.05 '.' 0.1 ' ' 1
Tukey multiple comparisons of means
95% family-wise confidence level

Fit: aov(formula = x ~ y, data = test)

```
$y
      diff      lwr      upr    p adj
2-1 0.071386837 0.02947088 0.11330279
0.0005777
3-1 0.006885835 -0.03682092 0.05059259
0.9211217
3-2 -0.064501003 -0.10739626 -0.02160575
0.0022610
```

[1] "Cd"

| | Df | Sum Sq | Mean Sq | F value | Pr(>F) |
|-----------|----|-----------|-----------|---------|------------|
| y | 2 | 3.120e-07 | 1.560e-07 | 6.449 | 0.00432 ** |
| Residuals | 33 | 7.981e-07 | 2.419e-08 | | |

Signif. codes: 0 '***' 0.001 '**' 0.01 '*' 0.05 '.' 0.1 ' ' 1
Tukey multiple comparisons of means
95% family-wise confidence level

Fit: aov(formula = x ~ y, data = test)

```
$y
      diff      lwr      upr    p adj
2-1 2.108623e-04 5.809608e-05 3.636286e-04
0.0051003
3-1 4.242769e-05 -1.168653e-04 2.017207e-04
0.7916640
3-2 -1.684347e-04 -3.247701e-04 -1.209925e-05
0.0325005
```

[1] "Co"

| | Df | Sum Sq | Mean Sq | F value | Pr(>F) |
|-----------|----|-----------|-----------|---------|------------|
| y | 2 | 1.409e-05 | 7.044e-06 | 8.207 | 0.00128 ** |
| Residuals | 33 | 2.832e-05 | 8.580e-07 | | |

Signif. codes: 0 '***' 0.001 '**' 0.01 '*' 0.05 '.' 0.1 ' ' 1

Tukey multiple comparisons of means
95% family-wise confidence level

Fit: aov(formula = x ~ y, data = test)

```
$y
      diff      lwr      upr    p adj
2-1 1.292038e-03 0.0003819984 0.0022020771
0.0039438
3-1 -2.136206e-05 -0.0009702817 0.0009275576
0.9983192
3-2 -1.313400e-03 -0.0022447008 -0.0003820988
0.0041961
```

[1] "Cr"

| | Df | Sum Sq | Mean Sq | F value | Pr(>F) |
|-----------|----|-----------|-----------|---------|--------------|
| y | 2 | 0.0005862 | 2.931e-04 | 9.208 | 0.000664 *** |
| Residuals | 33 | 0.0010504 | 3.183e-05 | | |

Signif. codes: 0 '***' 0.001 '**' 0.01 '*' 0.05 '.' 0.1 ' ' 1
Tukey multiple comparisons of means
95% family-wise confidence level

Fit: aov(formula = x ~ y, data = test)

```
$y
      diff      lwr      upr    p adj
2-1 0.007606777 0.002064729 0.013148825
0.0053620
3-1 -0.001473579 -0.007252404 0.004305246
0.8071319
3-2 -0.009080356 -0.014751886 -0.003408827
0.0011691
```

[1] "Cu"

| | Df | Sum Sq | Mean Sq | F value | Pr(>F) |
|-----------|----|-----------|-----------|---------|----------|
| y | 2 | 2.462e-05 | 1.231e-05 | 3.582 | 0.0391 * |
| Residuals | 33 | 1.134e-04 | 3.437e-06 | | |

Signif. codes: 0 '***' 0.001 '**' 0.01 '*' 0.05 '.' 0.1 ' ' 1
Tukey multiple comparisons of means
95% family-wise confidence level

Fit: aov(formula = x ~ y, data = test)

```
$y
      diff      lwr      upr    p adj
2-1 0.0002192223 -0.001601865 2.040310e-03
0.9531088
3-1 -0.0016704289 -0.003569320 2.284622e-04
0.0936180
3-2 -0.0018896511 -0.003753285 -2.601683e-05
0.0463312
```

[1] "Fe"

| | Df | Sum Sq | Mean Sq | F value | Pr(>F) |
|-----------|----|--------|---------|---------|--------------|
| y | 2 | 76.73 | 38.37 | 9.238 | 0.000652 *** |
| Residuals | 33 | 137.05 | 4.15 | | |

Signif. codes: 0 '***' 0.001 '**' 0.01 '*' 0.05 '.' 0.1 ' ' 1
Tukey multiple comparisons of means
95% family-wise confidence level

Fit: aov(formula = x ~ y, data = test)

```
$y
      diff      lwr      upr    p adj
2-1 3.08214439 1.080330 5.083959 0.0017747
3-1 0.09116731 -1.996172 2.178507 0.9936888
3-2 -2.99097708 -5.039561 -0.942393 0.0030247
```

[1] "Hg"

| | Df | Sum Sq | Mean Sq | F value | Pr(>F) |
|-----------|----|-----------|-----------|---------|--------|
| y | 2 | 3.240e-06 | 1.619e-06 | 1.15 | 0.329 |
| Residuals | 33 | 4.643e-05 | 1.407e-06 | | |

Tukey multiple comparisons of means

95% family-wise confidence level

Fit: aov(formula = x ~ y, data = test)

```
$y
      diff      lwr      upr    p adj
2-1 -0.0005448217 -0.001710040 0.0006203963
0.4924792
3-1 -0.0007090941 -0.001924095 0.0005059063
0.3364864
3-2 -0.0001642724 -0.001356714 0.0010281691
0.9390709
```

[1] "K"

```
      Df Sum Sq Mean Sq F value Pr(>F)
y         2  16.74   8.371   7.041 0.00284 **
Residuals 33  39.24   1.189
---
```

Signif. codes: 0 '***' 0.001 '**' 0.01 '*' 0.05 '.' 0.1 ' ' 1
Tukey multiple comparisons of means
95% family-wise confidence level

Fit: aov(formula = x ~ y, data = test)

```
$y
      diff      lwr      upr    p adj
2-1  1.37806260  0.3069599  2.4491653 0.0092705
3-1 -0.08367137 -1.2005355  1.0331928 0.9815530
3-2 -1.46173397 -2.5578613 -0.3656066 0.0068881
```

[1] "Mg"

```
      Df Sum Sq Mean Sq F value Pr(>F)
y         2   9.756   4.878   6.016 0.00592 **
Residuals 33  26.756   0.811
---
```

Signif. codes: 0 '***' 0.001 '**' 0.01 '*' 0.05 '.' 0.1 ' ' 1
Tukey multiple comparisons of means
95% family-wise confidence level

Fit: aov(formula = x ~ y, data = test)

```
$y
      diff      lwr      upr    p adj
2-1  1.0027057  0.1182019  1.8872094 0.0234797
3-1 -0.1537195 -1.0760125  0.7685735 0.9121733
3-2 -1.1564252 -2.0615940 -0.2512564 0.0098080
```

[1] "Mn"

```
      Df Sum Sq Mean Sq F value Pr(>F)
y         2  0.03445 0.01723   5.037 0.0123 *
Residuals 33  0.11285 0.00342
---
```

Signif. codes: 0 '***' 0.001 '**' 0.01 '*' 0.05 '.' 0.1 ' ' 1
Tukey multiple comparisons of means
95% family-wise confidence level

Fit: aov(formula = x ~ y, data = test)

```
$y
      diff      lwr      upr    p adj
2-1  0.06899011  0.01154752 0.1264327103
0.0157107
3-1  0.01093969 -0.04895707 0.0708364422
0.8955499
3-2 -0.05805043 -0.11683508 0.0007342236
0.0534970
```

[1] "Ni"

```
      Df Sum Sq Mean Sq F value Pr(>F)
y         2 1.964e-05 9.820e-06  6.602 0.00388 **
Residuals 33 4.909e-05 1.487e-06
---
```

Signif. codes: 0 '***' 0.001 '**' 0.01 '*' 0.05 '.' 0.1 ' ' 1
Tukey multiple comparisons of means
95% family-wise confidence level

Fit: aov(formula = x ~ y, data = test)

```
$y
      diff      lwr      upr    p adj
2-1  0.0012512995  5.327299e-05 0.0024493260
0.0391328
3-1 -0.0004859829 -1.735194e-03 0.0007632278
0.6102066
3-2 -0.0017372824 -2.963299e-03 -0.0005112658
0.0040154
```

[1] "P"

```
      Df Sum Sq Mean Sq F value Pr(>F)
y         2  0.0821 0.04105   5.905 0.00643 **
Residuals 33  0.2294 0.00695
---
```

Signif. codes: 0 '***' 0.001 '**' 0.01 '*' 0.05 '.' 0.1 ' ' 1
Tukey multiple comparisons of means
95% family-wise confidence level

Fit: aov(formula = x ~ y, data = test)

```
$y
      diff      lwr      upr    p adj
2-1  0.08965114  0.00774611 0.17155617 0.0294582
3-1 -0.01805213 -0.10345644 0.06735219 0.8628067
3-2 -0.10770326 -0.19152187 -0.02388465 0.0093655
```

[1] "Pb"

```
      Df Sum Sq Mean Sq F value Pr(>F)
y         2  0.0001192 5.962e-05   7.952 0.00152 **
Residuals 33  0.0002474 7.500e-06
---
```

Signif. codes: 0 '***' 0.001 '**' 0.01 '*' 0.05 '.' 0.1 ' ' 1
Tukey multiple comparisons of means
95% family-wise confidence level

Fit: aov(formula = x ~ y, data = test)

```
$y
      diff      lwr      upr    p adj
2-1 -0.004370206 -0.0070598655 -0.0016805465
0.0009931
3-1 -0.002181360 -0.0049859313 0.0006232121
0.1521872
3-2  0.002188846 -0.0005636528 0.0049413456
0.1404914
```

[1] "Sr"

```
      Df Sum Sq Mean Sq F value Pr(>F)
y         2  0.001955 0.0009774   3.059 0.0604 .
Residuals 33  0.010545 0.0003195
---
```

Signif. codes: 0 '***' 0.001 '**' 0.01 '*' 0.05 '.' 0.1 ' ' 1
Tukey multiple comparisons of means
95% family-wise confidence level

Fit: aov(formula = x ~ y, data = test)

```
$y
      diff      lwr      upr    p adj
2-1  0.017427777 -0.0001316656 0.034987221
0.0520744
3-1  0.006272016 -0.0120376315 0.024581664
0.6808451
3-2 -0.011155761 -0.0291254534 0.006813931
0.2932717
```

[1] "V"

```
      Df Sum Sq Mean Sq F value Pr(>F)
y         2  0.001675 0.0008376  10.81 0.000244 ***
Residuals 33  0.002556 0.0000775
---
```

Signif. codes: 0 '***' 0.001 '**' 0.01 '*' 0.05 '.' 0.1 ' ' 1
Tukey multiple comparisons of means
95% family-wise confidence level

Fit: aov(formula = x ~ y, data = test)

| | diff | lwr | upr | p adj |
|-----|-------------|--------------|--------------|-----------|
| 2-1 | 0.01271516 | 0.004070169 | 0.021360142 | 0.0028156 |
| 3-1 | -0.00272822 | -0.011742553 | 0.006286112 | 0.7401176 |
| 3-2 | -0.01544338 | -0.024290339 | -0.006596413 | 0.0004292 |

[1] "Zn"

| | Df | Sum Sq | Mean Sq | F value | Pr(>F) |
|-----------|----|----------|-----------|---------|----------|
| y | 2 | 0.001634 | 0.0008170 | 3.813 | 0.0324 * |
| Residuals | 33 | 0.007071 | 0.0002143 | | |

 Signif. codes: 0 '****' 0.001 '***' 0.01 '**' 0.05 '.' 0.1 ' ' 1
 Tukey multiple comparisons of means
 95% family-wise confidence level

Fit: aov(formula = x ~ y, data = test)

| | diff | lwr | upr | p adj |
|-----|--------------|--------------|------------|-----------|
| 2-1 | 0.015498855 | 0.001120268 | 0.02987744 | 0.0324046 |
| 3-1 | 0.003853134 | -0.011139759 | 0.01884603 | 0.8044317 |
| 3-2 | -0.011645721 | -0.026360241 | 0.00306880 | 0.1429630 |

[1] "Ca"

| | Df | Sum Sq | Mean Sq | F value | Pr(>F) |
|-----------|----|--------|---------|---------|--------|
| y | 2 | 10.4 | 5.212 | 0.426 | 0.657 |
| Residuals | 33 | 404.2 | 12.248 | | |

Tukey multiple comparisons of means
 95% family-wise confidence level

Fit: aov(formula = x ~ y, data = test)

| | diff | lwr | upr | p adj |
|-----|------------|-----------|----------|-----------|
| 2-1 | 1.0892602 | -2.348569 | 4.527090 | 0.7192777 |
| 3-1 | -0.0623572 | -3.647064 | 3.522349 | 0.9989960 |
| 3-2 | -1.1516174 | -4.669766 | 2.366532 | 0.7036849 |

[1] "Mo"

| | Df | Sum Sq | Mean Sq | F value | Pr(>F) |
|-----------|----|-----------|-----------|---------|----------|
| y | 2 | 1.786e-07 | 8.929e-08 | 7.544 | 0.002 ** |
| Residuals | 33 | 3.906e-07 | 1.184e-08 | | |

 Signif. codes: 0 '****' 0.001 '***' 0.01 '**' 0.05 '.' 0.1 ' ' 1
 Tukey multiple comparisons of means
 95% family-wise confidence level

Fit: aov(formula = x ~ y, data = test)

| | diff | lwr | upr | p adj |
|-----|---------------|---------------|---------------|-----------|
| 2-1 | 0.0001185738 | 1.170708e-05 | 2.254405e-04 | 0.0270196 |
| 3-1 | -0.0000473921 | -1.588245e-04 | 6.404034e-05 | 0.5551947 |
| 3-2 | -0.0001659659 | -2.753293e-04 | -5.660241e-05 | 0.0020599 |

[1] "AM241"

| | Df | Sum Sq | Mean Sq | F value | Pr(>F) |
|-----------|----|--------|---------|---------|------------|
| y | 2 | 7770 | 3885 | 7.097 | 0.00273 ** |
| Residuals | 33 | 18065 | 547 | | |

 Signif. codes: 0 '****' 0.001 '***' 0.01 '**' 0.05 '.' 0.1 ' ' 1
 Tukey multiple comparisons of means
 95% family-wise confidence level

Fit: aov(formula = x ~ y, data = test)

| | diff | lwr | upr | p adj |
|-----|------------|------------|-----------|-----------|
| 2-1 | 26.665385 | 3.682507 | 49.64826 | 0.0200680 |
| 3-1 | -7.022727 | -30.987519 | 16.94206 | 0.7540336 |
| 3-2 | -33.688112 | -57.207949 | -10.16827 | 0.0036315 |

Appendix T1.3 Model output for May seasonal differences

[1] "clay"

| | Df | Sum Sq | Mean Sq | F value | Pr(>F) |
|-----------|----|--------|---------|---------|----------|
| y | 2 | 36.84 | 18.421 | 3.488 | 0.0422 * |
| Residuals | 33 | 174.28 | 5.281 | | |

Signif. codes: 0 '***' 0.001 '**' 0.01 '*' 0.05 '.' 0.1 ' ' 1
Tukey multiple comparisons of means
95% family-wise confidence level

Fit: aov(formula = x ~ y, data = test)

\$y

| | diff | lwr | upr | p adj |
|-----|------------|------------|------------|-----------|
| 2-1 | 1.5944872 | -0.6629289 | 3.8519033 | 0.2081767 |
| 3-1 | -0.8280303 | -3.1818916 | 1.5258310 | 0.6669025 |
| 3-2 | -2.4225175 | -4.7326746 | -0.1123604 | 0.0382306 |

[1] "silt"

| | Df | Sum Sq | Mean Sq | F value | Pr(>F) |
|-----------|----|--------|---------|---------|----------|
| y | 2 | 1483 | 741.7 | 3.201 | 0.0536 . |
| Residuals | 33 | 7647 | 231.7 | | |

Signif. codes: 0 '***' 0.001 '**' 0.01 '*' 0.05 '.' 0.1 ' ' 1
Tukey multiple comparisons of means
95% family-wise confidence level

Fit: aov(formula = x ~ y, data = test)

\$y

| | diff | lwr | upr | p adj |
|-----|------------|-------------|-----------|-----------|
| 2-1 | 14.211154 | -0.7422888 | 29.164596 | 0.0651948 |
| 3-1 | 1.984091 | -13.6082182 | 17.576400 | 0.9477616 |
| 3-2 | -12.227063 | -27.5298694 | 3.075744 | 0.1380480 |

[1] "fine_sand"

| | Df | Sum Sq | Mean Sq | F value | Pr(>F) |
|-----------|----|--------|---------|---------|--------|
| y | 2 | 614 | 307.2 | 1.583 | 0.22 |
| Residuals | 33 | 6402 | 194.0 | | |

Tukey multiple comparisons of means
95% family-wise confidence level

Fit: aov(formula = x ~ y, data = test)

\$y

| | diff | lwr | upr | p adj |
|-----|-----------|------------|-----------|-----------|
| 2-1 | -9.867949 | -23.550142 | 3.814245 | 0.1954014 |
| 3-1 | -4.192424 | -18.459171 | 10.074323 | 0.7528583 |
| 3-2 | 5.675524 | -8.326332 | 19.677381 | 0.5853899 |

[1] "organic_matter"

| | Df | Sum Sq | Mean Sq | F value | Pr(>F) |
|-----------|----|--------|---------|---------|--------|
| y | 2 | 7.07 | 3.533 | 1.651 | 0.207 |
| Residuals | 33 | 70.63 | 2.140 | | |

Tukey multiple comparisons of means
95% family-wise confidence level

Fit: aov(formula = x ~ y, data = test)

\$y

| | diff | lwr | upr | p adj |
|-----|------------|------------|-----------|-----------|
| 2-1 | 1.0630769 | -0.3739706 | 2.5001245 | 0.1803245 |
| 3-1 | 0.5109091 | -0.9875344 | 2.0093526 | 0.6832461 |
| 3-2 | -0.5521678 | -2.0227897 | 0.9184541 | 0.6308835 |

[1] "carbonates"

| | Df | Sum Sq | Mean Sq | F value | Pr(>F) |
|-----------|----|--------|---------|---------|----------|
| y | 2 | 2.52 | 1.2600 | 3.227 | 0.0525 . |
| Residuals | 33 | 12.89 | 0.3905 | | |

Signif. codes: 0 '***' 0.001 '**' 0.01 '*' 0.05 '.' 0.1 ' ' 1
Tukey multiple comparisons of means
95% family-wise confidence level

Fit: aov(formula = x ~ y, data = test)

\$y

| | diff | lwr | upr | p adj |
|-----|------------|-------------|------------|-----------|
| 2-1 | 0.5277564 | -0.08606445 | 1.14157727 | 0.1032892 |
| 3-1 | -0.0455303 | -0.68557586 | 0.59451525 | 0.9833515 |
| 3-2 | -0.5732867 | -1.20144853 | 0.05487511 | 0.0792736 |

[1] "airkerma"

| | Df | Sum Sq | Mean Sq | F value | Pr(>F) |
|-----------|----|--------|---------|---------|----------|
| y | 2 | 35090 | 17545 | 3.013 | 0.0776 . |
| Residuals | 16 | 93183 | 5824 | | |

Signif. codes: 0 '***' 0.001 '**' 0.01 '*' 0.05 '.' 0.1 ' ' 1
17 observations deleted due to missingness
Tukey multiple comparisons of means
95% family-wise confidence level

Fit: aov(formula = x ~ y, data = test)

\$y

| | diff | lwr | upr | p adj |
|-----|-----------|------------|----------|-----------|
| 2-1 | 49.28571 | -60.269178 | 158.8406 | 0.4924003 |
| 3-1 | 108.00000 | -5.690485 | 221.6905 | 0.0639542 |
| 3-2 | 58.71429 | -50.840607 | 168.2692 | 0.3727730 |

[1] "ph"

| | Df | Sum Sq | Mean Sq | F value | Pr(>F) |
|-----------|----|--------|---------|---------|--------------|
| y | 2 | 0.8759 | 0.4380 | 14.76 | 2.63e-05 *** |
| Residuals | 33 | 0.9790 | 0.0297 | | |

Signif. codes: 0 '***' 0.001 '**' 0.01 '*' 0.05 '.' 0.1 ' ' 1
Tukey multiple comparisons of means
95% family-wise confidence level

Fit: aov(formula = x ~ y, data = test)

\$y

| | diff | lwr | upr | p adj |
|-----|------------|-------------|-------------|----------|
| 2-1 | -0.3679487 | -0.53713686 | -0.19876057 | 0.000020 |
| 3-1 | -0.2551515 | -0.43156801 | -0.07873502 | 0.003312 |
| 3-2 | 0.1127972 | -0.06034376 | 0.28593817 | 0.260448 |

[1] "CS137"

| | Df | Sum Sq | Mean Sq | F value | Pr(>F) |
|-----------|----|--------|---------|---------|----------|
| y | 2 | 5439 | 2719.7 | 3.136 | 0.0567 . |
| Residuals | 33 | 28622 | 867.3 | | |

Signif. codes: 0 '***' 0.001 '**' 0.01 '*' 0.05 '.' 0.1 ' ' 1
Tukey multiple comparisons of means
95% family-wise confidence level

Fit: aov(formula = x ~ y, data = test)

\$y

| | diff | lwr | upr | p adj |
|-----|-----------|-------------|----------|-----------|
| 2-1 | 29.38940 | 0.4598275 | 58.31897 | 0.0458421 |
| 3-1 | 12.73466 | -17.4308859 | 42.90021 | 0.5599269 |
| 3-2 | -16.65473 | -46.2602011 | 12.95073 | 0.3625481 |

[1] "Al"

| | Df | Sum Sq | Mean Sq | F value | Pr(>F) |
|-----------|----|--------|---------|---------|--------|
| y | 2 | 5.57 | 2.784 | 1.979 | 0.154 |
| Residuals | 33 | 46.41 | 1.407 | | |

Tukey multiple comparisons of means
95% family-wise confidence level

Fit: aov(formula = x ~ y, data = test)

\$y

| | diff | lwr | upr | p adj |
|-----|------------|------------|-----------|-----------|
| 2-1 | 0.9350456 | -0.2299287 | 2.1000199 | 0.1357412 |
| 3-1 | 0.3653161 | -0.8494302 | 1.5800625 | 0.7429102 |
| 3-2 | -0.5697295 | -1.7619216 | 0.6224626 | 0.4775376 |

```
[1] "As"
      Df Sum Sq Mean Sq F value Pr(>F)
y      2 1.070e-06 5.327e-07  0.344  0.712
Residuals 33 5.114e-05 1.550e-06
Tukey multiple comparisons of means
95% family-wise confidence level
```

Fit: aov(formula = x ~ y, data = test)

```
$y
      diff      lwr      upr    p adj
2-1 3.968734e-04 -0.0008259645 0.001619711
0.7078381
3-1 3.103639e-04 -0.0009647180 0.001585446
0.8225375
3-2 -8.650943e-05 -0.0013379169 0.001164898
0.9842695
```

```
[1] "Ba"
      Df Sum Sq Mean Sq F value Pr(>F)
y      2 0.005272 0.002636  10.46 0.000303 ***
Residuals 33 0.008315 0.000252
---
```

Signif. codes: 0 '***' 0.001 '**' 0.01 '*' 0.05 '.' 0.1 ' ' 1
 Tukey multiple comparisons of means
 95% family-wise confidence level

Fit: aov(formula = x ~ y, data = test)

```
$y
      diff      lwr      upr    p adj
2-1 0.0253863871 0.009793388 0.040979387
0.0009712
3-1 0.0004051877 -0.015854002 0.016664378
0.9979407
3-2 -0.0249811994 -0.040938505 -0.009023894
0.0014897
```

```
[1] "Cd"
      Df Sum Sq Mean Sq F value Pr(>F)
y      2 2.632e-07 1.316e-07  1.846  0.174
Residuals 33 2.353e-06 7.131e-08
Tukey multiple comparisons of means
95% family-wise confidence level
```

Fit: aov(formula = x ~ y, data = test)

```
$y
      diff      lwr      upr    p adj
2-1 1.949374e-04 -6.737358e-05 0.0004572485
0.1776659
3-1 4.292684e-05 -2.305911e-04 0.0003164448
0.9216983
3-2 -1.520106e-04 -4.204501e-04 0.0001164289
0.3578651
```

```
[1] "Co"
      Df Sum Sq Mean Sq F value Pr(>F)
y      2 7.130e-06 3.565e-06  1.968  0.156
Residuals 33 5.976e-05 1.811e-06
Tukey multiple comparisons of means
95% family-wise confidence level
```

Fit: aov(formula = x ~ y, data = test)

```
$y
      diff      lwr      upr    p adj
2-1 0.0010558625 -0.0002660129 0.0023777379
0.1382063
3-1 0.0003987638 -0.0009795870 0.0017771146
0.7593990
3-2 -0.0006570987 -0.0020098577 0.0006956602
0.4662610
```

```
[1] "Cr"
      Df Sum Sq Mean Sq F value Pr(>F)
```

```
y      2 0.0000621 3.106e-05  1.585  0.22
Residuals 33 0.0006466 1.959e-05
Tukey multiple comparisons of means
95% family-wise confidence level
```

Fit: aov(formula = x ~ y, data = test)

```
$y
      diff      lwr      upr    p adj
2-1 0.003086885 -0.001261230 0.007435000
0.2050308
3-1 0.001014800 -0.003519082 0.005548683
0.8475854
3-2 -0.002072084 -0.006521787 0.002377618
0.4952532
```

```
[1] "Cu"
      Df Sum Sq Mean Sq F value Pr(>F)
y      2 0.0000651 3.257e-05  1.567  0.224
Residuals 33 0.0006859 2.079e-05
Tukey multiple comparisons of means
95% family-wise confidence level
```

Fit: aov(formula = x ~ y, data = test)

```
$y
      diff      lwr      upr    p adj
2-1 0.0029494893 -0.001528964 0.007427942
0.2531969
3-1 0.0003415913 -0.004328198 0.005011380
0.9824049
3-2 -0.0026078979 -0.007190983 0.001975187
0.3544222
```

```
[1] "Fe"
      Df Sum Sq Mean Sq F value Pr(>F)
y      2 21.91 10.953  1.874  0.17
Residuals 33 192.90 5.845
Tukey multiple comparisons of means
95% family-wise confidence level
```

Fit: aov(formula = x ~ y, data = test)

```
$y
      diff      lwr      upr    p adj
2-1 1.8397729 -0.535171 4.214717 0.1543640
3-1 0.6359246 -1.840486 3.112335 0.8047081
3-2 -1.2038483 -3.634279 1.226582 0.4526729
```

```
[1] "Hg"
      Df Sum Sq Mean Sq F value Pr(>F)
y      2 2.480e-07 1.241e-07  0.394  0.677
Residuals 33 1.039e-05 3.148e-07
Tukey multiple comparisons of means
95% family-wise confidence level
```

Fit: aov(formula = x ~ y, data = test)

```
$y
      diff      lwr      upr    p adj
2-1 -5.461308e-05 -0.0006057193 0.0004964931
0.9679615
3-1 -2.017965e-04 -0.0007764480 0.0003728549
0.6678295
3-2 -1.471835e-04 -0.0007111654 0.0004167985
0.7990350
```

```
[1] "K"
      Df Sum Sq Mean Sq F value Pr(>F)
y      2 0.930 0.4650  2.054  0.144
Residuals 33 7.472 0.2264
Tukey multiple comparisons of means
95% family-wise confidence level
```

Fit: aov(formula = x ~ y, data = test)

```

$y
      diff      lwr      upr      p adj
2-1  0.35918602 -0.1082203 0.8265923 0.1587461
3-1  0.05892351 -0.4284521 0.5462991 0.9527135
3-2 -0.30026250 -0.7785890 0.1780640 0.2856342

```

```

[1] "Mg"
      Df Sum Sq Mean Sq F value Pr(>F)
y       2  11.47  5.735   3.411 0.045 *
Residuals 33  55.49  1.682
---
Signif. codes:  0 '***' 0.001 '**' 0.01 '*' 0.05 '.' 0.1 ' ' 1
Tukey multiple comparisons of means
 95% family-wise confidence level

```

Fit: aov(formula = x ~ y, data = test)

```

$y
      diff      lwr      upr      p adj
2-1  1.2821564  0.008371747 2.555941 0.0482420
3-1  0.2683358 -1.059869692 1.596541 0.8738334
3-2 -1.0138206 -2.317365296 0.289724 0.1522189

```

```

[1] "Mn"
      Df Sum Sq Mean Sq F value Pr(>F)
y       2  0.0696 0.03481  2.061 0.143
Residuals 33  0.5573 0.01689
Tukey multiple comparisons of means
 95% family-wise confidence level

```

Fit: aov(formula = x ~ y, data = test)

```

$y
      diff      lwr      upr      p adj
2-1  0.10366544 -0.02399243 0.23132331 0.1298862
3-1  0.03559436 -0.09751753 0.16870625 0.7902135
3-2 -0.06807107 -0.19871147 0.06256932 0.4170222

```

```

[1] "Ni"
      Df Sum Sq Mean Sq F value Pr(>F)
y       2 1.153e-05 5.765e-06  1.077 0.352
Residuals 33 1.767e-04 5.354e-06
Tukey multiple comparisons of means
 95% family-wise confidence level

```

Fit: aov(formula = x ~ y, data = test)

```

$y
      diff      lwr      upr      p adj
2-1  0.0013403687 -0.0009325981 0.003613335
0.3291683
3-1  0.0009013723 -0.0014687041 0.003271449
0.6234945
3-2 -0.0004389964 -0.0027650675 0.001887075
0.8889075

```

```

[1] "P"
      Df Sum Sq Mean Sq F value Pr(>F)
y       2  0.1421 0.07106  3.51 0.0415 *
Residuals 33  0.6681 0.02025
---
Signif. codes:  0 '***' 0.001 '**' 0.01 '*' 0.05 '.' 0.1 ' ' 1
Tukey multiple comparisons of means
 95% family-wise confidence level

```

Fit: aov(formula = x ~ y, data = test)

```

$y
      diff      lwr      upr      p adj
2-1  0.14380080  0.00403361 0.28356800 0.0426806
3-1  0.03340126 -0.11233731 0.17913982 0.8408589
3-2 -0.11039955 -0.25343218 0.03263309 0.1563410

```

```

[1] "Pb"
      Df Sum Sq Mean Sq F value Pr(>F)
y       2  0.0002181 1.091e-04  1.378 0.266

```

```

Residuals 33 0.0026110 7.912e-05
Tukey multiple comparisons of means
 95% family-wise confidence level

```

Fit: aov(formula = x ~ y, data = test)

```

$y
      diff      lwr      upr      p adj
2-1  0.005565727 -0.003171876 0.014303330
0.2756371
3-1  0.001091168 -0.008019738 0.010202074
0.9535745
3-2 -0.004474559 -0.013416303 0.004467185
0.4455194

```

```

[1] "Sr"
      Df Sum Sq Mean Sq F value Pr(>F)
y       2  0.001725 0.0008623  3.317 0.0487 *
Residuals 33  0.008580 0.0002600

```

```

---
Signif. codes:  0 '***' 0.001 '**' 0.01 '*' 0.05 '.' 0.1 ' ' 1
Tukey multiple comparisons of means
 95% family-wise confidence level

```

Fit: aov(formula = x ~ y, data = test)

```

$y
      diff      lwr      upr      p adj
2-1  0.016278811  0.0004396184 0.032118003
0.0429421
3-1  0.005414489 -0.0111014125 0.021930390
0.7029402
3-2 -0.010864322 -0.0270735724 0.005344929
0.2416241

```

```

[1] "V"
      Df Sum Sq Mean Sq F value Pr(>F)
y       2 0.0000345 1.723e-05  1.788 0.183
Residuals 33 0.0003181 9.639e-06
Tukey multiple comparisons of means
 95% family-wise confidence level

```

Fit: aov(formula = x ~ y, data = test)

```

$y
      diff      lwr      upr      p adj
2-1  0.0023271965 -0.0007225995 0.005376992
0.1626454
3-1  0.0009139856 -0.0022661090 0.004094080
0.7621101
3-2 -0.0014132108 -0.0045342606 0.001707839
0.5141497

```

```

[1] "Zn"
      Df Sum Sq Mean Sq F value Pr(>F)
y       2  0.002895 0.0014476  1.978 0.154
Residuals 33 0.024153 0.0007319
Tukey multiple comparisons of means
 95% family-wise confidence level

```

Fit: aov(formula = x ~ y, data = test)

```

$y
      diff      lwr      upr      p adj
2-1  0.021284058 -0.005291023 0.04785914
0.1368380
3-1  0.008073147 -0.019637320 0.03578361
0.7564830
3-2 -0.013210911 -0.040406877 0.01398506
0.4662322

```

```

[1] "Ca"
      Df Sum Sq Mean Sq F value Pr(>F)
y       2 167.7  83.85  4.766 0.0152 *
Residuals 33  580.5  17.59

```

Signif. codes: 0 '****' 0.001 '***' 0.01 '**' 0.05 '.' 0.1 ' ' 1
Tukey multiple comparisons of means
95% family-wise confidence level

Fit: aov(formula = x ~ y, data = test)

```
$y
      diff      lwr      upr    p adj
2-1 4.6120954 0.4920092 8.7321817 0.0255144
3-1 0.2590171 -4.0370945 4.5551287 0.9880106
3-2 -4.3530783 -8.5694240 -0.1367327 0.0418448
```

```
[1] "Mo"
      Df Sum Sq Mean Sq F value Pr(>F)
y      2 1.014e-08 5.072e-09  2.279 0.118
Residuals 33 7.345e-08 2.226e-09
Tukey multiple comparisons of means
95% family-wise confidence level
```

Fit: aov(formula = x ~ y, data = test)

```
$y
      diff      lwr      upr    p adj
2-1 -1.810169e-05 -6.444450e-05 2.824112e-05
0.6078113
3-1 -4.197309e-05 -9.029584e-05 6.349656e-06
0.0989093
3-2 -2.387140e-05 -7.129694e-05 2.355414e-05
0.4414199
```

```
[1] "AM241"
      Df Sum Sq Mean Sq F value Pr(>F)
y      2 4383 2191.4  4.164 0.0244 *
Residuals 33 17369 526.3
```

Signif. codes: 0 '****' 0.001 '***' 0.01 '**' 0.05 '.' 0.1 ' ' 1
Tukey multiple comparisons of means
95% family-wise confidence level

Fit: aov(formula = x ~ y, data = test)

```
$y
      diff      lwr      upr    p adj
2-1 26.006021  3.47034 48.541702 0.0208244
3-1  8.910252 -14.58824 32.408740 0.6252162
3-2 -17.095769 -40.15796  5.966423 0.1791243
```

Appendix T1.4 Model output for
September seasonal differences

[1] "clay"

| | Df | Sum Sq | Mean Sq | F value | Pr(>F) |
|-----------|----|--------|---------|---------|--------|
| y | 2 | 5.52 | 2.76 | 0.643 | 0.532 |
| Residuals | 33 | 141.56 | 4.29 | | |

 Tukey multiple comparisons of means
 95% family-wise confidence level

Fit: aov(formula = x ~ y, data = test)

\$y

| | diff | lwr | upr | p adj |
|-----|-------------|-----------|----------|-----------|
| 2-1 | 0.80884615 | -1.225662 | 2.843354 | 0.5972143 |
| 3-1 | -0.01318182 | -2.134612 | 2.108248 | 0.9998718 |
| 3-2 | -0.82202797 | -2.904069 | 1.260013 | 0.6013930 |

[1] "silt"

| | Df | Sum Sq | Mean Sq | F value | Pr(>F) |
|-----------|----|--------|---------|---------|--------|
| y | 2 | 339 | 169.5 | 1.118 | 0.339 |
| Residuals | 33 | 5004 | 151.7 | | |

 Tukey multiple comparisons of means
 95% family-wise confidence level

Fit: aov(formula = x ~ y, data = test)

\$y

| | diff | lwr | upr | p adj |
|-----|----------|-----------|----------|-----------|
| 2-1 | 3.886667 | -8.209989 | 15.98332 | 0.7126727 |
| 3-1 | 7.682121 | -4.931349 | 20.29559 | 0.3065478 |
| 3-2 | 3.795455 | -8.583821 | 16.17473 | 0.7343587 |

[1] "fine_sand"

| | Df | Sum Sq | Mean Sq | F value | Pr(>F) |
|-----------|----|--------|---------|---------|--------|
| y | 2 | 641 | 320.4 | 1.886 | 0.168 |
| Residuals | 33 | 5606 | 169.9 | | |

 Tukey multiple comparisons of means
 95% family-wise confidence level

Fit: aov(formula = x ~ y, data = test)

\$y

| | diff | lwr | upr | p adj |
|-----|------------|-----------|----------|-----------|
| 2-1 | -4.542308 | -17.34521 | 8.260596 | 0.6623367 |
| 3-1 | -10.550000 | -23.89989 | 2.799891 | 0.1437391 |
| 3-2 | -6.007692 | -19.10972 | 7.094331 | 0.5057050 |

[1] "organic_matter"

| | Df | Sum Sq | Mean Sq | F value | Pr(>F) |
|-----------|----|--------|---------|---------|----------|
| y | 2 | 24.58 | 12.290 | 4.888 | 0.0138 * |
| Residuals | 33 | 82.97 | 2.514 | | |

 Signif. codes: 0 '***' 0.001 '**' 0.01 '*' 0.05 '.' 0.1 ' ' 1
 Tukey multiple comparisons of means
 95% family-wise confidence level

Fit: aov(formula = x ~ y, data = test)

\$y

| | diff | lwr | upr | p adj |
|-----|------------|------------|------------|-----------|
| 2-1 | 1.8367949 | 0.2791978 | 3.39439190 | 0.0179139 |
| 3-1 | 0.2756061 | -1.3485373 | 1.89974941 | 0.9091199 |
| 3-2 | -1.5611888 | -3.1551767 | 0.03279904 | 0.0558739 |

[1] "carbonates"

| | Df | Sum Sq | Mean Sq | F value | Pr(>F) |
|-----------|----|--------|---------|---------|------------|
| y | 2 | 6.994 | 3.497 | 8.369 | 0.00115 ** |
| Residuals | 33 | 13.789 | 0.418 | | |

 Signif. codes: 0 '***' 0.001 '**' 0.01 '*' 0.05 '.' 0.1 ' ' 1
 Tukey multiple comparisons of means
 95% family-wise confidence level

Fit: aov(formula = x ~ y, data = test)

\$y

| | diff | lwr | upr | p adj |
|-----|-------------|------------|------------|-----------|
| 2-1 | -0.96871795 | -1.6036874 | -0.3337485 | 0.0019513 |
| 3-1 | -0.88969697 | -1.5517947 | -0.2275992 | 0.0064531 |
| 3-2 | 0.07902098 | -0.5707836 | 0.7288255 | 0.9521727 |

[1] "airkerma"

| | Df | Sum Sq | Mean Sq | F value | Pr(>F) |
|-----------|----|--------|---------|---------|--------------|
| y | 2 | 31964 | 15982 | 14.02 | 0.000304 *** |
| Residuals | 16 | 18240 | 1140 | | |

 Signif. codes: 0 '***' 0.001 '**' 0.01 '*' 0.05 '.' 0.1 ' ' 1
 17 observations deleted due to missingness
 Tukey multiple comparisons of means
 95% family-wise confidence level

Fit: aov(formula = x ~ y, data = test)

\$y

| | diff | lwr | upr | p adj |
|-----|-----------|-----------|-----------|-----------|
| 2-1 | -29.35714 | -77.82782 | 19.11354 | 0.2896734 |
| 3-1 | 68.50000 | 18.19960 | 118.80040 | 0.0076509 |
| 3-2 | 97.85714 | 49.38646 | 146.32782 | 0.0002403 |

[1] "ph"

| | Df | Sum Sq | Mean Sq | F value | Pr(>F) |
|-----------|----|--------|---------|---------|--------|
| y | 2 | 0.0534 | 0.02670 | 1.524 | 0.233 |
| Residuals | 33 | 0.5782 | 0.01752 | | |

 Tukey multiple comparisons of means
 95% family-wise confidence level

Fit: aov(formula = x ~ y, data = test)

\$y

| | diff | lwr | upr | p adj |
|-----|------------|-------------|-----------|-----------|
| 2-1 | 0.07275641 | -0.05727152 | 0.2027843 | 0.3663652 |
| 3-1 | 0.08946970 | -0.04611351 | 0.2250529 | 0.2518958 |
| 3-2 | 0.01671329 | -0.11635255 | 0.1497791 | 0.9490674 |

[1] "CS137"

| | Df | Sum Sq | Mean Sq | F value | Pr(>F) |
|-----------|----|--------|---------|---------|--------|
| y | 2 | 2290 | 1145 | 0.388 | 0.681 |
| Residuals | 33 | 97322 | 2949 | | |

 Tukey multiple comparisons of means
 95% family-wise confidence level

Fit: aov(formula = x ~ y, data = test)

\$y

| | diff | lwr | upr | p adj |
|-----|-----------|-----------|----------|-----------|
| 2-1 | 7.450682 | -45.89430 | 60.79567 | 0.9374291 |
| 3-1 | 19.826167 | -35.79791 | 75.45025 | 0.6598423 |
| 3-2 | 12.375485 | -42.21582 | 66.96679 | 0.8439998 |

[1] "Al"

| | Df | Sum Sq | Mean Sq | F value | Pr(>F) |
|-----------|----|--------|---------|---------|--------|
| y | 2 | 161.8 | 80.91 | 2.414 | 0.105 |
| Residuals | 33 | 1106.0 | 33.52 | | |

 Tukey multiple comparisons of means
 95% family-wise confidence level

Fit: aov(formula = x ~ y, data = test)

\$y

| | diff | lwr | upr | p adj |
|-----|-----------|------------|-----------|-----------|
| 2-1 | 3.467905 | -2.218927 | 9.1547372 | 0.3056653 |
| 3-1 | -1.567275 | -7.497069 | 4.3625196 | 0.7944758 |
| 3-2 | -5.035180 | -10.854876 | 0.7845157 | 0.1005822 |

[1] "As"

| | Df | Sum Sq | Mean Sq | F value | Pr(>F) |
|-----------|----|-----------|-----------|---------|--------|
| y | 2 | 3.350e-06 | 1.673e-06 | 0.758 | 0.476 |
| Residuals | 33 | 7.281e-05 | 2.206e-06 | | |

 Tukey multiple comparisons of means
 95% family-wise confidence level

Fit: aov(formula = x ~ y, data = test)

```

$y
      diff      lwr      upr    p adj
2-1 0.0006985612 -0.0007605015 0.0021576239
0.4762561
3-1 0.0001646355 -0.0013567638 0.0016860347
0.9619228
3-2 -0.0005339257 -0.0020270771 0.0009592257
0.6580940

```

```

[1] "Ba"
      Df Sum Sq Mean Sq F value Pr(>F)
y       2 0.00229 0.001144  0.607 0.551
Residuals 33 0.06216 0.001884
Tukey multiple comparisons of means
95% family-wise confidence level

```

Fit: aov(formula = x ~ y, data = test)

```

$y
      diff      lwr      upr    p adj
2-1 0.017621543 -0.02501125 0.06025433 0.5732680
3-1 0.002397276 -0.04205694 0.04685150 0.9903958
3-2 -0.015224267 -0.05885310 0.02840457 0.6711808

```

```

[1] "Cd"
      Df Sum Sq Mean Sq F value Pr(>F)
y       2 1.858e-07 9.289e-08  1.831 0.176
Residuals 33 1.674e-06 5.073e-08
Tukey multiple comparisons of means
95% family-wise confidence level

```

Fit: aov(formula = x ~ y, data = test)

```

$y
      diff      lwr      upr    p adj
2-1 1.245489e-04 -9.670128e-05 3.457990e-04
0.3620727
3-1 -4.316086e-05 -2.738636e-04 1.875419e-04
0.8907184
3-2 -1.677097e-04 -3.941291e-04 5.870959e-05
0.1795845

```

```

[1] "Co"
      Df Sum Sq Mean Sq F value Pr(>F)
y       2 5.900e-06 2.950e-06  1.821 0.178
Residuals 33 5.344e-05 1.619e-06
Tukey multiple comparisons of means
95% family-wise confidence level

```

Fit: aov(formula = x ~ y, data = test)

```

$y
      diff      lwr      upr    p adj
2-1 0.0007363332 -0.0005137468 0.0019864132
0.3299710
3-1 -0.0001909963 -0.0014944843 0.0011124918
0.9313700
3-2 -0.0009273295 -0.0022066156 0.0003519567
0.1923571

```

```

[1] "Cr"
      Df Sum Sq Mean Sq F value Pr(>F)
y       2 0.0001719 8.594e-05  1.351 0.273
Residuals 33 0.0020996 6.362e-05
Tukey multiple comparisons of means
95% family-wise confidence level

```

Fit: aov(formula = x ~ y, data = test)

```

$y
      diff      lwr      upr    p adj
2-1 0.0048773558 -0.002957938 0.012712649
0.2914120

```

```

3-1 0.0007848185 -0.007385228 0.008954865
0.9698636
3-2 -0.0040925373 -0.012110890 0.003925816
0.4316307

```

```

[1] "Cu"
      Df Sum Sq Mean Sq F value Pr(>F)
y       2 6.561e-05 3.281e-05  5.12 0.0116 *
Residuals 33 2.114e-04 6.410e-06
---

```

```

Signif. codes:  0 '***' 0.001 '**' 0.01 '*' 0.05 '.' 0.1 ' ' 1
Tukey multiple comparisons of means
95% family-wise confidence level

```

Fit: aov(formula = x ~ y, data = test)

```

$y
      diff      lwr      upr    p adj
2-1 0.001144912 -0.0013415440 0.003631368
0.5028747
3-1 0.003337306  0.0007446198 0.005929993
0.0092347
3-2 0.002192394 -0.0003521536 0.004736942
0.1023736

```

```

[1] "Fe"
      Df Sum Sq Mean Sq F value Pr(>F)
y       2 30.27 15.136  2.009 0.15
Residuals 33 248.63  7.534
Tukey multiple comparisons of means
95% family-wise confidence level

```

Fit: aov(formula = x ~ y, data = test)

```

$y
      diff      lwr      upr    p adj
2-1 1.89611047 -0.8001613 4.5923822 0.2109100
3-1 -0.02695313 -2.8384196 2.7845133 0.9996950
3-2 -1.92306360 -4.6823295 0.8362023 0.2165354

```

```

[1] "Hg"
      Df Sum Sq Mean Sq F value Pr(>F)
y       2 7.260e-07 3.631e-07  0.717 0.496
Residuals 33 1.671e-05 5.065e-07
Tukey multiple comparisons of means
95% family-wise confidence level

```

Fit: aov(formula = x ~ y, data = test)

```

$y
      diff      lwr      upr    p adj
2-1 -3.086497e-04 -0.0010077392 0.0003904399
0.5309138
3-1 -2.918189e-04 -0.0010207761 0.0004371383
0.5930151
3-2 1.683079e-05 -0.0006985919 0.0007322534
0.9981645

```

```

[1] "K"
      Df Sum Sq Mean Sq F value Pr(>F)
y       2 6.89  3.443  2.369 0.109
Residuals 33 47.97  1.454
Tukey multiple comparisons of means
95% family-wise confidence level

```

Fit: aov(formula = x ~ y, data = test)

```

$y
      diff      lwr      upr    p adj
2-1 0.7442748 -0.4400657 1.9286153 0.2848757
3-1 -0.2830185 -1.5179585 0.9519214 0.8408718
3-2 -1.0272933 -2.2393041 0.1847175 0.1096158

```

```

[1] "Mg"
      Df Sum Sq Mean Sq F value Pr(>F)
y       2 4.04  2.019  1.486 0.241

```

Residuals 33 44.84 1.359
Tukey multiple comparisons of means
95% family-wise confidence level

Fit: aov(formula = x ~ y, data = test)

```
$y
      diff      lwr      upr    p adj
2-1 0.68356730 -0.461507 1.8286416 0.3205578
3-1 -0.02777034 -1.221766 1.1662258 0.9982060
3-2 -0.71133764 -1.883165 0.4604895 0.3088503
```

```
[1] "Mn"
      Df Sum Sq Mean Sq F value Pr(>F)
y       2 0.1952 0.09762  4.64 0.0168 *
Residuals 33 0.6943 0.02104
```

Signif. codes: 0 '***' 0.001 '**' 0.01 '*' 0.05 '.' 0.1 ' ' 1
Tukey multiple comparisons of means
95% family-wise confidence level

Fit: aov(formula = x ~ y, data = test)

```
$y
      diff      lwr      upr    p adj
2-1 0.16602558 0.02354263 0.30850854 0.0194794
3-1 0.03118725 -0.11738310 0.17975761 0.8645487
3-2 -0.13483833 -0.28065018 0.01097352 0.0744979
```

```
[1] "Ni"
      Df Sum Sq Mean Sq F value Pr(>F)
y       2 5.320e-06 2.659e-06 0.678 0.515
Residuals 33 1.294e-04 3.921e-06
Tukey multiple comparisons of means
95% family-wise confidence level
```

Fit: aov(formula = x ~ y, data = test)

```
$y
      diff      lwr      upr    p adj
2-1 0.0005432812 -0.001401918 0.002488480
0.7736218
3-1 -0.0003920463 -0.002420352 0.001636259
0.8838253
3-2 -0.0009353275 -0.002925973 0.001055318
0.4891462
```

```
[1] "P"
      Df Sum Sq Mean Sq F value Pr(>F)
y       2 0.0535 0.02673  1.787 0.183
Residuals 33 0.4936 0.01496
Tukey multiple comparisons of means
95% family-wise confidence level
```

Fit: aov(formula = x ~ y, data = test)

```
$y
      diff      lwr      upr    p adj
2-1 0.06966045 -0.05047706 0.18979796 0.3410778
3-1 -0.01886954 -0.14413977 0.10640069 0.9276262
3-2 -0.08852999 -0.21147433 0.03441434 0.1963614
```

```
[1] "Pb"
      Df Sum Sq Mean Sq F value Pr(>F)
y       2 7.180e-06 3.590e-06 1.174 0.322
Residuals 33 1.009e-04 3.057e-06
Tukey multiple comparisons of means
95% family-wise confidence level
```

Fit: aov(formula = x ~ y, data = test)

```
$y
      diff      lwr      upr    p adj
2-1 0.0001514074 -0.0015660877 0.001868902
0.9745540
```

```
3-1 0.0010385271 -0.0007523457 0.002829400
0.3410038
3-2 0.0008871198 -0.0008705019 0.002644741
0.4394928
```

```
[1] "Sr"
      Df Sum Sq Mean Sq F value Pr(>F)
y       2 0.001961 0.0009804  1.936 0.16
Residuals 33 0.016709 0.0005063
Tukey multiple comparisons of means
95% family-wise confidence level
```

Fit: aov(formula = x ~ y, data = test)

```
$y
      diff      lwr      upr    p adj
2-1 0.012884466 -0.009219138 0.03498807
0.3373393
3-1 0.017703108 -0.005344844 0.04075106
0.1590091
3-2 0.004818642 -0.017801378 0.02743866
0.8608201
```

```
[1] "V"
      Df Sum Sq Mean Sq F value Pr(>F)
y       2 0.000627 0.0003136  1.999 0.152
Residuals 33 0.005178 0.0001569
Tukey multiple comparisons of means
95% family-wise confidence level
```

Fit: aov(formula = x ~ y, data = test)

```
$y
      diff      lwr      upr    p adj
2-1 0.007541904 -0.004762592 0.019846400
0.3021095
3-1 -0.002048795 -0.014878985 0.010781395
0.9190607
3-2 -0.009590699 -0.022182671 0.003001272
0.1636789
```

```
[1] "Zn"
      Df Sum Sq Mean Sq F value Pr(>F)
y       2 0.000102 5.076e-05 0.399 0.674
Residuals 33 0.004197 1.272e-04
Tukey multiple comparisons of means
95% family-wise confidence level
```

Fit: aov(formula = x ~ y, data = test)

```
$y
      diff      lwr      upr    p adj
2-1 0.002436575 -0.008641538 0.01351469
0.8523910
3-1 0.004172358 -0.007379054 0.01572377
0.6526011
3-2 0.001735783 -0.009601154 0.01307272
0.9253235
```

```
[1] "Ca"
      Df Sum Sq Mean Sq F value Pr(>F)
y       2 126.5 63.26 6.561 0.00399 **
Residuals 33 318.2 9.64
---
Signif. codes: 0 '***' 0.001 '**' 0.01 '*' 0.05 '.' 0.1 ' ' 1
Tukey multiple comparisons of means
95% family-wise confidence level
```

Fit: aov(formula = x ~ y, data = test)

```
$y
      diff      lwr      upr    p adj
2-1 0.663904 -2.3863217 3.714130 0.8551977
3-1 4.370400 1.1898576 7.550943 0.0053086
3-2 3.706496 0.5850067 6.827986 0.0170566
```

```
[1] "Mo"
      Df Sum Sq Mean Sq F value Pr(>F)
y      2 3.812e-08 1.906e-08  3.968 0.0285 *
Residuals 33 1.585e-07 4.803e-09
---
Signif. codes:  0 '***' 0.001 '**' 0.01 '*' 0.05 '.' 0.1 ' ' 1
Tukey multiple comparisons of means
 95% family-wise confidence level
```

Fit: aov(formula = x ~ y, data = test)

```
$y
      diff      lwr      upr  p adj
2-1 3.590167e-06 -6.448481e-05 7.166514e-05
0.9908124
3-1 -6.869865e-05 -1.396820e-04 2.284736e-06
0.0594479
3-2 -7.228882e-05 -1.419543e-04 -2.623380e-06
0.0406472
```

```
[1] "AM241"
      Df Sum Sq Mean Sq F value Pr(>F)
y      2 1669  834.7  0.492 0.616
Residuals 33 56002 1697.0
Tukey multiple comparisons of means
 95% family-wise confidence level
```

Fit: aov(formula = x ~ y, data = test)

```
$y
      diff      lwr      upr  p adj
2-1 15.825532 -24.64067 56.29173 0.6070859
3-1  4.493098 -37.70197 46.68816 0.9631059
3-2 -11.332434 -52.74406 30.07919 0.7815340
```

Appendix T1.5 Model output for December seasonal differences

[1] "clay"
 Df Sum Sq Mean Sq F value Pr(>F)
 y 2 6.57 3.286 0.691 0.508
 Residuals 33 156.90 4.755
 Tukey multiple comparisons of means
 95% family-wise confidence level

Fit: aov(formula = x ~ y, data = test)

\$y
 diff lwr upr p adj
 2-1 -0.6767949 -2.818727 1.465137 0.7205661
 3-1 -1.0492424 -3.282686 1.184201 0.4892545
 3-2 -0.3724476 -2.564423 1.819527 0.9088949

[1] "silt"
 Df Sum Sq Mean Sq F value Pr(>F)
 y 2 629 314.5 1.654 0.207
 Residuals 33 6273 190.1
 Tukey multiple comparisons of means
 95% family-wise confidence level

Fit: aov(formula = x ~ y, data = test)

\$y
 diff lwr upr p adj
 2-1 -2.850128 -16.39354 10.693282 0.8639181
 3-1 -10.182576 -24.30461 3.939459 0.1955556
 3-2 -7.332448 -21.19228 6.527383 0.4062357

[1] "fine_sand"
 Df Sum Sq Mean Sq F value Pr(>F)
 y 2 559 279.3 1.241 0.302
 Residuals 33 7427 225.1
 Tukey multiple comparisons of means
 95% family-wise confidence level

Fit: aov(formula = x ~ y, data = test)

\$y
 diff lwr upr p adj
 2-1 2.010833 -12.726019 16.74769 0.9401884
 3-1 9.401742 -5.964722 24.76821 0.3033622
 3-2 7.390909 -7.690246 22.47206 0.4600984

[1] "organic_matter"
 Df Sum Sq Mean Sq F value Pr(>F)
 y 2 15.82 7.908 4.662 0.0165 *
 Residuals 33 55.97 1.696

 Signif. codes: 0 '***' 0.001 '**' 0.01 '*' 0.05 '.' 0.1 ' ' 1
 Tukey multiple comparisons of means
 95% family-wise confidence level

Fit: aov(formula = x ~ y, data = test)

\$y
 diff lwr upr p adj
 2-1 0.07115385 -1.208139 1.35044677 0.9897868
 3-1 -1.40045455 -2.734404 -0.06650549 0.0379705
 3-2 -1.47160839 -2.780790 -0.16242679 0.0248319

[1] "carbonates"
 Df Sum Sq Mean Sq F value Pr(>F)
 y 2 2.054 1.027 8.851 0.000836 ***
 Residuals 33 3.829 0.116

 Signif. codes: 0 '***' 0.001 '**' 0.01 '*' 0.05 '.' 0.1 ' ' 1
 Tukey multiple comparisons of means
 95% family-wise confidence level

Fit: aov(formula = x ~ y, data = test)

\$y
 diff lwr upr p adj
 2-1 -0.1796154 -0.5142335 0.15500271 0.3959230
 3-1 -0.5859091 -0.9348233 -0.23699488 0.0006819
 3-2 -0.4062937 -0.7487296 -0.06385779 0.0171525

[1] "airkerma"
 Df Sum Sq Mean Sq F value Pr(>F)
 y 2 31581 15790 6.861 0.00705 **
 Residuals 16 36824 2301

 Signif. codes: 0 '***' 0.001 '**' 0.01 '*' 0.05 '.' 0.1 ' ' 1
 17 observations deleted due to missingness
 Tukey multiple comparisons of means
 95% family-wise confidence level

Fit: aov(formula = x ~ y, data = test)

\$y
 diff lwr upr p adj
 2-1 -17.35714 -86.226666 51.51238 0.7948419
 3-1 77.00000 5.530719 148.46928 0.0338793
 3-2 94.35714 25.487620 163.22667 0.0073215

[1] "ph"
 Df Sum Sq Mean Sq F value Pr(>F)
 y 2 0.1506 0.07528 5.801 0.00694 **
 Residuals 33 0.4282 0.01298

 Signif. codes: 0 '***' 0.001 '**' 0.01 '*' 0.05 '.' 0.1 ' ' 1
 Tukey multiple comparisons of means
 95% family-wise confidence level

Fit: aov(formula = x ~ y, data = test)

\$y
 diff lwr upr p adj
 2-1 -0.15493590 -0.26683634 -0.04303546 0.0049603
 3-1 -0.09053030 -0.20721154 0.02615094 0.1535137
 3-2 0.06440559 -0.05010922 0.17892041 0.3627182

[1] "CS137"
 Df Sum Sq Mean Sq F value Pr(>F)
 y 2 1745 872.5 0.956 0.395
 Residuals 33 30131 913.1
 Tukey multiple comparisons of means
 95% family-wise confidence level

Fit: aov(formula = x ~ y, data = test)

\$y
 diff lwr upr p adj
 2-1 2.676622 -27.00558 32.35882 0.9733913
 3-1 -13.527644 -44.47797 17.42269 0.5375213
 3-2 -16.204266 -46.57994 14.17141 0.4003273

[1] "Al"
 Df Sum Sq Mean Sq F value Pr(>F)
 y 2 175.9 87.97 4.131 0.0251 *
 Residuals 33 702.7 21.29

 Signif. codes: 0 '***' 0.001 '**' 0.01 '*' 0.05 '.' 0.1 ' ' 1
 Tukey multiple comparisons of means
 95% family-wise confidence level

Fit: aov(formula = x ~ y, data = test)

\$y
 diff lwr upr p adj
 2-1 1.579413 -2.953485 6.1123115 0.6719618
 3-1 -3.760686 -8.487246 0.9658750 0.1402134
 3-2 -5.340099 -9.978901 -0.7012963 0.0211741

[1] "As"
 Df Sum Sq Mean Sq F value Pr(>F)

y 2 3.426e-05 1.713e-05 7.462 0.00212 **
 Residuals 33 7.575e-05 2.295e-06

 Signif. codes: 0 '***' 0.001 '**' 0.01 '*' 0.05 '.' 0.1 ' ' 1
 Tukey multiple comparisons of means
 95% family-wise confidence level

Fit: aov(formula = x ~ y, data = test)

\$y

| | diff | lwr | upr | p adj |
|-----|---------------|---------------|---------------|-----------|
| 2-1 | 0.0006999554 | -0.0007883004 | 0.0021882111 | 0.4884810 |
| 3-1 | -0.0016570047 | -0.0032088443 | -0.0001051651 | 0.0343261 |
| 3-2 | -0.0023569600 | -0.0038799866 | -0.0008339335 | 0.0016826 |

[1] "Ba"

| | Df | Sum Sq | Mean Sq | F value | Pr(>F) |
|-----------|----|----------|-----------|---------|--------|
| y | 2 | 0.003934 | 0.0019672 | 2.153 | 0.132 |
| Residuals | 33 | 0.030147 | 0.0009135 | | |

Tukey multiple comparisons of means
 95% family-wise confidence level

Fit: aov(formula = x ~ y, data = test)

\$y

| | diff | lwr | upr | p adj |
|-----|-------------|-------------|-------------|----------|
| 2-1 | 0.00790379 | -0.02178611 | 0.037593694 | 0.791855 |
| 3-1 | -0.01743126 | -0.04838963 | 0.013527107 | 0.361918 |
| 3-2 | -0.02533505 | -0.05571861 | 0.005048513 | 0.117130 |

[1] "Cd"

| | Df | Sum Sq | Mean Sq | F value | Pr(>F) |
|-----------|----|-----------|-----------|---------|------------|
| y | 2 | 8.317e-07 | 4.158e-07 | 7.391 | 0.00223 ** |
| Residuals | 33 | 1.857e-06 | 5.630e-08 | | |

Signif. codes: 0 '***' 0.001 '**' 0.01 '*' 0.05 '.' 0.1 ' ' 1
 Tukey multiple comparisons of means
 95% family-wise confidence level

Fit: aov(formula = x ~ y, data = test)

\$y

| | diff | lwr | upr | p adj |
|-----|---------------|---------------|---------------|-----------|
| 2-1 | -0.0000629858 | -0.0002959859 | 0.0001700143 | 0.7861670 |
| 3-1 | -0.0003577629 | -0.0006007176 | -0.0001148082 | 0.0027833 |
| 3-2 | -0.0002947771 | -0.0005332208 | -0.0000563333 | 0.0126719 |

[1] "Co"

| | Df | Sum Sq | Mean Sq | F value | Pr(>F) |
|-----------|----|-----------|-----------|---------|------------|
| y | 2 | 2.428e-05 | 1.214e-05 | 5.659 | 0.00771 ** |
| Residuals | 33 | 7.079e-05 | 2.145e-06 | | |

Signif. codes: 0 '***' 0.001 '**' 0.01 '*' 0.05 '.' 0.1 ' ' 1
 Tukey multiple comparisons of means
 95% family-wise confidence level

Fit: aov(formula = x ~ y, data = test)

\$y

| | diff | lwr | upr | p adj |
|-----|---------------|--------------|---------------|-----------|
| 2-1 | 0.0001316018 | -0.001307093 | 0.0015702971 | 0.9726317 |
| 3-1 | -0.0017104013 | -0.003210563 | -0.0002102396 | 0.0225988 |
| 3-2 | -0.0018420031 | -0.003314311 | -0.0003696949 | 0.0115634 |

[1] "Cr"

| | Df | Sum Sq | Mean Sq | F value | Pr(>F) |
|---|----|-----------|-----------|---------|----------|
| y | 2 | 0.0005842 | 2.921e-04 | 4.918 | 0.0135 * |

Residuals 33 0.0019597 5.939e-05

 Signif. codes: 0 '***' 0.001 '**' 0.01 '*' 0.05 '.' 0.1 ' ' 1
 Tukey multiple comparisons of means
 95% family-wise confidence level

Fit: aov(formula = x ~ y, data = test)

\$y

| | diff | lwr | upr | p adj |
|-----|--------------|--------------|--------------|-----------|
| 2-1 | 0.003110751 | -0.004459066 | 0.010680567 | 0.5768919 |
| 3-1 | -0.006662979 | -0.014556206 | 0.001230248 | 0.1114654 |
| 3-2 | -0.009773730 | -0.017520403 | -0.002027056 | 0.0108302 |

[1] "Cu"

| | Df | Sum Sq | Mean Sq | F value | Pr(>F) |
|-----------|----|-----------|-----------|---------|----------|
| y | 2 | 0.0001428 | 7.142e-05 | 3.635 | 0.0374 * |
| Residuals | 33 | 0.0006484 | 1.965e-05 | | |

Signif. codes: 0 '***' 0.001 '**' 0.01 '*' 0.05 '.' 0.1 ' ' 1
 Tukey multiple comparisons of means
 95% family-wise confidence level

Fit: aov(formula = x ~ y, data = test)

\$y

| | diff | lwr | upr | p adj |
|-----|--------------|--------------|---------------|-----------|
| 2-1 | 0.002680642 | -0.001673572 | 0.0070348560 | 0.2990542 |
| 3-1 | -0.002188009 | -0.006728251 | 0.0023522338 | 0.4717444 |
| 3-2 | -0.004868650 | -0.009324594 | -0.0004127067 | 0.0297909 |

[1] "Fe"

| | Df | Sum Sq | Mean Sq | F value | Pr(>F) |
|-----------|----|--------|---------|---------|------------|
| y | 2 | 66.95 | 33.48 | 5.498 | 0.00869 ** |
| Residuals | 33 | 200.92 | 6.09 | | |

Signif. codes: 0 '***' 0.001 '**' 0.01 '*' 0.05 '.' 0.1 ' ' 1
 Tukey multiple comparisons of means
 95% family-wise confidence level

Fit: aov(formula = x ~ y, data = test)

\$y

| | diff | lwr | upr | p adj |
|-----|------------|-----------|-------------|-----------|
| 2-1 | 0.8056149 | -1.618177 | 3.22940698 | 0.6961435 |
| 3-1 | -2.4506210 | -4.977966 | 0.07672449 | 0.0588719 |
| 3-2 | -3.2562359 | -5.736656 | -0.77581565 | 0.0078599 |

[1] "Hg"

| | Df | Sum Sq | Mean Sq | F value | Pr(>F) |
|-----------|----|-----------|-----------|---------|--------|
| y | 2 | 9.540e-07 | 4.772e-07 | 0.848 | 0.437 |
| Residuals | 33 | 1.856e-05 | 5.626e-07 | | |

Tukey multiple comparisons of means
 95% family-wise confidence level

Fit: aov(formula = x ~ y, data = test)

\$y

| | diff | lwr | upr | p adj |
|-----|---------------|---------------|--------------|-----------|
| 2-1 | 0.0001749967 | -0.0005617857 | 0.0009117791 | 0.8302100 |
| 3-1 | -0.0002250937 | -0.0009933542 | 0.0005431668 | 0.7541087 |
| 3-2 | -0.0004000904 | -0.0011540866 | 0.0003539058 | 0.4041135 |

[1] "K"

| | Df | Sum Sq | Mean Sq | F value | Pr(>F) |
|-----------|----|--------|---------|---------|------------|
| y | 2 | 22.32 | 11.161 | 6.241 | 0.00503 ** |
| Residuals | 33 | 59.02 | 1.788 | | |

Signif. codes: 0 '***' 0.001 '**' 0.01 '*' 0.05 '.' 0.1 ' ' 1
Tukey multiple comparisons of means
95% family-wise confidence level

Fit: aov(formula = x ~ y, data = test)

```
$y
      diff      lwr      upr    p adj
2-1  0.07247917 -1.241152  1.3861104 0.9899487
3-1 -1.67048931 -3.040244 -0.3007348 0.0140370
3-2 -1.74296847 -3.087291 -0.3986463 0.0087083
```

[1] "Mg"
Df Sum Sq Mean Sq F value Pr(>F)
y 2 20.86 10.430 8.632 0.000966 ***
Residuals 33 39.87 1.208

Signif. codes: 0 '***' 0.001 '**' 0.01 '*' 0.05 '.' 0.1 ' ' 1
Tukey multiple comparisons of means
95% family-wise confidence level

Fit: aov(formula = x ~ y, data = test)

```
$y
      diff      lwr      upr    p adj
2-1  0.2317304 -0.848034  1.3114948 0.8589035
3-1 -1.5186575 -2.644553 -0.3927615 0.0062461
3-2 -1.7503879 -2.855379 -0.6453965 0.0013128
```

[1] "Mn"
Df Sum Sq Mean Sq F value Pr(>F)
y 2 0.2374 0.11872 6.967 0.00299 **
Residuals 33 0.5624 0.01704

Signif. codes: 0 '***' 0.001 '**' 0.01 '*' 0.05 '.' 0.1 ' ' 1
Tukey multiple comparisons of means
95% family-wise confidence level

Fit: aov(formula = x ~ y, data = test)

```
$y
      diff      lwr      upr    p adj
2-1 -0.01472715 -0.1429601  0.11350580 0.9572227
3-1 -0.18345894 -0.3171705 -0.04974740 0.0053796
3-2 -0.16873179 -0.2999607 -0.03750288 0.0093171
```

[1] "Ni"
Df Sum Sq Mean Sq F value Pr(>F)
y 2 5.598e-05 2.799e-05 4.404 0.0202 *
Residuals 33 2.097e-04 6.355e-06

Signif. codes: 0 '***' 0.001 '**' 0.01 '*' 0.05 '.' 0.1 ' ' 1
Tukey multiple comparisons of means
95% family-wise confidence level

Fit: aov(formula = x ~ y, data = test)

```
$y
      diff      lwr      upr    p adj
2-1  0.0001822638 -0.002294131  2.658659e-03 0.9821892
3-1 -0.0026073369 -0.005189533 -2.514094e-05 0.0474154
3-2 -0.0027896007 -0.005323853 -2.553484e-04 0.0284278
```

[1] "P"
Df Sum Sq Mean Sq F value Pr(>F)
y 2 0.4292 0.21458 9.164 0.000684 ***
Residuals 33 0.7727 0.02342

Signif. codes: 0 '***' 0.001 '**' 0.01 '*' 0.05 '.' 0.1 ' ' 1
Tukey multiple comparisons of means
95% family-wise confidence level

Fit: aov(formula = x ~ y, data = test)

```
$y
      diff      lwr      upr    p adj
2-1 -0.01220905 -0.1625246  0.13810649 0.9783542
3-1 -0.24311501 -0.3998526 -0.08637743 0.0016427
3-2 -0.23090596 -0.3847334 -0.07707853 0.0023009
```

[1] "Pb"
Df Sum Sq Mean Sq F value Pr(>F)
y 2 0.001519 0.0007596 21.25 1.17e-06 ***
Residuals 33 0.001179 0.0000357

Signif. codes: 0 '***' 0.001 '**' 0.01 '*' 0.05 '.' 0.1 ' ' 1
Tukey multiple comparisons of means
95% family-wise confidence level

Fit: aov(formula = x ~ y, data = test)

```
$y
      diff      lwr      upr    p adj
2-1 -0.010108342 -0.01598112 -0.0042355615 0.0005091
3-1 -0.015999015 -0.02212270 -0.0098753282 0.0000009
3-2 -0.005890674 -0.01190066  0.0001193148 0.0556574
```

[1] "Sr"
Df Sum Sq Mean Sq F value Pr(>F)
y 2 0.003276 0.0016379 5.791 0.00699 **
Residuals 33 0.009334 0.0002828

Signif. codes: 0 '***' 0.001 '**' 0.01 '*' 0.05 '.' 0.1 ' ' 1
Tukey multiple comparisons of means
95% family-wise confidence level

Fit: aov(formula = x ~ y, data = test)

```
$y
      diff      lwr      upr    p adj
2-1  0.005211024 -0.01130950  0.0217315499 0.7213740
3-1 -0.017455538 -0.03468188 -0.0002291941 0.0464980
3-2 -0.022666562 -0.03957306 -0.0057600600 0.0065804
```

[1] "V"
Df Sum Sq Mean Sq F value Pr(>F)
y 2 0.0009174 0.0004587 4.887 0.0138 *
Residuals 33 0.0030976 0.0000939

Signif. codes: 0 '***' 0.001 '**' 0.01 '*' 0.05 '.' 0.1 ' ' 1
Tukey multiple comparisons of means
95% family-wise confidence level

Fit: aov(formula = x ~ y, data = test)

```
$y
      diff      lwr      upr    p adj
2-1  0.004047899 -0.005469136  0.013564934 0.5551450
3-1 -0.008225211 -0.018148849  0.001698427 0.1199584
3-2 -0.012273110 -0.022012496 -0.002533724 0.0109326
```

[1] "Zn"
Df Sum Sq Mean Sq F value Pr(>F)
y 2 0.00705 0.003525 4.626 0.0169 *
Residuals 33 0.02515 0.000762

Signif. codes: 0 '***' 0.001 '**' 0.01 '*' 0.05 '.' 0.1 ' ' 1
Tukey multiple comparisons of means
95% family-wise confidence level

Fit: aov(formula = x ~ y, data = test)

```
$y
      diff      lwr      upr  p adj
2-1 0.001284838 -0.02583142 0.028401098
0.9925767
3-1 -0.029690055 -0.05796482 -0.001415287
0.0379283
3-2 -0.030974893 -0.05872468 -0.003225103
0.0259933
```

```
[1] "Ca"
      Df Sum Sq Mean Sq F value Pr(>F)
y      2  154.9   77.46   10.72 0.000258 ***
Residuals 33  238.4    7.22
```

```
---
Signif. codes:  0 '***' 0.001 '**' 0.01 '*' 0.05 '.' 0.1 ' ' 1
Tukey multiple comparisons of means
95% family-wise confidence level
```

Fit: aov(formula = x ~ y, data = test)

```
$y
      diff      lwr      upr  p adj
2-1 0.8510769 -1.789132  3.491286 0.7111106
3-1 -3.9947071 -6.747715 -1.241699 0.0032101
3-2 -4.8457840 -7.547677 -2.143891 0.0003066
```

```
[1] "Mo"
      Df Sum Sq Mean Sq F value Pr(>F)
y      2 2.030e-08 1.016e-08  0.662 0.523
Residuals 33 5.066e-07 1.535e-08
Tukey multiple comparisons of means
95% family-wise confidence level
```

Fit: aov(formula = x ~ y, data = test)

```
$y
      diff      lwr      upr  p adj
2-1 5.494705e-06 -0.0001162161 1.272055e-04
0.9932586
3-1 -4.847092e-05 -0.0001753816 7.843980e-05
0.6210317
3-2 -5.396563e-05 -0.0001785200 7.058874e-05
0.5432191
```

```
[1] "AM241"
      Df Sum Sq Mean Sq F value Pr(>F)
y      2  1568   784.0   1.649 0.208
Residuals 33 15686  475.3
Tukey multiple comparisons of means
95% family-wise confidence level
```

Fit: aov(formula = x ~ y, data = test)

```
$y
      diff      lwr      upr  p adj
2-1 1.548968 -19.86708 22.965019 0.9827944
3-1 -13.453326 -35.78435  8.877698 0.3141452
3-2 -15.002294 -36.91870  6.914110 0.2279696
```

Appendix T1.6 Model output for seasonal differences

[1] "clay"

| | Df | Sum Sq | Mean Sq | F value | Pr(>F) |
|-----------|-----|--------|---------|---------|--------------|
| y | 3 | 358.0 | 119.35 | 23.52 | 2.18e-12 *** |
| Residuals | 140 | 710.4 | 5.07 | | |

Signif. codes: 0 '***' 0.001 '**' 0.01 '*' 0.05 '.' 0.1 ' ' 1
Tukey multiple comparisons of means
95% family-wise confidence level

Fit: aov(formula = x ~ y, data = test)

\$y

| | diff | lwr | upr | p adj |
|-----|-----------|--------------|------------|-----------|
| 2-1 | 1.385833 | 0.005328311 | 2.7663384 | 0.0487316 |
| 3-1 | 4.264444 | 2.883939422 | 5.6449495 | 0.0000000 |
| 4-1 | 2.684722 | 1.304217200 | 4.0652272 | 0.0000078 |
| 3-2 | 2.878611 | 1.498106089 | 4.2591161 | 0.0000015 |
| 4-2 | 1.298889 | -0.081616133 | 2.6793939 | 0.0731991 |
| 4-3 | -1.579722 | -2.960227245 | -0.1992172 | 0.0179237 |

[1] "silt"

| | Df | Sum Sq | Mean Sq | F value | Pr(>F) |
|-----------|-----|--------|---------|---------|--------------|
| y | 3 | 11712 | 3904 | 21.5 | 1.64e-11 *** |
| Residuals | 140 | 25426 | 182 | | |

Signif. codes: 0 '***' 0.001 '**' 0.01 '*' 0.05 '.' 0.1 ' ' 1
Tukey multiple comparisons of means
95% family-wise confidence level

Fit: aov(formula = x ~ y, data = test)

\$y

| | diff | lwr | upr | p adj |
|-----|-----------|-----------|-----------|-----------|
| 2-1 | 2.842222 | -5.417025 | 11.101470 | 0.8075660 |
| 3-1 | 19.913333 | 11.654086 | 28.172581 | 0.0000000 |
| 4-1 | 18.740278 | 10.481030 | 26.999525 | 0.0000002 |
| 3-2 | 17.071111 | 8.811864 | 25.330358 | 0.0000019 |
| 4-2 | 15.898056 | 7.638808 | 24.157303 | 0.0000098 |
| 4-3 | -1.173056 | -9.432303 | 7.086192 | 0.9827335 |

[1] "fine_sand"

| | Df | Sum Sq | Mean Sq | F value | Pr(>F) |
|-----------|-----|--------|---------|---------|--------------|
| y | 3 | 8148 | 2715.9 | 15.28 | 1.18e-08 *** |
| Residuals | 140 | 24880 | 177.7 | | |

Signif. codes: 0 '***' 0.001 '**' 0.01 '*' 0.05 '.' 0.1 ' ' 1
Tukey multiple comparisons of means
95% family-wise confidence level

Fit: aov(formula = x ~ y, data = test)

\$y

| | diff | lwr | upr | p adj |
|-----|-------------|------------|-----------|-----------|
| 2-1 | -0.8783333 | -9.048306 | 7.291640 | 0.9923444 |
| 3-1 | -16.3611111 | -24.531084 | -8.191138 | 0.0000040 |
| 4-1 | -14.4591667 | -22.629140 | -6.289194 | 0.0000546 |
| 3-2 | -15.4827778 | -23.652751 | -7.312805 | 0.0000137 |
| 4-2 | -13.5808333 | -21.750806 | -5.410860 | 0.0001696 |
| 4-3 | 1.9019444 | -6.268029 | 10.071917 | 0.9302429 |

[1] "organic_matter"

| | Df | Sum Sq | Mean Sq | F value | Pr(>F) |
|-----------|-----|--------|---------|---------|------------|
| y | 3 | 224.2 | 74.75 | 39.58 | <2e-16 *** |
| Residuals | 140 | 264.4 | 1.89 | | |

Signif. codes: 0 '***' 0.001 '**' 0.01 '*' 0.05 '.' 0.1 ' ' 1
Tukey multiple comparisons of means
95% family-wise confidence level

Fit: aov(formula = x ~ y, data = test)

\$y

| | diff | lwr | upr | p adj |
|-----|------------|-------------|------------|-----------|
| 2-1 | 1.2900000 | 0.44779381 | 2.1322062 | 0.0006255 |
| 3-1 | 3.4391667 | 2.59696047 | 4.2813729 | 0.0000000 |
| 4-1 | 2.0827778 | 1.24057159 | 2.9249840 | 0.0000000 |
| 3-2 | 2.1491667 | 1.30696047 | 2.9913729 | 0.0000000 |
| 4-2 | 0.7927778 | -0.04942841 | 1.6349840 | 0.0730021 |
| 4-3 | -1.3563889 | -2.19859508 | -0.5141827 | 0.0002872 |

[1] "carbonates"

| | Df | Sum Sq | Mean Sq | F value | Pr(>F) |
|-----------|-----|--------|---------|---------|------------|
| y | 3 | 82.69 | 27.564 | 82.39 | <2e-16 *** |
| Residuals | 140 | 46.84 | 0.335 | | |

Signif. codes: 0 '***' 0.001 '**' 0.01 '*' 0.05 '.' 0.1 ' ' 1
Tukey multiple comparisons of means
95% family-wise confidence level

Fit: aov(formula = x ~ y, data = test)

\$y

| | diff | lwr | upr | p adj |
|-----|------------|-------------|-----------|-----------|
| 2-1 | 1.6869444 | 1.33246324 | 2.0414256 | 0.0000000 |
| 3-1 | 1.4827778 | 1.12829657 | 1.8372590 | 0.0000000 |
| 4-1 | 1.9522222 | 1.59774102 | 2.3067034 | 0.0000000 |
| 3-2 | -0.2041667 | -0.55864787 | 0.1503145 | 0.4416951 |
| 4-2 | 0.2652778 | -0.08920343 | 0.6197590 | 0.2138652 |
| 4-3 | 0.4694444 | 0.11496324 | 0.8239256 | 0.0041762 |

[1] "airkerma"

| | Df | Sum Sq | Mean Sq | F value | Pr(>F) |
|-----------|----|--------|---------|---------|--------|
| y | 3 | 14936 | 4979 | 1.182 | 0.323 |
| Residuals | 72 | 303167 | 4211 | | |

68 observations deleted due to missingness
Tukey multiple comparisons of means
95% family-wise confidence level

Fit: aov(formula = x ~ y, data = test)

\$y

| | diff | lwr | upr | p adj |
|-----|------------|-----------|----------|-----------|
| 2-1 | -35.421053 | -90.79155 | 19.94945 | 0.3403629 |
| 3-1 | -20.368421 | -75.73892 | 35.00208 | 0.7682723 |
| 4-1 | -4.263158 | -59.63366 | 51.10734 | 0.9970345 |
| 3-2 | 15.052632 | -40.31787 | 70.42313 | 0.8908352 |
| 4-2 | 31.157895 | -24.21261 | 86.52840 | 0.4547794 |
| 4-3 | 16.105263 | -39.26524 | 71.47576 | 0.8699083 |

[1] "ph"

| | Df | Sum Sq | Mean Sq | F value | Pr(>F) |
|-----------|-----|--------|---------|---------|------------|
| y | 3 | 7.820 | 2.6067 | 39.36 | <2e-16 *** |
| Residuals | 140 | 9.272 | 0.0662 | | |

Signif. codes: 0 '***' 0.001 '**' 0.01 '*' 0.05 '.' 0.1 ' ' 1
Tukey multiple comparisons of means
95% family-wise confidence level

Fit: aov(formula = x ~ y, data = test)

\$y

| | diff | lwr | upr | p adj |
|-----|------------|--------------|-------------|-----------|
| 2-1 | -0.1044444 | -0.262161158 | 0.05327227 | 0.3162409 |
| 3-1 | -0.5791667 | -0.736883381 | -0.42144995 | 0.0000000 |
| 4-1 | -0.4163889 | -0.574105603 | -0.25867218 | 0.0000000 |
| 3-2 | -0.4747222 | -0.632438936 | -0.31700551 | 0.0000000 |
| 4-2 | -0.3119444 | -0.469661158 | -0.15422773 | 0.0000053 |
| 4-3 | 0.1627778 | 0.005061064 | 0.32049449 | 0.0402624 |

[1] "CS137"

| | Df | Sum Sq | Mean Sq | F value | Pr(>F) |
|-----------|-----|--------|---------|---------|------------|
| y | 3 | 18220 | 6073 | 4.247 | 0.00661 ** |
| Residuals | 140 | 200193 | 1430 | | |

Signif. codes: 0 '***' 0.001 '**' 0.01 '*' 0.05 '.' 0.1 ' ' 1
Tukey multiple comparisons of means
95% family-wise confidence level

```

Fit: aov(formula = x ~ y, data = test)

$y
      diff      lwr      upr      p adj
2-1 -4.416994 -27.592189 18.75820 0.9599576
3-1 24.446464  1.271270 47.62166 0.0343874
4-1 12.176139 -10.999055 35.35133 0.5226900
3-2 28.863458  5.688264 52.03865 0.0080909
4-2 16.593133 -6.582061 39.76833 0.2493815
4-3 -12.270325 -35.445519 10.90487 0.5160550

[1] "Al"
      Df Sum Sq Mean Sq F value Pr(>F)
y       3  2477  825.7  37.94 <2e-16 ***
Residuals 140  3046  21.8
---
Signif. codes: 0 '***' 0.001 '**' 0.01 '*' 0.05 '.' 0.1 ' ' 1
Tukey multiple comparisons of means
 95% family-wise confidence level

```

```

Fit: aov(formula = x ~ y, data = test)

$y
      diff      lwr      upr      p adj
2-1 -5.644775 -8.5036910 -2.785859 0.0000055
3-1  5.724800  2.8658840  8.583716 0.0000040
4-1  2.385287 -0.4736292  5.244203 0.1369221
3-2 11.369575  8.5106589 14.228491 0.0000000
4-2  8.030062  5.1711458 10.888978 0.0000000
4-3 -3.339513 -6.1984293 -0.480597 0.0149462

[1] "As"
      Df Sum Sq Mean Sq F value Pr(>F)
y       3 7.539e-05 2.513e-05 11.8 6.14e-07 ***
Residuals 140 2.981e-04 2.129e-06
---
Signif. codes: 0 '***' 0.001 '**' 0.01 '*' 0.05 '.' 0.1 ' ' 1
Tukey multiple comparisons of means
 95% family-wise confidence level

```

```

Fit: aov(formula = x ~ y, data = test)

$y
      diff      lwr      upr      p adj
2-1 -0.0006978599 -0.0015921820 0.0001964622
0.1823447
3-1  0.0011748705  0.0002805484  0.0020691927
0.0045742
4-1  0.0007941541 -0.0001001680  0.0016884763
0.1008826
3-2  0.0018727304  0.0009784083  0.0027670525
0.0000013
4-2  0.0014920140  0.0005976919  0.0023863362
0.0001593
4-3 -0.0003807164 -0.0012750385  0.0005136057
0.6858998

[1] "Ba"
      Df Sum Sq Mean Sq F value Pr(>F)
y       3 0.1079 0.03595 23.86 1.57e-12 ***
Residuals 140 0.2110 0.00151
---
Signif. codes: 0 '***' 0.001 '**' 0.01 '*' 0.05 '.' 0.1 ' ' 1
Tukey multiple comparisons of means
 95% family-wise confidence level

```

```

Fit: aov(formula = x ~ y, data = test)

$y
      diff      lwr      upr      p adj
2-1 -0.042507628 -0.06629934 -0.018715914
0.0000455
3-1  0.034535981  0.01074427  0.058327695
0.0013370
4-1  0.002200117 -0.02159160  0.025991831
0.9950899

```

```

3-2 0.077043609 0.05325190 0.100835323
0.0000000
4-2 0.044707745 0.02091603 0.068499459
0.0000164
4-3 -0.032335865 -0.05612758 -0.008544151
0.0030849

[1] "Cd"
      Df Sum Sq Mean Sq F value Pr(>F)
y       3 8.500e-07 2.833e-07 4.794 0.00328 **
Residuals 140 8.275e-06 5.911e-08
---
Signif. codes: 0 '***' 0.001 '**' 0.01 '*' 0.05 '.' 0.1 ' ' 1
Tukey multiple comparisons of means
 95% family-wise confidence level

```

```

Fit: aov(formula = x ~ y, data = test)

$y
      diff      lwr      upr      p adj
2-1 1.414125e-04 -7.584029e-06 0.0002904091
0.0695189
3-1 1.818652e-04 3.286864e-05 0.0003308618
0.0098920
4-1 1.924178e-04 4.342122e-05 0.0003414143
0.0055259
3-2 4.045267e-05 -1.085439e-04 0.0001894492
0.8945964
4-2 5.100525e-05 -9.799131e-05 0.0002000018
0.8100067
4-3 1.055258e-05 -1.384440e-04 0.0001595491
0.9977740

[1] "Co"
      Df Sum Sq Mean Sq F value Pr(>F)
y       3 5.569e-05 1.856e-05 9.855 6.13e-06 ***
Residuals 140 2.637e-04 1.884e-06
---
Signif. codes: 0 '***' 0.001 '**' 0.01 '*' 0.05 '.' 0.1 ' ' 1
Tukey multiple comparisons of means
 95% family-wise confidence level

```

```

Fit: aov(formula = x ~ y, data = test)

$y
      diff      lwr      upr      p adj
2-1 5.485754e-04 -2.925526e-04 0.0013897035
0.3297657
3-1 1.456457e-03 6.153290e-04 0.0022975850
0.0000822
4-1 1.455593e-03 6.144652e-04 0.0022967212
0.0000831
3-2 9.078816e-04 6.675354e-05 0.0017490096
0.0289098
4-2 9.070178e-04 6.588976e-05 0.0017481458
0.0291230
4-3 -8.637778e-07 -8.419918e-04 0.0008402642
1.0000000

[1] "Cr"
      Df Sum Sq Mean Sq F value Pr(>F)
y       3 0.003665 0.0012216 23.88 1.53e-12 ***
Residuals 140 0.007161 0.0000511
---
Signif. codes: 0 '***' 0.001 '**' 0.01 '*' 0.05 '.' 0.1 ' ' 1
Tukey multiple comparisons of means
 95% family-wise confidence level

```

```

Fit: aov(formula = x ~ y, data = test)

$y
      diff      lwr      upr      p adj
2-1 -0.005475109 -0.009858159 -0.001092060
0.0078493
3-1 0.007110670 0.002727621 0.011493720
0.0002550

```

4-1 0.005979566 0.001596516 0.010362616
0.0029487
3-2 0.012585780 0.008202730 0.016968829
0.0000000
4-2 0.011454675 0.007071626 0.015837725
0.0000000
4-3 -0.001131104 -0.005514154 0.003251945
0.9078724

[1] "Cu"

| | Df | Sum Sq | Mean Sq | F value | Pr(>F) |
|-----------|-----|-----------|-----------|---------|----------|
| y | 3 | 0.0001353 | 4.511e-05 | 3.227 | 0.0245 * |
| Residuals | 140 | 0.0019574 | 1.398e-05 | | |

Signif. codes: 0 '***' 0.001 '**' 0.01 '*' 0.05 '.' 0.1 ' ' 1
Tukey multiple comparisons of means
95% family-wise confidence level

Fit: aov(formula = x ~ y, data = test)

\$y

| | diff | lwr | upr | p adj |
|-----|---------------|---------------|-------------|-----------|
| 2-1 | 0.0020670609 | -0.0002245440 | 0.004358666 | 0.0928339 |
| 3-1 | 0.0018561011 | -0.0004355038 | 0.004147706 | 0.1562323 |
| 4-1 | 0.0025577644 | 0.0002661594 | 0.004849369 | 0.0221234 |
| 3-2 | -0.0002109598 | -0.0025025648 | 0.002080645 | 0.9951550 |
| 4-2 | 0.0004907034 | -0.0018009016 | 0.002782308 | 0.9445634 |
| 4-3 | 0.0007016632 | -0.0015899418 | 0.002993268 | 0.8560885 |

[1] "Fe"

| | Df | Sum Sq | Mean Sq | F value | Pr(>F) |
|-----------|-----|--------|---------|---------|--------------|
| y | 3 | 220.9 | 73.63 | 10.57 | 2.61e-06 *** |
| Residuals | 140 | 975.3 | 6.97 | | |

Signif. codes: 0 '***' 0.001 '**' 0.01 '*' 0.05 '.' 0.1 ' ' 1
Tukey multiple comparisons of means
95% family-wise confidence level

Fit: aov(formula = x ~ y, data = test)

\$y

| | diff | lwr | upr | p adj |
|-----|------------|------------|-----------|-----------|
| 2-1 | 1.2366756 | -0.3809542 | 2.8543054 | 0.1975076 |
| 3-1 | 3.2427801 | 1.6251502 | 4.8604099 | 0.0000039 |
| 4-1 | 2.5127982 | 0.8951683 | 4.1304280 | 0.0005064 |
| 3-2 | 2.0061045 | 0.3884747 | 3.6237343 | 0.0084475 |
| 4-2 | 1.2761226 | -0.3415072 | 2.8937524 | 0.1744974 |
| 4-3 | -0.7299819 | -2.3476117 | 0.8876479 | 0.6446302 |

[1] "Hg"

| | Df | Sum Sq | Mean Sq | F value | Pr(>F) |
|-----------|-----|-----------|-----------|---------|--------|
| y | 3 | 7.100e-07 | 2.352e-07 | 0.339 | 0.797 |
| Residuals | 140 | 9.727e-05 | 6.948e-07 | | |

Tukey multiple comparisons of means
95% family-wise confidence level

Fit: aov(formula = x ~ y, data = test)

\$y

| | diff | lwr | upr | p adj |
|-----|---------------|---------------|--------------|-----------|
| 2-1 | -1.570451e-04 | -0.0006678805 | 0.0003537902 | 0.8546043 |
| 3-1 | -1.824619e-04 | -0.0006932973 | 0.0003283734 | 0.7894987 |
| 4-1 | -1.227694e-04 | -0.0006336048 | 0.0003880659 | 0.9239306 |
| 3-2 | -2.541683e-05 | -0.0005362522 | 0.0004854185 | 0.9992231 |
| 4-2 | 3.427567e-05 | -0.0004765597 | 0.0005451110 | 0.9981047 |

4-3 5.969250e-05 -0.0004511429 0.0005705279
0.9902222

[1] "K"

| | Df | Sum Sq | Mean Sq | F value | Pr(>F) |
|-----------|-----|--------|---------|---------|--------------|
| y | 3 | 80.7 | 26.899 | 18.78 | 2.72e-10 *** |
| Residuals | 140 | 200.6 | 1.433 | | |

Signif. codes: 0 '***' 0.001 '**' 0.01 '*' 0.05 '.' 0.1 ' ' 1
Tukey multiple comparisons of means
95% family-wise confidence level

Fit: aov(formula = x ~ y, data = test)

\$y

| | diff | lwr | upr | p adj |
|-----|------------|------------|------------|-----------|
| 2-1 | -0.9922810 | -1.7258433 | -0.2587187 | 0.0032642 |
| 3-1 | 0.5101642 | -0.2233981 | 1.2437265 | 0.2737703 |
| 4-1 | 1.0360735 | 0.3025113 | 1.7696358 | 0.0019164 |
| 3-2 | 1.5024452 | 0.7688829 | 2.2360075 | 0.0000023 |
| 4-2 | 2.0283546 | 1.2947923 | 2.7619168 | 0.0000000 |
| 4-3 | 0.5259093 | -0.2076529 | 1.2594716 | 0.2483008 |

[1] "Mg"

| | Df | Sum Sq | Mean Sq | F value | Pr(>F) |
|-----------|-----|--------|---------|---------|--------------|
| y | 3 | 37.7 | 12.567 | 8.257 | 4.26e-05 *** |
| Residuals | 140 | 213.1 | 1.522 | | |

Signif. codes: 0 '***' 0.001 '**' 0.01 '*' 0.05 '.' 0.1 ' ' 1
Tukey multiple comparisons of means
95% family-wise confidence level

Fit: aov(formula = x ~ y, data = test)

\$y

| | diff | lwr | upr | p adj |
|-----|------------|-------------|-----------|-----------|
| 2-1 | 0.25907682 | -0.49701639 | 1.0151700 | 0.8095646 |
| 3-1 | 1.08848034 | 0.33238714 | 1.8445735 | 0.0014938 |
| 4-1 | 1.18010657 | 0.42401337 | 1.9361998 | 0.0004709 |
| 3-2 | 0.82940352 | 0.07331032 | 1.5854967 | 0.0254634 |
| 4-2 | 0.92102975 | 0.16493655 | 1.6771230 | 0.0100886 |
| 4-3 | 0.09162623 | -0.66446697 | 0.8477194 | 0.9891230 |

[1] "Mn"

| | Df | Sum Sq | Mean Sq | F value | Pr(>F) |
|-----------|-----|--------|---------|---------|--------------|
| y | 3 | 0.8332 | 0.2777 | 15.78 | 6.78e-09 *** |
| Residuals | 140 | 2.4636 | 0.0176 | | |

Signif. codes: 0 '***' 0.001 '**' 0.01 '*' 0.05 '.' 0.1 ' ' 1
Tukey multiple comparisons of means
95% family-wise confidence level

Fit: aov(formula = x ~ y, data = test)

\$y

| | diff | lwr | upr | p adj |
|-----|-------------|-------------|-------------|-----------|
| 2-1 | 0.07111805 | -0.01018072 | 0.152416824 | 0.1089743 |
| 3-1 | 0.20686121 | 0.12556243 | 0.288159981 | 0.0000000 |
| 4-1 | 0.13010021 | 0.04880143 | 0.211398979 | 0.0003183 |
| 3-2 | 0.13574316 | 0.05444438 | 0.217041931 | 0.0001571 |
| 4-2 | 0.05898216 | -0.02231662 | 0.140280929 | 0.2385685 |
| 4-3 | -0.07676100 | -0.15805978 | 0.004537772 | 0.0717007 |

[1] "Ni"

| | Df | Sum Sq | Mean Sq | F value | Pr(>F) |
|-----------|-----|-----------|-----------|---------|--------------|
| y | 3 | 0.0001388 | 4.626e-05 | 9.853 | 6.15e-06 *** |
| Residuals | 140 | 0.0006574 | 4.700e-06 | | |

Signif. codes: 0 '***' 0.001 '**' 0.01 '*' 0.05 '.' 0.1 ' ' 1
Tukey multiple comparisons of means
95% family-wise confidence level

Fit: aov(formula = x ~ y, data = test)

\$y

| | diff | lwr | upr | p adj |
|--|------|-----|-----|-------|
|--|------|-----|-----|-------|

```

2-1 -0.0001180205 -0.0014460480 0.001210007
0.9956348
3-1 0.0018180240 0.0004899965 0.003146051
0.0028283
4-1 0.0019806431 0.0006526156 0.003308671
0.0009201
3-2 0.0019360445 0.0006080170 0.003264072
0.0012616
4-2 0.0020986635 0.0007706360 0.003426691
0.0003885
4-3 0.0001626191 -0.0011654084 0.001490647
0.9887869

```

[1] "P"

```

Df Sum Sq Mean Sq F value Pr(>F)
y      3 0.6783 0.2261 11.03 1.52e-06 ***
Residuals 140 2.8707 0.0205
---
```

Signif. codes: 0 '***' 0.001 '**' 0.01 '*' 0.05 '.' 0.1 ' ' 1
 Tukey multiple comparisons of means
 95% family-wise confidence level

Fit: aov(formula = x ~ y, data = test)

\$y

```

diff lwr upr p adj
2-1 0.005247912 -0.0825111267 0.09300695
0.9986551
3-1 0.092210181 0.0044511422 0.17996922
0.0353955
4-1 0.166541391 0.0787823520 0.25430043
0.0000133
3-2 0.086962269 -0.0007967701 0.17472131
0.0530947
4-2 0.161293479 0.0735344398 0.24905252
0.0000260
4-3 0.074331210 -0.0134278291 0.16209025
0.1276385

```

[1] "Pb"

```

Df Sum Sq Mean Sq F value Pr(>F)
y      3 0.004325 0.0014415 33.62 <2e-16 ***
Residuals 140 0.006003 0.0000429
---
```

Signif. codes: 0 '***' 0.001 '**' 0.01 '*' 0.05 '.' 0.1 ' ' 1
 Tukey multiple comparisons of means
 95% family-wise confidence level

Fit: aov(formula = x ~ y, data = test)

\$y

```

diff lwr upr p adj
2-1 0.010462220 0.006449244 0.014475195
0.0000000
3-1 -0.003005849 -0.007018825 0.001007127
0.2131606
4-1 0.007670850 0.003657874 0.011683826
0.0000114
3-2 -0.013468069 -0.017481045 -0.009455093
0.0000000
4-2 -0.002791370 -0.006804346 0.001221606
0.2736179
4-3 0.010676699 0.006663723 0.014689675
0.0000000

```

[1] "Sr"

```

Df Sum Sq Mean Sq F value Pr(>F)
y      3 0.01700 0.005665 14.67 2.34e-08 ***
Residuals 140 0.05408 0.000386
---
```

Signif. codes: 0 '***' 0.001 '**' 0.01 '*' 0.05 '.' 0.1 ' ' 1
 Tukey multiple comparisons of means
 95% family-wise confidence level

Fit: aov(formula = x ~ y, data = test)

\$y

```

diff lwr upr p adj
2-1 -0.014129222 -0.026174941 -0.002083503
0.0143957
3-1 0.015980407 0.003934689 0.028026126
0.0040931
4-1 0.005551103 -0.006494616 0.017596822
0.6289769
3-2 0.030109629 0.018063911 0.042155348
0.0000000
4-2 0.019680325 0.007634606 0.031726044
0.0002269
4-3 -0.010429304 -0.022475023 0.001616415
0.1147458

```

[1] "V"

```

Df Sum Sq Mean Sq F value Pr(>F)
y      3 0.01046 0.003485 33.87 <2e-16 ***
Residuals 140 0.01440 0.000103
---
```

Signif. codes: 0 '***' 0.001 '**' 0.01 '*' 0.05 '.' 0.1 ' ' 1
 Tukey multiple comparisons of means
 95% family-wise confidence level

Fit: aov(formula = x ~ y, data = test)

\$y

```

diff lwr upr p adj
2-1 -0.012389895 -0.018606290 -0.0061735002
0.0000045
3-1 0.010863677 0.004647282 0.0170800717
0.0000693
4-1 0.004610074 -0.001606321 0.0108264689
0.2209784
3-2 0.023253572 0.017037177 0.0294699670
0.0000000
4-2 0.016999969 0.010783574 0.0232163641
0.0000000
4-3 -0.006253603 -0.012469998 -0.0000372079
0.0480448

```

[1] "Zn"

```

Df Sum Sq Mean Sq F value Pr(>F)
y      3 0.01338 0.004460 8.642 2.66e-05 ***
Residuals 140 0.07225 0.000516
---
```

Signif. codes: 0 '***' 0.001 '**' 0.01 '*' 0.05 '.' 0.1 ' ' 1
 Tukey multiple comparisons of means
 95% family-wise confidence level

Fit: aov(formula = x ~ y, data = test)

\$y

```

diff lwr upr p adj
2-1 0.012945879 -0.0009765362 0.02686829
0.0783842
3-1 0.015043792 0.0011213764 0.02896621
0.0286659
4-1 0.027177306 0.0132548909 0.04109972
0.0000072
3-2 0.002097913 -0.0118245030 0.01602033
0.9795132
4-2 0.014231427 0.0003090115 0.02815384
0.0430741
4-3 0.012133514 -0.0017889011 0.02605593
0.1110492

```

[1] "Ca"

```

Df Sum Sq Mean Sq F value Pr(>F)
y      3 139.9 46.63 3.263 0.0234 *
Residuals 140 2000.9 14.29
---
```

Signif. codes: 0 '***' 0.001 '**' 0.01 '*' 0.05 '.' 0.1 ' ' 1
 Tukey multiple comparisons of means
 95% family-wise confidence level

Fit: aov(formula = x ~ y, data = test)

```
$y
      diff      lwr      upr    p adj
2-1 -0.9080923 -3.2250058 1.408821 0.7385481
3-1  0.4255551 -1.8913584 2.742469 0.9639256
4-1  1.8249679 -0.4919455 4.141881 0.1755933
3-2  1.3336474 -0.9832660 3.650561 0.4422339
4-2  2.7330603  0.4161468 5.049974 0.0136725
4-3  1.3994129 -0.9175006 3.716326 0.3988003
```

```
[1] "Mo"
      Df Sum Sq Mean Sq F value Pr(>F)
y       3 1.458e-07 4.86e-08  4.943 0.00271 **
Residuals 140 1.376e-06 9.83e-09
---
Signif. codes:  0 '***' 0.001 '**' 0.01 '*' 0.05 '.' 0.1 ' ' 1
Tukey multiple comparisons of means
 95% family-wise confidence level
```

Fit: aov(formula = x ~ y, data = test)

```
$y
      diff      lwr      upr    p adj
2-1 -8.526314e-05 -1.460281e-04 -2.449823e-05
0.0020833
3-1 -6.676528e-05 -1.275302e-04 -6.000364e-06
0.0251344
4-1 -4.473383e-05 -1.054987e-04  1.603108e-05
0.2268002
3-2  1.849786e-05 -4.226705e-05  7.926277e-05
0.8581975
4-2  4.052931e-05 -2.023561e-05  1.012942e-04
0.3099416
4-3  2.203144e-05 -3.873347e-05  8.279636e-05
0.7818646
```

```
[1] "AM241"
      Df Sum Sq Mean Sq F value Pr(>F)
y       3 17266  5755  6.577 0.000343 ***
Residuals 140 122512  875
---
Signif. codes:  0 '***' 0.001 '**' 0.01 '*' 0.05 '.' 0.1 ' ' 1
Tukey multiple comparisons of means
 95% family-wise confidence level
```

Fit: aov(formula = x ~ y, data = test)

```
$y
      diff      lwr      upr    p adj
2-1 -4.996945 -23.126525 13.132635 0.8903348
3-1  23.737417  5.607837 41.866997 0.0047485
4-1  9.562694 -8.566885 27.692274 0.5193113
3-2  28.734362  10.604782 46.863942 0.0003709
4-2  14.559639 -3.569940 32.689219 0.1620238
4-3 -14.174722 -32.304302  3.954858 0.1809210
```

Appendix T1.7 Model output for ²⁴¹Am for transect 1 season 1

[[1]]

Call:
lm(formula = substitute(log(Time.corrected.activity) ~ log(i),
list(i = as.name(x))), data = test)

Residuals:
Min 1Q Median 3Q Max
-0.28424 -0.09774 -0.04557 0.08212 0.38393

Coefficients:
Estimate Std. Error t value Pr(>|t|)
(Intercept) 2.0689 0.1522 13.59 9.85e-06 ***
log(clay) 1.0085 0.1273 7.92 0.000215 ***

Signif. codes: 0 '***' 0.001 '**' 0.01 '*' 0.05 '.' 0.1 ' ' 1

Residual standard error: 0.2141 on 6 degrees of freedom
Multiple R-squared: 0.9127, Adjusted R-squared: 0.8981
F-statistic: 62.72 on 1 and 6 DF, p-value: 0.0002152

[[2]]

Call:
lm(formula = substitute(log(Time.corrected.activity) ~ log(i),
list(i = as.name(x))), data = test)

Residuals:
Min 1Q Median 3Q Max
-0.26558 -0.09008 -0.01473 0.08930 0.29524

Coefficients:
Estimate Std. Error t value Pr(>|t|)
(Intercept) 1.60484 0.17152 9.357 8.45e-05 ***
log(silt) 0.70865 0.07467 9.491 7.80e-05 ***

Signif. codes: 0 '***' 0.001 '**' 0.01 '*' 0.05 '.' 0.1 ' ' 1

Residual standard error: 0.1811 on 6 degrees of freedom
Multiple R-squared: 0.9375, Adjusted R-squared: 0.9271
F-statistic: 90.08 on 1 and 6 DF, p-value: 7.797e-05

[[3]]

Call:
lm(formula = substitute(log(Time.corrected.activity) ~ log(i),
list(i = as.name(x))), data = test)

Residuals:
Min 1Q Median 3Q Max
-0.46143 -0.35957 -0.00713 0.40538 0.45004

Coefficients:
Estimate Std. Error t value Pr(>|t|)
(Intercept) 22.176 5.567 3.984 0.00725 **
log(fine_sand) -4.422 1.291 -3.425 0.01405 *

Signif. codes: 0 '***' 0.001 '**' 0.01 '*' 0.05 '.' 0.1 ' ' 1

Residual standard error: 0.4214 on 6 degrees of freedom
Multiple R-squared: 0.6617, Adjusted R-squared: 0.6053

F-statistic: 11.73 on 1 and 6 DF, p-value: 0.01405

[[4]]

Call:
lm(formula = substitute(log(Time.corrected.activity) ~ log(i),
list(i = as.name(x))), data = test)

Residuals:
Min 1Q Median 3Q Max
-0.76884 -0.18686 -0.02716 0.26839 0.66366

Coefficients:
Estimate Std. Error t value Pr(>|t|)
(Intercept) 3.5908 0.2328 15.425 4.69e-06 ***
log(organic_matter) 0.7048 0.2429 2.901 0.0273 *

Signif. codes: 0 '***' 0.001 '**' 0.01 '*' 0.05 '.' 0.1 ' ' 1

Residual standard error: 0.4674 on 6 degrees of freedom
Multiple R-squared: 0.5838, Adjusted R-squared: 0.5145
F-statistic: 8.418 on 1 and 6 DF, p-value: 0.02729

Appendix T1.8 Model output for ²⁴¹Am for transect 2 season 1

[[1]]

Call:
lm(formula = substitute(log(Time.corrected.activity) ~ log(i),
list(i = as.name(x))), data = test)

Residuals:
Min 1Q Median 3Q Max
-0.65965 -0.10742 0.05924 0.15417 0.43092

Coefficients:
Estimate Std. Error t value Pr(>|t|)
(Intercept) 1.6334 0.4276 3.820 0.005089 **
log(clay) 1.3420 0.2414 5.559 0.000535 ***

Signif. codes: 0 '***' 0.001 '**' 0.01 '*' 0.05 '.' 0.1 ' ' 1

Residual standard error: 0.3133 on 8 degrees of freedom
Multiple R-squared: 0.7943, Adjusted R-squared: 0.7686
F-statistic: 30.9 on 1 and 8 DF, p-value: 0.0005355

[[2]]

Call:
lm(formula = substitute(log(Time.corrected.activity) ~ log(i),
list(i = as.name(x))), data = test)

Residuals:
Min 1Q Median 3Q Max
-0.22834 -0.04193 0.01725 0.08989 0.15657

Coefficients:
Estimate Std. Error t value Pr(>|t|)
(Intercept) 0.5933 0.2320 2.557 0.0338 *
log(silt) 1.0690 0.0728 14.684 4.55e-07 ***

Signif. codes: 0 '***' 0.001 '**' 0.01 '*' 0.05 '.' 0.1 ' ' 1

Residual standard error: 0.1307 on 8 degrees of freedom
Multiple R-squared: 0.9642, Adjusted R-squared: 0.9598
F-statistic: 215.6 on 1 and 8 DF, p-value: 4.546e-07

[[3]]

Call:
lm(formula = substitute(log(Time.corrected.activity) ~ log(i),
list(i = as.name(x))), data = test)

Residuals:
Min 1Q Median 3Q Max
-0.53921 -0.12333 0.00581 0.12610 0.42332

Coefficients:
Estimate Std. Error t value Pr(>|t|)
(Intercept) 18.8473 2.3216 8.118 3.93e-05 ***
log(fine_sand) -3.6246 0.5643 -6.423 0.000204 ***

Signif. codes: 0 '***' 0.001 '**' 0.01 '*' 0.05 '.' 0.1 ' ' 1

Residual standard error: 0.2784 on 8 degrees of freedom
Multiple R-squared: 0.8376, Adjusted R-squared: 0.8173

F-statistic: 41.26 on 1 and 8 DF, p-value: 0.000204

[[4]]

Call:
lm(formula = substitute(log(Time.corrected.activity) ~ log(i),
list(i = as.name(x))), data = test)

Residuals:
Min 1Q Median 3Q Max
-0.22376 -0.07688 0.01878 0.09595 0.18966

Coefficients:
Estimate Std. Error t value Pr(>|t|)
(Intercept) 3.91355 0.04296 91.11 2.35e-13 ***
log(organic_matter) 1.38806 0.09828 14.12 6.14e-07 ***

Signif. codes: 0 '***' 0.001 '**' 0.01 '*' 0.05 '.' 0.1 ' ' 1

Residual standard error: 0.1356 on 8 degrees of freedom
Multiple R-squared: 0.9614, Adjusted R-squared: 0.9566
F-statistic: 199.5 on 1 and 8 DF, p-value: 6.141e-07

Appendix T1.9 Model output for ²⁴¹Am for transect 3 season 1

[[1]]

Call:
lm(formula = substitute(log(Time.corrected.activity) ~ log(i),
list(i = as.name(x))), data = test)

Residuals:
Min 1Q Median 3Q Max
-0.5042 -0.4173 0.1488 0.2842 0.6273

Coefficients:
Estimate Std. Error t value Pr(>|t|)
(Intercept) 2.5885 0.2780 9.310 6.47e-06 ***
log(clay) 0.5737 0.2726 2.105 0.0646 .

Signif. codes: 0 '***' 0.001 '**' 0.01 '*' 0.05 '.' 0.1 ' ' 1

Residual standard error: 0.417 on 9 degrees of freedom
Multiple R-squared: 0.3298, Adjusted R-squared: 0.2554
F-statistic: 4.429 on 1 and 9 DF, p-value: 0.06463

[[2]]

Call:
lm(formula = substitute(log(Time.corrected.activity) ~ log(i),
list(i = as.name(x))), data = test)

Residuals:
Min 1Q Median 3Q Max
-0.19136 -0.10539 -0.05888 0.06692 0.33984

Coefficients:
Estimate Std. Error t value Pr(>|t|)
(Intercept) 1.04277 0.25305 4.121 0.00259 **
log(silt) 0.83158 0.09961 8.349 1.57e-05 ***

Signif. codes: 0 '***' 0.001 '**' 0.01 '*' 0.05 '.' 0.1 ' ' 1

Residual standard error: 0.1722 on 9 degrees of freedom
Multiple R-squared: 0.8856, Adjusted R-squared: 0.8729
F-statistic: 69.7 on 1 and 9 DF, p-value: 1.572e-05

[[3]]

Call:
lm(formula = substitute(log(Time.corrected.activity) ~ log(i),
list(i = as.name(x))), data = test)

Residuals:
Min 1Q Median 3Q Max
-0.5932 -0.4930 0.1921 0.4150 0.6353

Coefficients:
Estimate Std. Error t value Pr(>|t|)
(Intercept) 2.3639 3.5982 0.657 0.528
log(fine_sand) 0.1786 0.8604 0.208 0.840

Residual standard error: 0.5081 on 9 degrees of freedom
Multiple R-squared: 0.004768, Adjusted R-squared: -0.1058
F-statistic: 0.04311 on 1 and 9 DF, p-value: 0.8401

[[4]]

Call:
lm(formula = substitute(log(Time.corrected.activity) ~ log(i),
list(i = as.name(x))), data = test)

Residuals:
Min 1Q Median 3Q Max
-0.39895 -0.29733 -0.02252 0.20549 0.67666

Coefficients:
Estimate Std. Error t value Pr(>|t|)
(Intercept) 3.6346 0.2145 16.945 3.9e-08 ***
log(organic_matter) 0.5928 0.2074 2.858 0.0188 *

Signif. codes: 0 '***' 0.001 '**' 0.01 '*' 0.05 '.' 0.1 ' ' 1

Residual standard error: 0.3688 on 9 degrees of freedom
Multiple R-squared: 0.4758, Adjusted R-squared: 0.4175
F-statistic: 8.169 on 1 and 9 DF, p-value: 0.01884

Appendix T1.10 Model output for
241 Am for transect 1 season 2

[[1]]

Call:
lm(formula = substitute(log(Time.corrected.activity) ~
log(i),
list(i = as.name(x))), data = test)

Residuals:
Min 1Q Median 3Q Max
-0.43356 -0.11042 0.02615 0.11534 0.30621

Coefficients:
Estimate Std. Error t value Pr(>|t|)
(Intercept) 2.0300 0.2203 9.217 7.03e-06 ***
log(clay) 0.7668 0.1496 5.125 0.000624 ***

Signif. codes: 0 '***' 0.001 '**' 0.01 '*' 0.05 '.' 0.1 ' ' 1

Residual standard error: 0.2108 on 9 degrees of
freedom
Multiple R-squared: 0.7448, Adjusted R-squared:
0.7164
F-statistic: 26.27 on 1 and 9 DF, p-value: 0.0006238

[[2]]

Call:
lm(formula = substitute(log(Time.corrected.activity) ~
log(i),
list(i = as.name(x))), data = test)

Residuals:
Min 1Q Median 3Q Max
-0.32766 -0.08896 -0.01822 0.08790 0.31242

Coefficients:
Estimate Std. Error t value Pr(>|t|)
(Intercept) 1.75725 0.21918 8.017 2.18e-05 ***
log(silt) 0.55688 0.08744 6.369 0.00013 ***

Signif. codes: 0 '***' 0.001 '**' 0.01 '*' 0.05 '.' 0.1 ' ' 1

Residual standard error: 0.1779 on 9 degrees of
freedom
Multiple R-squared: 0.8184, Adjusted R-squared:
0.7982
F-statistic: 40.56 on 1 and 9 DF, p-value: 0.00013

[[3]]

Call:
lm(formula = substitute(log(Time.corrected.activity) ~
log(i),
list(i = as.name(x))), data = test)

Residuals:
Min 1Q Median 3Q Max
-0.60031 -0.15275 -0.00098 0.19455 0.52518

Coefficients:
Estimate Std. Error t value Pr(>|t|)
(Intercept) 10.0614 4.0544 2.482 0.0349 *
log(fine_sand) -1.6270 0.9487 -1.715 0.1205

Signif. codes: 0 '***' 0.001 '**' 0.01 '*' 0.05 '.' 0.1 ' ' 1

Residual standard error: 0.3623 on 9 degrees of
freedom
Multiple R-squared: 0.2463, Adjusted R-squared:
0.1626

F-statistic: 2.941 on 1 and 9 DF, p-value: 0.1205

[[4]]

Call:
lm(formula = substitute(log(Time.corrected.activity) ~
log(i),
list(i = as.name(x))), data = test)

Residuals:
Min 1Q Median 3Q Max
-0.107318 -0.046724 -0.007716 0.017846 0.227378

Coefficients:
Estimate Std. Error t value Pr(>|t|)
(Intercept) 2.75290 0.03791 72.61 9.01e-14 ***
log(organic_matter) 1.11280 0.08213 13.55 2.72e-07 ***

Signif. codes: 0 '***' 0.001 '**' 0.01 '*' 0.05 '.' 0.1 ' ' 1

Residual standard error: 0.09022 on 9 degrees of
freedom
Multiple R-squared: 0.9533, Adjusted R-squared:
0.9481
F-statistic: 183.6 on 1 and 9 DF, p-value: 2.719e-07

Appendix T1.11 Model output for
²⁴¹Am for transect 2 season 2

F-statistic: 31.85 on 1 and 10 DF, p-value: 0.0002144

[[1]]

Call:
lm(formula = substitute(log(Time.corrected.activity) ~
log(i),
list(i = as.name(x))), data = test)

Residuals:
Min 1Q Median 3Q Max
-0.22455 -0.17268 -0.04668 0.08998 0.43001

Coefficients:
Estimate Std. Error t value Pr(>|t|)
(Intercept) 2.1594 0.4348 4.967 0.000564 ***
log(clay) 0.9027 0.2329 3.875 0.003084 **

Signif. codes: 0 '***' 0.001 '**' 0.01 '*' 0.05 '.' 0.1 ' ' 1

Residual standard error: 0.2251 on 10 degrees of
freedom
Multiple R-squared: 0.6003, Adjusted R-squared:
0.5603
F-statistic: 15.02 on 1 and 10 DF, p-value: 0.003084

[[2]]

Call:
lm(formula = substitute(log(Time.corrected.activity) ~
log(i),
list(i = as.name(x))), data = test)

Residuals:
Min 1Q Median 3Q Max
-0.27003 -0.04616 -0.03224 0.10156 0.16353

Coefficients:
Estimate Std. Error t value Pr(>|t|)
(Intercept) 1.3664 0.2981 4.584 0.001 **
log(silt) 0.7421 0.0893 8.311 8.42e-06 ***

Signif. codes: 0 '***' 0.001 '**' 0.01 '*' 0.05 '.' 0.1 ' ' 1

Residual standard error: 0.1266 on 10 degrees of
freedom
Multiple R-squared: 0.8735, Adjusted R-squared:
0.8609
F-statistic: 69.07 on 1 and 10 DF, p-value: 8.418e-06

[[3]]

Call:
lm(formula = substitute(log(Time.corrected.activity) ~
log(i),
list(i = as.name(x))), data = test)

Residuals:
Min 1Q Median 3Q Max
-0.23112 -0.11614 -0.06316 0.14702 0.29008

Coefficients:
Estimate Std. Error t value Pr(>|t|)
(Intercept) 8.9313 0.9062 9.856 1.82e-06 ***
log(fine_sand) -1.2518 0.2218 -5.643 0.000214 ***

Signif. codes: 0 '***' 0.001 '**' 0.01 '*' 0.05 '.' 0.1 ' ' 1

Residual standard error: 0.174 on 10 degrees of
freedom
Multiple R-squared: 0.761, Adjusted R-squared:
0.7371

[[4]]

Call:
lm(formula = substitute(log(Time.corrected.activity) ~
log(i),
list(i = as.name(x))), data = test)

Residuals:
Min 1Q Median 3Q Max
-0.20008 -0.11330 0.01540 0.08233 0.28856

Coefficients:
Estimate Std. Error t value Pr(>|t|)
(Intercept) 3.0642 0.1168 26.237 1.49e-10 ***
log(organic_matter) 0.8474 0.1212 6.992 3.75e-
05 ***

Signif. codes: 0 '***' 0.001 '**' 0.01 '*' 0.05 '.' 0.1 ' ' 1

Residual standard error: 0.1467 on 10 degrees of
freedom
Multiple R-squared: 0.8302, Adjusted R-squared:
0.8132
F-statistic: 48.89 on 1 and 10 DF, p-value: 3.751e-05

Appendix T1.12 Model output for ²⁴¹Am for transect 3 season 2

[[1]]

Call:
lm(formula = substitute(log(Time.corrected.activity) ~ log(i),
list(i = as.name(x))), data = test)

Residuals:
Min 1Q Median 3Q Max
-0.22455 -0.17268 -0.04668 0.08998 0.43001

Coefficients:
Estimate Std. Error t value Pr(>|t|)
(Intercept) 2.1594 0.4348 4.967 0.000564 ***
log(clay) 0.9027 0.2329 3.875 0.003084 **

Signif. codes: 0 '***' 0.001 '**' 0.01 '*' 0.05 '.' 0.1 ' ' 1

Residual standard error: 0.2251 on 10 degrees of freedom
Multiple R-squared: 0.6003, Adjusted R-squared: 0.5603
F-statistic: 15.02 on 1 and 10 DF, p-value: 0.003084

[[2]]

Call:
lm(formula = substitute(log(Time.corrected.activity) ~ log(i),
list(i = as.name(x))), data = test)

Residuals:
Min 1Q Median 3Q Max
-0.27003 -0.04616 -0.03224 0.10156 0.16353

Coefficients:
Estimate Std. Error t value Pr(>|t|)
(Intercept) 1.3664 0.2981 4.584 0.001 **
log(silt) 0.7421 0.0893 8.311 8.42e-06 ***

Signif. codes: 0 '***' 0.001 '**' 0.01 '*' 0.05 '.' 0.1 ' ' 1

Residual standard error: 0.1266 on 10 degrees of freedom
Multiple R-squared: 0.8735, Adjusted R-squared: 0.8609
F-statistic: 69.07 on 1 and 10 DF, p-value: 8.418e-06

[[3]]

Call:
lm(formula = substitute(log(Time.corrected.activity) ~ log(i),
list(i = as.name(x))), data = test)

Residuals:
Min 1Q Median 3Q Max
-0.23112 -0.11614 -0.06316 0.14702 0.29008

Coefficients:
Estimate Std. Error t value Pr(>|t|)
(Intercept) 8.9313 0.9062 9.856 1.82e-06 ***
log(fine_sand) -1.2518 0.2218 -5.643 0.000214 ***

Signif. codes: 0 '***' 0.001 '**' 0.01 '*' 0.05 '.' 0.1 ' ' 1

Residual standard error: 0.174 on 10 degrees of freedom
Multiple R-squared: 0.761, Adjusted R-squared: 0.7371

F-statistic: 31.85 on 1 and 10 DF, p-value: 0.0002144

[[4]]

Call:
lm(formula = substitute(log(Time.corrected.activity) ~ log(i),
list(i = as.name(x))), data = test)

Residuals:
Min 1Q Median 3Q Max
-0.20008 -0.11330 0.01540 0.08233 0.28856

Coefficients:
Estimate Std. Error t value Pr(>|t|)
(Intercept) 3.0642 0.1168 26.237 1.49e-10 ***
log(organic_matter) 0.8474 0.1212 6.992 3.75e-05 ***

Signif. codes: 0 '***' 0.001 '**' 0.01 '*' 0.05 '.' 0.1 ' ' 1

Residual standard error: 0.1467 on 10 degrees of freedom
Multiple R-squared: 0.8302, Adjusted R-squared: 0.8132
F-statistic: 48.89 on 1 and 10 DF, p-value: 3.751e-05

Appendix T1.13 Model output for
241 Am for transect 1 season 3

F-statistic: 57.86 on 1 and 10 DF, p-value: 1.827e-05

[[1]]

Call:
lm(formula = substitute(log(Time.corrected.activity) ~
log(i),
list(i = as.name(x))), data = test)

Residuals:
Min 1Q Median 3Q Max
-0.30093 -0.11711 0.00985 0.12073 0.24582

Coefficients:
Estimate Std. Error t value Pr(>|t|)
(Intercept) 1.0670 0.3705 2.880 0.0164 *
log(clay) 1.4427 0.1850 7.798 1.47e-05 ***

Signif. codes: 0 '***' 0.001 '**' 0.01 '*' 0.05 '.' 0.1 ' ' 1

Residual standard error: 0.1802 on 10 degrees of
freedom
Multiple R-squared: 0.8588, Adjusted R-squared:
0.8447
F-statistic: 60.81 on 1 and 10 DF, p-value: 1.472e-05

[[2]]

Call:
lm(formula = substitute(log(Time.corrected.activity) ~
log(i),
list(i = as.name(x))), data = test)

Residuals:
Min 1Q Median 3Q Max
-0.21305 -0.07335 0.01273 0.05205 0.22814

Coefficients:
Estimate Std. Error t value Pr(>|t|)
(Intercept) -0.3380 0.3492 -0.968 0.356
log(silt) 1.2323 0.1004 12.274 2.36e-07 ***

Signif. codes: 0 '***' 0.001 '**' 0.01 '*' 0.05 '.' 0.1 ' ' 1

Residual standard error: 0.1196 on 10 degrees of
freedom
Multiple R-squared: 0.9378, Adjusted R-squared:
0.9315
F-statistic: 150.6 on 1 and 10 DF, p-value: 2.362e-07

[[3]]

Call:
lm(formula = substitute(log(Time.corrected.activity) ~
log(i),
list(i = as.name(x))), data = test)

Residuals:
Min 1Q Median 3Q Max
-0.45788 -0.01544 0.04646 0.09810 0.20258

Coefficients:
Estimate Std. Error t value Pr(>|t|)
(Intercept) 9.5048 0.7351 12.929 1.44e-07 ***
log(fine_sand) -1.3979 0.1838 -7.606 1.83e-05 ***

Signif. codes: 0 '***' 0.001 '**' 0.01 '*' 0.05 '.' 0.1 ' ' 1

Residual standard error: 0.1841 on 10 degrees of
freedom
Multiple R-squared: 0.8526, Adjusted R-squared:
0.8379

[[4]]

Call:
lm(formula = substitute(log(Time.corrected.activity) ~
log(i),
list(i = as.name(x))), data = test)

Residuals:
Min 1Q Median 3Q Max
-0.39082 -0.09220 -0.04011 0.12561 0.38957

Coefficients:
Estimate Std. Error t value Pr(>|t|)
(Intercept) 2.685 0.206 13.036 1.34e-07 ***
log(organic_matter) 1.069 0.169 6.326 8.62e-05 ***

Signif. codes: 0 '***' 0.001 '**' 0.01 '*' 0.05 '.' 0.1 ' ' 1

Residual standard error: 0.2144 on 10 degrees of
freedom
Multiple R-squared: 0.8001, Adjusted R-squared:
0.7801
F-statistic: 40.01 on 1 and 10 DF, p-value: 8.619e-05

Appendix T1.14 Model output for
241 Am for transect 2 season 3

F-statistic: 220.9 on 1 and 11 DF, p-value: 1.254e-08

[[1]]

Call:
lm(formula = substitute(log(Time.corrected.activity) ~
log(i),
list(i = as.name(x))), data = test)

Residuals:
Min 1Q Median 3Q Max
-0.30013 -0.11977 -0.02857 0.09522 0.30181

Coefficients:
Estimate Std. Error t value Pr(>|t|)
(Intercept) 0.2300 0.3683 0.625 0.545
log(clay) 1.8699 0.1748 10.697 3.76e-07 ***

Signif. codes: 0 '***' 0.001 '**' 0.01 '*' 0.05 '.' 0.1 ' ' 1

Residual standard error: 0.1803 on 11 degrees of
freedom
Multiple R-squared: 0.9123, Adjusted R-squared:
0.9043
F-statistic: 114.4 on 1 and 11 DF, p-value: 3.756e-07

[[2]]

Call:
lm(formula = substitute(log(Time.corrected.activity) ~
log(i),
list(i = as.name(x))), data = test)

Residuals:
Min 1Q Median 3Q Max
-0.21243 -0.07679 0.00815 0.06123 0.33425

Coefficients:
Estimate Std. Error t value Pr(>|t|)
(Intercept) -0.5857 0.3902 -1.501 0.161
log(silt) 1.3276 0.1091 12.173 1e-07 ***

Signif. codes: 0 '***' 0.001 '**' 0.01 '*' 0.05 '.' 0.1 ' ' 1

Residual standard error: 0.1601 on 11 degrees of
freedom
Multiple R-squared: 0.9309, Adjusted R-squared:
0.9246
F-statistic: 148.2 on 1 and 11 DF, p-value: 1.004e-07

[[3]]

Call:
lm(formula = substitute(log(Time.corrected.activity) ~
log(i),
list(i = as.name(x))), data = test)

Residuals:
Min 1Q Median 3Q Max
-0.24481 -0.09418 0.04515 0.10976 0.14003

Coefficients:
Estimate Std. Error t value Pr(>|t|)
(Intercept) 11.7536 0.5140 22.87 1.26e-10 ***
log(fine_sand) -1.9530 0.1314 -14.86 1.25e-08 ***

Signif. codes: 0 '***' 0.001 '**' 0.01 '*' 0.05 '.' 0.1 ' ' 1

Residual standard error: 0.1326 on 11 degrees of
freedom
Multiple R-squared: 0.9526, Adjusted R-squared:
0.9483

[[4]]

Call:
lm(formula = substitute(log(Time.corrected.activity) ~
log(i),
list(i = as.name(x))), data = test)

Residuals:
Min 1Q Median 3Q Max
-0.079036 -0.045820 -0.019824 0.007267 0.211588

Coefficients:
Estimate Std. Error t value Pr(>|t|)
(Intercept) 1.82581 0.09604 19.01 9.20e-10 ***
log(organic_matter) 1.44473 0.05847 24.71 5.47e-11 ***

Signif. codes: 0 '***' 0.001 '**' 0.01 '*' 0.05 '.' 0.1 ' ' 1

Residual standard error: 0.081 on 11 degrees of
freedom

Multiple R-squared: 0.9823, Adjusted R-squared:
0.9807
F-statistic: 610.6 on 1 and 11 DF, p-value: 5.471e-11

Appendix T1.15 Model output for ²⁴¹Am for transect 3 season 3

[[1]]

Call:
lm(formula = substitute(log(Time.corrected.activity) ~ log(i),
list(i = as.name(x))), data = test)

Residuals:
Min 1Q Median 3Q Max
-0.9107 -0.0932 -0.0033 0.1292 1.3989

Coefficients:
Estimate Std. Error t value Pr(>|t|)
(Intercept) 3.82552 3.04210 1.258 0.244
log(clay) 0.08508 1.50934 0.056 0.956

Residual standard error: 0.6511 on 8 degrees of freedom
(1 observation deleted due to missingness)
Multiple R-squared: 0.000397, Adjusted R-squared: -0.1246
F-statistic: 0.003178 on 1 and 8 DF, p-value: 0.9564

[[2]]

Call:
lm(formula = substitute(log(Time.corrected.activity) ~ log(i),
list(i = as.name(x))), data = test)

Residuals:
Min 1Q Median 3Q Max
-0.75385 -0.25580 -0.06431 -0.02287 1.32488

Coefficients:
Estimate Std. Error t value Pr(>|t|)
(Intercept) 0.6310 2.4596 0.257 0.804
log(silt) 0.9096 0.6628 1.372 0.207

Residual standard error: 0.5859 on 8 degrees of freedom
(1 observation deleted due to missingness)
Multiple R-squared: 0.1905, Adjusted R-squared: 0.08936
F-statistic: 1.883 on 1 and 8 DF, p-value: 0.2072

[[3]]

Call:
lm(formula = substitute(log(Time.corrected.activity) ~ log(i),
list(i = as.name(x))), data = test)

Residuals:
Min 1Q Median 3Q Max
-0.50919 -0.20970 -0.05222 0.04412 1.31348

Coefficients:
Estimate Std. Error t value Pr(>|t|)
(Intercept) 11.705 4.002 2.925 0.0191 *
log(fine_sand) -2.033 1.054 -1.928 0.0900 .

Signif. codes: 0 '***' 0.001 '**' 0.01 '*' 0.05 '.' 0.1 ' ' 1

Residual standard error: 0.5381 on 8 degrees of freedom
(1 observation deleted due to missingness)
Multiple R-squared: 0.3173, Adjusted R-squared: 0.2319
F-statistic: 3.718 on 1 and 8 DF, p-value: 0.08998

[[4]]

Call:
lm(formula = substitute(log(Time.corrected.activity) ~ log(i),
list(i = as.name(x))), data = test)

Residuals:
Min 1Q Median 3Q Max
-0.37105 -0.21681 -0.06351 0.02776 1.01269

Coefficients:
Estimate Std. Error t value Pr(>|t|)
(Intercept) 1.9598 0.6018 3.257 0.01158 *
log(organic_matter) 1.5644 0.4513 3.467 0.00848 **

Signif. codes: 0 '***' 0.001 '**' 0.01 '*' 0.05 '.' 0.1 ' ' 1

Residual standard error: 0.4117 on 8 degrees of freedom
(1 observation deleted due to missingness)
Multiple R-squared: 0.6004, Adjusted R-squared: 0.5504
F-statistic: 12.02 on 1 and 8 DF, p-value: 0.008482

Appendix T1.16 Model output for
²⁴¹Am for transect 1 season 4

[[1]]

Call:
lm(formula = substitute(log(Time.corrected.activity) ~
log(i),
list(i = as.name(x))), data = test)

Residuals:
Min 1Q Median 3Q Max
-0.21117 -0.09705 0.02822 0.09294 0.20093

Coefficients:
Estimate Std. Error t value Pr(>|t|)
(Intercept) 1.6003 0.2234 7.165 3.05e-05 ***
log(clay) 1.2142 0.1177 10.320 1.19e-06 ***

Signif. codes: 0 '***' 0.001 '**' 0.01 '*' 0.05 '.' 0.1 ' ' 1

Residual standard error: 0.135 on 10 degrees of
freedom
Multiple R-squared: 0.9142, Adjusted R-squared:
0.9056
F-statistic: 106.5 on 1 and 10 DF, p-value: 1.191e-06

[[2]]

Call:
lm(formula = substitute(log(Time.corrected.activity) ~
log(i),
list(i = as.name(x))), data = test)

Residuals:
Min 1Q Median 3Q Max
-0.32382 -0.15836 -0.02742 0.14300 0.42983

Coefficients:
Estimate Std. Error t value Pr(>|t|)
(Intercept) 0.6489 0.6068 1.069 0.310010
log(silt) 0.8888 0.1664 5.342 0.000327 ***

Signif. codes: 0 '***' 0.001 '**' 0.01 '*' 0.05 '.' 0.1 ' ' 1

Residual standard error: 0.2347 on 10 degrees of
freedom
Multiple R-squared: 0.7405, Adjusted R-squared:
0.7145
F-statistic: 28.53 on 1 and 10 DF, p-value: 0.0003275

[[3]]

Call:
lm(formula = substitute(log(Time.corrected.activity) ~
log(i),
list(i = as.name(x))), data = test)

Residuals:
Min 1Q Median 3Q Max
-0.225501 -0.126275 0.007288 0.123488 0.208290

Coefficients:
Estimate Std. Error t value Pr(>|t|)
(Intercept) 8.1439 0.5366 15.176 3.13e-08 ***
log(fine_sand) -1.1122 0.1391 -7.998 1.18e-05 ***

Signif. codes: 0 '***' 0.001 '**' 0.01 '*' 0.05 '.' 0.1 ' ' 1

Residual standard error: 0.1694 on 10 degrees of
freedom
Multiple R-squared: 0.8648, Adjusted R-squared:
0.8513

F-statistic: 63.96 on 1 and 10 DF, p-value: 1.18e-05

[[4]]

Call:
lm(formula = substitute(log(Time.corrected.activity) ~
log(i),
list(i = as.name(x))), data = test)

Residuals:
Min 1Q Median 3Q Max
-0.22925 -0.11780 -0.09177 0.13933 0.27972

Coefficients:
Estimate Std. Error t value Pr(>|t|)
(Intercept) 3.0721 0.1313 23.405 4.59e-10 ***
log(organic_matter) 0.7570 0.1124 6.735 5.14e-05 ***

Signif. codes: 0 '***' 0.001 '**' 0.01 '*' 0.05 '.' 0.1 ' ' 1

Residual standard error: 0.1958 on 10 degrees of
freedom
Multiple R-squared: 0.8194, Adjusted R-squared:
0.8013
F-statistic: 45.36 on 1 and 10 DF, p-value: 5.137e-05

Appendix T1.17 Model output for
²⁴¹Am for transect 2 season 4

F-statistic: 109.5 on 1 and 11 DF, p-value: 4.68e-07

[[1]]

Call:
lm(formula = substitute(log(Time.corrected.activity) ~
log(i),
list(i = as.name(x))), data = test)

Residuals:
Min 1Q Median 3Q Max
-0.15033 -0.09939 -0.02233 0.07477 0.29596

Coefficients:
Estimate Std. Error t value Pr(>|t|)
(Intercept) 2.0594 0.1908 10.795 3.42e-07 ***
log(clay) 1.0548 0.1065 9.901 8.16e-07 ***

Signif. codes: 0 '***' 0.001 '**' 0.01 '*' 0.05 '.' 0.1 ' ' 1

Residual standard error: 0.1364 on 11 degrees of
freedom
Multiple R-squared: 0.8991, Adjusted R-squared:
0.8899
F-statistic: 98.03 on 1 and 11 DF, p-value: 8.164e-07

[[2]]

Call:
lm(formula = substitute(log(Time.corrected.activity) ~
log(i),
list(i = as.name(x))), data = test)

Residuals:
Min 1Q Median 3Q Max
-0.269325 -0.142901 -0.004937 0.153745 0.260624

Coefficients:
Estimate Std. Error t value Pr(>|t|)
(Intercept) 0.9328 0.4602 2.027 0.0676 .
log(silt) 0.8396 0.1288 6.516 4.33e-05 ***

Signif. codes: 0 '***' 0.001 '**' 0.01 '*' 0.05 '.' 0.1 ' ' 1

Residual standard error: 0.1948 on 11 degrees of
freedom
Multiple R-squared: 0.7943, Adjusted R-squared:
0.7756
F-statistic: 42.46 on 1 and 11 DF, p-value: 4.329e-05

[[3]]

Call:
lm(formula = substitute(log(Time.corrected.activity) ~
log(i),
list(i = as.name(x))), data = test)

Residuals:
Min 1Q Median 3Q Max
-0.27940 -0.08548 -0.01202 0.10778 0.15008

Coefficients:
Estimate Std. Error t value Pr(>|t|)
(Intercept) 8.8747 0.4756 18.66 1.12e-09 ***
log(fine_sand) -1.2732 0.1216 -10.47 4.68e-07 ***

Signif. codes: 0 '***' 0.001 '**' 0.01 '*' 0.05 '.' 0.1 ' ' 1

Residual standard error: 0.1297 on 11 degrees of
freedom
Multiple R-squared: 0.9087, Adjusted R-squared:
0.9005

[[4]]

Call:
lm(formula = substitute(log(Time.corrected.activity) ~
log(i),
list(i = as.name(x))), data = test)

Residuals:
Min 1Q Median 3Q Max
-0.20101 -0.09273 -0.03160 0.11472 0.19134

Coefficients:
Estimate Std. Error t value Pr(>|t|)
(Intercept) 2.93091 0.09989 29.34 8.49e-12

log(organic_matter) 0.88229 0.08395 10.51 4.49e-
07 ***

Signif. codes: 0 '***' 0.001 '**' 0.01 '*' 0.05 '.' 0.1 ' ' 1

Residual standard error: 0.1293 on 11 degrees of
freedom
Multiple R-squared: 0.9094, Adjusted R-squared:
0.9012
F-statistic: 110.4 on 1 and 11 DF, p-value: 4.491e-07

Appendix T1.18 Model output for ²⁴¹Am for transect 3 season 4

[[1]]

Call:
lm(formula = substitute(log(Time.corrected.activity) ~ log(i), list(i = as.name(x))), data = test)

Residuals:
Min 1Q Median 3Q Max
-0.57268 -0.10747 0.08928 0.15361 0.42883

Coefficients:
Estimate Std. Error t value Pr(>|t|)
(Intercept) 1.9698 0.5962 3.304 0.00917 **
log(clay) 0.9352 0.3421 2.734 0.02308 *

Signif. codes: 0 '***' 0.001 '**' 0.01 '*' 0.05 '.' 0.1 ' ' 1

Residual standard error: 0.3384 on 9 degrees of freedom
Multiple R-squared: 0.4537, Adjusted R-squared: 0.393
F-statistic: 7.474 on 1 and 9 DF, p-value: 0.02308

[[2]]

Call:
lm(formula = substitute(log(Time.corrected.activity) ~ log(i), list(i = as.name(x))), data = test)

Residuals:
Min 1Q Median 3Q Max
-0.47244 -0.12185 0.01739 0.15770 0.45751

Coefficients:
Estimate Std. Error t value Pr(>|t|)
(Intercept) 0.8048 0.8709 0.924 0.3795
log(silt) 0.8267 0.2583 3.201 0.0108 *

Signif. codes: 0 '***' 0.001 '**' 0.01 '*' 0.05 '.' 0.1 ' ' 1

Residual standard error: 0.3131 on 9 degrees of freedom
Multiple R-squared: 0.5323, Adjusted R-squared: 0.4804
F-statistic: 10.24 on 1 and 9 DF, p-value: 0.01082

[[3]]

Call:
lm(formula = substitute(log(Time.corrected.activity) ~ log(i), list(i = as.name(x))), data = test)

Residuals:
Min 1Q Median 3Q Max
-0.4737 -0.2345 0.1036 0.1246 0.4390

Coefficients:
Estimate Std. Error t value Pr(>|t|)
(Intercept) 9.9135 2.1768 4.554 0.00138 **
log(fine_sand) -1.5617 0.5358 -2.915 0.01718 *

Signif. codes: 0 '***' 0.001 '**' 0.01 '*' 0.05 '.' 0.1 ' ' 1

Residual standard error: 0.3283 on 9 degrees of freedom
Multiple R-squared: 0.4856, Adjusted R-squared: 0.4284

F-statistic: 8.495 on 1 and 9 DF, p-value: 0.01718

[[4]]

Call:
lm(formula = substitute(log(Time.corrected.activity) ~ log(i), list(i = as.name(x))), data = test)

Residuals:
Min 1Q Median 3Q Max
-0.50837 -0.08513 -0.04669 0.06937 0.53103

Coefficients:
Estimate Std. Error t value Pr(>|t|)
(Intercept) 2.8129 0.2160 13.021 3.83e-07 ***
log(organic_matter) 1.3133 0.3419 3.841 0.00396 **

Signif. codes: 0 '***' 0.001 '**' 0.01 '*' 0.05 '.' 0.1 ' ' 1

Residual standard error: 0.2818 on 9 degrees of freedom
Multiple R-squared: 0.6211, Adjusted R-squared: 0.5789
F-statistic: 14.75 on 1 and 9 DF, p-value: 0.003963

Appendix T1.19 Model output for
¹³⁷Cs for transect 1 season 1

[[1]]

Call:
lm(formula = substitute(log(Time.corrected.activity) ~
log(i),
list(i = as.name(x))), data = test)

Residuals:
Min 1Q Median 3Q Max
-0.33479 -0.13642 -0.05813 0.09958 0.49092

Coefficients:
Estimate Std. Error t value Pr(>|t|)
(Intercept) 1.9459 0.1909 10.191 5.2e-05 ***
log(clay) 1.1416 0.1597 7.149 0.000378 ***

Signif. codes: 0 '***' 0.001 '**' 0.01 '*' 0.05 '.' 0.1 ' ' 1

Residual standard error: 0.2685 on 6 degrees of
freedom
Multiple R-squared: 0.8949, Adjusted R-squared:
0.8774
F-statistic: 51.1 on 1 and 6 DF, p-value: 0.0003778

[[2]]

Call:
lm(formula = substitute(log(Time.corrected.activity) ~
log(i),
list(i = as.name(x))), data = test)

Residuals:
Min 1Q Median 3Q Max
-0.31467 -0.12713 -0.02507 0.10967 0.38818

Coefficients:
Estimate Std. Error t value Pr(>|t|)
(Intercept) 1.41691 0.21744 6.516 0.000623 ***
log(silt) 0.80394 0.09466 8.493 0.000146 ***

Signif. codes: 0 '***' 0.001 '**' 0.01 '*' 0.05 '.' 0.1 ' ' 1

Residual standard error: 0.2295 on 6 degrees of
freedom
Multiple R-squared: 0.9232, Adjusted R-squared:
0.9104
F-statistic: 72.13 on 1 and 6 DF, p-value: 0.0001458

[[3]]

Call:
lm(formula = substitute(log(Time.corrected.activity) ~
log(i),
list(i = as.name(x))), data = test)

Residuals:
Min 1Q Median 3Q Max
-0.50385 -0.38815 -0.01199 0.44814 0.47400

Coefficients:
Estimate Std. Error t value Pr(>|t|)
(Intercept) 25.389 6.088 4.170 0.00588 **
log(fine_sand) -5.163 1.412 -3.658 0.01061 *

Signif. codes: 0 '***' 0.001 '**' 0.01 '*' 0.05 '.' 0.1 ' ' 1

Residual standard error: 0.4609 on 6 degrees of
freedom
Multiple R-squared: 0.6904, Adjusted R-squared:
0.6388

F-statistic: 13.38 on 1 and 6 DF, p-value: 0.01061

[[4]]

Call:
lm(formula = substitute(log(Time.corrected.activity) ~
log(i),
list(i = as.name(x))), data = test)

Residuals:
Min 1Q Median 3Q Max
-0.88406 -0.20237 -0.02876 0.27396 0.80602

Coefficients:
Estimate Std. Error t value Pr(>|t|)
(Intercept) 3.6700 0.2689 13.65 9.61e-06 ***
log(organic_matter) 0.7997 0.2806 2.85 0.0292
*

Signif. codes: 0 '***' 0.001 '**' 0.01 '*' 0.05 '.' 0.1 ' ' 1

Residual standard error: 0.5399 on 6 degrees of
freedom
Multiple R-squared: 0.5751, Adjusted R-squared:
0.5043
F-statistic: 8.122 on 1 and 6 DF, p-value: 0.02919

Appendix T1.20 Model output for
¹³⁷Cs for transect 2 season 1

F-statistic: 35.97 on 1 and 8 DF, p-value: 0.0003244

[[1]]

Call:
lm(formula = substitute(log(Time.corrected.activity) ~
log(i),
list(i = as.name(x))), data = test)

Residuals:
Min 1Q Median 3Q Max
-0.57905 -0.10494 -0.00405 0.16231 0.50739

Coefficients:
Estimate Std. Error t value Pr(>|t|)
(Intercept) 1.4795 0.4342 3.407 0.009262 **
log(clay) 1.4799 0.2452 6.036 0.000311 ***

Signif. codes: 0 '***' 0.001 '**' 0.01 '*' 0.05 '.' 0.1 ' ' 1

Residual standard error: 0.3181 on 8 degrees of
freedom
Multiple R-squared: 0.82, Adjusted R-squared:
0.7975
F-statistic: 36.44 on 1 and 8 DF, p-value: 0.0003106

[[2]]

Call:
lm(formula = substitute(log(Time.corrected.activity) ~
log(i),
list(i = as.name(x))), data = test)

Residuals:
Min 1Q Median 3Q Max
-0.314183 -0.028766 0.001067 0.045773 0.172354

Coefficients:
Estimate Std. Error t value Pr(>|t|)
(Intercept) 0.38972 0.24991 1.559 0.158
log(silt) 1.16067 0.07842 14.800 4.28e-07 ***

Signif. codes: 0 '***' 0.001 '**' 0.01 '*' 0.05 '.' 0.1 ' ' 1

Residual standard error: 0.1407 on 8 degrees of
freedom
Multiple R-squared: 0.9648, Adjusted R-squared:
0.9604
F-statistic: 219 on 1 and 8 DF, p-value: 4.276e-07

[[3]]

Call:
lm(formula = substitute(log(Time.corrected.activity) ~
log(i),
list(i = as.name(x))), data = test)

Residuals:
Min 1Q Median 3Q Max
-0.61019 -0.15161 0.00192 0.16833 0.49959

Coefficients:
Estimate Std. Error t value Pr(>|t|)
(Intercept) 20.0139 2.6672 7.504 6.9e-05 ***
log(fine_sand) -3.8880 0.6483 -5.997 0.000324 ***

Signif. codes: 0 '***' 0.001 '**' 0.01 '*' 0.05 '.' 0.1 ' ' 1

Residual standard error: 0.3198 on 8 degrees of
freedom
Multiple R-squared: 0.818, Adjusted R-squared:
0.7953

[[4]]

Call:
lm(formula = substitute(log(Time.corrected.activity) ~
log(i),
list(i = as.name(x))), data = test)

Residuals:
Min 1Q Median 3Q Max
-0.23598 -0.10128 -0.03086 0.07322 0.35075

Coefficients:
Estimate Std. Error t value Pr(>|t|)
(Intercept) 3.99488 0.05695 70.14 1.90e-12

log(organic_matter) 1.49167 0.13031 11.45 3.07e-
06 ***

Signif. codes: 0 '***' 0.001 '**' 0.01 '*' 0.05 '.' 0.1 ' ' 1

Residual standard error: 0.1799 on 8 degrees of
freedom
Multiple R-squared: 0.9425, Adjusted R-squared:
0.9353
F-statistic: 131 on 1 and 8 DF, p-value: 3.069e-06

Appendix T1.21 Model output for
¹³⁷Cs for transect 3 season 1

[[1]]

Call:
lm(formula = substitute(log(Time.corrected.activity) ~ log(i),
list(i = as.name(x))), data = test)

Residuals:
Min 1Q Median 3Q Max
-0.5881 -0.4976 0.1799 0.3164 0.6821

Coefficients:
Estimate Std. Error t value Pr(>|t|)
(Intercept) 2.5277 0.3333 7.584 3.38e-05 ***
log(clay) 0.7147 0.3268 2.187 0.0565 .

Signif. codes: 0 '***' 0.001 '**' 0.01 '*' 0.05 '.' 0.1 ' ' 1

Residual standard error: 0.4998 on 9 degrees of freedom
Multiple R-squared: 0.3471, Adjusted R-squared: 0.2745
F-statistic: 4.784 on 1 and 9 DF, p-value: 0.05651

[[2]]

Call:
lm(formula = substitute(log(Time.corrected.activity) ~ log(i),
list(i = as.name(x))), data = test)

Residuals:
Min 1Q Median 3Q Max
-0.30003 -0.16686 -0.03560 0.07629 0.60651

Coefficients:
Estimate Std. Error t value Pr(>|t|)
(Intercept) 0.7828 0.4004 1.955 0.082322 .
log(silt) 0.9633 0.1576 6.111 0.000177 ***

Signif. codes: 0 '***' 0.001 '**' 0.01 '*' 0.05 '.' 0.1 ' ' 1

Residual standard error: 0.2726 on 9 degrees of freedom
Multiple R-squared: 0.8058, Adjusted R-squared: 0.7842
F-statistic: 37.35 on 1 and 9 DF, p-value: 0.0001768

[[3]]

Call:
lm(formula = substitute(log(Time.corrected.activity) ~ log(i),
list(i = as.name(x))), data = test)

Residuals:
Min 1Q Median 3Q Max
-0.7188 -0.5610 0.2462 0.4401 0.9396

Coefficients:
Estimate Std. Error t value Pr(>|t|)
(Intercept) 3.168679 4.380217 0.723 0.488
log(fine_sand) 0.002211 1.047348 0.002 0.998

Residual standard error: 0.6185 on 9 degrees of freedom
Multiple R-squared: 4.953e-07, Adjusted R-squared: -0.1111
F-statistic: 4.458e-06 on 1 and 9 DF, p-value: 0.9984

[[4]]

Call:
lm(formula = substitute(log(Time.corrected.activity) ~ log(i),
list(i = as.name(x))), data = test)

Residuals:
Min 1Q Median 3Q Max
-0.44093 -0.32890 -0.03683 0.20104 0.99735

Coefficients:
Estimate Std. Error t value Pr(>|t|)
(Intercept) 3.7923 0.2685 14.126 1.9e-07 ***
log(organic_matter) 0.6948 0.2596 2.676 0.0254 *

Signif. codes: 0 '***' 0.001 '**' 0.01 '*' 0.05 '.' 0.1 ' ' 1

Residual standard error: 0.4616 on 9 degrees of freedom
Multiple R-squared: 0.4432, Adjusted R-squared: 0.3813
F-statistic: 7.163 on 1 and 9 DF, p-value: 0.02536

Appendix T1.22 Model output for ¹³⁷Cs for transect 1 season 2

[[1]]

Call:
lm(formula = substitute(log(Time.corrected.activity) ~ log(i),
list(i = as.name(x))), data = test)

Residuals:
Min 1Q Median 3Q Max
-0.41997 -0.08577 0.00614 0.16113 0.24158

Coefficients:
Estimate Std. Error t value Pr(>|t|)
(Intercept) 2.0800 0.2124 9.792 4.26e-06 ***
log(clay) 0.7780 0.1443 5.392 0.000438 ***

Signif. codes: 0 '***' 0.001 '**' 0.01 '*' 0.05 '.' 0.1 ' ' 1

Residual standard error: 0.2033 on 9 degrees of freedom
Multiple R-squared: 0.7636, Adjusted R-squared: 0.7373
F-statistic: 29.07 on 1 and 9 DF, p-value: 0.0004378

[[2]]

Call:
lm(formula = substitute(log(Time.corrected.activity) ~ log(i),
list(i = as.name(x))), data = test)

Residuals:
Min 1Q Median 3Q Max
-0.31223 -0.06818 0.01101 0.09993 0.24766

Coefficients:
Estimate Std. Error t value Pr(>|t|)
(Intercept) 1.79933 0.20357 8.839 9.90e-06 ***
log(silt) 0.56664 0.08121 6.977 6.49e-05 ***

Signif. codes: 0 '***' 0.001 '**' 0.01 '*' 0.05 '.' 0.1 ' ' 1

Residual standard error: 0.1652 on 9 degrees of freedom
Multiple R-squared: 0.844, Adjusted R-squared: 0.8266
F-statistic: 48.68 on 1 and 9 DF, p-value: 6.486e-05

[[3]]

Call:
lm(formula = substitute(log(Time.corrected.activity) ~ log(i),
list(i = as.name(x))), data = test)

Residuals:
Min 1Q Median 3Q Max
-0.6106 -0.1462 0.0129 0.1649 0.4811

Coefficients:
Estimate Std. Error t value Pr(>|t|)
(Intercept) 11.095 3.863 2.872 0.0184 *
log(fine_sand) -1.854 0.904 -2.051 0.0706 .

Signif. codes: 0 '***' 0.001 '**' 0.01 '*' 0.05 '.' 0.1 ' ' 1

Residual standard error: 0.3453 on 9 degrees of freedom
Multiple R-squared: 0.3184, Adjusted R-squared: 0.2427

F-statistic: 4.205 on 1 and 9 DF, p-value: 0.07056

[[4]]

Call:
lm(formula = substitute(log(Time.corrected.activity) ~ log(i),
list(i = as.name(x))), data = test)

Residuals:
Min 1Q Median 3Q Max
-0.12192 -0.04741 -0.01824 0.03358 0.16284

Coefficients:
Estimate Std. Error t value Pr(>|t|)
(Intercept) 2.81630 0.03411 82.57 2.84e-14 ***
log(organic_matter) 1.12031 0.07389 15.16 1.03e-07 ***

Signif. codes: 0 '***' 0.001 '**' 0.01 '*' 0.05 '.' 0.1 ' ' 1

Residual standard error: 0.08117 on 9 degrees of freedom
Multiple R-squared: 0.9623, Adjusted R-squared: 0.9581
F-statistic: 229.9 on 1 and 9 DF, p-value: 1.027e-07

Appendix T1.23 Model output for
¹³⁷Cs for transect 2 season 2

F-statistic: 32.32 on 1 and 10 DF, p-value: 0.0002023

[[1]]

Call:
lm(formula = substitute(log(Time.corrected.activity) ~
log(i),
list(i = as.name(x))), data = test)

Residuals:
Min 1Q Median 3Q Max
-0.30823 -0.14458 -0.01982 0.05770 0.46083

Coefficients:
Estimate Std. Error t value Pr(>|t|)
(Intercept) 1.5033 0.4736 3.174 0.00992 **
log(clay) 1.2883 0.2538 5.077 0.00048 ***

Signif. codes: 0 '***' 0.001 '**' 0.01 '*' 0.05 '.' 0.1 ' ' 1

Residual standard error: 0.2452 on 10 degrees of
freedom
Multiple R-squared: 0.7205, Adjusted R-squared:
0.6925
F-statistic: 25.77 on 1 and 10 DF, p-value: 0.0004801

[[2]]

Call:
lm(formula = substitute(log(Time.corrected.activity) ~
log(i),
list(i = as.name(x))), data = test)

Residuals:
Min 1Q Median 3Q Max
-0.42252 -0.08296 0.02228 0.10780 0.19896

Coefficients:
Estimate Std. Error t value Pr(>|t|)
(Intercept) 0.7200 0.4220 1.706 0.119
log(silt) 0.9540 0.1264 7.546 1.96e-05 ***

Signif. codes: 0 '***' 0.001 '**' 0.01 '*' 0.05 '.' 0.1 ' ' 1

Residual standard error: 0.1792 on 10 degrees of
freedom
Multiple R-squared: 0.8506, Adjusted R-squared:
0.8357
F-statistic: 56.94 on 1 and 10 DF, p-value: 1.957e-05

[[3]]

Call:
lm(formula = substitute(log(Time.corrected.activity) ~
log(i),
list(i = as.name(x))), data = test)

Residuals:
Min 1Q Median 3Q Max
-0.24862 -0.19628 -0.07878 0.21670 0.29032

Coefficients:
Estimate Std. Error t value Pr(>|t|)
(Intercept) 10.5441 1.1738 8.983 4.21e-06 ***
log(fine_sand) -1.6336 0.2873 -5.685 0.000202 ***

Signif. codes: 0 '***' 0.001 '**' 0.01 '*' 0.05 '.' 0.1 ' ' 1

Residual standard error: 0.2254 on 10 degrees of
freedom
Multiple R-squared: 0.7637, Adjusted R-squared:
0.7401

[[4]]

Call:
lm(formula = substitute(log(Time.corrected.activity) ~
log(i),
list(i = as.name(x))), data = test)

Residuals:
Min 1Q Median 3Q Max
-0.16426 -0.12863 -0.01451 0.03869 0.42084

Coefficients:
Estimate Std. Error t value Pr(>|t|)
(Intercept) 2.8693 0.1362 21.07 1.29e-09 ***
log(organic_matter) 1.1261 0.1413 7.97 1.22e-05 ***

Signif. codes: 0 '***' 0.001 '**' 0.01 '*' 0.05 '.' 0.1 ' ' 1

Residual standard error: 0.171 on 10 degrees of
freedom
Multiple R-squared: 0.864, Adjusted R-squared:
0.8504
F-statistic: 63.52 on 1 and 10 DF, p-value: 1.217e-05

Appendix T1.24 Model output for ¹³⁷Cs for transect 3 season 2

[[1]]

Call:
lm(formula = substitute(log(Time.corrected.activity) ~ log(i),
list(i = as.name(x))), data = test)

Residuals:
Min 1Q Median 3Q Max
-0.36821 -0.17211 -0.07215 0.15475 0.60148

Coefficients:
Estimate Std. Error t value Pr(>|t|)
(Intercept) 1.7106 0.1763 9.703 4.60e-06 ***
log(clay) 1.2708 0.1342 9.469 5.62e-06 ***

Signif. codes: 0 '***' 0.001 '**' 0.01 '*' 0.05 '.' 0.1 ' ' 1

Residual standard error: 0.287 on 9 degrees of freedom
Multiple R-squared: 0.9088, Adjusted R-squared: 0.8986
F-statistic: 89.67 on 1 and 9 DF, p-value: 5.623e-06

[[2]]

Call:
lm(formula = substitute(log(Time.corrected.activity) ~ log(i),
list(i = as.name(x))), data = test)

Residuals:
Min 1Q Median 3Q Max
-0.28444 -0.12532 -0.07701 0.12880 0.33005

Coefficients:
Estimate Std. Error t value Pr(>|t|)
(Intercept) 1.35052 0.14870 9.082 7.93e-06 ***
log(silt) 0.80707 0.06004 13.443 2.91e-07 ***

Signif. codes: 0 '***' 0.001 '**' 0.01 '*' 0.05 '.' 0.1 ' ' 1

Residual standard error: 0.207 on 9 degrees of freedom
Multiple R-squared: 0.9526, Adjusted R-squared: 0.9473
F-statistic: 180.7 on 1 and 9 DF, p-value: 2.911e-07

[[3]]

Call:
lm(formula = substitute(log(Time.corrected.activity) ~ log(i),
list(i = as.name(x))), data = test)

Residuals:
Min 1Q Median 3Q Max
-0.70201 -0.63234 -0.00081 0.54497 0.67025

Coefficients:
Estimate Std. Error t value Pr(>|t|)
(Intercept) 8.5217 1.5082 5.650 0.000313 ***
log(fine_sand) -1.2984 0.3628 -3.579 0.005944 **

Signif. codes: 0 '***' 0.001 '**' 0.01 '*' 0.05 '.' 0.1 ' ' 1

Residual standard error: 0.6105 on 9 degrees of freedom
Multiple R-squared: 0.5873, Adjusted R-squared: 0.5414

F-statistic: 12.81 on 1 and 9 DF, p-value: 0.005944

[[4]]

Call:
lm(formula = substitute(log(Time.corrected.activity) ~ log(i),
list(i = as.name(x))), data = test)

Residuals:
Min 1Q Median 3Q Max
-0.24640 -0.12097 -0.02431 0.05134 0.36026

Coefficients:
Estimate Std. Error t value Pr(>|t|)
(Intercept) 2.73832 0.06574 41.66 1.32e-11 ***
log(organic_matter) 1.16078 0.08089 14.35 1.66e-07 ***

Signif. codes: 0 '***' 0.001 '**' 0.01 '*' 0.05 '.' 0.1 ' ' 1

Residual standard error: 0.1945 on 9 degrees of freedom
Multiple R-squared: 0.9581, Adjusted R-squared: 0.9535
F-statistic: 205.9 on 1 and 9 DF, p-value: 1.656e-07

Appendix T1.25 Model output for
¹³⁷Cs for transect 1 season 3

[[1]]

Call:
lm(formula = substitute(log(Time.corrected.activity) ~
log(i),
list(i = as.name(x))), data = test)

Residuals:
Min 1Q Median 3Q Max
-0.61800 -0.05557 0.05485 0.15307 0.25958

Coefficients:
Estimate Std. Error t value Pr(>|t|)
(Intercept) 0.5683 0.5141 1.105 0.295
log(clay) 1.6911 0.2567 6.588 6.17e-05 ***

Signif. codes: 0 '***' 0.001 '**' 0.01 '*' 0.05 '.' 0.1 ' ' 1

Residual standard error: 0.25 on 10 degrees of
freedom
Multiple R-squared: 0.8127, Adjusted R-squared:
0.794
F-statistic: 43.4 on 1 and 10 DF, p-value: 6.172e-05

[[2]]

Call:
lm(formula = substitute(log(Time.corrected.activity) ~
log(i),
list(i = as.name(x))), data = test)

Residuals:
Min 1Q Median 3Q Max
-0.66353 -0.05147 0.02589 0.17848 0.24404

Coefficients:
Estimate Std. Error t value Pr(>|t|)
(Intercept) -0.8185 0.7590 -1.078 0.306
log(silt) 1.3694 0.2182 6.276 9.19e-05 ***

Signif. codes: 0 '***' 0.001 '**' 0.01 '*' 0.05 '.' 0.1 ' ' 1

Residual standard error: 0.26 on 10 degrees of
freedom
Multiple R-squared: 0.7975, Adjusted R-squared:
0.7773
F-statistic: 39.39 on 1 and 10 DF, p-value: 9.188e-05

[[3]]

Call:
lm(formula = substitute(log(Time.corrected.activity) ~
log(i),
list(i = as.name(x))), data = test)

Residuals:
Min 1Q Median 3Q Max
-0.66698 -0.05785 0.08024 0.15304 0.23676

Coefficients:
Estimate Std. Error t value Pr(>|t|)
(Intercept) 10.4142 1.0425 9.990 1.60e-06 ***
log(fine_sand) -1.6273 0.2606 -6.245 9.57e-05 ***

Signif. codes: 0 '***' 0.001 '**' 0.01 '*' 0.05 '.' 0.1 ' ' 1

Residual standard error: 0.261 on 10 degrees of
freedom
Multiple R-squared: 0.7959, Adjusted R-squared:
0.7755

F-statistic: 39 on 1 and 10 DF, p-value: 9.572e-05

[[4]]

Call:
lm(formula = substitute(log(Time.corrected.activity) ~
log(i),
list(i = as.name(x))), data = test)

Residuals:
Min 1Q Median 3Q Max
-0.55975 -0.07509 -0.04177 0.10927 0.45375

Coefficients:
Estimate Std. Error t value Pr(>|t|)
(Intercept) 2.4239 0.2481 9.772 1.96e-06 ***
log(organic_matter) 1.2881 0.2035 6.330 8.57e-05 ***

Signif. codes: 0 '***' 0.001 '**' 0.01 '*' 0.05 '.' 0.1 ' ' 1

Residual standard error: 0.2582 on 10 degrees of
freedom
Multiple R-squared: 0.8003, Adjusted R-squared:
0.7803
F-statistic: 40.07 on 1 and 10 DF, p-value: 8.573e-05

Appendix T1.26 Model output for
¹³⁷Cs for transect 2 season 3

F-statistic: 258.5 on 1 and 10 DF, p-value: 1.792e-08

[[1]]

Call:
lm(formula = substitute(log(Time.corrected.activity) ~
log(i),
list(i = as.name(x))), data = test)

Residuals:
Min 1Q Median 3Q Max
-0.26039 -0.12238 -0.03128 0.12846 0.30398

Coefficients:
Estimate Std. Error t value Pr(>|t|)
(Intercept) 0.08414 0.39592 0.213 0.836
log(clay) 1.94474 0.18971 10.251 1.27e-06 ***

Signif. codes: 0 '***' 0.001 '**' 0.01 '*' 0.05 '.' 0.1 ' ' 1

Residual standard error: 0.1896 on 10 degrees of
freedom
Multiple R-squared: 0.9131, Adjusted R-squared:
0.9044
F-statistic: 105.1 on 1 and 10 DF, p-value: 1.266e-06

[[2]]

Call:
lm(formula = substitute(log(Time.corrected.activity) ~
log(i),
list(i = as.name(x))), data = test)

Residuals:
Min 1Q Median 3Q Max
-0.23899 -0.13059 -0.02981 0.09635 0.29199

Coefficients:
Estimate Std. Error t value Pr(>|t|)
(Intercept) -0.7763 0.4164 -1.864 0.0919 .
log(silt) 1.3847 0.1174 11.797 3.43e-07 ***

Signif. codes: 0 '***' 0.001 '**' 0.01 '*' 0.05 '.' 0.1 ' ' 1

Residual standard error: 0.1666 on 10 degrees of
freedom
Multiple R-squared: 0.933, Adjusted R-squared:
0.9263
F-statistic: 139.2 on 1 and 10 DF, p-value: 3.428e-07

[[3]]

Call:
lm(formula = substitute(log(Time.corrected.activity) ~
log(i),
list(i = as.name(x))), data = test)

Residuals:
Min 1Q Median 3Q Max
-0.21744 -0.08116 0.04599 0.07237 0.16872

Coefficients:
Estimate Std. Error t value Pr(>|t|)
(Intercept) 12.2056 0.5052 24.16 3.36e-10 ***
log(fine_sand) -2.0642 0.1284 -16.08 1.79e-08 ***

Signif. codes: 0 '***' 0.001 '**' 0.01 '*' 0.05 '.' 0.1 ' ' 1

Residual standard error: 0.1242 on 10 degrees of
freedom
Multiple R-squared: 0.9628, Adjusted R-squared:
0.959

[[4]]

Call:
lm(formula = substitute(log(Time.corrected.activity) ~
log(i),
list(i = as.name(x))), data = test)

Residuals:
Min 1Q Median 3Q Max
-0.11166 -0.05278 0.00121 0.03716 0.12885

Coefficients:
Estimate Std. Error t value Pr(>|t|)
(Intercept) 1.72123 0.10082 17.07 1.00e-08

log(organic_matter) 1.52277 0.06259 24.33 3.14e-
10 ***

Signif. codes: 0 '***' 0.001 '**' 0.01 '*' 0.05 '.' 0.1 ' ' 1

Residual standard error: 0.08293 on 10 degrees of
freedom
Multiple R-squared: 0.9834, Adjusted R-squared:
0.9817
F-statistic: 591.9 on 1 and 10 DF, p-value: 3.138e-10

Appendix T1.27 Model output for ¹³⁷Cs for transect 3 season 3

[[1]]

Call:
lm(formula = substitute(log(Time.corrected.activity) ~ log(i),
list(i = as.name(x))), data = test)

Residuals:
Min 1Q Median 3Q Max
-0.97959 -0.05117 0.00150 0.06010 1.65394

Coefficients:
Estimate Std. Error t value Pr(>|t|)
(Intercept) 4.9149 3.2529 1.511 0.165
log(clay) -0.4012 1.6110 -0.249 0.809

Residual standard error: 0.6983 on 9 degrees of freedom
Multiple R-squared: 0.006843, Adjusted R-squared: -0.1035
F-statistic: 0.06202 on 1 and 9 DF, p-value: 0.8089

[[2]]

Call:
lm(formula = substitute(log(Time.corrected.activity) ~ log(i),
list(i = as.name(x))), data = test)

Residuals:
Min 1Q Median 3Q Max
-0.92688 -0.22977 -0.10076 0.00554 1.56751

Coefficients:
Estimate Std. Error t value Pr(>|t|)
(Intercept) 1.5557 2.7892 0.558 0.591
log(silt) 0.6911 0.7537 0.917 0.383

Residual standard error: 0.6701 on 9 degrees of freedom
Multiple R-squared: 0.08544, Adjusted R-squared: -0.01617
F-statistic: 0.8408 on 1 and 9 DF, p-value: 0.3831

[[3]]

Call:
lm(formula = substitute(log(Time.corrected.activity) ~ log(i),
list(i = as.name(x))), data = test)

Residuals:
Min 1Q Median 3Q Max
-0.6874 -0.2653 -0.1701 0.1389 1.5228

Coefficients:
Estimate Std. Error t value Pr(>|t|)
(Intercept) 11.429 4.413 2.590 0.0292 *
log(fine_sand) -1.924 1.159 -1.661 0.1312

Signif. codes: 0 '***' 0.001 '**' 0.01 '*' 0.05 '.' 0.1 ' ' 1

Residual standard error: 0.6131 on 9 degrees of freedom
Multiple R-squared: 0.2345, Adjusted R-squared: 0.1495
F-statistic: 2.757 on 1 and 9 DF, p-value: 0.1312

[[4]]

Call:
lm(formula = substitute(log(Time.corrected.activity) ~ log(i),
list(i = as.name(x))), data = test)

Residuals:
Min 1Q Median 3Q Max
-0.4721 -0.3045 -0.1605 0.1724 1.2120

Coefficients:
Estimate Std. Error t value Pr(>|t|)
(Intercept) 2.1513 0.6959 3.092 0.0129 *
log(organic_matter) 1.5317 0.5319 2.880 0.0182 *

Signif. codes: 0 '***' 0.001 '**' 0.01 '*' 0.05 '.' 0.1 ' ' 1

Residual standard error: 0.5055 on 9 degrees of freedom
Multiple R-squared: 0.4796, Adjusted R-squared: 0.4217
F-statistic: 8.293 on 1 and 9 DF, p-value: 0.01818

Appendix T1.28 Model output for
¹³⁷Cs for transect 1 season 4

[[1]]

Call:
lm(formula = substitute(log(Time.corrected.activity) ~
log(i),
list(i = as.name(x))), data = test)

Residuals:
Min 1Q Median 3Q Max
-0.20650 -0.06206 -0.03350 0.08599 0.21115

Coefficients:
Estimate Std. Error t value Pr(>|t|)
(Intercept) 1.3428 0.2190 6.131 0.000111 ***
log(clay) 1.3920 0.1154 12.066 2.77e-07 ***

Signif. codes: 0 '***' 0.001 '**' 0.01 '*' 0.05 '.' 0.1 ' ' 1

Residual standard error: 0.1323 on 10 degrees of
freedom
Multiple R-squared: 0.9357, Adjusted R-squared:
0.9293
F-statistic: 145.6 on 1 and 10 DF, p-value: 2.775e-07

[[2]]

Call:
lm(formula = substitute(log(Time.corrected.activity) ~
log(i),
list(i = as.name(x))), data = test)

Residuals:
Min 1Q Median 3Q Max
-0.33577 -0.09842 -0.04147 0.10686 0.45221

Coefficients:
Estimate Std. Error t value Pr(>|t|)
(Intercept) 0.1564 0.6070 0.258 0.802
log(silt) 1.0453 0.1665 6.280 9.14e-05 ***

Signif. codes: 0 '***' 0.001 '**' 0.01 '*' 0.05 '.' 0.1 ' ' 1

Residual standard error: 0.2348 on 10 degrees of
freedom
Multiple R-squared: 0.7977, Adjusted R-squared:
0.7775
F-statistic: 39.44 on 1 and 10 DF, p-value: 9.14e-05

[[3]]

Call:
lm(formula = substitute(log(Time.corrected.activity) ~
log(i),
list(i = as.name(x))), data = test)

Residuals:
Min 1Q Median 3Q Max
-0.218063 -0.113141 0.007322 0.111819 0.219973

Coefficients:
Estimate Std. Error t value Pr(>|t|)
(Intercept) 8.9038 0.5050 17.631 7.33e-09 ***
log(fine_sand) -1.2905 0.1309 -9.861 1.81e-06 ***

Signif. codes: 0 '***' 0.001 '**' 0.01 '*' 0.05 '.' 0.1 ' ' 1

Residual standard error: 0.1594 on 10 degrees of
freedom
Multiple R-squared: 0.9067, Adjusted R-squared:
0.8974

F-statistic: 97.23 on 1 and 10 DF, p-value: 1.807e-06

[[4]]

Call:
lm(formula = substitute(log(Time.corrected.activity) ~
log(i),
list(i = as.name(x))), data = test)

Residuals:
Min 1Q Median 3Q Max
-0.18405 -0.11706 -0.04982 0.09749 0.26476

Coefficients:
Estimate Std. Error t value Pr(>|t|)
(Intercept) 2.99137 0.10426 28.69 6.16e-11 ***
log(organic_matter) 0.90459 0.08928 10.13 1.41e-06 ***

Signif. codes: 0 '***' 0.001 '**' 0.01 '*' 0.05 '.' 0.1 ' ' 1

Residual standard error: 0.1555 on 10 degrees of
freedom
Multiple R-squared: 0.9112, Adjusted R-squared:
0.9024
F-statistic: 102.7 on 1 and 10 DF, p-value: 1.409e-06

Appendix T1.29 Model output for
¹³⁷Cs for transect 2 season 4

[[1]]

Call:
lm(formula = substitute(log(Time.corrected.activity) ~
log(i),
list(i = as.name(x))), data = test)

Residuals:
Min 1Q Median 3Q Max
-0.18887 -0.10256 -0.03195 0.06684 0.33125

Coefficients:
Estimate Std. Error t value Pr(>|t|)
(Intercept) 1.5938 0.2257 7.06 2.10e-05 ***
log(clay) 1.3567 0.1261 10.76 3.53e-07 ***

Signif. codes: 0 '***' 0.001 '**' 0.01 '*' 0.05 '.' 0.1 ' ' 1

Residual standard error: 0.1614 on 11 degrees of
freedom
Multiple R-squared: 0.9133, Adjusted R-squared:
0.9054
F-statistic: 115.8 on 1 and 11 DF, p-value: 3.532e-07

[[2]]

Call:
lm(formula = substitute(log(Time.corrected.activity) ~
log(i),
list(i = as.name(x))), data = test)

Residuals:
Min 1Q Median 3Q Max
-0.32888 -0.16663 -0.03868 0.11641 0.45921

Coefficients:
Estimate Std. Error t value Pr(>|t|)
(Intercept) 0.1061 0.5446 0.195 0.849
log(silt) 1.0908 0.1525 7.154 1.86e-05 ***

Signif. codes: 0 '***' 0.001 '**' 0.01 '*' 0.05 '.' 0.1 ' ' 1

Residual standard error: 0.2305 on 11 degrees of
freedom
Multiple R-squared: 0.8231, Adjusted R-squared:
0.807
F-statistic: 51.18 on 1 and 11 DF, p-value: 1.86e-05

[[3]]

Call:
lm(formula = substitute(log(Time.corrected.activity) ~
log(i),
list(i = as.name(x))), data = test)

Residuals:
Min 1Q Median 3Q Max
-0.33466 -0.04282 -0.00826 0.04912 0.32387

Coefficients:
Estimate Std. Error t value Pr(>|t|)
(Intercept) 10.3421 0.5758 17.96 1.69e-09 ***
log(fine_sand) -1.6331 0.1473 -11.09 2.61e-07 ***

Signif. codes: 0 '***' 0.001 '**' 0.01 '*' 0.05 '.' 0.1 ' ' 1

Residual standard error: 0.1571 on 11 degrees of
freedom
Multiple R-squared: 0.9179, Adjusted R-squared:
0.9104

F-statistic: 123 on 1 and 11 DF, p-value: 2.606e-07

[[4]]

Call:
lm(formula = substitute(log(Time.corrected.activity) ~
log(i),
list(i = as.name(x))), data = test)

Residuals:
Min 1Q Median 3Q Max
-0.23420 -0.11781 -0.00028 0.08955 0.34391

Coefficients:
Estimate Std. Error t value Pr(>|t|)
(Intercept) 2.7181 0.1207 22.53 1.49e-10 ***
log(organic_matter) 1.1319 0.1014 11.16 2.44e-07 ***

Signif. codes: 0 '***' 0.001 '**' 0.01 '*' 0.05 '.' 0.1 ' ' 1

Residual standard error: 0.1561 on 11 degrees of
freedom
Multiple R-squared: 0.9189, Adjusted R-squared:
0.9115
F-statistic: 124.6 on 1 and 11 DF, p-value: 2.44e-07

Appendix T1.30 Model output for ¹³⁷Cs for transect 3 season 4

[[1]]

Call:
lm(formula = substitute(log(Time.corrected.activity) ~ log(i),
list(i = as.name(x))), data = test)

Residuals:
Min 1Q Median 3Q Max
-0.66062 -0.08105 0.04443 0.21510 0.51996

Coefficients:
Estimate Std. Error t value Pr(>|t|)
(Intercept) 1.6451 0.7026 2.342 0.0439 *
log(clay) 1.1753 0.4031 2.916 0.0171 *

Signif. codes: 0 '***' 0.001 '**' 0.01 '*' 0.05 '.' 0.1 ' ' 1

Residual standard error: 0.3987 on 9 degrees of freedom
Multiple R-squared: 0.4858, Adjusted R-squared: 0.4286
F-statistic: 8.502 on 1 and 9 DF, p-value: 0.01715

[[2]]

Call:
lm(formula = substitute(log(Time.corrected.activity) ~ log(i),
list(i = as.name(x))), data = test)

Residuals:
Min 1Q Median 3Q Max
-0.58217 -0.15271 0.00503 0.17960 0.55523

Coefficients:
Estimate Std. Error t value Pr(>|t|)
(Intercept) 0.2233 1.0304 0.217 0.83325
log(silt) 1.0263 0.3056 3.358 0.00841 **

Signif. codes: 0 '***' 0.001 '**' 0.01 '*' 0.05 '.' 0.1 ' ' 1

Residual standard error: 0.3704 on 9 degrees of freedom
Multiple R-squared: 0.5562, Adjusted R-squared: 0.5069
F-statistic: 11.28 on 1 and 9 DF, p-value: 0.008412

[[3]]

Call:
lm(formula = substitute(log(Time.corrected.activity) ~ log(i),
list(i = as.name(x))), data = test)

Residuals:
Min 1Q Median 3Q Max
-0.59164 -0.24510 0.07829 0.15866 0.57384

Coefficients:
Estimate Std. Error t value Pr(>|t|)
(Intercept) 11.7652 2.5057 4.695 0.00113 **
log(fine_sand) -1.9963 0.6168 -3.237 0.01021 *

Signif. codes: 0 '***' 0.001 '**' 0.01 '*' 0.05 '.' 0.1 ' ' 1

Residual standard error: 0.378 on 9 degrees of freedom
Multiple R-squared: 0.5379, Adjusted R-squared: 0.4866

F-statistic: 10.48 on 1 and 9 DF, p-value: 0.01021

[[4]]

Call:
lm(formula = substitute(log(Time.corrected.activity) ~ log(i),
list(i = as.name(x))), data = test)

Residuals:
Min 1Q Median 3Q Max
-0.54331 -0.13257 -0.06955 0.01986 0.73647

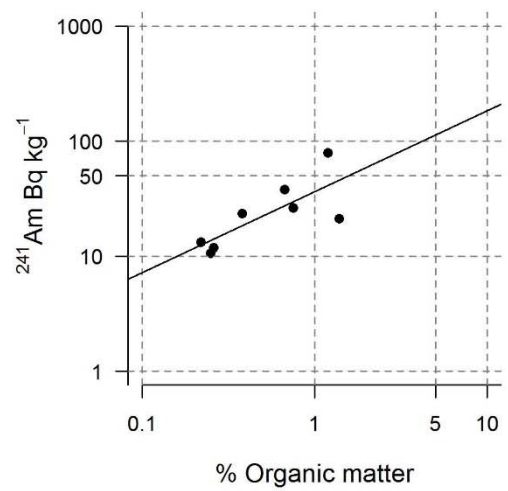
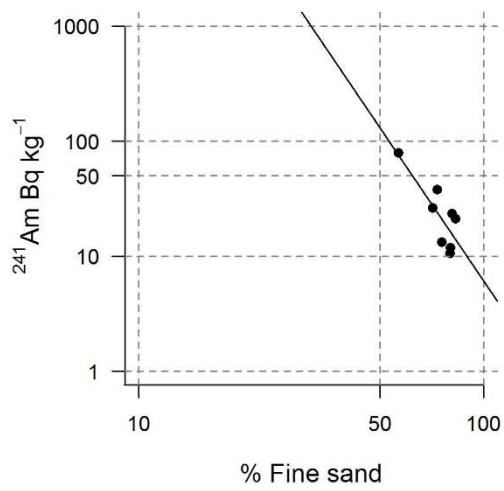
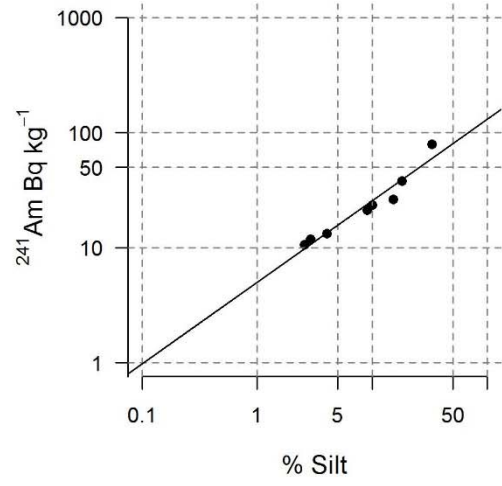
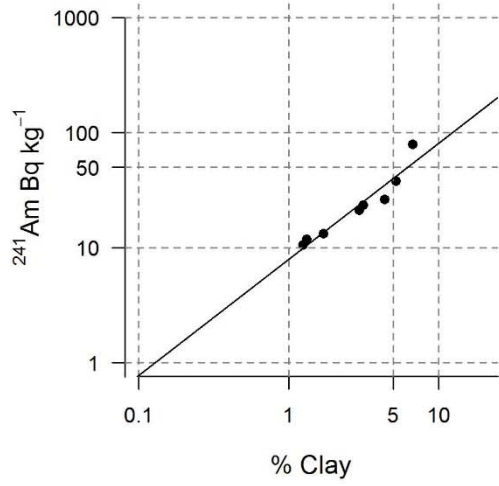
Coefficients:
Estimate Std. Error t value Pr(>|t|)
(Intercept) 2.7454 0.2663 10.31 2.77e-06 ***
log(organic_matter) 1.5804 0.4215 3.75 0.00458 **

Signif. codes: 0 '***' 0.001 '**' 0.01 '*' 0.05 '.' 0.1 ' ' 1

Residual standard error: 0.3474 on 9 degrees of freedom
Multiple R-squared: 0.6097, Adjusted R-squared: 0.5663
F-statistic: 14.06 on 1 and 9 DF, p-value: 0.004558

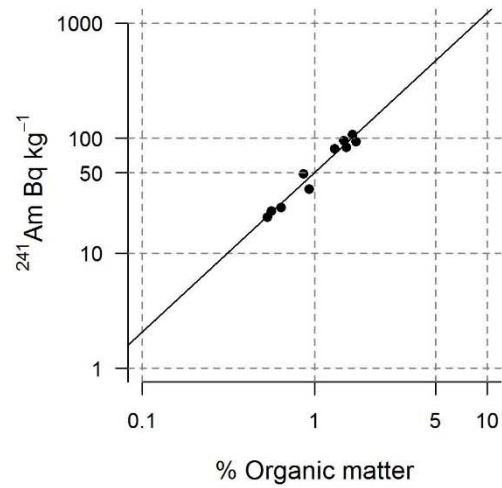
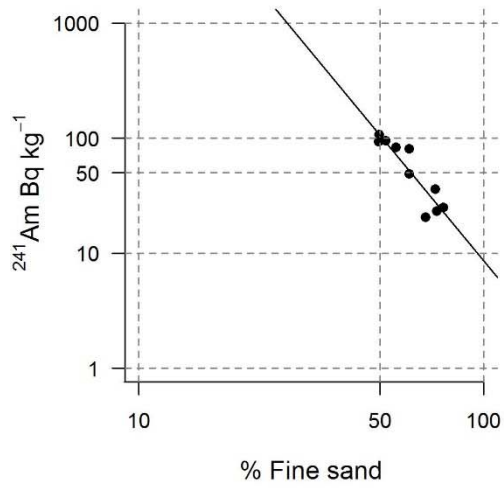
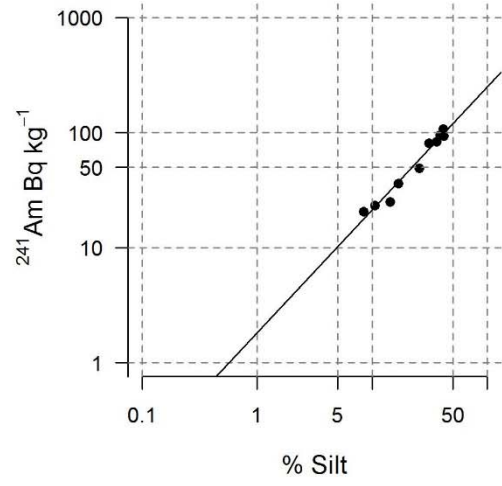
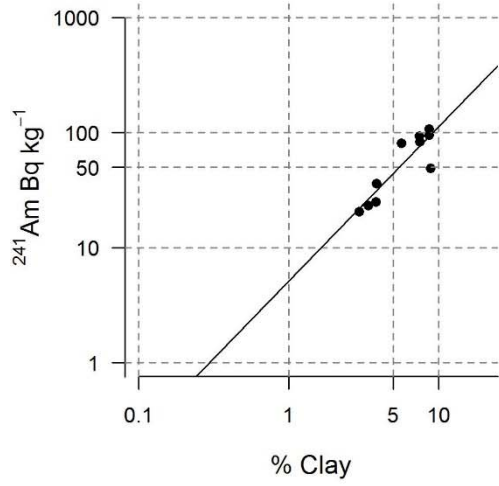
Appendix F1.1

Clay, silt, sand and organic matter regression models for ^{241}Am for transect 1 season 1



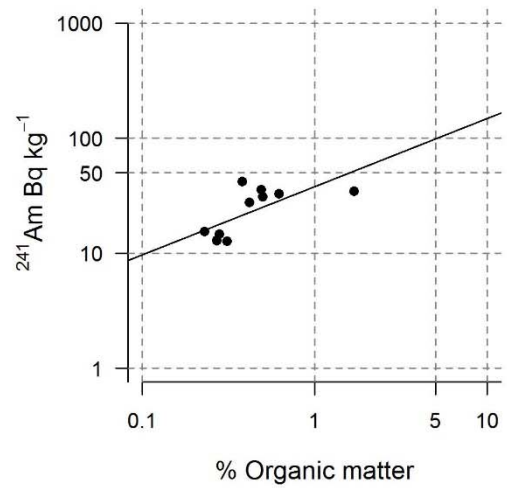
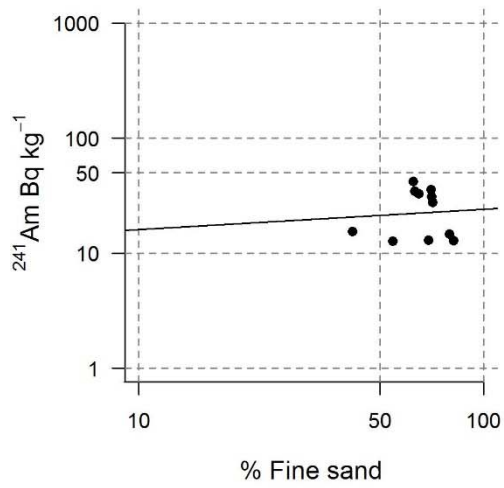
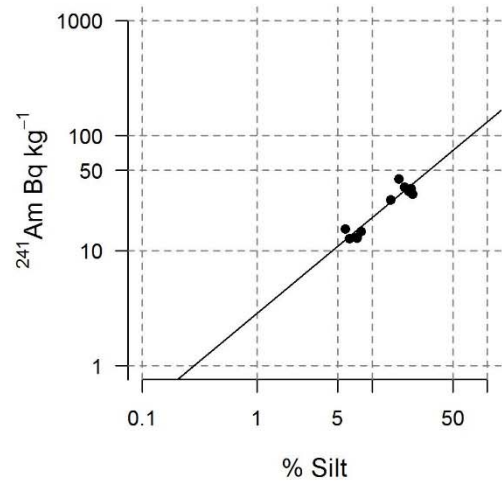
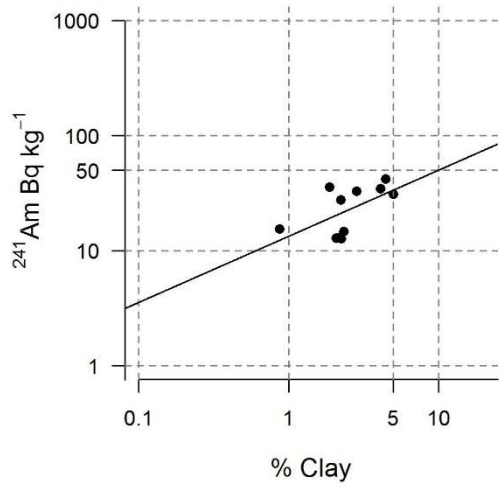
Appendix F1.2

Clay, silt, sand and organic matter regression models for ^{241}Am for transect 2 season 1



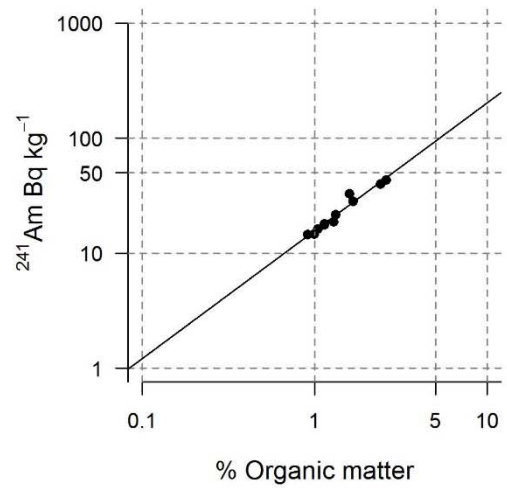
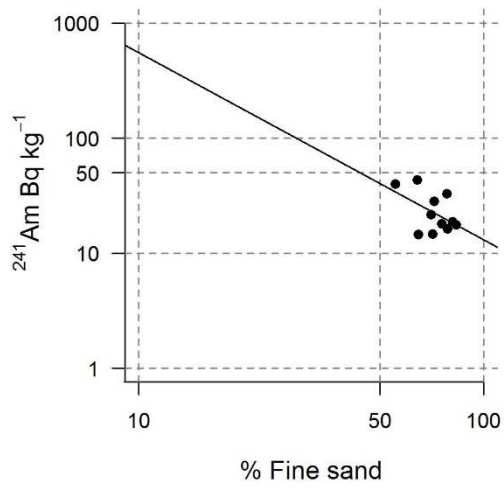
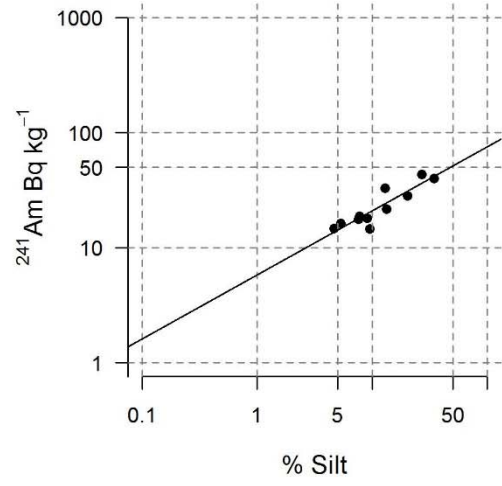
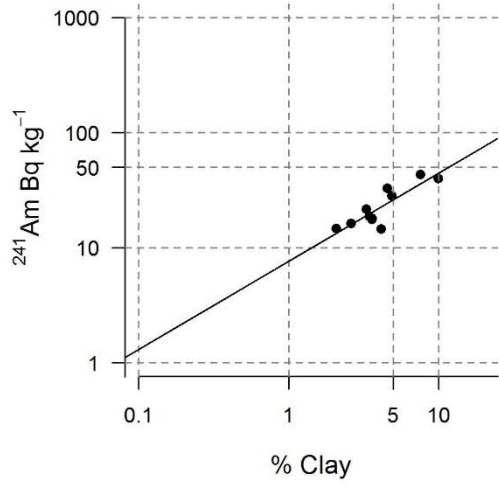
Appendix F1.3

Clay, silt, sand and organic matter regression models for ^{241}Am for transect 3 season 1



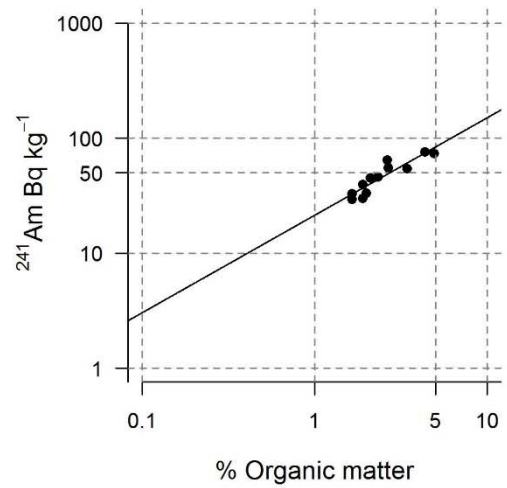
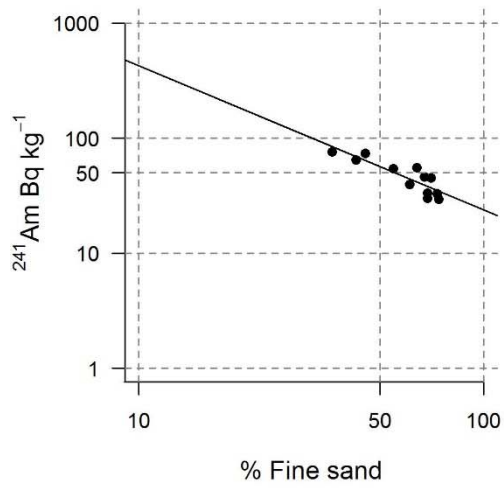
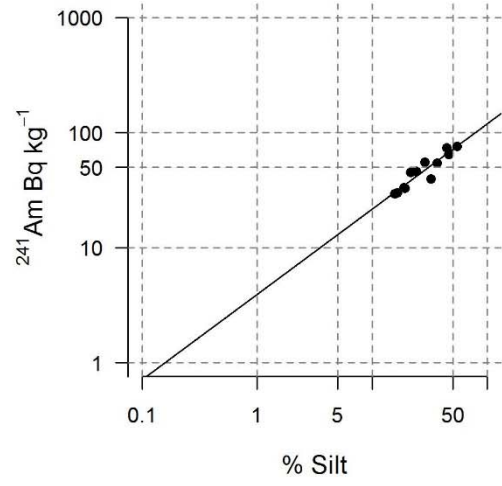
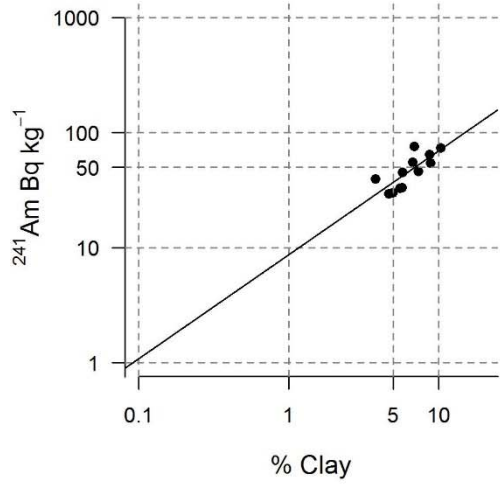
Appendix F1.4

Clay, silt, sand and organic matter regression models for ^{241}Am for transect 1 season 2



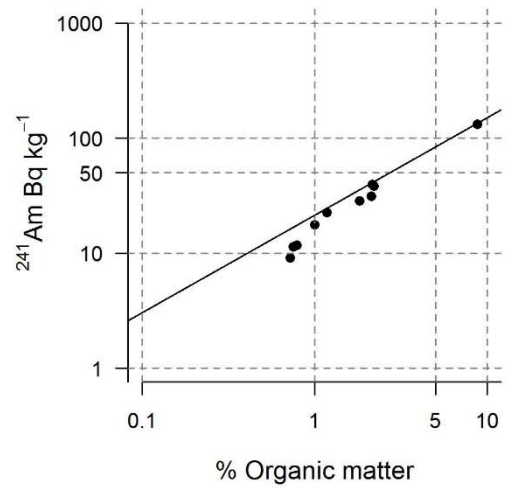
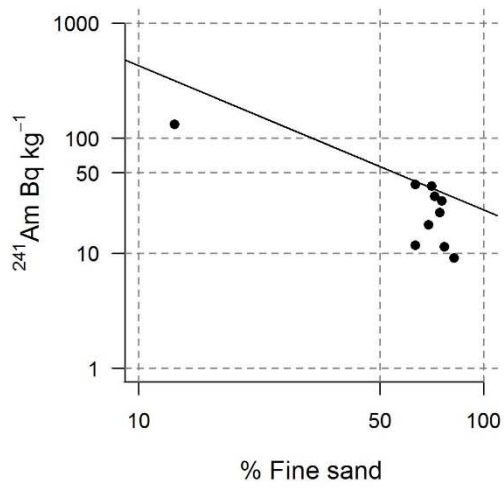
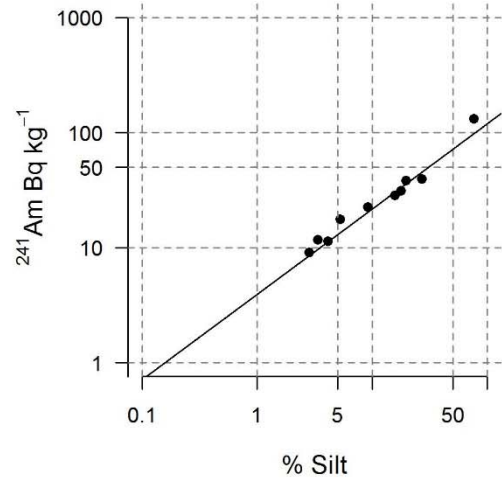
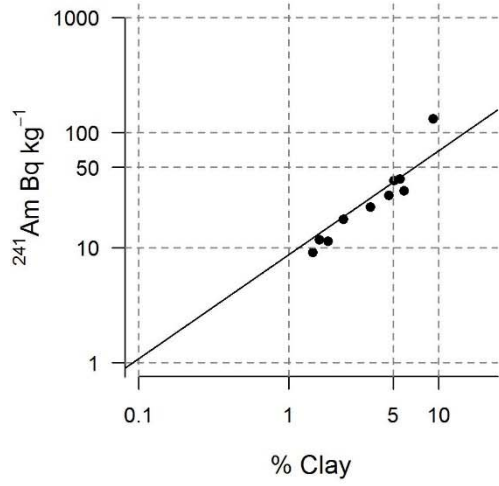
Appendix F1.5

Clay, silt, sand and organic matter regression models for ^{241}Am for transect 2 season 2



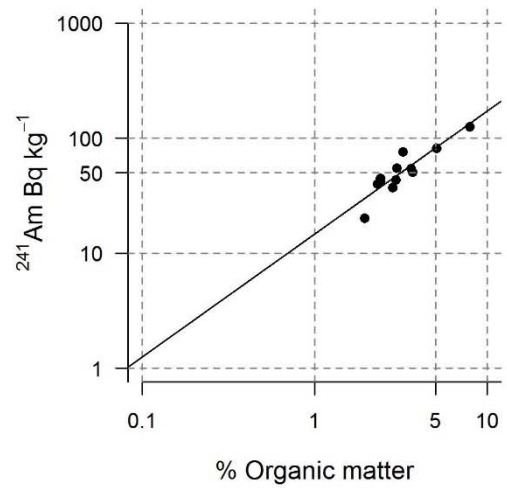
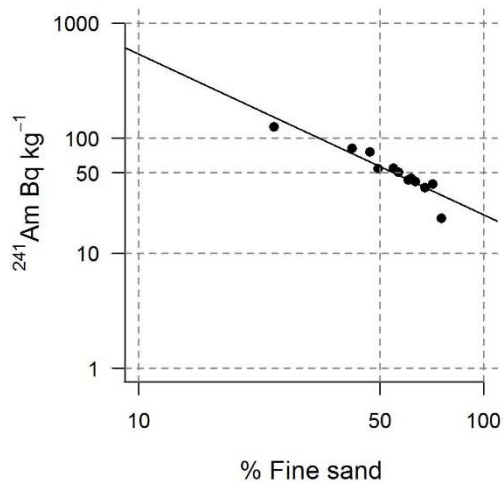
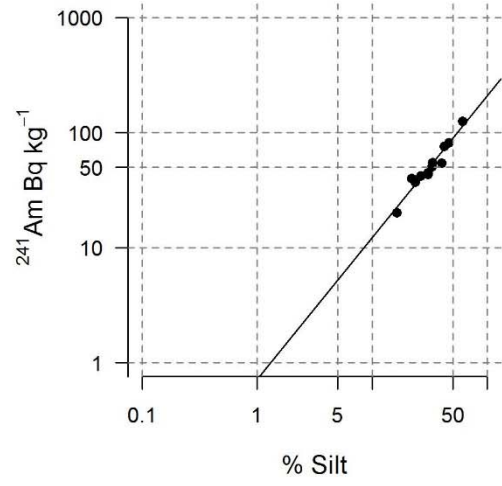
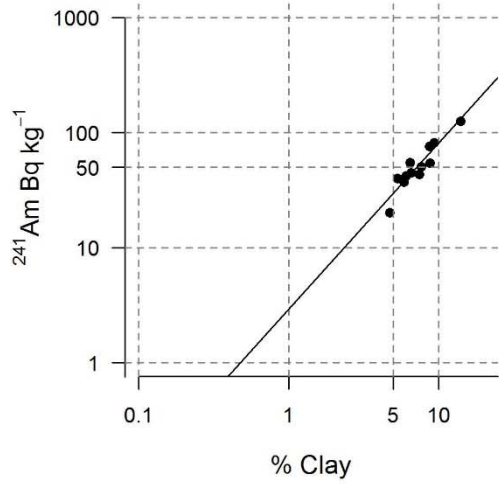
Appendix F1.6

Clay, silt, sand and organic matter regression models for ^{241}Am for transect 3 season 2



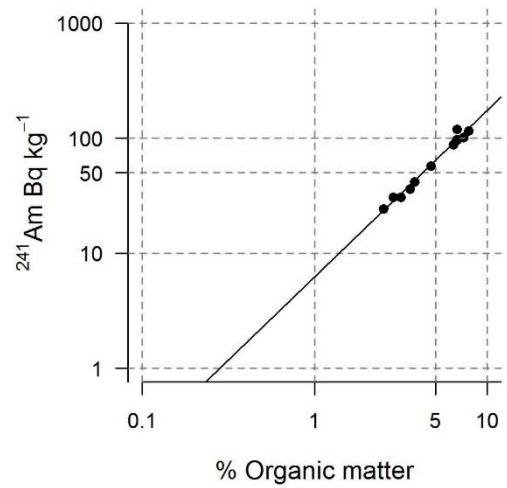
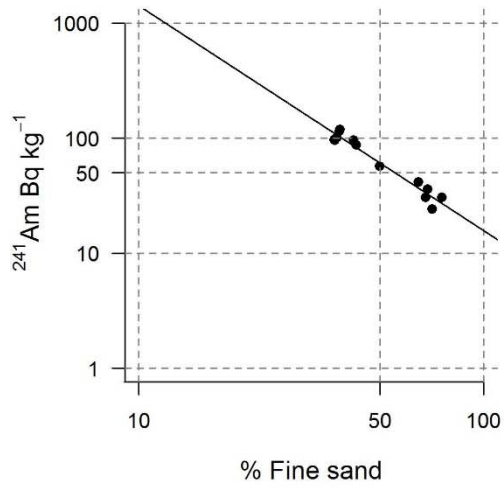
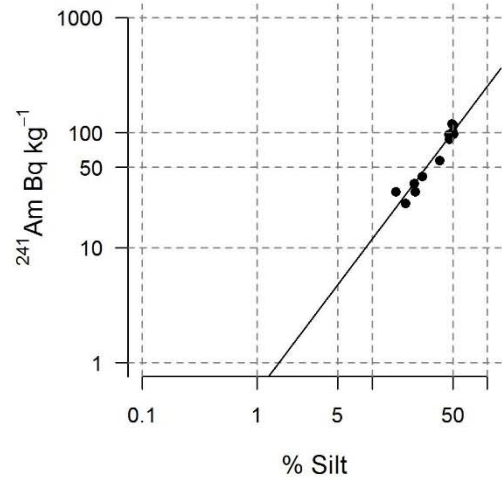
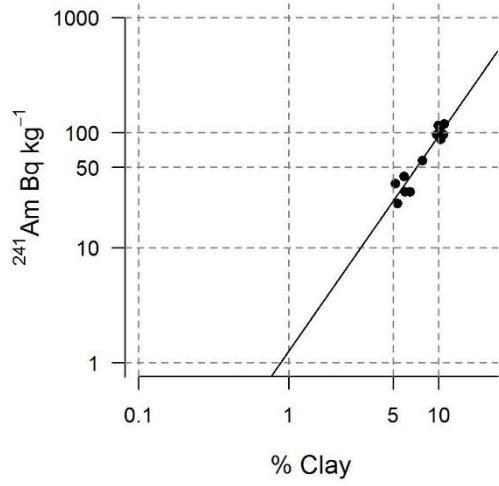
Appendix F1.7

Clay, silt, sand and organic matter regression models for ^{241}Am for transect 1 season 3



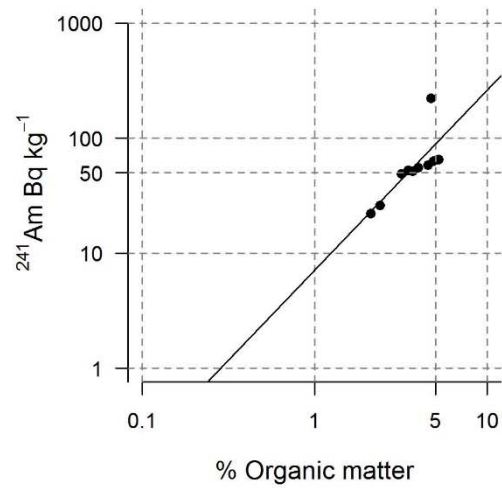
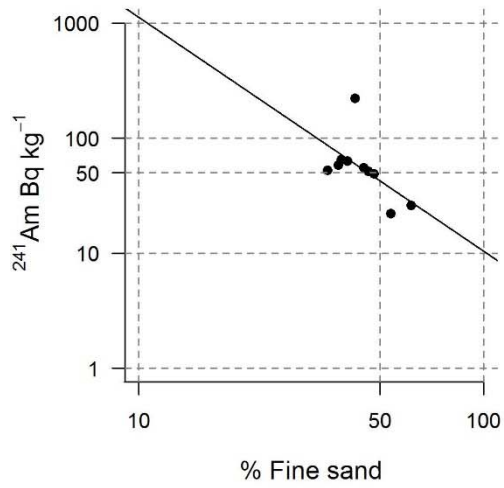
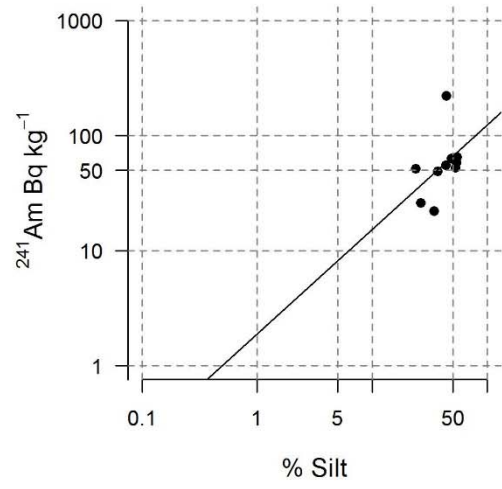
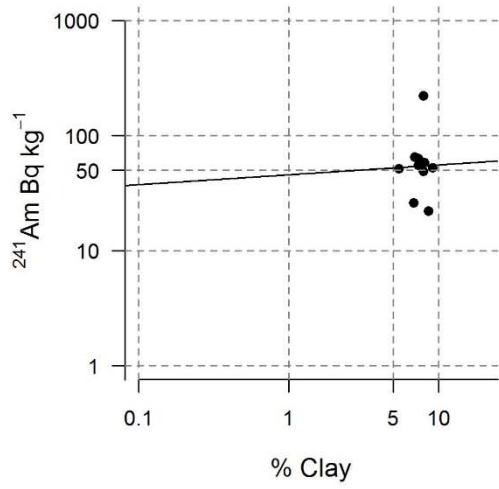
Appendix F1.8

Clay, silt, sand and organic matter regression models for ^{241}Am for transect 2 season 3



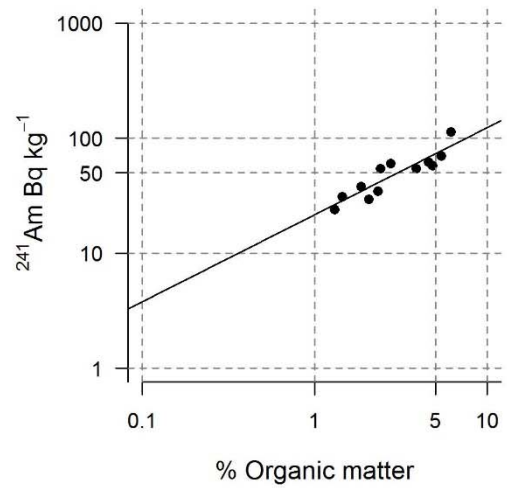
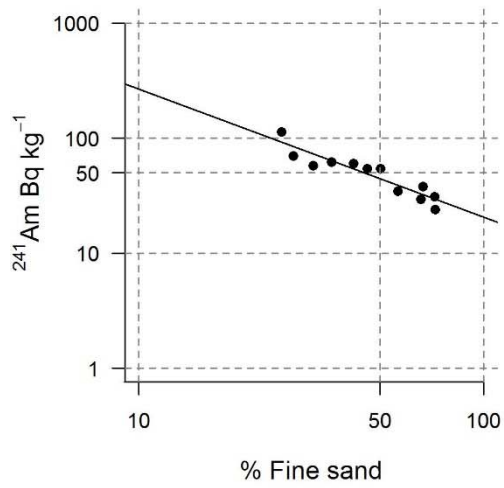
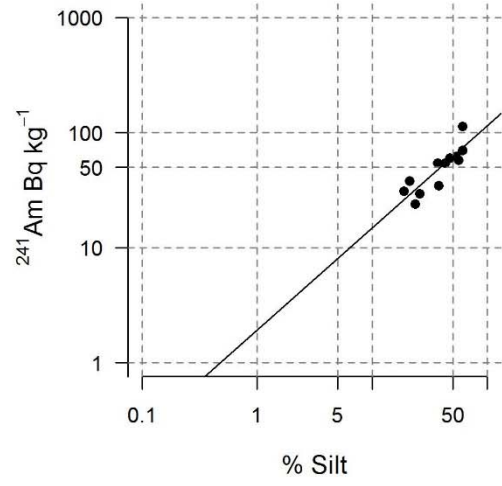
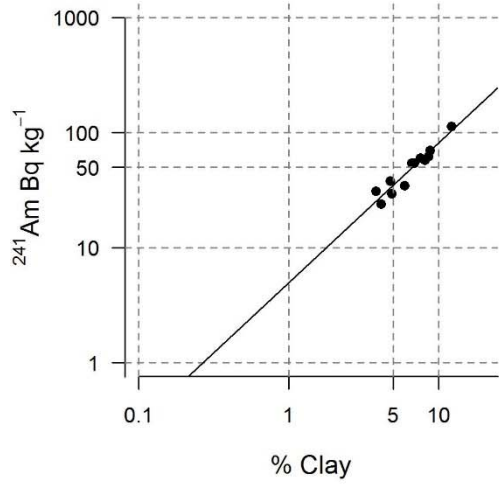
Appendix F1.9

Clay, silt, sand and organic matter regression models for ^{241}Am for transect 3 season 3



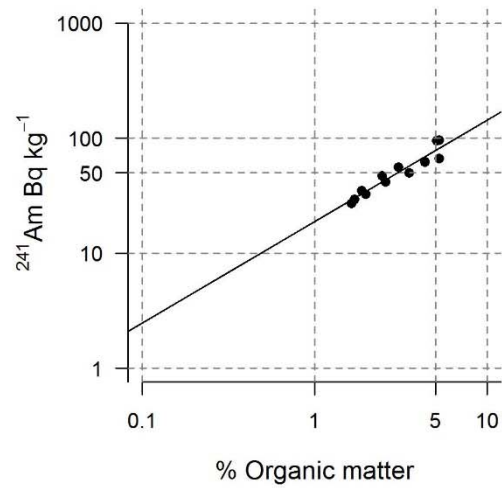
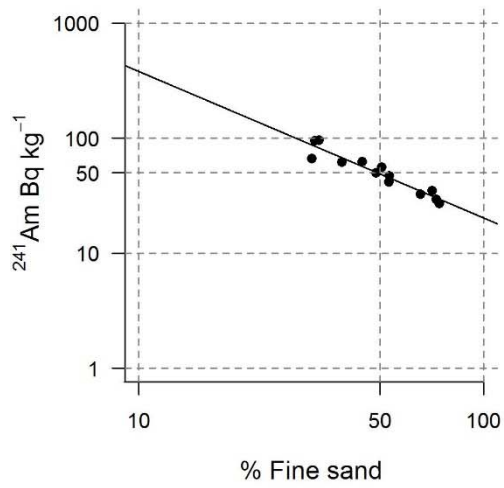
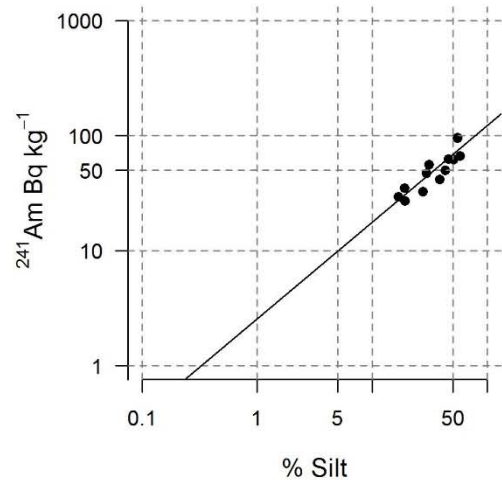
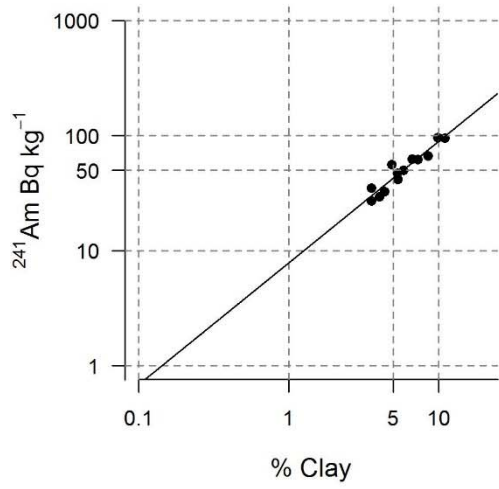
Appendix F1.10

Clay, silt, sand and organic matter regression models for ^{241}Am for transect 1 season 4



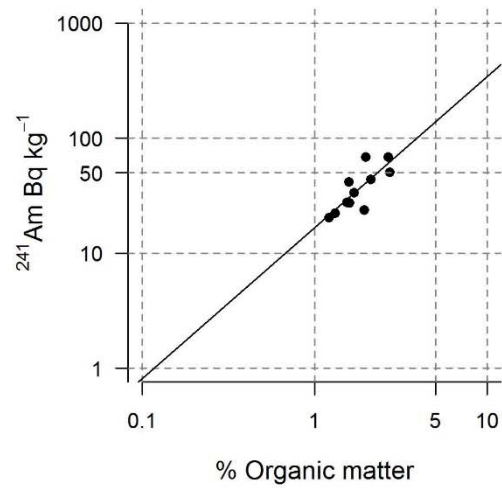
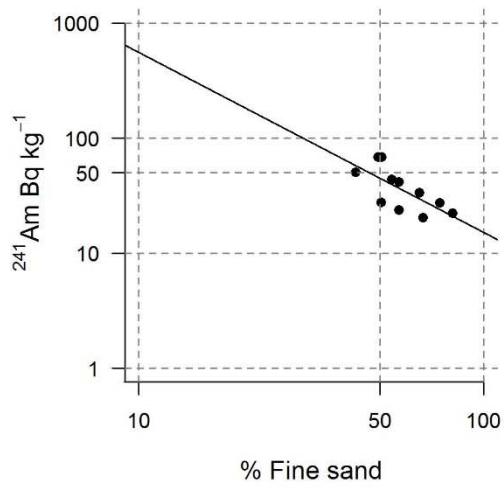
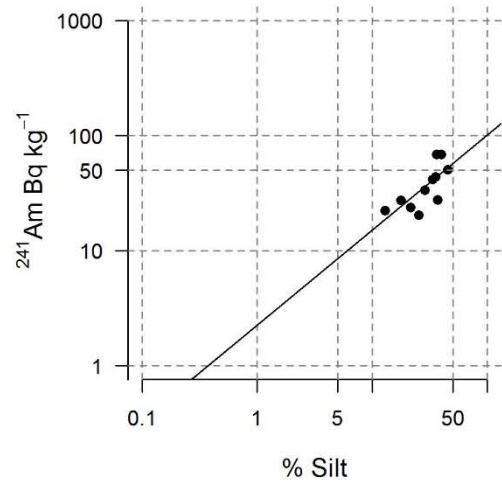
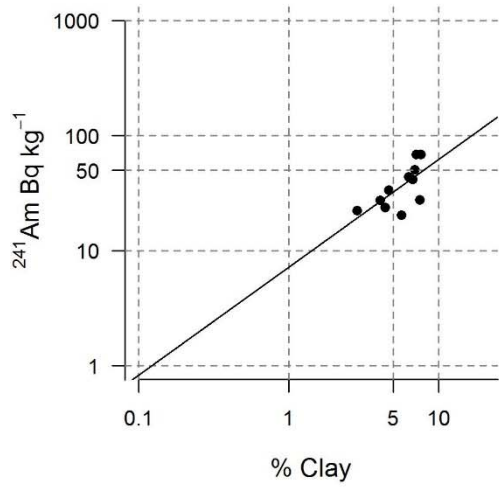
Appendix F1.11

Clay, silt, sand and organic matter regression models for ^{241}Am for transect 2 season 4



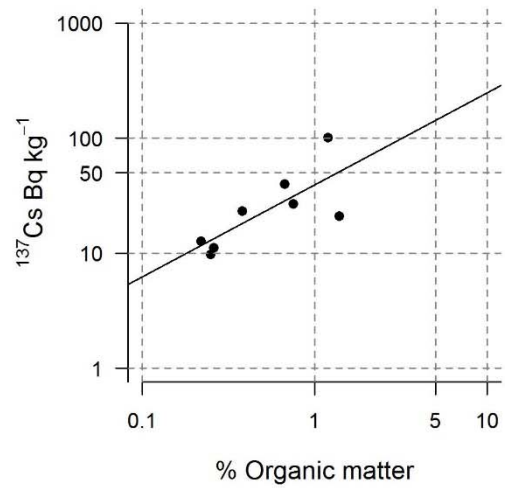
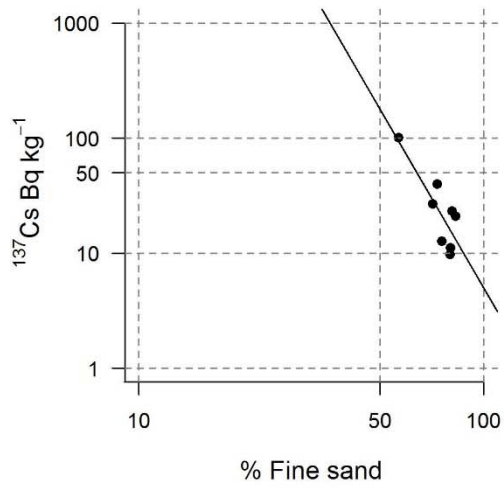
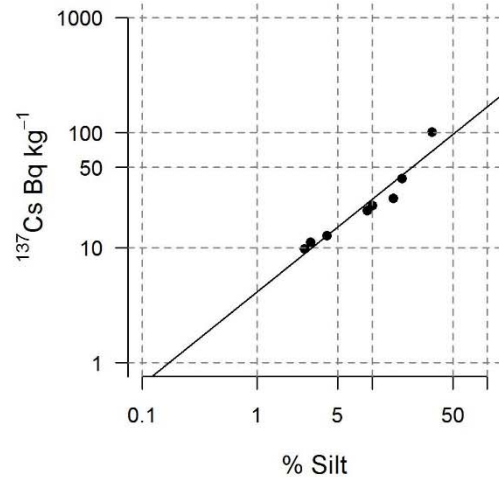
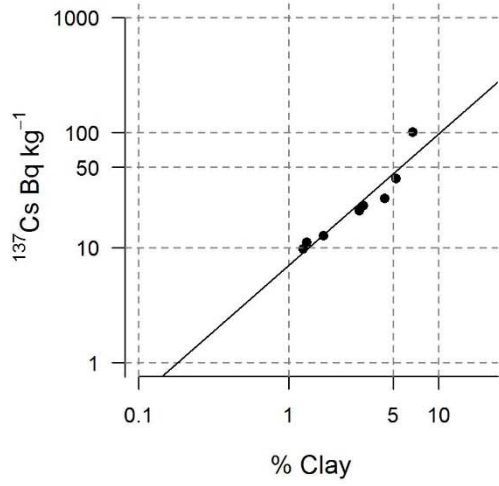
Appendix F1.12

Clay, silt, sand and organic matter regression models for ^{241}Am for transect 3 season 4



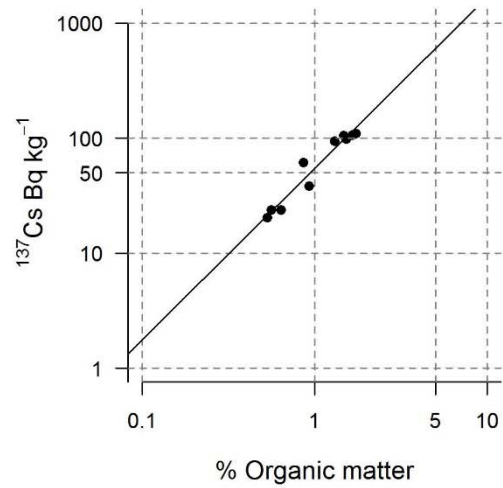
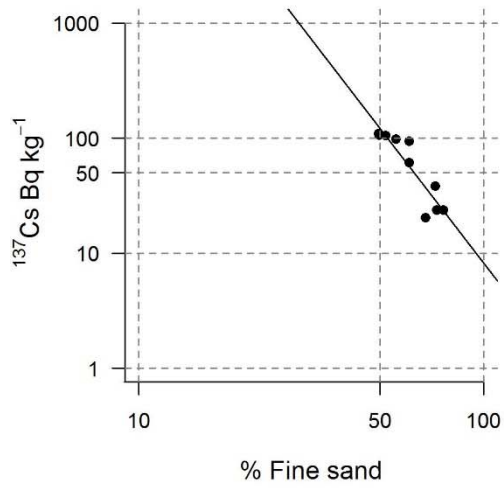
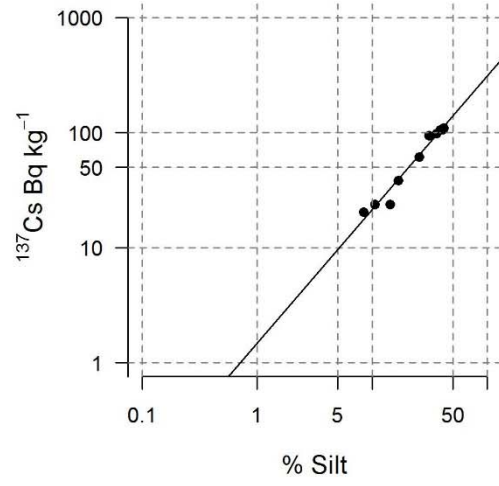
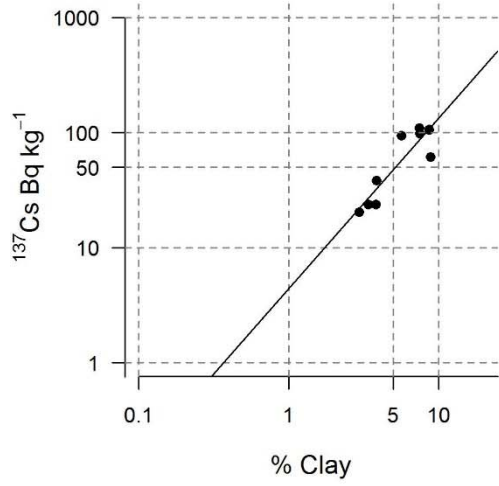
Appendix F1.13

Clay, silt, sand and organic matter regression models for ^{137}Cs for transect 1 season 1



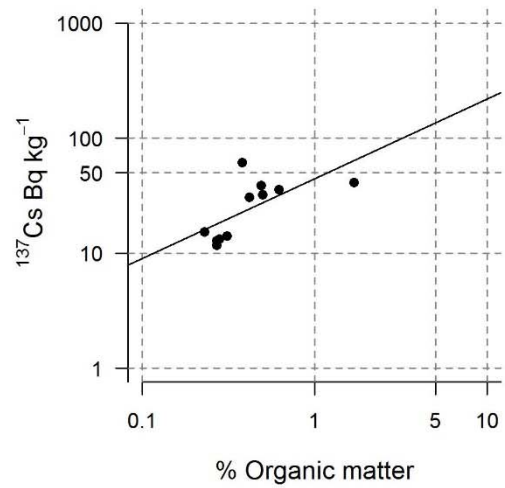
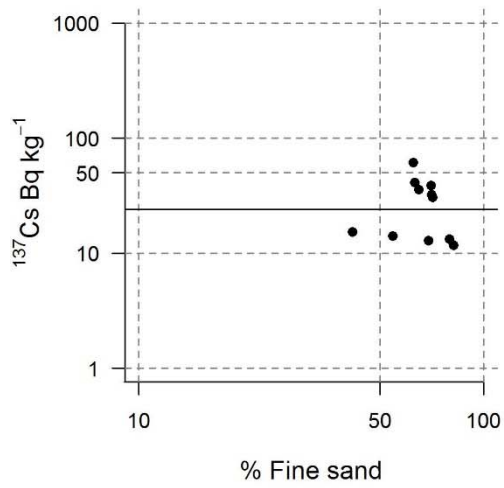
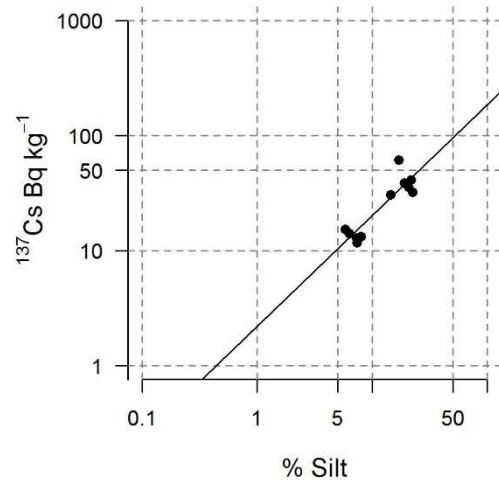
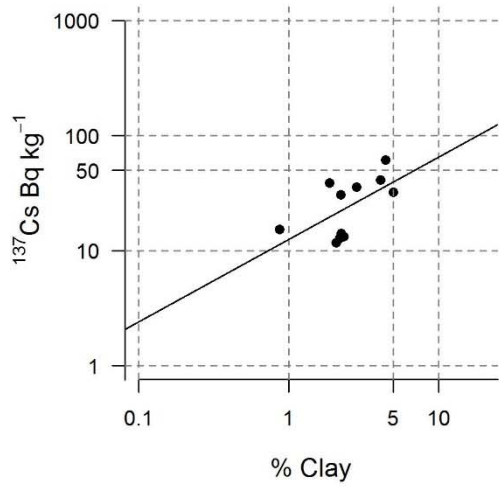
Appendix F1.14

Clay, silt, sand and organic matter regression models for ^{137}Cs for transect 2 season 1



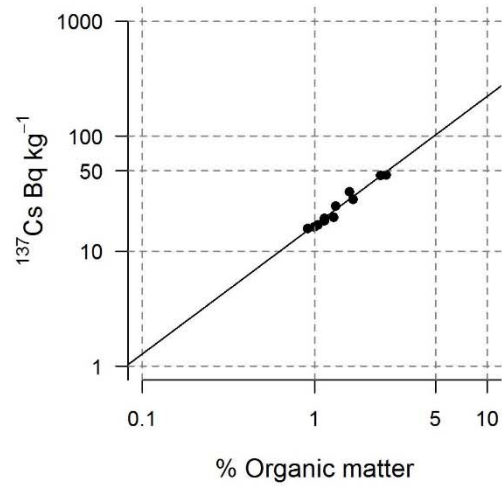
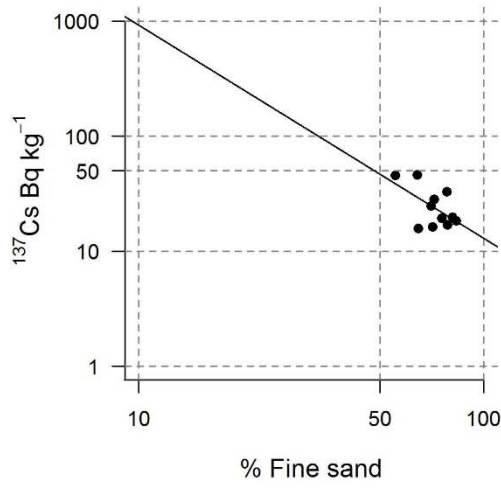
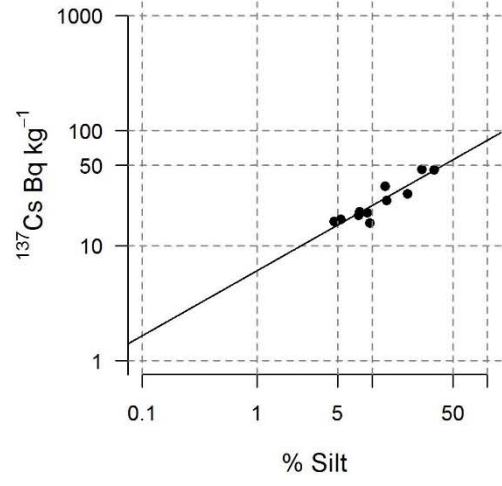
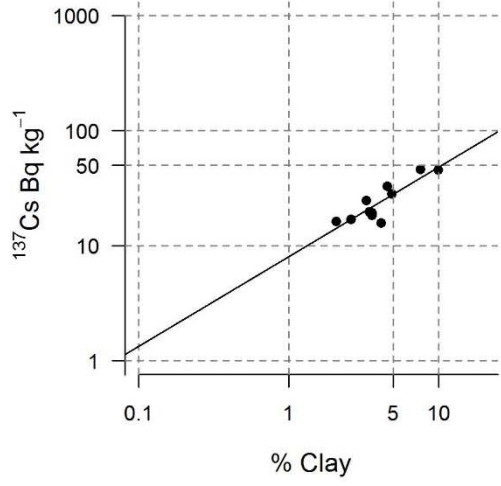
Appendix F1.15

Clay, silt, sand and organic matter regression models for ^{137}Cs for transect 3 season 1



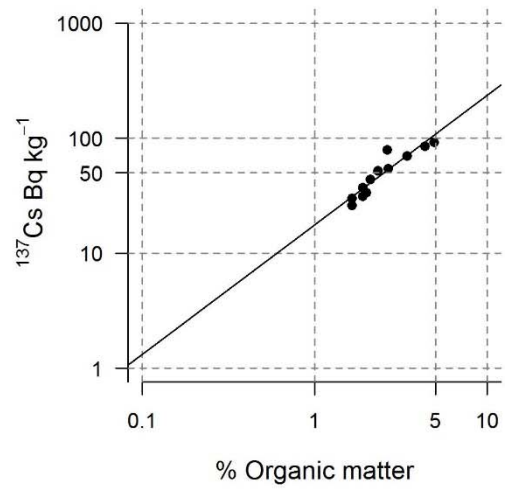
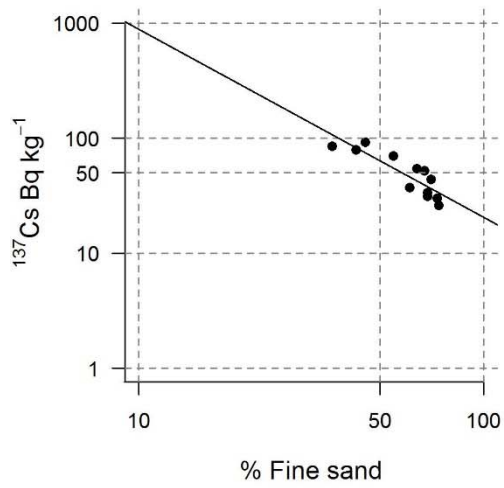
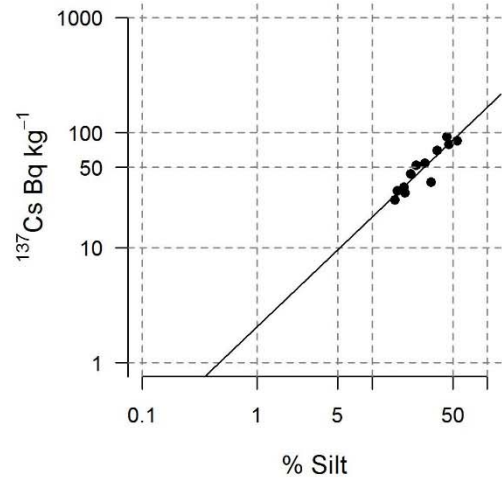
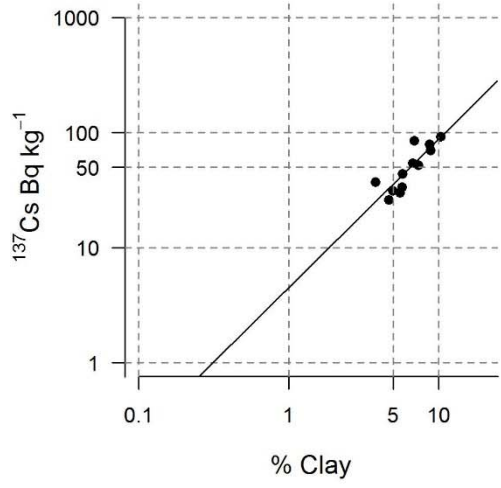
Appendix F1.16

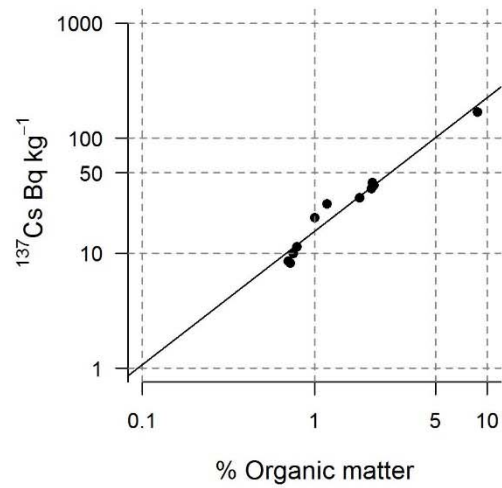
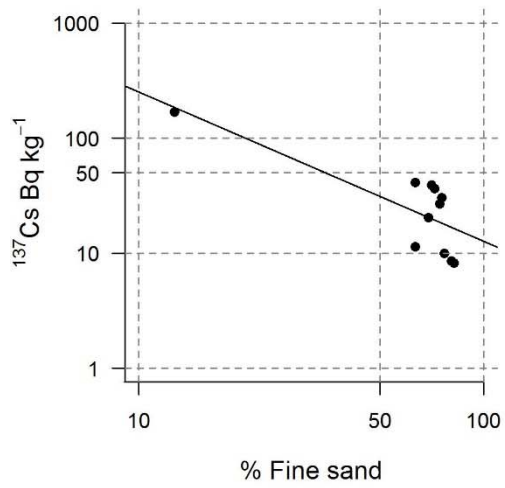
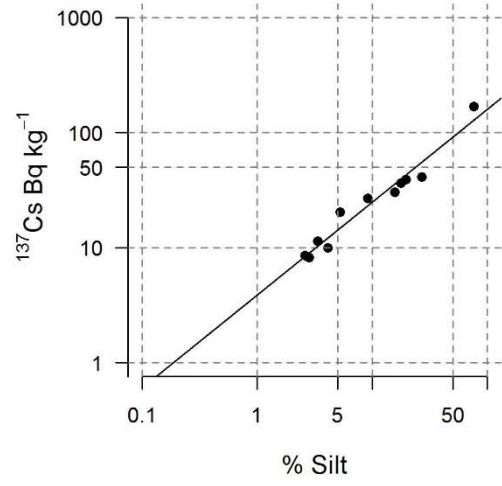
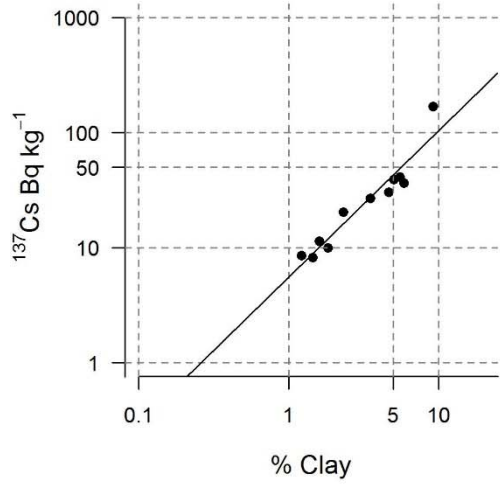
Clay, silt, sand and organic matter regression models for ^{137}Cs for transect 1 season 2



Appendix F1.17

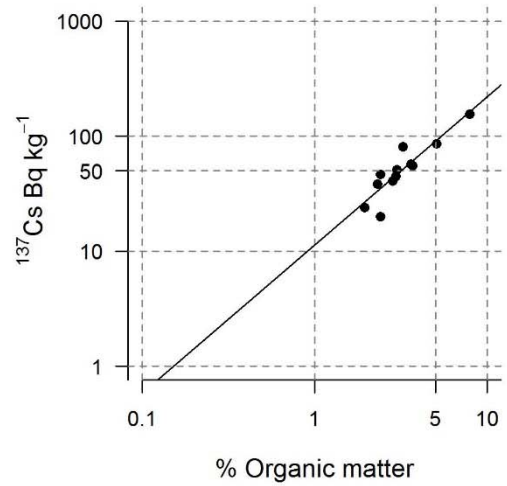
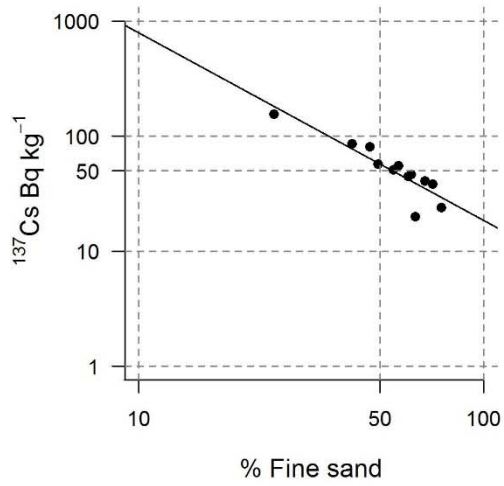
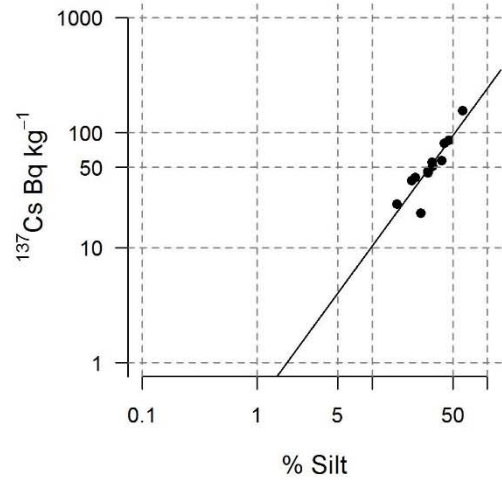
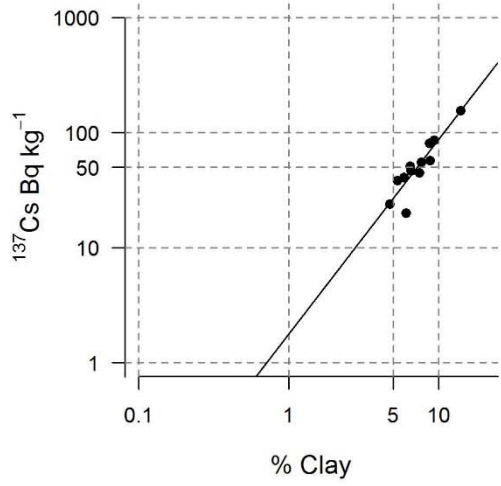
Clay, silt, sand and organic matter regression models for ^{137}Cs for transect 2 season 2





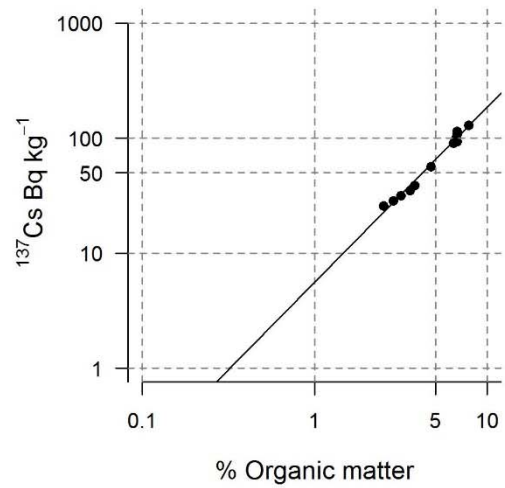
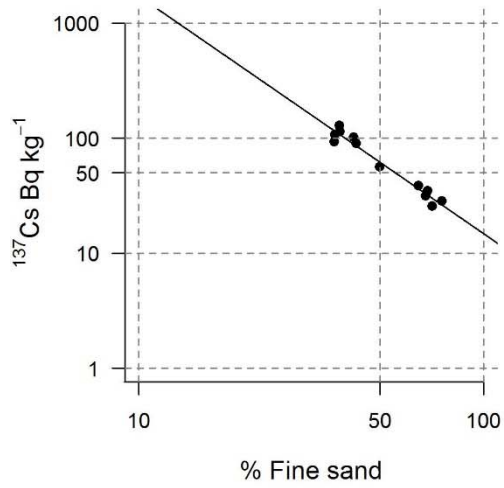
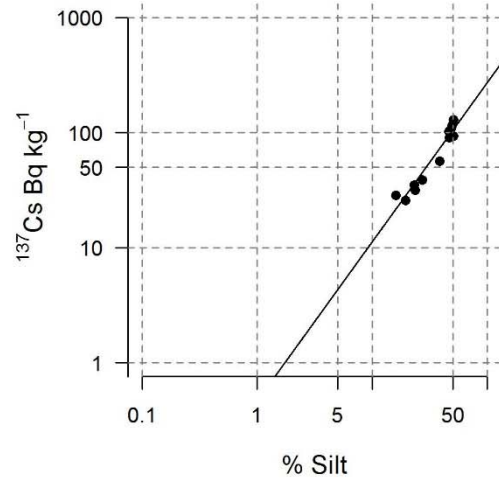
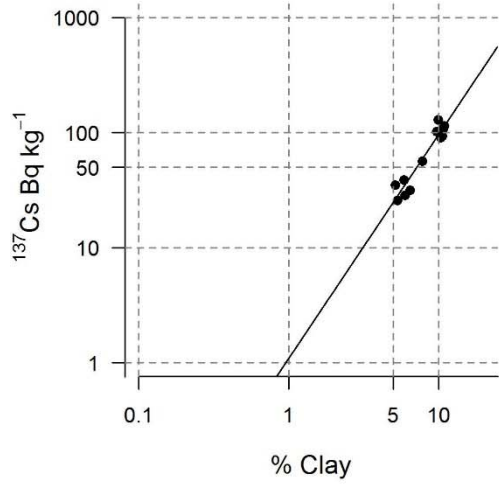
Appendix F1.19

Clay, silt, sand and organic matter regression models for ^{137}Cs for transect 1 season 3



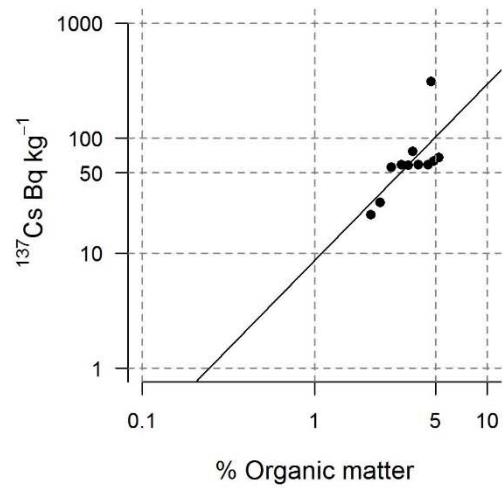
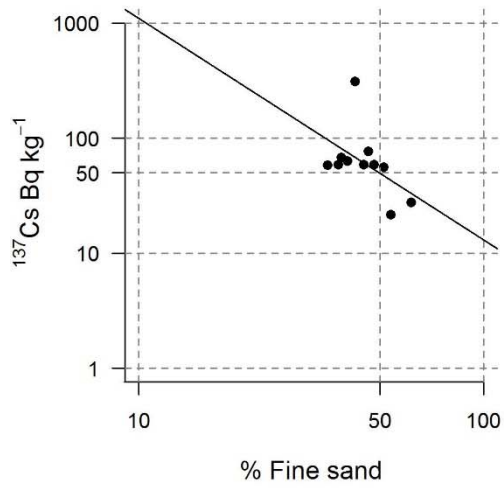
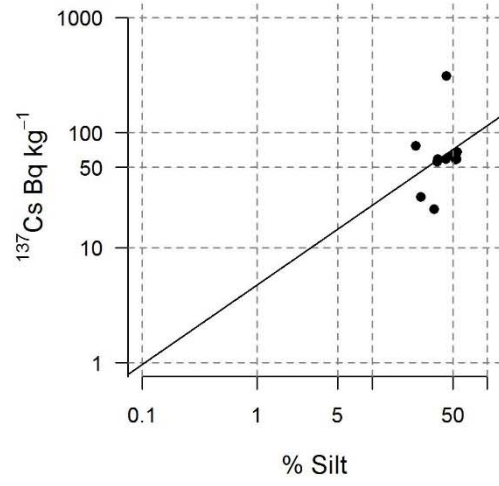
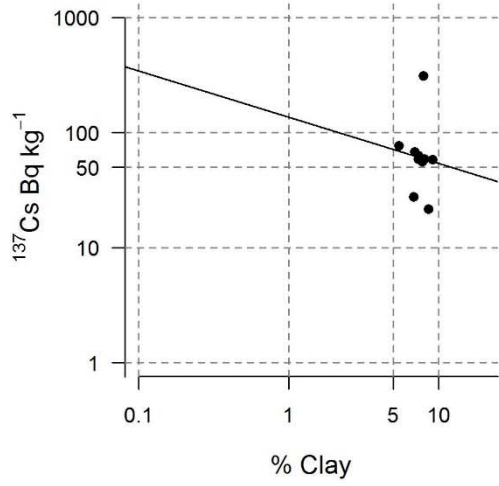
Appendix F1.20

Clay, silt, sand and organic matter regression models for ^{137}Cs for transect 2 season 3



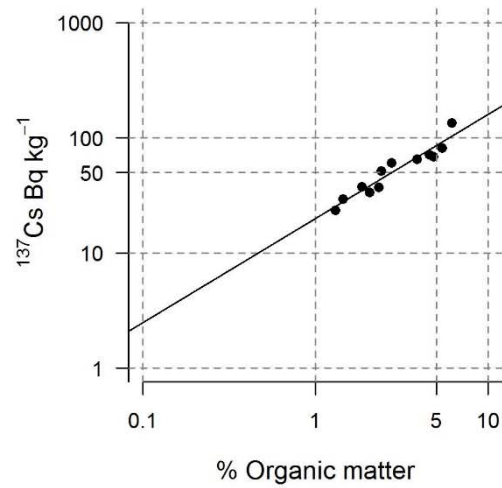
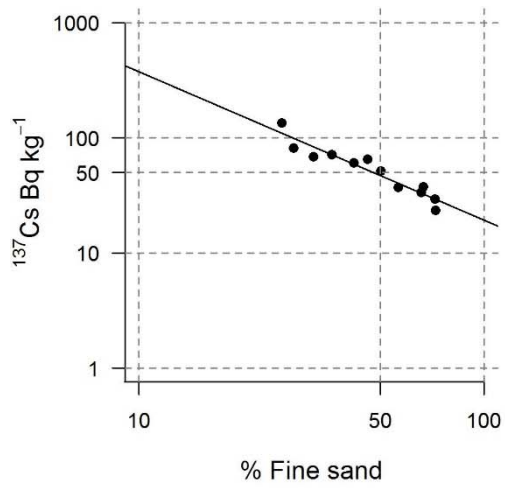
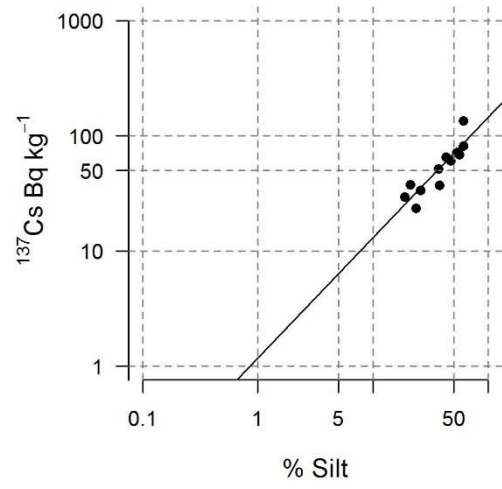
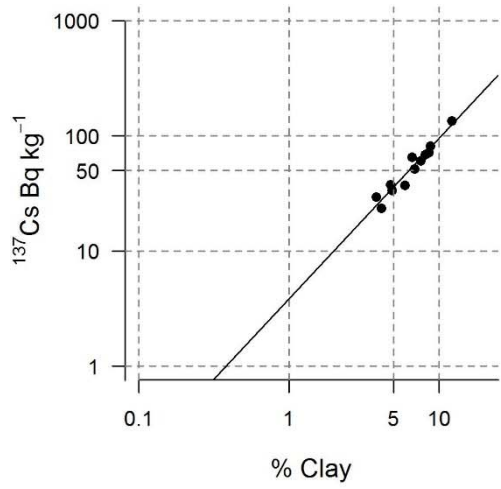
Appendix F1.21

Clay, silt, sand and organic matter regression models for ^{137}Cs for transect 3 season 3



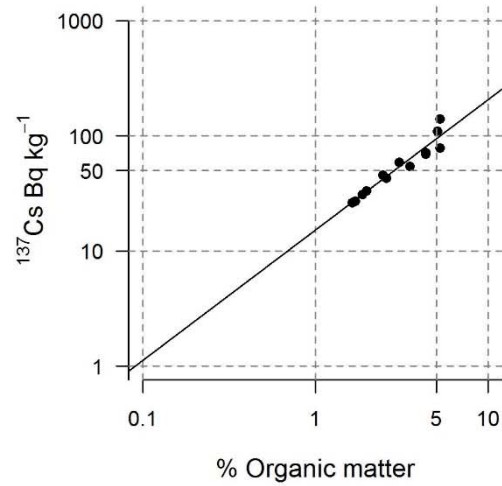
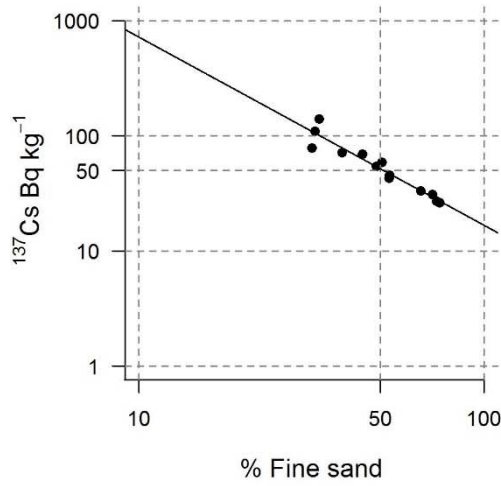
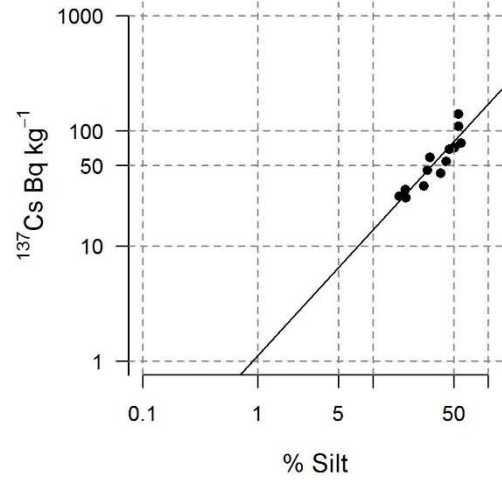
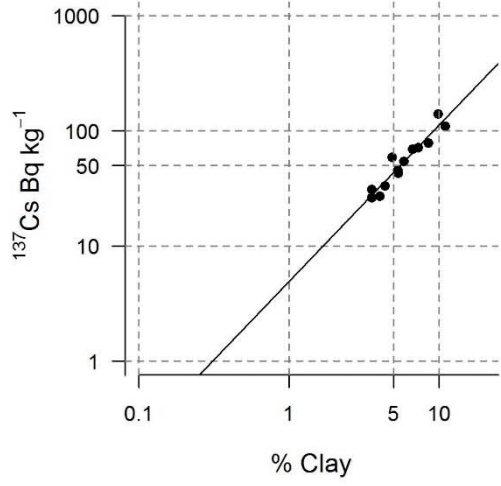
Appendix F1.22

Clay, silt, sand and organic matter regression models for ^{137}Cs for transect 1 season 4



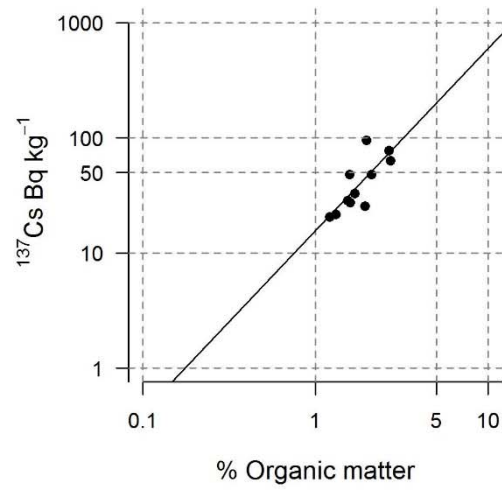
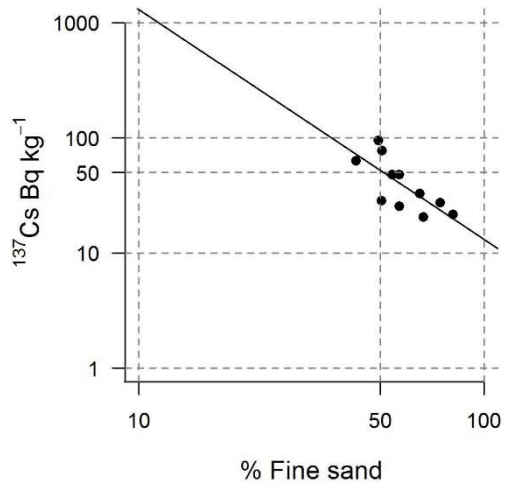
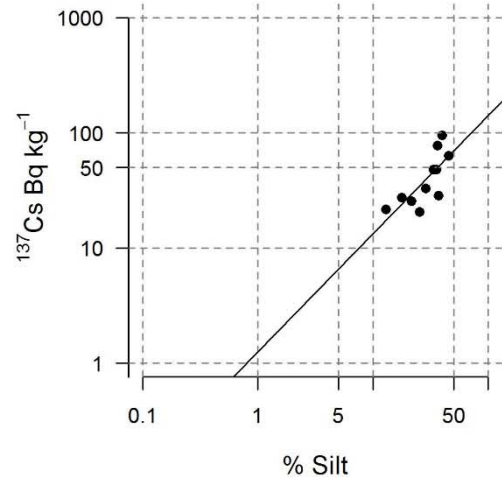
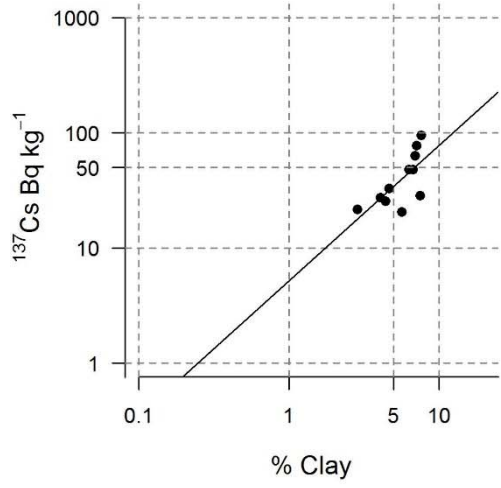
Appendix F1.23

Clay, silt, sand and organic matter regression models for ^{137}Cs for transect 2 season 4



Appendix F1.24

Clay, silt, sand and organic matter regression models for ^{137}Cs for transect 3 season 4



Appendix 2

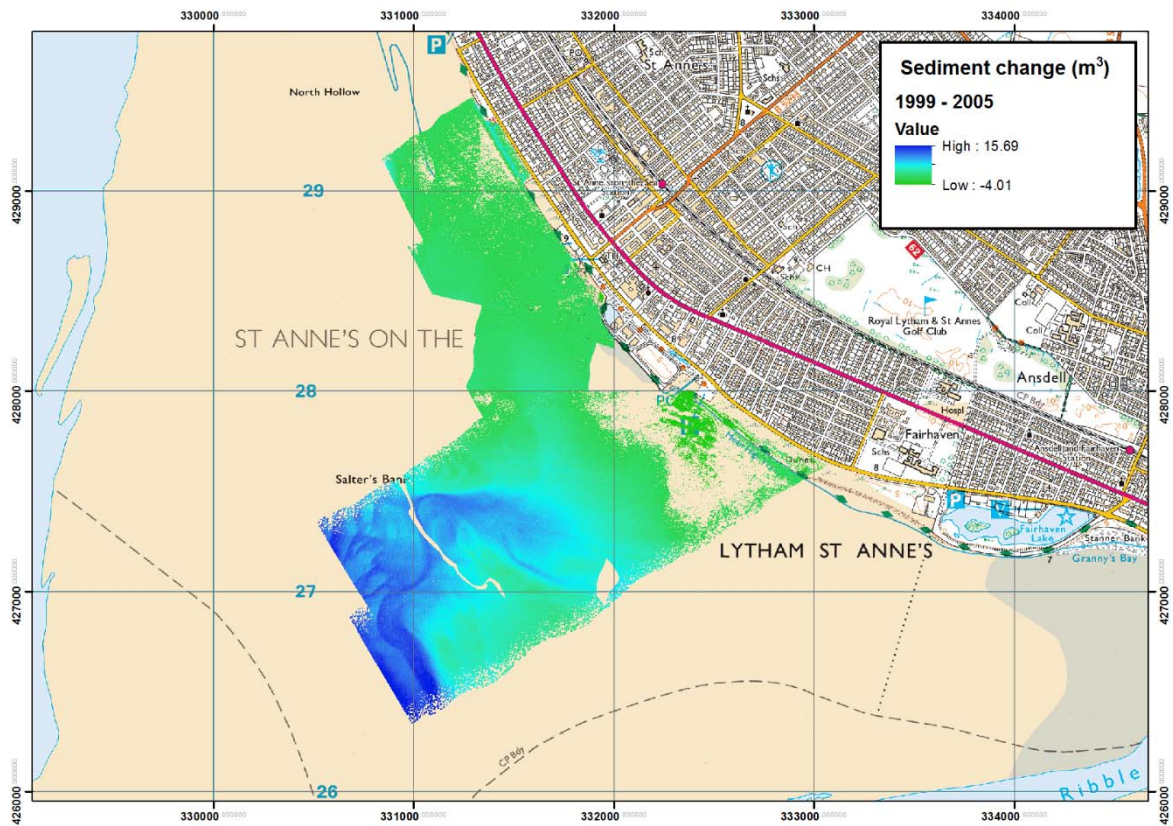


Figure A2.1 Map of change in volume (m^3) of sediment from 1999 – 2005 for the outer Ribble estuary sandbanks, each pixel has an area of 4m^2 . These data have had a limit of detection applied to them so that only significant movement is shown.

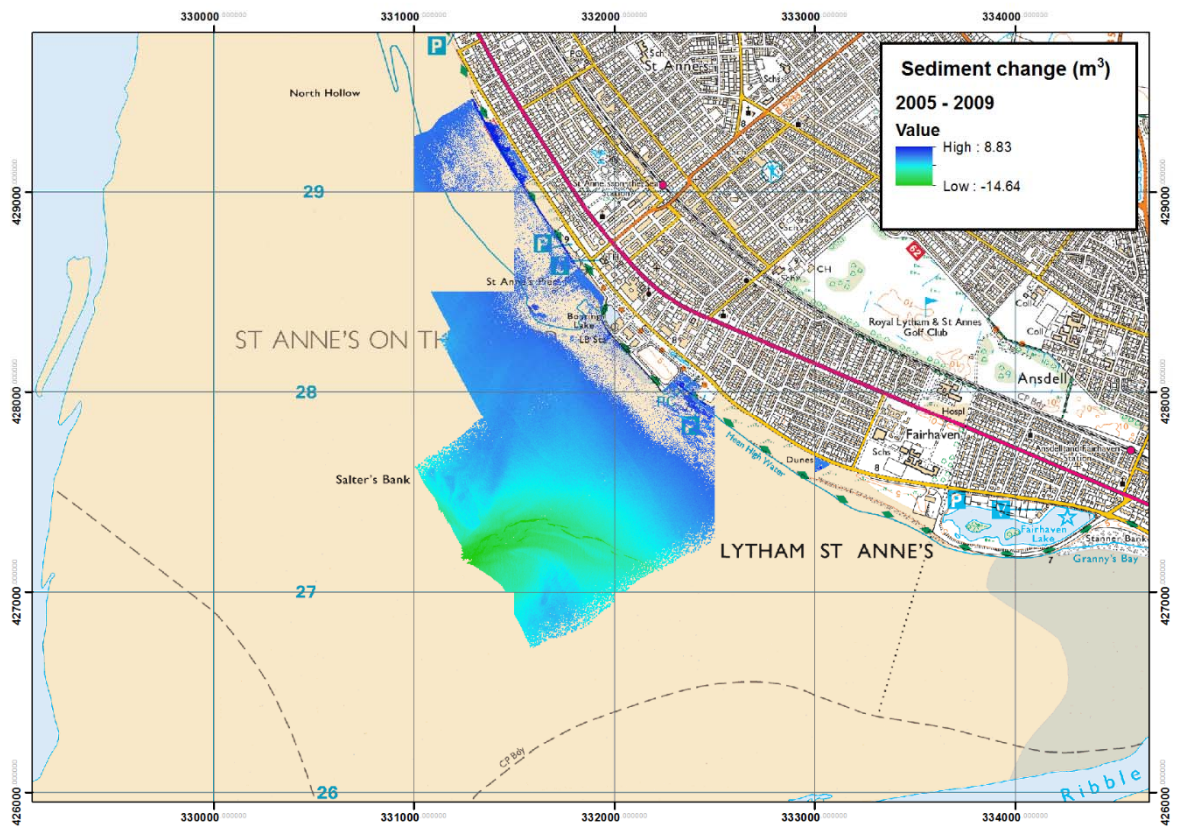


Figure A2.2 Map of change in volume (m³) of sediment from 2005 – 2009 for the outer Ribble estuary sandbanks, each pixel has an area of 4m². These data have had a limit of detection applied to them so that only significant movement is shown.

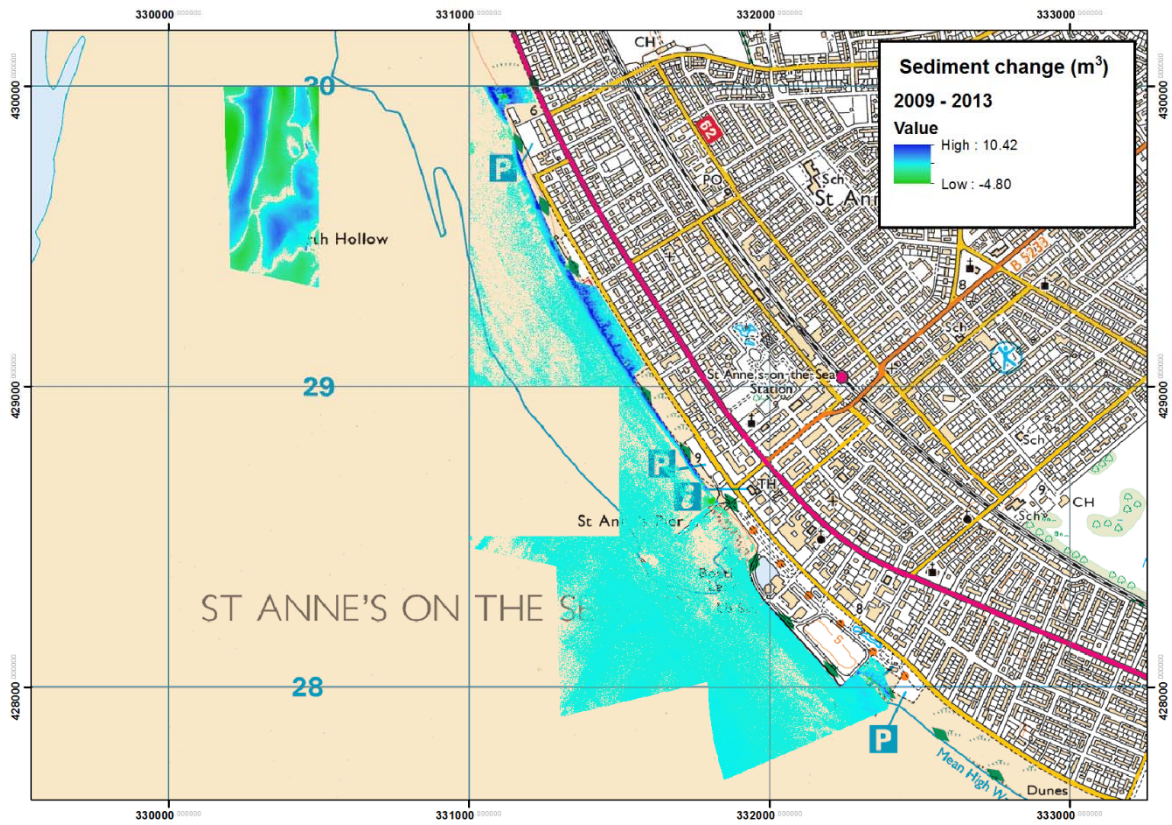


Figure A2.3 Map of change in volume (m³) of sediment from 2009 – 2013 for the outer Ribble estuary sandbanks, each pixel has an area of 4m². These data have had a limit of detection applied to them so that only significant movement is shown.

Appendix 3

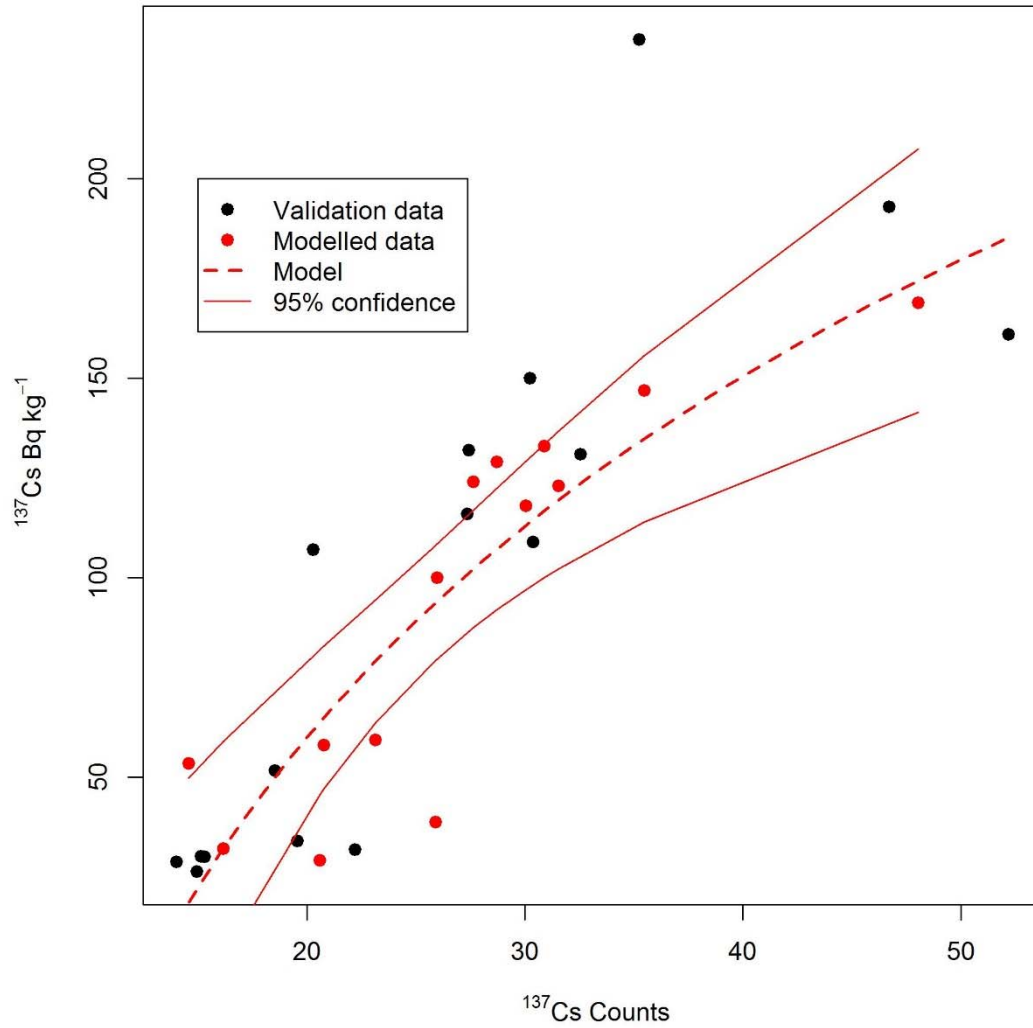


Figure A3.1 Total counts for the ^{137}Cs window from the MoGSS dataset are plotted against the ^{137}Cs Bq kg $^{-1}$ of the sediment scrapes from the old marsh. A regression model which used the log transformed MoGSS data was fitted to the data with 95% confidence intervals.

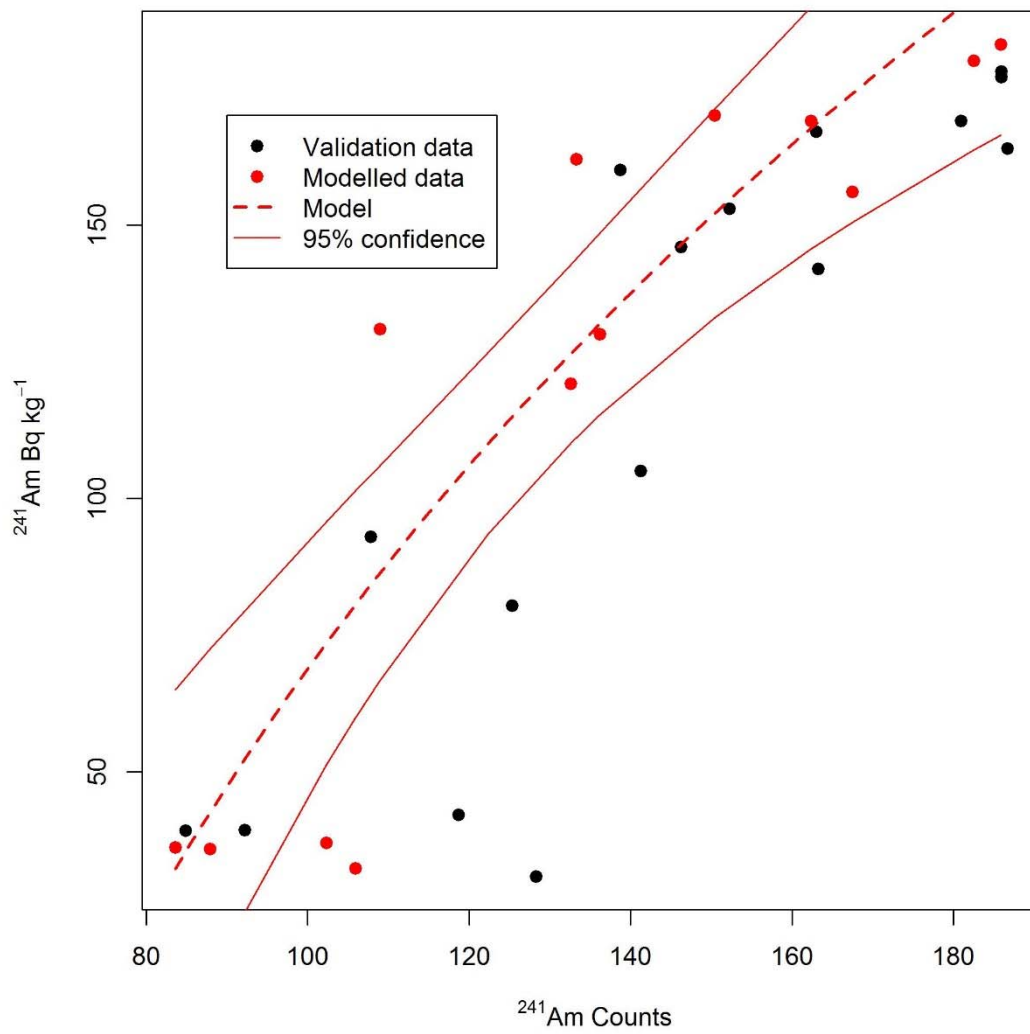


Figure A3.2 Total counts for the ²⁴¹Am window from the MoGSS dataset are plotted against the ¹³⁷Cs Bq kg⁻¹ of the sediment scrapes from the new marsh. A regression model which used the log transformed MoGSS data was fitted to the data with 95% confidence intervals.

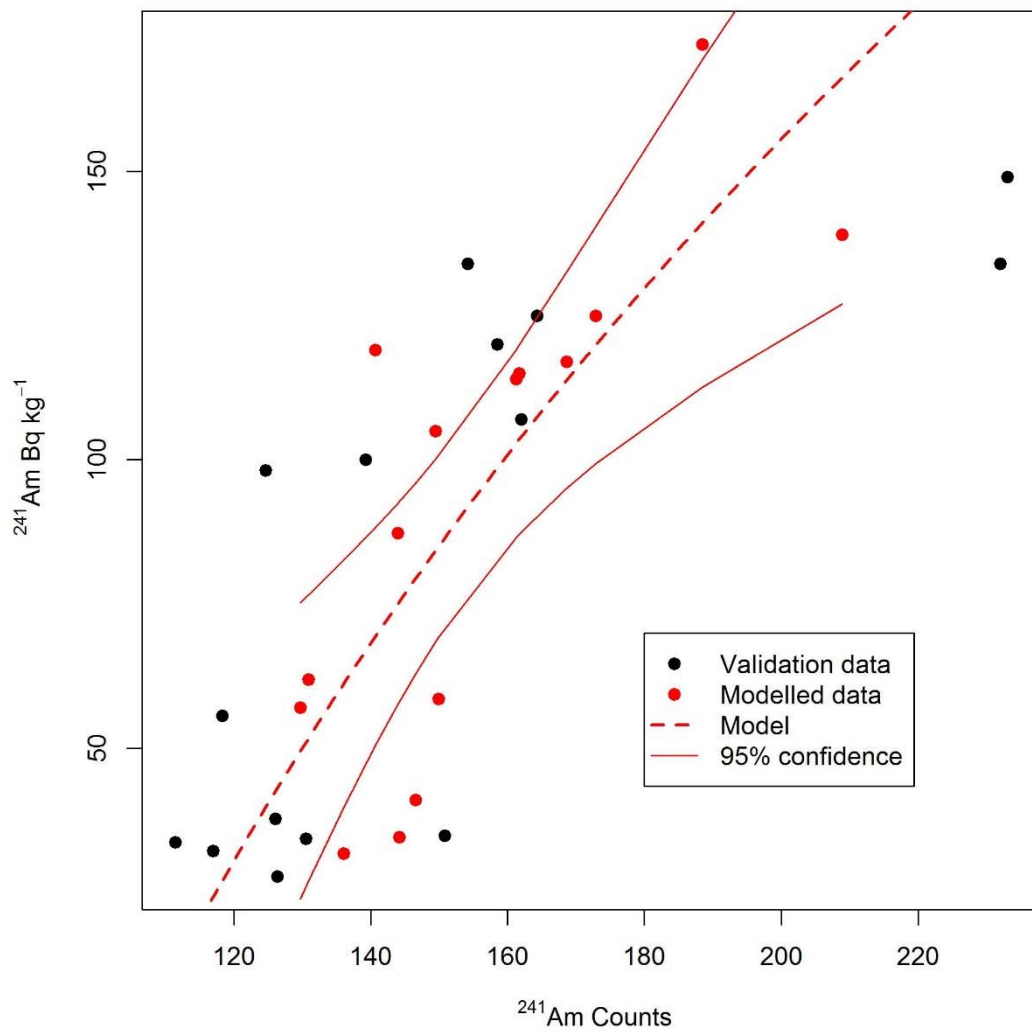


Figure A3.3 Total counts for the ^{241}Am window from the MoGSS dataset are plotted against the ^{137}Cs Bq kg^{-1} of the sediment scrapes from the old marsh. A regression model which used the log transformed MoGSS data was fitted to the data with 95% confidence intervals.

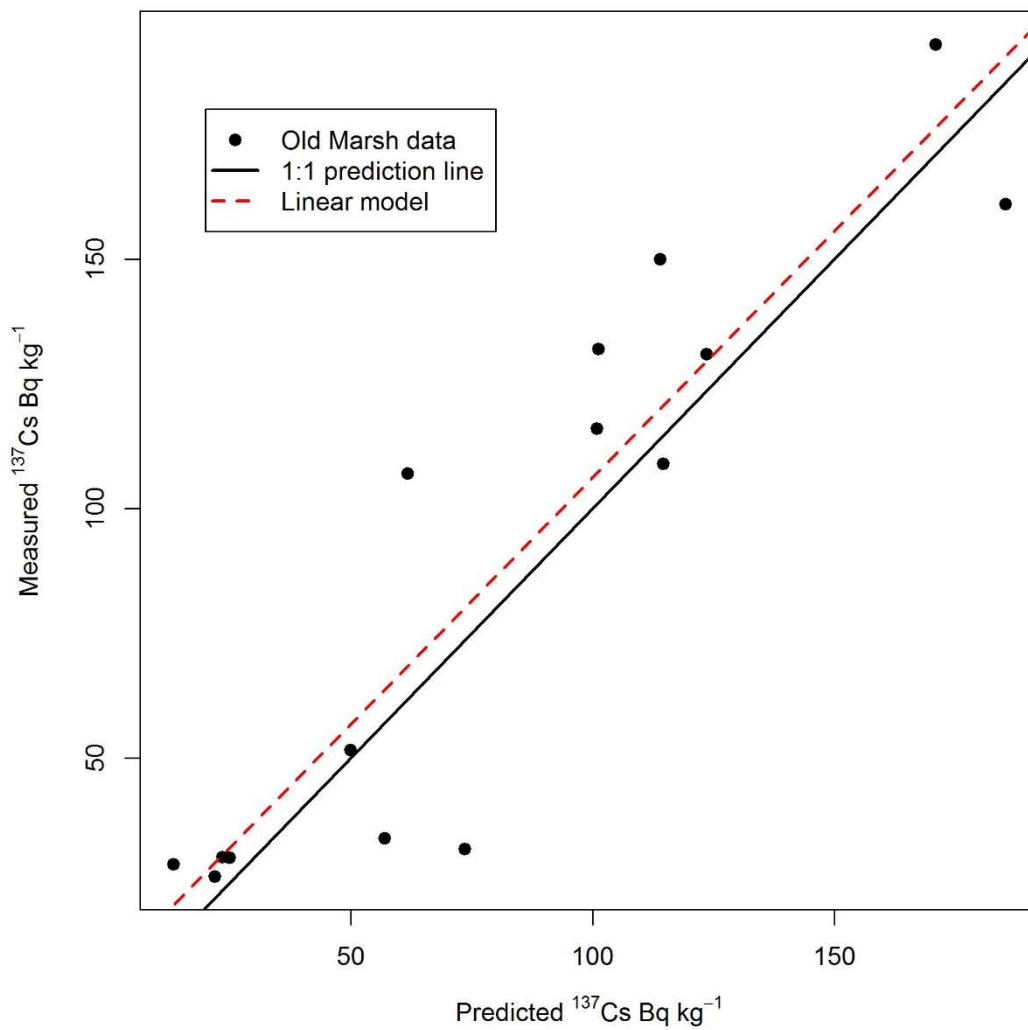


Figure A3.4 Comparison of estimated activity for ^{137}Cs in the old marsh (x axis) and measured activity (y axis) a linear model is fitted to these data to show the general trend in comparison to the 1:1 prediction line.

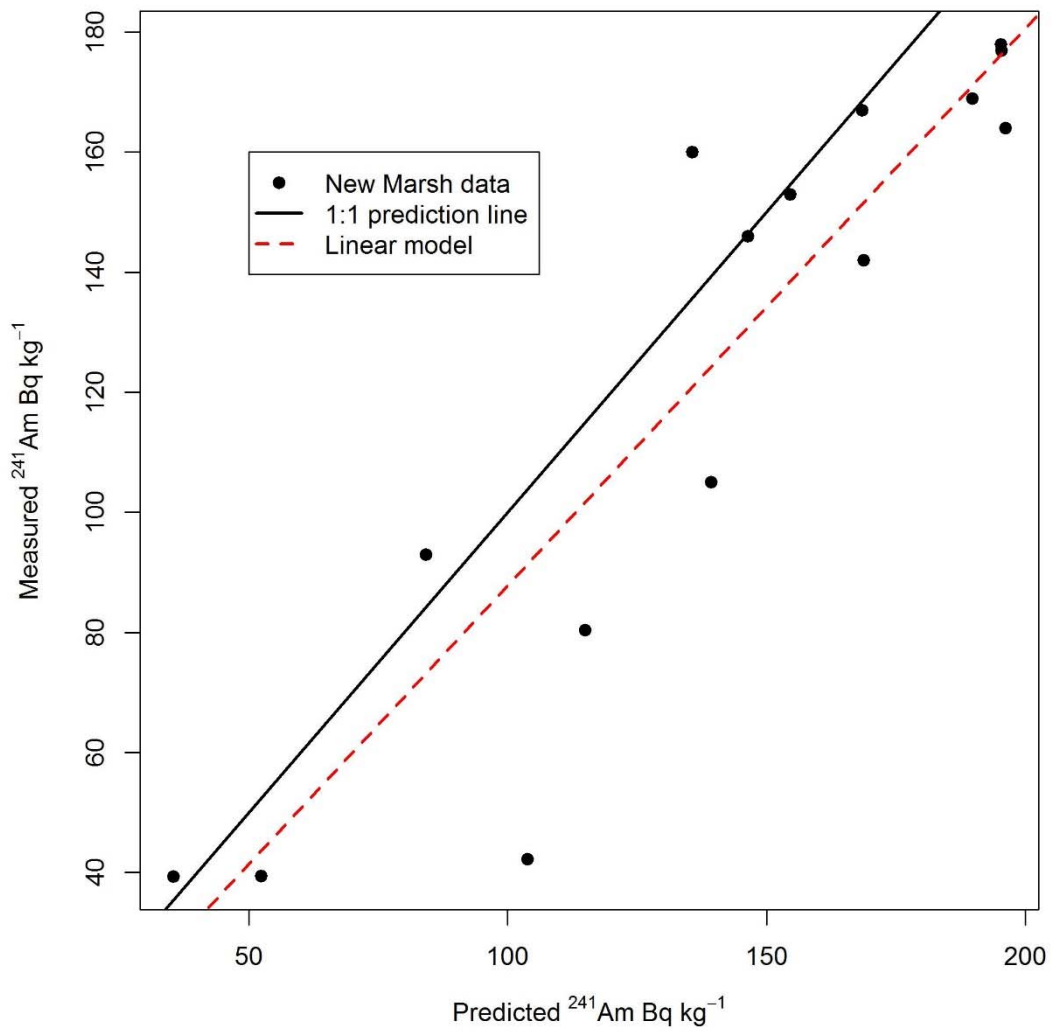


Figure A3.5 Comparison of estimated activity for ²⁴¹Am in the new marsh (x axis) and measured activity (y axis) a linear model is fitted to these data to show the general trend in comparison to the 1:1 prediction line.

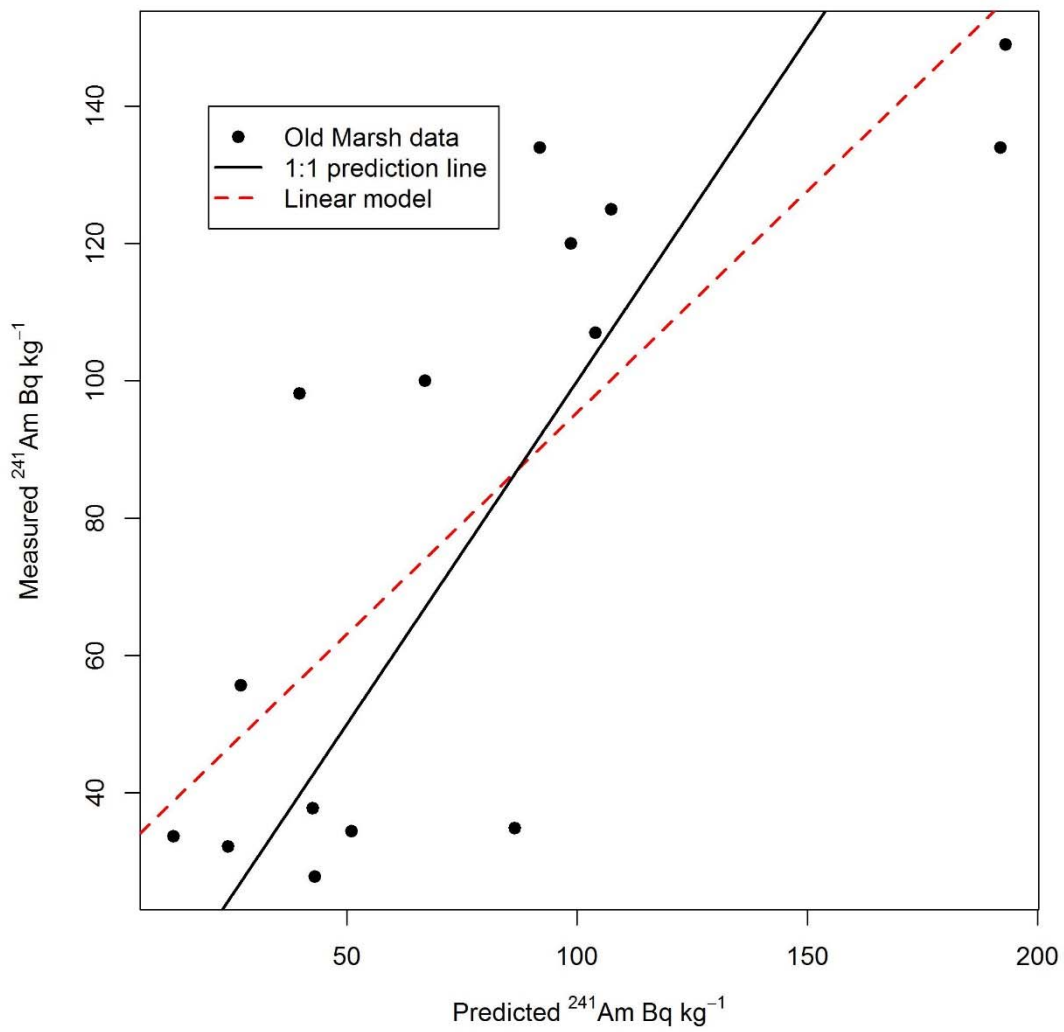


Figure A3.6 Comparison of estimated activity for ²⁴¹Am in the old marsh (x axis) and measured activity (y axis) a linear model is fitted to these data to show the general trend in comparison to the 1:1 prediction line.

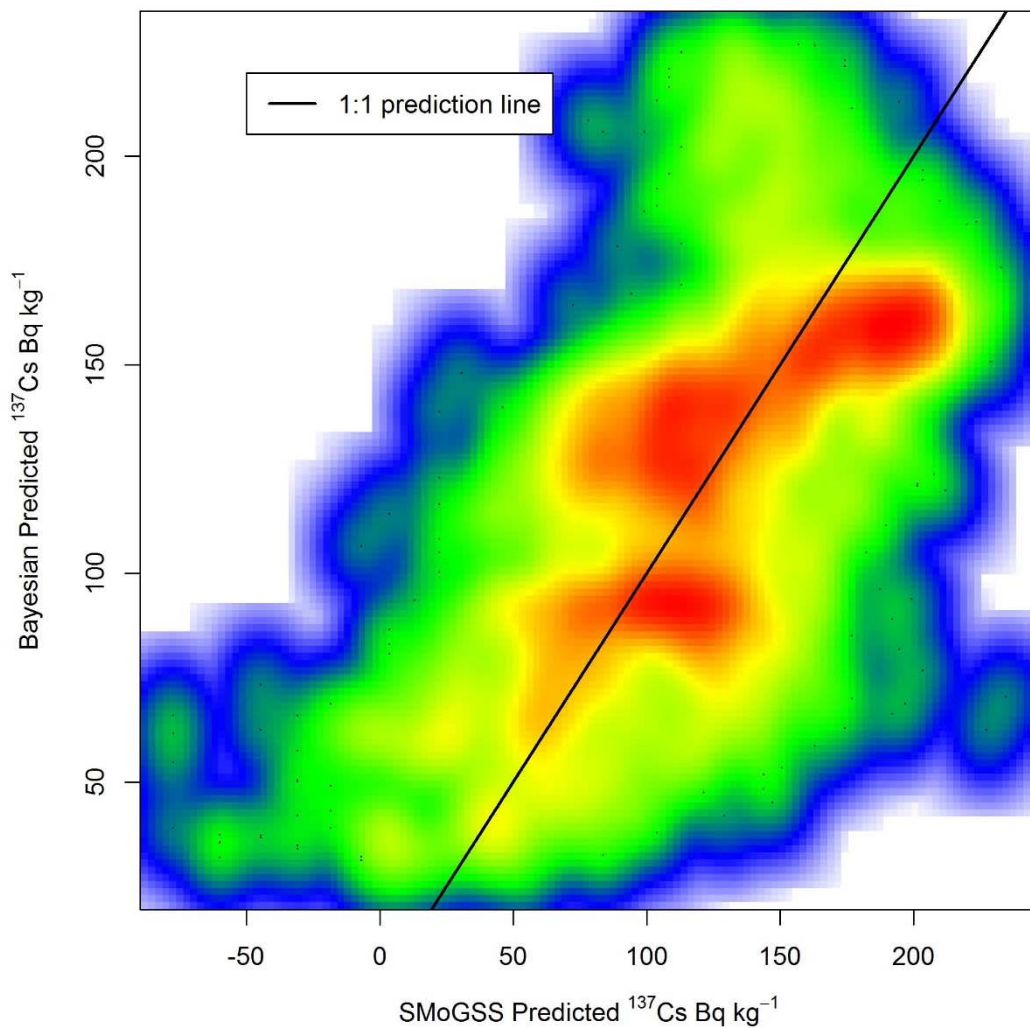


Figure A3.7 Plot of the old marsh MoGSS ^{137}Cs activity concentration data against the ^{137}Cs predicted by the spatial statistics model fitted to the sediment scrape data. The colour ramp from red to blue indicates the number of points at that location.

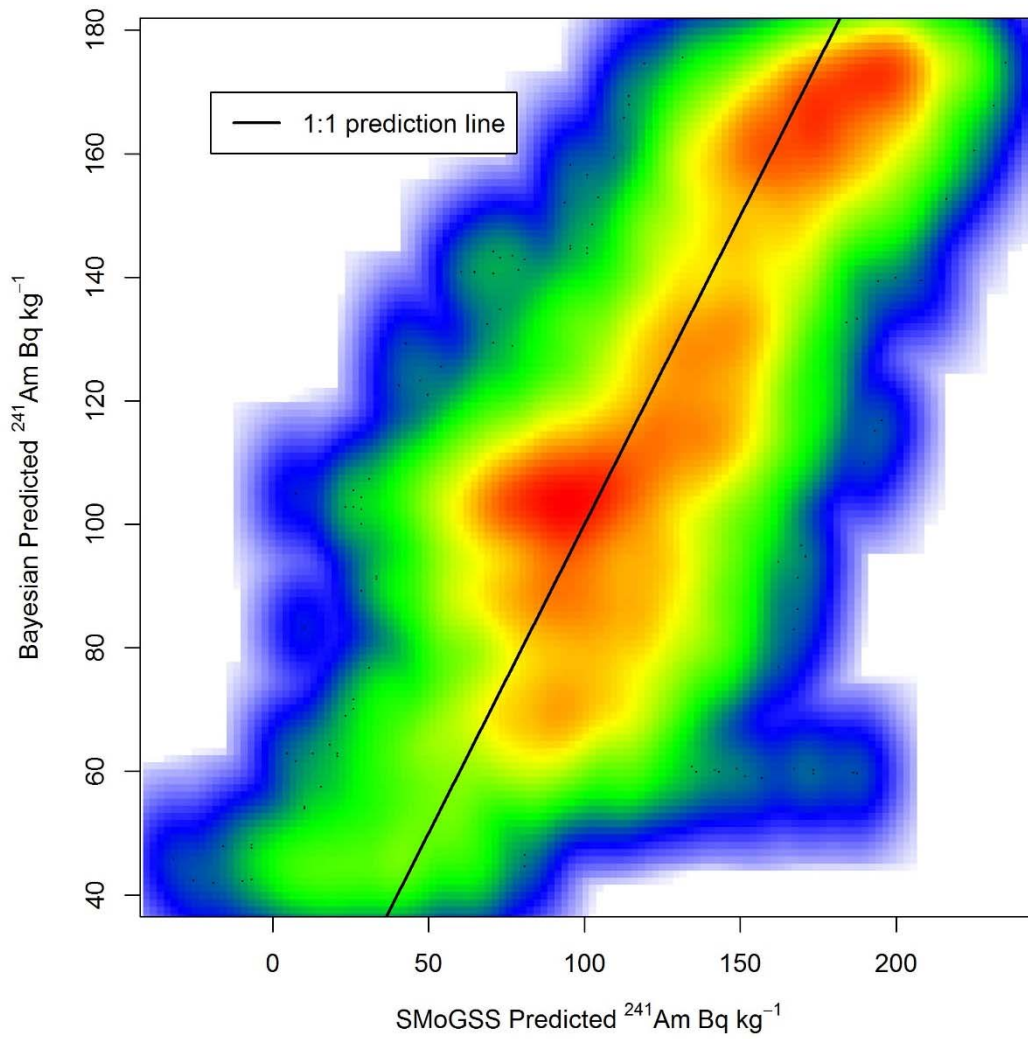


Figure A3.8 Plot of the new marsh MoGSS ^{241}Am activity concentration data against the ^{137}Cs predicted by the spatial statistics model fitted to the sediment scrape data. The colour ramp from red to blue indicates the number of points at that location.

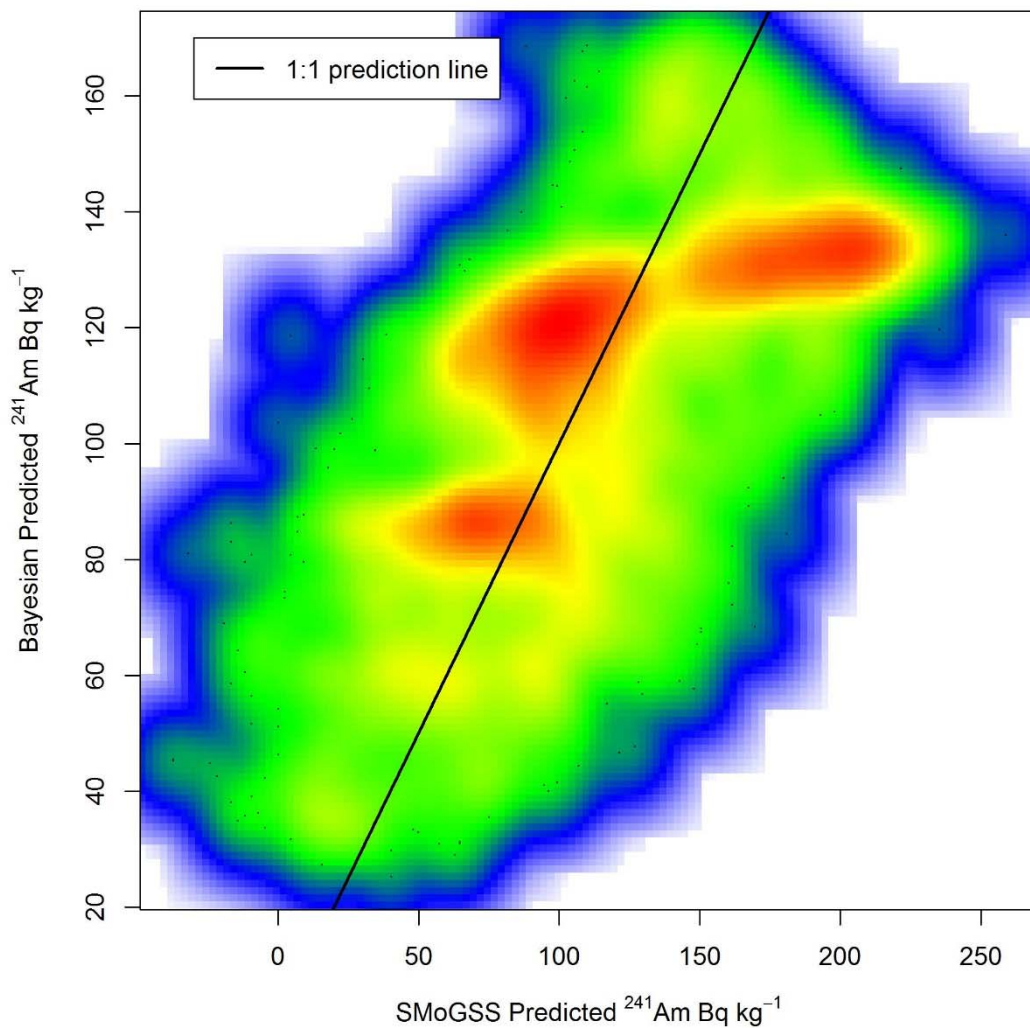


Figure A3.9 Plot of the old marsh MoGSS ²⁴¹Am activity concentration data against the ¹³⁷Cs predicted by the spatial statistics model fitted to the sediment scrape data. The colour ramp from red to blue indicates the number of points at that location.

References

- Adam, P. (1993) Saltmarsh ecology. Cambridge University Press.
doi:10.1017/CBO9780511565328
- Adams, P.N., Inman, D.L., Lovering, J.L. (2011). Effects of climate change and wave direction on longshore sediment transport patterns in Southern California. *Clim. Change* 109, 211–228.
doi:10.1007/s10584-011-0317-0
- Aldridge, J.N., Kershaw, P., Brown, J., McCubbin, D., Leonard, K.S., Young, E.F. (2003) Transport of plutonium ($^{239/240}\text{Pu}$) and caesium (^{137}Cs) in the Irish Sea: comparison between observations and results from sediment and contaminant transport modelling. *Cont. Shelf Res.* 23, 869–899. doi:10.1016/S0278-4343(03)00047-5
- Allen, J.R., Duffy, M. (1998) Temporal and spatial depositional patterns in the Severn Estuary, southwestern Britain: intertidal studies at spring–neap and seasonal scales, 1991–1993. *Mar. Geol.* 146, 147–171. doi:10.1016/S0025-3227(97)00124-2
- Allen, J.R.L., Pye, K. (1992) Coastal Saltmarshes: their nature and importance, in: Allen, J.R., Pye, K. (Eds.), *Saltmarshes: Morphodynamics, Conservation, and Engineering Significance*. Cambridge University Press, Cambridge, pp. 1–18.
- Assinder, D., Mudge, S., Bourne, G. (1997) Radiological assessment of the ribble estuary—I. Distribution of radionuclides in surface sediments. *J. Environ. Radioact.* 36, 1–19.
doi:10.1016/S0265-931X(96)00073-2
- Aston, S.R., Stanners, D.A. (1982) The transport to and deposition of americium in intertidal sediments of the ravenlass estuary and its relationship to plutonium. *Environ. Pollut. Ser. B, Chem. Phys.* 3, 1–9. doi:10.1016/0143-148X(82)90038-6
- Atkin, P.A. (2000) Sediment transport mechanisms in the Ribble Estuary using Airborne Remote Sensing. Thesis, University of Stirling.
- Attanasio, A., Pasini, A., Triacca, U. (2013) Granger Causality Analyses for Climatic Attribution. *Atmos. Clim. Sci.* 3, 515–522. doi:10.4236/acs.2013.34054
- Attanasio, A., Triacca, U. (2011) Detecting human influence on climate using neural networks based Granger causality. *Theor. Appl. Climatol.* 103, 103–107. doi:10.1007/s00704-010-0285-8
- Azevedo, I.C., Bordalo, A.A., Duarte, P.M. (2010) Influence of river discharge patterns on the hydrodynamics and potential contaminant dispersion in the Douro estuary (Portugal). *Water Res.* 44, 3133–3146. doi:10.1016/j.watres.2010.03.011
- Azhikodan, G., Yokoyama, K. (2015) Temporal and Spatial Variation of Mixing and Movement of Suspended Sediment in the Macrotidal Chikugo River Estuary. *J. Coast. Res.* 313, 680–689.
doi:10.2112/JCOASTRES-D-14-00097.1
- Bader, J., Mesquita, M.D.S., Hodges, K.I., Keenlyside, N., Østerhus, S., Miles, M. (2011) A review on Northern Hemisphere sea-ice, storminess and the North Atlantic Oscillation: Observations and projected changes. *Atmos. Res.* 101, 809–834.
doi:10.1016/j.atmosres.2011.04.007
- Barker, T. (2007) *Climate Change 2007 : An Assessment of the Intergovernmental Panel on Climate Change. Change, Synthesis Report 446*, 12–17. doi:10.1256/004316502320517344
- Beaumont, N.J., Jones, L., Garbutt, a., Hansom, J.D., Toberman, M. (2014) The value of carbon sequestration and storage in coastal habitats. *Estuar. Coast. Shelf Sci.* 137, 32–40.
doi:10.1016/j.ecss.2013.11.022

- Ben-Dor, E., Patkin, K., Banin, A., Karnieli, A. (2002) Mapping of several soil properties using DAIS-7915 hyperspectral scanner data - a case study over clayey soils in Israel. *Int. J. Remote Sens.* 23, 1043–1062. doi:10.1080/01431160010006962
- Bengtsson, L., Hodges, K.I., Roeckner, E. (2006) Storm Tracks and Climate Change. *J. Clim.* 19, 3518–3543. doi:10.1175/JCLI3815.1
- Blott, S.J., Pye, K., van der Wal, D., Neal, A. (2006) Long-term morphological change and its causes in the Mersey Estuary, NW England. *Geomorphology* 81, 185–206. doi:10.1016/j.geomorph.2006.04.008
- Boerema, A., Meire, P. (2017) Management for estuarine ecosystem services: A review. *Ecol. Eng.* 98, 172–182. doi:10.1016/j.ecoleng.2016.10.051
- Bolívar, J.P., García-Tenorio, R., Mas, J.L., Vaca, F. (2002) Radioactive impact in sediments from an estuarine system affected by industrial wastes releases. *Environ. Int.* 27, 639–645. doi:10.1016/S0160-4120(01)00123-4
- Bonnett, P.J.P., Cambray, R.S. (1991) The record of deposition of radionuclides in the sediments of Ponsoby Tarn, Cumbria. *Hydrobiologia* 214, 63–70. doi:10.1007/BF00050933
- Bossler, J.D., Campbell, J.B., McMaster, R.B., Rizos, C. (2010) *Manual of geospatial science and technology*. CRC Press/Taylor & Francis.
- Bradley, S., Clapham, P. (1998) Contemporary flux of radionuclides to contaminated saltmarshes in the Esk estuary, Cumbria. *Water. Air. Soil Pollut.* 175–184. doi:10.1023/A1019816808362
- Brooks, S.M., Spencer, T., Christie, E.K. (2017) Storm impacts and shoreline recovery: Mechanisms and controls in the southern North Sea. *Geomorphology* 283, 48–60. doi:10.1016/j.geomorph.2017.01.007
- Brooks, S.M., Spencer, T., McIvor, A., Möller, I. (2016) Reconstructing and understanding the impacts of storms and surges, southern North Sea. *Earth Surf. Process. Landforms* 41, 855–864. doi:10.1002/esp.3905
- Brown, J. (1997) *The behaviour of radionuclides in the Ribble Estuary, NW England*. Thesis, University of Reading.
- Brown, J.E., McDonald, P., Parker, A., Rae, J.E. (1999) The vertical distribution of radionuclides in a Ribble Estuary saltmarsh: transport and deposition of radionuclides. *J. Environ. Radioact.* 43, 259–275. doi:10.1016/S0265-931X(98)00041-1
- Brown, J.M., Ciavola, P., Masselink, G., McCall, R., Plater, A.J. (2016) Preface: Monitoring and modelling to guide coastal adaptation to extreme storm events in a changing climate. *Nat. Hazards Earth Syst. Sci.* 16, 463–467. doi:10.5194/nhess-16-463-2016
- Brown, J.M., Souza, A.J., Wolf, J. (2010) An 11-year validation of wave-surge modelling in the Irish Sea, using a nested POLCOMS–WAM modelling system. *Ocean Model.* 33, 118–128. doi:10.1016/j.ocemod.2009.12.006
- Brown, L.E., Chen, C.Y., Voytek, M.A., Amirbahman, A. (2015) The effect of sediment mixing on mercury dynamics in two intertidal mudflats at Great Bay Estuary, New Hampshire, USA. *Mar. Chem.* 177, 731–741. doi:10.1016/j.marchem.2015.10.011
- Browne, J.P. (2017) Long-Term Erosional Trends Along Channelized Salt Marsh Edges. *Estuaries and Coasts* 40, 1566–1575. doi:10.1007/s12237-017-0245-y

- Brunier, G., Fleury, J., Anthony, E.J., Gardel, A., Dussouillez, P. (2016) Close-range airborne Structure-from-Motion Photogrammetry for high-resolution beach morphometric surveys: Examples from an embayed rotating beach. *Geomorphology* 261, 76–88. doi:10.1016/j.geomorph.2016.02.025
- Buyukyildiz, M., Kumcu, S.Y. (2017) An Estimation of the Suspended Sediment Load Using Adaptive Network Based Fuzzy Inference System, Support Vector Machine and Artificial Neural Network Models. *Water Resour. Manag.* 31, 1343–1359. doi:10.1007/s11269-017-1581-1
- Cefas (2005) Radioactivity in food and the environment, 2005, Radioactivity in food and the environment 11.
- Chen, L., Yang, Y., Chen, J., Gao, S., Qi, S., Sun, C., Shen, Z. (2017) Spatial-temporal variability and transportation mechanism of polychlorinated biphenyls in the Yangtze River Estuary. *Sci. Total Environ.* 598, 12–20. doi:10.1016/j.scitotenv.2017.04.069
- Choi, K., Kim, D.H. (2016) Morphologic and hydrodynamic controls on the occurrence of tidal bundles in an open-coast macrotidal environment, northern Gyeonggi Bay, west coast of Korea. *Sediment. Geol.* 339, 68–82. doi:10.1016/j.sedgeo.2016.04.008
- Clifton, J., McDonald, P., Plater, A., Oldfield, F. (1999) Derivation of a Grain-size Proxy to Aid the Modelling and Prediction of Radionuclide Activity in Salt Marshes and Mud Flats of the Eastern Irish Sea. *Estuar. Coast. Shelf Sci.* 48, 511–518. doi:10.1006/ecss.1998.0461
- Coles, S.M. (1979) Benthic microalgal populations on intertidal sediments and their role as precursors to salt marsh development, in: Jeffries, R.L., Davy, A.J. (Eds.), *Ecological Processes in Coastal Environments*. Blackwell scientific publications, Oxford, pp. 25–42.
- Coughlan, M., Wheeler, A.J., Dorschel, B., Lordan, C., Boer, W., Gaever, P. V., Haas, H. D., Mörz, T. (2015) Record of anthropogenic impact on the Western Irish Sea mud belt. *Anthropocene* 9, 56–69. doi:10.1016/j.ancene.2015.06.001
- De Jonge, V., de Boer, W., De Jong, D., Brauer, V. (2012) Long-term mean annual microphytobenthos chlorophyll a variation correlates with air temperature. *Mar. Ecol. Prog. Ser.* 468, 43–56. doi:10.3354/meps09954
- DEFRA, 2012. Coastal Change Pathfinder Review Final Report 347.
- Deronde, B., Houthuys, R., Debruyne, W., Franssaer, D., Lancker, V. Van, Henriët, J.P. (2006) Use of Airborne Hyperspectral Data and Laserscan Data to Study Beach Morphodynamics along the Belgian Coast. *J. Coast. Res.* 225, 1108–1117. doi:10.2112/04-0264.1
- Deronde, B., Houthuys, R., J.P. Henriët, Lancker, V., Van (2008) Monitoring of the sediment dynamics along a sandy shoreline by means of airborne hyperspectral remote sensing and LIDAR: a case study in Belgium. *Earth Surf. ...* 294, 280–294. doi:10.1002/esp
- Desideri, D., Meli, M., Roselli, C., Testa, C., Degetto, S. (2001) Speciation of natural and anthropogenic radionuclides in different sea sediment samples. *Journal of Radioanalytical and Nuclear Chemistry.* 248, 3, 727–733.
- Dissanayake, P., Brown, J., Wisse, P., Karunarathna, H. (2015) Effects of storm clustering on beach/dune evolution. *Mar. Geol.* 370, 63–75. doi:10.1016/j.margeo.2015.10.010
- Doody, J.P. (2008) *Saltmarsh Conservation, Management and Restoration, Coastal Systems and Continental Margins*. Springer Netherlands, Dordrecht. doi:10.1007/978-1-4020-5748-9
- EPA. (2001) *Methods for Collection, Storage and Manipulation of Sediments for Chemical and Toxicological Analyses: Technical Manual*. EPA 823-B-01-002. U.S. Environ. Prot. Agency, Off. Water, Washington, DC. 1–208.

- Esri. (2012). Empirical Bayesian Kriging. last accessed 08/01/2017: <http://www.esri.com/news/arcuser/1012/empirical-byesian-kriging.html>
- Esteves, L.S., Williams, J.J., Brown, J.M. (2011) Looking for evidence of climate change impacts in the eastern Irish Sea. *Nat. Hazards Earth Syst. Sci.* 11, 1641–1656. doi:10.5194/nhess-11-1641-2011
- Falconer, R., Lin, B. (1997) Three-dimensional modelling of water quality in the Humber Estuary. *Water Res.* 31, 1092–1102. doi:10.1016/S0043-1354(96)00333-8
- Finegan, P., Vintró, L.L., Mitchell, P.I., Boust, D., Gouzy, A., Kershaw, P.J., Lucey, J. a. (2009) Accumulation, solid partitioning and remobilisation of ⁹⁹Tc in subtidal and intertidal sediments in the Irish Sea. *Cont. Shelf Res.* 29, 1995–2010. doi:10.1016/j.csr.2009.02.005
- Friend, P.L., Ciavola, P., Cappucci, S., Santos, R. (2003) Bio-dependent bed parameters as a proxy tool for sediment stability in mixed habitat intertidal areas. *Cont. Shelf Res.* 23, 1899–1917. doi:10.1016/j.csr.2002.12.001
- Gleizon, P., McDonald, P. (2010) Modelling radioactivity in the Irish Sea: from discharge to dose. *J. Environ. Radioact.* 101, 403–13. doi:10.1016/j.jenvrad.2010.02.013
- Gleizon, P., Punt, A., Lyons, M. (2003) Modelling hydrodynamics and sediment flux within a macrotidal estuary: problems and solutions. *Sci. Total Environ.* 314–316, 589–597. doi:doi.org/10.1016/S0048-9697(03)00075-5
- Goshawk, J. A, Clarke, S., Smith, C.N., McDonald, P. (2003) MEAD (part I)--a mathematical model of the long-term dispersion of radioactivity in shelf sea environments. *J. Environ. Radioact.* 68, 115–35. doi:10.1016/S0265-931X(03)00040-7
- Gosnell, K., Balcom, P., Ortiz, V., DiMento, B., Schartup, A., Greene, R., Mason, R. (2016). Seasonal Cycling and Transport of Mercury and Methylmercury in the Turbidity Maximum of the Delaware Estuary. *Aquat. Geochemistry* 22, 313–336. doi:10.1007/s10498-015-9283-x
- Greeves, C.Z., Pope, V.D., Stratton, R.A., Martin, G.M. (2007) Representation of Northern Hemisphere winter storm tracks in climate models. *Clim. Dyn.* 28, 683–702. doi:10.1007/s00382-006-0205-x
- Gutiérrez, O., Panario, D., Nagy, G.J., Bidegain, M., Montes, C. (2016) Climate teleconnections and indicators of coastal systems response. *Ocean Coast. Manag.* 122, 64–76. doi:10.1016/j.ocecoaman.2016.01.009
- Harvey, M.M., Hansom, J.D., MacKenzie, A. B. (2007) Constraints on the use of anthropogenic radionuclide-derived chronologies for saltmarsh sediments. *J. Environ. Radioact.* 95, 126–148. doi:10.1016/j.jenvrad.2007.02.005
- Holden, V.J.C., Worsley, A.T., Booth, C.A., Lymbery, G. (2011) Characterisation and sediment–source linkages of intertidal sediment of the UK’s north Sefton Coast using magnetic and textural properties: findings and limitations. *Ocean Dyn.* 61, 2157–2179. doi:10.1007/s10236-011-0448-x
- Horrill, A.D. (1983) The levels and point-to-point variation of the radionuclide burden in a cumbrian saltmarsh environment, in: Coughtrey, P.. (Ed.), *Ecological Aspects of Radionuclide Release*. Blackwell scientific publications, pp. 199–215.
- Hu, Z., Yao, P., Van der Wal, D., Bouma, T.J. (2017) Patterns and drivers of daily bed-level dynamics on two tidal flats with contrasting wave exposure. *Sci. Rep.* 7, 7088. doi:10.1038/s41598-017-07515-y
- Hunt, G.J. (1997) Radiation Doses to Critical Groups Since the Early 1950’s Due to Discharges of Liquid Radioactive Waste from Sellafield. *Health Phys.* 72.

- Hunt, J., Leonard, K., Hughes, L. (2013) Artificial radionuclides in the Irish Sea from Sellafield: remobilisation revisited. *J. Radiol. Prot.* 33, 261–79. doi:10.1088/0952-4746/33/2/261
- Inoue, M., Uemura, H., Kofuji, H., Fujimoto, K., Takata, H., Shirotani, Y., Kudo, N., Nagao, S. (2017) Spatial variation in low-level ^{134}Cs in the coastal sediments off central Honshu in the Sea of Japan: implications for delivery, migration, and redistribution patterns. *J. Oceanogr.* 73, 571–584. doi:10.1007/s10872-017-0437-x
- ISO 14688-1:2002 - Geotechnical investigation and testing -- Identification and classification of soil -- Part 1: Identification and description [WWW Document], 2013. http://www.iso.org/iso/iso_catalogue/catalogue_tc/catalogue_detail.htm?csnumber=25260 accessed 29/01/17.
- Jaud, M., Grasso, F., Le Dantec, N., Verney, R., Delacourt, C., Ammann, J., Deloffre, J., Grandjean, P. (2016) Potential of UAVs for Monitoring Mudflat Morphodynamics (Application to the Seine Estuary, France). *ISPRS Int. J. Geo-Information* 5, 50. doi:10.3390/ijgi5040050
- Jickells, T.D., Rae, J.E. (1997) Biogeochemistry of intertidal sediments. Cambridge University Press, Cambridge.
- Kang, J., Larsson, R. (2014) What is the link between temperature and carbon dioxide levels? A Granger causality analysis based on ice core data. *Theor Appl Clim.* 116, 537–548. doi:10.1007/s00704-013-0960-7
- Keim, B.D., Muller, R.A., Stone, G.W. (2004) Spatial and temporal variability of coastal storms in the North Atlantic Basin. *Mar. Geol.* 210, 7–15. doi:10.1016/j.margeo.2003.12.006
- Kershaw, P.J., Denoon, D.C., Woodhead, D.S. (1999a) Observations on the redistribution of plutonium and americium in the Irish Sea sediments, 1978 to 1996: concentrations and inventories. *J. Environ. Radioact.* 44, 191–221. doi:10.1016/S0265-931X(98)00134-9
- Kershaw, P.J., McCubbin, D., Leonard, K.S. (1999b) Continuing contamination of north Atlantic and Arctic waters by Sellafield radionuclides. *Sci. Total Environ.* 237–238, 119–132. doi:10.1016/S0048-9697(99)00129-1
- Knoll, G.F. (2010) Radiation Detection and Measurement, Phoenix Usa.
- Lagos-Avid, M.P., Bonilla, C.A. (2017) Predicting the particle size distribution of eroded sediment using artificial neural networks. *Sci. Total Environ.* 581–582, 833–839. doi:10.1016/j.scitotenv.2017.01.020
- Lansard, B., Grenz, C., Charmasson, S., Schaaff, E., Pinazo, C. (2005) Potential plutonium remobilisation linked to marine sediment resuspension: First estimates based on flume experiments. doi:10.1016/j.seares.2005.08.003
- Lee, B.J., Toorman, E., Molz, F.J., Wang, J. (2011) A two-class population balance equation yielding bimodal flocculation of marine or estuarine sediments. *Water Res.* 45, 2131–2145. doi:10.1016/j.watres.2010.12.028
- Leonard, K., Donaszi-Ivanov, A., Dewar, A., Ly, V., Bailey, T. (2017) Monitoring of caesium-137 in surface seawater and seafood in both the Irish and North Seas: trends and observations. *J. Radioanal. Nucl. Chem.* 311, 1117–1125. doi:10.1007/s10967-016-5071-3
- Leonard, K.S., McCubbin, D., Blowers, P., Taylor, B.R. (1999) Dissolved plutonium and americium in surface waters of the Irish Sea, 1973–1996. *J. Environ. Radioact.* 44, 129–158. doi:10.1016/S0265-931X(98)00132-5

- Lindahl, P., Worsfold, P., Keith-Roach, M., Andersen, M.B., Kershaw, P., Leonard, K., Choi, M.-S., Boust, D., Lesueur, P. (2011) Temporal record of Pu isotopes in inter-tidal sediments from the northeastern Irish Sea. *Sci. Total Environ.* 409, 5020–5025. doi:10.1016/j.scitotenv.2011.08.019
- Luo, J., Li, M., Sun, Z., O'Connor, B.A. (2013) Numerical modelling of hydrodynamics and sand transport in the tide-dominated coastal-to-estuarine region. *Mar. Geol.* 342, 14–27. doi:10.1016/j.margeo.2013.06.004
- Luo, J., Li, M., Sun, Z., Wang, W. (2015) Impacts of sea level rise on morphodynamics in Liverpool Bay. *Proc. Inst. Civ. Eng. - Marit. Eng.* 168, 3–19. doi:10.1680/maen.14.00012
- Lyons, M. (1997) The Dynamics of Suspended Sediment Transport in the Ribble Estuary. *Water, Air, Soil Pollut.* 99, 141–148. doi:10.1023/A:1018388517409
- M. Fox, W., S. Johnson, M., Jones, S.R., Leah, R.T., Coppelstone, D. (1999) The use of sediment cores from stable and developing salt marshes to reconstruct historical contamination profiles in the Mersey Estuary, UK. *Mar. Environ. Res.* 47, 311–329. doi:10.1016/S0141-1136(98)00123-8
- Mackenzie, A.B., Scott, R.D. (1993) Sellafield waste radionuclides in Irish sea intertidal and salt marsh sediments. *Environ. Geochem. Health* 15, 173–84. doi:10.1007/BF02627835
- MacKenzie, A.B., Cook, G.T., McDonald, P. (1999) Radionuclide distributions and particle size associations in Irish Sea surface sediments: implications for actinide dispersion. *J. Environ. Radioact.* 44, 275–296. doi:10.1016/S0265-931X(98)00137-4
- Mackenzie, A.B., Scott, R.D. (1993) Sellafield waste radionuclides in Irish sea intertidal and salt marsh sediments. *Environ. Geochem. Health* 15, 173–84. doi:10.1007/BF02627835
- Manning, A. j., Baugh, J. V., Soulsby, R.L., Spearman, J.R., Whitehouse, R.J.S. (2011) Cohesive Sediment Flocculation and the Application to Settling Flux Modelling, in: *Sediment Transport*. InTech. doi:10.5772/16055
- Marsden, O.J., Abrahamsen, L., Bryan, N.D., Philip Day, J., Keith Fifield, L., Gent, C., Goodall, P.S., Morris, K., Livens, F.R. (2006) Transport and accumulation of actinide elements in the near-shore environment: field and modelling studies. *Sedimentology* 53, 237–248. doi:10.1111/j.1365-3091.2005.00761.x
- Masselink, G., Russell, P. (2013) Impacts of climate change on coastal erosion. *MCCIP Sci. Rev.* 71–86. doi:10.14465/2013.arc09.071-086
- McDonald, P., Vives i Batlle, J., Bousher, A., Whittall, A., Chambers, N. (2001) The availability of plutonium and americium in Irish Sea sediments for re-dissolution. *Sci. Total Environ.* 267, 109–123. doi:10.1016/S0048-9697(00)00771-3
- Merriam-Webster. (2017) Hydrodynamics | Definition of Hydrodynamics [WWW Document]. Merriam-Webster. URL <https://www.merriam-webster.com/dictionary/hydrodynamics> (accessed 10.22.17).
- Mölter, T., Schindler, D., Albrecht, A., Kohnle, U. (2016) Review on the Projections of Future Storminess over the North Atlantic European Region. *Atmosphere (Basel)*. 7, 60. doi:10.3390/atmos7040060
- Montreuil, A.-L., Levoy, F., Bretel, P., Anthony, E.J. (2014) Morphological diversity and complex sediment recirculation on the ebb delta of a macrotidal inlet (Normandy, France): A multiple LiDAR dataset approach. *Geomorphology* 219, 114–125. doi:10.1016/j.geomorph.2014.05.008

- Morelli, G., Gasparon, M. (2015) Depositional variability of estuarine intertidal sediments and implications for metal distribution: An example from Moreton Bay (Australia). *Cont. Shelf Res.* 108, 41–54. doi:10.1016/j.csr.2015.07.017
- Morris, K., Butterworth, J.C., Livens, F.R. (2000) Evidence for the Remobilization of Sellafield Waste Radionuclides in an Intertidal Salt Marsh, West Cumbria, U.K. *Estuar. Coast. Shelf Sci.* 51, 613–625. doi:10.1006/ecss.2000.0705
- Mudge, S., Assinder, D., Bourne, G. (1997) Radiological assessment of the Ribble Estuary—III. Redistribution of radionuclides. *J. Environ. Radioact.* 36, 43–67. doi:10.1016/S0265-931X(96)00075-6
- National Oceanic and Atmospheric Administration (2017) Glossary of Terms for Detailed Wave Information [WWW Document]. URL <http://www.ndbc.noaa.gov/waveobs.shtml> (accessed 10.20.17).
- Oh, J.S., Warwick, P.E., Croudace, I.W. (2009) Spatial distribution of (241)Am, (137)Cs, (238)Pu, (239,240)Pu and (241)Pu over 17 year periods in the Ravenglass saltmarsh, Cumbria, UK. *Appl. Radiat. Isot.* 67, 1484–92. doi:10.1016/j.apradiso.2009.02.048
- Ord, J.K., Getis, A. (2010) Local Spatial Autocorrelation Statistics: Distributional Issues and an Application. *Geogr. Anal.* 27, 286–306. doi:10.1111/j.1538-4632.1995.tb00912.x
- Otosaka, S. (2017) Processes affecting long-term changes in 137Cs concentration in surface sediments off Fukushima. *J. Oceanogr.* 73, 559–570. doi:10.1007/s10872-017-0421-5
- Ouyang, Y., Higman, J., Campbell, D., Davis, J. (2003) Three-dimensional kriging analysis of sediment mercury distribution : a case study. *J. of the American Water Resources Association (JAWRA)*, 39(3):689-702.
- Pamba, S., Shaghude, Y.W., Muzuka, A.N.N. (2016) Hydrodynamic Modelling on Transport, Dispersion and Deposition of Suspended Particulate Matter in Pangani Estuary, Tanzania, in: *Estuaries: A Lifeline of Ecosystem Services in the Western Indian Ocean*. Springer, pp. 141–160. doi:10.1007/978-3-319-25370-1_9
- Periáñez, R. (2005) *Modelling the Dispersion of Radionuclides in the Marine Environment, Modelling the Dispersion of Radionuclides in the Marine Environment: An Introduction*. Springer Berlin Heidelberg, Berlin, Heidelberg. doi:10.1007/b138979
- Periáñez, R. (2003) Kinetic modelling of the dispersion of plutonium in the eastern Irish Sea: two approaches. *J. Mar. Syst.* 38, 259–275. doi:10.1016/S0924-7963(02)00242-7
- Pethick, J.S. (1992) Saltmarsh Geomorphology, in: Allen, J.R., Pye, K. (Eds.), *Saltmarshes: Morphodynamics, Conservation and Engineering Significance*. Cambridge University Press, New York, pp. 41–62.
- Pieterse, A., Puleo, J.A., McKenna, T.E., Figlus, J. (2017) In situ measurements of shear stress, erosion and deposition in man-made tidal channels within a tidal saltmarsh. *Estuar. Coast. Shelf Sci.* 192, 29–41. doi:10.1016/j.ecss.2017.04.028
- Pye, K., Blott, S.J. (2016) Assessment of beach and dune erosion and accretion using LiDAR: Impact of the stormy 2013–14 winter and longer term trends on the Sefton Coast, UK. *Geomorphology* 266, 146–167. doi:10.1016/j.geomorph.2016.05.011
- Pye, K., Blott, S.J. (2014) The geomorphology of UK estuaries: The role of geological controls, antecedent conditions and human activities. *Estuar. Coast. Shelf Sci.* 150, 196–214. doi:10.1016/j.ecss.2014.05.014

- Pye, K., Blott, S.J. (2008) Decadal-scale variation in dune erosion and accretion rates: An investigation of the significance of changing storm tide frequency and magnitude on the Sefton coast, UK. *Geomorphology* 102, 652–666. doi:10.1016/j.geomorph.2008.06.011
- Rahman, R., Plater, A.J., Nolan, P.J., Mauz, B., Appleby, P.G. (2013) Potential health risks from radioactive contamination of saltmarshes in NW England. *J. Environ. Radioact.* 119, 55–62. doi:10.1016/j.jenvrad.2011.11.011
- Rainey, M. (1999) Airborne remote sensing of estuarine intertidal radionuclide concentrations. Thesis, University of Stirling.
- Rainey, M., Tyler, A.N., Gilvear, D., Bryant, R., McDonald, P. (2003) Mapping intertidal estuarine sediment grain size distributions through airborne remote sensing. *Remote Sens. Environ.* 86, 480–490. doi:10.1016/S0034-4257(03)00126-3
- Rainey, M., Tyler, A.N., Bryant, R. (1999) Mapping intertidal radionuclide concentrations through airborne remote sensing- A comparison of techniques. *Exhib. 4 th/21 st ...* 345–352.
- Rainford, W.M. (1997) *The Sustainability of Sand Winning near Horse Bank in the Ribble Estuary.* Liverpool.
- Rangel-Buitrago, N.G., Thomas, T., Phillips, M.R., Anfuso, G., Williams, A.T. (2016) Wave Climate, Storminess, and Northern Hemisphere Teleconnection Patterns Influences: The Outer Bristol Channel, South Wales, U.K. *J. Coast. Res.* 322, 1262–1276. doi:10.2112/JCOASTRES-D-15-00166.1
- Ray, D. (2013) *Accumulation and Mobility of Radionuclides in the Sellafield Near-Shore.* Thesis, University of manchester.
- Revelle, W. (2016) Package “psych.” . accessed: 12/12/2016. <https://cran.r-project.org/web/packages/psych/psych.pdf>
- Ridgway, J. (2001) Distinguishing between natural and anthropogenic sources of metals entering the Irish sea : final report / J. Ridgway ... [et al.]. British Geological Survey, Nottingham.
- Robins, P.E., Skov, M.W., Lewis, M.J., Giménez, L., Davies, A.G., Malham, S.K., Neill, S.P., McDonald, J.E., Whitton, T.A., Jackson, S.E., Jago, C.F. (2016) Impact of climate change on UK estuaries: A review of past trends and potential projections. *Estuar. Coast. Shelf Sci.* 169, 119–135. doi:10.1016/j.ecss.2015.12.016
- Santos, P., Castel, J., Souzasantos, L. (1997) Spatial distribution and dynamics of microphytobenthos biomass in the Gironde estuary (France). *Ocean. Acta* 549–556.
- Schoellhamer, D.H., Mumley, T.E., Leatherbarrow, J.E. (2007) Suspended sediment and sediment-associated contaminants in San Francisco Bay. *Environ. Res.* 105, 119–131. doi:10.1016/j.envres.2007.02.002
- Schuerch, M., Vafeidis, A., Slawig, T., Temmerman, S. (2013) Modeling the influence of changing storm patterns on the ability of a salt marsh to keep pace with sea level rise. *J. Geophys. Res. Earth Surf.* 118, 84–96. doi:10.1029/2012JF002471
- Schumacher, B. (1990) A comparison of soil sample homogenisation techniques. USEPA. Office of reserch and development, 1-40
- Sierra, J.P., Casas-Prat, M. (2014) Analysis of potential impacts on coastal areas due to changes in wave conditions. *Clim. Change* 124, 861–876. doi:10.1007/s10584-014-1120-5

- Smith, M.J., Goodchild, M.F., Longley, P.A. (2008) *Geospatial Analysis: A Comprehensive Guide to Principles, Techniques, and Software Tools*, Second Edition - by Michael J. de Smith, Michael F. Goodchild, and Paul A. Longley, 2nd ed. Blackwell Publishing Ltd, Leicester. doi:10.1111/j.1467-9671.2008.01122.x
- Speakman, L., Macgregor, N., Van Dijk, N., Darch, G., Neale, A. (2013) *Assessing the potential consequences of climate change for England's landscapes: South East Northumberland*. Natural England Research Reports
- Stapleton, C., Wyer, M.D., Crowther, J., McDonald, A., Kay, D., Greaves, J., Wither, A., Watkins, J., Francis, C., Humphrey, N., Bradford, M. (2008) Quantitative catchment profiling to apportion faecal indicator organism budgets for the Ribble system, the UK's sentinel drainage basin for Water Framework Directive research. *J. Environ. Manage.* 87, 535–550. doi:10.1016/j.jenvman.2006.11.035
- Stark, J., Meire, P., Temmerman, S. (2017) Changing tidal hydrodynamics during different stages of eco-geomorphological development of a tidal marsh: A numerical modeling study. *Estuar. Coast. Shelf Sci.* 188, 56–68. doi:10.1016/j.ecss.2017.02.014
- Stark, K., Gómez-Ros, J.M., Vives i Batlle, J., Lindbo Hansen, E., Beaugelin-Seiller, K., Kapustka, L.A., Wood, M.D., Bradshaw, C., Real, A., McGuire, C., Hinton, T.G. (2017) Dose assessment in environmental radiological protection: State of the art and perspectives. *J. Environ. Radioact.* 175–176, 105–114. doi:10.1016/j.jenvrad.2017.05.001
- Still, D.A., Calbrade, N.A., Holt, C.A. (2014) *Review and analysis of changes in waterbird use of the Mersey Estuary SPA, Mersey Narrows & North Wirral Foreshore SPA and Ribble & Alt Estuaries SPA*. BTO
- Stive, M.J., Aarninkhof, S.G., Hamm, L., Hanson, H., Larson, M., Wijnberg, K.M., Nicholls, R.J., Capobianco, M. (2002) Variability of shore and shoreline evolution. *Coast. Eng.* 47, 211–235. doi:10.1016/S0378-3839(02)00126-6
- Symonds, A.M. (2006) *Impacts of coastal realignment on intertidal sediment dynamics: Freiston Shore, The Wash*. Thesis, University of Southampton.
- Toda, H.Y., Yamamoto, T. (1995) Statistical inference in vector autoregressions with possibly integrated processes. *J. Econom.* 66, 225–250. doi:10.1016/0304-4076(94)01616-8
- Tovey, E.L., Pontee, N.I., Harvey, R., Tovey, E.L., Harvey, R. (2009) *Managed Realignment at Hesketh Out Marsh West*. *Manag. Realignment Hesketh Out Marsh West* 162, 223–228. doi:10.1680/ensu.2009.162.4.223
- Tyler, A.N., Heal, K. V. (2000) Predicting Areas of ¹³⁷Cs Loss and Accumulation in Upland Catchments. *Water. Air. Soil Pollut.* 121, 271–288. doi:10.1023/A:1005219009425
- Valchev, N.N., Trifonova, E. V, Andreeva, N.K. (2012) Past and recent trends in the western Black Sea storminess. *Nat. Hazards Earth Syst. Sci.* 12, 961–977. doi:10.5194/nhess-12-961-2012
- Van der Wal, D., Herman, P., Forster, R., Ysebaert, T., Rossi, F., Knaeps, E., Plancke, Y., Ides, S. (2008) Distribution and dynamics of intertidal macrobenthos predicted from remote sensing: response to microphytobenthos and environment. *Mar. Ecol. Prog. Ser.* 367, 57–72. doi:10.3354/meps07535
- Van der Wal, D., Pye, K., Neal, A. (2002) Long-term morphological change in the Ribble Estuary, northwest England. *Mar. Geol.* 189, 249–266. doi:10.1016/S0025-3227(02)00476-0
- Van Manen, B., Coco, G., Bryan, K.R., Ruessink, B.G. (2010) The use of artificial neural networks to analyze and predict alongshore sediment transport. *Nonlinear Process. Geophys.* 17, 395–404. doi:10.5194/npg-17-395-2010

- Van Manen, B., Nicholls, R.J., French, J.R., Barkwith, A., Bonaldo, D., Burningham, H., Brad Murray, A., Payo, A., Sutherland, J., Thornhill, G., Townend, I.H., van der Wegen, M., Walkden, M.J.A. (2016) Simulating mesoscale coastal evolution for decadal coastal management: A new framework integrating multiple, complementary modelling approaches. *Geomorphology* 256, 68–80. doi:10.1016/j.geomorph.2015.10.026
- Villa, M., Mosqueda, F., Hurtado, S., Mantero, J., Manjón, G., Periañez, R., Vaca, F., García-Tenorio, R. (2009) Contamination and restoration of an estuary affected by phosphogypsum releases. *Sci. Total Environ.* 408, 69–77. doi:10.1016/j.scitotenv.2009.09.028
- Vintró, L., Smith, K., Lucey, J., Mitchell, P. (2000) The environmental impact of the Sellafield discharges, in: *SCOPE-RADSITE*, pp. 1–27.
- Vives I Batlle, J., Bryan, S., McDonald, P. (2008) A process-based model for the partitioning of soluble, suspended particulate and bed sediment fractions of plutonium and caesium in the eastern Irish Sea. *J. Environ. Radioact.* 99, 62–80. doi:10.1016/j.jenvrad.2007.06.012
- Wakefield, R. (2005) Sediment and associated radionuclide dynamics within the Ribble estuary, North West England. Thesis, University of Stirling.
- Wakefield, R., Tyler, A N., McDonald, P., Atkin, P. a, Gleizon, P., Gilvear, D. (2011) Estimating sediment and caesium-137 fluxes in the Ribble Estuary through time-series airborne remote sensing. *J. Environ. Radioact.* 102, 252–61. doi:10.1016/j.jenvrad.2010.11.016
- Wal, D. Van der, Herman, P. (2006) Quantifying the particle size of intertidal sediments with satellite remote sensing in the visible light, thermal infrared and microwave spectral domain. *Remote Sens. from pixels to*, 1–5.
- Wang, Q., Li, Y., Wang, Y. (2011) Optimizing the weight loss-on-ignition methodology to quantify organic and carbonate carbon of sediments from diverse sources. *Environ. Monit. Assess.* 174, 241–257. doi:10.1007/s10661-010-1454-z
- Warren, C., Duzgoren-Aydin, N.S., Weston, J., Willett, K.L. (2012) Trace element concentrations in surface estuarine and marine sediments along the Mississippi Gulf Coast following Hurricane Katrina. *Environ. Monit. Assess.* 184, 1107–1119. doi:10.1007/s10661-011-2025-7
- Wolanski, E., Moore, K., Spagnol, S., D'Adamo, N., Pattiaratchi, C. (2001) Rapid, Human-Induced Siltation of the Macro-Tidal Ord River Estuary, Western Australia. *Estuar. Coast. Shelf Sci.* 53, 717–732. doi:10.1006/ecss.2001.0799
- Wolters, M., Bakker, J.P., Bertness, M.D., Jefferies, R.L., Möller, I. (2005a) Saltmarsh erosion and restoration in south-east England: Squeezing the evidence requires realignment. *J. Appl. Ecol.* doi:10.1111/j.1365-2664.2005.01080.x
- Wolters, M., Garbutt, A., Bakker, J.P. (2005b) Salt-marsh restoration: evaluating the success of de-embankments in north-west Europe. *Biol. Conserv.* 123, 249–268. doi:10.1016/j.biocon.2004.11.013
- Wriedt, T. (2012) Mie Theory: A Review, in: Rhodes, W.. (Ed.), *Springer Series in Optical Sciences*. Springer US, pp. 53–71. doi:10.1007/978-3-642-28738-1_2
- Wright, J.E. (1971) *Irish Sea investigations, 1969-70*. H.M.S.O.
- Zar, J.H. (2010) *Biostatistical analysis*. Prentice-Hall/Pearson. UK
- Zeileis, A., Grothendieck, G., Ryan, J.A. (2016) S3 Infrastructure for Regular and Irregular Time Series (Z's Ordered Observations).

Zeileis, A., Hothorn, T. (2002) Diagnostic checking in regression relationships. R News 2, 7–10.
accessed 15/01/2017: https://cran.r-project.org/doc/Rnews/Rnews_2002-3.pdf